43rd LPSC

Lunar and Planetary Science Conference

March 19–23, 2012
The Woodlands, Texas

PROGRAM OF TECHNICAL SESSIONS

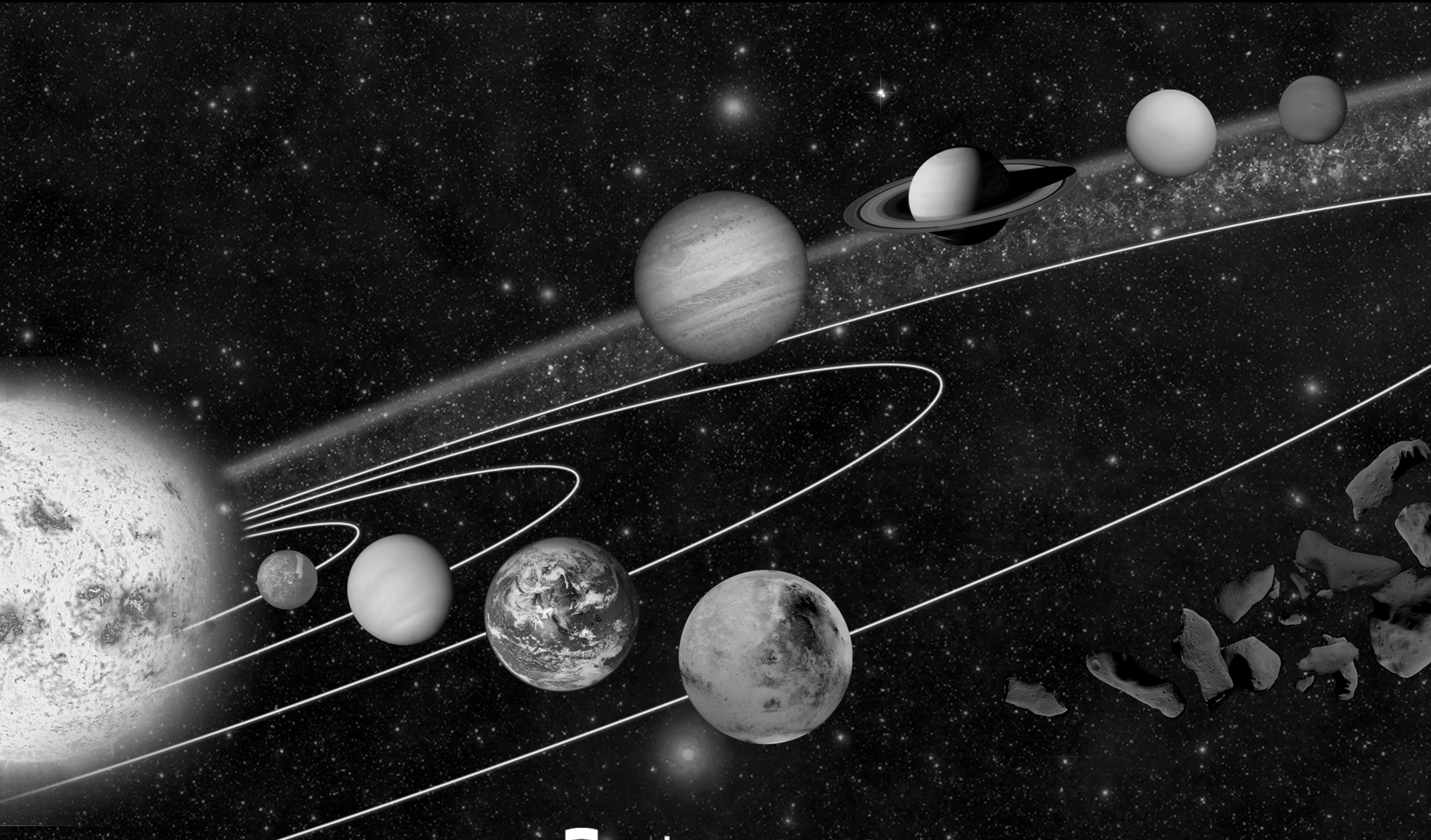

LUNAR AND PLANETARY INSTITUTE
NASA JOHNSON SPACE CENTER

Woodlands Waterway Convention Center Map

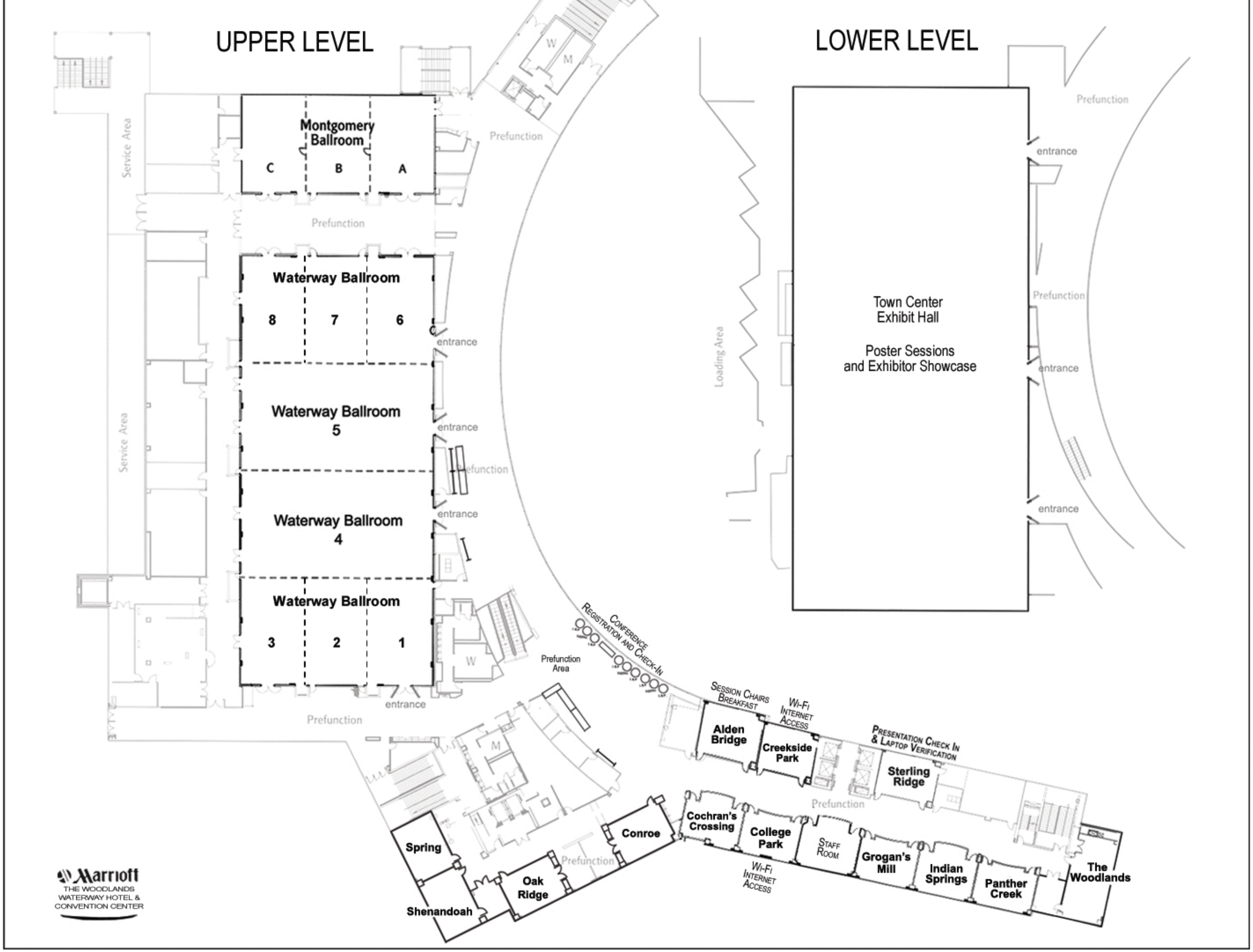

FORTY-THIRD LUNAR AND PLANETARY SCIENCE CONFERENCE

Program of Technical Sessions

March 19–23, 2012

The Woodlands Waterway Marriott Hotel and Convention Center
The Woodlands, Texas

Sponsored by
Lunar and Planetary Institute
NASA Johnson Space Center

Conference Co-Chairs
Stephen Mackwell, *Lunar and Planetary Institute*
Eileen Stansbery, *NASA Johnson Space Center*
David Draper, *NASA Johnson Space Center*

Program Committee

Neyda Abreu, *Pennsylvania State University*
Jeffrey Andrews-Hanna, *Colorado School of Mines*
Paul Archer, *NASA Johnson Space Center*
Janice Bishop, *SETI Institute/NASA Ames Research Center*
Veronica Bray, *University of Arizona/Lunar and Planetary Laboratory*
Debra Buczkowski, *Johns Hopkins University/Applied Physics Laboratory*
Devon Burr, *University of Tennessee*
Roy Christofferson, *NASA Johnson Space Center*
Catherine Corrigan, *Smithsonian Institution*
Dean Eppler, *NASA Johnson Space Center*
Juliane Gross, *American Museum of Natural History*
John Gruener, *NASA Johnson Space Center*
Justin Hagerty, *U.S. Geological Survey*
Rosalyn Hayward, *U.S. Geological Survey*
Veronika Heber, *University of California, Los Angeles*
Philipp Heck, *The Field Museum, Chicago*
Amanda Hendrix, *Jet Propulsion Laboratory*
Peter Isaacson, *University of Hawaii*
Jeffrey Kargel, *University of Arizona*
James Lyons, *University of California, Los Angeles*
Francis McCubbin, *University of New Mexico*
Andrew Needham, *Lunar and Planetary Institute*
Lan-Anh Nguyen, *Jacobs Engineering*
Paul Niles, *NASA Johnson Space Center*
Ryan Ogliore, *University of Hawaii*
Gordon Osinski, *Western University, Canada*
Louise Prockter, *The Johns Hopkins University Applied Physics Laboratory*
Jennifer Rapp, *Lunar and Planetary Institute*
Miriam Riner, *University of Hawaii*
Paul Schenk, *Lunar and Planetary Institute*
Susanne Schwenzer, *Open University*
Andrew Shaner, *Lunar and Planetary Institute*
Justin Simon, *NASA Johnson Space Center*
Steven Singletary, *Arizona State University*
Suzanne Smrekar, *Jet Propulsion Laboratory*
Timothy Titus, *U.S. Geological Survey*
Tomohiro Usui, *NASA Johnson Space Center*
James Van Orman, *Case Western Reserve University*
Channon Visscher, *Southwest Research Institute*
Renee Weber, *NASA Marshall Space Flight Center*
Catherine Weitz, *Planetary Science Institute*
Oliver White, *Lunar and Planetary Institute*

Produced by the Lunar and Planetary Institute (LPI), 3600 Bay Area Boulevard, Houston TX 77058-1113. Logistics, administrative, and publications support for the conference were provided by the Meeting and Publication Services Department of the LPI. The LPI is operated by the Universities Space Research Association under a cooperative agreement with the Science Mission Directorate of the National Aeronautics and Space Administration.

ABOUT LPSC

The Lunar and Planetary Science Conference brings together international specialists in petrology, geochemistry, geophysics, geology, and astronomy to present the latest results of research in planetary science. The five-day conference is organized by topical symposia and problem-oriented sessions.

The year 2012 will mark completion of the first 50 years of nuclear-powered spaceflight, which began with launch of the Transit 4A satellite in June 1961. In honor of this occasion, this year's LPSC is being held in conjunction with the Nuclear and Emerging Technologies for Space (NETS) topical meeting, which will take place March 21–23, 2012. Nuclear power has been an enabling technology for the most ambitious planetary missions in history. Holding the meetings together, with a joint plenary session on Wednesday evening, allows the planetary science community to learn more about the latest developments in nuclear power and propulsion, and see how new technologies could help their exploration efforts in the future.

LOGISTICAL INFORMATION

Venue Address and Phone Number

The conference is being held at The Woodlands Waterway Marriott Hotel and Convention Center, which is located at 1601 Lake Robbins Dr., The Woodlands TX 77380. The phone number for the hotel is 281-367-9797. Messages may be left for conference attendees by phoning the hotel and asking for the conference registration desk.

Please note that copy and printing services are not available at the conference registration desk, and must be arranged through the hotel business center. For your convenience, a minimal number of laptops and printers will be available in the Wi-Fi access rooms (see below).

Registration

Conference registration and check-in will be held on Sunday, March 18, from 4:00 to 8:00 p.m., and from 8:00 a.m. to 5:00 p.m. Monday through Friday, March 19 through 23. Conference badges provide access to all technical sessions, special events, and shuttle service. LPSC badges also grant access to all NETS technical sessions (and vice versa).

Internet Access

Complimentary Wi-Fi service will be available throughout the duration of the conference in the Creekside Park and College Park rooms (open only during conference hours), and in the Town Center Exhibit Area and immediate vicinity. Wi-Fi service will NOT be available in the oral session rooms. This restriction is (and has been) in place to curtail activities that could be distracting to speakers during their presentations.

Conference Shuttle Service

Conference shuttle bus service between the venue and the approved list of hotels will be provided on Sunday evening during the registration time and throughout the duration of the conference. Shuttle service will run before and immediately following all evening activities. Detailed shuttle schedules are available in the registration area and on the LPSC website at http://www.lpi.usra.edu/meetings/lpsc2012/travel/shuttleInfo/.

NEW THIS YEAR!!!

Poster Printing Available

AlphaGraphics will have a staffed booth at The Woodlands Waterway Marriott, just outside the Town Center Exhibit Area. Poster presenters can pick up pre-ordered posters or place orders for posters beginning on Sunday, March 18, at 4:00 p.m. The desk is located just outside the Town Center Exhibit Area on the first floor. For more information, visit their website at http://www.txagprinting.com/.

Personal Schedule

Create your own personal meeting schedule using the Personal Schedule tool found in the USRA Meeting Portal! Select the sessions you want to attend or talks you want to hear, then create a shareable schedule that can be viewed on your smart phone or shared with a colleague.

LIST OF EXHIBITORS

Cambridge University Press

www.cambridge.org/us
32 Avenue of the Americas
New York NY 10013-2473

Contact: James Murphy
212-924-3900
jmurphy@cambridge.org

Cambridge's publishing in books and journals combines state-of-the-art content with the highest standards of scholarship, writing and production. Visit our stand to browse new titles, available at a 20% discount, and to pick up sample issues of our journals. Visit our website to see everything we do: www.cambridge.org/us/.

Center for Space Nuclear Research

www.usra.csnr.edu
Universities Space Research Association
995 University Blvd.
Idaho Falls ID 83401

Contact: Delisa Rogers
208-526-5309
drogers@usra.edu

The Center for Space Nuclear Research (CSNR) is operated by the Universities Space Research Association (USRA) and Idaho National Laboratory (INL). The CSNR is a focus for engaging university research scientists in research and development of advanced space nuclear systems, including power/propulsion systems and radioisotope power generators. The CSNR creates opportunities for university researchers to collaborate with their counterparts at NASA and INL in projects to advance nuclear technologies for space exploration and other space applications.

Centre for Planetary Science and Exploration

www.cpsx.uwo.ca
Department of Earth Science
The University of Western Ontario
1151 Richmond Street
London Ontario N6A5B7 Canada

Contact: Alyssa Gilbert
519-661-2111
amoldow@uwo.ca

The goal of the Centre for Planetary Science and Exploration (CPSX) is to make The University of Western Ontario (Western) the focus for planetary science and exploration research in Canada, and to establish Western as a leading school for space systems design. The CPSX boasts the largest planetary science research group in Canada, consisting of over 50 faculty members and researchers, 10 post-docs, and 35 graduate students from 10 academic departments across the university.

Google Lunar X PRIZE

www.googlelunarxprize.org
X PRIZE Foundation
5510 Lincoln Blvd, Suite 100
Playa Vista CA 90094

Contact: Alexandra Hall
alex.hall@xprize.org

Before the end of 2015, robots will be landing on the surface of the Moon as competitors in the Google Lunar X PRIZE, vying to win some of a $30 million prize purse, and establish new efficient and effective ways to reach the Moon. Our 26 teams, from 16 countries, have a variety of options for taking small science payloads to the surface and are now seeking to partner with interested scientists!

Hamilton Sundstrand Rocketdyne
www.utc.com/units/hamilton.htm
6633 Canoga Ave.
Canoga Park CA 91309

Contact: Mike Tosca
818-586-0432
Mike.Tosca@hsr.utc.com

Hamilton Sundstrand Rocketdyne is currently working with NASA and the Department of Energy in defining and developing the latest radioisotope generators and nuclear power systems to power spacecraft and lunar surface systems, as well as advanced terrestrial nuclear power plants. We have been instrumental in bringing the necessary experience to energy and space exploration programs including innovative electrical power conversion, power management and distribution, heat transport, and thermal management as well as large-scale system integration, reliability and safety, and payload solutions.

Jacobs Technology
www.jacobstechnology.com
2224 Bay Area Blvd
Houston TX 77058

Contact: Glenn Ellis
281-461-5732
Glenn.Ellis@escg.jacobs.com

Jacobs Technology is the advanced technology division of Jacobs Engineering, one of the nation's largest engineering and technical services-only companies. With 70+ years of experience supporting government and commercial clients, we have earned a reputation for excellence and outstanding technical and managerial achievements in quality, performance, and safety. Our clients include the DOD, NASA, the U.S. Special Operations Command, the DOE, and dozens of commercial clients, such as Boeing, Lockheed Martin, Rolls-Royce, and General Motors.

JHU/Applied Physics Laboratory
civspace.jhuapl.edu
11100 Johns Hopkins Road
Laurel MD 20723

Contact: Margaret Simon
240-228-7150
Margaret.Simon@jhuapl.edu

The Johns Hopkins University's Applied Physics Laboratory (APL) leads several NASA planetary missions and conducts significant grant-based research on planetary, space, and Earth science interests. APL has built more than sixty-four spacecraft and instruments, including New Horizons, MESSENGER, STEREO, and RBSP.

JMARS — Mars Space Flight Facility — Arizona State University
jmars.mars.asu.edu
201 E. Orange Mall
Tempe AZ 85287

Contact: Scott Dickenshied
sdickens@mars.asu.edu

JMARS (Java Mission-planning and Analysis for Remote Sensing) is a Java-based geospatial information system developed by the Mars Space Flight Facility at Arizona State University. It is currently used for mission planning and scientific data analysis by several NASA missions, including Mars Odyssey, Mars Reconnaissance Orbiter, and the Lunar Reconnaissance Orbiter.

Lockheed Martin
www.lockheedmartin.com
P.O. Box 179
Mail Stop S8110
Denver CO 80201

Contact: Melissa Croswhite
303-971-9646
melissa.croswhite@lmco.com

Headquartered in Bethesda, Maryland, Lockheed Martin is a global security company that employs about 126,000 people worldwide and is principally engaged in the research, design, development, manufacture, integration, and sustainment of advanced technology systems, products, and services. Expanding our knowledge and understanding of the universe is a challenging endeavor that Lockheed Martin has been actively engaged in for five decades. We have developed and deployed numerous spacecraft and products supporting our understanding of Earth and Planetary Science, Heliophysics, and Astrophysics. We're accountable to one standard — 100% mission success. We understand the risks and will not shy away from the hard challenges associated with this mission.

NASA In-Space Propulsion Technology Program
spaceflightsystems.grc.nasa.gov/Advanced/ScienceProject/ISPT/
NASA Glenn Research Center
21000 Brookpark Rd, Mail Stop 142-5
Cleveland OH 44136

Contact: Daniel Vento
216-433-2834
Daniel.M.Vento@nasa.gov

Design Your Mission! NASA's In-Space Propulsion Technology program is sponsoring an opportunity to design your mission with the latest in NASA's Mission Design tools. Mission designers will be available to discuss your concept, potential methods of implementation, and design a notional trajectory to determine delivered capabilities and mission class estimate. The NASA ISPT Project provides advanced propulsion technology for planetary science missions. Technologies include advanced ion propulsion, advance chemical propulsion, and planetary ascent vehicles, as well as aerocapture and Earth entry vehicles.

NASA Radioisotope Power Systems

rps.nasa.gov
NASA/JPL
4800 Oak Grove Drive
Mail Stop 180-112
Pasadena CA 91109-8001

Contact: Eddie Gonzales
818-354-2326
edward.v.gonzales@jpl.nasa.gov

The Radioisotope Power Systems Program is an ongoing partnership between NASA and the U.S. Department of Energy to develop the next generation of reliable radioisotope power systems (RPS), enabling a broad range of science missions that could operate more widely and efficiently than their predecessors. This mission-driven technology development program is developing and validating two basic RPS units: the Multi-Mission Radioisotope Thermoelectric Generator (MMRTG) and the Advanced Stirling Radioisotope Generator (ASRG).

NASA's Eyes on the Solar System

solarsystem.nasa.gov/eyes
NASA/JPL
4800 Oak Grove Drive
Mail Stop 180-112
Pasadena CA 91109-8001

Contact: Eddie Gonzales
818-354-2326
edward.v.gonzales@jpl.nasa.gov

Almost everyone with a computer can now "ride along" with our planetary missions in a video-game like fashion. Using "Eyes on the Solar System," people everywhere can experience NASA and some ESA missions in real time or travel through time viewing missions from 1950 through 2050 using real mission data. New features and operation of NASA's "Eyes on the Solar System" and "Eyes on the Earth" online tools will be demonstrated.

National Nuclear Laboratory (UK)

www.nnl.co.uk
Chadwick House (5th Floor)
Birchwood Park
Warrington WA3 6AE
United Kingdom

Contact: Tim P Tinsley
tim.p.tinsley@nnl.co.uk

The UK's National Nuclear Laboratory (NNL) offers an unrivalled breadth of technical products and services to our customers across the whole nuclear industry. NNL covers the complete nuclear fuel cycle from fuel manufacture and power generation, to reprocessing, waste treatment, and disposal and including defence, new nuclear builds, and Homeland Security. NNL provides these services supported by an impressive range of facilities and links with international research organisations, academia, and other national laboratories.

NLSI-Center for Lunar Science and Exploration

www.lpi.usra.edu/nlsi/
USRA
3600 Bay Area Boulevard
Houston TX 77058

Contact: Julie Tygielski
281-486-2122
tygielski@lpi.usra.edu

The Center for Lunar Science and Exploration is an integral member of the NASA Lunar Science Institute and is designed to address the highest science priorities identified by the National Research Council for NASA, integrate lunar science with exploration activities to enhance mission productivity, generate expertise to meet the nation's needs, and provide a pipeline of knowledge for students and the public.

PDS Geosciences Node

pds-geosciences.wustl.edu
NASA
Washington University in St. Louis
One Brookings Dr., Campus Box 1169
St. Louis MO 63130

Contact: Susan Slavney
314-935-9295
geosci@wunder.wustl.edu

The Geosciences Node of NASA's Planetary Data System (PDS) archives and distributes data related to the study of the surfaces and interiors of terrestrial planetary bodies. We work with NASA missions to help them generate well-documented, permanent data archives. We provide data to NASA-sponsored researchers upon request, make data available using Analyst's Notebooks and Orbital Data Explorers, and provide expert assistance in using the data.

Regional Planetary Image Facility (RPIF) Network

science.nasa.gov/planetary-science/planetary-science-data/regional-planetary-image-facilities-rpif/
USGS Astrogeology Science Center
2255 N. Gemini Dr.
Flagstaff AZ 86001

Contact: David Portree
928-556-7037
dportree@usgs.gov

NASA's 17 U.S. and overseas Regional Planetary Image Facilities (RPIFs) supply planetary data to researchers, students, and the public. The RPIF Network was founded in 1977 to maintain photographic and digital data and mission documents. RPIF facilities, which are open to the public, are reference centers for browsing, studying, and selecting planetary data including images, maps, documents, and outreach materials. Experienced staff at each facility assist scientists, educators, students, media, and the public in accessing materials.

Smithsonian/NASA ADS
adslabs.org
Smithsonian Astrophysical Observatory
60 Garden Street, MS 83
Cambridge MA 02138

Contact: Donna Thompson
617-496-7660
dthompson@cfa.harvard.edu

The NASA Astrophysics Data System (ADS) is a Digital Library portal offering access to 9 million bibliographic records in Astronomy and Physics. The ADS provides access and links to a wealth of external resources, including electronic articles, data catalogs, and archives. Please stop by our booth for a demonstration of ADS Labs, our new search interface featuring filtering of results, visualization of bibliographic networks, article recommendations, and full-text searching. Find us online at http://adslabs.org.

Space Science in Wikipedia
www.lpi.usra.edu
Lunar and Planetary Institute
3600 Bay Area Blvd
Houston TX 77059

Contact: Mary Ann Hager
281-486-2136
mhager@hou.usra.edu

The Lunar and Planetary Institute (LPI) is a research institute that provides support services to NASA and the planetary science community, and conducts planetary science research under the leadership of staff scientists, visiting researchers, and postdoctoral fellows. LPI is available to assist the science community in sharing their knowledge and expertise worldwide on the world's most successful online encyclopedia, Wikipedia.

Springer
www.springer.com
233 Spring St.
6th Floor
New York NY 10013

Contact: Megan Ernst
212-460-1511
megan.ernst@springer.com

Our business is publishing. Throughout the world, we provide scientific and professional communities with superior specialist information — produced by authors and colleagues across cultures. We foster communication among our customers — researchers, students, and professionals. We think ahead, move fast, and promote change: Creative business models, inventive products, and mutually beneficial international partnerships have established us as a trusted supplier and pioneer in the information age.

The Boeing Company
www.boeing.com
Advanced Space Exploration
13100 Space Center Blvd
MC HB4-20
Houston TX 77059

Contact: Kurt Klaus
281-226-5707
kurt.k.klaus@boeing.com

Boeing Defense, Space & Security's Phantom Works group includes advanced programs, pursues new business, and executes new programs prior to their reaching the System Design and Development phase. In close collaboration with Boeing Research & Technology, Boeing's advanced research and development unit, Phantom Works develops and transitions advanced programs into the BDS business areas and ultimately to BDS' defense and space customers.

The University of Arizona Press
www.uapress.arizona.edu
1510 E. University Blvd
Tucson AZ 85721-0055

Contact: Arin Cumming
520-621-4913
acumming@uapress.arizona.edu

The University of Arizona Press publishes important research that bears great significance to the field of Space Science, including publications in our Space Science Series. Please visit our website, www.uapress.arizona.edu, for more information and visit us in our booth during to see a great selection of our books available for order at a special conference discount.

U.S. Geological Survey Astrogeology Science Center
astrogeology.usgs.gov/
2255 N. Gemini Dr
Bldg. 6
Flagstaff AZ 86001

Contact: Corey Fortezzo
928-556-7133
cfortezzo@usgs.gov

The United States Geological Survey Astrogeology Science Center is a community leader in planetary science research, image processing, cartography, geologic mapping, and geographic information system (GIS). Our mission is to serve the planetary community and public with research and technical expertise, analytical software, image products, digital and print maps, technical training, and education and public outreach programs.

LPSC WEEK AT A GLANCE

Day and Time	Waterway Ballroom 1	Waterway Ballroom 4	Waterway Ballroom 5	Waterway Ballroom 6	Montgomery Ballroom
Monday Morning, 8:30 a.m.	**SPECIAL SESSION:** A Season in the Saturn System I	New Views on Lunar Volatiles	Hot Stuff: Interplanetary Studies of Impact Melt	Chemical Processes in the Solar Nebula and Latest Genesis Results	Achondrites: From Core to Crust
Monday Afternoon, 1:30 p.m.		**PLENARY SESSION:** Masursky Lecture and Dwornik Award Presentations			
Monday Afternoon, 2:30 p.m.	**SPECIAL SESSION:** A Season in the Saturn System II	Mind the Gap: Lunar Petrology and Remote Sensing	Movers and Shakers: Planetary Dynamics and Tectonics	Recent Slope Processes on Mars: Sliding, Flowing, and Falling Down	
Monday Evening, 5:30 p.m.		**NASA Headquarters Briefing**			
Tuesday Morning, 8:30 a.m.	**SPECIAL SESSION:** Planetary Hydrology: Wet Worlds	Diverse Views of the Lunar Crust: An Orbital Perspective	Solar Nebula Mixing and CAIs	New Martian Meteorites and New Perspectives on Old Favorites	Venus Volcanism Viewpoints: Vague or Viable?
Tuesday Afternoon, 1:30 p.m.	Ice is Nice: Icy Satellite Landforms, Processes, and Structure	Opportunities for Scientist Participation in Education and Public Outreach	Isotopic Constraints on Early Solar System Chronology	Martian Hydrated Minerals and Volatiles from Mantle to Surface	
Tuesday Evening, 6:00 p.m. Town Center Exhibit Area Poster Session I					
Wednesday Morning, 8:30 a.m.	**SPECIAL SESSION:** MESSENGER's First Year in Orbit About Mercury	Airless Bodies Exposed: Space Environment Conditions and Surface Interactions	Impact Ejecta: Processes and Products	Primary and Secondary Martian Geochemistry	Primary and Secondary Martian Geochemistry
Wednesday Afternoon, 12:15 p.m. Panther Creek NETS Tutorial: Building the Bridge Between Science Missions and Nuclear Power Sources					
Wednesday Afternoon, 1:30 p.m.	Mercury Composition and Evolution from the Inside Out	Impact Craters: Peaks, Rings, and Basins	Small Body Studies I: Formation, Regolith, and Rubble Piles	Roving on Mars: Current and Future Sites	Chondrite Components and Primary Processes
Wednesday Evening, 5:30 p.m.		**Nuclear and Emerging Technologies for Space: Opening Plenary (Joint LPSC/NETS Plenary Session)**			
Thursday Morning, 8:30 a.m.	NETS SESSIONS	Lunar Chronology By Any Means Necessary	Small Body Studies II: Earth-Crossing to Main Belt	Water on Mars: Flowing, Flooding, and Freezing	Secondary Processes in Chondrites
Thursday Afternoon, 1:30 p.m.	NETS SESSIONS	Lunar Petrology and Geochemistry: From Core to Crust	**SPECIAL SESSION:** Dawn Over Vesta I	Planetary Brines and Alteration	Presolar Grains: Insight into Stellar Processes
Thursday Evening, 6:00 p.m. Town Center Exhibit Area Poster Session II					
Friday Morning, 8:30 a.m.	NETS SESSIONS	Lunar Geophysics and Internal Structure	**SPECIAL SESSION:** Dawn Over Vesta II: The HED-Vesta Connection	Mars Aeolian Processes: Prepare to be Blown Away! ***Followed at 10:00 a.m. by*** Mars Polar Processes: Very Cold and Really Cool	Cosmic Dust: Interstellar, Interplanetary, and Cometary Material
Friday Afternoon, 1:30 p.m.	NETS SESSIONS	Lunar Mapping ***Followed at 10:00 a.m. by*** Mars Climate Tales: Meteorites, Morphology, Models	**SPECIAL SESSION:** Dawn Over Vesta III: Regolith of a Transitional Planet	Young Solar System Cataclysm	Planetary Interiors: Dynamics and Differentiation

NETS Week at a Glance

Day and Time	Waterway Ballroom 1	Waterway Ballroom 2	Waterway Ballroom 3	Waterway Ballroom 4/5	Panther Creek
Wednesday Afternoon, 12:15 p.m.					NETS Tutorial: Building the Bridge Between Science Missions and Nuclear Power Sources
Wednesday Evening, 5:30 p.m.				Nuclear and Emerging Technologies for Space: Opening Plenary	
Thursday Morning, 8:30 a.m.	Fission Power Systems		Radioisotope Power Systems: Pu-238 Production and Analysis		
Thursday Morning, 10:30 a.m.	Advanced Concepts: Advanced Fission Concepts and Systems	Missions and Architectures: Space Radiation Shielding and Lunar Surface Concepts	Radioisotope Power Systems: Mission Simulation, Integration and Test		
Thursday Afternoon, 1:00 p.m	Fission Power Systems: Reactor Design and Simulation	Nuclear Thermal Propulsion: Program Overview	Radioisotope Power Systems: RPS Design Safety		
Thursday Afternoon, 3:30 p.m	Fission Power Systems: Heat Transfer and Thermal Control	Nuclear Thermal Propulsion: Modeling	Radioisotope Power Systems: Thermoelectric Energy Conversion		
Thursday Evening, 6:00 p.m. Town Center Exhibit Area Poster Session: Nuclear and Emerging Technologies for Space					
Friday Morning, 8:30 a.m.	Fission Power Systems: Power Conversion, Management, and Distribution	Nuclear Thermal Propulsion: NTP Fuels I	Radioisotope Power Systems: Stirling Generators		
Friday Morning, 10:30 a.m.	Fission Power Systems: Testing and Validation	Nuclear Thermal Propulsion: NTP Fuels II	Radioisotope Power Systems: Stirling Energy Conversion		
Friday Afternoon, 1:30 p.m.	Missions and Architectures: Space Policy and Risk Analysis	Advanced Concepts: Aneutronic Fusion Power and Propulsion	Radioisotope Power Systems: Alternative Fuels and Methods		
Friday Afternoon, 3:30 p.m.		Advanced Concepts: LENR, Anti-Matter, and New Physics	Radioisotope Power Systems: Future RPS Concepts		

Guide to Technical Program

POSTER SESSIONS

Tuesday Evening, March 20, 6:00 p.m.

Town Center Exhibit Area — Poster Session I

Thursday Evening, March 22, 6:00 p.m.

PRINT ONLY PRESENTATIONS

***** Denotes speaker**

SPECIAL SESSION:
A SEASON IN THE SATURN SYSTEM I
Monday, 8:30 a.m.   Waterway Ballroom 1

Chairs: **Dennis Matson and David Blackburn**

8:30 a.m. Spilker L. J. *
Cassini: Science Highlights from the Equinox and Solstice Missions **[#1358]**
The Cassini exploration of the Saturn system has returned a wealth of scientific data. Even after more than seven years of close study, the Cassini spacecraft still unveils new scientific discoveries that continue to captivate us.

9:00 a.m. West R. A. * Ovanessian A. Turtle E. P. Ray T. Balloch J. Dumont P. Lavvas P. Lorenz R. Rannou P.
Titan's Detached Haze and Polar Vortex: Large-Amplitude Seasonal Variations **[#2897]**
We present observations of Titan's detached haze showing large-amplitude seasonal variations. These observations and future observations from Cassini provide strong tests of dynamical and microphysical processes in Titan's atmosphere.

9:15 a.m. Teanby N. A. * Irwin P. G. J. Nixon C. A. de Kok R.
Seasonal Change at Titan's Poles **[#1500]**
We use seven years of data from Cassini to look for seasonal changes in the atmosphere of Saturn's largest moon — Titan. In particular we focus on the implications for atmospheric circulation as Titan moves from northern winter to northern summer.

9:30 a.m. Turtle E. P. * Perry J. E. Barnes J. W. McEwen A. S. Barbara J. M. Del Genio A. D. Hayes A. G. West R. A. Lorenz R. D. Schaller E. L. Lunine J. I. Ray T. L. Lopes R. M. C. Stofan E. R.
Evolution of Titan's Weather Patterns and Accompanying Surface Changes in the Wake of the Seasonal Shift of the Intertropical Convergence Zone **[#2555]**
After springtime rain / Titan's weather's quiet as / Northern summer looms.

9:45 a.m. Barnes J. W. * Buratti B. J. Turtle E. P. Bow J. Dalba P. A. Perry J. Rodriguez S. LeMouelic S. Baines K. H. Sotin C. Lorenz R. D. Malaska M. J. McCord T. B. Brown R. H. Clark R. N. Jaumann R. Hayne P. Nicholson P. D. Soderblom J. M. Soderblom L. A.
Cassini/VIMS Spectra and Time-Evolution of Precipitation-Associated Surface Brightenings on Titan **[#2762]**
Large areas of Titan's surface brightened at all wavelengths as seen from Cassini/VIMS for several months, then faded. The brightenings occurred after a large storm and rainfall event, and may relate to volatile refreezing due to evaporative cooling.

10:00 a.m. Mitchell K. L. * West R. D. Stiles B. W. Pappalardo R. T. Anderson Y. Lopes R. M. C. Wall S. D. Janssen M. A. Cassini Radar Team
The First High-Resolution SAR Observation of Enceladus by Cassini Radar **[#2760]**
We present SAR imagery and initial interpretations from the Cassini E16 fly-by of Enceladus. Different tectonic/radiometric domains are interpreted as the result of tectonic resurfacing and partial obfuscation by cryovolcanic plume deposition.

10:15 a.m. Hurford T. A. * Helfenstein P. Spitale J. N.
Tidal Control of Jet Eruptions Observed by Cassini ISS **[#2154]**
We examine the stresses on the Tiger Stripe active source regions to see how well diurnal tidal stress caused by Enceladus' orbital eccentricity may possibly correlate with and thus control the observed eruptions.

10:30 a.m. Buratti B. J. * Schenk P. M. Khurana K. Moore J. M.
Dione: The Evidence for Activity **[#1713]**
Several lines of evidence suggest that Dione is currently geologically active or has been recently.

10:45 a.m. Teolis B. D. * Waite J. H.
Cassini Measurements Show Seasonal O_2 — CO_2 Exospheres and Possible Seasonal CO_2 Frosts at Rhea and Dione **[#2923]**
We will present the recent finding of an O_2-CO_2 Dione exosphere by Cassini, and discuss modeling of the different north-south CO_2 density at Rhea, and the CO_2 abundance at Dione, indicating strongly seasonal CO_2 exospheres and polar frosts.

11:00 a.m. Esposito L. W. * Meinke B. K. Albers N. Sremcevic M.
A Season in Saturn's Rings: Cycling, Recycling and Ring History **[#2904]**
Cassini observations of Saturn's rings show a complex geophysical system. Recycling can allow the rings to be as ancient as the solar system.

11:15 a.m. Ferrari C. * Reffet E.
Temperature Gradients in Saturn's B Ring: Clue to its Thickness **[#2177]**
How vertical temperature gradients in very opaque rings can reveal their thickness and density.

NEW VIEWS ON LUNAR VOLATILES
Monday, 8:30 a.m. Waterway Ballroom 4

Chairs: James Greenwood and G. Jeffrey Taylor

8:30 a.m. Evans A. J. * Zuber M. T.
The Possible Role of Water in the Early Thermal Evolution of the Moon **[#2406]**
Recent work suggests a water concentration of at least 260 ppm was present in the lunar mantle ~3 Ga. Through a lunar convection model of post-magma ocean solidification, we examine the possible role of water and its effect on lunar thermal evolution.

8:45 a.m. Chen Y. * Zhang Y.
Initial Water Concentration and Degassing of Lunar Basalts Inferred from Melt Inclusions in Olivine **[#1361]**
We report preliminary data on water concentration in olivine-hosted melt inclusions in lunar basalts. Our results raise important questions about the budget and distribution of water in the Moon and its roles in the magma evolution.

9:00 a.m. Saal A. E. * Hauri E. H. Van Orman J. A. Rutherford M. J.
D/H Ratios of the Lunar Volcanic Glasses **[#1327]**
Here we report the first in-situ measurements of the isotopic composition of hydrogen dissolved in primitive volcanic glass and their melt inclusion samples recovered from the Moon by the Apollo 15 and 17 missions. We discuss the origin of the lunar water.

9:15 a.m. Greenwood J. P. * Itoh S. Sakamoto N. Warren P. H. Taylor L. A. Yurimoto H.
Towards a Wetter Moon: Implications of High Volatile Abundances in Lunar Apatite **[#2089]**
New results on water and D/H of lunar apatite are presented. Implications of high volatile abundances of lunar apatite for the water inventory of the Moon are considered in light of degassing of molecular hydrogen and low oxygen fugacities.

9:30 a.m. Taylor G. J. * Robinson K. L.
Distinct Volatile Reservoirs in the Moon: Evidence for Late Addition of Volatiles and Water **[#2443]**
Concentrations of highly volatile elements are roughly chondritic among pyroclastic glasses, mare basalts, and KREEP basalts and vary directly with water contents, suggesting late addition of a chondritic component containing a few tenths % water.

9:45 a.m. Sharp Z. D. * McCubbin F. M. Shearer C. K. Jr.
A Unifying Theory for H-Bearing Volatiles on the Moon **[#2751]**
The low oxygen fugacity of the Moon requires that H_2 gas is the dominant phase in the O-H system. H_2 is easily lost to space, so that the low H content of most basalts, high D/H ratios, presence of Fe(o) and high Cl-isotope ratios are all explained.

10:00 a.m. Liu Y. * Guan Y. Zhang Y. Rossman G. R. Eiler J. M. Taylor L. A.
Lunar Surface Water in Agglutinates: Origin and Abundances **[#1864]**
We report in situ measurements of the abundances and H-isotope compositions of lunar surface water stored in lunar soil samples.

10:15 a.m. Poston M. J. * Grieves G. A. Aleksandrov A. B. McLain J. L. Hibbitts C. A. Dyar M. D. Orlando T. M.
Formation and Time Evolution of Hydroxyl on Lunar Regolith by Proton Implantation and Diffusion **[#2801]**
A 1D discretized source-sink-transport simulation of solar wind proton implantation into lunar regolith. Trends with time of day, differing material, and differing latitude are described.

10:30 a.m. Dyar M. D. * Hibbitts K. A. King P. L. Breves E. A. Orlando T. M. Poston M. J. Grieves G. A. Tucker J. M. Seaman S. J.
Remote Sensing of H in Lunar Surface Materials: The Effect of Composition on Hydrogen Solubility and Quantification **[#2264]**
This paper explores the relationship between 3-µm band strength and the composition of lunar surface materials through transmission FTIR spectroscopy of a suite of synthetic lunar-analog glasses.

10:45 a.m. Miller R. S. * Nerurkar G. Lawrence D. J.
New Insights Into Hydrogen at the Lunar Poles from the Detection of Fast and Epithermal Neutron Signatures **[#1538]**
We report the first definitive detection of a fast-neutron signature consistent with enhanced lunar hydrogen abundances, and present new spatial distributions for epithermal-derived hydrogen at the lunar poles using a combined LP-LRO dataset.

11:00 a.m. Elphic R. C. * Paige D. A. Siegler M. A. Vasavada A. R. Teodoro L. A. Eke V. R.
Limits on the Abundance and Burial Depth of Lunar Polar Ice Deposits **[#1895]**
Water equivalent hydrogen abundances in the extensive subsurface cold traps must be less than 1 wt% generally, but can exceed this in specific locations. Observations of thermal neutrons help constrain abundance and burial depth.

11:15 a.m. Sanin A. B. * Mitrofanov I . G. Litvak M. L. Boynton W. V. Chin G. Droege G. Evans L. G. Garvin J. B. Golovin D. V. Harshman K. McClanahan T. P. Malakhov A. Mokrousov M. I. Milikh G. Sagdeev R. Z. Starr R. D.
Testing of Lunar Permanently Shadowed Regions for Water Ice **[#2134]**
The Lunar Exploration Neutron Detector (LEND) data have been used to look at distribution of neutron flux at the Moon's poles. LEND's narrow field of view provides the possibility to test the hypothesis if all major PSRs are reservoirs of hydrogen or water ice.

11:30 a.m. Eke V. R. * Teodoro L. F. A. Lawrence D. J. Elphic R. C. Feldman W. C.
What is the LEND Collimated Detector Really Measuring? **[#2211]**
A comprehensive analysis of data from the Lunar Exploration Neutron Detector Collimated Sensors for Epithermal Neutrons is performed, with significant implications for the lunar hydrogen distribution.

HOT STUFF: INTERPLANETARY STUDIES OF IMPACT MELT
Monday, 8:30 a.m. Waterway Ballroom 5

Chairs: Veronica Bray and Justin Hagerty

8:30 a.m. Osinski G. R. * Singleton A. C. Ozaruk A. Hansen J. R.
New Investigations of the Gow Lake Impact Structure, Saskatchewan, Canada: Impact Melt Rocks, Astronaut Training, and More **[#2367]**
New investigations of the Gow Lake impact structure has revealed an almost complete sequence of impactites from the crater floor upward through a series of melt-free and melt-bearing rocks. This research involved an astronaut training component.

8:45 a.m. Pittarello L. * Koeberl C.
New Insight into Impact Glasses from the El'gygytgyn Structure, Northern Siberia, Russia **[#1475]**
The El'gygytgyn impact structure provides the unique opportunity on Earth to study a meteorite impact in acidic volcanic rocks. Petrographic studies on the impact glasses improve our knowledge of the impact process and constrain the glass formation.

9:00 a.m. Singleton A. C. * Osinski G. R. Grieve R. A. F. Shaver C.
Characterization of Glasses in Impact Breccia Dykes at the Mistastin Lake Impact Structure, Labrador **[#2588]**
On Horseshoe Island in Mistastin Lake there exist dikes of impact melt bearing breccia containing melt clasts. The composition of these clasts varies from the melt sheet indicating that there is a missing component contributing to the melt clasts.

9:15 a.m. Tornabene L. L. * Osinski G. R. McEwen A. S. Boyce J. M. Bray V. J. Caudill C. M. Grant J. A. Hamilton C. W. Mattson S. Mouginis-Mark P. J. HiRISE Operations and Science Team
Wide-Spread Occurrence of Crater-Related Pitted Materials on Mars: Implications for the Role of Target Volatiles with Respect to the Impact Process **[#2418]**
The nearly global distribution of martian crater-related pitted materials, possibly representing a impact melt-rich deposit that is volatile-rich or interacted with volatile-rich materials, will be discussed.

9:30 a.m. Ostrach L. R. * Robinson M. S. Denevi B. W.
Distribution of Impact Melt on Mercury and the Moon **[#1113]**
We identified interior impact melt deposits within hundreds of craters on Mercury and the Moon. Our results show that for craters ≥40 km diameter, mercurian craters contain larger areal extents of interior ponded impact melt than lunar craters.

9:45 a.m. Stopar J. D. * Hawke B. R. Robinson M. S. Denevi B. W. Giguere T. A.
Distribution, Occurrence, and Degradation of Impact Melt Associated with Small Lunar Craters **[#1645]**
We characterize impact melt deposits at simple craters observed by LROC, especially craters D < 1 km. We also assess criteria for melt identification at small diameters, factors responsible for melt distribution, and changes in melt with degradation.

10:00 a.m. Neish C. D. * Glines N. Carter L. M. Bray V. J. Hawke B. R. Bussey D. B. J. Mini-RF Science Team
New Lunar Impact Melt Flows as Revealed by Mini-RF on LRO **[#2388]**
Lunar impact melts / Buried under regolith / First seen by radar.

10:15 a.m. Shankar B. * Osinski G. R. Antonenko I. Tornabene L. L.
Multispectral Analyses of the Olcott Crater with Recent High Resolution Datasets **[#1357]**
Characterizing the morphology and compositional details of impact materials associated with the Olcott crater on the lunar farside. We use data from Chandrayaan-1, Lunar Reconnaissance Orbiter, and Clementine for this study.

10:30 a.m. Dhingra D. * Pieters C. M.
Spectroscopy of Impact Melts — Results from Lunar Crater Tycho **[#1836]**
Compositional diversity among impact melts is illustrated using M^3 spectral data analysis of impact melts at crater Tycho. The observed spectral variation could be due to differences in crystallinity, clast fraction, or inefficient mixing of melt.

10:45 a.m. Keszthelyi L. P. *
Rate of Solidification of Silicate Melts on the Earth, Moon, Mars, and Beyond **[#2547]**
The sensitivity of the crust growth rate is investigated using a numerical model. The growth rate is extremely insensitive to environmental and intrinsic parameters of the melt, making crust thickness a robust geochronometer.

11:00 a.m. Darling J. R. * Moser D. E.
Impact Induced Crustal Differentiation: New Insights from the Sudbury Structure **[#2164]**
Hafnium isotope analysis reveals a common impact melting origin for igneous units within the Sudbury impact structure. The differentiated impact melt sheet allows for new insights into the effects of impact melting on planetary crusts.

11:15 a.m. Kring D. A. * Abramov O. Marchi S.
Impact Melt Production During the Basin-Forming Epoch **[#1615]**
For the first time, an analytical impact melt calculation, suitable for the most probable impact angle of 45°, is integrated with an observed ancient crater population to determine the melt volumes produced as a function of crater diameters.

11:30 a.m. Davison T. M. * Ciesla F. J. Collins G. S.
The Effect of Impact Obliquity on Porous Planetesimal Collisions **[#1235]**
We investigate the effect of impact obliquity on heating in collisions between porous planetesimals, and find that both the impact angle and the target curvature have a significant effect on the mass of material shock heated during a collision event.

CHEMICAL PROCESSES IN THE SOLAR NEBULA AND LATEST GENESIS RESULTS
Monday, 8:30 a.m. Waterway Ballroom 6

Chairs: Gerardo Dominguez and James Lyons

8:30 a.m. Huss G. R. * Nagashima K. Burnett D. S. Jurewicz A. J. G. Olinger C. T.
A New Upper Limit on the D/H Ratio in the Solar Wind **[#1709]**
We report measurements of D/H in solar wind from the Genesis B/C- and H-array collectors. Our new upper limit on D/H in the solar wind is a factor of >10 lower than previous sample-based estimates.

8:45 a.m. Desch S. J. *
Snow Lines in Externally Photoevaporated Protoplanetary Disks **[#2770]**
I calculate the effect of external photoevaporation on the radial distribution of water in a protoplanetary disk. I find the outward flow of gas prevents ice from drifting back into the inner disk even though temperatures are cold enough for ice.

9:00 a.m. Pascucci I. * Sterzik M. Alexander R. Sacco G.
Evidence for Disk Photoevaporation Driven by the Central Star — Impact on Planetary Architectures **[#1155]**
We present the first observational evidence for disk photoevaporation driven by the central star and discuss the implications of star-driven photoevaporation on the architecture of planetary systems.

9:15 a.m. Yang L. * Ciesla F. J. Alexander C. M. O'D.
The D/H Ratio of Water in a Forming and Evolving Protoplanetary Disk **[#2023]**
We explore how the D/H ratio of water would evolve in the solar nebula by coupling our model of transport in a growing protoplanetary disk with a kinetic study of chemical reactions involving hydrogen-bearing species.

9:30 a.m. Alexander C. M. O'D. * Bowden R. Fogel M. L. Howard K. T. Herd C. D. K.
The Origin of Water in Chondrites and Volatiles in the Terrestrial Planet Region **[#1929]**
The D/H ratios of water in CCs, Ocs, and Rs are inconsistent with models in which chondritic water and/or chondrites formed in the outer solar system.

9:45 a.m. Nuth J. A. III * Johnson N. M.
Will Organic Synthesis Within Icy Grains or on Dust Surfaces Within the Primitive Solar Nebula Completely Erase the Effects of Photochemical Self Shielding? **[#1495]**
Self shielding relies on the differential dissociation of CO and sequestration of ^{16}O-rich CO. Organic synthesis in the solar nebula starts with CO and hydrogen on grain surfaces, producing hydrocarbons and water. ^{16}O-rich CO cannot be sequestered.

10:00 a.m. Chakraborty S. * Yanchulova P. Thiemens M. H.
Laboratory Observation of Mass-Independent Oxygen Isotopic Composition in Solid Silicates Through Gas Phase Reaction: Cosmochemical Implications **[#2300]**
This abstract describes experiments of the gas phase oxidation reaction of SiO to form SiO_x and present isotope results from the gas and solid phase products and reactants. Mass-independent oxygen isotopic composition was observed in silicates.

10:15 a.m. Dominguez G. * Jackson T. Nunn M. Basov D. Thiemens M. H.
Low Temperature Mass-Independent Ozone Formation on Cold Surfaces **[#2403]**
We report the results of laboratory O_2 photolysis experiments that provide the first evidence that the formation of O_3, an important precursor to H_2O formation, on cold (T~32 K) surfaces is a mass-independent process.

10:30 a.m. Ozima M. * Suzuki T. K. Yamada A.
Genesis SW-Oxygen Corrected for SW/SUN Isotopic Fractionation is Closer to Earth Oxygen than to CAI **[#1194]**
The Genesis project gave a convincing isotopic composition of oxygen in bulk solar wind sample, but correction for putative isotopic fractionation between SW and the Sun is still needed to conclude the solar oxygen-isotopic composition.

10:45 a.m. Shi X. * Yin Q.-Z. Wiens R. Ng C.-Y.
Isotope Composition of Atomic Oxygen and Branching Ratio from CO Predissociation: Implications for Oxygen Isotope Evolution in the Early Solar Nebula **[#1403]**
We investigated the "self-shielding" effects by detecting atomic ^{16}O, ^{17}O, and ^{18}O as fragments from CO predissociation. Our photonion imaging results may help explain the different rare isotope enrichment between N and O reported by the Genesis team.

11:00 a.m. Lyons J. R. *
CO Self-Shielding by Various Stellar Sources **[#2818]**
CO self-shielding with two stellar sources is considered. Even though the stars have very different spectra in the FUV region, both predict oxygen isotope slopes ~0.9.

11:15 a.m. Chakraborty S. Jackson T. L. Muskatel B. H. Ahmed M. Levine R. D. Thiemens M. H. *
Nitrogen Isotopic Fractionation in VUV Photodissociation of N_2: Implications for the Early Solar System **[#2347]**
In this abstract we present the first experimentally determined N-isotopic fractionations during VUV photolysis of N_2 using the ALS synchrotron.

11:30 a.m. Milam S. N. * Charnley S. B.
Observations of Nitrogen Fractionation in Prestellar Cores: Nitriles Tracing Interstellar Chemistry **[#2618]**
Fractionated material found in primitive materials is suggested to originate from interstellar chemistry. We present observations of nitrogen and carbon fractionation in dense cores and will discuss these results as compared to primitive materials.

11:45 a.m. Wirström E. S. * Charnley S. B. Cordiner M. A. Milam S. N.
Spin-State-Dependent Ion-Molecule Chemistry as the Origin of ^{15}N and D Isotopic Anomalies in Primitive Matter **[#2457]**
We present calculations showing how different ortho/para ratios in interstellar H_2 can explain the highly variable D and ^{15}N enrichments observed in meteoritic material and IDPs.

MON ORALS

ACHONDRITES: FROM CORE TO CRUST
Monday, 8:30 a.m. Montgomery Ballroom

Chairs: Kathryn Gardner-Vandy and Deon van Niekerk

8:30 a.m. Goldstein J. I. * Huss G. R. Scott E. R. D.
Carbon Contents of Metallic Phases in Iron Meteorites **[#1339]**
To understand the effects of carbon on phase growth in iron meteorites, we measured the C distribution between kamacite, taenite, and plessite regions. Carbon concentrations were systematically lower in meteorites lacking graphite and carbides.

8:45 a.m. Scott E. R. D. * Goldstein J. I.
Occurrence of Carbides and Graphite in Iron Meteorites and Origin of C-Rich Irons **[#2671]**
Two carbides—cohenite Fe_3C and haxonite $Fe_{23}C_6$ — and graphite are abundant in groups IAB and IIICD, and totally absent in groups IVA and IVB reflecting nebular conditions during the formation of chondritic precursors.

9:00 a.m. Antonelli M. A. * Peters M. Farquhar J.
Sulfur Isotopic Compositions of Magmatic and Non-Magmatic Iron Meteorites **[#2081]**
We report the multiple sulfur isotopic compositions of fourteen iron meteorites from three different groups. We find that there are systematic differences in the sulfur isotopic composition of magmatic versus non magmatic iron meteorites.

9:15 a.m. Andreasen R. * Rehkämper M. Benedix G. K. Theis K. J. Schönbächler M. Smith C. L.
Lead-Thallium Chronology of IIAB and IIIAB Iron Meteorites and the Solar System Initial Abundance of Lead-205 **[#2902]**
Pb-Tl isotope data for the IIAB irons suggest that the IIAB metal segregated about 2 My after solar system formation and crystallized about 13 My later. Their initial Tl composition suggests slightly higher levels of ^{205}Pb than previously thought.

MON ORALS

9:30 a.m. Horstmann M. Humayun M. * Harries D. Langenhorst F. Chabot N. L. Bischoff A.
Wüstite in the Almahata Sitta Polymict Ureilite: Implications for Oxygen During Asteroidal Differentiation **[#1876]**
We report evidence for oxygen in metallic melt systems preserved as wüstite within Almahata Sitta MS-166 and the role of the Fe-S-O system during asteroidal differentiation. MS-166 might be a first sample of the S-rich metallic melt from the UPB.

9:45 a.m. Wilson L. * Goodrich C. A.
Melt Formation, Migration and Rapid Extraction from Differentiated Asteroid Interiors: Lessons from Ureilites Extended to All Asteroids **[#1128]**
We show that extraction of partial melts from the mantles of all differentiated asteroids was rapid, and was not strongly dependent on gas being present. Rapid melt transfer argues against magma oceans and for magma ponding in subcrustal sills.

10:00 a.m. Goodrich C. A. * Sutton S. R. Wirick S.
Valences of Cr in Ureilite Olivine and Implications for Ureilite Petrogenesis **[#1221]**
We use XANES to directly determine valences of Cr in olivine in ureilites. Results address the question of whether the large range of ureilite Fo corresponds to variation in oxidation state.

10:15 a.m. Jambon A. * Baghdadi B. Barrat J. A.
Peridotitic Angrites are Chimerolites **[#1758]**
Peridotitic (kamacite-bearing) angrites are annealed breccias made of angritic silicate and exogenous metal.

10:30 a.m. King P. L. * Spilde M. N. Wirick S. Lanzirotti A. Agee C. B.
Redox History of Early Solar System Planetesimals Recorded in the D'Orbigny Angrite **[#2436]**
V-valence state oxybarometry of the D'Orbigny angrite show that the crystalline and cavity pyroxenes in the rock formed at ~IW – 0.7, but that cross-cutting glass formed at IW + 2.9. Oxidation of the glass may be due to lowered H_2 on the parent body.

10:45 a.m. Gardner-Vandy K. G. * Lauretta D. S. McCoy T. J.
Formation History of the Brachinites: Partial Melts from an R Chondrite-Like Parent Body **[#1610]**
We present new thermodynamic data for brachinite formation conditions. We then discuss the implications of a series of 1-bar, gas-mixing, partial melting experiments of an R4 chondrite to the history and formation of the brachinites.

11:00 a.m. Hunt A. C. * Benedix G. K. Kreissig K. Hammond S. Strekopytov S. Rehkamper M.
Using Geochemical Data to Assess the Evolution of the Winonaite-IAB Parent Body **[#1818]**
We aim to produce a geochemical dataset for the winonaites to assess melting processes occurring on the winonaite-IAB parent body. New analyses suggest the winonaites are unmelted, implying heterogeneous heat distribution in the parent body.

11:15 a.m. Hidaka Y. * Yamaguchi A. Shirai N. Sekimoto S. Ebihara M.
Lithophile Element Characteristics of Acapulcoite-Lodranite and Winonaites: Implications for the Chemical Composition of Their Precursor Materials **[#1785]**
We have analyzed 13 primitive achondrites chemically and found one acapulcoite and two winonaites that show "primitive" characteristics. From their chemical data, we discuss the chemical composition of their precursor chondritic materials.

11:30 a.m. van Niekerk D. * Keil K.
Anomalous Enstatite Meteorites Queen Alexandra Range 94204 and Pairs: The Perplexing Question of Impact Melts or Partial Melt Residues, Either way, Unrelated to Yamato 793225 **[#2644]**
QUE 94204 and its seven pairs are anomalous enstatite meteorites that may either be impact melt products, or partial melt residues. We explore the petrology of these meteorites and present new findings.

PLENARY SESSION:
MASURSKY LECTURE AND DWORNIK AWARD PRESENTATIONS
Monday, 1:30 p.m. Waterway Ballroom 4 and 5

Chairs: Stephen Mackwell and Eileen Stansbery

Presentation of the 2011 GSA Stephen E. Dwornik Award Winners

Best Graduate Oral Presentation:
Kelsey J. Zabrusky, Colorado School of Mines, "*The Distribution and Depositional History of Sedimentary Deposits in Arabia Terra*"

Honorable Mention, Graduate Oral Presentation:
Debra M. Hurwitz, Brown University, "*Modeling Affects of Lunar Surface Slope, Temperature, and Material Properties on the Efficiency of Erosion During the Formation of Rima Prinz*"

Best Graduate Poster Presentation:
Christina E. Viviano, University of Tennessee, "*Using THEMIS to Address Discrepancies Between OMEGA/CRISM and TES Detections of Phyllosilicates*"

Best Undergraduate Poster Presentation:
Sarah Christian, Bryn Mawr College, "*Frequency Analysis of SHARAD Reflectors Within the North Polar Layered Deposits, Mars and Implications for the Link Between Radar and Optical Data*"

Honorable Mention, Undergraduate Poster Presentation:
Niina Jamsja, Portland State University, "*Presence of Hydrous Phases in Two R Chondrites, Northwest Africa 6491 and 6492*"

Presentation of the 2012 LPI Career Development Award Winners

Rebecca Bast, *Westfälische Wilhelms-Universität Münster, Germany*
Robert Beauford, *University of Arkansas*
Elmar Buhl, *Albert-Ludwigs-Universität Freiburg, Germany*
Michael Chaffin, *University of Colorado at Boulder*
Carolyn Crow, *University of California Los Angeles*
Dirk Elbeshausen, *Forshung Museum für Naturkunde, Germany*
Amy L. Fagan, *University of Notre Dame*
Roger R. Fu, *Massachusetts Institute of Technology*
Emmanuel Jacquet, *Laboratoire de Minéralogie et Cosmochimiedu Muséum, France*
Matthew E. Sanborn, *Arizona State University*
Stephen Seddio, *Washington University in St. Louis*
Bhairavi Shankar, *University of Western Ontario, Canada*
Priyanka Sharma, *University of Arizona*
Matthew R. Smith, *University of Washington*
Veerle Jasmin Sterken, *MPIK-Staubgruppe, Germany*
Kun Wang, *Washington University in St. Louis*
Nathan Robert Williams, *Arizona State University*
Kelsey Young, *Arizona State University*
Gang Yu, *Harvard University*
Michael R. Zanetti, *Washington University in St. Louis*

Masursky Lecture:

Masursky Lecture by Head J. W. III *

Mars Climate History: A Geological Perspective **[#2582]**

Deciphering the climate history of Mars requires multiple disciplines and approaches; geological observations provide important guidelines and constraints.

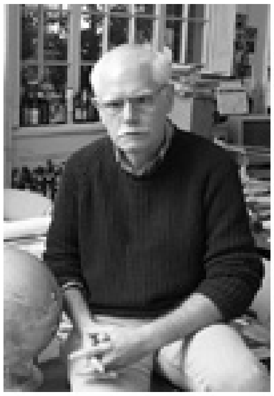

Professor James W Head III is the Louis and Elizabeth Scherck Distinguished Professor of Geological Sciences at Brown University in Providence, Rhode Island. He came to Brown University in 1973, following his work with the NASA Apollo program, in which he analyzed potential landing sites, studied returned lunar samples and data, and provided training for the Apollo astronauts. His current research centers on the study of the processes that form and modify the surfaces, crusts and lithospheres of planets, how these processes vary with time, and how such processes interact to produce the historical record preserved on the planets. Comparative planetology, the themes of planetary evolution, and application of these to the study of early Earth history are also of interest. He has followed up his research on volcanism, tectonism and glaciation with field studies on active volcanoes in Hawaii and at Mount St. Helens, on volcanic deposits on the seafloor with three deep sea submersible dives, and during five field seasons in the Antarctic Dry Valleys. Since 1984, Head has convened the Vernadsky Institute/Brown University microsymposia, held twice yearly in Moscow and Houston. He has served as an investigator with NASA and Russian space sissions, such as the Soviet Venera 15/16 and Phobos missions, and the U.S. Magellan (Venus), Galileo (Jupiter), Mars Surveyor, Russian Mars 1996, and space shuttle missions. Head is currently a co-investigator for the NASA MESSENGER mission to Mercury and Moon Mineralogy Mapper (M3), as well as the European Space Agency's Mars Express Mission.

SPECIAL SESSION: A SEASON IN THE SATURN SYSTEM II
Monday, 2:30 p.m. Waterway Ballroom 1

Chairs: Linda Spilker and Jani Radebaugh

2:30 p.m. Matson D. L. * Johnson T. V. Davies A. G. Castillo-Rogez J. C. Lunine J. I.
Enceladus' Gas Budget and Ocean Temperature **[#2411]**
The relationships between water, carbon dioxide, and heat in Enceladus are used to obtain the temperatures of water in the plume-formation chambers and in the subsurface ocean.

2:45 p.m. Blackburn D. G. * Goguen J. D. Buratti B. J. Clark R. N. Howell R. R. Spencer J. R.
Detection of Thermal Emission from Enceladus' Tiger Stripes with Cassini VIMS **[#1532]**
We announce the detection of thermal emission from Damascus and Cairo with the Cassini VIMS in the 4–5 µm region of the spectrum. These new spectra put strong constraints on the emitting area at the hottest temperatures.

3:00 p.m. Ducci M. * Iess L. Armstrong J. W. Asmar S. W. Jacobson R. A. Lunine J. I. Racioppa P. Rappaport N. J. Stevenson D. J. Tortora P.
The Geodesy of the Main Saturnian Satellites from Range Rate Measurements of the Cassini Spacecraft **[#2200]**
During Cassini's eight-year tour in the saturnian system, the gravity field of the main satellites was inferred from range rate measurements of the spacecraft. Here we present our latest results and an overview of our analysis methods.

3:15 p.m. Hendrix A. R. * Buratti B. J.
Multi-Wavelength Photometry of the Icy Saturnian Satellites **[#2722]**
We present an analysis of solar phase curves of Enceladus and Dione as measured by Cassini UVIS and VIMS. Results have implications for surface scattering properties and effects from exogenic processes.

3:30 p.m. Waite J. H. Jr. * Bell J. M. Lorenz R. Achterberg R. Flasar F. M.
A New Titan Atmospheric Model for Mission Engineering Applications **[#1232]**
Titan's polar regions and hydrocarbon lakes are of interest for future exploration. This paper describes a new engineering model of Titan's atmospheric structure with particular reference to the proposed Titan Mare Explorer mission.

3:45 p.m. Castillo-Rogez J. C. * Lunine J. I.
Tidal Response of Titan's Interior Models Consistent with Cassini-Derived Constraints **[#1707]**
The goal of this paper is to identify to what extent tidal Love number and dissipation factor data can help distinguish between the models proposed so far to explain Titan's moment of inertia derived from Cassini Radio Science observations.

4:00 p.m. Radebaugh J. * Le Gall A. Barnes J. W. Lorenz R. D. Lunine J. I. Kirk R. L. Cassini Radar Team
Stabilized Dunes on Titan Indicate Changes in Climate and Surface Processes **[#2224]**
Dune-like landforms, similar in morphology but not radar backscatter to dunes, have been detected at Titan's mid-high latitudes. We propose they are dunes that were once active but are now immobilized by more recent surface deposits.

4:15 p.m. Neish C. D. * Kirk R. L. Lorenz R. D. Bray V. J. Schenk P. Stiles B. Turtle E. Cassini Radar Team
Crater Topography on Titan: Implications for Landscape Evolution **[#2412]**
Titan crater depths / Shallower than Ganymede / Like whatever, man.

4:30 p.m. Kirk R. L. * Howington-Kraus E. Redding B. Callahan P. S. Hayes A. G. LeGall A. Lopes R. M. C. Lorenz R. D. Lucas A. Mitchell K. L. Neish C. D. Aharonson O. Radebaugh J. Stiles B. W. Stofan E. R. Wall S. D. Wood C. A. Cassini Radar Team
Topographic Mapping of Titan: Latest Results **[#2759]**
High resolution topomapping of Titan's surface reveals a mystery among the dunes and a fresh central peak crater. High precision elevations on the shores of Ligeia Mare and a host of maps of the southern hemisphere are in the works.

MIND THE GAP: LUNAR PETROLOGY AND REMOTE SENSING
Monday, 2:30 p.m. Waterway Ballroom 4

Chairs: Juliane Gross and Rachel Klima

2:30 p.m. Ohtake M. * Takeda H. Mastunaga T. Yokota Y. Haruyama J. Morota T. Yamamoto S. Ogawa Y. Hiroi T. Karouji Y. Saiki K. Lucey P. G.
Primitive Farside Highland Materials Detected by Mg Number **[#1977]**
We utilize a new algorithm that derives Mg# from spectral reflectance data to derive a global map of Mg#. The derived Mg# distribution of the lunar highlands clearly indicates its dichotomic distribution, with a higher Mg# in the farside highlands than in the nearside.

2:45 p.m. Takeda H. * Nagaoka H. Ohtake M. Kobayashi S. Yamaguchi A. Morota T. Karouji Y. Haruyma J. Katou M. Hiroi T. Nyquist L. E.
Comparisons of Mineralogy of Lunar Meteorites Possibly from the Farside and the Kaguya Remote Sensing Data to Reconstruct the Earliest Anorthositic Crust of the Moon **[#1379]**
Comparisons of mineralogy of lunar meteorites (Dhofar 911, etc.) from the farside and the Kaguya Th concentrations a to reconstruct the earliest, asymmetric anorthositic crust of the Moon. We propose that these meteorites might have come from the Dirichlet-Jackson basin.

3:00 p.m. Isaacson P. J. * Hiroi T. Pieters C. M. Liu Y. Patchen A. Taylor L. A.
Spectroscopy of Lunar Meteorites for Expanded Sample Collection Diversity: Initial Results of Component Analyses **[#1668]**
We present spectral reflectance and associated geochemistry/abundance data for mineral/lithic components of lunar meteorites. These results will enable investigation of the geologic context of the meteorite samples through remote sensing.

3:15 p.m. Davenport J. D. * Neal C. R.
Revisiting the Lunar Magma Ocean Crystallization: Creating a Unified Hybrid Model **[#1546]**
Lunar magma ocean theory (LMO) has been given much consideration recently. This study uses work on modeling the LMO to create a hybrid model. This will give insight into the formation of the Moon as well as using it for comparative planetary studies.

3:30 p.m. Prissel T. C. * Parman S. W. Jackson C. R. M. Dhingra D. Ganskow G. Cheek L. C. Rutherford M. J. Hess P. Pieters C. M.
Melt-Wallrock Reactions on the Moon: Experimental Constraints on the Formation of Newly Discovered Mg-Spinel Anorthosites **[#2743]**
Here, we provide experimental evidence suggesting the formation of newly discovered lunar Mg-rich spinel anorthosite via melt-wallrock reaction between known lunar basalts and an anorthositic crust.

3:45 p.m. Jackson C. R. M. * Cheek L. C. Parman S. W. Cooper R. F. Pieters C. M.
Compositional Constraints on Lunar Spinel Anorthosite: Synthesis of Spinel with Variable Iron Content **[#2335]**
Fe-bearing spinels were synthesized under reducing conditions applicable to the Moon. The spectra of these minerals will place improved compositional constraints on the newly identified spinel anorthosite (M^3).

4:00 p.m. Jolliff B. L. * Zanetti M. Shirley K. A. Accardo N. J. Lauber C. Robinson M. S. Greenhagen B. T.
Compton-Belkovich Volcanic Complex **[#2097]**
We present new information on volcanic features at the Compton-Belkovich Volcanic Complex, and we discuss timing and petrogenesis, including intrusion and inflation, effusion, magma chamber collapse, and emplacement of late-stage differentiates.

4:15 p.m. Klima R. L. * Lawrence D. Cahill J. T. S. Hagerty J.
Bullialdus Crater: Correlations Between KREEP and Local Mineralogy **[#2517]**
We explore the pyroxenes in and around Bullialdus Crater, examining relationships between lithology, thorium content, and hydroxylated material to help constrain about the source region and character of KREEP on the lunar nearside.

4:30 p.m. Nekvasil H. * Ustunisik G. Lindsley D. H.
Large Scale Lunar Magmatism: Inferences from the Moscoviense Basin **[#2178]**
Phase equilibria computations have constrained the compositions of parental liquids that can give rise the lithologies observed by M^3 at Moscoviense Basin and indicated evolution of residual melts to rhyolitic compositions.

MOVERS AND SHAKERS: PLANETARY DYNAMICS AND TECTONICS
Monday, 2:30 p.m. Waterway Ballroom 5

Chairs: Jeffrey Andrews-Hanna and H. Jay Melosh

2:30 p.m. Morschhauser A. * Grott M. Lesur V.
A New Model of the Lithospheric Field of Mars Using MGS-MPO Data and L1-Regularization **[#1963]**
We present a SH model (degree 90) of the martian lithospheric field. The model was regularized using a L1-Norm. Hence, strong anomalies are well represented, while still accounting for the normal distribution of errors in the data.

2:45 p.m. Sandu C. * Kiefer W. S.
Crustal Growth and Degassing of the Martian Mantle: Constraints from Numerical Experiments **[#1310]**
We used a one-dimensional parameterized convection thermal evolution model to calculate the thermal evolution of Mars and the effect of temperature and water content on the crustal and degassing evolution.

3:00 p.m. Karimi M. * Dombard A. J. Williams R. M.
A Study of the Thermal Evolution of Mars via Viscoelastic Relaxation of Large Craters **[#2712]**
We constrain Mars' heat flux by simulating deformation of large craters. Our results reveal a secular cooling of Mars and a regional variation consistent with higher heat fluxes closer to the Crustal Dichotomy boundary persisting to the mid-Noachian.

3:15 p.m. Weller M. B. * Lenardic A.
Plate Tectonics on Terrestrial Planets: A Hysteresis of States in Mantle Convection Systems **[#1557]**
The viability of plate tectonics (PT) have been argued for extrasolar terrestrial planets. The modeling results are: (1) Most will have PT; and (2) most will not have PT. Can both results be correct? We explore path dependence to explain the hysteresis.

3:30 p.m. Lognonne P. * Banerdt W. B. Hurst K. Mimoun D. Garcia R. Lefeuvre M. Gagnepain-Beyneix J. Wieczorek M. Mocquet A. Panning M. Beucler E. Deraucourt S. Giardini D. Boschi L. Christensen U. Goetz W. Pike T. Johnson C. Weber R. Larmat K. Kobayashi N. Tromp J.
Insight and Single-Station Broadband Seismology: From Signal and Noise to Interior Structure Determination **[#1983]**
The goal of the InSight Seismometer is to determine interior structure and seismic activity of the planet. We summarize the flow from instrument performance to expected science performance in terms of interior structure and activity determination.

3:45 p.m. Melosh H. J. * Blair D. M. Freed A. M.
Origin of Superisostatic Gravity Anomalies in Lunar Basins **[#2596]**
Superisostatic gravity anomalies in lunar basins are the inevitable consequence of the cooling and contraction of deep melt pools formed by large impacts into a warm early Moon.

4:00 p.m. Andrews-Hanna J. C. *
The Origin of Non-Mare Mascon Gravity Anomalies on the Moon **[#2804]**
Some lunar basins possess mascon gravity anomalies in excess of that which can be explained by mare loading. These are shown to result from the flexural uplift of an annulus of thickened but sub-isostatic crust surrounding the basin.

4:15 p.m. Han L. * Showman A. P.
On the Formation of the Hemispheric Dichotomy of Enceladus **[#2028]**
We present three-dimensional models of Enceladus that demonstrate (1) how localized active regions can result from brittle deformation, and (2) how topography on the silicate core can modulate convection and allow tectonic activity to be focused in one hemisphere.

4:30 p.m. Matsuyama I. M. *
Tidal Dissipation in the Subsurface Oceans of Icy Satellites **[#2068]**
Previous studies considering tidal dissipation in the subsurface oceans of icy satellites ignore the effect of an overlying ice shell. We extend these studies by taking into account the presence of an overlying ice shell.

RECENT SLOPE PROCESSES ON MARS: SLIDING, FLOWING, AND FALLING DOWN
Monday, 2:30 p.m. Waterway Ballroom 6

Chairs: Joseph Levy and Norbert Schorghofer

2:30 p.m. Raack J. * Reiss D. Ruesch O. Hiesinger H.
Present Day Activity of South Polar Gullies on Mars **[#1801]**
We report on the first clearly identified seasonal changes of gullies in the south polar region on Mars. With new imaging, temperature, and spectral data we analyze the timing and mechanism that initiate gully activity in the last two martian years.

2:45 p.m. Palucis M. C. * Dietrich W. E. Howard A. Nishiizumi K. Kring D. A.
How Much Water is Needed to Make Gullies on Mars: A Conceptual Model **[#1499]**
We propose a general morphodynamic model for gully and fan systems formed by flowing water that may be applicable to some martian gullies. Our quantitative observations at Meteor Crater substantiate the conceptual model.

3:00 p.m. Jouannic G. * Conway S. J. Gargani J. Costard F. Patel M. R. Ori G. G.
Experimental Investigation of Gully Formation Under Low Pressure and Low Temperature Conditions **[#1509]**
The aim of this study is to develop a experiments both under martian atmospheric pressure and terrestrial atmospheric pressure in order to reproduce the variability of the observed martian gullies under well-constrained experimental conditions.

3:15 p.m. ElShafie A. * Heggy E. Dixon J. C. Chevrier V. F. Dennis N.
Investigating the Effect of Mechanical and Electrical Regolith Properties on Geomorphological Shape Formations **[#2573]**
We simulated gully formation under different bulk densities with the objective of correlating mechanical and electrical properties of the regolith to gully shape which enhances our knowledge, analysis and interpretation of previous, current and future surface forms.

3:30 p.m. Schorghofer N. * Rottas K. M. Bergonio J. R.
A Balanced Slope Streak Population on Mars: Comparison of CTX and Viking Images **[#1109]**
We study slope streak activity based on images separated in time by at least three decades. The number of new slope streaks nearly equals the number of disappeared slope streaks and the turnover time of the population is estimated to be four decades.

3:45 p.m. Kereszturi A. Sik A. Bérczi Sz. * Horvath A.
Comparison of Recent Water or Brine Related Flow Features on Mars **[#1787]**
Comparison of three types of recent flow-like surface features on Mars are presented, including DDS-seepages, slope streaks, and recurring slope lineae. Their characteristics are compatible with the models of brine-related wet formation mechanism.

4:00 p.m. Ojha L. * McEwen A. Dundas C. Mattson S. Byrne S. Schaefer E. Masse M.
Recurring Slope Lineae on Mars: Updated Global Survey Results **[#2591]**
Recurring Slope Lineae (RSL) are recently discovered features on Mars that are observed to form and grow during warm seasons and fade in colder seasons. We present results from our global survey for RSL in HiRISE images and their attributes.

4:15 p.m. Levy J. S. * Fountain A. G.
Hydrological Characteristics of Recurrent Slope Lineae on Mars Based on Time-Resolved HiRISE Analyses and Comparisons with Fluid Flow Through an Antarctic Terrestrial Analog Regolith **[#1029]**
We test the “wet” (brine-related) RSL formation mechanism by using repeat HiRISE images to determine whether a simple Darcy flow model can explain the spatial pattern of RSL darkening. This remote hydrogeological tool is verified in Antarctic soil.

4:30 p.m. Dickson J. L. * Head J. W. III
Active-Layer Drainage Without Surface Erosion: Time-Lapse Photography of Antarctic Slope Lineae and Implications for the Flow of Water on Mars **[#1085]**
The McMurdo Dry Valleys of Antarctica host features very similar to “recurring slope lineae” on Mars. We synchronize time-lapse photography observations and soil moisture measurements to track fluvial activity associated with these features.

SPECIAL SESSION: PLANETARY HYDROLOGY: WET WORLDS
Tuesday, 8:30 a.m. Waterway Ballroom 1

Chairs: **Karl Mitchell and Giles Marion**

8:30 a.m. Richardson M. I. * Newman C. E. Soto A. S.
Climate, Precipitation, and Aridity on the Terrestrial Bodies **[#2913]**
We discuss the climate constraints on the hydrological cycles on the terrestrial bodies.

8:45 a.m. Andrews-Hanna J. C. * Soto A. Richardson M. I.
Meridiani Planum and Gale Crater: Hydrology and Climate of Mars at the Noachian-Hesperian Boundary **[#2706]**
We combine GCM predictions of rainfall patterns on early Mars with hydrological models of groundwater flow to investigate the formation of sulfate-rich sedimentary deposits at Meridiani Planum and Gale Crater.

9:00 a.m. Halevy I. * Head J. W. III
Punctuated Volcanism, Transient Warming and Global Change in the Late Noachian-Early Hesperian **[#1908]**
The dynamics of atmospheric sulfur chemistry during phases of episodic volcanism, punctuated by long quiescent periods, warmed the surface of Mars for multiple episodes of tens to hundreds of years during the late Noachian and early Hesperian.

9:15 a.m. Carter J. * Poulet F.
Global Investigation of Hydrated Exposures on Mars: Evidence for a Clay Cycle **[#1436]**
Global-scale investigation of hydrated minerals on Mars reveal the possible existence of a clay cycle similar to Earth's on early Mars.

9:30 a.m. Popa C. * Di Achille G. Esposito F. Mennella V. Colangeli L.
Evidences of Possible Hydrothermal Alteration in Xanthe Terra: Implications for Surface Water on Early Mars **[#2516]**
The work traces the early Noachian alteration in the western part of Xanthe Terra, Mars, and tries to build a rationale for alteration type and time of pristine rock types, in connection to channel and deltaic systems formation.

9:45 a.m. McEwen A. S. * Keszthelyi L. P. Grant J. A.
Have There Been Large, Recent (Mid-Late Amazonian) Water Floods on Mars? **[#1612]**
Sparsely-cratered units in martian outflow channels date post-channel lava flows rather than water flooding events, so there isn't clear evidence for a deep, extant groundwater table.

10:00 a.m. Kargel J. S. * Furfaro R.
A Frozen Lake/Glaciolacustrine Model of Crater Greg (Mars) **[#2629]**
Crater Greg (near Hellas, Mars) exhibits some of the most compelling evidence of glaciation on Mars. The depositional environment and paleoclimatic implications are not clear. Here we propose a frozen lake model of glacier-like flow formation.

10:15 a.m. Stofan E. R. Lunine J. I. Lorenz R. D. Kirk R. L. Aharonson O. Hayes A. G. Lucas A. Turtle E. P. Wall S. D. * Wood C. A.
Shorelines of Ligeia Mare, Titan **[#1556]**
The general morphology of the shorelines of Ligeia Mare, Titan, can be interpreted using Earth analogues to better understand their possible modes of formation and modification.

10:30 a.m. Lucas A. * Aharonson O. Hayes A. G. Deledalle C. Wye L. Kirk R. Howington-Kraus E. Cassini Radar Science Team
Clues to Titan Hydrology from Enhanced SAR Image Processing **[#2566]**
In order to quantify the interactions of fluvial/marine processes on Titan with the topography we present new insights based on an adapted algorithm for de-noising images. The data reveals details of submerged valleys and gradients in the bathymetry.

10:45 a.m. Drummond S. A. * Burr D. M. Cartwright R. Black B. A. Perron J. T.
Morphologic Classification and Geologic Implications of Titan Fluvial Features **[#2868]**
Drainage pattern analysis of fluvial networks on Titan indicates a predominance of rectangular networks. Through comparison with terrestrial analogs, we infer a tectonic influence and suggest possible stress mechanisms.

11:00 a.m. Lorenz R. D. * Turtle E. P.
How Often Does it Rain on Titan? **[#2472]**
Titan's methane rains / Just days in a century / Perhaps TiME will tell.

11:15 a.m. Vance S. * Sotin C. Choukroun M. Mitchell K.
Titan's Subsurface Alkanology **[#2939]**
Hydrocarbon flows / Through Titan's cold lithosphere / Are explored herein.

11:30 a.m. Moore J. M. * Nimmo F.
Does Titan's Landscape Betray the Late Acquisition of Its Current Atmosphere? **[#1248]**
Titan may have acquired its massive atmosphere relatively recently in solar system history. The appearance of a thick atmosphere may have changed Titan's global topography. This change may be expressed in the latitudinal distribution of landforms.

DIVERSE VIEWS OF THE LUNAR CRUST: AN ORBITAL PERSPECTIVE
Tuesday, 8:30 a.m. Waterway Ballroom 4

Chairs: Paul Lucey and Joshua Cahill

8:30 a.m. Lucey P. G. * Greenhagen B. T. LRO Diviner Team
Lunary Mineral Maps Integrating Thermal and Near Infrared Multispectral Imaging **[#1736]**
Global lunar mineral maps were produced combining near-infrared and Diviner thermal infrared multispectral data for improved accuracy. Plagioclase, ortho- and clinopyroxene, and olivine maps at 2 km resolution were produced, as well as Mg number.

8:45 a.m. Song E. * Bandfield J. L. Lucey P. G. Greenhagen B. T. Paige D. A.
Bulk Mineralogy of Lunar Crater Central Peaks — Results from Diviner Lunar Radiometer **[#2553]**
A survey of CF values from the Diviner Lunar Radiometer Experiment has been performed for the central peaks of 135 complex craters on the Moon, providing global and regional observations of the heterogeneity of crustal compositions.

9:00 a.m. Donaldson Hanna K. L. * Cheek L. C. Pieters C. M. Mustard J. F. Wyatt M. B. Greenhagen B. T.
Global Identifications of Crystalline Plagioclase Across the Lunar Surface Using M^3 *and Diviner Data* **[#1968]**
An integrated NIR and TIR approach is used to identify the local and global distribution of crystalline plagioclase across the lunar surface and to determine its composition.

9:15 a.m. Cheek L. C. * Pieters C. M.
Variations in Anorthosite Purity at Tsiolkovsky Crater on the Moon **[#2624]**
In contrast to the highly pure (<2% pyroxene) anorthosite reported for numerous lunar highland craters, we present M^3 data showing that the central peak of Tsiolkovsky Crater exposes a wide range of anorthosite mineralogy.

9:30 a.m. Yamamoto S. * Nakamura R. Matsunaga T. Ogawa Y. Ishihara Y. Morota T. Hirata N. Ohtake M. Hiroi T. Yokota Y. Haruyama J.
Global Distribution Trend of Purest Anorthosite on the Moon Revealed by SELENE Spectral Profiler **[#1356]**
We report the global distribution trend and the modes of occurrence of purest anorthosite (PAN) on the Moon revealed by the Spectral Profiler onboard the Japanese lunar explorer SELENE (Kaguya).

9:45 a.m. Cahill J. T. S. * Blewett D. T. Nguyen N. V. Xu K. Lawrence S. J. Denevi B. W.
Determination of Iron Metal Optical Constants: Implications for Lunar Remote Sensing **[#2215]**
New measurements of the optical constants of Fe metal represent important improvements over previous data, and have significant implications for interpretation and Hapke modeling of lab and remote spectra of surfaces containing nano or macro iron.

10:00 a.m. Greenhagen B. T. * Thomas I. R. Bowles N. E. Allen C. C. Donaldson Hanna K. L. Foote E. J. Paige D. A.
Compositional Ground Truth of Diviner Lunar Radiometer Observations **[#2092]**
Returned lunar soil samples from Apollo offer an unique opportunity to “ground truth” of Diviner Lunar Radiometer compositional interpretations. Here we compare Diviner observations of Apollo sites to laboratory measurements of Apollo soil samples.

10:15 a.m. Glotch T. D. * Greenhagen B. T. Lucey P. G. Bandfield J. L. Hayne P. O. Allen C. C. Elphic R. C. Paige D. A.
Observations of Lunar Swirls by the Diviner Lunar Radiometer Experiment **[#1951]**
We have made daytime and nighttime measurements of lunar swirls with the Diviner Lunar Radiometer Experiment. Diviner data are consistent with the solar wind standoff mechanism for swirl formation.

10:30 a.m. Bussey D. B. J. * Schulze R. Jakowatz C. V. Nolan M. Jensen R. Turner F. S. Wahl D. E. Yocky D. A. Cahill J. T. S. Raney R. K. Patterson G. W. Mini-RF Team
Bistatic Radar Observations of the Moon Using the Arecibo Observatory and the Mini-RF Instrument on LRO **[#2586]**
Using Arecibo as the transmitter and Mini-RF as the receiver we are collecting the first ever non beta-zero bistatic radar images of the Moon. These data provide new insight into volatiles, regolith and pyroclastic deposits.

10:45 a.m. Raney R. K. * Cahill J. T. S. Patterson G. W. Bussey D. B. J. Mini-RF Team
Characterization of Lunar Craters Using M-Chi Decompositions of Mini-RF Radar Data **[#2676]**
LRO’s Mini-RF S-band radar data set is used to better characterize lunar crater ejecta deposits and for the presence of water-ice using a new (to radar astronomy) method of polarimetric data analysis, known as an m-chi decomposition.

11:00 a.m. Litvak M. L. * Mitrofanov I. G. Sanin A. B. Boynton W. V. Chin G. Evans L. Harshman K. Droege G. Malakhov A. Milikh G. McClanahan T. Sagdeev R. Starr R.
Global Maps of the Moon Neutron Flux from LEND Instrument Onboard LRO **[#2101]**
Latest neutron spectroscopy observations made by LEND onboard LRO mission during more then 1 year of mapping phase (started at September 2009) are used to create global maps of lunar neutron fluxes in different energy ranges.

11:15 a.m. McClanahan T. P. * Mitrofanov I. G. Boynton W. V. Chin G. Droege G. Evans L. G. Garvin J. Harshman K. Litvak M. L. Malakhov A. Livengood T. Milikh G. M. Nandikotkur G. Neumann G. Smith D. Sagdeev R. Sanin A. G. Starr R. D. Trombka J. I. Zuber M. T.
Correlated Observations of Epithermal Neutrons and Polar Illumination Models from Orbital Neutron Detectors **[#2341]**
This paper is a correlative study of Illumination modeling derived from LOLA topography with Orbital Neutron Detectors: the Lunar Exploration Neutron Detector (LEND) and the Lunar Prospector Neutron Spectrometer (LPNS).

11:30 a.m. Ashley J. W. * Robsinson M. S. Boyd A. K. Wagner R. V. Speyerer E. J. Hawke B. R. Hiesinger H. van der Bogert C. H. Burns K. Sato H.
LROC Imaging of Thin Layering in Lunar Mare Deposits **[#2115]**
LROC NAC imaging is producing an emerging picture of widespread thin layering in lunar mare deposits from exposures in crater walls, steep-walled pits, and rilles. Layers 3 to 14 m thick are common, and may represent individual flows or flow lobes.

SOLAR NEBULA MIXING AND CAIs
Tuesday, 8:30 a.m. Waterway Ballroom 5

Chairs: Justin Simon and Hiroko Nagahara

8:30 a.m. Boss A. P. * Alexander C. M. O'D. Podolak M. Ebel D. S.
Particle Trajectories During FU Orionis Outbursts by the Protosun **[#1249]**
Marginally gravitationally unstable disks lead to FU Orionis outbursts while simultaneously forcing particles on trajectories that loop around much of the solar nebula, leading to extensive mineralogical and isotopic alteration, as seen in some CAIs.

8:45 a.m. Wozniakiewicz P. J. * Ishii H. A. Bradley J. P. Kearsley A. T. Burchell M. Price M. C.
Grain Size Sorting in the Outer Nebula Accretion Disk **[#2392]**
We report that rρ relations indicative of aerodynamic sorting are found in cometary CP IDPs and Comet 81P/Wild 2, demonstrating that efficient, nebula-wide aerodynamic sorting of crystalline grains occurred prior to accretion of asteroids and comets.

9:00 a.m. Simon J. I. * Matzel J. E. P. Simon S. B. Weber P. K. Grossman L. Ross D. K. Hutcheon I. D.
Coordinated Oxygen Isotopic and Petrologic Studies of CAIs Record Varying Composition of Protosolar Gas **[#1340]**
High-resolution O-isotopic zoning profiles obtained by NanoSIMS indicate a progressive and cyclic record of exchange between CAIs and distinct nebular gases. Numerical models are used to constrain conditions and duration of these exchange events.

9:15 a.m. MacPherson G. J. * Nagashima K. Ivanova M. A. Krot A. N.
Primary Reverse Oxygen-Isotope Evolution of Pyroxene in Compact Type A CAIs from the Efremovka and NWA-3118 CV3 Chondrites: Insights into Internal CAI Mixing Lines **[#2415]**
^{16}O-depleted Ti-Al-rich pyroxenes in compact Type A CAIs reflect the composition of the perovsites from which they first formed. Perovsite apparently exchanged oxygen very early, prior to melilite exchange and to initial melting of the CAIs.

9:30 a.m. Young E. D. * Shahar A.
Magnesium, Silicon, and Oxygen Isotopic Consequences of CAI Evaporation and Inversion for Primordial Melt Compositions **[#1693]**
We show how realistic activity-composition relationships in CMAS melts can be used to invert silicon- and magnesium-isotope ratios for evaporation histories of CAIs. Results suggest igneous CAIs were indeed condensates from a solar gas.

9:45 a.m. Nagahara H. * Ozawa K.
The Role of Isotopic Exchange Reaction in Oxygen Isotope Evolution in the Protosolar Disk **[#1277]**
We quantitatively examine the role of exchange reactions in mass-dependent oxygen isotope fractionation during evaporation and recondensation of silicate melt. The results are applied to the CCAM line, FUN inclusions, and chondrules.

10:00 a.m. Marin-Carbonne J. McKeegan K. D. * Davis A. D. MacPherson G. J. Mendybaev R. A. Richter F. M.
O, Si and Mg Isotopic Compositions of FUN Inclusion Vigarano 1623-5 **[#1687]**
FUN inclusion Vigarano 1623-5 shows the first unequivocal correlated petrologic and isotopic evidence for volatilization. O-, Si-, and Mg-isotopic compositions reveal that 1623-5 has experienced several evaporation events and an isotopic exchange of O.

10:15 a.m. Zhang J. * Huang S. Davis A. M. Dauphas N. Jacobsen S. B. Hashimoto A.
Calicium and Titanium Mass-Dependent Isotope Fractionation During Evaporation of $CaTiO_3$ **[#2132]**
We study evaporation effects on highly refractory elements, Ca and Ti, during evaporation of perovskite. Our results suggest that some CAIs experienced evaporation at such high temperature that even highly refractory elements evaporated.

10:30 a.m. Krot A. N. * Makide K. Nagashima K. Huss G. R. Hellebrand E. Petaev M. I.
Heterogeneous Distribution of ^{26}*Al at the Birth of the Solar System: Evidence from Corundum-Bearing Refractory Inclusions* **[#2255]**
Corundum-bearing CAIs recorded heterogeneous distribution of ^{26}Al at the birth of the solar system. We suggest that ^{26}Al was injected into the protosolar molecular cloud core by a wind from a massive star and was later homogenized through the disk.

10:45 a.m. Mishra R. * Chaussidon M.
Mg Isotopic Study of CA-, Al-Rich Inclusions from Carbonaceous Chondrites: Constraints on ^{26}*Al Distribution in the Accretion Disk and Accretion Processes* **[#1942]**
Variations in ^{26}Al/^{27}Al ratios and Mg-isotopic compositions of CV CAIs, AOAs, and chondrules constrain the level of homogeneity of ^{26}Al and Mg isotopes in the accretion disk and/or the timing of formation of the first condensates.

11:00 a.m. Brennecka G. A. * Borg L. E. Wadhwa M.
Combined Stable Isotope Signatures in Allende CAIs: The Nucleosynthetic Conundrum **[#2006]**
We report isotope compositions of Sr and Mo in Allende CAIs for which the isotopics of Ba, Nd, and Sm were previously obtained. We show that the combined isotopic signatures of normal CAIs requires a more complicated scenario beyond *r*-process addition.

11:15 a.m. Steele R. C. J. * Elliott T. Coath C. D. Regelous M. Russell S. S.
Neutron-Poor Ni Isotope Anomalies in Bulk Meteorites and Their Nucleosynthetic Significance **[#2354]**
Study of isotope anomalies in meteorites can yield information about the nucleosynthetic origins of the solar system. Neutron-poor Ni-isotope anomalies in bulk meteorites show evidence of input from the Si/S zone of an SNII to the early solar system.

11:30 a.m. Fischer-Gödde M. * Burkhardt C. Kleine T.
Ruthenium Isotope Anomalies in Meteorites and the Cosmic Mo-Ru Correlation **[#2492]**
Ruthenium-isotope anomalies obtained for IVB iron meteorites, the ungrouped iron meteorite Chinga, and the CB chondrite Gujba fall on the cosmic Mo-Ru correlation and indicate a deficit in *s*-process isotopes.

NEW MARTIAN METEORITES AND NEW PERSPECTIVES ON OLD FAVORITES
Tuesday, 8:30 a.m. Waterway Ballroom 6

TUE ORALS

Chairs: Juliane Gross and Francis McCubbin

8:30 a.m. Irving A. J. * Kuehner S. M. Tanaka R. Herd C. D. K. Chen G. Lapen T. J.
The Tissint Depleted Permafic Olivine-Phyric Shergottite: Petrologic, Elemental and Isotopic Characterization of a Recent Fall in Morocco **[#2510]**
The first witnessed martian meteorite fall in 49 years is a primitive olivine-phyric shergottite.

8:45 a.m. Agee C. B. * Wilson N. V. McCubbin F. M. Sharp Z. D. Ziegler K.
Basaltic Breccia NWA 7034: New Ungrouped Planetary Achondrite **[#2690]**
NWA 7034 is a basaltic breccia with petrology and geochemistry that resembles SNC meteorites, however its oxygen isotope values are anomalous compared to SNC meteorites. Aqueous alteration or a non-martian origin could account for this discrepancy.

9:00 a.m. Roszjar J. * Bischoff A. Llorca J. Pack A.
Ksar Ghilane 002 (KG 002) — A New Shergottite: Discovery, Mineralogy, Chemistry and Oxygen Isotopes **[#1780]**
We report on the discovery, mineralogical, chemical, and isotopic characteristics of a new basaltic shergottite: Ksar Ghilane 002.

9:15 a.m. Cartwright J. A. * Merchel S. Rugel G. Fimiani L. Ludwig P. Llorca J. Ott U.
The 100th Martian Meteorite Ksar Ghilane 002 (KG 002): Noble Gases and Radionuclides Point to a Strong Relationship with Los Angeles **[#1213]**
We report noble gas and radionuclide data for new martian meteorite KG 002, including cosmic-ray exposure ages. Our results show that KG 002 has striking similarities with the shergottite Los Angeles, and may hint at a similar ejection event.

9:30 a.m. Gross J. * Filiberto J. Treiman A. H. Herd C. D. K. Melwani Daswani M. Schwenzer S. P.
Petrography, Mineral Chemistry, and Crystallization History of Olivine-Phyric Shergottite NWA6234: A New Intermediate Melt Composition **[#2693]**
The new martian meteorite NWA 6234 is an olivine-phyric shergottite and may have special significance. It appears to represent a magma composition and new group of shergottites that is neither depleted nor enriched in incompatible trace elements.

9:45 a.m. Filiberto J. * Chin E. Day J. M. D. Gross J. Penniston-Dorland S. C. Schwenzer S. P. Treiman A. H.
Geochemistry of Intermediate Olivine-Phyric Shergottite Northwest Africa 6234 **[#1139]**
Here we present major- and trace-element geochemistry, Li-isotope composition and abundance, and Re-Os isotope and highly siderophile element abundance data for the ol-phyric shergottite Northwest Africa 6234.

10:00 a.m. Udry A. * McSween H. Y. Jr.
Paired Nakhlites MIL 090030, 090032, 090136 and 03346: New Insights into the Cumulate Pile **[#1047]**
Pairing of the nakhlites MIL 090030, MIL 090032, MIL 090136, and MIL 03346 has been confirmed. However, modal abundances indicate that MIL 03346 is not representative of the parent sample.

10:15 a.m. Mikouchi T. * Makishima J. Kurihara T. Hoffmann V. H. Miyamoto M.
Relative Burial Depth of Nakhlites Revisited **[#2363]**
We calculated cooling rates of olivine in newly discovered nakhlites to reappraise our model for relative burial depth in a single cumulus pile. The obtained cooling rates suggest that all mesostasis-rich samples have similar burial depths (<2 m).

10:30 a.m. Goodrich C. A. * Treiman A. H. Filiberto J. Gross J. Jercinovic M. J.
K_2O-Rich Melt from the Martian Mantle? **[#1276]**
We conclude from a study of melt inclusions that the melt trapped in olivine cores in Nakhla was unusually K_2O-rich compared to most martian magmas. We discuss possible origins of this melt.

10:45 a.m. Taylor L. A. * Liu Y. Balta J. B. Goodrich C. A. McSween H. Y. Jr.
New Constraints on the Formation of Shergottite EET 79001 Lithology **[#2456]**
Since the martian meteorite EET 79001 contains two lithologies, an olivine-phyric portion and a basaltic portion, in an apparent igneous contact, several models have been proposed for the formation of EET 79001.

11:00 a.m. Sears D. W. G. *
Thermoluminescence Measurements and the Thermal History of Martian Meteorites **[#1853]**
The TL data indicate high-temperature feldspar is present in all four shergottites measured. This places important constraints on the post-shock thermal history of these meteorites.

11:15 a.m. Brandon A. D. *
Old Versus Young Shergottites from a Re-Os Isotope Perspective **[#2454]**
Re-Os isotopes can be used to assess the old versus young age debate for martian shergottites. These data are inconsistent with the younger ages produced via shock. Instead, Re-Os indicates the young ages result from igneous crystallization.

11:30 a.m. Moser D. E. * Chamberlain K. R. Tait K. T. Schmitt A. K. Barker I. R. Hyde B. C. Darling J. R.
Microstructure and U-Pb Dates of Martian Baddeleyite Rimmed by Zircon Indicate a 'Young' Igneous and Metamorphic History for Shergottite NWA 5298 **[#2173]**
Resolution of the shergottite "age paradox" through integrated SIMS and electron nanobeam (e.g., CL, EBSD) analysis of primary igneous baddeleyite and later metamorphic zircon.

VENUS VOLCANISM VIEWPOINTS: VAGUE OR VIABLE?
Tuesday, 8:30 a.m. Montgomery Ballroom

Chairs: Virgil Sharpton and Mark Bullock

8:30 a.m. Saunders R. S. *
Venus Resurfacing — Its Not Just About the Craters **[#1961]**
Complicated analyses of the venusian plains crater population are largely irrelevant to the issue of resurfacing. Resurfacing occurred prior to plains emplacement in a global tectonic event.

TUE ORALS

8:45 a.m. Hansen V. L. *
Constraints A–Z for the Surface Evolution of Venus, and Proposed History **[#1877]**
This contribution summarizes constraints A through Z for surface evolution of Venus, as derived from geologic mapping and analysis from a wide range of studies. All viable resurfacing models must be able to accommodate each of these constraints.

9:00 a.m. Ivanov M. A. * Head J. W. III
Evolution of Volcanism on Venus **[#1037]**
Spatial and temporal distributions of main volcanic units show that the types and intensity of internal activity on Venus were strongly time-dependent.

9:15 a.m. Sharpton V. L. *
Resolving the Volcanic History of Venus: Data Needs and Current Limitations **[#1246]**
Long-standing debate over the volcanic history of Venus suggests that current data are inadequate for resolving this important issue. I present SAR image resolution requirements for volcanic centers to be detected and characterized adequately.

9:30 a.m. Campbell B. A. * Campbell D. B. Carter L. M. Nolan M.
Long-Term Monitoring of Venus Volcanism Using Earth-Based Radar **[#2027]**
Radar mapping using the Arecibo telescope in 1988 provided a 1–2-km-resolution image of Venus. At the close approach in June 2012, we have a 24-year baseline to search for surface changes due to volcanism.

9:45 a.m. Kohler E. * Gavin P. Chevrier V. F. Johnson N.
Experimental Investigation into the Radar Anomalies on the Surface of Venus **[#2749]**
Preliminary results from experiments constraining the origins of the radar anomalies in the venusian highlands are presented.

10:00 a.m. Smrekar S. E. * Sotin C.
Implications of Recent Hotspot Volcanism on Venus for the Interior, Surface, and Atmosphere **[#2830]**
The presence of ~9 active mantle plumes implies that the mantle of Venus is relatively hot and possibly heating up. These plumes could provide observed atmospheric water vapor, and may also imply a transition from more widespread plains volcanism.

10:15 a.m. Piskorz D. * Elkins-Tanton L. T. Smrekar S. E.
Corona Formation on Venus via Extension and Lithospheric Instability **[#1982]**
We demonstrate that a mantle plume associated with a rift can create melt that intrudes the lower lithosphere and causes dripping into the upper mantle, extension, surface stresses, and the creation of off-rift coronae at Parga Chasma on Venus.

10:30 a.m. Basilevsky A. T. * Shalygin E. V. Titov D. V. Markiewicz W. J. Scholten F. Roatsch Th. Kreslavsky M. A. Moroz L. V. Ignatiev N. I. Fiethe B. Osterloh B. Michalchik H. Mironov N. L.. Head J. W. III
Possible Felsic Summit of Tuulikki Mons, Venus: Evidence from 1-Micron Surface Emissivity and Magellan-Viewed Morphology **[#1092]**
Based on the data taken by the Venus Monitoring Camera it was found that the summit of Tuulikki Mons volcano shows the 1-µm emissivity lower than that of the main body of the volcano. This suggests that the volcano summit material may be close to felsic.

10:45 a.m. Glaze L. S. * Baloga S. M. Stofan E. R.
Emplacement Scenarios for Volcanic Domes on Venus **[#1074]**
Effects of different boundary conditions on solutions for pressure-driven flow are explored. Results indicate a lava viscosity of 10^{12}–10^{13} Pa-s and dome emplacement times of ~2–16 years, both significantly less than prior estimates.

11:00 a.m. Santos A. R. * Agee C. B. McCubbin F. M.
The Effect of CO_2 on Melt Density and its Relevance to Magmatism on Venus **[#1592]**
The densities of anhydrous melts with different amounts of CO_2 (0–12 wt%) were determined experimentally over a range of pressures up to 9 GPa. The results were then applied to magmatic activity on Venus.

11:15 a.m. Miller D. M. * Gregg T. K. P.
Geologic Characteristics and Stratigraphic Relationships of Shield Fields Versus Shield Plains on Venus **[#2311]**
This study examines the stratigraphic relationships and characteristics between the two types of shield volcano clusters on Venus: shield fields and shield plains.

11:30 a.m. Davey S. C. * Ernst R. E. Samson C. Grosfils E. B.
Pit Crater Chain Clustering in Ganiki Planitia, Venus: Observations and Implications **[#1681]**
Clusters of pit crater chains in Ganiki Planitia, Venus, are examined and compared to lithology, structure, and volcanic features.

TUE ORALS

ICE IS NICE: ICY SATELLITE LANDFORMS, PROCESSES, AND STRUCTURE
Tuesday, 1:30 p.m. Waterway Ballroom 1

Chairs: Louise Prockter and Michael Bland

1:30 p.m. McKinnon W. B. * Singer K. N. Schenk P. M. Moore J. M.
Massive Ice Avalanches on Iapetus, and the Mechanism of Friction Reduction in Long-Runout Landslides **[#2823]**
We report numerous long-runout landslides on Iapetus, and its extremely cold, airless surface provides an excellent control on landslide friction reduction compared with Earth and Mars, as there is little role for either trapped air or groundwater.

1:45 p.m. Wood S. E. * Moore J. M. Ivarson K. L. Danilina I. Johnson M.
A New Hypothesis for the Origin of Mass Movements on Callisto **[#2901]**
We will describe a new hypothesis for the origin of the large lobate mass movements seen on Callisto but not other Galilean satellites. The mechanism involves near-surface condensation of CO_2 vapor driven upward by the geothermal gradient.

2:00 p.m. Hammond N. P. * Phillips C. B. Nimmo F. Kattenhorn S. A.
Determining Elastic Thickness on Dione from Flexure **[#2374]**
Using stereo-derived digital elevation models, we measure flexure across tectonic features on Dione, an icy satellite of Saturn, in order to estimate local elastic thickness and corresponding heat flux.

2:15 p.m. Barr A. C. *
Grooved Terrain Formation on Ganymede Driven by Mobile-Lid Convection **[#1319]**
Mobile-lid convection in Ganymede's ice shell is shown to be a possible means of driving the formation of its grooved terrain.

2:30 p.m. Prockter L. M. * Shirley J. H. Dalton J. B. Kamp L. W.
Apparent Resurfacing of a Pull-Apart Band in Argadnel Regio, Europa, Resulting from Trough Formation **[#2286]**
We use Galileo SSI and NIMS data to investigate a distinctive wedge-shaped band within Europa's Argadnel Regio. The band appears to have been resurfaced along its northern portion as the result of the formation of a large regional depression.

TUE ORALS

2:45 p.m. Schmidt B. E. * Blankenship D. D. Patterson G. W. Schenk P. M.
Insights into Europa's Shallow Water Mobility from Thrace and Thera Macula **[#2667]**
Comparison of Thera and Thrace Macula shows evidence for shallow water mobility within Europa's crust and places constraints on the timescales and direction of hydraulic water flow, as well as the material properties of the ice.

3:00 p.m. Gavin P. * Vance S.
Modeling Hydrothermal Vents on Europa **[#1683]**
Simulations of potential hydrothermal vents at Europa's ocean floor are presented. The effects of differing initial rock composition and temperature are explored with respect to mineral formation and vent fluid composition.

3:15 p.m. Castillo-Rogez J. C. * Choukroun M. Young J. B.
Opening the Black Box: A Laboratory-Based Dissipation Model for Water Ice — Description and Implications **[#2100]**
We will introduce a new model for ice dissipation in the conditions of stress amplitude and frequency relevant to outer planet satellites.

3:30 p.m. Singer K. N. * Bland M. T. McKinnon W. B. Schenk P. M.
Relaxed Impact Craters on Ganymede: Not All Sulci Are Created Equal **[#2775]**
Relaxed craters on Ganymede indicate heat flows in excess of 40 mW/m^2 averaged over 2 Ga, which suggests even higher heat flows if they occurred over a shorter interval. Mapping of four areas illuminates possible regional differences in heating.

3:45 p.m. Bland M. T. * Singer K. N. McKinnon W. B. Schenk P. M.
Crater Relaxation on Enceladus: Tales of High Heat Fluxes in Unexpected Places **[#2168]**
Enceladus craters aren't deep, modified by slow viscous creep. High heat flows, they say, relax craters away, so thermal gradients must have been steep.

4:00 p.m. Phillips C. B. * Hammond N. P. Robuchon G. Nimmo F. Beyer R. A. Roberts J.
Stereo Imaging, Crater Relaxation, and Thermal Histories of Rhea and Dione **[#2571]**
We use crater relaxation as a probe for subsurface temperature structure on satellites of Saturn. Crater relaxation from Cassini DEM crater profiles is compared with theoretical results. We find Rhea and Dione were warmer than predicted by our model.

4:15 p.m. Wagner R. J. * Neukum G. Schmedemann N.
Double and Multiple Craters on the Satellites of Saturn and Their Size Distribution **[#2469]**
Double and multiple craters on the satellites of Saturn are identified and their crater size frequency is measured.

4:30 p.m. Hoogenboom T. * Schenk P. White O. L.
Investigation of Secondary Craters in the Saturnian System **[#2579]**
To derive accurate ages using impact craters, the impact source must be determined. We investigate secondary crater size, frequency, distribution, formation, and crater chain formation on icy satellites throughout the Jupiter and Saturn systems.

OPPORTUNITIES FOR SCIENTIST PARTICIPATION IN EDUCATION AND PUBLIC OUTREACH
Tuesday, 1:30 p.m. Waterway Ballroom 4

Chairs: Sanlyn Buxner and Brooke Hsu

1:30 p.m. Shipp S. * Buxner S. Dalton H. CoBabe-Ammann E. Boonstra D. Ristvey J. Halligan E. Shupla C. Wessen A. Zimmerman-Brachman R. Igel C. Bleacher L. V. Scalice D.
Planetary Science Education and Public Outreach: How Scientists can get Involved! **[#2771]**
NASA SMD's Planetary Science E/PO Forum supports scientists who are involved and are interested in getting involved in education and public outreach.

1:45 p.m. Williams S. H. *
Planetary Science E/PO in 2012: The Year of the Solar System, Fifty Years of Solar System Exploration, and More **[#2564]**
The successful Year of the Solar System E/PO program will be followed by one themed to Fifty Years of Solar System Exploration. These programs, key astronomical events, and other factors will make 2012 a banner year for solar system programming.

2:00 p.m. CoBabe-Ammann E. Shipp S. S. Dalton H.
The Higher Education Clearinghouse for Space Sciences (HECl) **[#1634]**
The Higher Education Clearinghouse (HECl) is a searchable database of undergraduate classroom materials for faculty teaching planetary sciences and solar and space physics at both the introductory and upper division levels.

2:15 p.m. Benfield M. P. J. * Turner M. W. Farrington P. A. Mitchell B. K.
Developing Partnerships for an Undergraduate Design Program on Planetary Science Mission Concept Development **[#1657]**
Innovative undergraduate educational experience.

2:30 p.m. Klug Boonstra S. L. * Christensen P. R.
Engaging Scientists from the Top Down (Practicing Scientists) and Bottom Up (Graduate and Undergraduate Science Students): Creating a Rich Culture of STEM Learning to Benefit Multiple Stakeholders in the Middle **[#2445]**
Learn some keys for successfully engaging scientists to be more effective in working with educational audiences. Find out some of the success stories that have changed both the scientist and educator in surprising ways.

2:45 p.m. *Discussion led by Brooke Hsu*

3:15 p.m. Smith H. Coe L. Reyes M. McKay C. Rask J. Heldman J. Warren-Rhodes K.
Spaceward Bound — Training the Next Generation of Field Scientists **[#2763]**
Spaceward Bound, an educational program sponsored by NASA Ames Research Center, pairs K–12 teachers, students, and graduate students with interdisciplinary field scientists to provide a hands on learning experience.

3:30 p.m. Graff P. V. * Stefanov W. L. Willis K. J. Runco S.
Bridging the Gap Between Scientists and Classrooms: Scientist Engagement in the Expedition Earth and Beyond Program **[#2358]**
The Expedition Earth and Beyond Program bridges the gap between scientists and classrooms. Scientists work with students as mentors, participate in student presentations, and interact with students through distance learning events.

3:45 p.m. Buxner S. *
Engaging Scientists in Meaningful Education and Public Outreach Partnerships: Examples from the Planetary Science Institute **[#2876]**
Successful education and public outreach (E/PO) programs require collaboration with professional scientists. This presentation highlights a portfolio of E/PO activities at the Planetary Science Institute that effectively engage scientists.

4:00 p.m. Cohen J. P. * Ding W. Sable J. Li R. Stepinski T.
Mars Weekend: A Panel and Games at the Museum of Science Boston **[#1023]**
This ongoing outreach project uniquely combines the data, systems, and resources of four existing NASA-funded research projects: MER Participating Scientist project, ExoMars PanCam project, AISR Crater Detection project, and lunar mapping.

4:15 p.m. Cobabe-Ammann E. * [INVITED]
Navigating SMD EPO: A Practical Guide to SMD EPO Funding Opportunities

4:30 p.m. *Discussion led by Sanlyn Buxner*

ISOTOPIC CONSTRAINTS ON EARLY SOLAR SYSTEM CHRONOLOGY
Tuesday, 1:30 p.m. Waterway Ballroom 5

Chairs: Herbert Palme and Naomi Marks

TUE ORALS

1:30 p.m. Gounelle M. * Chaussidon M. Rollion-Bard C.
The Be-B, Al-Mg and Oxygen Isotopes Systematics of Isheyevo (CH/CB) Calcium-, Aluminium-Rich Inclusions **[#1912]**
Be-B, Al-Mg, and O isotope systematics of Isheyevo CAIs are reported. Isheyevo CAIs with ^{16}O-rich oxygen isotopic composition contain large ^{10}B excesses, possibly due to ^{10}Be decay or to spallogenic ^{10}B. They have recorded extreme irradiation processes.

1:45 p.m. Tang H. * Dauphas N.
Low Abundance and Homogeneous Distribution of ^{60}Fe in the Early Solar System **[#1703]**
Issue of ^{60}Fe abundance and homogeneity is still unclear. We measured ^{58}Fe and ^{60}Ni abundances in many meteorites, from which we derive a much lower initial ^{60}Fe/^{56}Fe ratio and show that ^{60}Fe was homogeneously distributed among planetary bodies.

2:00 p.m. Telus M. * Huss G. R. Nagashima K. Ogliore R. C. Tachibana S.
Reevaluating Our Understanding of the ^{60}Fe-^{60}Ni System in Chondrites **[#2733]**
We summarize our findings regarding the Fe and Ni isotopic composition of chondrules from primitive ordinary chondrites and discuss important constraints on the initial abundance of ^{60}Fe in the solar system.

2:15 p.m. Spivak-Birndorf L. J. * Wadhwa M. Janney P. E.
^{60}Fe–^{60}Ni Systematics of Chainpur Chondrules and the Plutonic Angrites Northwest Africa 4590 and 4801 **[#2861]**
We present ^{60}Fe-^{60}Ni isotope systematics for bulk Chainpur chondrules and plutonic angrites. The Chainpur chondrule data are used to estimate an upper limit on the initial solar system ^{60}Fe/^{56}Fe $< \sim 1 \times 10^{-7}$.

2:30 p.m. Papanastassiou D. A. * Chen J. H. Weiss B P.
Mn-Cr Isotopic Systematics in the Eagle Station Pallasite Metal **[#2504]**
We report large cosmic ray spallation effects for ^{53}Cr and ^{54}Cr in Eagle Station metal, which may affect the Mn-Cr chronometer interpretation and possible link of Eagle Station to CO3 and CV3 chondrites.

2:45 p.m. Palme H. * Kleine T. Rubie D. C.
Early Volatile Depletion and Rapid Core Formation in the Earth: Evidence from the ^{53}Mn–^{53}Cr System **[#2163]**
The ^{53}Mn-^{53}Cr system of Earth compared to meteorites indicates volatile depletion in Earth within the first million years. Core formation began at the same time. The Cr-isotopic composition of the core is different from the mantle.

3:00 p.m. Horan M. F. * Carlson R. W. Blichert-Toft J.
An Evaluation of the Palladium-Silver Isotope Systematics in the Oldest Differentiated Planetesimal: Beyond Shock **[#1116]**
Pd-Ag isotopic systematics in Muonionlusta (Group IVA iron meteorite, troilite Pb-Pb age = 4565.3 ± 0.1 Ma) yield an initial solar system abundance of 107Pd/108Pd of $(2.8 \pm 0.4) \times 10^{-5}$, despite heterogeneous shock effects in troilite.

3:15 p.m. Sanborn M. E. * Carlson R. W. Wadhwa M.
Internal Lu-Hf Isochrons for the Quenched and Plutonic Angrites and Their Chronological Implications **[#2039]**
We present the initial results of our investigation of the ^{176}Lu-^{176}Hf systematics in mineral separates and whole-rock fractions of the D'Orbigny quenched angrite and the NWA 4590 and NWA 4801 plutonic angrites.

3:30 p.m. Bast R. * Scherer E. E. Taetz S. Sprung P. Mezger K. Srinivasan G.
Internal Lu-Hf Isotope Systematics of the Eucrites Millbillillie and Piplia Kalan **[#2542]**
Internal Lu-Hf isochron data for the eucrites Piplia Kalan and Millbillillie were acquired to help determine the cause of the commonly observed discordance between U-Pb and Lu-Hf ages in meteorites and their components.

3:45 p.m. Burkhardt C. * Kleine T. Dauphas N. Wieler R.
Origin of Nucleosynthetic Isotope Heterogeneity in the Solar Nebula Inferred from Mo and W Isotopes in Acid Leachates from Murchison **[#2405]**
The first W-isotopic data of chondrite leachates are presented. Implications for the distribution of nucleosynthetic carriers, the origin of planetary-scale nucleosynthetic anomalies, and the solar system initial ε^{182}W are discussed.

4:00 p.m. Kruijer T. S. * Fischer-Gödde M. Sprung P. Leya I. Wieler R. Kleine T.
Neutron Capture on Pt and W Isotopes in Iron Meteorites: Implications for Hf-W Chronometry **[#1529]**
We report the first precise Pt-isotope data for extraterrestrial materials. The Pt-isotope anomalies in IVB iron meteorites are neutron-capture induced. The combined Pt- and W-isotope results are used here to quantify cosmic-ray effects on W isotopes.

4:15 p.m. Wittig N. * Humayun M. Huang S. Brandon A. D.
Revised Tungsten Isotope Chronology of IVB Iron Meteorites from W-Os Systematics **[#1482]**
W-Os isotope systematics of 12 IVB iron meteorites, including five newly characterized samples, are correlated and used to derive a pre-irradiation ε^{182}W of -3.37 ± 0.19, which is indistinguishable from CAIs.

4:30 p.m. Walker R. J. * Touboul M.
Improved Constraints on the Relative Timing of Metal Segregation in the Early Solar System Using Coupled W-Os Isotopes **[#1166]**
^{182}W has been used to place age constraints on early metal-silicate segregation. New high-precision W measurements, coupled with Os-isotope constraints on cosmic ray exposure history, allow small differences in ages among iron groups to be resolved.

MARTIAN HYDRATED MINERALS AND VOLATILES FROM MANTLE TO SURFACE
Tuesday, 1:30 p.m. Waterway Ballroom 6

Chairs: Tomohiro Usui and Joseph Michalski

1:30 p.m. Channon M. B. * Boyce J. W. Stolper E. M. Eiler J. M.
Abundances of Cl, F, H, and S in Apatites from Martian Meteorites **[#2845]**
Apatites from basaltic shergottites have higher abundances of water and sulfur than other SNC rock types, and match (in the case of water) or exceed (in the case of sulfur) abundances of terrestrial igneous mafic rocks.

TUE ORALS

1:45 p.m. McCubbin F. M. * Hauri E. H. Elardo S. M. Vander Kaaden K. E. Wang J. Shearer C. K. Jr.
Hydrous Melting of the Martian Mantle Produced Both Depleted and Enriched Shergottites **[#1121]**
Water contents of apatite from a depleted and an enriched shergottite indicate that hydrous melting of the martian interior occurred for both sources. Elevated water contents in the depleted source indicate early storage of water in Mars' interior.

2:00 p.m. Jones J. H. * Usui T. Alexander C. M. O'D. Simon J. I. Wang J.
Provenance and Concentration of Water in the Shergottite Mantle **[#2560]**
H_2O and Na_2O abundances in shergottite Y980459, coupled with simple melting models, imply that the water content of the depleted shergottite source region is 16–33 ppm. The D/H ratio of this water is approximately chondritic, or "Earthlike."

2:15 p.m. Usui T. * Alexander C. M. O'D. Wang J. Simon J. I. Jones J. H.
Evidence from Olivine-Hosted Melt Inclusions that the Martian Mantle has a Chondritic D/H Ratio and that Some Young Basalts have Assimilated Old Crust **[#1341]**
Olivine-hosted melt inclusions from a depleted shergottite (Y-980459) possess undegassed water with near-chondritic δD of ~275‰. In contrast, a melt inclusion from an enriched shergottite (LAR 06319) exhibits an atmospheric/surficial δD of ~5000‰.

2:30 p.m. Hallis L. J. * Taylor G. J. Nagashima K. Huss G. R.
Magmatic Water in Martian Meteorites **[#2317]**
We studied the hydrogen-isotope composition of Nakhla apatites in an attempt to measure the primordial martian D/H ratio.

2:45 p.m. Stanley B. D. * Hirschmann M. M.
Solubility of C-O-H Volatiles in Graphite-Saturated Martian Basalts **[#2050]**
We investigate the solubility of carbon dioxide in martian analogue basaltic melts with graphite present to constrain the magmatic outgassing fluxes of carbon dioxide during martian atmospheric evolution.

3:00 p.m. Mustard J. F. * Poulet F. Ehlman B. E. Milliken R. E. Fraeman A.
Sequestration of Volatiles in the Martian Crust Through Hydrated Minerals: A Significant Planetary Reservoir of Water **[#1539]**
We derive a first-order estimate of the size of the water reservoir in the martian crust defined by hydrous minerals integrating data and results from orbital, lander data of Mars and meteorite analyses.

3:15 p.m. Smith M. R. * Bandfield J. L.
Hydrated Silica on Mars: Near-IR and Thermal-Infrared Spectroscopic Investigation Into the Diversity of Martian Silica **[#1641]**
We are using near-infrared and thermal infrared spectroscopy to examine the range of martian hydrated silica compositions and find that there are variable compositions among detected silicas.

3:30 p.m. McKeown N. K. * Mazurok J. Kamanos K. Wray J. J.
Mineralogies of the Amenthes-Northern Terra Cimmeria Region, Mars **[#2670]**
Amenthes and northern Terra Cimmeria have been studied geomorphically but the mineralogy has not yet been studied in detail. Our preliminary studies indicate the presence of olivine, low-calcium pyroxene, and a hydrated mineral (possibly carbonate).

3:45 p.m. Bishop J. L. * Rampe E. B.
Allophane Identified at Mawrth Valles in CRISM and TES Datasets and Implications for the Ancient Phyllosilicate-Rich Rocks **[#2277]**
Allophane has been identified at Mawrth Vallis in the upper Al/Si-rich clay unit using CRISM data and in the region at ~10% through modeling of TES data. This implies the presence of young, well-drained soils in neutral to mildly acidic conditions.

4:00 p.m. Che C. * Glotch T. D.
Characterizing Dehydrated and Dehydroxylated Phyllosilicates on Mars Using Thermal and Near IR Spectroscopy **[#1377]**
The objective of this work is to identify, map, and characterize dehydrated and dehydroxylated clays on Mars, using TES and CRISM data. The significant suite of our previous laboratory spectra will be the basis for our TES and CRISM data analysis.

4:15 p.m. Flahaut J. * Quantin C. Bishop J. L. Fueten F. Allemand P. Mangold N. Poulet F. Bibring J.-P.
Mineralogic Investigation of Capri/Ganges/Eos Chasmata, Mars: Insights into the Geologic History of Valles Marineris **[#1823]**
We present here detailed analyses of Ganges, Capri, and Eos chasmata (Valles Marineris eastern end) using high-resolution morphologic and mineralogic data from the Mars Reconnaissance Orbiter (MRO) mission.

4:30 p.m. Michalski J. R. * Rogers A. D. Wright S. P. Niles P. B. Cuadros J.
Sporadic Groundwater Upwelling in Deep Martian Craters: Evidence for Lacustrine Clays and Carbonates **[#1431]**
We searched for evidence of groundwater upwelling in deep martian craters and found only rare evidence for such processes. However, some cases suggest that groundwater-fed lakes have existed and led to the formation of lacustrine clays and carbonates.

SPECIAL SESSION: MESSENGER'S FIRST YEAR IN ORBIT ABOUT MERCURY
Wednesday, 8:30 a.m. Waterway Ballroom 1

Chairs: Sean Solomon and David Paige

8:30 a.m. Johnson C. L. * Purucker M. E. Anderson B. J. Winslow R. M. Al Asad M. Korth H. Slavin J. A. Alexeev I. I. Ritzer J. A. Phillips R. J. Zuber M. T. Solomon S. C.
MESSENGER Observations of Mercury's Magnetic Field Structure **[#1355]**
We use orbital magnetic field data from MESSENGER to constrain Mercury's internal dipolar field and large-scale, time-averaged magnetopause and magnetotail fields. We investigate mechanisms that may account for structure in the residual fields.

8:45 a.m. Purucker M. E. * Johnson C. L. Winslow R. M. Nicholas J. B. Anderson B. J. Korth H. Head J. W. III Zuber M. T. Solomon S. C. Slavin J. A. Alexeev I. I. Phillips R. J. Paige D. A.
Evidence for a Crustal Magnetic Signature on Mercury from MESSENGER Magnetometer Observations **[#1297]**
Magnetic fields from low-altitude MESSENGER observations over the northern pole reveal an anomaly that can be reproduced with a crustal layer magnetized in a direction opposite to that of the present main field. We present possible interpretations.

9:00 a.m. Mazarico E. * Lemoine F. G. Goossens S. J. Smith D. E. Zuber M. T. Neumann G. A. Torrence M. H. Rowlands D. D. Solomon S. C.
The Gravity Field of Mercury from MESSENGER **[#2189]**
A gravity field of Mercury is developed from MESSENGER orbital observations. In addition to the radiometric tracking data, altimetric crossovers base on the MLA data are used.

9:15 a.m. Hauck S. A. II * Solomon S. C. Margot J.-L. Lemoine F. G. Mazarico E. Peale S. J. Perry M. E. Phillips R. J. Smith D. E. Zuber M. T.
Mercury's Internal Structure as Constrained by MESSENGER Observations **[#1170]**
We discuss the implications of Mercury's gravity field as revealed by MESSENGER and Earth-based measurements of its spin-state for the planet's internal structure. Results indicate that Mercury has a large core with a potentially unique structure.

9:30 a.m. Michel N. C. * Hauck S. A. II Solomon S. C. Phillips R. J. Roberts J. H. Zuber M. T.
Implications of MESSENGER Observations for Mantle Convection on Mercury **[#1671]**
We investigate the implications of MESSENGER observations for the evolution of Mercury's interior by modeling convection in a mantle constrained to be relatively thin.

9:45 a.m. James P. B. * Zuber M. T. Phillips R. J.
Viscosity Structure of Mercury and Implications for Support of the Northern Rise **[#2425]**
Models for support of the Northern Rise are tested against viscosity profiles of Mercury's mantle. Additionally, we address the role of lithospheric stresses in the support of topography and we compare our results to crater tilts measured by MLA.

10:00 a.m. Solomon S. C. * Klimczak C. Byrne P. K. Hauck S. A. II Balcerski J. A. Dombard A. J. Zuber M. T. Smith D. E. Phillips R. J. Head J. W. III Watters T. R.
Long-Wavelength Topographic Change on Mercury: Evidence and Mechanisms **[#1578]**
Orbital observations by the MESSENGER spacecraft show that Mercury experienced marked changes in long-wavelength topography more recently than the end of late heavy bombardment and the volcanic emplacement of the largest expanses of smooth plains.

10:15 a.m. Byrne P. K. * Şengör A. M. C. Klimczak C. Solomon S. C. Watters T. R.
Large-Scale Crustal Deformation on Mercury **[#2118]**
We map laterally extensive sets of contractional landforms on Mercury as fold-and-thrust belts. In places these belts correlate to regions of high topography, and may play a role in the distribution of thicker crustal blocks on the innermost planet.

10:30 a.m. Chabot N. L. * Ernst C. M. Harmon J. K. Murchie S. L. Solomon S. C. Blewett D. T. Denevi B. W.
Craters Hosting Radar-Bright Deposits in Mercury's North Polar Region **[#1476]**
All radar-bright features near Mercury's north pole are confined to shadowed areas in MESSENGER images to date, consistent with the water-ice hypothesis, although low-latitude and small craters provide challenging thermal environments.

10:45 a.m. Talpe M. J. * Zuber M. T. Neumann G. A. Mazarico E. Solomon S. C. Vilas F.
Characterization of the Morphometry of Impact Craters Hosting Polar Deposits in Mercury's North Polar Region **[#1600]**
We characterize the shape of 274 craters between 6.08 and 207 km in diameter and located in Mercury's north polar region from MLA observations. Thirty-five craters host radar-bright deposits and are statistically deeper than craters that don't host deposits.

11:00 a.m. Neumann G. A. * Cavanaugh J. F. Sun X. Mazarico E. Smith D. E. Zuber M. T. Solomon S. C. Paige D. A.
Dark Material at the Surface of Polar Crater Deposits on Mercury **[#2651]**
All Mercury radar-bright deposits correspond to poleward-facing slopes in permanently shadowed regions north of 68°N. The Mercury Laser Altimeter on the MESSENGER spacecraft sees these regions as darker than their surroundings at 1064 nm wavelength.

11:15 a.m. Paige D. A. * Harmon J. K. Smith D. E. Zuber M. T. Neumann G. A. Solomon S. C.
Thermal Stability of Frozen Volatiles in the North Polar Region of Mercury **[#2875]**
We examine the thermal stability of water ice and other frozen volatiles in the north polar region of Mercury using topographic profiles obtained by the MESSENGER MLA instrument in conjunction with a three-dimensional ray-tracing thermal model.

11:30 a.m. Lawrence D. J. * Feldman W. C. Evans L. G. Goldsten J. O. McNutt R. L. Jr. Nittler L. R. Peplowski P. N. Prettyman T. H. Solomon S. C.
Hydrogen at Mercury's North Pole? Update on MESSENGER Neutron Measurements **[#1802]**
The MESSENGER Neutron Spectrometer (NS) is being used to identify and measure putative hydrogen deposits of Mercury's north pole. The NS data analysis is in progress and an update will be provided.

AIRLESS BODIES EXPOSED: SPACE ENVIRONMENT CONDITIONS AND SURFACE INTERACTIONS
Wednesday, 8:30 a.m. Waterway Ballroom 4

Chairs: Roy Christoffersen and William Farrell

8:30 a.m. Hurley D. M. * Killen R. M. Sarantos M.
Monte Carlo Model Insights into the Lunar Sodium Exosphere **[#1594]**
We model the sodium exosphere of the Moon and compare the distribution to telescope data to determine how sodium interacts with the lunar regolith. We investigate sticking, thermal accommodation, and reemission.

8:45 a.m. Farrell W. M. * Zimmerman M. I. Poppe A. Halekas J. S. Delory G. T.
The Lunar Photoelectron Sheath: A Change in Trapping Efficiency During a Solar Storm **[#1816]**
We examine the trapping efficiency of the photoelectric sheath at the Moon when the local environmental plasma is undergoing an extreme event: a solar storm.

9:00 a.m. Horanyi M. * Sternovsky Z. Lankton M. James D. Szalay J. Drake K. Shu A. Colette A. Gruen E. Kempf S. Srama R. Mocker A.
The Dust Environment of the Moon: Expectations for the Lunar Dust Experiment (LDEX) **[#2635]**
The lunar dust exosphere is sustained by interplanetary dust bombardment and by electromagnetic effects induced by the solar wind and UV radiation. We present the expectations for the observations by LDEX to be launched onboard the LADEE mission.

9:15 a.m. Spence H. E. * Blake J. B. Case A. W. Golightly M. J. Kasper J. C. Looper M. D. Mazur J. E. Schwadron N. A. Townsend L. W. Zeitlin C. J.
Energy Spectral Properties and Implications of the Lunar Energetic Proton Albedo **[#2692]**
We use CRaTER observations to quantify the energy spectrum of the newly-discovered lunar energetic proton albedo. We discuss aspects of this unanticipated albedo, including implications for similar interactions with other airless planetary objects.

9:30 a.m. Jordan A. P. * Stubbs T. J. Zeitlin C. Spence H. E. Schwadron N. A. Zimmerman M. I. Farrell W. M.
On the Interaction Between Highly Energetic Charged Particles and the Lunar Regolith **[#2619]**
In this study we explore how galactic cosmic rays and solar energetic particles contribute to deep dielectric charging within the lunar regolith and how these particles affect lunar surface charging in tenuous plasma environments.

9:45 a.m. Noble S. K. * Keller L. P. Christoffersen R. Rahman Z.
Space Weathering of Lunar Rocks **[#1239]**
Like lunar soils, exposed rocks also incur the effects of space weathering. A TEM study of the space-weathered patina of three Apollo 17 rocks provides a glimpse into the similarities and differences between soil and rock weathering.

10:00 a.m. Thompson M. S. * Christoffersen R. Noble S. K. Keller L. P.
Comparative Mineralogy, Microstructure and Compositional Trends in the Sub-Micron Size Fractions of Mare and Highland Lunar Soils **[#2384]**
Analytical TEM methods have been used to systematically compare and contrast the microstructure and mineralogy of the smallest grains in highland and mare lunar soils.

10:15 a.m. Wang K. * Moynier F. Podosek F. A. Foriel J.
Iron Isotope and the Origin of Nanophase Iron in Lunar Regolith **[#1148]**
We report the iron-isotopic composition of nanophase iron in lunar regolith. It is highly enriched in heavy isotopes of Fe (δ^{56}Fe up to 0.71‰). It is due to the preferential loss of light isotopes to space during vaporization by micrometeorite impacts.

10:30 a.m. Hemingway D. * Garrick-Bethell I.
Insights into Lunar Swirl Morphology and Magnetic Source Geometry: Models for the Reiner Gamma and Airy Anomalies **[#1735]**
We use Lunar Prospector and Clementine data along with our own equivalent source models to support the solar wind deflection model for swirl formation and to show how magnetic field direction influences small-scale swirl morphology.

10:45 a.m. Rout S. S. * Stockhoff T. Moroz L. V. Hofsäss H. Dohmen R. Zhang K. Baither D. Schade U. Bischoff A. Hiesinger H.
High Temperature, Nanoscale Changes in Films Produced by Irradiation of Iron Bearing Silicates: Laboratory Simulations of Space Weathering in Hermean Environment **[#1998]**
Thin film on a silicon substrate was deposited by Ar-ion irradiation of the San Carlos olivine. This silicate film contains nanoinclusions of Fe, Cu, and Ni that increased in size when heated to 450°, relevant to Mercury.

11:00 a.m. Bradley J. P. * Ishii H. A. Aguiar J. Borg L. E. Shearer C. K.
Amorphous Silicates Produced During Space Weathering: Insight from Monochromated Valence Electron Energy-Loss Spectroscopy **[#1941]**
Monochromated valence electron energy-loss spectroscopy enables distinction between otherwise indistinguishable amorphous silicates in lunar regolith soils and interplanetary dust particles formed by different mechanisms during space weathering.

11:15 a.m. Poppe A. R. * Halekas J. S. Delory G. T. Farrell W. M.
Particle-in-Cell Simulations of Plasma Interaction with Lunar Crustal Magnetic Anomalies **[#1526]**
We present results from a kinetic plasma simulation on the interaction of ambient plasma with lunar crustal magnetic anomalies. We discuss implications of this work for physical phenomena at the Moon, such as lunar swirls and proton implantation.

11:30 a.m. Noguchi T. * Kimura M. Hashimoto T. Konno M. Nakamura T. Nakato A. Ogami T. Ishida H. Sagae R. Tsujimoto S. Tsuchiyama A. Zolensky M. E. Tanaka M. Fujimura A. Abe M. Yada T. Mukai T. Ueno M. Okada T. Shirai K. Ishibashi Y. Okazaki R.
Space Weathering Products Found on the Surfaces of the Itokawa Dust Particles: A Summary of the Initial Analysis **[#1896]**
We report a summary of the initial analysis of space weathering of the Itokawa particles. In addition to the two-layered nanoparticle-bearing rims, we found vesicular rims with nanoparticles and quite thin vapor deposition layers on intact minerals.

IMPACT EJECTA: PROCESSES AND PRODUCTS
Wednesday, 8:30 a.m. Waterway Ballroom 5

Chairs: Gordon Osinski and Steven Goderis

8:30 a.m. Hermalyn B. * Schultz P. H. Heineck J. T.
Experimental Studies of the Ejecta Velocity Distribution from Oblique Impacts: Towards an Analytical Model **[#2022]**
A novel three-dimensional particle tracking technique enables temporal measurement of the early-to main-stage ejecta velocity distribution from experimental oblique impacts at the AVGR. A physically based scaling model incorporating obliquity is proposed.

8:45 a.m. Sommer F. D. * Reiser F. Dufresne A. Poelchau M. H. Kenkmann T. Deutsch A.
Ejection Behavior During Variation of Impact Energy and Target Water Saturation — The MEMIN Project **[#2035]**
Ejection behavior in experimental impacts into sandstone was analysed and specific characteristics were identified with changes in target pore space saturation, projectile velocity, and projectile mass.

9:00 a.m. Ong L. * Melosh H. J.
Nonlinear Shock Interactions Produce High-Velocity, Low-Pressure Spall **[#2031]**
We simulate the interactions of impact-induced nonlinear shock waves in the near-surface of the target. Shocks interact with the free surface to produce lightly-shocked ejecta with velocities 1.5 times the particle velocities in the shock front.

9:15 a.m. Barlow N. G. * Boyce J. M.
Distribution and Characteristics of Martian Low Aspect Ratio Layered Ejecta (LARLE) Craters **[#1253]**
We are conducting a global survey of the distribution and characteristics of an unusual crater morphology that we have termed low aspect ratio layered ejecta (LARLE) craters. LARLE craters appear to be related to pedestal craters.

9:30 a.m. Piatek J. L. * Nolan R. T. Tornabene L. L.
Thermophysical Properties of Layered Crater Ejecta Deposits on Mars **[#2098]**
The complex relationship between layered and ballistically emplaced ejecta deposits of fresh craters on Mars is examined using thermal inertia results from THEMIS images with analysis of visible morphology from HiRISE/CTX images.

9:45 a.m. Bandfield J. L. * Song E. Hayne P. O. Ghent R. R. Paige D. A.
Lunar "Cold Spots": A New Class of Thermophysically and Morphologically Distinct Craters **[#1487]**
A class of lunar craters are surrounded by a highly insulating regolith layer that can extend over 100 crater radii from the source. Visible images do not show this layer but display layered near-crater ejecta with fluidized flow morphologies.

10:00 a.m. Kalleson E. * Riis F. Setsaa R. Dypvik H.
Ejecta Distribution and Stratigraphy — Field Evidence from the Ritland Impact Structure **[#1351]**
An ejecta layer from the 2.7-km-diameter Cambrian, Ritland impact structure has been studied in the field. The layer consists of crystalline clasts ejected during impact, mixed with Cambrian dark clays.

10:15 a.m. Bierhaus E. B. * Dones L.
Cratering by Impact Ejecta, from Mercury to the Asteroids **[#2451]**
We estimate the relative importance of secondary cratering in the inner solar system. Notably, we find that Mercury should have the most secondary craters, perhaps the most in the solar system, and that the largest asteroids should also have secondaries.

10:30 a.m. Plescia J. B. *
Uncertainties in the <3 Ga Lunar Impact Cratering Chronology **[#1614]**
Self-cratering results in the use of crater counts on ejecta of dated craters of dubious value to constrain the impact flux as the number does not reflect a primary flux. This has implications for a martian flux as it is extrapolated from the Moon.

10:45 a.m. Zanetti M. * Jolliff B. van der Bogert C. H. Hiesinger H.
Equal-Area Radial Crater Counts at Large Copernican Impact Craters: Implications for Late-Stage Ejecta Emplacement **[#2131]**
The distribution of small impact craters in the continuous ejecta of Copernican craters using equal-area counts oriented radially to the rim show a trend of decreasing age with increasing distance, suggesting an influence of self-secondary cratering.

11:00 a.m. Johnson B. C. * Melosh H. J.
Distal Impact Ejecta: Melt Droplets, Impact Lapilli, and Tektites **[#1456]**
We describe the formation of melt droplets, impact lapilli, and tektites. We also make size estimates of these ejecta products that are consistent with observations and predict that non-global ejecta layers should be an aggregate of these particles.

11:15 a.m. Davatzes A. K. * Byerly G. R.
Insight into Archean Spherule Growth from Geochemistry and 3D Imaging **[#2093]**
MicroCT three-dimensional imaging of the spherules shows no unusual shapes or surface agglutination. Electron microprobe line scans show geochemical differences in layered spherules, indicating growth by collision while still partially molten.

WED ORALS

11:30 a.m. Deutsch A. * Artemieva N.
Tracking down Traces of the Chicxulub Projectile in K-Pg Boundary Deposits **[#2087]**
Flat and unfractionated REE distribution patterns of impact spherules from K-Pg sites in northeast Mexico, Alabama, and ODP 207 substantiate the so far unknown but significant contribution of the Chicxulub bolide to these ejecta sites.

PRIMARY AND SECONDARY MARTIAN GEOCHEMISTRY
Wednesday, 8:30 a.m. Waterway Ballroom 6

Chairs: Melissa Lane and Paul Archer Jr.

8:30 a.m. Clenet H. * Quantin C. Ceamanos X. Flahaut J. Allemand P. Pinet P. C. Daydou Y.
Crustal Composition in the Vicinity of Valles Marineris, Mars, as Seen from the Central Peaks of Impact Craters **[#1486]**
We studied impact craters central peaks with CRISM data. MGM is used to extract chemical composition of mafic minerals. There is a relationship between depth of sampled crust and orthopyroxene composition. Link with alteration is also investigated.

8:45 a.m. Wilson J. H. * Mustard J. F.
Extensive Exposures of Olivine-Rich Volcanic Rocks in Noachian-Aged Surfaces on Mars **[#2090]**
Noachian-aged volcanics on Mars are difficult to identify, so their composition hasn't been addressed in detail. Volcanics identified on a Noachian surface, east of Ares Vallis, are studied to address the character and scope of ancient volcanics.

9:00 a.m. Ody A. * Poulet F. Langevin Y. Bibring J.-P. Gondet B. Carter J.
Olivine Detections in the Martian Northern Plains with OMEGA/Mex **[#2430]**
Based on data from the imaging spectrometer MEx/OMEGA, olivine was detected in crater ejectas and extended deposits within the martian northern plains, thus allowing some constraints to be put on the global geological history of these northern plains.

9:15 a.m. Huang J. * Edwards C. S. Christensen P. R. Horgan B. H. Xiao L.
Thermally Distinct Olivine-Rich Dikes in Thaumasia Planum, Mars **[#2577]**
We report several new occurrences of dikes in Thaumasia Planum, which have distinct thermophysical and compositional characteristics. They are important for understanding the magmatic properties and processes in early martian geological time.

9:30 a.m. Pan C. * Rogers A. D.
Thermal and Near-Infrared Analyses of Central Uplifts of Martian Impact Craters **[#2312]**
We analyze martian impact craters with central uplifts globally using TIR and NIR data. Comparisons between spectrally distinct crater central uplifts and their surrounding regions are also discussed.

9:45 a.m. McLennan S. M. *
Constraints on the Age, Composition and Size of the Martian Sedimentary Mass **[#1869]**
The overall martian sedimentary mass is ancient, of mafic composition, and approximately 2–20% of the size of the terrestrial sedimentary record.

10:00 a.m. Karunatillake S. * Gasnault O. McLennan S. M. Rogers A. D. Wray J. J. Squyres S. W. Boynton W. V.
The Hydration State of Sulfates on Mars **[#2940]**
We assess the hydration state of sulfates using Mars Odyssey Gamma Ray Spectrometer (GRS) derived H_2O and S mass fraction distributions in the mid-latitudinal subsurface at decimeter depths.

10:15 a.m. Robertson K. M. * Bish D. L.
Stability of Phases in the $CaSO_4 \bullet nH_2O$ System and Implications for Their Occurrence on Mars **[#1547]**
Experimental results are presented here that provide a clearer understanding of phase stabilities in the $CaSO_4 \bullet nH_2O$ system under martian conditions that help constrain the association between observable hydrous phases and current and past climates.

10:30 a.m. Franz H. B. * Farquhar J. Irving A. J.
Clues to the Martian Sulfur Cycle Revealed Through Isotopic Analysis of Shergottites, Nakhlites, and Chassigny **[#2232]**
We report results of an extensive study to characterize the isotopic composition of both reduced and oxidized sulfur-bearing mineral phases in 27 shergottites, the Y-000593 nakhlite, and Chassigny, which we will compare to other solar system bodies.

10:45 a.m. Cannon K. M. * Sutter B. Ming D. W. Boynton W. V. Quinn R. C.
Possible Calcite and Magnesium Perchlorate Interaction in the Mars Phoenix Thermal and Evolved Gas Analyzer (TEGA) **[#2008]**
Laboratory experiments simulating TEGA analysis indicate that a lower-temperature carbon dioxide release detected by TEGA may have be caused by an inorganic reaction between magnesium perchlorate and calcite in the instrument ovens.

11:00 a.m. Archer P. D. Jr. * Lauer H. V. Jr. Sutter B. Ming D. W. Niles P. B. Boynton W. V.
A Possible Organic Contribution to the Low Temperature CO_2 Release seen in Mars Phoenix Thermal and Evolved Gas Analyzer Data **[#2276]**
Organic combustion by perchlorate-produced oxygen could contribute to the low-temperature CO_2 release detected by the TEGA instrument on the Mars Phoenix Lander.

11:15 a.m. Hanley J. * El Senousy A. Chevrier V. F. Farris H.
Analysis of the Salt Assemblage from WCL at the Phoenix Landing Site **[#2574]**
Ion concentrations obtained from WCL were modeled to determine the original salts present at the Phoenix landing site, as well as their implications for the stability of liquid water.

11:30 a.m. Meslin P.-Y. * Hamara D. K. Boynton W. V. Sabroux J.-C. Gasnault O.
Analysis of Uranium and Thorium Lines in Mars Odyssey Gamma Spectra and Refined Mapping of Atmospheric Radon **[#2852]**
A new analysis of Mars Odyssey GRS spectra confirms the presence of radon in the atmosphere of Mars, and allowed us to map it and to observe its time variations.

CHONDRULE FORMATION AND DISK CHEMISTRY
Wednesday, 8:30 a.m. Montgomery Ballroom

Chairs: Harold Connolly Jr. and Brigitte Zanda

8:30 a.m. Hood L. L. * Weidenschilling S. J.
The Planetesimal Bow Shock Model for Chondrule Formation: Sizes of Highly Eccentric Planetesimals and Initial Simulations for a Radially Migrating Jupiter **[#2110]**
Improved simulations of planetesimal orbital evolution in the presence of jovian resonances are reported to better evaluate the conditions under which chondrules may have formed in bow shocks of highly eccentric planetesimals.

8:45 a.m. Zanda B. * Humayun M. Hewins R. H.
Chemical Composition of Matrix and Chondrules in Carbonaceous Chondrites: Implications for Disk Transport **[#2413]**
LA-ICP-MS analyses of unaltered matrix, chondrules, and bulk CM and CR chondrites show that the preaccretionary matrix had a CI composition. Chondrules could have formed in the inner disk and been transported to be embedded in matrix further out.

9:00 a.m. Morris M. A. * Desch S. J. Boley A. C.
The Chemical Environment Experienced by Chondrules Formed in Planetary Embryo Bow Shocks **[#2782]**
We investigate the chemical environment of chondrules formed in planetary embryo bow shocks. We find that many aspects of chondrule formation are explained by interaction of chondrules with volatiles outgassed from the protoplanet's magma ocean.

9:15 a.m. Fedkin A. V. Grossman L. * Ciesla F. J.
Extreme Conditions Required for Suppression of Alkali Evaporation During Chondrule Formation **[#2565]**
Na retention during formation of FeO-bearing chondrules requires very high nebular pressures, and very large enrichments of dust and water. This is suggestive of formation in vapor + liquid + solid plumes generated by impacts on icy planetesimals.

9:30 a.m. Armytage R. M. G. * Georg R. B. Williams H. M. Halliday A. N.
Silicon Isotopic Composition of Allende Chondrules and Nebular Processes **[#1971]**
We present new high-precision silicon isotope data for chondrules from Allende. The variations observed are consistent with either sampling precursor heterogeneities in the nebula or evaporation and recondensation chondrule formation processes.

WED ORALS

9:45 a.m. Mendybaev R. A. * Richter F. M. Marin-Carbonne J. McKeegan K. D.
Crystallization of Evaporating Forsterite-Rich Melts: Texture and Magnesium and Silicon Isotopic Compositions of the Evaporation Residues **[#2482]**
We present first results on texture and isotopic compositions of residues produced by cooling Fo-rich materials in vacuum. The results show that it is evaporation that controls the textures and Mg- and Si-isotopic compositions of crystallized phases.

10:00 a.m. Schrader D. L. * Connolly H. C. Jr. Lauretta D. S. Nagashima K. Huss G. R. Davidson J. Domanik K.
O-Isotope Composition of the Gas Present During Chondrule Formation as Recorded in CR Chondrites **[#1627]**
We present observations that constrain the O-isotope composition of the gas reservoir that exchanged with ferromagnesian chondrules from CR chondrites.

10:15 a.m. Nagashima K. * Krot A. N. Huss G. R.
Oxygen-Isotope Compositions of Chondrules and Matrix Grains in the LEW 87232, Kakangari-Like Chondrite **[#1768]**
In LEW 87232 K-chondrite, most chondrule grains have $\Delta^{17}O \sim 0‰$ while matrix is isotopically heterogeneous, with the ^{16}O-poor grains having $\Delta^{17}O \sim -2‰$. The chondrules and ^{16}O-poor matrix grains appear to have sampled different O-isotope reservoirs.

10:30 a.m. Tenner T. J. * Nakashima D. Ushikubo T. Kita N. T. Weisberg M. K.
Oxygen Isotopes of Chondrules in the Queen Alexandra Range 99177 CR3 Chondrite: Further Evidence for Systematic Relationships Between Chondrule Mg# and $\Delta^{17}O$ and the Role of Ice During Chondrule Formation **[#2127]**
QUE 99177 chondrules steadily rise in $\Delta^{17}O$ (–5 to –1 ‰) as Mg# decreases (99 to 97). Addition of + $\Delta^{17}O$ H_2O ice to dry precursors could reduce chondrule Mg# (by oxidation during formation) while increasing $\Delta^{17}O$. Estimated H_2O ice $\Delta^{17}O$ is 0.5 to 6‰.

10:45 a.m. Soulié C. * Libourel G. Tissandier L. Hiver J.-M.
Kinetics of Olivine Dissolution in Chondrule Melts: An Experimental Study **[#1840]**
We present three-dimensional X-ray microtomography images of partially resorbed forsterites in different silicate melts at high temperature that allow us to calculate the dissolution rates of olivines in chondrule melts.

11:00 a.m. Barcena H. * Connolly H. C. Jr.
Constraining the Nature of Type-I Chondrules: I. Chemical Models **[#2506]**
We explore the chemical reactions that took place during the melt synthesis of ferromagnesian chondrules, the expected molecular species released to the ambient environment, and the heterogeneous reactions that occurred with the surrounding gas.

11:15 a.m. Connolly H. C. Jr. * Barcena H. Domanik K. Nagashima K. Nagashima K. Huss G. R. Ash R. D. Weisberg M. K.
Constraining the Nature of Type-I Chondrules from UOC's: A Detailed In Situ Petrologic and Geochemical Investigation **[#2204]**
We investigated type-I chondrules from two L3.05 UOCs and determined the petrography; major, minor, and oxygen isotopic abundances of their silicates and spinels; plus siderophile-element abundances of the FeNi metal to constrain their formation.

11:30 a.m. Tachibana S. *
Nucleation and Growth of Iron Sulfide on Metallic Iron Particles Under Low-Pressure Protoplanetary Disk Conditions **[#1814]**
Nucleation and growth kinetics of iron sulfide on 1-µm-sized metallic iron grains were experimentally investigated in the He-H_2S gas at 1 Pa. Nucleation seems to occur as fast as the further growth process at the present experimental condition.

MERCURY COMPOSITION AND EVOLUTION FROM THE INSIDE OUT
Wednesday, 1:30 p.m. Waterway Ballroom 1

Chairs: Patrick Peplowski and Miriam Riner

1:30 p.m. Peplowski P. N. * Evans L. G. Hamara D. K. Lawrence D. J. Rhodes E. A. Sprague A. L. Solomon S. C.
Compositional Variability on the Surface of Mercury: Results from the MESSENGER Gamma-Ray Spectrometer **[#1541]**
MESSENGER's Gamma-Ray Spectrometer has been used to examine variations in the surface composition of Mercury for the elements Si, K, O, Ca, and S.

1:45 p.m. Weider S. Z. * Nittler L. R. Starr R. D. Byrne P. K. Hamara D. K. McCoy T. J. Solomon S. C.
Compositional Heterogeneity on Mercury's Surface Revealed by MESSENGER's X-Ray Spectrometer **[#1472]**
MESSENGER X-ray spectrometer data reveal that Mercury's northern volcanic plains are different in composition (especially in terms of Mg/Si) to the surrounding terrain.

2:00 p.m. McCubbin F. M. * Riner M. A. Vander Kaaden K. E. Elardo S. M. Shearer C. K. Jr.
Is Mercury Volatile Enriched or Volatile Depleted? New Insights from Combining MESSENGER X-Ray, Neutron, and Gamma-Ray Spectrometer Data **[#1270]**
Is Mercury volatile enriched or volatile depleted? The data from the MESSENGER mission may not be sufficient for answering this question when data from all the instruments is considered together. Experimental work is needed to determine the answer.

2:15 p.m. Izenberg N. R. * Holsclaw G. M. Domingue D. L. McClintock W. E. Klima R. L. Blewett D. T. Kochte M. C. Helbert J. D'Amore M. Sprague A. L. Vilas F. Solomon S. C.
Ultraviolet Through Near-Infrared Reflectance Variation on Mercury and the Search for Mineralogical Telltales **[#2365]**
We examine ultraviolet through near-infrared reflectance spectra of Mercury from the MASCS VIRS instrument, and find variations possibly indicative of differing iron contents in different units.

2:30 p.m. Riner M. A. * Lucey P. G.
Intense Space Weathering on Mercury: Are There Any Surface Exposures of Immature Material? **[#2866]**
Application of a new space weathering model to multi-spectral images of Mercury suggest accumulation space weathering derived iron is substantially higher than on the Moon and large deposits of immature material may not occur at the surface.

2:45 p.m. Helbert J. * Maturilli A. D'Amore M. Vaughan W. M. Head J. W. III Klima R. L. Blewett D. T. McCoy T. J.
Spectral Reflectance Measurements of Sulfides at the Planetary Emissivity Laboratory — Analogs for Hollow-Forming Material on Mercury? **[#1381]**
We present spectral reflectance measurements at visible and near-infrared wavelengths of fresh and heated samples of MnS, CaS, and MgS, as well as elemental sulfur. We infer that sulfides display a diagnostic feature at or near 0.6 µm.

3:00 p.m. Malavergne V. * Brunet F. Righter K. Zanda B. Avril C. Borensztajn S. Berthet S.
Experimental Behavior of Sulfur Under Primitive Planetary Differentiation Processes, the Sulfide Formations in Enstatite Meteorites and Implications for Mercury **[#1860]**
We have simulated different models of CaS-FeS-MgS sulfide formation and determine the solubility of sulfur in silicate melts at high pressure and high temperatures. We will present their implications for planetary differentiation and Mercury.

3:15 p.m. Charlier B. * Grove T. L. Zuber M. T.
Composition and Differentiation of 'Basalts' at the Surface of Mercury **[#1400]**
New experiments on surface compositions of Mercury obtained by MESSENGER and relevant phase equilibria constrain the composition and crystallization paths of "basaltic" rocks that cover most
of the planet.

3:30 p.m. Vaughan W. M. * Helbert J. Blewett D. T. Head J. W. III Murchie S. L. Gwinner K. McCoy T. J. Solomon S. C.
Hollow-Forming Layers in Impact Craters on Mercury: Massive Sulfide or Chloride Deposits Formed by Impact Melt Differentiation? **[#1187]**
We map the geology of the heavily hollowed crater Kertesz and show that hollows in this crater develop in a 30-meter-thick hollow-forming layer derived from impact melt. This layer may be a massive sulfide or chloride impact melt differentiate.

3:45 p.m. Grott M. * Breuer D. Spohn T.
The Thermo-Chemical Evolution of Mercury Revisited **[#1376]**
The thermo-chemical evolution of Mercury is revisited. New constraints on the abundance of heat-producing elements and core size are taken into account. The evolution of Mercury is found to be compatible with a komatiitic composition.

4:00 p.m. Brown S. M. * Elkins-Tanton L. T.
The Early Dynamics and Density Structure of Mercury's Mantle **[#2062]**
We numerically model Mercury's mantle to investigate the fate of high-density minerals that fractionally crystallize from a magma ocean. We produce different density profiles based on initial composition of a given formation mechanism.

4:15 p.m. Head J. W. III * Solomon S. C. Fassett C. I. Murchie S. L. Prockter L. M. Robinson M. S. Blewett D. T. Denevi B. W. Watters T. R. Whitten J. L. Goudge T. A. Baker D. M. H. Hurwitz D. M. Byrne P. K. Klimczak C.
Effusive Volcanism on Mercury from MESSENGER Mission Data: Nature and Significance for Lithospheric Stress State and Mantle Convection **[#1451]**
MESSENGER data are interpreted to mean that the small vertical extent of Mercury's mantle may inhibit convection and favor sublithospheric magma buildup and extensional lithospheric stresses on regional scales in the planet's early history.

4:30 p.m. Chapman C. R. * Merline W. J. Marchi S. Prockter L. M. Fassett C. I. Head J. W. Solomon S. C. Xiao Z.
The Young Inner Plains of Mercury's Rachmaninoff Basin Reconsidered **[#1607]**
Smooth plains within Rachmaninoff Basin's peak ring were interpreted from MESSENGER flyby images as very young (~1 Ga). Orbital images now show many secondaries D = 0.8–2 km, so the plains are not so young, but still younger than the basin itself.

IMPACT CRATERS: PEAKS, RINGS, AND BASINS
Wednesday, 1:30 p.m. Waterway Ballroom 4

Chairs: **Henning Dypvik and Ludovic Ferrière**

1:30 p.m. Ernst C. M. * Barnouin O. S. Gaskell R. W.
The Morphology of Craters on 433 Eros **[#2393]**
Large craters on Eros show a correlation between their d/D and their radial distances from Shoemaker, supporting the Thomas et al. model for the removal of small craters by seismic shaking and indicating the presence of significant loose regolith.

1:45 p.m. Herrick R. R. *
Martian Craters at the Simple-Complex Transition Diameter **[#2380]**
The simple-complex crater transition on Mars occurs over a large diameter range, so there are craters with similar diameter that have widely varying morphologies. I show that the variations are determined primarily by specific target properties.

2:00 p.m. Milam K. A. * Perkins J. W.
The Obliquity of the Flynn Creek Impact Event **[#2294]**
Structural and elevation data from the target rock exposures of the Flynn Creek impact crater were used to map and assess the obliquity of the causal impact event.

2:15 p.m. Kenkmann T. * Wulf G. Poelchau M. H.
Structural Indicators for Oblique Impact Trajectories found in Martian and Terrestrial Impact Craters **[#1440]**
It is possible to derive the trajectory of oblique impacts even if the ejecta blanket is not preserved. We document that strike and dip of strata as well as fault and fold orientations in the central uplift correlate with the trajectory.

2:30 p.m. Vasconcelos M. A. R. * Crósta A. P. Maziviero M. V. Molina E. C. Reimold W. U.
Geophysical Signatures of the Riachão Impact Structure, Brazil **[#1120]**
The Riachão is a complex impact structure of ~4 km diameter located in Brazil. Its geophysical signatures show a rim with low level of K, Th, and U and an annular basin with short wavelength magnetic anomalies and two positive gravity anomalies.

2:45 p.m. Baker D. M. H. * Head J. W. Prockter L. M. Fassett C. I. Neumann G. A. Smith D. E. Solomon S. C. Zuber M. T. Oberst J. Preusker F. Gwinner K.
New Morphometric Measurements of Peak-Ring Basins on Mercury and the Moon: Results from the Mercury Laser Altimeter and Lunar Orbiter Laser Altimeter **[#1238]**
We use new topography data from MESSENGER and LRO to calculate the depths and peak-ring heights of peak-ring basins on Mercury and the Moon. New trends in these parameters as a function of basin diameter may be related to peak-ring formation.

3:00 p.m. Bray V. J. * Atwood-Stone C. McEwen A. S.
Lunar Crater Peak and Peak-Ring Volumes from the LROC Global Lunar DTM 100 **[#1694]**
Measurements of peak and peak-ring diameter in impact craters have been used to support a wide variety of peak-ring formation models. We present volume and height data that may be important for further assessing the various formation theories.

3:15 p.m. Sori M. M. * Zuber M. T.
Anomalous Shallowing of Lunar Impact Craters in the South Pole-Aitken Basin from Lunar Orbiter Laser Altimeter (LOLA) Observations **[#2707]**
Analysis of topographic data obtained from LOLA reveal that impact structures in the South Pole-Aitken Basin are anomalously shallow. We analyze potential mechanisms to explain this, including viscous relaxation and cryptomaria deposits.

3:30 p.m. Bierhaus M. * Wünnemann K. Elbeshausen D.
Numerical Modeling of Basin-Forming Impacts: Implications for the Heat Budget of Planetary Interiors **[#2174]**
Basin-forming impacts create shock waves travelling through a whole planet. We carried out a suite of three-dimensional models of inclined impacts using the iSALE-3D hydrocode to study the effect of oblique impacts on planetary interiors.

WED ORALS

3:45 p.m. Potter R. W. K. * Collins G. S. Kiefer W. S. McGovern P. J. Kring D. A.
Further Modeling of Lunar Multi-Ring Basin Formation: Insights into Thermal Conditions During the Lunar Basin-Forming Epoch **[#1383]**
Numerical models of lunar basin-forming impacts are compared to observations and used to estimate features for a number of lunar basins. From this, tentative suggestions of thermal conditions during the lunar basin-forming epoch are made.

4:00 p.m. Stewart S. T. *
Impact Basin Formation and Structure from 3D Simulations **[#2865]**
3D simulations of basin formation produce large-scale features in excellent agreement with observations of South Pole-Aitken and suggest limited post-impact modification.

4:15 p.m. Wünnemann K. * Marchi S. Nowka D. Michel P.
The Effect of Target Properties on Impact Crater Scaling and the Lunar Crater Chronology **[#1805]**
We present numerical models of impact crater formation on a layered lunar crust to refine existing scaling laws and to improve dating of planetary surfaces by the size-frequency-distribution of the observed crater record.

4:30 p.m. Ivanov B. A. * Kamyshenkov D.
Impact Cratering: Scaling Law and Thermal Softening **[#1407]**
Numerical modeling of impacts into rock-like targets with a dry friction shows that dry friction and its shock softening result in the additional dependence on the impact velocity. Craters on Mars and Mercury may be slightly different in shape.

SMALL BODY STUDIES I: FORMATION, REGOLITH, AND RUBBLE PILES
Wednesday, 1:30 p.m. Waterway Ballroom 5

Chairs: **Seth Jacobson and Linda Elkins-Tanton**

1:30 p.m. Cuzzi J. N. * Hogan R. C.
Primary Accretion by Turbulent Concentration: The Rate of Planetesimal Formation and the Role of Vortex Tubes **[#2536]**
We present a new fundamental timescale for direct formation of 10–100-km-diameter asteroids and TNOs by concentration of small particles in turbulence, and show how vortex tubes acting on large scales may explain the properties of numerical simulations.

1:45 p.m. Elkins-Tanton L. T. *
The Fate of Water in Early-Accreting Internally Heated Planetesimals **[#1582]**
Partial differentiation in early-forming planetesimals results in bulk densities and water compositions that vary by total mass, time of accretion, and bulk radiogenic content. Crusts will be heterogeneous in density and water content.

2:00 p.m. Brown P. * Kikwaya J. B. Campbell-Brown M. D.
An Electro-Optical Survey of Meteoroid Bulk Density: Evidence for Widespread Radial Mixing in the Early Solar Nebula **[#1576]**
Based on precise observations of 92 meteors, we have estimated bulk densities of meteoroids. We find that Jupiter family comet-type meteoroids have chondritic-like bulk densities, while many asteroidal-type meteoroids are nearly pure iron.

2:15 p.m. Scheeres D. J. * Jacobson S. A.
Comet Rotational Relaxation and Interior Stresses and Loads **[#2169]**
Comet outgassing excites complex rotation of nuclei, causing time-varying internal stresses and strains that damp over time toward uniform rotation. The internal stresses and loads change during dissipation and may be related to comet bursting.

2:30 p.m. Steckloff J. K. * Melosh H. J.
Cometary Jet Collimation Without Physical Confinement **[#2548]**
The prevailing view of cometary jets is that collimation requires physical confinement. Here we show that this this is not that case, but rather that collimation can result from a porous, flat surface.

2:45 p.m. Singerling S. A. * McSween H. Y. Jr.
A Comparison of Glasses on Airless Bodies: The Moon vs. Vesta **[#1180]**
The purpose of this research is to analyze glasses in howardites and distinguish their origin (impact-melt-derived or pyroclastic) based on textural and chemical differences observed in lunar glasses. The Moon is used as a proxy for Vesta.

3:00 p.m. Delbo M. Libourel G. Michel P. * Ganino C. Verati C.
Temperature Shocks at the Origin of Regolith on Asteroids **[#1776]**
Here we study how regolith on asteroids develop via thermal fatigue cracking of rocks at the surface of these bodies due to the huge number of day/night temperature cycles that asteroids experience during their lifetime.

3:15 p.m. Vahidinia S. V. * Cuzzi J. N. Draine B. D. Marouf E. M.
Radiative Transfer in Closely Packed Realistic Regoliths **[#2880]**
We present a regolith radiative transfer model that is essential for near-to-far infrared observations of all airless solar system bodies with granular surfaces. We show the role of porosity on layer reflectivity and problematic spectral bands.

3:30 p.m. Sanchez P. * Scheeres D. J.
Granular "van der Waals Bridges" and the Cohesion of Rubble-Pile Asteroids **[#1620]**
Fine regolith in rubble pile asteroids may act as a sort of "van der Waals concrete" that forms bridges that bind larger boulders and strengthens small asteroids, allowing them to rotate more rapidly. We test these ideas using DEM simulations.

3:45 p.m. Richardson D. C. Munyan S. K. Schwartz S. R. * Michel P.
Comparison of Discrete Element Methods for Simulating Low-Speed Rubble Pile Collisions: First Results **[#2195]**
We compared low-speed rubble-pile collisions using hard- and soft-sphere methods. Results are similar, although differences exist during the peak of the impact shock.

4:00 p.m. Jacobson S. A. * Scheeres D. J.
Formation of the Asynchronous Binary Asteroids **[#2737]**
We find three pathways to form asynchronous binaries: they are born that way, are formed from planetary flybys, and are formed due to BYORP/tidal expansion. The YORP effect on the secondary can play an important role for each of these pathways.

4:15 p.m. Rossi A. * Marzari F. Scheeres D. J. Jacobson S.
Effects of YORP-Induced Rotational Fission on the Asteroid Size Distribution at the Small Size End **[#2095]**
The asteroid belt size distribution was shaped by collisions grinding the population into smaller bodies via cratering or fragmentation. At the small size end YORP may contribute by accelerating the spin of the bodies beyond the disruption limit.

4:30 p.m. Takir D. * McSween H. Y. Jr. Emery J. P. Clark R. N. Pearson N.
Constraints on the Nature and the Degree of Aqueous Alteration in Outer Main Belt Asteroids **[#1354]**
In order to constraint the nature and the degree of aqueous alteration in outer main belt asteroids ($2.5 < a < 4.0$ AU) , we investigated the geochemical/petrological parameters and the spectral properties of 10 CM/CI carbonaceous chondrites.

ROVING ON MARS: CURRENT AND FUTURE SITES
Wednesday, 1:30 p.m. Waterway Ballroom 6

Chairs: Matthew Golombek and Paul Niles

1:30 p.m. Squyres S. W. * Athena Science Team
Initial Opportunity Rover Results at Endeavour Crater, Mars **[#1892]**
Initial findings from the Mars Exploration Rover Opportunity at Endeavour Crater include a variety of impact breccias in the crater rim, and gypsum veins emplaced by aqueous fluids.

1:45 p.m. Crumpler L. S. * MER Science Team
Field Geologic Context of Gypsum Veins and Impactites on the Rim of Endeavour Crater, Cape York, MER Opportunity Rover **[#1258]**
Rocks at the geologic unconformity between the rim of Endeavour crater and the Meridiani plains are separated significantly within the global stratigraphic sequence. We now have direct outcrop evidence of conditions existing early in martian geologic time.

2:00 p.m. Herkenhoff K. E. * Ashley J. W. Johnson J. R. Parker T. J. Athena Science Team
Recent Athena Microscopic Imager Results **[#2802]**
The Mars Exploration Rover Opportunity arrived at the rim of Endeavour Crater in August 2011. This presentation summarizes Opportunity Microscopic Imager observations of ejecta, bedrock, a gypsum vein, and other materials in the crater rim rocks.

2:15 p.m. Farrand W. H. * Johnson J. R. Bell J. F. III Rice M. S.
Visible and Near Infrared Spectral Classes of Rocks Observed at Cape York, Endeavour Crater, Mars **[#2280]**
VNIR spectral classes of rocks observed on the rim of Endeavour crater by Opportunity's multispectral Pancam are described. These spectral classes include those indicative of basaltic compositions, and some unlike previously observed rock spectra.

2:30 p.m. Golombek M. P. *
Timescale of Small Crater Modification on Meridiani Planum, Mars **[#2267]**
Field observations by the Opportunity rover and HiRISE images of small craters on Meridiani Planum, Mars, yields a timescale for their formation (10 yr to 10 Ma) based on crater retention age, modification by granule ripples, and degradational state.

2:45 p.m. Bustard A. * Elliott B. E. Spray J. G. Thompson L. M.
Crater Count Mapping and Regional Geologic Context of the Area Surrounding the Gale Impact Structure, Mars **[#2297]**
Crater counting has been employed to understand the regional geologic context of a 500,000-square-kilometer area surrounding Gale Crater. The goal is to place the Gale landing site in a broader setting to complement results obtained from focused MSL rover activities.

3:00 p.m. Calef F. J. III * Day M. Buhler P. Grotzinger J. P.
Small Crater Ejecta Retention Ages Inside Gale Crater: Recent Erosional History and Potential Sampling Locations for the Mars Science Laboratory **[#2674]**
We recorded all fresh craters with ejecta or blocks outside their crater rim within or near the MSL Gale landing ellipse in a GIS. Ejecta retention rates are <10 m.y. for craters D < 100 m. These craters would be ideal for sample acquisition by MSL.

3:15 p.m. Silvestro S. * Vaz D. A. Rossi A. P. Flahaut J. Fenton L. K. Ewing R. Geissler P. E.
Active Aeolian Processes Along Curiosity's Traverse in Gale Crater **[#1804]**
In this report we demonstrate that aeolian activity is quite vigorous within the landing ellipse of the MSL mission, by describing and quantifying a variety of aeolian modifications to several dunes located in the NW portion of Gale Crater's floor.

3:30 p.m. Poulet F. * Carter J.
Mineral Abundances of the Final Four MSL Landing Sites and Implications for Their Formation **[#1397]**
We present the modal mineralogy of the major phyllosilicate-bearing deposits of the final four MSL landing sites derived from the modeling of CRISM spectra using a radiative transfer model and then discuss the implications for their formation processes.

3:45 p.m. Fergason R. L. *
Surface Properties of the Mars Science Laboratory Landing Site Gale Crater: Characterization from Orbit and Predictions **[#2606]**
This work integrates a variety of data sets to identify and assess surface materials within the MLS Gale landing ellipse and surrounding region, and to determined how thermophysical variations correspond to morphology, and when applicable mineralogical diversity.

4:00 p.m. Putzig N. E. * Campbell B. A. Phillips R. J. Mellon M. T.
SHARAD Sounding and Surface Roughness of Once and Future Mars Landing Sites **[#2864]**
The Shallow Radar instrument on MRO maps out likely subsurface returns at the Phoenix site and Gale Crater. Gale and the other sites proposed for MSL Curiosity are rougher than past landing sites at the scale of meters to tens of meters.

4:15 p.m. Niles P. B. * Michalski J.
Origin and Evolution of Sediments in Gale Crater Through Ice-Hosted Processes **[#2575]**
The Gale Crater sediments on Mars were formed by ice-dust deposition, weathering, and diagenesis. This is supported by modeling, geomorphic relationships, and comparisons to similar martian sedimentary deposits and will be tested by MSL.

4:30 p.m. Léveillé R. J. *
Integrated Mineralogical and Geochemical Studies of Authigenic Magnesium-Phyllosilicates by the Curiosity Rover at Gale Crater **[#2608]**
Mg-phyllosilicates are proposed as priority targets for detailed geochemical and mineralogical investigation by the Curiosity rover at Gale Crater as these minerals may provide key information on habitability.

CHONDRITE COMPONENTS AND PRIMARY PROCESSES
Wednesday, 1:30 p.m. Montgomery Ballroom

Chairs: Michael Weisberg and Simon Clemett

1:30 p.m. Haenecour P. * Floss C.
Stardust in Fine-Grained Chondrule Rims and Matrix in LaPaz 031117: Insights Into the Conditions of Dust Accretion in the Solar Nebula **[#1107]**
Abundances of presolar SiC and oxides are similar in the matrix and a chondrule rim of LAP 031117, but presolar silicate abundances are higher in the matrix. Silicates may have been destroyed during accretion of the rim onto a still hot chondrule.

1:45 p.m. Leitner J. * Hoppe P. Zipfel J.
The Stardust Inventories of Graves Nunataks 95229 and Renazzo: Implications for the Distribution of Presolar Grains in CR Chondrites **[#1835]**
We report the discovery of presolar silicates, oxides and SiC in fine-grained chondrule rims in GRA 95229 and Renazzo, supporting the idea that the fine-grained material was accreted from the solar nebula prior to parent body formation.

2:00 p.m. Leroux H. *
TEM Investigation of Fine-Grained Components in the Matrix of the Bishunpur (LL3.1) Chondrite **[#1761]**
We report an analytical TEM study of the matrix of the LL3.1 Bishunpur chondrite. Although parent body secondary alteration phases are present, amorphous material is frequent and reveals a nonequilibrium formation, likely during a nebular process.

2:15 p.m. Verchovsky A. B. * Pearson V. K. Fisenko A. V. Semenova L. F. Sephton M. A. Wright I. P.
Separation of Q from Carbon in CR Meteorites During Stepped Combustion **[#2645]**
During metamorphism of CR meteorites Q carrier, in contrast to most of the macromolecular material, is encased into the matrix and therefore can be separated from the organic carbon by stepped combustion. Q may not be carbonaceous.

2:30 p.m. Amari S. * Matsuda J.
Noble Gas Study of Q-Rich Fractions from Saratov (L4) **[#1051]**
We separated Q-rich fractions from Saratov (L4). One of the fractions, AJ, has the highest ^{132}Xe concentration (2.1^{-6} cm^3 STP/g) that has ever been measured in any extraterrestrial material.

WED ORALS

2:45 p.m. Clemett S. J. * Messenger S. R. Thomas-Keprta K. L. Nakamura-Messenger K.
The Spatial Distribution of Organic Matter and Mineralogical Relationships in Carbonaceous Chondrites **[#2889]**
Microprobe two-step laser mass spectrometry utilizing a novel vacuum UV photoionization source has been applied to mapping the spatial distribution of organic species in carbonaceous chondrite matrices at micron spatial resolutions.

3:00 p.m. Yokoyama T. * Ito N. Fukami Y. Okui W.
Strontium Isotope Anomalies in Allende and Tagish Lake Meteorites: Results for Sequential Acid Leaching Experiments **[#1897]**
We performed sequential acid leaching for Allende (CV3) and Tagish Lake (C2) meteorites, and precisely measured Sr isotopes in the leachates. We found that the main carriers of isotopically anomalous Sr are CAI for Allende and presolar grains for Tagish Lake.

3:15 p.m. Jacquet E. * Gounelle M. Alard O.
Trace Element Microdistribution in Carbonaceous Chondrite Chondrules **[#1102]**
We present LA-ICP-MS analyses of silicate phases in chondrules of CR and CV chondrites. Olivine/mesostasis REE partitioning approach equilibrium for the coarser-grained chondrules. Pyroxene data offer further evidence of gas-melt interaction.

3:30 p.m. Chen J. H. * Papanastassiou D. A. Zhang J. Dauphas N. Davis A. M.
Correlated Ca, Ti, and Cr Isotopic Anomalies in Meteorites **[#2607]**
We present new ^{48}Ca isotopic anomalies, correlated with ^{50}Ti in the same whole meteorites. The effects are compatible with wide distribution of neutron rich supernova Ia products and may have "filled" significant deficits in the solar system.

3:45 p.m. Huang S. * Jacobsen S. B.
Calcium Isotopic Variations in Chondrites: Implications for Planetary Isotope Composition **[#1334]**
We present mass-dependent Ca isotopic effect in chondrites.

4:00 p.m. Davidson J. * Lauretta D. S. Schrader D. L.
Compositional Variations in Silicate Phases Within the CV and CK Carbonaceous Chondrites **[#1494]**
We present compositional data for chondrule olivine in a number of CV3 and CK3 chondrites to investigate their chondrule formation conditions. Several lines of evidence suggest they do not share a common origin.

4:15 p.m. Brearley A. J. *
MIL 07687 — An Intriguing, Very Low Petrologic Type 3 Carbonaceous Chondrite with a Unique Style of Aqueous Alteration **[#1233]**
MIL 07687 is a unique low petrologic type carbonaceous chondrite with a very high abundance of matrix (~68 wt%) and unusual style of alteration. Chondrules contain primary glass, but matrix has been extensively replaced by a fibrous Fe-oxyhydroxide.

4:30 p.m. Weisberg M. K. * Ebel D. S. Kita N. T. Nakashima D.
Petrology and Oxygen Isotopes of Chondrules in NWA 5492 and GRO 95551: A New Type of Metal-Rich Chondrite **[#1463]**
NWA 5492 and GRO 95551 are the first samples of a new type of metal-rich chondrite and possibly new parent body. Their silicates are mostly reduced and oxygen isotope ratios of their chondrules plot between the TF and Y-R lines in three-isotope space.

NUCLEAR AND EMERGING TECHNOLOGIES FOR SPACE: OPENING PLENARY
Wednesday, 5:30 p.m. Waterway Ballroom 4 and 5

What Can Nuclear Power Sources Do for Science?

Moderators: **Leonard Dudzinski** (NASA Headquarters)
Wade Carroll (Department of Energy Headquarters)

Panel Members: **Ralph L. McNutt Jr., Michael Meyer, and Steve Squyres**

The NETS opening plenary will take an in-depth look at what nuclear power sources have offered to science missions in the past, how they are being employed today, and what might be on the horizon for the future.

5:30 p.m. ***Ralph L. McNutt Jr.*** (Science and Analysis Branch, Chief Scientist for Space Science, Johns Hopkins University Applied Physics Laboratory)
Historical Overview of RPS-Enabled Planetary Science Missions

5:55 p.m. ***Michael Meyer*** (Lead Scientist for NASA's Mars Exploration Program, NASA Headquarters)
Current Applications of Radioisotopes in Science Missions

6:20 p.m. ***Steve Squyres*** (Goldwin Smith Professor of Astronomy, Cornell University)
What Does the Future Hold?

LUNAR CHRONOLOGY BY ANY MEANS NECESSARY
Thursday, 8:30 a.m. Waterway Ballroom 4

Chairs: **Herbert Frey and Nicolle Zellner**

8:30 a.m. Hiesinger H. * van der Bogert C. H. Pasckert J. H. Schmedemann N. Robinson M. S. Jolliff B. Petro N.
New Crater Size-Frequency Distribution Measurements of the South Pole-AitkenBasin **[#2863]**
We performed new crater size-frequency distribution (CSFD) measurements for the South Pole-Aitken basin (SPA) and several superposed craters and basins. Our crater counts indicate an absolute model age of 4.26 Ga for SPA.

8:45 a.m. van der Bogert C. H. * Hiesinger H. Banks M. E. Watters T. R. Robinson M. S.
Derivation of Absolute Model Ages for Lunar Lobate Scarps **[#1847]**
Crater size-frequency distribution measurements indicate that the Mandel'shtam and Lee-Lincoln scarps were active as recently as ~91 Ma and ~75 Ma, respectively. These results confirm that lobate scarps are some of the youngest features on the Moon.

9:00 a.m. Ambrose W. A. *
Ejecta Distribution and Relative Ages of the Imbrium, Serenitatis, and Crisium Basins **[#1048]**
Ejecta features (asymmetric secondary craters, scours, and crater chains), imaged from LOLA data, indicate that terrain east of Mare Serenitatis is dominated by Imbrium ejecta, suggesting a Pre-Nectarian age for the Serenitatis Basin.

9:15 a.m. Frey H. V. *
Preliminary Crater Retention Ages for an Expanded Inventory of Large Lunar Basins **[#1852]**
The distribution of N(50) crater retention ages for an expanded inventory of 95 candidate large lunar basins shows two distinct and separable peaks, even when weaker candidate basins are eliminated.

9:30 a.m. Kreslavsky M. A. * Werner S. C. Head J. W. III Fassett C. I.
New Observational Evidence of Nonuniform Cratering of the Moon **[#1193]**
Ananlysis of spatial distributions of rayed craters and craters with steep walls confirms the predicted apex/antapex asymmetry in cratering rate; however, the spatial distribution also shows statistically significant patchiness of unknown origin.

9:45 a.m. Souders A. K. * Sylvester P. J. Osinski G. R.
Effect of Impact-Related Processes on the Lead Isotope Systematics of Anorthosites: A Lunar Analogue Study at Mistastin Lake Crater, Labrador **[#1909]**
The elemental and Pb isotope systematics of magmatic plagioclase, shocked plagioclase, and maskelynite from terrestrial anorthosites of Mistastin Lake Crater are evaluated to assess the potential effects of impact-related processes on lunar samples.

10:00 a.m. Zhang A. C. * Taylor L. A. Wang R. C. Li Q. L. Li X. H. Patchen A. D. Liu Y.
SIMS Pb/Pb Ages of Baddeleyite and Zirconolite in Apollo 17 Norite 78235: Implications for Shock Histories of Extraterrestrial Rocks **[#1036]**
Our dating results on baddeleyite and zirconolite in the unbrecciated lunar rock Apollo 17 norite 78235 indicate that impact events in natural system could reset Pb/Pb ages of baddeleyite.

10:15 a.m. Shaulis B. J. * Righter M. Lapen T. J. Korotev R. L. Irving A. J. Kuehner S. M.
Baddeleyite Chronology of Northwest Africa 6950: A 3.1 Ga Lunar Olivine Gabbro Paired with NWA 2977 and the Cumulate Mare Gabbro Lithology in NWA 773 **[#2236]**
NWA 6950 is closely related to the NWA 773 clan of meteorites, a group of paired and/or petrographically related stones. New U-Pb and Pb-Pb ages of baddeleyite in NWA 6950 confirm petrogenetic linkages with olivine gabbro in NWA 2977 and NWA 773.

10:30 a.m. Nyquist L. E. * Shih C.-Y. Reese Y. D.
Redetermination of the Sm-Nd Age and Initial Epsilon-Nd of Lunar Troctolite 76535: Implications for Lunar Crustal Development **[#2416]**
The Sm-Nd age of 4335 ± 71 Ma and ε^{143}Nd = +0.23 ± 0.44 for lunar troctolite 76535 are consistent with early lunar formation accompanied by early differentiation of urKREEP if the initial lunar ε^{143}Nd was similar to that in cumulate eucrites.

10:45 a.m. Hui H. * Neal C. R. Shih C.-Y. Nyquist L. E.
Derivation of Apollo 14 High-Al Basalts at Discrete Times: Rb-Sr Isotopic Constraints **[#2662]**
Four eruption episodes were identified for A-14 high-Al basalts. Rb-Sr isotopic data and ITE ratios show that their parental melt compositions of are correlated through mixing of evolved components with a relatively primitive magma ocean cumulate.

11:00 a.m. Shih C. -Y. * Nyquist L. E. Reese Y.
Rb-Sr and Sm-Nd Isotopic Studies of Lunar Green and Orange Glasses **[#1606]**
Rb-Sr and Sm-Nd isotopic results of green and orange glassy samples are presented. Green and orange glass, and mare basalt source mineralogies, are discussed in the context of the lunar magma ocean dynamics.

11:15 a.m. Zellner N. E. B. * Norman M. D.
Compositions and Ages of Apollo 15 Lunar Impact and Volcanic Glasses: First Results **[#1711]**
We present the first results of compositional studies of impact glasses from the Apollo 15 landing site, as well as compositional information about the well-studied Apollo 15 volcanic glasses. Ages for select glasses will also be presented.

11:30 a.m. Norman M. D. * Zellner N. E. B. Adena K.
A New Approach to Dating Lunar Spherules Using U-Th-Pb Chemical Ages **[#1370]**
Chemical ages based on U-Th-Pb concentrations provide a promising approach to dating volcanic and impact glasses. Young (≥500 Ma) impacts appear to dominate the regolith population but the role of gardening requires further clarification.

SMALL BODY STUDIES II: EARTH-CROSSING TO MAIN BELT
Thursday, 8:30 a.m. Waterway Ballroom 5

Chairs: Lucy Lim and Andrew Rivkin

8:30 a.m. Lim L. F. * Emery J. P. Moskovitz N. A. Granvik M.
The Near-Earth Encounter of 2005~YU55: Thermal Infrared Observations from Gemini North **[#2202]**
We conducted thermal infrared photometry and spectroscopy (7.9–14 and 18–22 µm) of the C-type NEO 2005 YU55 using the Michelle instrument at Gemini North. Temperature and thermal inertia will be discussed.

8:45 a.m. Moskovitz N. A. * Yang B. Lim L. F. Emery J. P. Granvik M. Sheppard S. S. Willman M. McMillan M.
The Near-Earth Encounter of Asteroid 2005 YU55: Visible and Near-Infrared Spectroscopy **[#2080]**
In Nov. 2011 the asteroid 2005 YU55 passed between Earth and the Moon. During this encounter we conducted an observing campaign to study this object's chemical and physical properties. Here we present visible and near-infrared spectroscopic results.

9:00 a.m. Nakamura E. * Makishima A. Moriguti T. Kobayashi K. Tanaka R. Kunihiro T. Tsujimori T. Sakaguchi C. Kitagawa H. Ota T. Yachi Y. Yada T. Abe M. Fujimura A. Ueno M. Mukai T. Yoshikawa M. Kawaguchi J.
Space Environment of an Asteroid Preserved on Micro-Grains Returned by the Hayabusa Spacecraft **[#1375]**
In this paper, we summarize the results of our comprehensive initial analysis of the sizes, morphology, mineralogy, and geochemistry of five lithic grains from Itokawa.

9:15 a.m. Zolensky M. E. * Nakamura T. Mikouchi T. Hagiya K. Ohsumi K. Tanaka K. Noguchi T. Kimura M. Tsuchiyama A. Nakato A. Ogami T. Ishida H. Uesugi M. Yada T. Shirai K. Fujimura A. Okazaki R. Ishibashi Y. Abe M. Okada T. Ueno M. Mukai T. Yoshikawa M. Kawaguchi J.
The Shock State of Itokawa Samples **[#1477]**
We made a determination of the impact shock state of the recovered Itokawa samples.

9:30 a.m. Mazrouei S. * Daly M. Barnouin O. Ilnicki M. Kahn E.
Distribution of Boulders on Asteroid 25143 Itokawa **[#2404]**
The objective is to confirm and update any previously identified trends in the global and regional distributions of boulders on Itokawa. Trends found should provide insights to Itokawa's current state following the disruption of its parent body.

9:45 a.m. Fraeman A. A. * Arvidson R. E. Murchie S. L. Rivkin A. S. Bibring J.-P. Gondet B. Manaud N. Langevin Y. Choo T. Humm D.
Analysis of CRISM and OMEGA Observations of Phobos and Deimos **[#2525]**
Data from CRISM and OMEGA provide the highest-spatial-resolution spectra of Phobos ever acquired and the first disk-resolved hyperspectral observation of Deimos. We discuss these data and analyze them for clues to the moons' surface compositions.

10:00 a.m. Chappaz L. * Melosh H. J. Vaquero M. Howell K. C.
Material Transfer from the Surface of Mars to Phobos and Deimos **[#1422]**
The Russian Phobos-Grunt mission originally planned to return 200 grams of surface material from Phobos. An analysis of the possibility that such a sample may also contain material ejected from the surface of Mars by large impacts is performed.

10:15 a.m. Ramsley K. R. * Head J. W. III
The Origins of Phobos Grooves from Ejecta Launched from Impact Craters on Mars: Tests of the Hypothesis **[#1054]**
With modeling techniques, we test six major predictions of the J. Murray hypothesis (that the main groove-forming process on Phobos is the intersection of Phobos with ejecta from primary impact events on Mars to produce chains of secondary craters).

10:30 a.m. Hergenrother C. W. * Scheeres D. J. Nolan M. d'Aubigny C. Barucci M. A. Clark B. E. Dotto E. Emery J. P. Lauretta D. S. Licandro J. Rizk B.
Lightcurve and Phase Function Photometry of the OSIRIS-REx Target (101955) 1999 RQ36 **[#2219]**
We present visible wavelength photometry of the OSIRIS-REx target asteroid (101955) 1999 RQ36. We find a rotation period of 4.2968 ± 0.0017 hr and phase slope of 0.039 mag/deg. YORP induced rotation rate changes should be detectable by OSIRIS-REx.

10:45 a.m. Rivkin A. S. * Howell E. S. DeMeo F. E. Vervack R. J. Binzel R. P. Magri C. Nolan M. C. Fernandez Y. R. Cheng A. F. Barucci M. A. Michel P.
New Observations and Proposed Meteorite Analogs of the MarcoPolo-R Target Asteroid (175706) 1996 FG3 **[#1537]**
CV chondrites show spectra like the target of MarcoPolo-R.

11:00 a.m. Binzel R. P. * Polishook D. DeMeo F. E. Emery J. P. Rivkin A. S.
Marco Polo-R Target Asteroid (175706) 1996 FG3: Possible Evidence for an Annual Thermal Wave **[#2222]**
Pre- and post-perihelion spectral measurements (0.8–2.5 µm) of 1996 FG3 show substantially different thermal fluxes. We may be detecting deep absorption and re-radiation of the annual thermal wave rather than just diurnal thermal flux balance.

11:15 a.m. Barucci M. A. * Belskaya I. Fulchignoni M. Fornasier S. Leyrat C.
Surface Composition of Asteroid (21) Lutetia: Lesson Learned from the Rosetta Flyby **[#1586]**
During the close encounter of the Rosetta spacecraft with (21) Lutetia on July 10, 2010, the instruments OSIRIS, VIRTIS, ALICE, and MIRO were turned on to characterize the surface properties of the asteroid.

11:30 a.m. Shepard M. K. * Taylor P. A. Nolan M. C. Howell E. S. Benner L. A. M. Giorgini J. D. Warner B. D. Harris A. W. Clark B. E. Ockert-Bell M. Coley D.
Radar Observations of Seven X/M-Class Main-Belt Asteroids **[#1228]**
Using the Arecibo radar, we observed seven new X/M-class MBAs. We find 40% of 26 total observed have metal-like radar albedos. Four W-class (hydrated M's) have metal-like radar albedos. Forty percent of X/M MBAs show evidence of bifurcation.

11:45 a.m. Fieber-Beyer S. K. * Gaffey M. J. Blagan J. R.
Near-Infrared Spectroscopy of 3:1 Kirkwood Gap Asteroids (660) Crescentia, (797) Montana, (879) Ricarda, (1391) Carelia, and (1644) Rafita **[#1530]**
The 3:1 Kirkwood gap asteroids are a mineralogically diverse set of asteroids located in a region that delivers meteoroids into Earth-crossing orbits.

WATER ON MARS: FLOWING, FLOODING, AND FREEZING
Thursday, 8:30 a.m. Waterway Ballroom 6

Chairs: Edwin Kite and Gordon Osinski

8:30 a.m. Scanlon K. E. * Head J. W. III Madeleine J.-B. Wordsworth R. D. Forget F.
Orographic Precipitation in Terra Cimmeria: Towards New Constraints on the Climate of Noachian Mars **[#1287]**
To test the idea that Mars' valley networks were precipitation-sourced, we compared Terra Cimmeria's valleys with the predictions of an orographic precipitation model. We hope to develop new constraints on the Noachian climate using this framework.

8:45 a.m. Mangold N. * Adeli S. Conway S. Ansan V. Langlais B.
A Chronology of Mars Hydrological Evolution from Impact Degradation **[#1210]**
Degradation of impact craters >20 km is studied in two Noachian regions. Results show a shift in degradation at 3.7 Gy. Craters with alluvial fans are distinct from the most degraded by being better preserved, and being formed during the Hesperian.

9:00 a.m. Grant J. A. * Wilson S. A.
A Synoptic Source of Water for Late Alluvial Fan Activity in Southern Margaritifer Terr, Mars? **[#2064]**
Deposition of sediments exposed on widely distributed alluvial deposits in southern Margaritifer Terra was likely related to a relatively late period of synoptic precipitation rather than local impact induced degradation.

9:15 a.m. Hurwitz D. M. * Head J. W. III
Testing the Late-Stage Outflow Channel Origin Hypothesis: Investigating Both Water Erosion and Lava Erosion Origins for Athabasca Valles, Mars **[#1056]**
Analytical models estimate the fluid volumes, effusion rates, and erosion rates required to erode Athabasca Valles by water and by lava. Results are put in context with geomorphologic observations to assess the potential for each origin hypothesis.

9:30 a.m. Warner N. H. * Sowe M. Gupta S. Dumke A. Goddard K.
Connecting Valles Marineris to the Northern Plains: Linkage by Lake Overspill and Catastrophic Flooding **[#1237]**
We demonstrate that linkage of basins east of Valles Marineris occurred by lake spillover and was controlled by the base level of each basin. The data indicate a mechanism for the formation of an extensive regional flow routing system on Mars.

9:45 a.m. Kite E. S. *
Evidence for Melt-Fed Meandering Rivers in the Gale-Aeolis-Zephyria Region, Mars **[#2778]**
Here I describe watershed-scale topographic relations that suggest the presence of large near-surface ice bodies at the time the Gale-Aeolis-Zephyria rivers were flowing, and evidence that Gale-Aeolis-Zephyria rivers were fed by seasonal melt.

10:00 a.m. Lefort A. * Burr D. M. Beyer R. A. Howard A. D.
Sinuous Ridges as Tools to Investigate Post-Flow Modification in the Aeolis–Zephyria Plana, Western Medusae Fossae Formation, Mars **[#1953]**
The longitudinal profiles of inverted fluvial features located in the Medusa Fossae Formation exhibit undulations that we interpret as evidence of post-fluvial deformation of the region. We propose and evaluate possible deformation processes.

10:15 a.m. Hobley D. E. J. * Howard A. D. Moore J. M.
Geomorphology of Fluvioglacial Features in the Martian Sounthern Midlatitudes, Northeastern Noachis Terra **[#1344]**
We map and analyze a suite of 761 small-scale, post-Noachian channel segments in the martian southern midlatitudes, over an area 320 × 560 km. Scaling and distribution of the channels is most consistent with formation under a thick ice cover.

10:30 a.m. Goudge T. A. * Mustard J. F. Head J. W. III Fassett C. I.
Constraints on the History of Open-Basin Lakes on Mars from the Timing of Volcanic Resurfacing **[#1328]**
The morphology, physical attributes, and mineral composition of 30 martian open-basin lakes indicates the basins are volcanically resurfaced. Dating of these units suggests the resurfacing likely began shortly after the end of valley network activity.

10:45 a.m. Haltigin T. W. * Pollard W. H. Dutilleul P. Osinski G. R.
Morphometric Evidence of Co-Evolving Polygonal and Scalloped Terrains in Southwestern Utopia Planitia, Mars **[#2689]**
This project provides various quantitative analyses of polygonal and scalloped terrain morphologies in Utopia Planitia, demonstrating that these two landforms interact as they evolve.

11:00 a.m. Orloff T. C. * Kreslavsky M. A. Asphaug E. I.
Possible Mechanism for Boulder Clustering on Thermal Contraction Polygons **[#1652]**
We propose that the CO_2 frost formed in martian winters locks boulders in place during the contraction phase of the seasonal cycle, and then in summer, boulders shift outward with expanding surface material leading to clustering in polygon margins.

THU ORALS

11:15 a.m. Costard F. * Sejourne A. Kargel J. Soare R.
Shallow Melting and Underground Drainage in Utopia Planitia, Mars **[#1822]**
Based on the identification of sinuous and elongated pits in Utopia Planitia, we suggest that shallow melting and underground drainage are possible. We test that hypothesis using a thermal model that comprises a thick insulating dusty layer.

11:30 a.m. Osinski G. R. * Capitan R. D. Kerrigan M. Barry N. Blain S.
Late Amazonian Glaciations in Utopia Planitia, Mars **[#1957]**
We present evidence from western Utopia Planitia, including lineated valley fill and lobate debris aprons, for widespread glaciations over a large expanse of the northern plains and dichotomy boundary during Late Amazonian times.

SECONDARY PROCESSES IN CHONDRITES
Thursday, 8:30 a.m. Montgomery Ballroom

Chairs: Jon Friedrich and Alexander Ruzicka

8:30 a.m. Ciesla F. J. * Davison T. M. Collins G. S.
Combined Impact and Radiogenic Heating of Early Planetesimals **[#1676]**
We investigate the thermal evolution of planetesimals heated by both impacts and ^{26}Al. Impacts affected all bodies in the first ~100 m.y. of the solar system, and had important consequences for the global thermal evolution of these bodies.

8:45 a.m. Ivanova M. A. * Lorenz C. A. Bychkov A. Yu. Sevastyanov V. S. Franchi I. A.
Experimental Simulation of Formation Processes of Metamorphosed Carbonaceous Chondrites **[#1591]**
We report results of experimental investigations of oxygen-isotopic composition of terrestrial olivine undergoing hydration-dehydration process to test the hypothesis of multiple processing of the metamorphosed CCs parent asteroid.

9:00 a.m. Ruzicka A. * Hutson M. Floss C. Hildebrand A.
Large Silica-Rich Igneous-Textured Inclusions in the Buzzard Coulee (H4) Chondrite **[#1630]**
Buzzard Coulee (H4) contains two types of large, igneous inclusions that are best explained by igneous differentiation, but which also show evidence for cooling and vapor phase phenomena consistent with transit through a space environment.

9:15 a.m. Bullock E. S. * McCoy T. J. Corrigan C. M.
Discovery of Keilite in Type 3 Enstatite Chondrites: Influence of Metamorphic Temperature on Formation **[#2225]**
The discovery of keilite, previously observed in type 4–6 enstatite chondrites, in shock- or impact-melted type 3 enstatite chondrites, constrains the post-shock equilibration temperatures experienced by these meteorites to the range of 400°–500°C.

9:30 a.m. Abreu N. M. *
Low and High Temperature Aqueous Alteration of the Matrices of CR Chondrites: Nano-SEM, EPMA, and TEM Study **[#2739]**
Composition of CR matrices are proposed to have evolved along two different tracks as a consequence of aqueous alteration. In Track 1, Fe content decreases via progressive formation of magnetite. In Track 2, Fe increases as metal dissolves.

9:45 a.m. Rubin A. E. *
Impact-Induced Aqueous Alteration of CM and CV Carbonaceous Chondrites **[#1058]**
CMs have a strong correlation between the degree of alteration and the extent of particle alignment; water was retained preferentially in rocks that experienced greater impact-induced shear. CV3s with petrofabrics are more shocked than those without.

10:00 a.m. Dobrică E. * Brearley A. J.
Complex Heterogeneous Aqueous Alteration in the Matrices of Unequilibrated Ordinary Chondrites by Low Temperature Hydrothermal Solutions **[#2212]**
Distinct, coarse-grained phyllosilicate-rich objects formed by aqueous alteration occur in the matrix of UOC, MET 00526. Rims and veins of ferroan olivine replace these phyllosilicates by low-temperature hydrothermal solutions.

10:15 a.m. Friedrich J. M. * Ruzicka A. Ebel D. S. Thostenson J. Rudolph R. A. Rivers M. L. Macke R. J. Britt D. T.
Three Dimensional Petrography of Kernouvé: A Story of Vein Formation, Compaction, and Metamorphism **[#1197]**
We use the 3D technique X-ray microtomography to investigate the structures of metallic veins in the Kernouvé H chondrite. The striking complexity of shape of these large (>1 cm) vein structures indicates a pre-metamorphic impact origin.

10:30 a.m. Matsumoto T. M. * Tsuchiyama A. T. Gucsik A. G. Noguchi R. N. Matsuno J. M. Nagano T. N. Imai Y. I. Shimada A. S. Uesugi M. U. Uesugi K. U. Nakano T. N. Takeuchi A. T. Suzuki Y. S. Nakamura T. N. Noguchi T. N. Mukai T. M. Abe M. A. Yada T. Y. Fujimura A. F.
Micro-Structures of Particle Surfaces of Itokawa Regolith and LL Chondrite Fragments **[#1969]**
In this study, observations of particle surfaces of Itokawa regolith and LL chondrites were made using a field emission-scanning electron microscope together with three-dimensional structures using X-ray microtomography to understand surface processes on Itokawa.

10:45 a.m. Tsuchiyama A. * Uesugi M. Uesugi K. Nakano T. Noguchi R. Matsumoto T. Matsuno J. Nagano T. Imai Y. Shimda A. Takeuchi A. Suzuki Y. Nakamura T. Noguchi T. Mukai T. Abe M. Yada T. Fujimura A.
Three-Dimensional Structures of Itokawa Particles Using Micro-Tomography: Comparison with LL5 and LL6 Chondrites **[#1870]**
Three-dimensional structures of Itokawa samples from the first sampling site show no difference from those from the second sampling site. Most of Itokawa samples are consistent with LL5 and 6 chondrites even if grain size, voids, and cracks are taken into consideration.

11:00 a.m. Ross D. K. * Simon J. I. Simon S. B. Grossman L.
Ca-Fe and Alkali-Halide Alteration of an Allende Type B CAI: Aqueous Alteration in Nebular or Asteroidal Settings? **[#2466]**
Petrographic and chemical observations of secondary alteration products in a CAI constrain the physical and temporal setting of the alteration. Andradite, hedenbergite, sodalite, and nepheline alteration pre-dated assembly of the Allende chondrite parent body.

11:15 a.m. Ziegler K. * Zolensky M. Young E. D. Ivanov A.
Oxygen Isotope Compositions of the Kaidun Meteorite — Indications for Aqueous Alteration of E-Chondrites **[#2414]**
The Kaidun microbreccia meteorite contains E-chondrite clasts with signs of pre-Kaidun aqueous alterations that vary in type and degree. Oxygen-isotope and mineralogical data attest to the presence of water in E-chondrite parent bodies.

11:30 a.m. Herd C. D. K. * Sharp Z. D. Alexander C. M. O'D. Blinova A.
Oxygen Isotopic Composition of Tagish Lake Lithologies: Insights into Parent Body Alteration **[#1688]**
Whole-rock oxygen isotope compositions of four Tagish Lake specimens define a mass fractionation trend with a greater range in variation than any other carbonaceous chondrite. The range is consistent with varying degrees of aqueous alteration.

11:45 a.m. Changela H. * Stroud R. M. Peeters Z. Nittler L. R. Alexander C. M. O'D. De Gregorio B. T. Cody G. D.
Morphological Study of Insoluble Organic Matter Residues from Primitive Chondrites **[#2745]**
By studying the morphologies of IOM residues from a range of CM and CR chondrites, we have identified a coarsening in the texture of IOM from the more altered chondrites. Thus, parent body alteration altered/formed IOM in the CM and CR chondrites.

LUNAR PETROLOGY AND GEOCHEMISTRY: FROM CORE TO CRUST
Thursday, 1:30 p.m. Waterway Ballroom 4

Chairs: Willem van Westrenen and Clive Neal

1:30 p.m. van Westrenen W. * de Meijer R. J. Anisichkin V. F. Voronin D. V.
Forming the Moon from Terrestrial Silicate-Rich Material — 2012 Edition **[#1738]**
Moon formation models have to be consistent with lunar chemistry. Current versions of the giant impact model are not. We provide a (radical) alternative hypothesis in which the Moon is formed from terrestrial material.

1:45 p.m. Rai N. * van Westrenen W.
Constraints on the Formation of a Lunar Core from Metal-Silicate Partitioning of Siderophile Elements **[#1781]**
Using metal-silicate partitioning behaviour of siderophile elements, we model lunar core formation and examine whether a consistent set of P-T-fO_2-X conditions can be obtained to match observed siderophile-element depletions in the silicate Moon.

2:00 p.m. Sprung P. * Kleine T. Scherer E. E.
Lu-Hf Evolution of the Moon — Importance of Neutron Capture Effects **[#2194]**
New Hf-isotope and Lu-Hf data show that neutron capture (NC) has falsified the measured Lu-Hf systematics in 9 out of 13 analyzed lunar rock samples. This frequent occurrence of NC effects calls for a reinvestigation of the lunar Lu-Hf systematics.

2:15 p.m. Rapp J. F. * Draper D. S.
Experimental Fractional Crystallization of the Lunar Magma Ocean **[#2048]**
We have experimentally simulated fractional crystallization of the lunar magma ocean, and present the resultant crystallizing assemblages. These experiments will provide insight into the mechanisms of lunar evolution.

2:30 p.m. Gross J. * Treiman A. H. Mercer C. M.
Sinking the Lunar Magma Ocean: New Evidence from Meteorites and the Return of Serial Magmatism **[#2306]**
Current understanding of lunar evolution is built on the lunar magma ocean hypothesis and the assumption that ferroan anorthosites are globally distributed. Anorthosites in lunar meteorites are inconsistent with a global lunar magma ocean.

2:45 p.m. Liang Y. * Yao L. Sun C. Hess P. C.
A REE-in-Two-Pyroxene Thermometer for Mafic and Ultramafic Rocks from the Earth, Moon (FANs and Mg-Suite Rocks), and Other Planetary Bodies: Promises and Challenges **[#1987]**
A REE-in-two-pyroxene thermometer for mafic and ultramafic rocks is developed. Applications to samples from Earth and the Moon (FANs) show both promising and surprising results that may shed new light on the thermal history of the samples.

3:00 p.m. Hui H. * Neal C. R.
Preliminary Study of Olivine Melt Inclusions of Apollo 12 and 14 Basalts **[#2563]**
The goal of this study is to use composition of melt inclusion to infer parental melt composition. The major elements suggest that the magma was saturated with several phases at the time of incorporation into the olivine crystals.

3:15 p.m. Elardo S. M. * McCubbin F. M. Shearer C. K. Jr.
The Origin of Chromite Symplectites in Lunar Troctolite 76535: A New Look at an Old Rock **[#1028]**
The origin of Cr-rich symplectites in 76535 has been debated and bears relevance to the extremely low Cr-content of its cumulus olivine. Here we assess previously proposed formation mechanisms and show that open system addition of Cr may be required.

3:30 p.m. Shearer C. K. Jr. * Borg L. E. Burger P. V. Connelly J. N. Bizarro M.
Timing and Duration of the Mg-Suite Episode of Lunar Crustal Building. Part 1: Petrography and Mineralogy of a Norite Clast in 15445 **[#1421]**
We examine the ambiguity between crystallization ages derived from FANs and Mg-suite lithologies and implications for building the early lunar crust.

3:45 p.m. Treiman A. H. * Gross J.
Lunar Cordierite-Spinel Troctolite: Igneous History, and Volatiles **[#1196]**
Apollo sample 15295,101 contains a cordierite spinel troctolite (Marvin et al., 1989). The cordierite is volatile-free, at least by EMP — more precise analyses are in progress. The troctolite may be a partial melt of a spinel-rich igneous cumulate.

4:00 p.m. Neal C. R. * Davidson J.
A New Look at the Origin and Evolution of Mare Basalts Using REE Profiles **[#1832]**
A method is presented to use the shape and slope of REE profiles to examine source characteristics and post-magma-generation processes.

4:15 p.m. Donohue P. H. * Neal C. R.
Apollo 17 High-Ti Basalt Evolution: Whole Rock vs. Mineral Crystallization Trends **[#2827]**
In-situ trace element geochemical studies are a leading edge in petrologic research, allowing a high level of fidelity in evaluating basalt evolution. We analyzed major phases in a representative suite of samples to unravel A17 basalt crystallization.

4:30 p.m. Zeigler R. A. * Korotev R. L. Jolliff B. L.
Pairing Relationships Among Feldspathic Lunar Meteorites from Miller Range, Antarctica **[#2377]**
The Miller Range ice fields have yielded five feldspathic lunar meteorites. Here we examine the pairing relationships among the Miller Range feldspathic lunar meteorites using petrography in concert with trace- and major-element compositions.

SPECIAL SESSION: DAWN OVER VESTA I
Thursday, 1:30 p.m. Waterway Ballroom 5

Chairs: Carol Raymond and Ernesto Palomba

1:30 p.m. Russell C. T. * Raymond C. A. Jaumann R. McSween H. Y. Dawn Science Team
Dawn at Vesta: Accomplishments and Plans **[#1633]**
The current discoveries and near-term plans of the Dawn mission are described and the following presentations introduced.

1:45 p.m. Jaumann R. * Pieters C. M. Raymond C. A. Yingst R. A. Williams D. A. Schenk P. Buczkowski D. L. Denevi B. W. Neukum G. Mottola S. O'Brien D. P. Garry W. B. Blewett D. T. Roatsch T. Preusker F. Krohn K. Stephan K. Nathues A. Sykes M. V. De Sanctis M. C. McSween H. Y. Keller H. U. Schmedemann N. Hiesinger H. Marchi S. McCord T. B. Zuber M. T.
Mapping Vesta: A Geological Overview **[#1788]**
Geomorphology and distribution of surface features provide evidence for impact cratering, tectonic activity, regolith, and probable volcanic processes on Vesta. In general, Vesta's geology is more like the Moon and rocky planets than other asteroids.

2:00 p.m. Raymond C. A. * Asmar S. W. Konopliv A. S. Park R. S. Jaumann R. Preusker F. Russell C. T. Smith D. E. Toplis M. J. Zuber M. T.
Geophysical Exploration of Vesta **[#1007]**
Dawn's data have detrained the shape and gravity field of Vesta, revealing correlations between topography and gravity anomalies and providing evidence for a significant iron core.

2:15 p.m. Asmar S. W. * Konopliv A. S. Park R. S. Bills B. G. Gaskell R. Raymond C. A. Russell C. T. Smith D. E. Toplis M. J. Zuber M. T.
The Gravity Field of Vesta and Implications for Interior Structure **[#2600]**
Paper describes results from the Dawn gravity investigation at Vesta. When correlated with a shape model, these data can constrain the interior structure. Determination of GM is highly accurate for a gravity field of degree 8 with 140-km resolution.

2:30 p.m. Fu R. R. * Weiss B. P. Li L. Suavet C. Gattacceca J. Lima E. A.
Magnetic Fields on 4 Vesta as Recorded in Two Eucrites **[#1946]**
We conduct paleomagnetic studies on two eucrites, believed to originate from asteroid 4 Vesta. We find evidence of magnetic fields on Vesta most consistent with the existence of a past dynamo.

2:45 p.m. Solano J. M. Kiefer W. S. * Mittlefehldt D. W.
Modelling the Thermal History of the Asteroid 4 Vesta **[#2063]**
Modeling of Vesta has been undertaken to investigate its evolution from an unconsolidated chondritic body to a differentiated body. Both melt migration and heat transfer are modelled to investigate the evolution of Vesta into a differentiated body.

3:00 p.m. Toplis M. J. * Mizzon H. Forni O. Monnereau M. Barrat J. A. Prettyman T. H. McSween H. Y. McCoy T. J. Mittlefehldt D. W. De Sanctis M. C. Raymond C. A. Russell C T.
Chondritic Models of 4 Vesta: Comparison of Predicted Internal Structure and Surface Composition/Mineralogy with Data from the Dawn Mission **[#2152]**
This work explores the consequences of different chondritic bulk compositions on the internal structure and surface mineralogy/composition of Vesta. This analysis provides a useful reference frame for interpretation of data from the Dawn mission.

3:15 p.m. Schenk P. * Marchi S. O'Brien D. P. Buczkowski D. L. Jaumann R. Yingst A. McCord T. Gaskell R. Roatsch T. Keller H. E. Raymond C. A. Russell C. T.
Mega-Impacts into Planetary Bodies: Global Effects of the Giant Rheasilvia Impact Basin on Vesta **[#2757]**
Vesta has been hammered by large impacts, including two large (400–500 km) basins at the South Pole, the largest basins in proportion to target radius so far seen in the solar system. Here we examine the global effects of impacts at planetary scales.

3:30 p.m. Vincent J.-B. * Hoffman M. Nathues A. Sierks H. Gaskell R. W. Marchi S. O'Brien D. Schenk P. Fulchignoni M. Keller H. U. Raymond C. Sykes M.
Crater Depth-to-Diameter Ratio and Surface Properties of (4) Vesta **[#1415]**
We report on the depth-to-diameter ratio of craters on the surface of Vesta, currently visited by the Dawn spacecraft. We discuss how d/D can be use to understand better the surface properties and evolution, and we compare with other small bodies.

3:45 p.m. Marchi S. * McSween H. Y. O'Brien D. Schenk P. De Sanctis M. C. Gaskell R. Hiesinger H. Jaumann R. Mottola S. Preusker F. Raymond C. A. Roatsch T. Russell C. T. Yingst R. A.
Vesta Collisional History Revealed by Dawn: Building a Vesta Global Crater Catalog **[#1617]**
This abstract presents a global catalog of craters on Vesta, as revealed by Dawn observations. Implications of these findings are discussed.

4:00 p.m. O'Brien D. P. * Marchi S. Schenk P. Russell C. T. Raymond C. A.
The Impact History of Vesta: Developing and Testing an Absolute Cratering Chronology **[#2688]**
With crater counts from Dawn imaging and topography data, along with insights provided by dynamical models and constraints from the HED meteorites, we are working towards developing an absolute cratering chronology for Vesta's surface.

4:15 p.m. Bottke W. F. * Marchi S. Vokrouhlicky D. Cohen B. A.
Reconciling Asteroid Collision Ages with the Late Heavy Bombardment **[#2191]**
Most main belt asteroids hit each other too slowly to produce much heat or reset Ar-Ar ages. Instead, we show LHB-era impact heating events likely came from asteroids pushed onto deep Earth-crossing orbits by late giant planet migration.

4:30 p.m. Schmedemann N. * Kneissl T. Michael G. Neukum G. Nathues A. Sierks H. Wagner R. Krohn K. Reddy V. Hiesinger H. Jaumann R. Raymond C. A. Russell C. T.
Crater Size-Frequency Distribution (CSFD) and Chronology of Vesta — Crater Counts Matching HED Ages **[#2544]**
We compare crater size-frequency distributions and chronologies between the Moon, Vesta, and smaller asteroids. The derived crater retention ages on Vesta match with high probable K/Ar-Ar ages of HED meteorites.

PLANETARY BRINES AND ALTERATION
Thursday, 1:30 p.m. Waterway Ballroom 6

Chairs: Jeffrey Kargel and Susanne Schwenzer

1:30 p.m. Sapers H. M. * Osinski G. R. Buitenhuis E. Banerjee N. R. Flemming R. L. Hainge J. Blain S.
The Ries Post-Impact Hydrothermal System: Spatial and Temporal Mineralogical Variation **[#1915]**
Mineralogical data from surficial suevite, Nördlingen, and Wörnitzostheim drill cores used to assess the extent of the Ries post-impact hydrothermal system suggest that the system outside the crater rim is more extensive than previously reported.

1:45 p.m. Dypvik H. * Hellevang H. Kalleson E.
Alteration of Impact Melts **[#1072]**
In this project we study the alteration processes of melt rocks, impact melt in particular. Experimental analyses, succeeded by mineralogical and geochemical modeling, explain the formation of alterations products, e.g., smectites, saponite, zeolites.

2:00 p.m. McCollom T. * Moskowitz B. Berquo T. Hynek B.
Acid-Sulfate Alteration of Basalt in Fumarolic Environments on Earth and Mars **[#1574]**
A combined field, experimental, and model study of acid-sulfate alteration indicates that the initial stage of alteration of martian basalt in fumarole environments should be dominated by amorphous silica, gypsum, Fe-rich natroalunite, and kieserite.

2:15 p.m. Bridges J. C. * Schwenzer S. P.
The Nakhlite Hydrothermal Brine **[#2328]**
The nakhlite martian hydrothermal brine reached 100°C, pH 8–9.5, and a low water rock ratio <10. These constraints were determined with a thermochemical model (using CHILLER) based on the known nakhlite hydrothermal assemblage.

2:30 p.m. Mangold N. * Carter J. Poulet F. Dehouck E. Ansan V. Loizeau D.
Hydrothermal Alteration in a Late Hesperian Impact Crater on Mars **[#1209]**
The 45-km-diameter Majuro Crater shows an alluvial fan containing phyllosilicates. Observations suggest alteration occurred during the Hesperian by hydrothermal circulation due to the impact heat coupled to snow precipitation.

2:45 p.m. Noe Dobrea E. Z. * Swayze G. A.
Hydrothermal Alteration Products in the Circum-Hellas Region: Targets for Future Landing Missions **[#1009]**
This work presents an analysis of the regional geologicial and mineralogical context for prehnite detected in the NW Hellas rim, in support of Mars Exploration's Critical Data Produces program.

3:00 p.m. Schmidt M. E. * Flemming R. L. Stickles J. Morena J.
Hydraulic Properties Control Phyllosilicate and Zeolite Formation in Basaltic Tuffs: Implications for Detection and Alteration Processes on Mars **[#1226]**
Basaltic hydrovolcanic tuffs from central Oregon illustrate how primary porosity and permeability control hydrothermal fluid flow and alteration assemblages.

3:15 p.m. Hausrath E. M. * Adcock C. T. Tu V.
Phosphate Records Environmental Conditions Important to Habitability in Soils and Rocks on Mars **[#2719]**
Phosphate, an important terrestrial nutrient, behaves differently under different conditions of pH, water: rock ratio, time and oxidation state, and may preserve characteristics important to habitability in soils and rocks on Mars.

3:30 p.m. Gough R. V. * Chevrier V. F. Tolbert M. A.
Deliquescence of Perchlorate/Chloride Mixtures: Implications for Stable and Metastable Aqueous Solutions on Mars **[#1706]**
Raman microscopy is used to study the deliquescence (solid to aqueous transition) and efflorescence (aqueous to solid transition) of three ClO_4^-/Cl^- mixed salt systems. We find that aqueous phases form at low RH values and may occur on current Mars.

3:45 p.m. Barge L. M. * Doloboff I. J. Kanik I. Russell M. J.
Electrochemistry of Inorganic Membranes at Alkaline Hydrothermal Vents — Energy Sources for Emerging Life on Wet Rocky Planets **[#2489]**
We present electrochemical studies of iron sulfide membranes precipitated in simulated alkaline hydrothermal systems. The electrochemical/chemiosmotic energy in such membranes may be sufficient to drive the emergence of metabolism on rocky planets.

THU ORALS

4:00 p.m. Doloboff I. J. * Barge L. M. Russell M. J. Kanik I.
Characterization of Electrochemical and Morphological Properties of Iron-Phosphate-Silicate Chemical Garden Structures **[#2646]**
Examination of the growth of Fe^{2+}, phosphate, and silicate chemical garden structures to understand properties of similar structures that may have formed at Hadean alkaline hydrothermal vents which may play an important role in the emergence of life.

4:15 p.m. Schwenzer S. P. * Anand M. Franchi I. A. Gibson J. M. Greenwood R. C. Hammond S. Haubold R. Herrmann S. Kelley S. P. Ott U. Tindle A. G.
Cold Desert Alteration of Martian Meteorites: Mixed News from Noble Gases, Trace Elements and Oxygen Isotopes **[#1954]**
We investigated rim and interior subsamples from the martian meteorites ALH A77005 and RBT 04261 and found terrestrial alteration to influence mineralogy and heavy noble gases but less so oxygen isotopes and trace elements.

4:30 p.m. Wang A. *
Subsurface Hydrous Salts and Obliquity Cycle on Mars **[#2172]**
We correlate the dehydration and rehydration rates of Mg-sulfates (derived from experimental data) with Mars obliquity cycles and evaluate the preservation potential of highly hydrated sulfates in the subsurface of equatorial regions on Mars.

PRESOLAR GRAINS: INSIGHT INTO STELLAR PROCESSES
Thursday, 1:30 p.m. Montgomery Ballroom

Chairs: Philipp Heck and Christine Floss

1:30 p.m. Hoppe P. * Zinner E.
Sulfur-Isotopic Signature of Presolar SiC Grains of Type X **[#1414]**
We report here results of S-isotope measurements on presolar SiC X grains made in order to gain further insights into the S-isotopic signature of SN dust and the chemical and physical processes taking place in SNII ejecta.

1:45 p.m. Orthous-Daunay F.-R. * Gyngard F. Moynier F. Zinner E.
Multi-Element Isotopic Compositions of Presolar SiC Grains from the Indarch Meteorite **[#2679]**
We present a NanoSIMS study of grains isolated from Indarch with sizes between 0.4 and 1 µm. Si and C isotopic compositions of more than thousand particles were measured. Grains with extreme anomalies were selected for multi-element investigation.

2:00 p.m. Heck P. R. * Hoppe P. Huth J.
Sulfur Isotopic Analysis of 24 Sulfur-Rich Dust Impact Craters from Comet Wild 2 **[#1794]**
All but one crater have normal S-isotopic compositions indicative of a solar system origin. A small anomaly in one crater could be a mixture between a presolar supernova sulfide and a normal sulfide; or due to fractionation or a statistical outlier.

2:15 p.m. Trappitsch R. * Savina M. R. Willingham D. G. Liu N. Pellin M. J. Dauphas N. Davis A. M.
Iron Isotopic Abundances in Presolar Grains **[#2497]**
Iron-isotope abundances in 12 presolar grains were measured using RIMS. Our data do not show isotope anomalies predicted by AGB star models. Contamination with solar system material or galactic chemical evolution might mask AGB contribution.

THU ORALS

2:30 p.m. Ávila J. N. Ireland T. R. * Lugaro M. Gyngard F. Zinner E. Mallmann G. Holden P.
U-Th-Pb Isotopic Compositions in Stardust SiC Grains from the Murchison Meteorite **[#2709]**
U-Th-Pb isotopic compositions have been measured from presolar SiC grains from Murchison. Pb isotopic compositions are dominated by an *s*-process component. U and Th concentrations are quite variable.

2:45 p.m. Zinner E. * Jadhav M.
Internal "Isochrones" Within Presolar Dust Grains **[#1122]**
NanoSIMS depth profiles of parent and daughter isotopes of radioactive nuclides in presolar graphite grains let us construct isochrone-type plots. The perfect correlation of such plots indicates quantitative retention of the daughter isotopes.

3:00 p.m. Groopman E. * Wopenka B. Bernatowicz T. J. Zinner E.
Heterogeneous Distributions of C, N, and O Isotopes and Raman Signatures in Low-Density Supernova Graphite Grains from Orgueil **[#2126]**
We observe heterogeneities in the C-, N-, and O-isotopic compositions of low-density graphite grains from Orgueil. We make the first observations of highly anomalous and spatially-correlated hotspots in $^{18}O/^{16}O$ and $^{15}N/^{14}N$ delta values.

3:15 p.m. Daulton T. L. * Bernatowicz T. J. Croat T. K.
Electron Energy Loss Spectral Imaging of TiC Formed by Supernovae: A Scanning Transmission Electron Microscopy Study of Grain Formation and Alteration Mechanisms **[#2247]**
Micrometer-sized spherules of graphite formed by supernovae contain numerous TiC and Fe-Ni subgrains. These subgrains often have disordered surface rims. The mechanism(s) of rim formation on these subgrains is studied by transmission electron microscopy.

3:30 p.m. Croat T. K. * Berg T. Bernatowicz T. J. Jadhav M.
Presolar Refractory Metal Nuggets **[#1503]**
Presolar RMN microstructures show they are primary high T circumstellar condensates, which are then encapsulated in graphite at 1580–1815 K. Similarities between presolar RMNs and isolated RMNs suggest the latter are among the first primary solar system condensates.

3:45 p.m. Nguyen A. N. * Keller L. P. Rahman Z. Messenger S.
Mineralogical Studies of a Highly ^{17}O-Depleted and a ^{17}O-Rich Presolar Grain from the Acfer 094 Meteorite **[#2755]**
We report the mineralogical characterization by transmission electron microscopy (TEM) of two presolar O-rich grains that have different stellar origins.

4:00 p.m. Floss C. * Noguchi T. Yada T.
Ultracarbonaceous Antarctic Micrometeorites: Origins and Relationships to Other Primitive Extraterrestrial Materials **[#1217]**
Isotopic analyses of micrometeorite TT54B397 show the presence of abundant presolar grains, but normal N (and C) isotopic compositions. The carbonaceous matter in this (and other) UCAMMs may have a solar nebular, rather than interstellar, origin.

4:15 p.m. Nittler L. R. * Wang J. Alexander C. M. O'D.
Confirmation of Extreme ^{54}Cr Enrichments in Orgueil Nano-Oxides and Correlated O-Isotope Measurements **[#2442]**
We confirm extreme ^{54}Cr enrichments previously inferred for Orgueil nano-oxides. Normal O in the same grains rules out direct formation in supernovae. Hundreds of new presolar grains were also found, including the most ^{17}O-rich sample ever measured.

4:30 p.m. Zega T. J. * Nittler L. R. Stroud R. M. Alexander C. M. O'D. Kilcoyne A. L. D.
Measurement of the Oxidation State of Ti in Solar and Presolar Hibonite **[#2338]**
We report measurement of the oxidation state of Ti in solar and presolar hibonite. We infer the oxygen fugacity under which the grains formed or last equilibrated.

LUNAR GEOPHYSICS AND INTERNAL STRUCTURE
Friday, 8:30 a.m. Waterway Ballroom 4

Chairs: Paul Warren and Walter Kiefer

8:30 a.m. Zuber M. T. * Smith D. E. Asmar S. W. Konopliv A. S. Lemoine F. G. Melosh H. J. Neumann G. A. Phillips R. J. Solomon S. C. Watkins M. M. Wieczorek M. A. Williams J. G.
Gravity Recovery and Interior Laboratory (GRAIL) Mission: Status at the Initiation of the Science Mapping Phase **[#1489]**
The Gravity Recovery And Interior Laboratory (GRAIL) mission is on track to initiate its science phase on March 8, 2012. GRAIL will determine the structure of the lunar interior, and advance understanding of lunar thermal evolution.

8:45 a.m. Zhong S. J. * Qin C. A G. R. Wahr J.
Coupling of Tidal Force with Heterogeneous Mantle Structure and its Implications for Using GRAIL Observations to Constrain Lunar Interior Structure **[#2754]**
Tidal force may produce non-degree-2 gravity and radial displacement responses for a planetary body with a heterogeneous mantle. We show how this mechanism can be explored to use GRAIL results to constrain lunar interior structures.

9:00 a.m. McGovern P. J. *
An Intrusive Origin for Lunar Mascons: Magma Ascent Theory, Gravitational Signatures, and Tests for GRAIL **[#2937]**
I explore the idea that intrusive bodies beneath lunar impact basins are responsible for the immense “mascon” gravity anomalies.

9:15 a.m. Kiefer W. S. * Macke R. J. Britt D. T. Irving A. J. Consolmagno G. J.
Regional Variability in the Density of Lunar Mare Basalts and Implications for Lunar Gravity Modeling **[#1642]**
Lunar mare basalts show considerable variability in both composition and density. We show how sample and remote sensing data can be combined to estimate lunar basalt densities, providing improved constraints on gravity model parameters.

9:30 a.m. Grimm R. E. *
Thermal Models of the Lunar Procellarum KREEP Terrane: Geophysical Implications **[#2313]**
Subcrustal KREEP heating sufficient to explain mare volcanism would produce a residual gravity anomaly today that is not observed. KREEP heating must be distributed within the crust, and mare volcanism explained by secular cooling.

9:45 a.m. Nimmo F. * Faul U.
Lunar Mantle Temperature Structure from Seismic and Geodetic Observations and Laboratory Dissipation Experiments **[#1564]**
The observed dissipation and k_2 Love number of the Moon can be reconciled with laboratory measurements by invoking a relatively cold Moon, in which two-thirds of the radiogenic elements are in the crust. A deep zone of partial melt is not needed.

10:00 a.m. Tikoo S. M. * Weiss B. P. Grove T. L. Fuller M. D.
Decline of the Ancient Lunar Core Dynamo **[#2691]**
The lunar dynamo likely produced at most weak (<7 microtesla) to null surface magnetic fields 3.2–3.3 billion years ago (Ga). This indicates a decline in field intensity from the ~65 paleofield inferred for samples aged 3.6–3.7 Ga.

10:15 a.m. Suavet C. * Weiss B. P. Fuller M. Gattacceca J. Grove T. L. Shuster D. L.
Persistence of the Lunar Dynamo Until 3.6 Billion Years Ago **[#1925]**
Mare basalt 10017 provides a paleomagnetic record of a lunar core dynamo 3.6 billion years ago. These results extend the lifetime of the lunar dyamo by 100 million years and challenge current planetary dynamo models.

10:30 a.m. Richmond N. C. * Hood L. L.
Further Constraints on the History of the Lunar Dynamo Field from Lunar Prospector Magnetometer Data **[#1898]**
Lunar Prospector MAG data will be presented for the Serenitatis and Schrodinger basins, which both show evidence of basin-related magnetization. The results will be used to provide constraints on the time period of lunar core dynamo operation.

10:45 a.m. Aharonson O. * Goldreich P. Sari R.
Why do We See the Man in the Moon? **[#2532]**
Numerical simulations and analysis show that the Moon locks into resonance with a statistical preference of facing either the current nearside or farside toward Earth.

11:00 a.m. Nakajima M. * Stevenson D. J.
The Initial State of the Moon Forming Disk and the Earth's Mantle Based on SPH Simulations **[#2627]**
We have performed giant impact simulations with SPH and derived thermal profiles of 2D impact-generated disks. A mechanical mixing process between the mantle materials originating from the proto-Earth and those from an impactor is also investigated.

11:15 a.m. Perera V. * Garrick-Bethell I.
Lunar Symmetry: The True Shape of the Moon? **[#2634]**
We present a new center-of-figure referenced map of lunar topography, which shows that the nearside and the farside are more symmetric than previously inferred.

11:30 a.m. Warren P. H. *
Constraints on the Impact-Accreted Carapace Hypothesis for the Lunar Farside Highlands **[#2941]**
The recent proposal that the an impact-accreted carapace accounts for the greater thickness of the Moon's farside highlands crust is not plausible. The carapace would not have appropriately low density, nor the appropriate Al_2O_3-rich composition.

SPECIAL SESSION: DAWN OVER VESTA II: THE HED-VESTA CONNECTION
Friday, 8:30 a.m. Waterway Ballroom 5

Chairs: Michael Toplis and David Lawrence

8:30 a.m. Le Corre L. * Reddy V. Nathues A. Li J.-Y. Denevi B. W. Buratti B. J. Sierks H. Schröder S. E. Pieters C. M. Gaskell R. Becker K. J. Gutiérrez Marqués P. Russell C. T. Raymond C. A.
Vesta Terrains Seen by the Dawn Framing Camera Color Filters **[#1624]**
We present an analysis of the different terrains on Vesta using latest data from the color filters of the Dawn Framing Camera. Preliminary understanding of the nature and origin of these bright, dark, gray and orange/red materials will be presented.

8:45 a.m. De Sanctis M. C. * Ammannito E. Capria M. T. Capaccioni F. Carraro F. Fonte S. Frigeri A. Magni G. Marchi S. Palomba E. Tosi F. Zambon F. McCord T. B. McFadden L. A. McSween H. Y. Jr. Mittlefehldt D. W. Pieters C. M. Raymond C. A. Russell C. T.
Overview of Vesta Mineralogy Diversity **[#1444]**
Vesta's spectrum has strong absorption centered near 0.9 and 1.9 µm, indicative of Fe-bearing pyroxenes. Data from the Dawn VIR characterize and map the mineral distribution on Vesta, providing new insights into Vesta's formation and evolution.

9:00 a.m. Prettyman T. H. * Beck A. Feldman W. C. Forni O. Joy S. P. Lawrence D. J. McCoy T. J. McFadden L. A. McSween H. Y. Mittlefehldt D. W. Polanskey C. A. Rayman M. D. Raymond C. A. Reedy R. C. Russell C. T. Titus T. N. Toplis M. J. Yamashita N.
The GRaND Geochemistry of 4 Vesta: First Results **[#2389]**
We present first results of the analysis and interpretation of geochemical data acquired by the NASA Dawn mission's Gamma Ray and Neutron Detector in the low-altitude mapping orbit around 4 Vesta.

9:15 a.m. Mittlefehldt D. W. * Prettyman T. H. Reedy R. C. Beck A. W. Blewett D. T. Gaffey M. J. Lawrence D. J. McCoy T. J. McSween H. Y. Jr. Toplis M. J. Dawn Science Team
Do Mesosiderites Reside on 4 Vesta? An Assessment Based on Dawn GRaND Data **[#1655]**
We will use GRaND data from the Dawn spacecraft to test the hypothesis that mesosiderites are a lithologic component of the vestan crust.

9:30 a.m. Wasson J. T. *
Vesta, Iron Meteorites from Extensively Differentiated Asteroids, and the Provenance of the HED Meteorites **[#2931]**
There were many extensively differentiated asteroids thus Vesta is unlikely to be the source of the HEDs. If the GRAND instrument measures K it may be able to show that Vesta cannot be the HED parent.

9:45 a.m. McSween H. Y. Jr. * Mittlefehldt D. W. Beck A. W. McCoy T. J. Marchi S. De Sanctis M. C. Ammannito E. Raymond C. A. Russell C. T.
Dawn and the Vesta-HED Connection **[#1433]**
The hypothesis that Vesta is the parent body of HED meteorites is consistent with, and strengthened by, the geologic context for HEDs provided by Dawn.

10:00 a.m. Barrat J. A. * Bodenan J. D. Yamaguchi A. Buchanan P. C. Toplis M.
What Can We Learn on Vesta from the Petrology of Impact Melts? **[#1438]**
Geochemistry of impact melts suggests that some of them formed from targets unlike HEDs.

10:15 a.m. Roszjar J. * Srinivasan G. Whitehouse M. Bischoff A. Mezger K.
Hf-W Analyses of Eucrite Zircon: New Crystallization Timescales for the Eucrite Parent Body **[#1774]**
In situ ^{182}Hf-^{182}W isotope analyses of zircon grains were performed in order to determine the timing of crystallization of basaltic eucrites.

10:30 a.m. Erb I. R. * Boesenberg J . S.
Integrating Elemental X-Ray Mapping and Mineral Analysis Techniques to Estimate the Provenance of the Howardites on Vesta **[#1531]**
We compare howardite mineral modes from clasts and fragments in the large and small fractions to obtain an estimate of whether the individual meteorites derive from one or more provenances. Correlations are made between mapping and mineral chemistry.

10:45 a.m. Beck A. W. * Sunshine J. M. McCoy T. J. Hiroi T.
Challenges to Finding Olivine on the Surface of 4 Vesta **[#2218]**
Here we examine laboratory spectra of harzburgitic and orthopyroxenitic diogenites. In the VNIR, these two meteorites are indistinguishable; suggesting that vestan Ol-rich terranes will be difficult to identify using the VIR spectrometer on Dawn.

11:00 a.m. Sarafian A. R. * Roden M. F. Patiño-Douce A. E.
The Nature of Volatiles in Vesta: Clues from Apatite in Eucrites **[#1175]**
We used the electron and ion probe to measure the volatile content of apatite in eucrites. We found several distinct volatile reservoirs in eucrites: degassed and undegassed basalts and two possible late-stage fluids.

11:15 a.m. Combe J.-Ph. * McCord T. B. Palomba E. De Sanctis M. C. Prettyman T. H. Pieters C. M. Ammannito E. Capaccioni F. Capria M. T. Raymond C. A. Russell C. T.
Water and Other Volatiles on Vesta After the Lunar Case **[#2463]**
Reflectance spectra of the surface of Vesta from the Visible and Near-Infrared Mapping Spectrometer (VIR) onboard the Dawn spacecraft are being analyzed for the search of volatiles, in the context of recent discoveries of OH and H_2O on the Moon.

11:30 a.m. Stubbs T. J. * Wang Y.
On the Presence of Water at the Asteroid 4 Vesta **[#1350]**
We investigate the average solar illumination and surface temperatures at the asteroid 4 Vesta, and assess the implications for the presence of water in the subsurface and on the surface of the regolith.

MARS AEOLIAN PROCESSES: PREPARE TO BE BLOWN AWAY!
Friday, 8:30 a.m. Waterway Ballroom 6

Chairs: Nathan Bridges and Candice Hansen

8:30 a.m. Geissler P. E. * HiRISE Team
Persistent Surface Changes in Solis Lacus, Mars **[#2598]**
Orbital monitoring has shown that the Solis Lacus region experiences continual, drastic albedo changes due to eolian activity. Images from HiRISE help explain the activity, and show evidence for lateral surface transport of dust deposits.

8:45 a.m. Bridges N. T. * Ayoub F. Avouac J-P. Leprince S. Lucas A. Mattson S.
High Sand Fluxes and Abrasion Rates on Mars Determined from HiRISE Images **[#1322]**
We derive the reptation and saltation sand fluxes in Nili Patea, Mars. The dunes have unexpectedly high fluxes that are like those in Victoria Valley, Antarctica, implying that rates of landscape modification on Mars and Earth are similar.

9:00 a.m. Feldman W. C. * Bourke M. C. Teodoro L. F. A.
Water Equivalent Hydrogen variability in the North Polar Region: The Potential Influence of Katabatic Winds **[#2170]**
North polar dune sediment is subject to dessication by polar katabatic winds.

9:15 a.m. Bourke M. C. *
Seasonal Change in Polar Dune Morphology **[#2885]**
Cryo-aeolian processes play an important role in the North Polar dune morphology changes observed between Mars year 29 and 30.

9:30 a.m. Brothers T. C. * Holt J. W. Spiga A.
Abalos Mensa, Planum Boreum, Mars: A Constructional, Aeolian History Derived from Radar and Optical Stratigraphy, Reinforced by Atmospheric Modeling **[#1452]**
Radar and HiRISE data have unveiled a new formation scenario for Abalos Mensa only requiring observed atmospheric processes. Analysis of both radar and optical stratigraphy has revealed a constructional formation for Abalos Mensa.

9:45 a.m. Horgan B. * Sullivan R. Bell J. F. III
Seasonally Active Dune Slipface Avalanches on Mars: Evidence for a Wind-Related Origin **[#1631]**
The origin of slipface avalanches on some martian dunes has been previously attributed to spring CO_2 sublimation. However, we show that the timing, morphology, and orientations of the features support an aeolian origin in mid- to late summer.

MARS POLAR PROCESSES: VERY COLD AND REALLY COOL
Friday, 10:00 a.m. Waterway Ballroom 6

Chairs: Candice Hansen and Nathan Bridges

10:00 a.m. Brown A. J. * Calvin W. M.
Water Ice Grain Size Evolution on Martian North Polar Residual Layered Deposits for Late Summer MY28 AND 30 from CRISM/MARCI Observations **[#1742]**
We report on the late summer evolution of the the NPLD. We used CRISM data to identify an increase in VNIR albedo that we attribute to a decrease in ice grain size from L_s = 132–167 in MY28. MARCI data indicate this is not likely due to clouds or dust.

10:15 a.m. Calvin W. M. * James P. B. Hansen C. J.
Seasonal Variation in Volatile Ices in the North Polar Region of Mars **[#2278]**
Spring and summer CRISM observations of selected sites in the north polar region are examined to explore volatile ice composition and grain size evolution with season. The polar layered deposits are diverse with both seasonal and annual variability.

10:30 a.m. Plaut J. J. * Frigeri A. Orosei R.
Compositional Constraints on the Martian North Polar Basal Unit from MARSIS Radar Sounding Data **[#2458]**
Data from the 2011 north polar MARSIS campaign allow estimation of the dielectric constant of the basal unit of the polar plateau. The values suggest a component of lithic material as high as 50%.

10:45 a.m. Holt J. W. * Greve R. Smith I. B. Steel L. E. Cowan T. C.
Stratigraphic and Modeling Evidence in Support of a Young Age for the North Polar Layered Deposits, Mars **[#2879]**
Internal radar stratigraphy of the NPLD is consistent with modeling results that indicate its deposition of the northern polar ice within the past 4 million years.

11:00 a.m. Frigeri A. * Orosei R. Cartacci M. Cicchetti A. Mitri G. Giuppi S. Noschese R. Picardi G. Plaut J. J.
Three Dimensional Structure and Possible Lateral Inhomogeneities of the Mars North Polar Basal Unit **[#2922]**
MARSIS subsurface radar sounder data from 2011 allowed us to start to map in three deminsions the internal structure of the North Pole of Mars, and in particular we are exploring the structure of the Basal Unit.

11:15 a.m. Hansen C. J. * Bourke M. C. McEwen A. Mellon M. Pommerol A. Portyankina G. Thomas N.
Year 3 HiRISE Observations of Sublimation of the Northern Seasonal Polar Cap on Mars **[#2386]**
HiRISE has imaged the sublimation of Mars' northern seasonal polar cap for three years. The processes by which the dunes are reshaped every year are explored with high-resolution color images of the same locations as spring progresses.

11:30 a.m. Becerra P. * Byrne S. HiRISE Team
CO_2 Frost Halos on the South Polar Residual Cap of Mars **[#2513]**
We present observational analysis, and a numerical model to explain the formation of bright CO_2 frost halos seen by HiRISE on the edges of scarps and "swiss cheese" features in the south polar residual cap of Mars.

COSMIC DUST: INTERSTELLAR, INTERPLANETARY, AND COMETARY MATERIAL
Friday, 8:30 a.m. Montgomery Ballroom

Chairs: Lindsay Keller and Rhonda Stroud

8:30 a.m. Sterken V. J. * Westphal A. J. Altobelli N. Postberg F. Srama R. Grün E.
Interstellar Dust Simulations for the Stardust Mission **[#1878]**
In 2006, Stardust returned dust grains from Comet 81P/Wild2 as well as (candidate) interstellar dust grains. We simulated the flow of interstellar dust through the solar system and calculated impact velocities and directions on Stardust.

8:45 a.m. Westphal A. J. * Achilles C. Allen C. Ansari A. Bajt S. Bassim N. Bastien R. Bechtel H. A. Borg J. Brenker F. E. Bridges J. Brownlee D. E. Burchell M. Burghammer M. Butterworth A. Changela H. Cloetens P. Davis A. M. Floss C. Flynn G. Fougeray P. Frank D. Gainsforth Z. Gruen E. Heck P. R. Hillier J. K. Hoppe P. Hudson B. Huss G. R. Huth J. Hvide B. Kearsley A. King A. J. Lai B. Leitner J. Lemelle L. Leonard A. Leroux H. Lettieri R. Marchant W. Nittler L. R. Ogliore R. Postberg F. Price M. C. Sandford S. A. Sans Tresseras J.-A. Schmitz S. Schoonjans T. Schreiber K. Silversmit G. Simionovici A. Sole V. A. Srama R. Stephan T. Sterken V. Stodolna J. Stroud R. M. Sutton S. Treiloff M. Tsou P. Tsuchiyama A. Tyliszczak T. Vekemans B. Vincze L. Wordsworth N. Zevin D. Zolensky M. E. >30,000 Stardust@home dusters
Status of the Stardust ISPE and the Origin of Four Interstellar Dust Candidates **[#2084]**
Here we apply quantitative tests to constrain the origin of four interstellar dust candidates from the Stardust interstellar collector.

9:00 a.m. Gainsforth Z. * Simionovici A. Brenker F. E. Schmitz S. Burghammer M. Cloetens P. Lemelle L. Sans Tresseras J.-A. Schoonjans T. Silversmit G. Sole V. A. Vekemans B. Vincze L. Achilles C. Allen C. Ansari A. Bajt S. Bassim N. Bastien R. S. Bechtel H. A. Borg J. Bridges J. Brownlee D. E. Burchell M. Butterworth A. Changela H. Davis A. M. Floss C. Flynn G. Fougeray P. Frank D. Grun E. Heck P. R. Hillier J. K. Hoppe P. Hudson B. Huss G. R. Huth J. Hvide B. Kearsley A. King A. J. Lai B. Leitner J. Leonard A. Leroux H. Lettieri R. Marchant W. Nittler L. R. Ogliore R. Postberg F. Price M. C. Sandford S. A. Schreiber K. Srama R. Stephan T. Sterken V. Stodolna J. Stroud R. M. Sutton S. Trieloff M. Tsou P. Tsuchiyama A. Tyliszczak T. Westphal A. J. Wordsworth N. Zevin D. Zolensky M. E. >30,000 Stardust@home dusters
Identification of Crystalline Material in Two Interstellar Dust Candidates from the Stardust Mission **[#2336]**
Two interstellar dust candidates from the Stardust mission are found by synchrotron X-ray nanodiffraction to contain crystalline components. Analysis of the X-ray diffraction patterns determines the most likely mineral candidates.

9:15 a.m. Stroud R. M. * Achilles C. Allen C. Ansari A. Bajt S. Bassim N. Bastien R. Bechtel H. A. Borg J. Brenker F. E. Bridges J. Brownlee D. E. Burchell M. Burghammer M. Butterworth A. Changela H. Cloetens P. Davis A. M. Floss C. Flynn G. Fougeray P. Frank D. Gainsforth Z. Grün E. Heck P. R. Hillier J. K. Hoppe P. Hudson B. Huss G. R. Huth J. Hvide B. Kearsley A. King A. J. Lai B. Leitner J. Lemelle L. Leonard A. Leroux H. Lettieri R. Marchant W. Nittler L. R. Ogliore R. Ong W. J. Postberg F. Price M. C. Sandford S. A. Sans Tresseras J.-A. Schmitz S. Schoonjans T. Schreiber K. Silversmit K. Simionovici A. Solé V. A. Srama R. Stephan T. Sterken V. Stodolna J. Sutton S. Trieloff M. Tsou P. Tsuchiyama A. Tyliszczak T. Vekemans B. Vincze L. Westphal A. J. Wordsworth N. Zevin D. Zolensky M. E.
Constraining the Origin of Impact Craters on Al Foils from the Stardust Interstellar Dust Collector **[#2001]**
We present results from the elemental analysis of 24 craters in Al foil from the Stardust interstellar dust collector, and discuss the possible origins of 4 craters that are identified as candidate interstellar dust impacts.

9:30 a.m. Henkel T. * Lyon I. C. Kearsley A. T. Price M. C. Cole M. J. Burchell M.
Survival of Organic Compounds on Al Foil Under Stardust Conditions **[#2158]**
Organic material was captured on the Al foils of the Stardust collector. We studied the survival of organic material under Stardust conditions to understand the processing that organic crater residues, found on the flight foils, must have undergone.

9:45 a.m. Kearsley A. T. * Price M. C. Burchell M. Cole M. J. Foster N. J.
How the Shape and Volume of Impact Tracks in Stardust Aerogel Reflect Cometary Dust Properties: Experimental Evidence **[#1398]**
Stardust aerogel track shape was controlled by impactor internal structure, subgrain size and overall strength, rather than bulk grain density. Carbonaceous chondrite powders make Type B tracks; organics can make distinctive, squat “carrot” tracks.

10:00 a.m. Nakamura-Messenger K. * Keller L. P. Messenger S. Clemett S. J. Nguyen A. N. Frank D.
Coordinated Analyses of Diverse Components in Whole Stardust Cometary Tracks **[#2551]**
We are performing systematic examinations of entire Stardust tracks to discern the representative mineralogy and origins of comet Wild 2 components and to search for well preserved fine grained materials.

10:15 a.m. Joswiak D. J. * Brownlee D. E. Matrajt G. Nakashima D. Ushikubo T. Kita N. T. Gainsforth Z. Westphal A.
Diverse Source Regions for Fragments from a Single Stardust Track: A Mineralogical and Isotopic Study of Track 77 **[#2395]**
TEM studies of large fragments from Stardust track 77 indicate that Comet Wild 2 is mineralogically heterogeneous on the micrometer scale. Isotopic measurements further suggest the fragments were derived from diverse source regions in the nebula.

10:30 a.m. Starkey N. A. * Franchi I. A. Davidson J.
Insight into the Oxygen Reservoirs of the Comet Forming Region: Oxygen Isotope study of Interplanetary Dust Particles **[#1764]**
We present NanoSIMS O-isotopes on a set of IDPs. Most anhydrous IDPs have values similar to carbonaceous chondrites or their components, including FUN-like material. However, evidence exists for a distict group with more solar-like compositions.

10:45 a.m. Messenger S. * Keller L. P. Nakamura-Messenger K. Clemett S. J.
Pristine Stratospheric Collection of Cosmic Dust **[#2696]**
We report initial mineralogical and chemical studies of interplanetary dust particles collected in the stratosphere using a polyurethane foam substrate, without the use of silicone oil.

11:00 a.m. Stodolna J. * Butterworth A. Leroux H. Gainsforth Z. Tyliszczak T. Jacob D. Westphal A. J.
Iron Valence State Distribution at the Nano-Scale in Comet Wild2 Material from the Stardust Mission — A Coordinated TEM/STEM EDX/STXM Study **[#1212]**
We characterize the Fe valence state distribution of the GEMS-like material and combine the results with TEM characterization to better understand the chemical modifications during capture versus the primary nature of the Wild 2 fine-grained material.

11:15 a.m. Keller L. P. * Messenger S.
Formation and Processing of Amorphous Silicates in Primitive Carbonaceous Chondrites and Cometary Dust **[#1880]**
Amorphous silicates in CR 3.0 chondrites and Acfer 094 are compared and contrasted with GEMS grains in IDPs. Parent body oxidation and hydration reactions have modified the meteoritic amorphous silicates.

11:30 a.m. Bridges J. C. * Hicks L. J. Gurman S. J.
Space Weathering in Stardust Comet Wild2 Samples **[#2214]**
The Stardust Track 170 terminal grain is shown by XANES and EXAFS to be an Fe-metal and silicate assemblage that originated through space weathering on the surface of Wild 2.

LUNAR MAPPING
Friday, 1:30 p.m. Waterway Ballroom 4

Chairs: **Lisa Gaddis and C. K. Shum**

1:30 p.m. Archinal B. A. * Kirk R. L. Gaddis L. R. Rosiek M. R.
Unifying Lunar Topographic and Other Datasets **[#2394]**
This abstract describes the steps needed to ensure development of high-value lunar products based on information fusion of data from multiple missions by national and international space agencies permitting comparative and synergistic use of the data.

1:45 p.m. Rosiek M. R. * Lee E. M. Howington-Kraus E. T. Fergason R. L. Weller L. A. Galuszka D. M. Redding B. L. Thomas O. H. Saleh R. A. Richie J. O. Shinaman J. R. Archinal B. A. Hare T. M.
USGS Digital Terrain Models and Mosaics for LMMP **[#2343]**
This abstract describes the USGS DTMs and mosaics produced for the Lunar Mapping and Modeling Program. The primary initial objective was to support exploration missions by making LRO-derived products useful and accessible to the Constellation Program.

2:00 p.m. Nefian A. V. * Moratto Z. Beyer R. A. Kim T. Broxton M. Fong T.
Apollo Metric Zone Terrain Reconstruction **[#2184]**
Using advanced and fully automated mapping and image processing techniques the Intelligent Robotics Group at NASA Ames has recently released the terrain map of the Apollo Metric zone that covers 18% of the lunar surface at 30 m/pixel.

2:15 p.m. Gusakova E. * Karachevtseva I. Shingareva K. Oberst J. Peters O. Wählisch M. Robinson M. S.
Mapping and GIS-Analyses of the Lunokhod-1 Landing Site **[#1750]**
Using GIS tools and high-resolutiom DEM derived from LRO NAC various morphometric parameters of the Lunokhod-1 area were calculated. The results of geoanalyses can be used for cartography at high level of detail as support of future landing mission.

2:30 p.m. Shum C. K. * Fok H. S. Yi Y. Dai C. L. Shang K. Wang L. Araki H. Matsumoto K. Sasaki S. Iz H. B. Ding X. L. Ping J. S.
Lunar Topography Model Determined by Integrating Laser Altimetry from Multiple Orbiters **[#2407]**
Multiple lunar orbiters carrying laser altimeters have distinct sampling and accuracy. We used the differenced altimeter technique for orbit adjustments to develop a combined lunar topography model with improved accuracy and resolution (1.89 km).

2:45 p.m. Retherford K. D. * Gladstone G. R. Stern S. A. Egan A. F. Miles P. F. Parker J. Wm. Kaufman D. E. Greathouse T. K. Versteeg M. H. Steffl A. J. Mukherjee J. Davis M. W. Slater D. C. Bayless A. J. Rojas P. M. Karnes P. L. Feldman P. D. Hurley D. M. Pryor W. R. Hendrix A. R.
LRO-Lyman Alpha Mapping Project (LAMP) Maps of Lunar Far-UV Albedo **[#2292]**
LAMP measurements indicate ~1–2% surface water frost abundances in a few PSRs based on spectral color comparisons, and we find that many PSRs may have porosities of ~0.7 based on relatively low albedos at Lyman-α.

3:00 p.m. Sato H. * Denevi B. W. Robinson M. S. Hapke B. W. McEwen A. S. LROC Science Operation Team
Photometric Parameter Maps of the Moon from LROC WAC Observations **[#1771]**
Photometric parameter maps in 2 × 2° tiles for global and 0.05 × 0.05° tiles near the Apollo 17 site were derived using 20 months of LROC WAC images. Variations of surface optical properties detected by parameter b,c (H-G double lobe) and hc will be presented.

MARS CLIMATE TALES: METEORITES, MORPHOLOGY, MODELS
Friday, 3:15 p.m. Waterway Ballroom 4

Chairs: Laura Kerber and Robina Shaheen

3:15 p.m. Shaheen R. * Niles P. B. Corrigan C. M. Thiemens M. H.
The Carbonates in ALH 84001 Record the Evolution of the Martian Atmosphere through Multiple Formation Events **[#2594]**
A new Ca-rich carbonte phase highly enriched in C and O isotopes is reported. The O isotopic anomaly ($\Delta\ ^{17}O$ = 0.7‰‰) indicates incorporation of oxygen from an atmospheric source of martian origin.

3:30 p.m. Manga M. Patel A. Dufek J. Kite E. S. *
Wet Surface and Dense Atmosphere on Early Mars Suggested by the Bomb Sag at Home Plate **[#1241]**
We use analogue experiments to interpret the volcanic bomb sag at Home Plate, and infer a wet surface at the time of impact. The modest penetration depth suggests a dense atmosphere.

3:45 p.m. Kerber L. * Forget F. Madeleine J. B. Wordsworth R. Head J. W. III Wilson L.
The Effect of Atmospheric Pressure on the Dispersal of Pyroclasts from Martian Volcanoes **[#1295]**
Explosive eruptions into the martian atmosphere are modeled under various atmospheric pressures using a Mars global climate model adapted to paleoatmospheric applications.

4:00 p.m. Madeleine J.-B. * Forget F. Head J. W. Navarro T. Millour E. Spiga A. Colaitis A. Montmessin F. Määttänen A.
Amazonian Glacial Cycles on Mars: Response of the New LMD Global Climate Model to Orbital Variations **[#1661]**
The goal of this study is to analyze the response of the Mars climate system to changes in the orbital conditions using the new version of the LMD/GCM, and to better understand glacial cycles as represented in the geological record.

4:15 p.m. Haberle R. M. * Kahre M. A. Hollingsworth J. L. Schaeffer J. Montmessin F. Phillips R. J.
A Cloud Greenhouse Effect on Mars: Significant Climate Change in the Recent Past? **[#1665]**
Under favorable orbital conditions, a cloud atmospheric greenhouse effect may have warmed Mars by several tens of degrees Kelvin in the recent geological past.

4:30 p.m. Bills B. G. * Mischna M. A.
Mars Gravity and Climate **[#2369]**
We examine the measurement accuracy required for Mars gravity field variations, as seen from an orbiting spacecraft, in order to constrain Mars climate models. It appears that among existing techniques, gravity gradiometry is most promising.

SPECIAL SESSION: DAWN OVER VESTA III: REGOLITH OF A TRANSITIONAL PLANET
Friday, 1:30 p.m. Waterway Ballroom 5

Chairs: Debra Buczkowski and Harald Hiesinger

1:30 p.m. Denevi B. W. * Blewett D. T. Capaccioni F. De Sanctis M. C. Garry W. B. Li J. Y. Marchi S. McCoy T. J. Nathues A. Petro N. E. Raymond C. A. Russell C. T. Schenk P. Scully J. E. C. Sunshine J. M. Williams D. A. Yingst R. A.
Dawn Observations of Marcia Crater, Vesta **[#2308]**
We present observations of geologic features associated with Marcia, a young, irregularly shaped crater ~70 km in diameter on Vesta.

1:45 p.m. Capaccioni F. De Sanctis M. C. * Ammannito E. Li J. Y. Longobardo A. Mittlefehldt D. W. Palomba E. Pieters C. M. Schroeder S. E. Tosi F. Hiesinger H. Blewett D. T. Russell C. T. Raymond C. A.
Spectral Characterization of Bright Materials on Vesta **[#2217]**
The surface of Vesta displays large geological and mineralogical variability; dark and bright areas are very diverse and often associated with specific geologic features. We report on the spectral characterization of the "bright areas."

2:00 p.m. Schroder S. E. * Li J.-Y. Mittlefehldt D. W. Pieters C. M. De Sanctis M. C. Hiesinger H. Blewett D. T. Russell C. T. Raymond C. A. Keller H. U.
Visible Color and Photometry of Bright Materials on Vesta **[#2459]**
We report a detailed investigation of visible color and photometric properties of the bright materials found on Vesta.

2:15 p.m. Li J.-Y. * Mittlefehldt D. W. Pieters C. M. De Sanctis M. C. Schroder S. E. Hiesinger H. Blewett D. T. Russell C. T. Raymond C. A. Keller H. U.
Investigating the Origin of Bright Materials on Vesta: Synthesis, Conclusions, and Implications **[#2381]**
We report the synthesis analysis and preliminary results to investigate the origin of relatively bright areas on Vesta.

2:30 p.m. Jaumann R. * Krohn K. McCord T. B. Williams D. A. Raymond C. A. Blewett D. T. Hiesinger H. Yingst R. A. Garry W. B. McSween H. Y. Denevi B. W. Palomba E. Roatsch T. Stephan K. Russell C. T.
Investigating the Origin of Dark Material on Vesta: Locations and Geological Context **[#1807]**
Deposits of dark material (DM) appear on Vesta's surface as lower-albedo features in the visible wavelength. DM are distributed unevenly and are often associated with impact craters as outcrops in walls and mass-wasting deposits as well as ejecta.

2:45 p.m. Reddy V. * Le Corre L. Nathues A. Cloutis E. A. Gaffey M. J. Becker K. J. McCord T. B. Combe J.-Ph. Palomba E. Blewett D. T. McSween H. Y. Jr. Raymond C. A. Williams D.
Investigating the Origin of Dark Material on Vesta Using Dawn Framing Camera **[#1587]**
We report first results from the origin and nature of enigmatic dark material on Vesta as observed by the Dawn Framing Camera. Laboratory spectral analysis of meteorites is used to pinpoint the source of this dark material on Vesta.

3:00 p.m. Palomba E. * Combe J.-Ph. McCord T. B. De Sanctis M. C. Ammannito E. Longobardo A. Tosi F. Capaccioni F. Blewett D. T. Jaumann R. McSween H. Raymond C. A. Reddy V. Williams D. Russell C. T. Dawn Team
Composition and Mineralogy of Dark Material Deposits on Vesta **[#1930]**
Unusual regions of very low albedo (DMD) on Vesta's surface were discovered by the Dawn mission.We present a catalogue of DMD detected by combining visible and IR images taken by the VIR instrument. We discuss their spectral behavior and composition.

3:15 p.m. McCord T. B. * Combe J.-Ph. Jaumann R. Palomba E. Reddy V. Blewett D. T. McSween H. Y. Jr. Raymond C. A. Williams D. Dawn Team
Dark Material on Vesta: Synthesis and Interpretations from Dawn Observations **[#1352]**
Dark material on Vesta is interpreted to be one of only two endmember materials, when mixed in various proportions, that are needed to model most of Vesta's surface. The material is likely from infall of carbonaceous chondrite material and from impact melt.

3:30 p.m. De Sanctis M. C. Nathues A. * Ammannito E. Capaccioni F. Frigeri A. Le Corre L. Jauman R. Palomba E. Pieters C. M. Reddy V. Stephan K. Tosi F. Yingst A. Zambon F. Barucci M. A. Blewett D. T. Capria M. T. Combe J.-Ph. Denevi B. W. Keller H. U. Marchi S. McCord T. B. McFadden L A. McSween H. Raymond C. A. Russell C. T. Sunshine J. Toplis M. Li J. Y.
First Mineralogical Maps of 4 Vesta **[#1902]**
FC color ratio data from Survey with a resolution of 250 m/pixel and VIR hyperspectral images from Approach and Survey with resolutions of 1300 and 700 m/pixel,respectively, provided information on surface mineralogical and lithologic distributions.

3:45 p.m. Capria M. T. * Tosi F. Capaccioni F. De Sanctis M. C. Palomba E. Ammannito E. Titus T. N. Combe J.-Ph. Toplis M. Sunshine J. Russell C. T. Raymond C. A.
Thermal Inertia Variations on the Surface of Vesta from the Dawn Data **[#1863]**
Temperature information has been obtained from the VIR spectra. When combined with a thermophysical model, these temperatures can be used to derive surface thermal properties, thus leading to the characterization of surface and regolith properties.

4:00 p.m. Capaccioni F. * Li J. Y. De Sanctis M. C. Ammannito E. Capria M. T. Carraro F. Fonte S. Frigeri A. Magni G. Palomba E. Longobardo A. Tosi F. Zambon F. Buratti B. J. Schroeder S. E. Hicks M. D. Reddy V. Nathues A. Hoffman M. Denevi B. W. Jorda L. Mottola S. Pieters C. Raymond C. A. Sykes M. V. Palmer E. Russell C. T. Titus T. N. Roatsch T. Mastrodemos N.
Analysis of Photometric Properties of the Vesta Surface Materials **[#2091]**
Analysis of band depth as a function of the phase angle show a clear positive correlation. This result, although supported by similar data from the Framing Camera, is intriguing as it is contrary to the expectations from radiative transfer theories.

4:15 p.m. Pieters C. M. * Blewett D. T. Gaffey M. Mittlefehldt D. W. De Sanctis M. C. Reddy V. Nathues A. Denevi B. W. Li J. Y. McCord T. B. Marchi S. Palmer E. E. Sunshine J. M. Ammannito E. Raymond C. A. Russell C. T.
Space Weathering on 4 Vesta: Processes and Products **[#1254]**
The presence of space weathering processes are evident at Vesta, but the character and form are controlled by the unique environment and geologic history of this small body.

4:30 p.m. Cartwright J. A. * Mittlefehldt D. W. Quinn J. E. Ott U.
The Continuing Quest for "Regolithic" Howardites **[#1211]**
We report the latest results from our noble gas analysis of howardites, to better establish the regolithic nature of these meteorites. Of our samples, at least one contains clear evidence for both solar wind and mixing with a planetary component.

YOUNG SOLAR SYSTEM CATACLYSM
Friday, 1:30 p.m. Waterway Ballroom 6

Chairs: Catherine Corrigan and Marc Norman

1:30 p.m. Norman M. D. * Nemchin A. A.
Heavy Bombardment of the Moon at ~4.2 Ga: Evidence from Ages of Lunar Melt Breccias and Zircons **[#1368]**
U-Pb ages of apatite and zirconalite in 67955 confirm an age of 4.2 Ga followed by a thermal overprint at 3.9 Ga. Lunar zircon ages imply episodic bombardment of the Moon between 3.8 and 4.4 Ga. Some lunar basins are likely older than 3.9 Ga.

1:45 p.m. Crow C. A. * McKeegan K. D. Gilmour J. D. Crowther S. A. Taylor D. J.
Are Apollo Zircons Witness to a Lunar Cataclysm? **[#1639]**
To investigate the proposed lunar cataclysm, we obtained preliminary U-Pu-Xe analyses for lunar zircons with Pb-Pb crystallization ages pre-dating the 3.9 Ga cataclysm. We find no contribution from ^{244}Pu and little or no contribution from ^{235}U.

2:00 p.m. Cohen B. A. *
The Vestal Cataclysm **[#1265]**
Heavy bombardment / Stoked the hearth of the goddess / Now frozen in time.

2:15 p.m. Abramov O. * Mojzsis S. J.
Modeling of Impact Ejecta Temperatures on the Earth and the Moon **[#2723]**
We model the thermal state of impact ejecta deposited on the surface to further understand the mechanism(s) behind impact-induced modifications of radiogenic systems. The ultimate aim of this work is to constrain the LHB duration and intensity.

2:30 p.m. Liu J. G. * Galenas M. G. Puchtel I. S. Walker R. J.
Late Heavy Bombardment of the Moon: Evidence from Os Isotope and Highly Siderophile Element Characteristics of Lunar Impact-Melt Breccias **[#2366]**
New HSE results for lunar impact melt breccias, in combination with previously published data, show the variable, chemical, and isotopic nature of impactors that contributed to basin-forming events on the Moon.

2:45 p.m. Robbins S. J. * Hynek B. M.
Impact History of Large Bolides at Mars: Implications for the Late-Heavy Bombardment and Isochron Uncertainties **[#1649]**
We have age dated 78 large craters and basins on Mars using multiple chronologies and found no evidence for a late heavy bombardment event since ~4.0 Ga on Mars. We also illustrate many of the internal disagreements between chronology systems.

3:00 p.m. Michael G. G. * Platz T. Kneissl T. Schmedemann N.
Planetary Surface Dating from Crater Size-Frequency Distribution Measurements: Spatial Randomness and Clustering **[#2486]**
We suggest the routine use of a spatial randomness analysis when making crater counts to ensure that the populations used for assessing ages or assessing the impactor flux are consistent with the uniformity and independence assumptions.

3:15 p.m. Richardson J. E. * Minton D. A. Thomas P. C. Kirchoff M.
Uncovering the Impactor Population for the Outer Solar System from Saturnian Satellite Cratering Records **[#2585]**
We use crater counts for seven saturnian satellites to constrain the outer solar system impactor population, showing the Kuiper Belt as the most likely source, and that impactor flux levels 2–3 decades higher than current are needed to model the records.

3:30 p.m. Minton D. A. * Richardson J. E. Thomas P. Kirchoff M. Schwamb M. E.
Combining Saturnian Craters and Kuiper Belt Observations to Build an Outer Solar System Impactor Size-Frequency Distribution **[#2669]**
Using Cassini mission imagery of the icy satellites of Saturn, numerical simulations, and telescopic observation data we produce a model size frequency distribution for outer solar system impactors spanning tens of meters to thousands of kilometers.

3:45 p.m. Nimmo F. * Korycansky D. G.
Impact-Driven Ice Loss in Outer Solar System Satellites: Consequences for the Late Heavy Bombardment **[#1580]**
The Nice model late heavy bombardment (LHB) was sufficient to completely strip Enceladus, Mimas, and Miranda of ice. Either these bodies formed after the LHB was complete, or the LHB delivered ~10 times less mass than the standard model.

4:00 p.m. *Panel Discussion*

PLANETARY INTERIORS: DYNAMICS AND DIFFERENTIATION
Friday, 1:30 p.m. Montgomery Ballroom

Chairs: Valerie Hillgren and Rajdeep Dasgupta

1:30 p.m. Kendall J. D. * Melosh H. J.
Fate of Iron Cores During Planetesimal Impacts **[#2699]**
Chemical equilibrium in the Earth's mantle depends critically on the emulsification of cores of impacting planetesimals. We show that the impact process greatly disperses cores and allows for greater emulsification.

1:45 p.m. Fei Y. * Zhang C.
Imaging Percolation During Core Formation by High-Resolution 3D Tomography **[#2242]**
We present a new imaging technique to visualize the distribution of liquid metal in silicate matrix in three-dimensions, providing a new way to investigate the efficiency of metal percolation in a real silicate mantle and core formation process.

2:00 p.m. Zhang Y. G. Yin Q.-Z. *
Light Elements in the Core and Degree of Chemical Equilibration During Core-Mantle Segregation: A Window Through First-Principles Molecular Dynamics **[#1360]**
We use first-principles molecular dynamics to calculate light-element contents in the core and gauge the degree of chemical equilibrium between metallic core and silicate mantle during accretion using light-element contents as the constraint.

2:15 p.m. Roskosz M. * Bouhifd M. A. Jephcoat A. P. Marty B. Mysen B. O.
Nitrogen Solubility in Molten Metal and Silicate at High Pressure and Temperature: A First Experimental Approach **[#1497]**
Nitrogen solubility is studied up to 18 GPa on a mixture of molten Fe-bearing silicates and Fe-Ni metal alloy. Nitrogen depletion relative to other volatiles can be accomplished by a moderately efficient segregation into the core-forming material.

2:30 p.m. Hillgren V. J. * Fei Y.
The Partitioning of Si Between Metal and Silicate: Implications for Planetary Cores **[#2886]**
We experimentally examine the the partitioning of Si between metal and silicate. We apply the results to the core of Mercury.

2:45 p.m. Shahar A. * Kaufman L. A. Horan M. F. Mock T. D. Deng L. Macris C. A.
Iron Isotope Fractionation During Planetary Differentiation **[#2049]**
Experiments at high pressure and temperature reveal an iron isotopic fractionation between metal and silicate, where the metal is more enriched in $^{57}Fe/^{54}Fe$. This result agrees with the direction of fractionation seen in pallasites.

3:00 p.m. Dasgupta R. * Chi H. Shimizu N. Buono A. Walker D.
Carbon Cycling in Shallow Magma Oceans of Terrestrial Planets Constrained by High P-T Experiments **[#1767]**
High-pressure-temperature experiments are performed to constrain the solubility, speciation,and partitioning of carbon between metallic and silicate liquid in a magma ocean environment. We discuss the role of magma ocean processes on the deep C-cycle.

3:15 p.m. Li J. * Liu J. Chen B. Li Z. Wang Y.
Chemical Convection in the Lunar Core from Melting Experiments on the Iron-Sulfur System **[#2474]**
Experimental results on the liquidus curve of the Fe-S system at the pressures of the lunar core provide constraints on the Moon's thermal and chemical states and the role of chemical convection in the origin of early lunar core dynamo.

3:30 p.m. Jing Z. * Wang Y. Yu T. Sakamaki T. Kono Y. Park C.
Density and Sound Velocity of Iron-Sulfur Alloying Liquids at High Pressures and Implications to Planetary Cores **[#2813]**
We determine the density and sound velocity of Fe-S liquids at high P-T conditions up to 8 GPa and 2173 K. The results can be compared with geophysical observations to constrain the composition and structure of the cores of Moon and Mercury.

3:45 p.m. Yu G. * Jacobsen S. B.
Core Formation Memory of Siderophile Elements in Earth and Mars **[#1573]**
We define a concept-core formation memory of a siderophile element as to how far back in a planet's core formation history the current mantle content of the element can record. The memories of siderophile elements in Earth and Mars are reported.

4:00 p.m. Righter K. * Humayun M.
Volatile Siderophile Elements in Shergottites: Constraints on Core Formation and Magmatic Degassing **[#2465]**
A suite of martian shergottites has been analyzed for 73 elements. We focus on the volatile siderophile elements, derive martian mantle abundances, and evaluate early differentiation scenarios for Mars.

4:15 p.m. Touboul M. * Liu J. G. O'Neil J. Puchtel I. S. Walker R. J.
Time Constraints on Late Accretion to the Earth and Moon, and New Evidence for Early Mantle Differentiation Derived from Coupled Investigations of W and Os Isotope Compositions **[#1923]**
We report ^{182}W excesses in ~4.2-Ga-old rocks from the Nuvvuagittuq greenstone belt. Combined with HSE and ^{142}Nd data, these isotopic anomalies indicate differentiation of Earth's mantle earlier than the giant impact and the formation of the Moon.

4:30 p.m. Jacobsen S. B. * Yu G.
Extinct Isotope Heterogeneities in the Mantles of Earth and Mars: Implications for Mantle Stirring Rates **[#2210]**
On the basis of both extinct (^{182}Hf-^{182}W and ^{146}Sm-^{142}Nd) and long-lived (Sr and Nd) isotope systems we have shown that the mantles of Earth and Mars exhibit substantially different mixing or stirring rates (~500 m.y. and 2000 m.y., respectively).

TUE POSTERS

POSTER SESSION I
Tuesday, 6:00 p.m. Town Center Exhibit Area

SOLAR NEBULA MIXING AND CAIS

Yamada K. Inaba S.
On Low-Mass Planetary Migration in an Optically Thick Disk **[#1126]**
A protoplanet embedded in a gas disk experiences a torque from the disk that generally changes its orbit elements. We numerically examine the torque exerted on a planet by an optically thick accretion disk for various values of the opacity and the accretion rate.

Pascussi I. Apai D.
Stellar-Mass-Dependent Evolution of Planet Forming Disks **[#1244]**
We present new and archival observational data demonstrating that disk evolution is stellar-mass-dependent. We discuss the implications of this finding for the formation of giant and terrestrial planets around stars of different masses.

Fujita T. Ohtsuki K. Tanigawa T.
Capture of Planetesimals by Circumplanetary Disks **[#1378]**
We examine orbital evolution of planetesimals approaching a growing giant planet with a circumplanetary disk by integrating Hill's equation including the gas drag term, and evaluate the capture probability.

Suetsugu R. Ohtsuki K.
Global Orbital Integration for Temporary Capture of Planetesimals by a Giant Planet: Implication for Their Source Region **[#1157]**
We use a three-body system that consists of the Sun, a planet, and a test particle, and perform global orbital integration to examine effects of a high-mass planet on temporary capture.

Perry J. Kimery J. Matthews L. S. Hyde T. W.
Effects of Monomer Shape on the Formation of Fractal Aggregates Under a Power Law Distribution **[#2615]**
Studies modeling the coagulation of dust particles typically assume spherical monomers, which may not always be valid. This work compares morphologies of aggregates built from spherical monomers as well as prolate and oblate ellipsoidal monomers.

Kropf A. Libourel G.
Condensation Processes in the Early Solar Nebula — Experimental Approaches **[#1920]**
We present a new technical setup to study high-T/low-P condensation from a gas under early solar nebula conditions in order to get an experimental condensation sequence and an experimental proxy of the young stellar environment.

Archer G. J. Walker R. J.
Highly Siderophile Element and Rhenium-Osmium Isotope Systematics of Calcium-Aluminum Rich Inclusions: Evidence for Early Solar System Properties and Processes **[#2379]**
Highly siderophile element abundances and Re-Os isotope systematics were determined for six Allende CAIs. HSE abundances were consistent with previously published results for these CAIs. Several CAIs plot off a primordial Re-Os isochron.

Williams C. D. Wadhwa M. Janney P. E. Hines R. R. Bullock E. S. MacPherson G. J.
The Measurement of Titanium Isotopic Compositions of Allende Refractory Inclusions by LA-MC-ICPMS **[#2523]**
We report on the in situ measurement of titanium isotope ratios by LA-MC-ICPMS in nine Allende CAIs. Matrix-matched glass standards were synthesized and used for the correction of matrix-effects and isobaric interferences.

Haring M. M.   Flemming R. L.   Terskikh V.   Grossman L.   Simon S. B.
Crystal Structure and Cation Ordering in Fassaite from Type B CAI TS62B in Allende CV3 **[#2601]**
We report cation ordering data of fassaite from Allende Type B TS62B by ^{29}Si and ^{27}Al Magic Angle Spinning (MAS) and triple quantum (3Q) MAS Nuclear Magnetic Resonance spectroscopy. This is the first such data reported for meteoritic fassaite.

Hamilton V. E.   Connolly H. C. Jr.
In Situ Microspectroscopy of a Type B CAI in Allende: Mineral Identification in Petrographic Context **[#2495]**
We show that IR µ-spectroscopy (7–25 µm) offers a powerful approach to identifying and mapping the distribution of individual minerals in meteorites at the 50-µm scale, avoiding the loss of petrographic context that occurs with powdered preparations.

Chizmadia L. J.   Bravo-Ruiz H.
QUE97416 and A-88882094, Two CO3 Breccias: Evidence from Petrologic Subtypes Determined from Amoeboid Olivine Inclusions **[#2918]**
AOIs in QUE 97416 and Asuka -882094 have differing ratios of Fe:Mg olivine which seems to indicate a range of subtypes from 3.2 to 3.6. This can be best explained if these meteorites are brecciated representatives of the CO3 parent body asteroid.

Ivanova M. A.   Ivanov A. V.   Lorenz C. A.   MacPherson G. J.
An Unusual Type B2 CAI and a P-Ca-Rich Clast from Kaidun **[#2262]**
We report results on petrology, mineral chemistry, and bulk composition of one Kaidun sample, #A3-9, a rare CAI that encloses an unusual P,Ca-rich object of unclear origin.

Han J.   Brearley A. J.
Microstructural Observations of Spinel-Pyroxene Refractory Inclusions from the ALHA 77307 CO3.0 Carbonaceous Chondrite: Comparison with CAI-Like Objects in an Amoeboid Olivine Aggregate **[#1324]**
We report TEM observations of CAIs from the ALHA 77307 CO3.0 chondrite and discuss their origin and thermal histories. Additionally, we compare these observations with those from refractory CAI-like objects in an AOA.

Han J.   Brearley A. J.
The Microstructure and Microchemistry of Amoeboid Olivine Aggregates from the ALHA 77307 CO3.0 Carbonaceous Chondrite: Constraints on Formation and Thermal Histories **[#1323]**
We present new microstructural and microchemical observations obtained by TEM on olivine and refractory Ca-Al-rich phases in AOAs from the ALHA 77307 CO3.0 chondrite and discuss their implications for the formation and thermal histories of the AOAs.

CHONDRULE FORMATION AND DISK CHEMISTRY

Luu T.-H.   Chaussidon M.   Birck J.-L.
Mg Isotopic Constraints on the Origin of Mg-Rich Olivines in Allende Matrix and Porphyritic Type I Chondrules **[#2201]**
Mg-rich olivines from Allende (CV3.2) were analyzed for their O- and Mg-isotopic compositions using ion microprobes. The goal of the present study is to put some new constraints on the origin of these objects, which remains an open question.

Ingalls S. C.   Young E. D.   Gounelle M.
Do Magnesium Isotope Systematics of Al-Rrich Chondrules Offer Insights into the History of Chondrule Formation in General? **[#2665]**
We describe new magnesium isotope data for Al-rich chondrules from Allende and Krymka. Results suggest these objects may provide important new constraints on chondrule formation in general.

TUE POSTERS

Miura H. Tsukamoto K.
Numerical Simulation of Solidification of Chondrules: Formation of Olivine Bars in Mg_2SiO_4-Fe_2SiO_4 System **[#1715]**
We numerically simulated formation of olivine bars observed in barred olivine chondrules. The parallel set of bars was reproduced from a platy seed crystal by morphological instability. The calculated Mg/Fe zoning is compared with experiments.

Dwyer C. A. Nimmo F. Asphaug E.
A Physical Model for Simultaneous Production of CH and CB Chondrules During an Impact Event **[#2291]**
We present a physical, analytical model for determining impactor diameter and velocity of impact events capable of simultaneously generating CH chondrules (modeled to be vapor condensates) and CB chondrules (modeled to be melt droplets).

Rocha S. E. Jones R. H.
An Experimental Study of the Conditions of Type II Chondrule Formation in Ordinary Chondrites **[#2595]**
We report experiments that reproduce type II chondrule textures at slow cooling rates. Since plagioclase is not observed in type II chondrules, the conditions under which plagioclase crystallizes place a lower limit on chondrule cooling rates.

Marrocchi Y. Libourel G.
Evidence of High-Temperature Formation of Sulfide Phases of Chondrules **[#1386]**
We report a systematic petrographic and mineralogical study of sulfides in type I chondrules of the carbonaceous chondrite Vigarano (CV3). Our results suggest that sulfides were inherited from the high-temperature chondrule-forming event.

Bigolski J. N. Weisberg M. K. Connolly H. C. Jr. Ebel D. S.
Microchondrule-Bearing, Iron-Rich Chondrule Rims in Northwest Africa 5717 **[#2426]**
Observations of the ungrouped chondrite Northwest Africa 5717 reveal a preponderance of microchondrules, along with mineral and lithic fragments, within Fe-rich rims that surround host chondrules, providing new insight into accretionary processes.

Dobrică E. Brearley A. J.
Glassy Vesiculated Microchondrule-Like Spherules in the Matrix of Unequilibrated Ordinary Chondrites **[#2197]**
In the matrix of UOCs (MET 00526 and Semarkona) we have identified a number of glassy vesiculated microchondrule-like spherules. Their distinct texture and chemical compositions suggest that they were formed by extremely rapid heating and cooling.

Lehner S. W. Petaev M. I. Buseck P. R.
Relation Between Silicate Chondrules and Metal-Sulfide Nodules in EH3 Chondrites **[#2252]**
We compare the composition of sulfides in MSN and chondrules, report spheroidal aggregates of silicates, silica, metal, and sulfides, and the variation in the abundance of opaque and non-opaque minerals comprising MSN and silicate chondrules.

Feng L. ElGoresy A. Zhang J. Hao J. Boyet M. Yang L.
Excess ^{36}S in Lawrencite and Nitrogen Isotopic Compositions of Sinoite from Almahata Sitta MS-17 EL3 Chondrite Fragment **[#1766]**
Excess ^{36}S in lawrencite and N isotopes in sinoite from an EL3 fragment of Almahata Sitta were analyzed by NanoSIMS 50L. The isotopic compositions provide information on the formation and evolution processes of the early solar system and Earth.

Das J. P. Meshik A. P. Pravdivtseva O. Hohengberg C. M.
Trapped Noble Gases in Magnetic and Non-Magnetic Separates from Allende Chondrules: Clues for Noble Gas Fractionation during Chondrule Formation **[#2346]**
Magnetic (M) and non-magnetic (NM) phases were separated from big and small chondrules from Allende. M phases carry higher trapped noble gases, suggesting fractionation of noble gas during chondrule formation. Also, big chondrules are less homogenized.

Beyersdorf-Kuis U. Trieloff M. Cartwright J. A. Bennett J. Ott U.
Cosmogenic Noble Gases in Single Chondrules from CV and CR Chondrites **[#1763]**
We present noble gas data from single chondrules and associated matrix to look for evidence of pre-irradiation. Our data suggest a pre-irradiation of Vigarano and El Djouf 001 chondrules.

Huber L. Metzler K. Maden C. Vogel N. Wieler R.
Cosmic Ray Irradiation History of Individual Murchison Chondrules Analyzed by UV-Laser Ablation **[#1420]**
We analyzed noble gases of Murchison chondrules with in situ laser ablation to investigate the position of pre-irradiated chondrules in respect to primary rock fragments and lithic clasts.

EARLY SOLAR SYSTEM CHRONOLOGY

Marhas K. K. Randhawa J. S.
Production of Short Lived Radionuclides: Late-Stage Irradiation in the Early Solar System **[#2410]**
Production of short-lived radionuclides, ^{26}Al, ^{36}Cl, and ^{10}Be in late irradiation scenario at asteroidal distances with target material of sodalite composition.

Meyer B. S. Yu T.
Dynamical Weak Statistical Equilibrium and the Neutron-Rich Iron-Group Isotopes **[#2727]**
Calcium-48 has substantial production in expansions of low-entropy matter, which probably occurs in dense thermonuclear supernovae. We explore the weak statistical equilibrium in such environments to constrain their neutron richness.

Yu T. Meyer B. S.
On Production of Neutron-Rich Iron-Group Isotopes in Simple Models of Dense Thermonuclear Supernovae **[#2293]**
We presented a simple thermonuclear (Type Ia) supernovae model that shows for high initial density (low entropy) most of the yield would be neutron-rich iron-group isotopes. This may help to explain the excesses and deficits correlation in FUN CAIs.

Bowers M. Collon P. Kashiv Y. Lu W.
^{33}S(α,p)^{36}Cl Cross Section Measurement for Production in the Early Solar System **[#1700]**
The ^{33}S(α,p) ^{36}Cl reaction is one of the most important for the creation of ^{36}Cl in the early solar system. We measured the averaged reaction cross section in the energy range 1.84–2.04 MeV/A.

Bricker G. E. Jr. Caffee M. W.
Incorporation of ^{7}Be, ^{10}Be, ^{14}C, ^{26}Al, ^{36}Cl, ^{41}Ca, and ^{53}Mn into Early Solar System Materials in the Solar Wind Implantation Model **[#1599]**
We consider the short-lived radionuclides ^{7}Be, ^{10}Be, ^{14}C, ^{26}Al, ^{36}Cl, ^{41}Ca, and ^{53}Mn in calcium-aluminum-inclusions (CAIs) in primitive meteorites in accordance with a solar wind implantation model.

Blinova A. Alexander C. M. O'D. Wang J. Herd C. D. K.
Mineralogy and Mn-Cr Extinct Radionuclide Dating of a Dolomite from the Pristine Tagish Lake Meteorite **[#1188]**
We present Mn-Cr data for a large carbonate grain found in pristine Tagish Lake meteorite. These data give us insights into the timing of alteration on the Tagish Lake parent body.

Englert P.
^{53}Mn and Cosmic Ray Track Production Rates: Contributions of Exposure Histories of Djermaia and Lost City **[#1729]**
A ^{53}Mn CRT relationship is presented as a useful tool for the analysis shielding depth, preatmospheric size, and exposure history of meteorites.

TUE POSTERS

Jörg G. Amelin Y. Kossert K. v. Gostomski C. L.
Direct Determination of the Half-Life of ^{41}Ca **[#1757]**
The half-life of ^{41}Ca is determined at 9937 ± 146 years using double spike isotope dilution TIMS, and liquid scintillation counting using triple-to-double coincidence ratio method on a radiochemically pure, carrier-free ^{41}Ca.

Marks N. E. Borg L. E. Hutcheon I. D. Jacobsen B. Clayton R. N. Mayeda T. K.
Temporal and Spatial Heterogeneities in the Solar Nebula Reflected in Rb-Sr and Sm-Nd Systematics of Al3S4, an Allende Type B CAI **[#2259]**
We have measured the Rb-Sr, ^{174}Sm-^{143}Nd and ^{147}Sm-^{142}Nd isotope compositions of a type B CAI. These data indicate that CAIs and Earth have the same ^{142}Nd/^{144}Nd composition and that carbonaceous chondrites are distinct from both Earth and CAIs.

Ito M.
THE JAMSTEC NanoSIMS 50L Ion Microprobe: Applications to Earth, Planetary and Life Sciences **[#1752]**
The JAMSTEC NanoSIMS 50L has been installed at Kochi Institute for Core Sample Research end of 2011. We will investigate variety of samples from extraterrestrial, terrestrial, and biology samples. Some initial isotopic measurements will be presented.

Liu M.-C. Chaussidon M.
Calcium-41 Revisited: Development of Potassium Isotope Mass Spectrometry on CAMECA 1280HR2 **[#1890]**
We developed mass spectrometry on CAMECA 1280HR2 to measure the potassium-isotopic compositions of CAIs in hopes of confirming the existence and initial abundance of ^{41}Ca in the early solar system.

Kööp L. Davis D. W.
Classification and U-Pb Isotopic Study of Northwest Africa 6514 **[#2066]**
In addition to results from a U-Pb isotopic study of different components of ordinary chondrite NWA 6514 by laser ablation inductively coupled plasma mass spectrometry, we present a petrographic description and the classification of this meteorite.

Tissot F. L. H. Dauphas N.
^{238}U/^{235}U Ratios of Anagrams: Angrites and Granites **[#1981]**
We report ^{238}U/^{235}U ratios of five angrites and give the corresponding Pb-Pb ages of D'Orbigny and Angra Dos Reis. The U-isotopic composition of terrestrial granites (I, S, and A types) is also assessed to determine the influence of the protolith.

Burnett D. S. Paque J. M. Beckett J. R. Guan Y.
On the Origin of Li Isotopic Variations in Ca-Al-Rich Inclusions (CAIs) **[#2159]**
Li isotopes in relatively unaltered CAIs show that the incorporation of Li occurred subsequent to evaporation event(s), and occurred independently of whatever process produced ^{16}O-poor melilite in most CAIs. No evidence for in situ ^{7}Be is found.

Van Orman J. A. Cherniak D. J. Kita N. T.
Magnesium Diffusion in Plagioclase **[#1467]**
We present experimental data showing that Mg diffusion increases systematically with decreasing anorthite content. Mg diffusion in An23 is two orders of magnitude faster than in pure anorthite, and the closure temperature is more than 100 K lower.

Ireland T. J. Dauphas N. Tissot F. L. H.
Development of an Automated All-Teflon HPLC System for the Analysis of Precious Geological and Extraterrestrial Materials **[#2141]**
We outline the development and progress toward building an automated all-Teflon HPLC system for the analysis of precious geological and extraterrestrial samples. Our system has several traits that distinguish it from traditional column setups.

CHEMICAL PROCESSES IN THE SOLAR NEBULA AND LATEST GENESIS RESULTS

Yamada A. Nanbu S. Ozima M.
Quantum Chemical Calculations on Photo-Dissociation of CO: $E^1\Pi \leftarrow X^1\Sigma^+$ with Non-Adiabatic Transition **[#2714]**
We report fractionation factors using calculated cross section for photo-dissociation of CO isotopologues by using quantum chemical calculations.

Wirström E. S. Charnley S. B. Geppert W. D. Persson C. M.
Observations of Carbon Isotopic Fractionation in Interstellar Formaldehyde **[#1611]**
While solar system organics exhibit small fluctuations in $\delta^{13}C$ as compared to $\delta^{15}N$ and δD, an interstellar origin cannot be excluded. This study off ^{13}C fractionation in the cold, dense ISM reveals an enrichment in H_2CO that remains to be explained.

Contreras C. S. Salama F.
Laboratory Simulation of the Formation and Destruction Processes of Extraterrestrial Carbonaceous Materials **[#2853]**
Experimental mass spectral studies of the formation of PAHs under conditions that simulate circumstellar and interstellar mediums.

Lyons J. R.
Isotope Signatures in Organics due to CO and N_2 Self-Shielding **[#2858]**
CO and N_2 self-shielding models are used to predict enrichments in simple organic compounds. Methanol and formaldehyde are both depleted in ^{17}O due to formation from CO. HCN is enriched in ^{15}N due to formation from N_2.

Rodriguez M. C. Allton J. H. Burkett P. J.
Using Image Pro Plus Software to Develop Particle Mapping on Genesis Solar Wind Collector Surfaces **[#2750]**
The Genesis curatorial facility at JSC provides optical analysis of collector array surfaces as cleaning steps progress in an updated master cleaning plan coordinated by the Genesis mission PI Don Burnett.

Schmeling M. Burnett D. S. Choi Y. Eng P. J. Stubbs D. E. Tripa C. E. Veryovkin I. V.
Study of Genesis Solar Wind Samples by Laboratory Based Total Reflection X-Ray Fluorescence Spectrometry and Synchrotron Based Grazing Incidence X-Ray Fluorescecence **[#2209]**
Genesis solar wind samples were analyzed by TXRF and GI-XRF for evaluation of cleaning procedures and discrimation between surface contamination and solar wind.

Baryshev S. V. Zinovev A. V. Tripa C. E. Pellin M. J. Burnett D. S. Veryovkin I. V.
Fine Structure of Near-Surface Solar Wind Depth Profile by SNMS/SEM Imaging **[#2909]**
In this work, we report results of Genesis Si coupons investigations conducted by laser post-ionization secondary neutral mass spectrometry (LPI SNMS) based on dual beam depth profiling with low energy normal incidence sputtering (lenisDB).

Wiens R. C. Olinger C. T. Reisenfeld D. B. Heber V. Burnett D. S.
Ion Trajectory Simulations of the Genesis Solar Wind Concentrator: Li, C, Mg, S **[#1369]**
The Genesis Solar Wind Concentrator may be used to analyze Li, C, Mg, and S isotopes. We have performed ion trajectory simulations to determine instrumental fractionation for these elements.

Heber V. S. Jurewicz A. J. G. Janney P. Wadhwa M. McKeegan K. D. Burnett D. S.
Magnesium Isotopic Composition of Solar Wind as Test for Sun-Solar Wind Isotopic Fractionation: A Progress Report **[#2921]**
We present preliminary data on the solar wind Mg isotopic composition in Genesis collectors to quantify the isotopic fractionation between solar wind and the Sun's photosphere.

Wimpenny J.   Yin Q. Z.   Burnett D. S.   Jurewicz A. J. G.   Woolum D. S.
Measuring the Mg Fluence of the Solar Wind Using LA-ICP-MS Depth Profiling **[#1857]**
We investigate the Mg fluence in the solar wind by analysing Genesis flight samples by LA-ICP-MS. This technique allows us to depth profile slowly through the silicon or sapphire samples, and to measure a wide range of elements very rapidly.

Veryovkin I. V.   Baryshev S. V.   Burnett D. S.   Pellin M. J.   Tripa C. E.   Zinovev A. V.
Dual Beam Sputter Depth Profiling of Genesis Solar Wind Collectors by RIMS **[#2296]**
We achieved a breakthrough in accuracy of the RIMS method applied to analyses of Genesis solar wind (SW) samples. For the first time, we measured depth profiles of Mg, Ca, and Cr corresponding to different SW regimes and determined their fluences.

Veryovkin I. V.   Baryshev S. V.   Becker N. G.   Burnett D. S.   Choi Y.   Eng P. J.   Stubbs J. E.   Schmeling M.   Toyoda N.   Tripa C. E.   Yamada I.   Zinovev A. V.
Cleaning Genesis Samples with Gas Cluster Ion Beams: Method Evaluation by Comparative Studies with RIMS, GI-XRF and Other Surface Characterization Techniques **[#2732]**
We conducted concerted and all-rounded evaluation of the efficiency of Gas Cluster Ion Beam technology applied to cleaning of contaminated surfaces of Genesis Solar Wind samples. We compared results obtained with RIMS, GI-XRF and other techniques.

CHONDRITE COMPONENTS AND PRIMARY PROCESSES

Kebukawa Y.   Cody G. D.
Deuterium-Hydrogen Exchange Kinetics: Implications for Early Chemical Evolution of Chondritic Insoluble Organic Matter **[#1034]**
We report D-H exchange kinetics obtained using laboratory synthesized organic polymers, in order to evaluate the D-H exchange between D enriched organic polymers and D depleted water. Our results explain well the known chondritic δD values.

Gasda P. J.   Taylor G. J.
The Distribution of Organic Carbon in CR2 Chondrite EET 92161 **[#1677]**
We present Raman spectral maps of EET 92161 CR2 chondrite to understand the distribution and petrographic context of organics in carbonaceous chondrites to learn how these compounds are affected by aqueous alteration on meteorite parent bodies.

Peeters Z.   Changela H.   Stroud R. M.   Alexander C. M. O'D.   Nittler L. R.
Coordinated Analysis of In Situ Organic Material in the CR Chondrite QUE 99177 **[#2612]**
We report the results of a coordinated analysis of several FIB lift-out sections by XANES, TEM and nanoSIMS, investigating the chemical, structural, and isotopic nature of in situ organic matter in QUE 99177.

Okabayashi S.   Yokoyama T.   Hirata T.
Iron Isotopic Signature for Fe-Ni Metal of Ordinary Chondrite Using Newly Developed Technique; LAL-MC-ICPMS **[#1871]**
Fe-isotopic compositions of Fe-Ni metals in ordinary chondrites were measured using laser ablation in liquid (LAL)-MC-ICPMS technique. We found that Fe-Ni metals in H chondrites have slightly lighter Fe-isotopic signature than L and LL chondrites.

Petaev M. I.   Lehner S. W.   Buseck P. R.
Chemical Fractionation During Processing of Silicates in S-Rich Systems: Implications for the Origin of Enstatite Chondrites **[#2229]**
We review physicochemical conditions of silicate sulfidation in EH chondrites that resulted in chemical fractionations of major elements relevant to the origin and chemical compositions of enstatite chondrites.

Lehner S. W.   Petaev M. I.   Buseck P. R.
Sulfidation of Enstatite in the Fine-Grained Matrix of EH3 Sahara 97072 **[#2309]**
We report TEM results of a S-enriched area where niningerite and silica occur surrounded by enstatite. The mineralogy and chemistry can be explained by reaction of enstatite and FeNi metal with S_2 and CO gas at ~1000 and –1100K.

Varela M. E.   Zinner E.
Silica-Rich Objects in Acfer 128: A SIMS Study **[#1405]**
We report the results of major- and trace-element studies of some silica-bearing objects in Acfer 182.

Parai R.   Huang S.   Jacobsen S. B.
Precise Determination of Calcium Isotope Variations in Meteoritic and Planetary Materials **[#1625]**
Large mass-dependent Ca-isotope effects have been found in planetary materials. We use a Monte Carlo model to explore the precision and accuracy of Ca double spike techniques that are used to correct for mass-dependent fractionation during analysis.

Kaltenbach A.   Stirling C. H.   Amelin Y.
Uranium Isotopic Composition of Carbonaceous Chondrites **[#1691]**
We present uranium isotope and concentration data of 12 carbonaceous chondrites, analyzed by MC-ICPMS.Minor variations in the $^{238}U/^{235}U$ ratios are detected, showing that it is necessary for a reliable Pb-Pb chronology to analyze U and Pb isotopes.

Fukami Y.   Yokoyama T.
Tellurium Isotope Anomalies in Carbonaceous Chondrites: Results for Sequential Acid Leaching Experiments **[#1861]**
We present preliminary data of Te-isotopic compositions in acid leachates of the Murchison meteorite (CM2) measured by N-TIMS. No isotope anomalies were found in all leachates but one that potentially shows depletion of *s*-process Te.

Crowther S. A.   Filtness M. J.   Gilmour J. D.
Pathways of Iodine and Xenon into Terrestrial Planets **[#1919]**
Our understanding of the behaviour of halogens and noble gases on planetesimals is limited. We focus on the I-Xe systematics of primitive meteorites, seeking to understand their incorporation into and subsequent processing on planetesimals.

Isa J.   Rubin A. E.   Wasson J. T.
Bulk Compositions of CV and CK Chondrites: Support for a Close Relationship **[#2809]**
The CV and CK chondrites do not seem to be separate groups; they may have originated in the same asteroidal parent body.

Teplyakova S. N.   Humayun M.   Lorenz C. A.   Ivanova M. A.
A Common Parent for IIE Iron Meteorite and H Chondrites **[#1130]**
We report new siderophile element abundances for the metal in the IIE irons — Watson, Tobychan, Elga, Verkhne Dnieprovsk, and Miles — to examine the possible genetic relations between IIE metal and H chondritic precursors.

Humayun M.   Weisberg M. K.
A Possible Ordinary Chondrite Affinity for Metal from the Unique Chondrite NWA 5492 **[#1458]**
NWA 5492 metal is compositionally similar to that from the unique chondrite GRO 95551, and both are linked to H-chondrite siderophile-element composition despite the more extreme state of reduction in NWA 5492.

Ebihara M.   Sekimoto S.   Shirai N.   Nakamura T.   Tsuchiyama A.   Abe M.   Fujimura A.
Mukai T.   Yada T.
Neutron Activation Analysis of Rocky Grains Recovered by the Hayabusa Spacecraft — Revisited **[#1986]**
Two additional small rocky grains recovered by the Hayabusa spacecraft were analyzed by instrumental neutron activation analysis. These grains were shown to be chondritic in elemental composition.

Nagano T. Tsuchiyama A. Shimobayashi N. Seto Y. Noguchi R. Imai Y. Matsumoto T. Matsuno J.
Homogeneity of LL5 and LL6 Chondrites in Relation to Hayabusa Sample Analysis **[#2500]**
Statistical analysis of LL chondrite textures shows that difference between the mineral abundance of Itokawa samples from that of LL chondrites is due to errors of a small amount of samples, and Itokawa surface material is consistent with LL chondrites.

Monnereau M. Toplis M. J. Baratoux D. Guignard J.
Thermal Constraints on the Time and Duration of Accretion of the H-Chondrite Parent Body **[#2046]**
Thermal evolution of the H-chondrite parent body is modeled and compared to available thermochronological constraints, with a focus on the effects of non-instantaneous accretion. Results point to accretion times that are unlikely to be >0.5 m.y.

Melanson D. Samson C. Herd R. K. Fry C. McCausland P. J. A. Umoh J. Holdsworth D. W.
X-Ray Micro-Computed Tomography Imaging of the Buzzard Coulee Chondrite **[#1506]**
This abstract outlines research and some results of X-ray micro-computed tomography imaging of the Buzzard Coulee H4 chondrite. A comparison of bulk density results and an analysis of radio-density profile curves are discussed.

Christoffersen P. A. Simon J. I. Ross D. K. Friedrich J. M. Cuzzi J. N.
Particle Size Distributions Obtained Through Unfolding 2D Sections: Towards Accurate Distributions of Nebular Solids in the Allende Meteorite **[#2058]**
Nebular components of Allende were characterized using high-resolution X-ray maps. Data were processed by matrix inversion to transform two-dimensional particle section areas into volumes. The algorithm was calibrated on the particle size standard NIST 1019b.

Lunning N. G. Corrigan C. M. Welzenbach L. C. McCoy T. J.
Using Immersion Oils to Classify Equilibrated Ordinary Chondrites from Antarctica **[#1566]**
This abstract describes the oil immersion method used at the Smithsonian Institution to classify the equilibrated ordinary chondrites in the U.S. Antarctic Meteorite collection.

ACHONDRITES: FROM CORE TO CRUST

McDermott K. H. Greenwood R. C. Franchi I. A. Anand M. Scott E. R. D.
The IIE Iron Meteorite Family Tree: A Study of the Petrography and Oxygen Isotopes of the Non-Magmatic Group **[#1799]**
Petrographic and isotopic analysis have shown three distinct relationships exist between the ordinary chondrites and IIE silicates, expanding our concept of the parent body and the thermal history it encountered.

Van Roosbroek N. Goderis S. Debaille V. Valley J. W. Claeys Ph.
Formation of the Mont Dieu IIE Non Magmatic Iron Meteorite, and Origin of its Silicate Inclusions **[#1773]**
Mont Dieu is an IIE nonmagmatic iron meteorite showing primitive features such as preserved chondrules and glass. SEM and geochemical analyses demonstrate that it most likely originated from an H-chondrite parent body impacted by a Fe-Ni projectile.

Winfield T. B. Goldstein J. I. Scott E. R. D.
Cooling Rate Estimates for IAB and IIICD Iron Meteorites **[#1307]**
The scanning electron microscope was used to measure the size of the high-Ni island phase in 10 members of groups IAB and IIICD iron meteorites. These size measurements were used to determine the relative cooling rates of these meteorites.

Dietderich J. E.   Walker R. J.
Modeling Fractional Crystallization of Group IIAB Iron Meteorites **[#1195]**
This research examined the abundances of highly siderophile elements present in group IIAB iron meteorites. A model of fractional crystallization was developed to account for variations of concentrations for Re, Os, Ir, Ru, Pt, and Pd.

Worsham E. A.   Walker R. J.   Corrigan C. M.   McCoy T. J.
The Tishomingo Iron Meteorite and a Possible Genetic Link to Group IVB Iron Meteorites — Evidence from Molybdenum Isotopes **[#2678]**
Using Mo isotopes to support or reject a genetic link between the ungrouped iron meteorite Tishomingo and the IVB iron meteorite group is explored. Implications of the possible relationship for the evolution of the IVB parent body are also outlined.

Campbell T. J.   Humayun M.
Siderophile Element Abundances in the Ni-Rich Ataxites Gebel Kamil, Dumont and Tinnie **[#2833]**
New siderophile element abundances are reported for Gebel Kamil (ungrouped) and the IVB irons Tinnie and Dumont.

Fry C.   Samson C.   McCausland P. J. A.   Herd R. K.
3D Laser Imaging of Iron Meteorites **[#2703]**
Seven fragments of four different iron meteorites have been imaged in 3D with a laser camera, to produce volumetrically accurate models. From this, iron meteorite density can be readily measured.

Arai T.   Kasuga T.   Otsuka K.
Mm-Cm Scale Chemical Heterogeneity of Partially-Molten Planetismals: Evidences from Meteorites and Meteors **[#2932]**
Studies of primitive achondrites and observation of meteors indicate mm-cm scale chemical heterogeneity induced by partial melting on planetismals.

Ness P. K.   Miyamoto H.
Possible Under-Sampling of Meteorites Inferred from a New Database of Meteorite and Terrestrial Rock **[#1388]**
Whole classes of meteorites seem to have no asteroid counterpart and vice versa. To determine if any meteorites types could be undersampled, we compiled meteorite and terrestrial rock chemical abundances and compared statistical characteristics.

Hutchins K. I.   Agee C. B.
Microprobe Analyses of Two Almahata Sitta Ureilites **[#2435]**
We have analyzed two of the Almahata Sitta meteorites. They are both ureilites. One is coarse grained and the other is fine grained. They are both dominated by olivine, with a very minor amount of pyroxene. They both have Fe metal that is low in Ni.

Wang K.   Moynier F.   Dauphas N.   Barrat J. A.   Craddock P. R.   Sio K.
Iron Isotopic Compositions of Angrites and Stannern-Trend Eucrites **[#1146]**
We report high-resolution iron isotopic compositions of angrite, martian, and HED meteorites. Angrite and Stannern-trend eucrite has shown significant enrichment in heavy iron isotopes. The mechanism is discussed as an igneous process on parent bodies.

Warren P. H.   Rubin A. E.
The Miller Range 090340 Dunite: Not a Uniquely Ferroan Ureilite, not even a Ureilite **[#2528]**
Mineralogical data show that MIL 090340, originally classed as a dunitic and uniquely ferroan ureilite, is more likely a brachinite, and certainly not a ureilite. Carbon is absent. Olivine Cr and Ca contents are vastly lower than the ureilite range.

Charon E.   Aléon J.   Rouzaud J. N.
Early History of Acapulco and Lodran Constrained by the Nanostructure and C, N Isotopic Composition of Their Carbons **[#2734]**
New results of structure and C, N isotopes of carbons on A-L meteorites allows us to defend an original history of A-L parent body benefiting of previous interpretations implying shock after the peak temperature and seeding by an exogenous carbons.

Sipiera P. P.   Irving A. J.   Kuehner S. M.   Tanaka R.
Acapulcoite PCA 01026 and Other Meteorites Collected in a 2002 Expedition to Pecora Escarpment, Antarctica **[#1516]**
Specimens collected on a PSF-funded expedition to Antarctica contribute to the knowledge base of planetary materials.

Jambon A.   Humayun M.   Barrat J. A.
Northwest Africa 6693: A Unique Achondritic Cumulate **[#2099]**
Northwest Africa 6693 is an igneous cumulate. The high Ni content of metal suggests a high oxidation state on the parent body.

Ma C.   Beckett J. R.   Rossman G. R.
Discovery of Buseckite, (Fe,Zn,Mn)S, a New Mineral in Zakłodzie, an Ungrouped Enstatite-Rich Achondrite **[#1520]**
We report here new mineral buseckite (Fe,Zn,Mn)S with a wurtzite-type hexagonal structure, and consider the origin of this phase and implications through its formation and survival for the evolution of the Zakłodzie meteorite.

LUNAR REMOTE SENSING: DIVERSE VIEWS OF BASALTS

Jawin E. R.   Kiefer W. S.   Bussey D. B. J.   Cahill J. T. S.   Dyar M. D.   Fassett C. I.   Spudis P. D.
Analyzing the Evolution of Surface Roughness of Lunar Mare **[#1343]**
We studied the relationship between surface roughness and age of lunar mare in relation to regolith development. To do this we compared CPR and various measurements from LOLA data. This allows us to analyze roughness on a range of length scales.

Jawin E. R.   Kiefer W. S.   Bussey D. B. J.   Cahill J. T. S.   Dyar M. D.   Fassett C. I.
Lawrence S.   Spudis P. D.
The Relationship Between Radar Scattering and Surface Roughness of Lunar Volcanic Domes **[#1333]**
We explore the relationship between surface roughness and radar signatures of various lunar geologic features. In order to quantify this relationship, we compared radar CPR values with topographic variation attained from LOLA data.

Kumamoto A.   Ono T.   Kobayashi T.
A Study of the Lunar Subsurface Echo Intensity for Evaluation of the Maximum Detection Depth of the Kaguya Lunar Radar Sounder **[#1465]**
The lunar subsurface echo power was estimated based on the reflectance at the buried regolith layers and attenuation rate in the basalt lava flow layers. The maximum detection depth of Kaguya/LRS was also evaluated based on it.

Bando Y.   Kumamoto A.   Nakamura N.   Nagahama H.
Subsurface Magnetized Source Layers Underneath the Mare Crisium Observed by Lunar Radar Sounder **[#1380]**
We evaluated subsurface stratification and its thickness as magnetized source layers by using Lunar Radar Sounder data. Our results imply lunar core dynamo had been driven at least during 3.47 Ga to 3.67 Ga.

Meyer J. A. Hurtado J. M.
Detecting Subsurface Lunar Lava Tubes Using Thermal Inertia **[#1636]**
In this study we create a thermal inertia map over a known lunar lava tube candidate in northern Oceanus Procellarum, demonstrating a thermal inertia low created by the subsurface void space.

Roberts C. E. Gregg T. K. P.
Quantitative Comparisons of Lunar Sinuous Rilles in the Marius Hills and Aristarchus Plateau Regions: Insights into Formation and Evolution **[#1685]**
Morphometric analyses of lunar sinuous rilles in the Marius Hills and Aristarchus Plateau regions provided insight into possible controls on rille morphometry and emplacement.

Feng D. C. Ye C. Huang Y. Xiang S. M. Yuan Y. F. Zhang J. B. Huang D. H. Yang R. Y. Zhu P. M.
The Characteristic of Lunar Rilles Around Mare Imbrium **[#1419]**
Lunar rilles were caused by a combination of both volcanism and tectonism. The different proportion of volcanism and tectonism both for forming the different morphology. The superposition and transection relations of the rilles may be identify its age.

Whitten J. L. Head J. W. III Neumann G. A. Zuber M. T. Smith D. E.
Volcanic Flooding Experiments in Impact Basins and Heavily Cratered Terrain Using LOLA Data: Patterns of Resurfacing and Crater Loss **[#1470]**
We use models to flood lunar topography to understand the thicknesses and volumes required to form mare-like deposits. Information gleaned from the experiments is applied to partially filled lunar basins to understand their early volcanic histories.

Gaddis L. Hawke B. R. Giguere T. Klem S. Gustafson J. O. Lawrence S. J. Stopar J. D.
Volcanism Within Floor-Fractured Atlas Crater **[#2787]**
Recent observations of the crater Atlas by imaging instruments on the LRO and SELENE missions allow us to examine in detail two small pyroclastic volcanic deposits in the crater floor.

Arimoto T. Ohtake M. Haruyama J. Iwata T.
Composition of Dark Mantle Deposit on the Aristarchus Plateau **[#1572]**
It is important to know the lunar mantle composition. In this study, by using MI spectral data of SELENE, we estimated the composition and crystallinity of dark mantle deposits on the Aristarchus Plateau, which originated in magma from deeper mantle.

Hawke B. R. Giguere T. A. Gaddis L. R. Gustafson O. Lawrence S. J. Stopar J. D. Peterson C. A. Bell J. F. III Robinson M. S. LROC Science Team
Localized Pyroclastic Deposits in the Grimaldi Region of the Moon **[#1749]**
LRO Camera WAC and NAC images were used to identify and characterize previously unknown localized pyroclastic deposits in the Grimaldi region. Some are among the smallest pyroclastic deposits yet identified on the lunar surface.

Hawke B. R. Giguere T. A. Lawrence S. J. Glotch T. D. Greenhagen B. T. Hagerty J. J. Braden S. E. Gaddis L. R. Jolliff B. L. Lucey P. G. Stopar J. D. Peterson C. A. Paige D. A. Robinson M. S. LROC Science Team
The Geology and Composition of Hansteen Alpha **[#1754]**
LROC images, LRO Diviner data, and Clementine UVVIS images were used to investigate the geology and composition of Hansteen α, a Th-rich, spectral anomaly on the Moon.

Accardo N. J. Jolliff B. L. Lawrence S. J.
Boulder Densities at the Compton-Belkovich Volcanic Complex **[#1656]**
We measure boulder densities at three volcanic mounds in the Compton-Belkovich Volcanic Complex (CBVC) to better understand the rock properties of boulders, to distinguish the style of eruption, and to understand the properties of the CBVC materials.

TUE POSTERS

Stooke P. J.
Lunar Meniscus Hollows **[#1011]**
The famous Ina or D-Caldera is not alone on the Moon. A few other examples were noted by Schultz in 1976. Now LROC images reveal these features in many places, usually near volcanic centers. Twenty-seven locations are identified and illustrated.

Garcia J. H. Hurtado J. M. Jr.
Phreatomagmatic Activity on the Moon: Possibility of Pseudocraters on Mare Frigoris **[#1390]**
Pseudocraters are volcanic features that form as a result of steam explosions from the interaction between lava and water. On the Moon the mechanism of formation could be triggered by the interaction between mare lava flows and ice in the regolith.

Lawrence S. J. Stopar J. D. Hawke B. R. Jolliff B. L. Robinson M. S. Spudis P. D. Giguere T. A.
Characterizing Volcanic Cones in the Marius Hills Region **[#2432]**
We present a comprehensive survey of volcanic cones in the Marius Hills complex using Lunar Reconnaissance Orbiter Camera data, including a detailed morphological classification scheme, and discuss implications for volcanism in the region.

LUNAR REMOTE SENSING: VISIBLE, INFRARED, AND BEYOND

Allen C. C. Greenhagen B. T. Donaldson Hanna K. L. Oehler D. Z. Paige D. A.
Derivation of FeO Abundances in Lunar Pyroclastic Deposits Using LRO Diviner **[#1504]**
Lab and Diviner thermal IR data correlate closely with FeO abundances across the range of soil and pyroclastic glass in the Apollo sample collection. Such data have the potential to analyze FeO concentrations in unsampled lunar pyroclastic deposits.

Otake H. Ohtake M. Hirata N.
Lunar Iron and Titanium Abundance Algorithms Based on SELENE (Kaguya) Multiband Imager Data **[#1905]**
We present algorithms for deriving the abundances of iron and titanium on the lunar surface based on SELENE (Kaguya) Multiband Imager's high-spatial-resolution data that have been calibrated and released to the public.

Bhatt M. Mall U. Bugiolacchi R.
Iron Abundance Estimation of the Lunar Surface Using VIS-NIR Spectrometers On-Board Chandrayaan-1 **[#1409]**
Our method of estimating iron abundance is based on an empirical relation between the 2-μm absorption parameters and the laboratory measured FeO wt%. A comparison of results from our method and Clementine-derived maps are in good agreement.

Moriarty D. P. III Pieters C. M. Petro N. Isaacson P. J.
Compositional Heterogeneity Within Lunar Central Peaks **[#2399]**
The purpose of this study is to characterize the compositional heterogeneity across lunar central peaks in order to determine properties of the source region of central peak material.

Cheek L. C. Donaldson Hanna K. L. Pieters C. M. Head J. W. Whitten J. L.
Anorthosite Exposures in the Inner Rook Mountains of the Lunar Orientale Basin **[#2731]**
Moon Mineralogy Mapper (M^3) spectra over the Orientale Basin show that crystalline plagioclase is pervasive throughout the IRM while mafic signatures are lacking. This indicates that an extensive, coherent layer of highly pure anorthosite was sampled by the impact.

Bugiolacchi R. Mall U. Bhatt M.
NIR Spectral Characterisation of the Northern Imbrium Region from SIR-2 Data **[#1462]**
We have developed a classification method of spectral characterization that appears to differentiate reliably between heterogeneous lunar surface materials; here we present a preliminary report, focused on six of the most recurrent spectral shapes.

Yamamoto A. Ohtake M. Haruyama J. Matsunaga T.
Kaguya LISM/MI Data Analysis for the Menelaus Crater Region of the Moon **[#1449]**
We used Japanese lunar orbiter "Kaguya" multiband imager data for classification analysis study about the Menelaus crater region on the moon. Nine-band multispectral data is useful to interpret geological history around the crater.

Kaur P. Chauhan P. Bhattacharya S. Ajai Kumar A.S. K.
Compositional Diversity at Tycho Crater: Mg-Spinel Exposures Detected from Moon Mineralogical Mapper (M^3) Data **[#1434]**
We report for the first time detection of Mg-spinel from Tycho crater along with crystalline plagioclase, olivine, and high-Ca pyroxene from the Tycho crater using M^3 data onboard Chandrayaan-1.

Arivazhagan S. Anbazhagan S.
Lithological Discrimination of Apollo 17 Landing Site Using Chandrayaan1 Moon Mineralogical Mapper Data **[#1751]**
Apollo 17 landing site lithology discriminated using Chandrayaan M^3 data standard band ratio, spectral profiles, and FeO/ TiO_2 estimation. The results were compared with the previously published data.

Lemelin M. Germain M. Morisset C.-E. Hipkin V. Goïta K.
Ilmenite Detection on the Moon by Remote Sensing: An Integration of Multisensor Datasets over Mare Australe and Mare Ingenii Regions **[#1972]**
We propose a method to map ilmenite concentrations on the Moon using integrated Lunar Reconnaissance Orbiter Wide Angle Camera and Clementine UVVIS/NIR datasets to take advantage of the unique spectral characteristics of ilmenite in the UV.

Standart D. L. Hurtado J. M. Jr.
Lunar Mineralogy Exploration Using Moon Mineralogy Mapper (M^3) Hyperspectral Imagery **[#2142]**
Moon Mineralogy Mapper imagery is used to develop iron band ratios for ilmenite exploration. We compare the index images created from these band ratios with ultraviolet/visible light index images from the LROC Wide Angle Camera to check our results.

Boyd A. K. Robinson M. S. Mahanti P.
Automatic Lunar Smooth Plains Classification Using LRO and Clementine Mission Data **[#2917]**
An automatic classification of units on the moon using the WAC 7 band photometrically corrected mosaic, GLD100, and clementine date. Classifications include maria, smooth plains, and highlands material.

Isaacson P. J. Petro N. E. Pieters C. M. Besse S. Boardman J. W. Clark R. N. Green R. O. Lundeen S. Malaret E. McLaughlin S. Sunshine J. M. Taylor L. A. M3 Team
Absolute Ferrous Absorption Band Strength in the Lunar Feldspathic Highlands Terrane from the Moon Mineralogy Mapper **[#1740]**
We evaluate the ferrous band strength in the feldspathic highlands terrane with M^3 data. We find that the ground truth correction delivered with the M^3 PDS archive improves consistency between data collected over different phases of the mission.

Powell K. E. McGovern P. J. Kramer G. Y.
Olivine Detections at the Rim of Crisium Basin with Moon Mineralogy Mapper **[#1689]**
We address the origin and transport of olivine at Crisium using spectra from the Moon Mineralogy Mapper (M^3) onboard Chandrayaan-1.

Wiseman S. M. Donaldson Hanna K. L. Mustard J. F. Isaacson P. J. Pieters C. M. Jolliff B.
Origin of Aristarchus Olivine Based on M^3 and Diviner Analyses **[#2515]**
Olivine-bearing material is exposed in ejecta deposits on the SE portion of the Aristarchus crater wall. We investigate the nature of these deposits with M^3 and Diviner and compare them to other olivine-bearing deposits in the vicinity of Imbrium.

TUE POSTERS

Mustard J. F.   Donaldson Hanna K. L.   Wiseman S.   Pieters C. M.
Visible-Near Infrared and Morphologic Character of High Silica Areas Identified by Diviner in the Aristarchus Crater: Association with Impact Melt **[#2246]**
The unusual short wavelength Christiansen Feature materials identified with Diviner near Aristarchus crater are analyzed with M^3 and LROC data. These materials are strongly correlated with the distribution and abundance of impact melt.

Foote E. J.   Paige D. A.   Shepard M. K.   Johnson J. R.   Grundy W. M.   Biggar S. F.
Greenhagen B. T.   Allen C. C.
Laboratory and Diviner Bidirectional Reflectance Measurements of Apollo Soils **[#2357]**
We compare laboratory reflectance measurements of Apollo soil samples to LRO Diviner observations of the landing sites.

Goguen J. D.
Apollo Soils Physical Properties Linked to M^3 Spectra Combined with ROLO Photometry **[#2568]**
Forward radiative transfer models are used to link the known size distributions and composition of the returned Apollo lunar soil samples to remote sensing measurements of the lunar sites from which they were collected.

Boyd A. K.   Robinson M. S.   Sato H.
Lunar Reconnaissance Orbiter Wide Angle Camera Photometry: An Empirical Solution **[#2795]**
The Lunar Reconnaissance Orbiter Wide Angle Camera is constantly imaging illuminated moon. A mostly continuous –63 to 63 latitude photometrically corrected 7 band color mosaic was created.

Yokota Y.   Matsunaga T.   Yamamoto S.   Ohtake M.   Haruyama J.   Nakamura R.   Ogawa Y.   Morota T.
Honda C.   Saiki K.   Nagasawa K.   Kitazato K.   Sasaki S.   Iwasaki A.   Demura H.   Hirata N.   Hiroi T.
Honda R.   Iijima Y.   Mizutani H.
Lunar Photometric Properties at Wavelength over 1.7 Microns Acquired by SELENE Spectral Profiler NIR-2 Sensor **[#2810]**
We present photometric correction method for SELENE SP NIR-2 sensor.

Cheng A. F.   Domingue D. L.
Photometric Modeling of Particulate Surfaces: A New Radiative Transfer Approach **[#1568]**
Opposition effects, roughness, and porosity effects can be treated within the framework of radiative transfer modeling. Geometric albedo may be a robust measure of surface reflectivity and spectral dependence, relatively unaffected by viewing geometry and by porosity.

Arnold J. A.   Glotch T. D.   Wolff M. J.
Exact Calculation of the Scattering Properties of Wavelength-Sized Particles **[#2529]**
We are interested in the light-scattering properties of planetary surfaces composed of fine-grained particulates, such as the lunar regolith. Here we focus on modeling the infrared emission spectra of quartz using a T matrix scattering code.

Banks M. E.   Watters T. R.   Robinson M. S.   Tornabene L. L.   Tran T.   Ojha L.
Williams N. R.   LROC Team
Morphometric Analysis of Small-Scale Lobate Scarps on the Moon Using Data from the Lunar Reconnaissance Orbiter **[#2817]**
LROC images and DTMs and LOLA altimetry are used to measure the relief and characterize the morphology of lunar lobate scarps. Results indicate that the scarps typically exhibit tens of meters of relief and are tens of kilometers or less in length.

Mahanti P.   Burns K.   Tran T.   Robinson M. S.
Measurement of Highland Pond Melt Volumes from LRO NAC DEMs **[#2807]**
DEM's obtained from NAC stereo-pair images is used to obtain melt pond volumes in highland area by image processing. Variation of melt volumes with pond area is studied.

Antonenko I.
Leathery Texture in the Bose, Bhabha, and Stoney Crater Region of South Pole-Aitken Basin on the Moon **[#2581]**
LROC data shows fine-scaled leathery texture throughout the central SPA area. A survey of the region was conducted to assess the extent of this texture. Observations are consistent with the texture forming by seismic shaking from small local impacts.

Jin Y. Q.
Diurnal Temperature Changes of Cratered Lunar Surface Inverted from Chinese Chang'E-1 Multi-Channel Radiometer Observations **[#1004]**
Based on a three-layer radiative transfer model, the brightness temperature data of Chinese Chang'E-1 multi-channel microwave radiometer are first studied and applied to invert the diurnal temperatures changes of some specific cratered areas.

Holsclaw G. M.   Snow M.   McClintock W. E.
Disk-integrated Polarization of the Moon in the Ultraviolet **[#2832]**
We have obtained the first disk-integrated measurement of the lunar polarization at ultraviolet wavelengths and only the second polarization measurement of the Moon to date.

Hendrix A. R.   Vilas F.   Holsclaw G. M.   Feldman P. D.
Ultraviolet Spectroscopy of the Moon: A New Look at Some Not-so-New Data Sets **[#2839]**
We present an analysis of several previously untapped ultraviolet datasets of the Moon: IUE, Apollo 17 UVS, Galileo UVS and Cassini UVIS. We use these data to look into compositional and weathering effects across the surface.

Cahill J. T. S.   Bussey D. B. J.   Patterson G. W.   Turner F. S.   Lopez N. R.   Raney R. K.
Neish C. D.   Mini-RF Science Team
Global Mini-RF S-Band CPR and M-Chi Decomposition Observations of the Moon **[#2590]**
We report on analyses Mini-RF global S-band radar maps using a unique and complimentary method of polarimetric data analysis, known as an m-chi decomposition.

Aldridge T. M.   Thomson B. J.   Stoddard P. R.   Cahill J. T. S.   Bussey D. B. J.   Mini-RF Science Team
A Mini-RF Radar Analysis of the Moon's South Pole-Aitken Basin **[#2493]**
Using Mini-RF S-band zoom we derive the Stokes (S1), circular polarization ratio (CPR), and same sense (SC) parameters of the South Pole-Aitken basin for comparison with Clementine UVVIS-NIR derived TiO_2 maps.

Baloga S. M.   Glaze L. S.   Spudis P. D.
Inferred Lunar Boulder Distributions at Decimeter Scales **[#1647]**
Block size distributions for Linné crater and Surveyor III and VII sites were analyzed. Statistical properties of these distributions are determined as well as methods for reliably extrapolating from NAC data down to decimeter scales relevant to CPR.

Hayne P. O.   Aharonson O.   Bandfield J. L.   Greenhagen B. T.   Paige D. A.
The Surface Roughness of the Moon from Diviner Infrared Observations **[#2829]**
Surface roughness maps derived from Diviner infrared data present a unique record of geologic processes on the Moon, from lunar swirls to anomalous impact features known as "cold spots".

LUNAR REMOTE SENSING: THE LUNAR CRUST THROUGH DIVERSE REMOTE SENSING TECHNIQUES

Wilson J. K. Spence H. E. Case A. W. Blake J. B. Golightly M. J. Kasper J. Looper M. D. Mazur J. E. Schwadron N. Townsend L. W. Zeitlin C.
First Cosmic Ray Albedo Proton Map of the Moon **[#2373]**
We have used the CRaTER instrument on LRO to make a cosmic-ray albedo proton map of the Moon. We find no obvious albedo features corresponding to regional differences in elemental composition of the regolith, such as between maria and highlands.

Case A. W. Kasper J. C. Spence H. E. Golightly M. J. Schwadron N. E. Blake J. B. Looper M. Mazur J. E. Townsend L. W. Zeitlin C. J.
An Unidentified Lunar Cosmic Ray Signal that Depends on Altitude and Solar Zenith Angle **[#2479]**
Using the CRaTER instrument, an unidentified lunar cosmic ray signal is investigated. This signal shows a dependence on altitude and on the orientation of the detectors with respect to the Sun. This signal may be caused by solar X-ray photons.

Yamashita N. Reedy R. C. Hareyama M. Kobayashi M. Hasebe N. Nagaoka H. Karouji Y. Kobayashi S. d'Uston C. Gasnault O. Forni O. Kim K. J. Hamara D. K. Kaguya Gamma Ray Spectrometer Team
Peaks in Kaguya Gamma-Ray Spectra and Gamma Rays Used to Get Elemental Abundances **[#1283]**
The Kaguya gamma-ray spectrum near peaks used for elemental abundances (K, Th, U, Fe, Si, Ca, Mg, Ti, and Al) in the Moon are described. Most are easy to analyze.

McClanahan T. P. Mitrofanov I. G. Boynton W. V. Chin G. Livengood T. Starr R. D. Evans L. G. Neumann G. Mazarico E. Smith D. E. LEND Team LOLA Team
Estimation of Orbital Neutron Detector Spatial Resolution by Systematic Shifting of Differential Topographic Masks **[#2302]**
We present a method and preliminary results related to estimating the spatial resolution of orbital neutron detectors by systematically convolving epithermal neutron maps with differential topographic masks.

Hagerty J. J. Lawrence D. J. Cahill J. T. S. Klima R. L. Gillis-Davis J. J.
Analysis of Global Lunar Iron Abundances: A Systematic Comparison of Lunar Prospector and Clementine Data **[#1933]**
Analyses of Lunar Prospector and Clementine global iron maps show significant differences between these datasets for specific portions of the lunar surface. We use forward modeling of gamma ray data to investigate discrepant regions of interest.

LUNAR VOLATILES: FROM THE SURFACE TO THE INTERIOR

Schorghofer N.
On the Theory of Migration of Water on the Moon **[#1110]**
It has been suggested and questioned that water molecules on the lunar surface move on ballistic trajectories. I investigate the migration process in and on the Moon with an improved physical model of H_2O-regolith interaction.

Livengood T. A. Mitrofanov I. G. Boynton W. V. Chin G. McClanahan T. P. Starr R. D. Evans L. G. LEND Team
A Search for Hydrogen near the Lunar Terminator at Low Latitude **[#2643]**
We search for the signature of hydrogen in the lunar regolith in the near-equatorial region as a function of local time. Concentrations of water suggested by reflectance spectroscopy are consistent with the LEND instrument on LRO.

Lemelin M. Roberts C. E. Blair D. M. Runyon K. D. Nowka D. Paige D. A.
Spudis P. D. Kring D. A.
Finding Volatiles in the Lunar Surface: An Innovative Multi-Source ArcGIS-Based Approach **[#1067]**
We evaluated locations optimally suited for exploration of lunar polar volatiles using spatial analyst in ArcGIS. We propose four regions at each pole for lunar polar volatile examination.

Thompson T. W. Ustinov E. A. Spudis P. D. Fessler B. W.
Modeling of Radar Backscatter from Icy and Rough Lunar Craters **[#1069]**
Our model for radar backscattering from lunar craters was examined for 4 nonpolar craters and 12 polar craters using LRO Mini-RF 13-cm wavelength data. Results indicate that icy craters can be distinguished from young rough craters.

Boynton W. V. Droege G. F. Harshman K. Schaffner M. A. Mitrofanov I. G.
McClanahan T. P. LEND Team
Constraints on Lunar Hydrogen Mobility Provided by High Spatial Resolution Studies of Epithermal Neutron Emission **[#2244]**
The enhanced H content in the polar regions that is not associated with NSRs is due to differences in thermal volatilization rates, which are a strong function of surface temperature.

Mitchell E. H. Schaible M. J. Raut U. Fulvio D. Dukes C. A. Baragiola R. A.
Photodesorption of Adsorbed Water on the Moon **[#2362]**
We experimentally examine the removal of adsorbed water from lunar highland soil by Lyman-α (121.6-nm) photons and by 193-nm photons. These results will yield lifetimes of H_2O/OH species on the lunar regolith due to the solar photon flux.

Runyon K. D. Blair D. M. Lemelin M. Nowka D. Roberts C. E. Paige D. A. Spudis P. Kring D. A.
Volatiles at the Lunar South Pole: A Case Study for a Mission to Amundsen Crater **[#1619]**
The in situ study of lunar polar volatiles is a high National Research Council priority. Amundsen crater is a prime south-polar location for a landed mission to study volatiles.

Smith D. E. Zuber M. T. Head J. W. Neumann G. A. Mazarico E. Torrence M. H. Aharonson O. Tye A. R.
Fassett C. I. Rosenburg M. A. Melosh H. J.
Brightening and Volatile Distribution within Shackleton Crater Observed by the LRO Laser Altimeter **[#1663]**
The Shackleton crater is in almost permanent shadow and brighter than the surrounding terrain. The walls are the brightest part of the crater. Crater counts suggest the floor is over 3 billion years old.

McGovern J. A. Bussey D. B. J. Greenhagen B. T. Paige D. A. Cahill J. T. S. Siegler M. Spudis P. D.
Mapping and Characterization of Non-Polar Permanent Shadows on the Lunar Surface **[#2550]**
We have discovered permanent shadows as far from the pole as ±58° of latitude. Here we report the results of our analyses of these areas, specifically evaluating whether they are cold enough to harbor volatile deposits.

Speyerer E. J. Robinson M. S. Lawrence S. J. Burns K. Stopar J. D.
In Search of Shade in Persistently Illuminated Regions near the Lunar Poles **[#2633]**
The Moon's slightly tilted spin axis relative to the ecliptic normal provides a unique lighting environment near the lunar poles. Using LROC images, we identify both persistently illuminated and shadowed features in close proximity to one another.

Siegler M. A. Bills B. G. Paige D. A.
Spatio-Temporal Evolution of Lunar Polar Cold Traps **[#2376]**
We model the spatial, temporal, and quantitative variability of lunar ice. In this study we develop components of a comprehensive thermal-diffusion model of ice migration and stability, which evolves as a function of changes in the lunar orbit.

Hurley D. M.   Lawrence D. J.   Bussey D. B. J.   Vondrak R. R.   Elphic R. C.   Gladstone G. R.
Two-Dimensional Distribution of Ice in the Lunar Regolith — Modeling and Interpretation **[#1145]**
We model ice in lunar cold traps under the effects of space weathering. Impacts poke holes creating dry spots at early times. Later, holes outnumber wet spots. Finally, the distribution becomes homogenized. Lateral coherence disappears quickly.

Alford J. A.   Hodges A. R.   Heggy E.   Crotts A. P. S.
Exploring Volatile Deposition in Lunar Regolith **[#2938]**
Various evidence indicates volatiles trapped in the regolith near the lunar poles. We present results from two studies useful in understanding these processes: radar exploration of hydrated regolith and regolith buildup in low-lying areas.

Jacob S. R.   Mercer C. N.
Tracking the Process of Volatile Release from the Lunar Highland Breccia Meteorite Northwest Africa 2996 Using Vesicle Size Distributions **[#1291]**
Vesicles are frozen records of degassing processes in magmas. We apply quantitative textural analysis methods, commonly used to study gas exsolution in terrestrial volcanism, to explore the role of volatiles in generating vesicular lunar rocks.

Robinson K. L.   Taylor G. J.   Hellebrand E.   Nagashima K.
Water in Evolved Lunar Rocks: Implications for Water Distribution in the Lunar Mantle **[#1727]**
Water concentrations in lunar pyroclastics, mare basalts, and our analyses of KREEP-related rocks indicate that water is distributed heterogeneously in the lunar mantle.

Barnes J. J.   Anand M.   Franchi I. A.   Starkey N. A.   Ota Y.   Sano Y.   Russell S. S.   Tartese R.
The Hydroxyl Content and Hydrogen Isotope Composition of Lunar Apatites **[#1797]**
We report δD values and hydroxyl contents of apatite grains from Apollo mare basalt 12064 and lunar mare basalt meteorite Miller Range MIL 05035.

Liu Y.   Mosenfelder J. L.   Guan Y.   Rossman G. R.   Eiler J. M.   Taylor L. A.
Sims Analysis of Water Abundance in Nominally Anhydrous Minerals in Lunar Basalts **[#1866]**
Preliminary examination of Fe-rich NAMs in lunar basalts shows promising results.

Nunn M. H.   Thiemens M. H.
High Precision Oxygen Isotopic Measurements of Water Extracted from Selected Lunar Samples **[#2752]**
We present here the first high precision measurements of oxygen isotopic ratios in water extracted from lunar material and discuss scenarios of water production, transport, and delivery that explain the observed ratios.

Treiman A. H.   Gross J.
Abundant Apatite in Granulite 79215: Spoor of Another Volatile-Rich Lunar Fluid **[#1223]**
Lunar granulite 79215 contains abundant apatite concentrated in curvilinear traces, implying deposition from fluid. The fluid was rich in P, F, and Cl, but was not KREEPy; 79215 has P/Sm >> KREEP. Most likely, the fluid was aqueous or a dense vapor.

Ustunisik G.   Nekvasil H.   Lindsley D. H.   McCubbin F. M.
Vapor Phase Evolution During Sequential Degassing of Cl-, F-, H_2O- and S-Bearing Lunar Magams: Insights from Time Studies **[#1879]**
Experiments were conducted as time studies to monitor the changes in relative volatile contents during successive intervals of degassing. The first vapor (after 1 hr) was water-rich; the successive vapor was dry but rich in metal chlorides and fluorides.

Shearer C. K. Jr. Sharp Z. D. McCubbin F. M. Steele A. Burger P. V. Provencio P. P. Papike J. J.
Chlorine Distribution and Its Isotope Composition, Alteration Mineralogy, and Micro-Textural Analysis of "Rusty Rock" 66095. Implications for the Petrogenesis of "Rusty Rock", Origin of "Rusty" Alteration, and Volatile Element Behavior on the Moon **[#1416]**
We examine the isotope composition and distribution of Cl in 66095, and the associated alteration mineralogy to gain additional insights into its petrogenesis, and transport of volatiles in the lunar crust and on the lunar surface.

Boyce J. W. Ma C. Eiler J. M. Baker M. B. Liu Y. Stolper E. M. Taylor L. A.
Sulfur Speciation in Lunar and Terrestrial Apatite **[#2675]**
Apatite from 14072,16, 14053,61, and 14053,241 have S Kα peak shifts consistent with incorporation of both sulfide and sulfate. Sulfur concentration is inversely correlated with the percentage of sulfide.

Wetzel D. T. Jacobsen S. D. Rutherford M. J. Hauri E. H. Saal A. E.
The Solubility and Speciation of Carbon in Lunar Picritic Magmas **[#1535]**
Lunar green glass experiments give new information about the speciation and solubility of carbon in hydrogen-bearing, graphite-saturated picritic melts for a range in oxygen fugacity and pressure at liquidus temperatures.

Newcombe M. Brett A. Beckett J. R. Baker M. B. Newman S. Stolper E. M.
Solubility and Diffusivity of H-Bearing Species in Lunar Basaltic Melts **[#2777]**
We have measured the solubility and diffusivity of water in silicate melts similar in composition to lunar magmas under conditions similar to those thought to exist on the Moon.

PERSPECTIVES ON LUNAR GEOCHEMISTRY FROM SAMPLES

Fimiani L. Cook D. L. Faestermann T. Gomez Guzman J. M. Hain K. Herzog G. F. Korschinek G. Ligon B. Ludwig P. Park J. Reedy R. C. Rugel G.
Sources of Live ^{60}Fe, ^{10}Be, and ^{26}Al in Lunar Core 12025, Core 15008, Skim Sample 69921, Scoop Sample 69941, and Under-Boulder Sample 69961 **[#1279]**
Relatively high concentrations of live ^{60}Fe ($T_{1/2}$ = 2.62 ± 0.04 Ma) in lunar surface samples confirm earlier work and suggest the arrival of supernova (SN) debris on the Moon about 2 Ma ago.

Joy K. H. Nagashima K. Huss G. R. Zolensky M. E. Kring D. A.
Mineral Chemistry and Oxygen Isotope Analysis of a Chondritic Projectile in Lunar Meteorite Pecora Escarpment 02007 **[#1021]**
We report oxygen isotope data from a chondritic meteorite particle in lunar meteorite PCA 02007. The fragment provides direct evidence of asteroid projectile debris being delivered to the lunar surface.

Korotev R. L. Irving A. J. Bunch T. E.
Keeping Up With the Lunar Meteorites — 2012 **[#1152]**
We discuss several new lunar meteorites.

Kuehner S. M. Irving A. J. Korotev R. L.
Petrology and Composition of Lunar Meteorite Northwest Africa 7022: An Unusually Sodic Anorthositic Gabbroic Impact Melt Breccia with Compositional Similarities to Miller Range 090036 **[#1524]**
We characterize a new type of relatively sodic impact melt breccia from the Moon.

Demidova S. I. Nazarov M. A. Ivanova M. A. Lorenz K. A. Kononkova N. N.
New Lunar Meteorite from the Sahara Desert: North West Africa 6888 **[#1726]**
The new lunar meteorite NWA 6888 is a mingled breccia containing highland rocks and VLT mare basalts with no KREEP. We report the first data on petrography and mineralogy of the rock. NWA 6888 appears to be one of the most altered NWA meteorites.

Kent J. J.   Brandon A. D.   Lapen T. J.   Peslier A. H.   Irving A. J.   Coleff D. M.
In Situ Chemical Characterization of Mineral Phases in Lunar Granulite Meteorite Northwest Africa 5744 **[#2559]**
NWA 5744 is compared to other magnesian lunar granulites by the chemistry of situ phases and aided by a CT density volume. NWA 5744 may be linked to FAN composition materials, and magnesian granulites as a whole probably have diverse origins.

Shirai N.   Ebihara M.   Sekimoto S.   Yamaguchi A.   Nyquist L.   Shih C.-Y.   Park J.   Nagao K.
Geochemistry of Lunar Highland Meteorites MIL 090034, 090036 and 090070 **[#2003]**
Bulk chemical compositions of newly found lunar meteorites (MIL 090034, 090036 and 090070) were determined by using INAA. Based on chemical compositions, we compared three MIL lunar meteorites with the other lunar highland meteorites.

Kuehner S. M.   Irving A. J.   Korotev R. L.
Petrology and Composition of Lunar Mare Ferroan Gabbro Breccia Northwest Africa 7007: New Insights into the Complex Petrogenesis of Northwest Africa 773 and Siblings **[#1519]**
This lunar meteorite is comprised mainly of a gabbro lithology previously not well-characterized in related specimens of the "NWA 773 clan."

Gorman J.   Gross J.
Spinel-Rich Lithologies on the Moon: An Experimental Study of Possible Precursor Melt Compositions **[#1125]**
Here we present data of liquidus/crystallization experiments at low pressure to provide constraints on the origin and formation history of Mg-Al spinel-rich and spinel-bearing lunar highland samples.

Elardo S. M.   Shearer C. K. Jr.   Fagan A. L.   Neal C. R.   Burger P. V.   Borg L. E.
Diversity in Low-Ti Mare Magmatism and Mantle Sources: A Perspective from Lunar Meteorites NWA 4734, NWA 032, and LAP 02205 **[#2648]**
Lunar meteorites NWA 4734, NWA 032, and LAP 02205 have the potential to expand our knowledge of the compositional diversity among low-Ti basaltic magmas and source regions on the Moon.

Fagan A. L.   Neal C. R.
Apollo 11-Type Basalts from Apollo 16: A New Type of High-Ti Basalt? **[#1429]**
Rare basalt clasts from Apollo 16 are similar in composition to Apollo 11 high-Ti basalts, but display distinct differences as well indicating the possibility of a new type of lunar high-Ti basalt.

Donohue P. H.   Neal C. R.
Crystal Stratigraphy of Olivine Cumulate 71597: Tracing the Crystallization History of a High-Ti Basalt Lava Flow **[#2077]**
We performed a petrographic and in situ trace-element characterization study of major phases of high-titanium basalt 71597, and present a detailed crystallization history for one of the few mare basalt samples with evidence for a cumulate origin.

Morisset C.-E.   Jackson S.   Williamson M.-C.   Hipkin H. J.
Trace Element Concentrations of Ilmenite in Samples Selected from the Six Apollo Landed Missions **[#2018]**
We report the trace-element concentrations of ilmenite contained in 12 selected samples from the 6 Apollo landing sites using a Laser-Ablation–Inductively Coupled Plasma–Mass Spectrometer (LA-ICP-MS).

Macke R. J.   Kiefer W. S.   Britt D. T.   Irving A. J.   Consolmagno G. J.
Density and Porosity of Apollo Lunar Basalts and Breccias **[#1299]**
We report results of density and porosity measurements on 22 Apollo lunar samples. These include specimens from all six missions, and represent diverse types including low-Ti and high-Ti basalts, impact-melt breccias, regolith breccias, and others.

Barker D. C.   Snow J. E.
Phenocryst Growth and Compositional Inhomogeneity of Apollo 17 Glass Spherules **[#2926]**
Phenocryst growth in Apollo 17 lunar glasses has been examined using Field Emission Scanning Electron Microprobe (FESEM) and Electron Probe Micro Analysis (EMPA) instruments.

Cronberger K. Neal C. R.
The Textural Pristinity of KREEP Basalts: The Role of Impact Melting and Volcanic Eruptions **[#2203]**
A new method using quantitative petrology is being used on samples of a KREEPy basaltic composition to determine their textural pristinity.

Simmons S T. Lapen T J.
Trace Element Geochemistry of Apollo Sample 78236: Possible Connections with Other Mg-Suite Norites **[#2622]**
New high precision ICP-MS trace element analysis of Apollo 17 Mg-suite sample 78236 indicates that it is geochemically identical to some norite clasts in other Apollo 17 samples potentially allowing geochemical distinctions among Mg-suite norites.

Seddio S. M. Korotev R. L. Jolliff B. L.
Two Appollo 12 Granit Rock Fragments: Evidence for the Priximal Coexistence of High-Th Impact Melt Breccia and Granite **[#1006]**
We characterize a lunar granite fragment and a granitic breccia. The breccia's granitic component is that of the granite fragment if it equilibrated with a more mafic lithology. We infer a source region with granite and high-Th impact melt breccia.

LUNAR REMOTE SENSING: TECHNIQUES AND LABORATORY GROUND TRUTH

Wong U. H. Wu Y. Z.
A Monte Carlo Ray Tracing Model for Lunar Soil and Its Applications to Chang'e-1 Topography Data and LSCC Data Set **[#1222]**
In this paper, a Monte Carlo ray tracing model for lunar soils is proposed for the purpose of simulating the reflection of electromagnetic radiation in the lunar surface. The reflectance spectrum is calculated using Hapke model with the LSCC data.

Serventi G. Carli C. Sgavetti M. Pompilio L.
Effects of Plagioclase Chemistry and Modal Abundance on Spectral Properties of Multimineral Fe,Mg Mixtures **[#1404]**
In this abstract we show plagioclase effects on three different Fe,Mg mixtures. The spectra of these mixtures were analyzed via decomposition with an EGO algorithm in order to determine band spectral parameters, particularly in the 1.2-μm region.

Hiroi T. Kaiden H. Misawa K. Kojima H. Uemoto K. Ohtake M. Arai T. Sasaki S. Takeda H. Nyquist L. E. Shih C.-Y.
Diversity in the Visible-NIR Absorption Band Characteristics of Lunar and Asteroidal Plagioclase **[#1168]**
Visible and NIR reflectance spectra of plagioclase in lunar anorthosites and basalt samples, and lunar and HED meteorites, have been analyzed using the modified Gaussian model. Lunar anorthosite 60015 shows an unusually short band center wavelength.

Mall U. Korokhin V. Bugiolacchi R. Shkuratov Y.
Towards a Quantitative Determination of the Modal Mineralogy of Planetary Surfaces Using Near-Infrared Spectroscopic Data from the Moon **[#1893]**
We investigate data returned from the SIR-2 NIR spectrometer on the Chandrayaan-1 mission with the Shkuratov spectral model. We selected from measured lunar samples an optimal set of seven mineral components for describing the lunar soil composition.

Cavanagh P. D. Li. L.
Band Selection Method Applied to Moon Mineralogy Mapper (M^3) **[#2742]**
A previously developed band selection method identified 15 bands that describe the greatest variability of the M^3 hyperspectral dataset from the Apollo 17 landing site. The 15 bands accurately reconstructed the 74 original bands with minimal error.

Thomas I. R.   Bowles N. E.   Warren T.   Greenhagen B. T.   Donaldson Hanna K. L.   Paige D. A.
Thermal Infrared Emission and Goniometric Laboratory Measurements **[#2637]**
This presentation describes the thermal-infrared laboratory experiments that have been constructed: a simulated lunar environment chamber, multiple-angle reflectance apparatus, and goniometer. Results from these experiments are presented.

Donaldson Hanna K. L.   Pieters C. M.   Patterson W. R. III   Hiroi T.   Moriarty D.
Wyatt M. B.   Thompson C.
Asteroid and Lunar Environment Chamber (ALEC): Simulated Asteroid and Lunar Environments for Measuring Analog Materials **[#2241]**
First light results from the Asteroid and Lunar Environment Chamber (ALEC) at Brown University. ALEC will simulate asteroid and lunar environments to enable spectral measurements of analog materials.

Crites S.   Lucey P. G.
Characterization of Lunar Soils Using Infrared Microscopic Hyperspectral Imaging **[#1653]**
We present a study to characterize mineralogy of lunar soils at an individual grain level using a thermal infrared hyperspectral imaging system equipped to take data in both emission and reflectance, and a near-infrared hyperspectral imaging system.

Taylor G. J.   Martel L. M. V.   Lucey P. G.   Crites S.   Blake D. F.
Modal Analyses of Apollo 16 Soils by X-Ray Diffraction **[#2316]**
Modal mineralogy of 30 Apollo 16 soils confirms the Descartes highlands are more feldspathic than the Cayley plains and the chemical differences between the mineral and glass components in each. This affects calibration of remote sensing data.

Retherford K. D.   Davis M. W.   Winters G. S.   Patrick E. L.   Escobedo S. M.   Nagengast M. E.   Gladstone G. R.
Miles P. F.   Parker J. Wm.   Stern S. A.   Hendrix A. R.
Lunar Ultraviolet Reflectance Experiment (LURE): Far-UV Signatures of Water Ice **[#2190]**
The Lunar Ultraviolet Reflectance Experiment (LURE) conducts laboratory measurements of the far-ultraviolet (115–200 nm) spectral signatures of water ice and lunar simulants over various reflectance angles to characterize their BRDF.

LUNAR IMPACT CRATERS

Yokota Y.   Gwinner K.   Oberst J.   Haruyama J.   Matsunaga T.   Morota T.   Noda H.   Araki H.   Ohtake M.
Yamamoto S.
Lunar Surface Roughness at Baseline 0.15–100 km and the Impact History of the Highlands **[#2843]**
We report roughness measurement results at the baseline scale from 0.15 to 100 km, using the digital topography data derived from the SELENE Laser Altimeter (LALT) and Terrain Camera (TC).

Jozwiak L. M.   Head J. W. III   Neumann G. A.   Zuber M. T.   Smith D. E.
Lunar Floor-Fractured Craters: Classification, Distribution, and Implications for Magmatism and Shallow Crustal Structure **[#1512]**
A study classifying and mapping the distribution of all lunar floor-fractured craters. We then use the crater distribution and morphology to investigate proposed formation mechanisms, favoring shallow magmatic intrusion over viscous relaxation.

Frey H. V.   Meyer H. M.   Romine G. C.
Improving the Inventory of Large Lunar Basins: Using LOLA Data to Test Previous Candidates and Search for New Ones **[#1848]**
LOLA topographic and LOLA-based crustal thickness data were used to eliminate 23 candidate basins previously suggested based on older data. The newer data also suggest there may be an additional 20 possible basins, for a working inventory of 95.

Ishihara Y. Morota T. Saruwatari Y. Sawada A. Hiramatsu Y.
A Determination of Characteristics of Impact Basins from "Kaguya" Geodetic Data **[#1723]**
We propose a new quantitative and objective procedure to measure the impact basin's characteristics based on a (localized) spherical function model, and show its application result for actual lunar data.

Kinoshita T. Honda C. Hirata N. Morota T. Demura H. Asada N.
Evaluation of Spatial Distribution of Craters on Lunar Surface for Detection of Secondary Craters **[#1829]**
For crater chronology, we should evaluate quantitatively the region that contains secondary craters. The clustered secondary craters could be evaluated non-random spatial distribution of craters quantitatively by our clustering analysis.

Thomson B. J. Bussey D. B. J. Cahill J. T. S. Neish C. D. Kirk R. Patterson G. W. Raney R. K. Spudis P. D.
Excess Numbers of Enhanced CPR Craters in the Lunar Polar Regions **[#2104]**
The abundance of craters with a polarization signature consistent with roughness or small ice fractions is greater at the poles vs. the equator by a ratio of ~1.6:1, suggesting roughness alone is not responsible for the polar crater observations.

Martin-Wells K. S. Campbell D. B. Campbell B. A. Carter L. M.
The Relationship Between Debris Flow and Enhanced Radar Circular Polarization Ratio Values in Lunar Secondary Crater Clusters **[#2272]**
Recent work has shown that lunar secondary craters are sometimes associated with streaks of enhanced radar circular polarization ratio (CPR) compared to surrounding terrains. We examine the origin of enhanced CPR in relation to secondary cratering.

Kramer G. Y. Ohman T. Nahm A. L. McGovern P. J.
Pre- and Post-Impact Influences on Schrödinger Basin's Structural Geology **[#1734]**
Schrodinger Basin hosts a series of fractures that exhibit complex cross-cutting relationships with each other and the basin floor materials. Some of these fractures are evidence of deep faulting, and some are associated with late-onset volcanism.

Xiao Z. Strom R. G. Chapman C. R. Head J. W.
New Comparisons Between Fresh Impact Craters on Mercury and the Moon **[#2130]**
Impact ejecta on Mercury and the Moon is affected by both surface gravity and impact velocity.

Miura Yas.
Formation of Moon-Type Rocks by Multiple Impacts with Porous, Crystals and Glassy Soils **[#1203]**
Lunar rocks are checked by two data of (a) density, porosity, and age; and (b) FeO, Ni, Co, and C contents and age. The results indicate that primordial FAN anorthosites are relatively brecciated on heterogeneous surface with multiple impact process.

Basilevsky A. T. Abdrakhimov A. M. Ivanov M. A. Zabalueva E. V. Karachevtseva I. P. Shingareva K. B. Gusakova E. N. Oberst J. Waehlisch M. Robinson M.
Identification and Measurements of Small Impact Craters in the Lunokhod 1 Study Area, Mare Imbrium **[#1481]**
Analyzing LROC NAC images and DTM for the Lunokhod 1 area, we consider a problem of craters identification on images taken at different solar elevations, measure crater D/H ratios, and make profiles through craters having different morphological prominence.

Herrick R. R.
Antoniadi is an Unusual Lunar Protobasin **[#2409]**
I examined several lunar craters around 150 km in diameter, where protobasins begin to form. Antoniadi is quite different from similar-sized craters and may provide some unique insights into peak ring formation and lunar subsurface properties.

Petro N. E.
Formation of South Pole-Aitken Basin as the Result of an Oblique Impact: Implications for Melt Volume and Source of Exposed Materials **[#2656]**
South Pole-Aitken (SPA) is the largest and oldest identified basin on the Moon. The source of impact melt and the effects of oblique impact on the depth of origin of melted material are investigated. Ultimately, a large volume of melt is produced and retained in SPA.

Dhingra D. Pieters C. M. Head J. W. Isaacson P. J.
Large Flow Feature at Copernicus Crater — Implications for Impact Melt Evolution and Emplacement Chronology **[#2339]**
Analysis of M^3 data for Copernicus Crater suggests the presence of a large impact melt flow extending from northern wall and terminating at the central peaks. The reasoning for this interpretation and implications for melt evolution are discussed.

EDUCATION AND PUBLIC OUTREACH: THE MOON

Robbins S. J. Antonenko I. Gay P. L. Lehan C. Moore J.
Cataloging the Moon with the CosmoQuest Moon Mappers Citizen Science Project **[#2856]**
We present the early results from a citizen science -based approach to cataloging lunar features, primarily craters. Setup, data reduction, and validation of crowd-sourced data will be discussed with these results.

Runyon C. J. Hall C. Joyner E. Daou D. Hurd D. Boyce K. Garver K.
Generating STEAM with Engaging Lunar Exploration Education/Public Outreach Activities **[#1944]**
Our E/PO activities and programs present the ongoing story of lunar exploration and discovery and help teachers engage students in learning how the Moon and planetary surfaces form. Outreach materials highlight not just STEM, but also fine arts.

Hsu B. C. Bleacher L. V. Daou D. Day B. Jones A. Mitchell B. Shaner A. Shipp S.
Reaching an International Audience with Lunar Science Through International Observe the Moon Night **[#2021]**
On 08 October 2011, over 627 events were held in 57 countries for International Observe the Moon Night (InOMN). This represents an 25% increase in the number of events held in 2010. InOMN is a great opportunity to share lunar science with the public.

LaConte K. Shupla C. Barr A. Shipp S. Bottke W. F.
Public Engagement in the Science of NLSI's Center for Lunar Origin and Evolution (CLOE) **[#2874]**
The Center for Lunar Origin and Evolution (CLOE) team is sharing CLOE research about the Moon's formation and evolution, NLSI science, and excitement about space science with high-school students and the general public.

Shaner A. J. Shupla C. Shipp S. Halligan E. Allen J. Kring D. A. LaConte K.
Bringing You the Moon: Lunar Education Efforts of the Center for Lunar Science and Education **[#2603]**
The Center for Lunar Science and Exploration has developed a variety of programs and products, including Lunar Traveling Exhibits and the High School Lunar Research Project, featured at http://www.lpi.usra.edu/nlsi/education/.

MARTIAN CRATERS

Landis M. E. Barlow N. G.
Analysis of Impact Craters in the 0–20N, 0–30E Region of Arabia Terra, Mars and Implications for Volatiles **[#1255]**
We are classifying ejecta and interior morphologies of all craters 1 km and larger in the 0–20N 0–30E region of Arabia Terra to investigate the role of subsurface and surficial volatiles on this area. We find small craters are excessively deep.

Malinski P. T. Brusnahan H. Milam K. A.
A Morphometric Analysis of Martian Impact Craters 21–30 km in Diameter **[#2848]**
An ongoing MOLA analysis of the morphology of complex impact craters on Mars is being conducted to identify temporal changes in morphometric relationships between crater landforms.

Garner K. M. L. Barlow N. G.
Distribution of Rimmed, Partially Rimmed, and Non-Rimmed Central Floor Pits on Mars **[#1256]**
We have classified 798 central floor pit craters on Mars as to whether the pit is rimmed, partially rimmed, or non-rimmed. Our results suggest that target characteristics strongly influence the production of rimmed and non-rimmed pits.

Bamberg M. Jaumann R. Asche H.
Floor Fractured Craters Around Syrtis Major, Mars **[#1833]**
Floor-fractured craters can be found around Syrtis Major. The appearance of the craters is diverse, so it is likely that they were formed and modified by different geologic processes. Crater classification is used to analyze these processes.

Tewelde Y. Zuber M. T.
Determining the Fill of the Ghost Craters of Mars' Lowlands **[#2475]**
Many of the craters of Mars' lowlands are partially or completely buried by volcanic and sedimentary fill of unknown relative proportions. By using MOLA data we can determine minimum fill volumes and estimate a minimum volume for the northern plains.

Brusnahan H. M. Milam K. A.
How do the Relationships Between Crater Landforms Change over Time on a Geologically Dynamic Planet? **[#2811]**
In this study, we have subdivided the crater population into groups that correspond to the three martian geologic periods and have measured crater dimensions of each age population in an effort to track changes in crater morphometry over time.

Williams J.-P. Pathare A. V.
Scaling Effective Diameters of Small Impact Crater Clusters on Mars **[#2881]**
Approximately half of the fresh craters on Mars are observed to be crater clustersresulting from disruption of the projectile prior to impacting the surface. We explore how this can influence the crater size-frequency distribution.

Daubar I. J. McEwen A. S. Byrne S. Kennedy M. R.
Seasonal Variation in Current Martian Impact Rate **[#2740]**
Thirty-eight new craters on Mars have well-constrained formation dates. We present an updated prediction for an increased impactor population at aphelion, and examine whether such an aphelion enhancement is detectable in the current impact rate data.

MARS GEOMORPHOLOGY: MAPPING

Audouard J. Poulet F. Vincendon M. Bibring J.-P. Gondet B. Langevin Y.
Remote Sensing of the Thermophysical Properties of the Martian Surface with Visible and Near-Infrared Orbital Measurements **[#2125]**
We present the first study of the thermophysical properties of the martian surface using the OMEGA dataset. The elliptical orbit of Mars Express yields a novel sampling of the thermal cycles, different from TES and THEMIS heliosynchronous datasets.

Bandfield J. L. Edwards C. S. Brand B. D. Montgomery D. R.
The Physical Nature of the Upper Martian Crust **[#1483]**
The pre-Hesperian martian crust is typically composed of poorly consolidated, particulate materials. Material akin to what might be derived from lava flows is much less substantial but appears to have become more common later in martian history.

Jasiewicz J. Stepinski T. F.
Global Geomorphometric Map of Mars **[#1347]**
A global geomorphometric map of Mars is generated from DEM using a novel computer algorithm. This map provides a new valuable tool for terrain analysis and objective quantification of surface units. Auto-mapping of surface units is a future application.

Coles K. S. Tanaka K. L. Christensen P. R. Dohm J. M. Fortezzo C. M. Skinner J. A. Jr. Hare T. M. Blue J. S.
A New Atlas of Mars **[#2530]**
A new atlas of Mars includes base maps created from merged, multiple datasets, global views of geology and composition, and features of interest in each region.

Crown D. A. Berman D. C.
Geologic Mapping of MTM -35137 Quadrangle: Daedalia Planum Region of Mars **[#2055]**
Geologic mapping in the SW Daedalia Planum region of Mars reveals an extensive history of volcanism. The most recent phase in the Middle Amazonian Epoch emplaced vast sheet flows that exhibit evidence for flow inflation along their margins.

Crown D. A. Ramsey M. S. Berman D. C.
Morphologic and Chronologic Studies of Lava Flow Fields in the Southern Tharsis Region of Mars **[#2138]**
The current investigation examines styles and sequences of volcanism in southern Tharsis, Mars. Geologic and flow field mapping reveal changes in flow morphology and age from south of Arsia Mons to the southern extent of Daedalia Planum.

Mouginis-Mark P. J.
A New 1:200,000-Scale Geologic Map of Tooting Crater, Mars **[#1562]**
A geologic map of Tooting Crater, Mars, is presented. This 27-km-diameter crater is very young (<3 m.y.) and displays numerous landforms (impact melt, four ejecta layers, water release from walls) that might also have existed at older craters on Mars.

Tanaka K. L. Dohm J. M. Fortezzo C. M. Irwin R. P. Kolb E. J. Skinner J. A. Jr. Hare T. M. Platz T. Michael G. Robbins S.
The Geology of Mars: What the New Global Map Shows **[#2702]**
We describe how post-Viking data sets and our comprehensive, digital, team-based mapping approach have resulted in more robust unit identification, stratigraphic analysis, and understanding of geologic materials and features on Mars.

Tanaka K. L. Rodriguez J. A. P. Fortezzo C. M. Platz T. Michael G. Robbins S.
Geologic History of Valles Marineris, Mars, Revisited **[#2821]**
Geologic mapping and other investigations using post-Viking image and topographic data reveal some fundamental new insights regarding the geologic history of Valles Marineris.

Ismailos C. Fueten F. Stesky R. Flahaut J. Rossi A. Hauber E.
Layer Thickness Determination of the Interior Layered Deposit within Ganges Chasma, Mars **[#1533]**
Layer thicknesses measured over 3 km of stratigraphy on the large ILD within Ganges Chasma indicate that layering is on average 1.26 m thick. These layer thickness measurements are less than similar measurements made on layers in Candor Mensa.

Guallini L. Gilmore M. S. Marinangeli L.
Geologic and Geomorphologic Map of Iani Chaos (Mars) **[#1410]**
We present the first high-resolution geologic and geomorphologic map of Iani Chaos. Chaotic, LLD, and fluvial units have been defined. Ares Vallis outflow systems erode LLD and control their elevation. The deposition of LLD was coeval to chaos formation.

Stoddard Crile M. B.   Howard D. A.
Geographic Survey of Martian Chaotic Terrain **[#2340]**
GIS analysis evaluates spatial correlations between chaos sites on Mars and associated occurrence properties. These sites are examined from a broad perspective, to determine if there are global trends in the occurrences of chaotic terrain.

Platz T.   Michael G. G.   Skinner J. A.   Tanaka K. L.   Kneissl T.   Fortezzo C. M.
Absolute Age Determinations for Regional Geologic Units: A Case Study of the Middle Noachian Unit in the Arabia-Sabaea-Noachis Terrae Region, Mars **[#2686]**
This study shows how well-selected type locations of regional geologic units can be used for detailed crater counts to derive representative unit model ages.

Dohm J. M.   Robbins S. J.   Hynek B. M.
Recent Geological and Hydrological Activity in Amazonis and Elysium Basins and Their Link, Marte Valles (AME): Prime Target for Future Reconnaissance **[#1948]**
Amazonis and Elysium basins and their link, Marte Vallis (AME), uniquely point to a geologically and hydrologically active Mars. We will present evidence for why AME reconnaissance can help address whether Mars is geologically, hydrologically, and biologically active.

Golder K. B.   Gilmore M. S.
Geomorphological Mapping of Eastern Eridania Basin and Associated Subbasins, Mars **[#2661]**
We performed a geomorphological analysis of the eastern Eridania region using contemporary image data to create a new geologic map at ~1:1.4 M scale to determine the timing of the sequence of events within the basin.

Signorella J. D.   de Wet A. P.   Bleacher J. E.   Collins A.   Schierl Z. P.   Schwans B.
Volcanic or Fluvial Channels on Ascraeus Mons: Focus on the Source Area of Sinuous Channels on the Southeast Rift Apron **[#2773]**
This study focuses on the source area of sinuous channels on the southeast rift apron on Ascraeus Mons, Mars and attempts to understand whether the channels were formed through volcanic or fluvial processes.

Kostama V. -P.   Ivanov M. A.   Rauhala A. I.   Törmänen T.   Korteniemi J.   Raitala J.
Martian Volcanic and Sedimentary Layer Study: Morphologic and Morphometric Criteria for Different Origins **[#1843]**
Layers exposed in volcanic and sedimentary key sites were used as a foundation for morphologic and morphometric identification criteria. Criteria were used for several test sites and results compared to determine the origin of the observed layering.

Voelker M.   Platz T.   Tanaka K. L.   Fortezzo C. M.   Fergason R. L.   Hare T. M.
Geological Mapping of Havel Vallis, Xanthe Terra, Mars: Stratigraphy and Reconstruction of Valley Formation **[#2738]**
Havel Vallis is related to the formation of Juventae and Baetis chaoses and the Maja Valles systems. We present the first geological map of Havel Vallis by characterising its deposits.

Bleamaster L. F. III   Chuang F. C.   Crown D. A.
Geologic Mapping of Locations Formerly Known as MSL Landing Sites: Nili Fossae and Mawrth Vallis, Mars **[#1478]**
Geologic mapping at 1:1-million-scale of Nili Fossae and Mawrth Vallis is being used to assess geologic materials (including a variety of mineral detections) and processes that shape the highlands along the Arabia Terra dichotomy boundary.

Korteniemi J.   Kukkonen S.   Kostama V.-P.
Morphology and Ages of Units on the Floor of Dao Vallis Head, Mars: Preliminary Results **[#2034]**
Preliminary results of CTX/HiRISE scale geologic mapping and age estimates on the various floor units of Dao Vallis head, Mars. We have identified a complex and distinct feature set from an area previously considered as a single unit.

Zimbelman J. R.   Scheidt S. P.
Crater Retention Ages Indicate a Hesperian Age for Western and Central Portions of the Medusae Fossae Formation, Mars **[#2052]**
Impact craters were counted on the THEMIS IR base map for MFF map units. Results suggest that units from both the lower and middle members of MFF were emplaced during the Hesperian rather than the Amazonian.

Capitan R. D.   Osinski G. R.   Van De Wiel M. J.   Kerrigan M.   Barry N.   Blain S.
Mapping Utopia Planitia: Morphometric and Geomorphologic Mapping at a Regional Scale **[#2237]**
A new mapping concept based on elevation datasets and imagery visualization is applied to regional surfaces on Mars, in Utopia Planitia.

Dohm J. M.   Kargel J. S.
Geologic Mapping Investigation of the Argyre and Surrounding Regions of Mars **[#2468]**
A post-Viking-era geologic mapping investigation of the Argyre impact basin and surroundings at 1:5,000,000 scale is ongoing to address important questions concerning the impact event and its subsequent influence on the geology and hydrology of the region.

El Maarry M. R.   Thomas N.   Pommerol A.
Banded Terrain and Associated Geology at the NW of Hellas Basin, Mars **[#2653]**
We describe and map a peculiar formation we call the "banded terrain" that is located in the NW part of Hellas Basin, Mars, as well as the associated geological units to investigate the possible formation mechanisms of this unit.

Fortezzo C. M.   Skinner J. A. Jr.
Geologic Evolution of the Runanga-Jorn Basin, Northeast Hellas, Mars **[#2681]**
The Runanga-Jorn Basin provides insight into the evolution of the northeast Hellas Basin rim region. This development includes megaregolith, volcanic deposits, and stratified sediments with preserved vertical and lateral channel cross sections.

RECENT SLOPE PROCESSES ON MARS

Raack J.   Reiss D.   Hiesinger H.
Gullies and Their Relationships to the Dust-Ice Mantle in the Northwestern Argyre Basin, Mars **[#1798]**
We investigated gullies and their relationship to the atmospherically derived dust-ice mantle and aeolian features in the northwestern part of the Argyre basin and constrained stratigraphic relationships and relative ages of gullies.

Capitan R. D.   Osinski G. R.   Van De Wiel M. J.   Kerrigan M.   Barry N.   Blain S.
Distribution of Gullies in Utopia Planitia, Mars **[#2240]**
Gullies in Utopia Planitia are distributed mainly within craters in the eastern part of this region.

Conway S. J.   Mangold N.   Balme M. R.   Ansan V.
Comparison of the Morphology of Crater-Slopes with Gullies to those Without Gullies **[#2281]**
We use HRSC topography in three regions to quantify the slope and curvature of craters with and without gullies. Gullies form on steeper more concave slopes for a given orientation and latitude. Gullies in the northern hemisphere are less developed.

Schaefer E. I.   McEwen A. S.   Ojha L.   Mattson S. S.
Comprehensive Survey of Recurring Slope Lineae in Tivat Crater, Mars **[#2558]**
We are conducting a comprehensive survey of the evolution of recurring slope lineae (RSL) in Tivat Crater in the southern midlatitudes of Mars over two martian years. The results will help to constrain the as yet unknown formation mechanism for RSL.

VOLCANISM ON MARS AND BEYOND: NEW INSIGHTS FROM GEOLOGIC MAPPING, EMPLACEMENT DYNAMICS, AND MODELS

Jodlowski P.   Platz T.   Michael G. G.
Preliminary Eruption History of the Syrtis Major Volcanic Province, Mars **[#2494]**
In our ongoing study to unlock the eruption history of Mars we present first results of the Syrtis Major volcanic province.

Harrison T. N.
Evidence for Volcanism in and Near the Chaotic Terrains East of Valles Marineris, Mars **[#1057]**
Volcanic features associated with martian chaotic regions, including small shield volcanoes and extensive lava flows, have been documented using the Mars Reconnaissance Orbiter (MRO) Context Camera (CTX).

Richardson J. A.   Bleacher J. E.   Connor C. B.   Connor L. J.
Using Spatial Density to Characterize Volcanic Fields on Mars **[#2314]**
Kernel density estimation is presented as a new, non-parametric method for quantifying the spatial arrangement of volcanic fields. It is applied to two vent fields in Tharsis Province, Mars, to produce insightful spatial density functions.

Schierl Z. P.   Spencer P.   Signorella J.   Collins A.   Schwans B.   de Wet A. P.   Bleacher J. E.
Origin of Sinuous Channels on the SW Apron of Ascraeus Mons and the Surrounding Plains, Mars **[#1602]**
We used a variety of spacecraft imagery to determine the most likely origin for a network of sinuous channels found on the southwest apron of Ascraeus Mons and that extend out onto the surrounding plains.

Collins A.   de Wet A. P.   Bleacher J. E.   Schierl Z.   Schwans B.   Signorella J.   Judge S.
A Comparison and Analog-Based Analysis of Sinuous Channels on the Rift Aprons of Ascraeus Mons and Pavonis Mons Volcanoes, Mars **[#1686]**
The origin of sinuous channels on the rift aprons of Mars' Tharsis volcanos is debated. We show that the channels on the flanks of Ascraeus Mons and Pavonis Mons were likely formed by comparable processes, which were probably volcanic in nature.

Bleacher J. E.   Williams D. A.   Shean D.   Greeley R.
Geologic Mapping of the Olympus Mons Volcano, Mars **[#2186]**
We discuss the current status for our project, geologic mapping of the Olympus Mons volcano, Mars.

Michalski J. R.   Wright S. P.   Bleacher J. E.
Discovery of a Possible Large Caldera in Northwestern Arabia Terra: Implications for Recognizing Ancient Volcanic Source Regions on Mars **[#1392]**
We present evidence for the presence of a large, ancient, previously unrecognized caldera in northwestern Arabia Terra.

Williams D. A.   Garry W. B.   Bleacher J. E.   Shean D.   Greeley R.
Geologic Mapping of Arsia and Pavonis Montes **[#1528]**
This presentation will discuss our progress in geologic mapping of Arsia and Pavonis Montes, Mars, and their surrounding lava flow fields.

Simon M. N.   Carter L. M.   Campbell B. A.   Phillips R. J.   Mattei S.
Studies of Lava Flows in Mars' Tharsis Region Using SHARAD Radar **[#1595]**
Models show that Tharsis area lavas, including long flows near Ascraeus and Pavonis Montes, had viscosities consistent with basaltic flows. We surveyed SHARAD radar data across the area to understand the composition and stratigraphy of these flows.

Lehmann T. R.   Platz T.   Michael G. G.
Ages of Lava Flows in the Hesperia Volcanic Province, Mars **[#2526]**
In our ongoing effort to unlock the eruption history of Mars we present first results from the Hesperia volcanic province.

Dundas C. M.   Keszthelyi L. P.
Modeling of Steam Pressure Under Martian Lava Flows **[#2554]**
We model the buildup of steam pressures under lava flows during heating of martian ground ice. Shallow ice tables allow pressures to build high enough to drive rootless eruptions.

Ramsey M. S.   Crown D. A.   Price M. A.
Decoupling Lava Flow Composition and Emplacement Processes from Eolian Mantling Deposits Using Thermal Infrared Data **[#2013]**
Eolian processes influence Mars and cover many lava surfaces with sand and dust. We present recent results examining unusual thermophysical variations of the Arsia Mons lava flows and focus on a terrestrial analog study examining mantled lava flows.

Keszthelyi L. P.
Revisiting Simple Models Relating Lava Flow Dimensions, Emplacement, and Rheology **[#2567]**
A simple relationship linking the fluidity of a flow to the ratio of flow thickness and length and another linking effusion rate to flow area are derived. These appear to better match observed trends than previous formulations.

Graff M. A.   Zimbelman J. R.
A Search for Inflated Lava Flows on Mars **[#1144]**
A search for inflated lava flows in the Tharsis Montes region of Mars identified five candidate flows out of 314 randomly selected CTX frames, indicating <2% of the frames included probable inflated flows.

Diniega S.   Sigelmann L.   Sangha S.   Smrekar S. E.
Identification and Survey of Martian Lava Inflationary Features **[#2537]**
We are generating a comprehensive/global survey of martian inflationary features — positive topographic features found on basaltic flows that yield a useful connection between surface morphology of a lava field and subsurface/past lava dynamics.

Zimbelman J. R.   Garry W. B.   Bleacher J. E.   Crumpler L. S.
Terraced Margins on the Inflated McCartys Basalt Lava Flow, New Mexico: Constraints on Emplacement Mechanisms **[#1831]**
Terraces along the margin of the McCartys lava flow have distinct topographic characteristics that indicate the features are one manifestation of the lava flow inflation process.

Diniega S.   Smrekar S. E.   Anderson S.   Stofan E.
Lava Flow Dynamics Driven by Temperature-Dependent Viscosity Variations **[#2556]**
We investigate whether a viscosity-driven dynamic instability plays a significant role in initializing lava tubes and channels. This may improve interpretation of lava flow morphology and make it easier to compare flows in different sites/planets.

Ryan A. J.   Christensen P. R.
Lava Coils and Drifting Patterned Ground in Cerberus Palus, Mars **[#2552]**
Lava coils have been identified in Cerberus Palus, Mars. The patterned ground here has also fractured and drifted, like a crust. These two observations indicate that the structures in Cerberus Palus are primarily volcanic, rather than ice-related.

Milazzo M. P.   Weiss D. K.   Jackson B.   Barnes J.
Columnar Jointing on Mars: Earth Analog Studies **[#2726]**
Terrestrial analog modeling of martian columnar jointing suggests that some martian lavas cooled, in the persistent presence of liquid water, over a period of several to tens of years.

Weiss D. K. Jackson B. Milazzo M. P. Barnes J. W.
A New Look at Cooling Models for Martian Flood Basalt Columns **[#1150]**
We describe preliminary inferences of Martian basalt columns' thermal histories and emplacement conditions, and report on a field expedition to the CRBG, where we surveyed basalt column outcrops from the ground and air to ground-truth our data.

Mège D. Purcell P. G. Jourdan F.
Dikes and Linear Troughs: New Observations on the Somali Plate **[#1317]**
Linear troughs ("narrow grabens") are common on planetary surfaces, and are sometimes interpreted as dike emplacement. Linear troughs observed above individual dikes on the Somali Plate give new ideas as to the possible nature of their relationships.

Manfredi L. Greeley R.
Origin of Ridges Seen in Tempe Terra, Mars **[#2599]**
The authors investigate a regionally small unit in Tempe Terra (~15,000 km^2) that is distinguished from nearby units by ridges that have no obvious formation process. These ridges are compared to terrestrial analogs to determine their origin.

Wyrick D. Y. Watson-Morris M. J. Morris A. P.
Physical Analog Modeling of Martian Dike-Induced Deformation **[#2396]**
Analog models of dike injection were performed to determine style and magnitude of structural deformation associated with the dike. Primary deformation style is contraction rather than extension, indicating that martian dikes may not create grabens.

MOVERS AND SHAKERS: PLANETARY DYNAMICS AND TECTONICS

Pendleton M. W. Hansen L. N. Zimmerman M. E. Kohlstedt D. L.
Anisotropic Viscosity of Olivine-Chromite-MORB Aggregates **[#2036]**
Experiments were performed at high P-T conditions to quantify the viscous anisotropy of olivine-MORB aggregates. Our results provide insight into the effect of melt segregation on geodynamic processes and help constrain models of planetary interiors.

Tielke J. A. Zimmerman M. E. Kohlstedt D. L.
The Influence of Hydrogen Content on the Viscosity of Olivine Single Crystals Under Lithospheric Conditions **[#2616]**
In order to more fully characterize the rheological properties of the lithospheric mantles of terrestrial planets, an investigation is underway to derive constitutive equations that describe the flow behavior of hydrous olivine single crystals.

Schulson E. M. Fortt A. L.
Friction of Ice **[#1502]**
New results: The kinetic coefficient friction of ice sliding slowly upon itself at temperatures from 98 to 263 K varies from 0.15 to 0.76, independent of grain size and texture, but not of roughness. Pressure-aging raises the static coefficient.

Walker C. C. Bassis J. N.
Mechanical Failure of the Icy Moons: Modeling Planetary Ice with Discrete Ice Sheet Fracture Models **[#2928]**
We describe the use of a new model developed for terrestrial ice sheet fracture as applied to the ice shells of Enceladus and Europa.

Soderlund K. M. Schmidt B. E. Blankenship D. D.
Convective Heat Transfer in Europa's Ocean and the Formation of Chaos Terrain **[#2903]**
This work implies that thermal gradients along the bottom of the ice shell due to underlying ocean circulation are important to consider for the formation of chaos terrain and evolution of Europa's ice shell.

Tyler R.
Estimates of the Dissipative Heat Generated by Oceans on Icy Satellites in the Outer Solar System **[#2701]**
We show that in the case of several of the icy satellites with potential oceans tidal resonant states with elevated tidal heat are not only possible but may be typical.

Sekhar P.   King S. D.
Non-Newtonian Convection Modeling and the Possibility of Present Day Internal Activity on Ceres? **[#2017]**
Using a three-dimensional spherical shell convection model to understand the internal activity of Ceres. Also, to analyze the geoid, topography and heat flow from our models and compare it with observational data from Dawn when it arrives at Ceres in 2015.

Sterenborg M. G.   Crowley J. W.
Thermal Evolution of Early Solar System and the Possibility of Sustained Dynamos **[#2361]**
We investigate the possibility of a small-body dynamo powered by thermal convection and seek to determine which parameters are relevant for its occurrence and duration as suggested by paleomagnetic analyses of certain meteorites.

Shebalin J. V.
Magnetic Helicity and Planetary Dynamos **[#1147]**
A model of a planetary dynamo based on the Boussinesq approximation along with homogeneous boundary conditions is considered. A statistical theory describing a large-scale MHD dynamo is found, in which magnetic helicity is the critical parameter.

Williams J.-P.
Stagnant Lid Heterogeneity on Mars **[#2847]**
The mantle of Mars is in the stagnant lid convection regime where most of the cold upper boundary layer is immobile and conductive. It is shown here how crust thickness can influence the thickness and heat flow of the lid.

Jiang W.   Roberts J. H.   Kuang W.
Effects of Basin-Forming Impacts on the Historical Martian Dynamo **[#1561]**
We simulate the martian dynamo with a heterogeneous heat flux across the boundary arising from the impacts. Our results show that both the location and the intensity of the impacts have significant effects on the subcritical martian dynamo.

Boutin D.   Arkani-Hamed J.
Low-Magnetic Early Noachian Crust of Mars **[#1667]**
We show that the crust of several old Noachian regions of Mars are very low magnetic. This implies that there was no strong magnetic field on Mars during the formation and cooling of the primordial crust of Mars.

Langlais B.   Thébault E.   Ostanciaux E.   Mangold N.
A Late Martian Dynamo Cessation Time 3.77 Gy Ago **[#1231]**
A new analysis of the magnetic field signature over appropriately sized impact basins and volcanoes on Mars prove that the dynamo lasted until 3.77 Ga, which may explain why most of the liquid water surface activity persisted through that epoch.

Yin A.
High Mantle Viscosity Controls the Enormous Size of Martian Volcanoes: A Hypothesis Based on Inferences from Rayleigh-Taylor Instability Theory **[#1309]**
The size and spacing of Tharsis volcanoes increase with time. This is explained by an increase in mantle viscosity with time that controls volcano spacing assuming eruption centers were initiated by Rayleigh-Taylor instability.

Anderson R. C.   Dohm J. M.   Robbins S.   Hynek B.   Andrews-Hanna J.
Terra Sirenum: Window into Pre-Tharsis and Tharsis Phases of Mars Evolution **[#2803]**
The Terra Sirenum region contains some of the oldest stratigraphic units on Mars. Detailed examination of the structures and units provides an excellent window into identifying the processes that influenced the early geologic evolution of Mars.

Karasozen E. Andrews-Hanna J. C. Dohm J. M. Anderson R. C.
The Formation Mechanism of the South Tharsis Ridge Belt, Mars **[#2592]**
Origin of ridges in the South Tharsis ridge belt is evaluated, using evidence from topographic profiles,deformed craters,tectonic modeling, and crustal thickness.Though no one model explains all aspects of ridges,results support an extensional origin.

Kromuszczyńska O. Mège D. Lucas A. Gurgurewicz J.
Giant Sackung in Valles Marineris **[#1161]**
New CTX-derived DEMs allows quantitative analysis of gravitational spreading of topography in Valles Marineris. In southeast Valles Marineris, 20–40% of vertical fault displacement is estimated to be of gravitational origin.

Zhang Y. X.
Is Valles Marineris a Spreading Basin Due to a Divergent Plate Boundary? **[#1346]**
I propose that Valles Marineris is a narrow basin due to spreading of a divergent plate boundary on Mars, similar to the Red Sea on Earth.

Watkins J. Yin A.
Spatial and Temporal Relationships of Landslides in Valles Marineris, Mars: Constraints on Their Triggering Mechanisms **[#1719]**
Two distinguishable martian landslide types, thick-skinned and thin-skinned, are characterized through systematic mapping of surface morphology, spectral data, and runout ratio in order to constrain landslide trigger and emplacement mechanisms.

Akers C. Schedl A. D. Mundy L.
What Caused the Landslides in Valles Marineris, Mars? **[#1932]**
Our work suggests that Mars-quakes produced most of the landslides in Valles Marineris.

Hooper D. M. Smart K. J.
Morphometric Analysis of a Subset of Landslides in Valles Marineris, Mars **[#2323]**
Morphometric analysis was conducted on four landslides in Valles Marineris indicating complex mass wasting events. Topographic texture, defined as the standard deviation of elevation, serves as a measure of local relief or surface roughness.

Weller M. B. McGovern P. J. Fournier T. Morgan J. K. Katz O.
Eastern Olympus Mons Basal Scarp: A Landslide Story? **[#1565]**
Olympus Mons is surrounded by aureole deposit landforms that may be the result of catastrophic failures of the edifice. We examine the stability of the eastern basal scarp to evaluate a landslide mechanism for the formation of the aureole lobes.

Okubo C. H.
Discovery of Deformation Band Damage Zones on Mars **[#1077]**
High-resolution structural mapping within the layered deposits in west Candor Chasma provide the first detailed documentation of fault-related damage zones on Mars. These damage zones are interpreted to be largely composed of deformation bands.

Clark J. D. Hurtado J. M. Jr.
Characterization of Thrust Fault on the Moon Using Thermoelastic Stress Calculations and 3D Visualizations **[#2895]**
An investigation on lunar thrust fault scarps to determine better constraints on the amount of crustal shortening and improve understanding of the stress state of the Moon with thermoelastic equations and 3D visualizations.

Williams N. R. Bell J. F. III Watters T. R. Banks M. E. Robinson M. S.
Tectonic Mapping of Mare Frigoris Using Lunar Reconnaissance Orbiter Camera Images **[#2708]**
New populations of lobate scarps, wrinkle ridges, and graben have been discovered and mapped in and around Mare Frigoris using Lunar Reconnaissance Orbiter Camera images.

Teanby N. A.   Wookey J.
Meteor Impacts as a Seismic Source on Mars **[#1492]**
There is currently great interest in missions to Mars that include a seismometer. Here we investigate if meteorite impacts provide a viable source for studying Mars' interior.

Stark A.   Oberst J.   Preusker F.   Gwinner K.   Peale S. J.   Margot J.-L.   Zuber M. T.   Solomon S. C.
In-Situ Measurement of Mercury's Physical Librations Using Image and Laser Altimeter Data from MESSENGER: General Approach and Sensitivity Analysis **[#1389]**
We present the analysis of an idea for direct measurement of Mercury's physical librations by combining in situ laser altimeter and image data obtained by the MESSENGER spacecraft.

Van Hoolst T.   Rivoldini A.   Baland R.-M.   Yseboodt M.
The Effect of Tides and an Inner Core on the Forced 88 day Libration of Mercury **[#2082]**
Mercury's librations depend on the moment of inertia of its silicate shell and contain information on the interior structure and composition of Mercury. Here we study the effect of tides and the existence of a solid inner core on the librations.

Rivoldini A.   Van Hoolst T.
Constrainst on Mercury's Core Size and Composition **[#2234]**
We determine to what precision Mercury's core radius and core light-element concentration can be constrained from its global gravity field measured by MESSENGER and from radar measurements about its spin state.

MARTIAN HYDRATED MINERALOGY AND MORPHOLOGY

Gross C.   Wendt L.   Combe J.-Ph.   Jodlowski P.   Marzo G. A.   Roush T. L.   McCord T.
Halbach P.   Neukum G.
Investigating the Pyllosilicate Bearing Micoud Crater in the Northern Plains of Mars **[#1795]**
Micoud crater shows important phyllosilicate detections. Our objective is to identify several types of phyllosilicates and other hydrated minerals in order to test the hypothesis of impact-induced hydrothermalism versus excavation models.

Gross C.   Sowe M.   Wendt L.   Bishop J. L.   Fairén A. G.
Phyllosilicates in Bamberg Crater, Mars **[#2356]**
Hydrated silicates have been identified in several impact craters in the northern plains of Mars. Bamberg is a ~55-km-diameter impact crater located roughly 60 km north of the highlands/lowlands boundary north of Arabia Terra.

Wendt L.   Bishop J. L.   Neukum G.
Knob Fields in the Terra Cimmeria/Terra Sirenum Region of Mars: Stratigraphy, Mineralogy, Morphology **[#2024]**
This study of textural and mineralogical features of light-toned exposures at the knob fields around Ariadnes Colles produced a new stratigraphy that integrates past conflicting models of the region.

Bishop J. L.   Tirsch D.   Tornabene L. L.   McGuire P. C.   Ody A.   Poulet F.   Hash C.   Mustard J. F.   Jaumann R.
Murchie S. L.
Fe/Mg-Smectite, Carbonate and Al-Smectite in Ancient Aqueous Outcrops at Libya Montes and Their Association with Fluvial Features and Mafic Rocks **[#2330]**
Libya Montes hosts Noachian to Amazonian surface rocks featuring Fe/Mg-smectite, carbonate, and Al-smectite resulting from fluvial activity and chemical alteration. Stratigraphy of the aqueous and mafic minerals are shown using HiRISE and HRSC DTMs.

Crumpler L. S.
Mars Landing Sites in Phyllosilicate, Carbonate, and Ancient Wet Noachian Terrains of Bibya Montes **[#1261]**
This is about results from the Mars Landing site "critical data products" study effort.

Greenberger R. N.   Mustard J. F.   Kumar P. S.   Dyar M. D.   Speicher E. A.   Skulte E. C.
Mineral Assemblages of Deccan Basalts and Al-Phyllosilicate Deposits on Mars: Implications for Leaching Processes on Mars **[#1907]**
On Earth, leaching basalt ultimately forms a kaolinite + Fe-oxide assemblage. We are using CRISM to look for an association of Fe-oxides and Al-phyllosilicates on Mars to test the leaching hypothesis for the formation of Al clays over Fe/Mg smectite.

Farrand W. H.   Rice J. W. Jr.
South of Mawrth Vallis: A Potential Future Landing Site with Extensive Exposures of the Mawrth Vallis Stratigraphy **[#1965]**
An area south of the main Mawrth Vallis channel and outcrops, that also displays the diverse Mawrth Vallis stratigraphy, is described. This area lies south of 20N latitude and would allow a solar-powered rover to explore that stratigraphy.

Stein A. J.   Bushick K. M.   Oliver A. R.
Utilization of Sulfates and Hydroxide Minerals as a Determinant of the Acidity of Water on Mars **[#1345]**
Ancient Mars was host to liquid water, which, when tested, shows a negative correlation between the monohydrated sulfates and the hydroxides and helps conclude that the water on Mars trended toward acidity.

Murchie S. L.   Johnson J. R.   Seelos F. P.
MRO/CRISM Observations of Interior Layered Deposits of Tithonium Chasma, Mars **[#1553]**
We report first results from analysis of CRISM data covering western Tithonium Chasma, including a a far-western outlier of the Valles Marineris interior layered deposits, whose location tests proposed genetic mechanisms and regional relations.

Weitz C. M.   Williams R. M. E.   Noe Dobrea E.   Baldridge A.
Hydrated Minerals and Fluvial Features In and Around the Melas Chasma Basin **[#2304]**
Using a synergy of mineralogy derived from CRISM data and morphology interpreted from HiRISE and CTX images, we map geologic units within and around the Melas basin. Numerous hydrated minerals and fluvial features indicate a complex aqueous history.

Liu Y.   Arvidson R. E.   Li R.   Wang W.
Hydrated Minerals Associated with Interior Layered Deposits Near the Southern Wall of Melas Chasma, Valles Marineris, Mars **[#2572]**
We identified a sequence of interior layered deposits over a portion of the southern wall and nearby floor of Melas Chasma using MRO CRISM data. Polyhydrated sulfates, monohydrated sulfates, and jarosite were identified in the ILDS.

Ackiss S. E.   Wray J. J.
Hydrated Sulfates in the Southern High Latitudes of Mars **[#2434]**
CRISM data reveal new hydrated sulfates including gypsum in the southern high latitudes of Mars. Their distribution and spectral features suggest two formation processes: volcanism and/or minor melting of ice.

Amador E. S.   Bandfield J. L.
Elevated Bulk Silica Compositions Associated with Olivine Rich Basalts in Nili Fossae, Mars **[#2508]**
The analysis of bulk rock composition in Nili Fossae has shown the association of high bulk silica surfaces with olivine-rich basalts. When compared to the phyllosilicate mineralogy in the area, a more complicated alteration history is presented.

Horgan B.   Bell J. F. III
Widespread Weathered Glass on the Surface of Mars **[#1622]**
Near-infrared spectra of the northern plains of Mars are consistent with leached glass, potentially implying widespread acidic leaching and a history of explosive volcanism.

HIGH-TEMPERATURE MARTIAN GEOCHEMISTRY

Ody A. Poulet F. Langevin Y. Bibring J.-P. Gondet B. Loizeau D.
Evidence for Analogue Mineralogical Site at Mars to the Los Angeles Basaltic Shergottite **[#2350]**
We identify, map, and characterize possible analogue source regions for the SNC martian meteorites using specral data from the near-infrared imaging spectrometer MEx/OMEGA.

Stephen N. R. Benedix G. K. Genge M.
The Effect of Composition and Zoning on Infra-Red Spectra of the Martian Silicate Minerals **[#2199]**
We isolate mid-IR spectral characteristics of the minerals most abundant in the shergottite meteorites (pyroxene and olivine) and aim to illustrate variable compositions within their hosts are reflected in their spectra with respect to Fe, Mg, and Ca.

Irving A. J. Kuehner S. M. Chen G. Herd C. D. K. Tanaka R. Lapen T. J.
Petrologic, Elemental and Isotopic Characterization of Two Unusual Martian Meteorites: Depleted Permafic Microgabbroic Shergottite Northwest Africa 7032 and Intermediate Permafic Intersertal Shergottite Northwest Africa 7042 **[#2496]**
Two more shergottites found in Northwest Africa emphasize the growing diversity among igneous rocks from Mars.

Wilson N. V. Agee C. B. Sharp Z. D.
New Martian Shergottite NWA 6963 **[#1696]**
NWA 6963 is a newly classified martian shergottite. It has pyroxene compositional trends similar to Shergotty. Oxygen isotopes were also determined on NWA 6963 and they plot on the SNC fractionation array.

Alpert S. P. Harvey R. P. Karner J. M. Hull D. R.
Pairing in Martian Meteorites RBT 04261 and RBT 04262: Olivine's Story **[#2673]**
Pairing in two martian meteorites is explored through comparison of olivine grains. Poikilitic and cumulate textures are compared using petrographic microscope and electron microprobe data.

Righter K. Keller L. P. Rahman Z. Christoffersen R.
Exsolution of Iron-Titanium Oxides in Magnetite in Miller Range (MIL) 03346 Nakhlite: Evidence for Post Crystallization Reduction in the Nakhlite Cumulate Pile **[#2417]**
Fine ilmenite lamellae in titanomagnetite in the MIL 03346 nakhlite define a low temperature and oxygen fugacity. When combined with literature data a cooling and reduction trend is revealed.

Danielson L. Righter K. Pando K. Morris R. V. Graff T. Agresti D. Martin A. Sutton S. Newville M. Lanzirotti A.
Unusual Iron Redox Systematics of Martian Magmas **[#2419]**
Magnetite has been proposed as the dominant FeO-bearing mineral at many MER sites, and may be igneous in origin. We have conducted a series of experiments to determine magnetite stability and the ferric iron abundance in shergottite glasses.

O'Sullivan K. M. Neal C. R. Simonetti A.
A New Petrogenetic Model for the Shergotty Meteorite **[#2307]**
Using crystal stratigraphy, a new petrogenetic model is proposed for the crystallization of the Shergotty meteorite.

Aaron P. M. Shearer C. K. Jr. Burger P. V.
Ghost in the Crystal: Reconstructing the Petrogenic History of Olivine Megacrysts in Martian Basalts Using Phosphorous Zoning **[#1059]**
A reconstruction of early chemical and thermal histories in an REE enriched martian meteorite and an REE depleted martian meteorite by examining P zoning in large olivine megacrysts.

Burger P. V. Shearer C. K. Jr. Papike J. J. McCubbin F. M.
Crystal Chemistry of Merrillite in Martian Basalts and Its Significance to Interpreting Basalt Petrogenesis **[#1178]**
We examine the variation in chemistry of “merrillite-whitlockite” from a variety of martian basalts, compare them to similar phosphates in lunar basalts, and decipher the petrogenetic significance of their crystal chemistry.

Vander Kaaden K. E. McCubbin F. M. Whitson E. S. Hauri E. H. Wang J.
Partitioning of F, Cl, and H_2O Between Apatite and a Synthetic Shergottite Liquid (QUE 94201) at 1.0 GPa and 990°–1000°C **[#1247]**
Apatite/melt partitioning experiments on a QUE 94201 composition were conducted at 1 GPa and 990°–1000°C in a piston-cylinder press. The partition coefficients for F, Cl, and H_2O are highly variable and seem to correlate strongly with melt F content.

Schaub D. R. Stanley B. D. Hirschmann M. M.
Experimental Investigation of CO_2 Solubility in Primitive Martian Basalts Similar to Yamato 980459 and Implications for Martian Atmospheric Evolution **[#2265]**
Experimental studies on a synthetic material similar to martian meteorite Yamato 980459 showed lower than expected CO_2 solubility, implying that models of an early martian greenhouse that are dependent on CO_2 may need reexamination.

Nekvasil H. Ustunusik G. Lindsley D. H.
Degassing of Volatile-Bearing Martian Magma into a CO_2-Rich Atmosphere **[#2640]**
Shallow degassing into a CO_2-rich atmosphere was experimentally simulated in order to assess the contribution of magmatic volatiles to the martian atmosphere and the retention of volatiles in martian basalts upon extrusion.

Rapp J. F. Draper D. S. Mercer C.
Crystallization of Yamato 980459 at 0.5 GPa: Are Residual Liquids like QUE 94201 **[#2108]**
We have experimentally crystallized the Y-980459 composition, and find that the liquid evolves to a very similar composition to that of QUE 94201. This implies that these two meteorites sample geochemically similar source regions.

Collinet M. Médard E. Devouard B. Peslier A.
Constraints on the Parental Melts of Enriched Shergottites from Image Analysis and High Pressure Experiments **[#2269]**
Element map analysis provides accurate bulk rock compositions of LAR 06319 and NWA 1068 that allow the investigation of parental melt compositions. This method shows that olivine-melt disequilibrium cannot be explained by simple olivine accumulation.

Barnett R. G. Jones J. H. Draper D. S. Le L.
An Experimental Investigation of the Shergottite NWA 6162 **[#1523]**
Experiments on the shergottite NWA 6162 indicate that it is a partial olivine cumulate.

Balta J. B. McSween H. Y. Jr.
High Silica Contents in Martian Basalts and Its Relationship to Magmatic Water **[#1190]**
The presence of a thick crust and volatile elements such as Cl or CO_2 should produce basalts with low silica contents. We demonstrate that martian basalts appear silica enriched compared to Earth, and suggest this enrichment is due to magmatic water.

Walton-Hauck E. L.
The Occurrence of Ringwoodite in Shock Veins of the Elephant Moraine 79001 Martian Meteorite **[#1697]**
Ringwoodite in EET A79001 has been confirmed using optical microscopy and raman spectroscopy. This phase occurs as polycrystalline aggregates within and adjacent to shock veins. A shock pressure of 18–23 GPa is estimated for EET A79901 lithology A.

Huber L.   Irving A. J.   Maden C.   Wieler R.
Noble Gas Cosmic Ray Exposure Ages of Four Unusual Martian Meteorites: Shergottites NWA 4797, NWA 5990, NWA 6342 and Nakhlite NWA 5790 **[#1408]**
We measured He, Ne, and Ar of three shergottites and one nakhlite and present their corresponding cosmic-ray-exposure ages.

Lindsay F.   Turrin B.   Herzog G. F.   Swisher C. III   Emge T.
$^{39}Ar/^{40}Ar$ Ages of Single Grains from Shergottite NWA 2626: Pushing the Limits of Laser Step-Heating **[#2836]**
Using laser step heating we measured $^{39}Ar/^{40}Ar$ ages for grains (4.5–35 µg) separated from martian meteorite NWA 2626. Plateau ages for four grains and an isochron age for all samples yield a concordant age of ~500 Ma.

MARTIAN SPECTROSCOPY NITTY GRITTY

Rogers A. D.   Bandfield J. L.   Smith M. D.   Christensen P. R.
Maximizing Information Extraction from the Mars Global Surveyor Thermal Emission Spectrometer Data **[#1650]**
MGS TES surface-atmosphere separation methods are improved by removing minor CO_2 and water vapor absorptions and working with an expanded spectral range. One of the new advantages is ability to assess global spectral variability at >1300 cm^{-1}.

Bell J. F. III   Wolfe E. M.   Horgan B. N. H.   Joseph J.   Araki S.
Kilometer-Scale VIS-NIR Spectral Variations on Mars from Global Mapping and Analysis of Mars Express OMEGA Data **[#1739]**
We report initial results from our work on global mapping and analysis of Mars Express OMEGA hyperspectral imaging data at approximately 1 km/pixel spatial resolution.

Schmidt F.   Bourguignon S.   Le Mouëlic S.   Dobigeon N.   Tréguier E.
Constraining Martian Mineralogical Compositions Using Hyperspectral Images **[#1872]**
Constraining the martian surface composition using hyperspectral images is a difficult task due to the high diversity of the potential minerals. Here we present hypothesis, rationale, and results in the Syrtis Major region.

Wiseman S. M.   Arvidson R. E.   Wolff M. J.   Seelos F. P.   Smith M. D.   Humm D.
Murchie S. L.   Mustard J. F.
Retrieval of Atmospherically Corrected CRISM Spectra Using Radiative Transfer Modeling **[#2146]**
Atmospheric correction of CRISM spectra of the martian surface is necessary for interpretation of mineralogy. We present an iterative radiative transfer procedure that overcomes difficulties to atmospheric correction presented by the CRISM dataset.

Glotch T. D.   Arnold J. A.   Wolff M. J.   Lucey P. G.
Exact Calculation of the Scattering Properties of Olivine in a Salt Matrix: Application to Mars and Trojan Asteroids **[#2652]**
We use the Multiple Sphere T Matrix Model to calculate the scattering properties of olivine in a transparent matrix at mid-IR wavelengths. This work has implications for halite salt deposits on Mars and proposed salty surfaces of Trojan asteroids.

Sklute E. C.   Glotch T. D.   Dyar M. D.
VNIR Optical Constant Determination of Synthetic Jarosites for Quantitative Abundance Analysis of Remote Sensing Datasets **[#1508]**
Preliminary values for the wavelength-dependent, imaginary index of refraction, k, are calculated in the VNIR wavelength range for three compositionally distinct synthetic jarosites using Lucey's 1998 treatment of Hapke scattering theory.

Baldridge A. M.   Bandfield J. L.   Smith M. D.
Effects of Dehydration on TIR Spectra of Chlorides and Implications for Mars **[#2250]**
We measured emissivity spectra for samples from Death Valley to study the spectral characteristics of chlorides in natural environments. By comparison with remote sensing data, we hope to constrain the mineralogy of the putative martian chlorides.

Maturilli A.   Helbert J.   Roush T. L.   D'Amore M.
Influence of Moisture Content on Albedo Changes of JSC-Mars1 Martian Simulant: A Lesson for HiRISE? **[#1406]**
Albedo depends upon the moisture level of the surface, but this relation is not fully understood. In the Planetary Emissivity Laboratory we measured VIS reflectance spectra of a JSC Mars-1 martian soil simulant under several different moisture contents.

Jo I.   Elam J.   Pokuri K.   Garcia V.
Thermal Model Comparison of Fine Grain Sized Sediments with Respect to Moisture Content **[#1336]**
The goal of the Mars Outreach for North Carolina Students research program in 2011–2012 was to find the effects of water on the thermal inertias of fine grain size sediments to develop a model that could determine moisture saturation levels on Mars.

Pokuri J.   Kelley K.   Brownstein N.   Jowell A.   Storch J.
Thermal Modeling of Fine Gravel at Different Saturation Levels **[#1800]**
This study was performed in hope of exploring the possibility of significant amounts of water on Mars. By measuring and modeling the thermal inertia of typical martian sediments, we can potentially identify moisture on or below the surface of Mars.

Sharp T. G.   Michalski J. R.   Dyar M. D.   Bish D. L.   Friedlander L. R.   Glotch T.
Effects of Shock Metamorphism on Phyllosilicate Structures and Spectroscopy **[#2806]**
Clays detected on Mars indicate formation in the early history of Mars. Because the surface of Mars is also heavily cratered, clays on Mars have experienced shock metamorphism. Here we describe shock experiments and structural and spectral characterization fo shocked clays.

Friedlander L. R.   Glotch T.   Michalski J. R.   Sharp T. G.   Dyar M. D.   Bish D. L.
Spectroscopic Studies of Nontronite After Impacts at Three Pressures **[#2520]**
We exposed three phyllosilicate minerals to impacts at high pressure. We present structural and spectroscopic changes in the UV/vis and mid-IR spectra of nontronite. Our observations may explain variability among clay detections on Mars.

Rampe E. B.   Lanza N. L.
Application of Principal Component Analysis to NIR Spectra of Phyllosilicates: A Tool for Identifying Phyllosilicates on Mars **[#2570]**
Principal component analysis (PCA) models of phyllosilicate NIR data demonstrate that PCA can be used to differentiate between types of phyllosilicates and can help identify phyllosilicate compositions on Mars.

Mann J. P.   Cloutis E. A.   Rice M. S.   Craig M. A.   Berard G. M.
Variations in Reflectance Spectra Associated with Exposure of Hydrated Minerals to Simulated Mars Surface Conditions **[#2351]**
This study was designed to have a better understanding of the stability of hydrated minerals on the surface of Mars and to quantify their spectral changes associated within their desiccation process.

Hardgrove C.   Rogers A. D.
Thermal Infrared Spectra of Microcrystalline Sedimentary Phases: Effects of Natural Surface Roughness on Spectral Feature Shape **[#1675]**
Thermal infrared spectral features of common microcrystalline phases (chert, alabaster, micrite) are presented. Spectra are sensitive to mineralogy and micron-scale (~1–25 µm) surface roughness. Roughness is on the scale of the average crystal size.

MARS GEOMORPHOLOGY: ANALOGS, LABORATORY STUDIES, AND SCIENCE TOOLS

Mattson S. Russell P. Byrne S. Kirk R. L. Herkenhoff K. McEwen A. S.
Production and Error Analysis of Polar Digital Terrain Models from HiRISE **[#2659]**
Digital Terrain Models of polar scarps from HiRISE are used to analyze the climate history of Mars. Techniques used to understand image noise and its effects in the DTM also have applications to analyzing the topographic data in a quantitative sense.

Walter S. Kirk R. L. Stenzel O. J. McGuire P. C. Neukum G.
HRSC Topographic Correction by Empirical Photometric Modeling **[#2322]**
We want to use the bundle adjusted orientation information of the High Resolution Stereo Camera (HRSC) together with the terrain model to derive an empirical photometric model of the image and use it for eliminating the topographic shading effects.

Poole W. Muller J-P. Gupta S.
On the Calibration of MOLA Pulse-Width Surface Roughness Estimates Using High-Resolution DTMs **[#1854]**
Surface roughness estimates from MOLA pulse-width data have been compared against surface roughness estimates from high-resolution DTMs to assess the potential of MOLA pulse-width data for landing site selection.

Pedrosa M. M. Silva E. A. Nogueira J. R.
Impact Crater Detection on Mars from Digital Image **[#2004]**
The approach we present aims to detect impact craters on Mars. To this purpose, we applied techniques of mathematical morphology, following the step of pattern recognition that uses the technique of template matching via fast Fourier transform.

Jung J. H. Kim C. J. Heo J. Luo W.
Estimating Volume of Martian Valleys Using Axelsson Algorithm **[#2205]**
A progressive TIN densification algorithm is adapted to estimate the volume martian valley networks (VN) based MOLA point data. This method can be used to estimate the global water inventory associated with VN.

Katz J. Peterson C. M. Viswanathan A. Tedder R. E. Jowell A.
Water Presence Detection Through Thermal Inertia Analysis in Coarse Sediment **[#2019]**
The thermal inertia of coarse sand was examined with varying levels of an artificial water table. Water had an impact on the thermal inertia of the samples. The higher the water table, the lower the change in temperature that was observed.

Jowell A. Jowell A. Pokuri K.
Thermal Modeling of Fine Gravel, Coarse Sand and Fine Sand Sediments with Varying Amounts of Saturated Layers **[#2672]**
This abstract discusses the thermal signatures models of different sediments with various levels of saturation.

De Hon R. A.
Significance of Maars on Mars: Terrestrial Analogs to Martian Monogenic Volcanism **[#1075]**
Monogenic volcanic fields on Earth provide insights into the significance of cinder cones, maars, and pseudocraters in interpreting martian groundwater or permafrost environment and as sampling sites for subjacent geology.

Hooper D. M. Dinwiddie C. L. McGinnis R. N. Smart K. J. Roberts M. M.
Observations of Debris Flows at the Great Kobuk Sand Dunes, Alaska: Implications for Analogous Features on Mars **[#2040]**
Debris flows with fresh-appearing gullies occur on the slopes of several dune fields on Mars. They bear a striking resemblance to small meltwater-induced debris flows observed on slopes of dunes at the Great Kobuk Sand Dunes in Alaska.

Souness C. J. Abramov A.
The Volcanic Terrains of Kamchatka, Eastern Russia: A Glacial and Periglacial Environment with Potential for Mars Analog-Based Research **[#1071]**
The high, glacierized volcanoes of eastern Russia's Kamchatka region host a broad range of glacial and periglacial landscapes which, occurring as they do in association with scoria deposits, offer opportunity for Mars analog-based research.

Reiss D. Raack J. Maturilli A. Rossi A. P. Erkeling G.
Dust Devil Tracks in the Turpan Depression Desert (China): Implications for their Formation on Mars **[#2227]**
We report about laboratory analyses of soil samples of investigated terrestrial dust devils tracks (DDTs). The aim of this study is to constrain the influence of compositional differences of the soil and dust properties in the formation of DDTs.

VENUS ATMOSPHERE AND IONOSPHERE

Luhmann J. G. Villarreal M. Ma Y. J. Russell C. T. Wei H. Y. Zhang T. L.
The Venus Solar Wind Interaction — Is It Purely Ionospheric? **[#1521]**
Reanalysis of magnetic fields observed on Pioneer Venus Orbiter suggests the presence of a persistent hemispheric radial magnetic field bias in the wake above ~250 km. We use a model to ask how a planet-centered weak dipole would manifest itself.

Russell C. T. Strangeway R. J. Leinweber H. Wei H. Y. Daniels J. T. M. Zhang T. L.
Dispersion Measurements of Whistler Mode Signals Observed in the Venus Ionosphere with the Venus Express Magnetometer **[#1635]**
Whistler mode signals produced by lightning have a distinct falling tone at the Earth. Venus whistler mode signals in the ionosphere has a similar "dispersion" consistent with their shorter travel path.

Markiewicz W. J. Petrova E. Shalygina O. Almeida M. Titov D. V. Limaye S. S. Ignatiev N.
Venus Glory and the Unknown UV Absorber **[#2043]**
We report on the first observation of a complete glory on top of the Venus clouds captured with the Venus Monitoring Camera (VMC) when the Sun was almost directly behind the Venus Express spacecraft.

Gao P. Zhang X. Crisp D. Bardeen C. G. Yung Y. L.
Bimodal Distribution of H_2SO_4 Aerosols in the Upper Atmosphere of Venus **[#2906]**
The upwelling of cloud particles and the nucleation of meteoric dust are investigated as possible sources of the bimodal size distribution in the haze particles of Venus' upper atmosphere.

Limaye S. S. Krauss R. J. Rozoff C. Markiewicz W. J.
New Insights into the Hemispheric Vortex Structure and the Cloud Level Circulation of Venus Observed by the Venus Monitoring Camera on Venus Express Orbiter **[#2720]**
Since April 2006, the long term imaging coverage of Venus from the Venus Monitoring Camera (on the Venus Express Orbiter) continues to provide new insights into the dynamics of the Venus atmosphere.

VENUS TOPOGRAPHY, MODELING, AND GEOLOGY

Mitchell K. L. Hensley S. Nunes D. C. Shaffer S. J. Deen R. Ansar A.
Automated Stereogrammetry of Venus **[#2744]**
We automate F-BIDR stereo processing to obtain precise and extensive terrain data, complete with formal error calculation and updated ephemerides. Results will eventually be released to the community with a viewing/editing tool.

TUE POSTERS

Shang K.   Shum C. K.   Fok H. S.   Guo J. Y.   Matsumoto K.   Yi Y.
Venus Topography and Potential k_2 Modeling Using Planet-Wide Differenced Altimeter Measurement **[#1973]**
PVO and Magellan provided Venus altimetry with distinct accuracy. We combined both data using differenced altimetry for orbit adjustment to develop a topography model. Simulation indicates that k_2 estimation may be feasible using altimetry.

Murphy B. S.   Metcalfe K. S.   Ruiz G.   Curtin L. G.   Chestler S. R.   Penido J. C.
Muller J. K.   Grosfils E. B.
Magma Reservoir Rupture Beneath a Venusian Edifice: When Does Lithospheric Flexure Become Significant? **[#1060]**
This FEM study assesses the conditions for which lithospheric flexure beneath a volcanic edifice affects the characteristics of magma reservoir failure on Venus. We examine variable elastic thickness, edifice geometry, and magma reservoir geometry.

Galgana G. A.   McGovern P. J.   Grosfils E. B.
The Formation of Giant Radiating Dike Systems on Venus: Insights from Elastoplastic Flexural Models **[#1662]**
This research presents modes of radial dike formation, magma ascent, and propagation within the venusian lithosphere using elastoplastic finite element models.

Matiella Novak M. A.   Buczkowski D. L.
Structural Mapping Around Irnini Mons, Venus **[#2070]**
An investigation of the numerous structures around Irnini Mons at the highest possible resolution (75 m/pixel) is likely to reveal the relative timing of the structures and thus shed light on the deformation history of this region of Venus.

Shaw B. G. R.   Bleamaster L. F. III
Structural Mapping of Devana Chasma, Venus: Implications for Coronae/Chasmata Relations **[#2088]**
Structural analysis of Devana Chasma for a comparative assessment of styles of coronae and other volcano-tectonic manifestations in rift zones with other extensively studied chasmata with ArcGIS mapping at a scale of 1:1,000,000 of surface features.

Lang N. P.   Lopez I.
Constraints of the Evolution of Three Venusian Coronae **[#1552]**
Volcanism at venusian coronae manifests itself in a variety of ways including large-scale flows, small volcanic constructs or shields, and steep-sided domes or tholi. Our work presented here aims to constrain the causes of this volcanic diversity.

McGowan E. M.   McGill G. E.
Geologic Map of the Lachesis Tessera Quadrangle (V-18), Venus **[#1517]**
Preliminary geologic mapping results for the Lachesis Tessera (V-18) quadrangle on Venus are presented.

Pierce N. P.   Lang N. P.
Preliminary Geological Overview of the Mahuea Tholus Quadrangle (V49), Venus **[#1682]**
This is an introduction to the geology of the Mahuea Tholus quadrangle (V49) on Venus. Topics of interest include the volcano Mahuea Tholus, canali, coronae, and rifting.

Guseva E. N.   Basilevsky A. T.   Head J. W.
Photogeologic Mapping of the Thetis Regio Quadrangle (V-36), Venus **[#1384]**
The results of this work permitted us to identify and map 13 material and 3 structural units, two of which (material of lineated plains and material of rift plains) are specific to this region.

A SEASON IN THE SATURN SYSTEM: TITAN, RINGS, AND OTHER THINGS

Jia Y.-D. Russell C. T. Khurana K. K. Gombosi T. I.
Constraining Seasonal Changes of the Enceladus Plume **[#2620]**
We have deduced the outgassing rates by comparing calculated and observed plasma and field values using our MHD models but no significant variations are found.

Martin E. S. Kattenhorn S. A.
Crater Induced Fracture Reorientation on Enceladus **[#2883]**
We present characterization of crater fracture interactions on Enceladus in order to understand what is driving a crater's ability to reorient fractures.

Patthoff D. A. Kattenhorn S. A. Cooper C. M.
Effects of Nonsynchronous Rotation Stresses on the South Polar Terrain of Enceladus **[#2527]**
Nonsynchronous rotation and diurnal tidal stresses for the SPT of Enceladus are modeled to show how fracture initiation in the ice shell could occur. These results demonstrate how fracture sets of differing ages can coexist in the SPT.

Miller M. S. Martin E. S. Patthoff D. A. Kattenhorn S. A.
Pit Chains on Enceladus: An Experimental Test of the Impact of Fault Geometry on Pit Chain Growth **[#2925]**
We present experimental work examining the effect of segmented pit chain geometries on pit nucleation. Our modified experimental setup will allow us to determine if segmented fault systems result in larger or more numerous pits.

Travis B. J. Schubert G.
Hydrothermal Flow Within Enceladus **[#2695]**
A numerical model of fluid flow and heat and salt transport in Enceladus results in long-lasting transient flow restricted to polar regions with a very non-uniform ice shell distribution.

Wood C. A. Radebaugh J.
Trouble on Titan — Speculative Interpretation of How It Works as a World **[#1628]**
Titan has few identified volcanoes but based on planetary comparisons and degassing it may have other unrecognized volcanic terrains. Boring mid-latitude plains may be fluid lavas, accounting for the paucity of craters and the replenishment of CH_4.

Liu Z. Y. C. Radebaugh J. Harris R. Christiansen E. H. Kirk R. L. Neish C. D. Lorenz R. D. Stofan E. R. Cassini Radar Team
Evidence for an Endogenic Origin of Mountains on Titan **[#2378]**
The purpose of this study is to test the hypothesis of the origin of mountains (exogenic vs. endogenic) on Titan by analyzing (1) mountain heights and (2) structural mapping.

Cook C. Barnes J. W. Radebaugh J. Hurford T. Kattenhorn S. A.
Global Patterns of Tectonism from Mountain Ranges to Virgae **[#2484]**
This research is focused on global patterns of tectonism on the surface of Titan. The orientations of mountain chains and virgae, which are of possible tectonic origin, may provide clues to the dominate mechanism driving tectonism on Titan.

Mills N. T. Radebaugh J. Savage C. J. Le Gall A.
Ongoing Measurements of Dune Width and Spacing on Titan Reveal Dune Field Properties **[#2812]**
Modeling of dune parameters on Titan, such as dune width and spacing have yielded important results concerning dune field maturity. New measurements have been made on the T25 swath that use new methods that better correlate width and spacing.

Arnold K. Radebaugh J. Le Gall A. Turtle E. P. Lorenz R. D. Cassini Radar Team
Sand Volume Estimates on Titan from Cassini Radar and ISS: Fensal and Aztlan Sand Seas **[#2893]**
This is the first detailed study of sand sea areas using images from Cassini's ISS in conjunction with Cassini SAR images. Preliminary results for the total area of dunes in Fensal/Aztlan is about 2.3 million km^2 and total volume is ~70,000 km^3.

Dalba P. A. Buratti B. J. Baines K. H. Barnes J. Brown R. H. Clark R. N. Nicholson P. D. Sotin C.
The Rain in the Plain on Titan **[#1717]**
Analysis of spectral changes as revealed by the Cassini Visual Infrared Mapping Spectrometer (VIMS) instrument shows that between 2009 and 2011 hydrocarbon rainstorms occurred in the Senkyo region of Titan.

Wasiak F. C. Androes D. Blackburn D. G. Chevrier V. F. Dixon J.
Characterization of Ligeia Mare in the North Polar Region of Titan **[#1720]**
The characterization of Titan's Ligeia Mare and surrounding geologically diverse terrain, including active processes.

Larson E. J. L. Sekine Y. Sugita S. Sasamori T. McKay C. P.
Tholin Sensitivity to Atmospheric Methane Abundance and the Implications for Multiple Stable States of Titan's Climate System **[#1427]**
We investigated the effect of methane concentration in tholin production and tholin optical constants in laboratory experiment. We used these results in a simple model to explore the stability of Titan's climate.

Rodriguez S. Le Mouélic S. Barnes J. W. Hirtzig M. Rannou P. Sotin C. Brown R. H. Bow J. Vixie G. Cornet T. Bourgeois O. Narteau C. Courrech du Pont S. Griffith C. A. Jauman R. Stephan K. Buratti B. J. Clark R. N. Baines K. H. Nicholson P. D. Coustenis A.
Singular Regional Brightening Events on Titan as Seen by Cassini/VIMS **[#1158]**
We present here the observation with VIMS of intense brightening at Titan's tropics, very close to the equinox. These events all appear spectrally and morphologically distinct from all previous observed surface features or atmospheric phenomena.

Le Mouélic S. Cornet T. Rodriguez S. Sotin C. Barnes J. W. Brown R. H. Baines K. H. Buratti B. J. Clark R. N. Lefèvre A. Nicholson P. D.
Investigating the Surface of Titan in the 1–2.8 µm Range with CassiniI/VIMS Hyperspectral Images **[#1745]**
We focus in this presentation on the global mapping of the surface of Titan using data from the Visual and Infrared Mapping Spectrometer (VIMS) onboard Cassini. The objective is to produce seamless mosaics in the short-wavelength surface windows.

Wasiak F. C. Luspay-Kuti A. Welivitiya W. D. D. P. Roe L. Chevrier V. F. Blackburn D. G. Cornet T.
A Facility for Simulating Titan's Surface Environment **[#1374]**
We simulate Titan conditions within our laboratory and subject relevant samples to experiments under those conditions. The properties of our facility are presented, including experimental results.

Blackburn D. G. Buratti B. J. Rivera-Valentin E. G.
Exploring the Impact of Thermal Segregation on Dione Through a Bolometric Bond Albedo Map **[#1536]**
Next to Iapetus, Dione exhibits the greatest albedo dichotomy of any object in the solar system. We explore whether the dichotomy on Dione, which is probably exogenically created by the E-ring, can be sustained by a thermal transport mechanism.

Stephan K. Jaumann R. Wagner R. Clark R. N. Cruikshank D. P. Dalle Ore C. Brown R. H. Giese B. Roatsch T. Matson D. Baines K. Filacchione G. Capaccione F. Buratti B. J. Nicholson P. D.
Spectral Properties of the Saturnian Satellites Tethys as Derived from Cassini-VIMS Data **[#2119]**
Results of the spectroscopic analysis of the saturnian satellite Tethys will be presented.

West R. Mitchell K. Stiles B. Anderson Y. Le Gall A. Hayes A. Janssen M. Kirk R. Lopes R. Lorenz R. Wall S. Wye L. Zebker H.
Observation Design and Early Results from Cassini Radar SAR Imaging of Enceladus **[#2602]**
On November 6, 2011, Cassini RADAR obtained a unique data set during a flyby of Enceladus. We will discuss the observation design and processing and present the data in preliminary form.

Hansen G. B. Romain J.
Modeling of Layers of Micron Sized Water Ice Over Enceladus Surface to Fit the 1 to 5 Micron Spectra From the Cassini VIMS Instrument **[#2625]**
We are modeling Enceladus surface as larger grained (>5 μm) ice covered by a fine-grained ice with a roughly monolayer depth. This accurately fits the >3 μm VIMS spectrum and provides a more accurate estimate of the underlying grain size.

Galuba G. G. Denk T. Neukum G.
Dark Terrains on Iapetus: From the Local to the Global Perspective and Back **[#2153]**
The surface of Iapetus is famous for its global albedo dichotomy. A thermal feedback process is proposed as cause. For the proposed global instance of this effect and a local one the triggering mechanism must differ in their characteristic lengths.

Rivera-Valentin E. G. Blackburn D. G. Ulrich R. K.
On the Mass Balance at Iapetus' Poles: Exploring the Limiting Effects of the Dark Overburden **[#1033]**
By modeling the mass balance at the Iapetian poles including the limiting effects of the overburden on Cassini Regio, we show there exists sufficient inbound ice to overcome exogenic darkening.

Rivera-Valentin E. G. Schenk P. White O. L.
Small Diameter Crater Shapes and Geometry on Iapetus and Rhea **[#2042]**
We use high-resolution topography maps of Iapetus and Rhea in order to investigate their small diameter crater d/D ratio, specifically comparing the two satellites and analyzing the Iapetian equatorial ridge.

Reffet E. Ferrari C.
Comparison of Cassini-CIRS Thermal Observations of Saturn's B Ring to a New Multi-Scale Heat Transfer Model **[#1979]**
The thermal evolution of Saturn's B ring has been monitored using the Cassini-CIRS spectrometer. Confrontation to a new multiscale heat transfer model allows retrieval of the physical properties of the particles and the structure of the ring.

Tseng W.-L. Elrod M. K. Johnson R. E.
Seasonal Variability of Saturn's Ring Atmosphere and Its Effects **[#1975]**
We predicted would-be seasonal variations in the ring atmosphere due to the orientation of the ring plane to the Sun. Therefore, it would exhibit seasonal variations in the magnetospheric O_2^+ ion density. We also confirmed the result by CAPS data.

Poppe A. R. Horanyi M.
On the Edgeworth-Kuiper Belt Dust Flux to Saturn **[#1365]**
We describe the model-predicted flux of Edgeworth-Kuiper belt dust grains into the saturnian system. We compare our model with previous estimates of the incoming dust flux and discuss implications for physical processes in the saturnian system.

ICY SATELLITES: CLAYS AND CHEMISTRY

Hibbitts C. A. Hagaman S. Greenspon A.
The Adsorption of Gases onto Refractory Materials: CO_2 onto Clays and Their Relevance to the Icy Galilean Satellites **[#2400]**
We explore the spectral nature and thermal stability of CO_2 adsorbed onto cryogenic clays as an analog to processes potentially occurring on the Galilean satellites.

Hibbitts C. A. McAdam M. M. Greenspon A.
The Effects of Vacuum Desiccation and Temperature on the Near-Infrared Spectra of Clays **[#1704]**
We investigate the spectral characteristics of carbon dioxide adsorbed by clays at low temperatures to better understand the mechanism responsible for the carbon dioxide on the Galilean and saturnian satellites.

Fortes A. D. Wood I. G. Tucker M. G. Marshall W. G.
An Empirical Equation of State for Ice-VI with Application to Planetary Modelling and Impact Simulations **[#1061]**
We report a thermal equation of state for ice-VI fitted to high-pressure powder diffraction data, which will improve the accuracy of both internal structure models for icy planetary bodies and simulations of the impact cratering process.

Maynard-Casely H. E. Brand H. E. A. Wallwork K. S.
Sulfuric Acid Octahydrate Formation from a Water Rich Environment: A Powder Diffraction Study **[#1363]**
This study has shown that a water-rich sulfuric acid hydrate will form from a “drowned” solution and persist over a large range of temperatures, making it likely to be an important stable phase applicable to the subsurface region of Europa.

Dougherty A. J. Avidon J. A. Hogenboom D. L. Kargel J. S.
Eutectic Temperatures for Low and High Pressure Phases of Sodium Sulfate Hydrates with Applications to Europa **[#2321]**
We use optical images of crystallization in the Na_2SO_4-H_2O system, coupled with measurements of pressure, temperature, and volume changes, to report eutectic transitions for pressures up to 375 MPa, with implications for modeling Europa’s ocean.

Bollengier O. Choukroun M. Grasset O. Le Menn E. Tobie G. Bellino G. Bezacier L. Morizet Y. Oancea A. Taffin C.
The H_2O–CO_2 System up to 1.7 GPa: Implications for Large Icy Moons **[#2162]**
New experiments have been carried out in the H_2O-CO_2 system over the 0–1.7 GPa and 255–330 K ranges to constrain the CO_2 hydrates stability and CO_2 solubility. Implications for the large outer solar system icy bodies (e.g., Ganymede) are discussed.

ICY SATELLITES: HEATING, FAULTING, RHEOLOGY, AND WEATHERING

Patterson G. W. Paranicas C. Prockter L. M.
Characterizing Electron Bombardment of Europa’s Surface by Location and Depth **[#2447]**
We characterize the bombardment of energetic electrons onto Europa’s surface, thereby isolating and quantifying a major contributor to exogenic processes that influence the surface albedo, chemistry, and astrobiological potential of the satellite.

Rathbun J. A. Spencer J. R. Howett C. J. A.
Galileo PPR Observations of Europa: Correlations of Thermophysical Properties with Surface Features **[#2610]**
We will compare Galileo Photopolarimeter-Radiometer (PPR) temperature data to thermal models and a geologic map to determine if there are correlations between thermophysical properties and surface features.

Walker M. E. Mitchell J. L.
A Model for the Elastic Libration of Europa’s Ice Shell **[#1099]**
Decoupled from its synchronously rotating interior, Europa’s ice shell experiences oscillations. Using tidal potential theory and the resulting stresses we evaluate the elastic restoring torque and the shell’s librational amplitude and frequency.

Cameron M. E. Nahm A. L. Smith-Konter B. R. Pappalardo R. T.
Tidally Driven Coulomb Failure Along Europa’s Agenor Linea **[#1718]**
We investigate the relationship between shear and normal stresses at Agenor Linea to better understand the role of tidal (diurnal + NSR) stress sources and implications for shear failure of fractures on Europa.

Quick L. C. Marsh B. D.
Dynamics of Europan Volcanism: Constraints from Heat Transfer and Phase Equilibria **[#2549]**
Using initial melt volume, melt chemistry, cryomagma ascent rate, and potential ascent mechanisms as constraints, we explore conditions under which cryomagma transfer in Europa's interior may lead to cryovolcanism at the surface.

Johnston S. A. Montési L. G.
The Role of Dike Intrusions in Ridge Formation on Europa **[#2538]**
Deformation of the Europan crust around a crystallizing intrusion produces a ridge at the surface. We show in numerical models that the cross section of the intrusion controls the morphology of the ridge (single or double ridge).

Beddingfield C. B. Burr D. M. Emery J. P.
Evidence for a Listric Extensional Fault System Bounding Arden Corona on Uranus' Moon Miranda **[#1366]**
We use multiple lines of evidence to test the hypothesis that the boundary of Arden Corona on Uranus' moon Miranda consists of a listric fault geometry. Our results support this hypothesis and may indicate a subsurface detachment.

Gao P. Stevenson D. J.
How Does Nonhydrostaticity Affect the Determination of Icy Satellites' Moment of Inertia? **[#1701]**
The effects of degree-2 nonhydrostatic structures on the accuracy of the Radau Darwin method of moment of inertia estimation is investigated for large icy satellites.

Io: Volcanism, Global Shape, and Atmosphere

Spencer J. R. Jessup K. L. Tsang C. C. C. Cunningham N. Retherford K.
Evidence for Volcanic Support of Io's Jupiter-Facing Atmosphere from Constraints on Post-Eclipse Atmospheric Changes **[#2420]**
New Hubble observations of Io's atmosphere show minimal changes in atmospheric density as Io warms after Jupiter eclipse. The simplest explanation of this surprising result is that the atmosphere on the this side of Io is volcanically supported.

Tsang C. C. C. Spencer J. R. Jessup K. L.
Io's Atmosphere in 2010: Synergistic Observations of Longitudinal Distribution in the Near-Ultraviolet and the Mid-Infrared **[#2789]**
Here, we present a unique analysis of quasi-simultaneous observations of Io's atmosphere in 2010, from the near-ultraviolet HST-COS and the mid-infrared, IRTF-TEXES, concerning the longitudinal variability of Io's atmosphere.

Hamilton C. W. Beggan C. D. Still S. Beuthe M. Lopes R. M. C. Williams D. A. Radebaugh J. Wright W.
Cluster Analysis of Volcanoes on Io: Implications for Tidal Heating and Magma Ascent **[#1041]**
Distance-based clustering of volcanoes on Io supports asthenospheric-dominated tidal heating models but reveals a significant eastward offset between volcano concentrations and the tidal axis that may imply lateral advection in a global magma ocean.

Nadezhdina I. Oberst J. Patraty V. Shishkina L. Zubarev A.
New Control Point Network and Global Shape Estimates for Io **[#1039]**
We have analyzed Galileo and Voyager images of Io to derive a new geodetic control point network for this innermost jovian satellite. Also we determined best-fit spheres, spheroids, and triaxial ellipsoids.

White O. L. Schenk P. M. Hoogenboom T.
New Topographic Maps of Io Using Voyager and Galileo Stereo Imaging and Photoclinometry **[#2429]**
Stereo and photoclinometry processing have been applied to Voyager and Galileo images of Io in order to derive regional- and local-scale topographic maps of 20% of the moon's surface to date. We present initial mapping results.

Davies A. G. White O. L. Schenk P. Radebaugh J.
Ionian Paterae Volumes and Slopes Derived from New Photoclinometry and Stereo Products **[#2112]**
Measurements of 18 ionian paterae depths (~1 km) and relatively shallow wall slopes yield estimates of volumes of material removed, ranging from ~2000 km^3 to over 10,000 km^3. These numbers will allow the testing of formation models.

Veeder G. J. Davies A. G. Matson D. L. Johnson T. V. Williams D. A. Radebaugh J.
Distribution of Io's Volcanic Thermal Emission from Galileo and Ground-Based Data **[#2085]**
We have estimated thermal emission from 240 individual Io thermal sources. These include many dark areas seen by Galileo that did not exhibit obvious anomalous thermal emission, yet their low albedo suggests that these features are at least warm.

Bunte M. K. Lin Y. Saripalli S. Greeley R.
Autonomous Detection of Transient Phenomena on Planetary Bodies **[#2180]**
Autonomous supervised classification techniques detect 73–95% of transient geophysical phenomena such as volcanic plumes on Io and Enceladus and outgassing on Comet 103/P Hartley 2 and differentiate features such as mountain slopes and plumes.

PLANETARY HYDROLOGY: WET WORLDS

Cornet T. Bourgeois O. Le Mouélic S. Rodriguez S. Sotin C. Lefèvre A. Barnes J. W. Brown R. H. Baines K. H. Buratti B. J. Clark R. N. Nicholson P. D.
Shaping Titan's Landscapes by Dissolution and Evaporation: The Case of Ontario Lacus, a High-Latitude Semi-Arid Karst-Playa Landsystem **[#1914]**
The comparison between Ontario Lacus (Titan) and the Etosha Pan (Namibia), a semi-arid karst-playa landsystem, infer that dissolution/evaporation processes shaped Ontario Lacus' region until the present day, and perhaps as a whole, other Titan's lakes.

Cornet T. Magar S. S. Luspay-Kuti A. Wasiak F. C. Chevrier V. F. Welivitiya W. D. D. P. Roe L. Bourgeois O. Le Mouélic S.
Infrared Monitoring of Liquid/Solid Hydrocarbons Under Titan Simulated Conditions **[#1849]**
We investigate the spectral behavior of Titan relevant liquid/solid hydrocarbon compounds, between 1.0 and 2.6 µm, under Titan simulated conditions (1.5 bar of N_2, 90–95 K).

Luspay-Kuti A. Wasiak F. C. Chevrier V. F. Welivitiya W. D. D. P. Roe L. A. Cornet T. Magar S. S.
Liquid Hydrocarbon Evaporation Under Simulated Titan Conditions **[#2408]**
Ethane and methane-ethane mixtures are condensed and monitored in our Titan simulation chamber, under Titan surface conditions. Results on the evaporation rate of these liquids that are most probably the main components of the lakes are presented.

Luspay-Kuti A. Wasiak F. C. Chevrier V. F. Magar S. S. Welivitiya W. D. D. P. Roe L. A. Cornet T.
Experimental Simulations of Liquid Methane Evaporation Under Titan Surface Conditions **[#2287]**
We simulate Titan surface conditions and the evaporation of methane, a major component of liquids. Our results may well quantitatively characterize methane liquid formed at the arid equatorial regions in possible occasional, heavy rainfall events.

Malaska M. Radebaugh J. Barnes J. Mitchell K.
Titan in a Fume Hood: Room-Temperature Simulation of a Titan Evaporite Playa Using a Multi-Component Mixture of Organic Compounds **[#2139]**
A multi-component mixture of organic compounds in heptanes was evaporated to simulate the formation of an evaporite playa on Titan. The deposition sequence of the analog materials and their implications for Titan geology will be presented.

Welivitiya W. D. D. P. Wasiak F. Tullis J. A. Blackburn D. G. Chevrier V. F.
A Remote Sensing and GIS Approach for Change Detection on Titan's Lakes Using Cassini Orbiter's SAR Data **[#1678]**
We present the results obtained by applying RS and GIS techniques to identify changes in Titan lakes using Cassini SAR data. We detected a transient change in an estuary-like feature in the Kraken Mare area on Titan.

Vixie G. Barnes J. W. Jackson B. Wilson P.
Temperate Lakes Discovered on Titan **[#2766]**
We have discovered two temperate lakes on Titan using Cassini's Visual and Infrared Mapping Spectrometer (VIMS). Three key features help to identify these surface features as lakes: morphology, albedo, and specular reflection.

Sharma P. Byrne S.
Modeling of Titan's Surface Processes Constrained by Shoreline Fractal Analysis and Comparison with Terrestrial Analogs **[#1567]**
We have carried out statistical analyses of Titan's north polar lake shorelines and terrestrial analogs, to constrain the spatial distribution of surface process types on Titan and perform landscape evolution modeling.

Harrison K. P.
Thermokarst Processes in Titan's Lakes: Comparison with Terrestrial Data **[#2271]**
Qualitative comparisons between Titan's lakes and terrestrial thermokarst depressions have revealed some intriguing similarities. A quantitative study of lake outlines provides further evidence that thermokarst processes modified Titanian lakes.

Magar S. S. Chevrier V. F. Ulrich R. Howe K. L.
Numerical Modeling of Titan Fluvial Channels **[#2348]**
Model for brines flowing in martian gullies will be modified under Titan conditions. It will place minimum constrains on the fluid properties within Titan's large channels in order to identify the maximum boulder sizes the channel could support.

Choukroun M. Sotin C.
Is Titan's Shape Caused by its Meteorological and Carbon Cycle? **[#1760]**
We show that Titan's global shape can result from the chemical interactions between the products of it atmospheric chemistry with subsurface materials, by subsidence associated to clathrate formation/substitution.

Parsons R. A. Moore J. M. Howard A. D.
Hydrology of Hesperian/Amazonian-Aged Valleys in Newton Basin, Mars: How Much Water for How Long? **[#1728]**
Applying sediment transport theory to martian valleys for a range of channel depths and sediment grain sizes suggest that the cumulative duration of fluvial activity lasted 0.5 to 10 years, and the largest valleys were cut by 1 km^3 of water.

Head J. W. III
Mars Planetary Hydrology: Was the Martian Hydrological Cycle and System Ever Globally Vertically Integrated? **[#2137]**
New data (atmosphere models, mineralogy, surface geology, terrestrial analogs, and the influence of volcanism on the atmosphere) combine to suggest that the hydrological system of Mars might not have been vertically integrated in the Late Noachian.

Baker D. M. H. Head J. W.
Geology and Chronology of the Ma'adim Vallis-Eridania Basin Region, Mars: Implications for the Noachian-Hesperian Hydrologic Cycle **[#1252]**
We assess the hydrologic evolution of a large paleolake basin on Mars by analyzing the character of units and valleys within the basin's watershed. This analysis places constraints on the environmental conditions near the Noachian/Hesperian boundary.

Di Achille G. Hoke M. R. T. Rossi A. P. Hynek B. M. Esposito F. Hutton E. W. H. Kettner A. J.
Process-Response Sedimentary Modeling of Ancient Martian Deltas 1: Introduction and Case Studies **[#2120]**
We are carrying out a comprehensive study of the hydrology and sedimentology of martian deltas by using modified versions of state of the art terrestrial models whose concepts have been successfully tested in several different terrestrial settings.

Hoke M. R. T. Hynek B. M. Di Achille G. Hutton E.
Process-Response Sedimentary Modeling of Ancient Martian Deltas 2: Offshore Sedimentation and Formation Timescales **[#2254]**
We use a comprehensive three-dimensional model (Sedflux2.0) to explore the conditions of delta formation on ancient Mars. Our results show significant offshore sedimentation and longer formation timescales than otherwise determined by bulk transport calculations.

Erkeling G. Reiss D. Hiesinger H. Poulet F. Carter J. Ivanov M. A. Hauber E. Jaumann R.
Valleys, Paleolakes and Possible Shorelines at the Libya Montes/Isidis Boundary: Implications for the Hydrologic Evolution of Mars **[#1762]**
We describe the results of our morphologic, stratigraphic, and mineralogic investigations of fluvial landforms, paleolakes, and possible shoreline morphologies at the Libya Montes/Isidis Planitia boundary between 85°/86.5°E and 1.8°/5°N.

Carter J. Poulet F. Mangold N. Ansan V. Dehouck E. Bibring J.-P. Murchie S.
Composition of Deltas and Alluvial Fans on Mars **[#1978]**
A systematic survey for all alluvial fans and deltas on MARS using the CRISM imaging spectrometer reveals the presence of opaline silica, an alteration product formed in situ in an arid environment.

Petau A. Tirsch D. Jaumann J.
Geomorphological Analysis of Mass Balances of Martian Valley Networks in Western Terra Sirenum **[#1834]**
The intention of this study focuses on a geomorphological analysis of valley networks in the Western part of Terra Sirenum presenting calculations to improve the insight at a time in which there must have been other environmental and climate conditions.

Mercier D. Lowell R. P.
Ice Melting Above a Convecting, Crystallizing Magmatic Sill on Mars **[#2275]**
We investigate the melting of an ice layer above a vigorously convecting, crystallizing magmatic sill intruded in the martian crust. We show that the melt layer is 3.5 times the sill thickness, assuming crystals remain suspended in the melt.

Rhodes N. Hurtado J. M. Jr.
A Magnetic Survey of Kilbourne Hole, Southern New Mexico: Implications for Near Surface Geophysical Exploration of Mars and the Moon **[#2914]**
A detailed magnetic survey of Kilbourne Hole, a phreatomagmatic crater, to map the boundary of eruptive material, in order to quatify the size of the groundwater reservoir related to the magma-water interactions that caused the eruption.

Jupiter and Beyond the Infinite

Simon-Miller A. A.   Rogers J. H.   Gierasch P. J.   Choi D.   Allison M. D.   Adamoli G.   Mettig H.-J.
Longitudinal Variation and Waves in Jupiter's South Equatorial Wind Jet **[#1104]**
Jupiter's south equatorial winds and clouds are consistent with a high frequency, gravity-inertia, wave. A second, westward-moving, Rossby wave was also identified. Asymmetry with the north equatorial clouds are likely due to the Great Red Spot.

Wilson H. F.   Militzer B.
Rocky Core Erosion in Jupiter and Giant Exoplanets **[#2873]**
We present ab initio calculations which predict significant solubility of rocky materials at the core-mantle boundaries of Jupiter. This implies that cores of Jupiter and larger exoplanets are likely to be at least partially eroded.

Thom N.   Jackson B.
Atmospheric Mass Loss and Orbital Evolution of Exoplanets **[#2717]**
The distribution and evolution of exoplanets are a product of many factors, including atmospheric mass loss and tidal forces. These two effects are coupled here in order to explain the gaps in the distribution of mass and semi-major axes.

Education and Public Outreach: Outer Planets, Satellites, and Rings

Dyches P.   Zimmerman-Brachman R.   Spear K.   Simon M.   Bechtel R.
Knowledge is Power: Radioisotope Power Systems Education and Public Outreach at NASA **[#1640]**
The education and public outreach effort for NASA's Radioisotope Power Systems Program raises awareness of the long, safe history of exploration enabled by space nuclear power technologies and emphasizes their importance for future exploration.

Mercury: Compositional Remote Sensing and Analysis

D'Amore M.   Helbert J.   Maturilli A.   Head J. W. III   Sprague A. L.   Izenberg N. R.   Holsclaw G. M.   McClintock W. E.   Vilas F.   Solomon S. C.
Global Classification of MESSENGER Spectral Reflectance Data and a Detailed Look at Rudaki Plains **[#1413]**
We suppose that Mercury surface compositional information can be derived from spectral reflectance measurements of MESSENGER/MASCS via statistical techniques. Unsupervised hierarchical clustering successfully identify surface region and relationship.

Domingue D. L.   Holsclaw G. M.   Izenberg N. R.   Vilas F.
Photometric Analysis of Selected Regions on Mercury from MESSENGER Orbital Observations of Spectral Reflectance **[#2498]**
Photometric analysis of MASCS observations provide corrections to surface spectral observations and give insight into the variations in photometric properties among difference surface units.

Domingue D. L.   Vilas F.   Travnicek P. M.   Benna M.   Schriver D.   Sarantos M.
A Search for Latitudinal Variation in Space Weathering on Mercury's Surface **[#1646]**
Bombardment by charged solar wind particles contributes to space weathering of regoliths. Observations from MESSENGER indicate latitudinal variability in the surface ion flux, raising the possibility of latitudinal variability in spectral effects.

D'Incecco P.   Helbert J.   Head J. W.   D'Amore M.   Maturilli A.   Izenberg N. R.
Holsclaw G. M.   Domingue D. L.
Kuiper Crater on Mercury — An Opportunity to Study Recent Surface Weathering Trends with MESSENGER **[#1815]**
The ~55–60-km-diameter, unusually fresh impact crater Kuiper displays one of the highest albedos of any area on the surface of Mercury and is thus an excellent candidate for an end member for the study of "space weathering" effects on Mercury.

Blewett D. T.   Chabot N. L.   Denevi B. W.   Ernst C. M.   Murchie S. L.   Izenberg N. L.   Xiao Z.
Vaughan W. M.   Head J. W. III   Helbert J.
Spectral and Morphological Studies of Mercury's Hollows **[#1329]**
High-reflectance depressions found in and around impact structures on Mercury occur in several morphological types and in association with a dark global color unit. We compare spectra of Mercury surfaces with lab spectra of analog minerals.

Xiao Z.   Strom R. G.   Blewett D. T.   Chapman C. R.   Denevi B. W.   Head J. W.   Fassett C. I.   Braden S. E.
Gwinner K.   Solomon S. C.   Murchie S. L.   Watters T. R.   Banks M. E.
The Youngest Geologic Terrains on Mercury **[#2143]**
We have identified bright-haloed hollows, dark spots, and volcanic vents that appear to be younger than rayed craters.

Vilas F.   Domingue D. L.   Sprague A. L.   Izenberg N. R.   Klima R. L.   Jensen E. A.   Helbert J.   D'Amore M.
Stockstill-Cahill K. R.   Solomon S. C.
Search for Absorption Features in Mercury's Visible Reflectance Spectra: Recent Results from MESSENGER **[#1330]**
MESSENGER visible reflectance data are searched for absorption features. Most reflectance spectra show no obvious absorption features. Subtle absorption features are seen in spectra of high-albedo material associated with younger features.

Greenspon A. S.   Hibbitts C. A.   Dyar M. D.
Compositional Dependencies in Ultraviolet Reflectance Spectra of Synthetic Glasses Relevant to Airless Bodies **[#2490]**
We characterize the reflectance UV spectra (130–400 nm) of synthetic glasses relevant to airless bodies and relate identifiable spectral features to the chemical composition of each sample. Spectra are taken under high vacuum.

Maturilli A.   Helbert J.   St. John J.   D'Amore M.
Visible-Infrared Reflectance and Emissivity Spectra of a Terrestrial Komatiite as a Guide to Observations at Mercury **[#1394]**
From MESSENGER X-ray measurements, Mercury's crust is comparable to terrestrial komatiites. At the Planetary Emissivity Laboratory (PEL) we measured the VIS and IR spectra of a terrestrial komatiite sample under a range of environmental conditions.

Stockstill-Cahill K. R.   McCoy T. J.   Nittler L. R.   Weider S. Z.
Magnesium-Rich Compositions of Mercury: Implications for Magmatism from Petrologic Modeling **[#2107]**
Petrologic modeling of Mercury's NVP and non-NVP compositions suggests eruption of low-viscosity, high-temperature magmas and reveals mineralogical variation between these two units.

Rhodes E. A.   Peplowski P. N.   Evans L. G.   Hamara D. K.   Solomon S. C.
Element Abundances from MESSENGER's Gamma-Ray Spectrometer: Background Normalization **[#1555]**
Element abundances from Mercury orbital gamma-ray spectrometer data will be presented, for Ca, S, and Al, and perhaps Fe and Cl. Data normalization methods used to derive these abundances will be described, particularly models of spacecraft background.

Starr R. D. Nittler L. R. Weider S. Z. Rhodes E. A. Schriver D. Schlemm C. E. II Solomon S. C.
MESSENGER X-Ray Spectrometer Detection of Electron-Induced X-Ray Fluorescence from Mercury's Surface **[#1176]**
X-ray emissions observed from the dark side of Mercury are the result of ~1–10 keV electrons impinging on the planet's surface. Knowledge of the precipitating electron distribution makes it possible to infer surface composition from the measured fluorescent spectra.

Meslin P.-Y. Déprez G.
Radon Exhalation as a Possible Explanation to the Low Th/U Ratio Measured by MESSENGER GRS on Mercury **[#2800]**
The Th/U ratio recently measured by MESSENGER GRS is puzzling, because it is much lower than its chondritic value. A possible explanation is an increase of the apparent uranium concentration measured by the GRS resulting from the outgassing of radon.

MERCURY: VOLCANISM AND MAPPING

Wilson L. Head J. W. III
Volcanic Eruption Processes on Mercury **[#1316]**
Data from MESSENGER on the presence, absence, and distribution of volcanic features, along with geochemical information on crustal composition, allow us to model the processes controlling the generation, ascent, and eruption rates of magma on Mercury.

Hurwitz D. M. Head J. W. III Byrne P. K. Xiao Z.
Potential for Lava Erosion on Mercury: Modeling the Formation of Both Small and Large Lava Channels **[#1055]**
Features consistent with channelized lava flow and erosion have been identified in images collected by MESSENGER. Analytical models are used to estimate potential erosion rates and eruption durations required to form these observed channels.

Goudge T. A. Head J. W. III Kerber L. Blewett D. T. Denevi B. W. Murchie S. L. Izenberg N. R. McClintock W. E. Holsclaw G. M. Domingue D. L. Gillis-Davis J. J. Xiao Z. Strom R. G. Helbert J. Solomon S. C.
Global Inventory and Characterization of Pyroclastic Deposits on Mercury: New Insights into Pyroclastic Activity from MESSENGER Orbital Data **[#1325]**
MESSENGER orbital data of previously identified pyroclastic deposits show detailed aspects of vent morphologies, relative ages, compositions, and geologic associations. Evidence for newly identified pyroclastic deposits are also presented.

Zambon F. De Sanctis M. C. Capaccioni F. Filacchione G. Carli C. Ammannito E. Frigeri A.
Pyroclastic Deposits in the Rudaki's Area **[#2069]**
We distinguished a bright spot in the Rudaki's Area on Mercury with the minimum distance classification method. We compared this region with some pyroclastic deposits using RGB analysis to investigate the spectral properties of this spot.

Buczkowski D. L. Seelos K. D.
A Map of the Intra-Ejecta Plains of the Caloris Basin, Mercury **[#1844]**
This presentation outlines the progress associated with a mapping project of Caloris basin, intended to improve our knowledge of the geology and geologic history of the basin.

Whitten J. L. Head J. W. III Murchie S. L. Blewett D. T. Denevi B. W. Neumann G. A. Zuber M. T. Smith D. E. Solomon S. C.
Intercrater Plains on Mercury: Topographic Assessment with MESSENGER Data **[#1479]**
MESSENGER data are used to complete hypsometry/flooding/chronology analyses on multiple intercrater plains regions on Mercury. This data is used to assess the formation mechanism of these plains, distinguishing between impact and volcanic processes.

Becker K. J.   Weller L. A.   Edmundson K. L.   Becker T. L.   Robinson M. S.   Enns A. C.   Solomon S. C.
Global Controlled Mosaic of Mercury from MESSENGER Orbital Images **[#2654]**
The USGS is constructing a global, controlled monochrome base map of Mercury from MESSENGER orbital data. A digital elevation model is created from this process that will aid in the creation of map products.

MERCURY: TECTONICS, TOPOGRAPHY, AND IMPACT CRATERING

Elgner S.   Oberst J.   Perry M. E.   Zuber M. T.   Robinson M. S.   Solomon S. C.
Analysis of Mercury Limb Profiles from MESSENGER Images: Results from Least-Squares Adjustments of Crossover Heights **[#1469]**
We have analyzed images of Mercury's limb obtained by MESSENGER's Mercury Dual Imaging System for studies of the planet's global shape.

Di Achille G.   Popa C.   Massironi M.   Ferrari S.   Giacomini L.   Mazzotta Epifani E.   Pozzobon R.   Zusi M.   Cremonese G.   Palumbo P.
Mapping Mercury's Tectonic Features at the Terminator: Implications for Radius Change Estimates and Thermal History Models **[#2176]**
We mapped Mercury's tectonic features at the terminator thus under optimal lighting geometry for their observation. This favorable illumination allowed us to infer reliable estimates of the average contractional strain and planetary radius decrease.

Watters T. R.   Solomon S. C.   Robinson M. S.   Head J. W.   Strom R. G.   Klimczak C.   Byrne P. K.   Enns A. C.   Ernst C. M.   Prockter L. M.   Murchie S. L.   Oberst J.   Preusker F.   Zuber M. T.   Hauck S. A. II   Phillips R. J.
Tectonic Features on Mercury: An Orbital View with MESSENGER **[#2121]**
Oribital images combined with topographic data obtained from MESSENGER are revealing tectonic landforms, their morphometry, and topographic settings in unprecedented detail.

Dickson J. L.   Head J. W. III   Whitten J. L.   Fassett C. I.   Neumann G. A.   Smith D. E.   Zuber M. T.   Phillips R. J.
Topographic Rise in the Northern Smooth Plains of Mercury: Characteristics from MESSENGER Image and Altimetry Data and Candidate Modes of Origin **[#2249]**
MESSENGER Mercury Laser Altimeter (MLA) data has revealed a broad topographic rise ~1000 km across in the northern smooth plains and more than 1.5 km high; we characterize the rise and outline a range of hypotheses for its origin.

Balcerski J. A.   Hauck S. A. II   Sun P.   Klimczak C.   Byrne P. K.   Dombard A. J.   Barnouin O. S.   Zuber M. T.   Phillips R. J.   Solomon S. C.
Tilted Crater Floors: Recording the History of Mercury's Long-Wavelength Deformation **[#1850]**
Analysis of MESSENGER MLA profiles of flat-floored craters in Mercury's northern hemisphere indicates that a significant fraction have been tilted from horizontal. We find geographic correlations between these craters and long-wavelength topography.

Byrne P. K.   Watters T. R.   Murchie S. L.   Klimczak C.   Solomon S. C.   Prockter L. M.   Freed A. M.
A Tectonic Survey of the Caloris Basin, Mercury **[#1722]**
We map the tectonic structures of Caloris, the largest impact basin on Mercury, at unprecedented detail. Its extensional and contractional landforms are more complex than previously described, and do not appear to correlate to its unusual topography.

Klimczak C.   Ernst C. M.   Byrne P. K.   Solomon S. C.   Watters T. R.
Fault Restriction in the Caloris Smooth Plains: Implications for Mechanical Stratigraphy **[#1959]**
Fault displacement profiles from shadow measurements across graben in the Caloris smooth plains, Mercury, reveal the mechanical stratigraphy of the volcanic plains that fill the Caloris basin.

Blair D. M. Freed A. M. Byrne P. K. Klimczak C. Solomon S. C. Watters T. R. Prockter L. M. Melosh H. J. Zuber M. T.
Thermally Induced Graben in Peak-Ring Basins and Ghost Craters on Mercury **[#2501]**
The graben patterns seen in the interiors of mercurian peak-ring basins Rachmaninoff, Raditladi, and Mozart, and in the ghost craters of the northern plains of Mercury, can be attributed to thermal stresses in the cooling volcanic fill.

Massironi M. Di Achille G. Ferrari S. Giacomini L. Popa C. Pozzobon R. Zusi M. Cremonese G. Palumbo P.
Strike-Slip Kinematics on Mercury: Evidences and Implications **[#1924]**
Mercury is classically dominated by contractional features at a global scale. Nonetheless, numerous evidences of strike-slip kinematics have been found on Mercury Dual Imaging System (MDIS) camera images.

Banks M. E. Watters T. R. Strom R. G. Solomon S. C. Braden S. E. Chapman C. R. Xiao Z. Barlow N. G.
Stratigraphic Relationships Between Lobate Scarps and Young Impact Craters on Mercury: I mplications for the Duration of Lobate Scarp Formation **[#2684]**
New results from MESSENGER MDIS images suggest that lobate scarp formation and development on Mercury occurred more recently than the formation of some Class 1 craters (Mansurian in age or younger) and may have continued into the Kuiperian system.

Preusker F. Oberst J. Blewett D. T. Gwinner K. Head J. W. Murchie S. L. Robinson M. S. Watters T. R. Zuber M. T. Solomon S. C.
Topography of Mercury from Stereo Images: First Samples from MESSENGER Orbital Mapping **[#1913]**
From stereo photogrammetric analysis using MDIS NAC/WAC stereo images from MESSENGER's orbital mapping we derived digital terrain models (DTM) with lateral spacing of 330 m/pixel and a vertical accuracy of 50 m.

Strom R. G. Xiao Z. Blewett D. T. Chapman C. R. Denevi B. W. Head J. W. III Fassett C. I. Braden S. E. Solomon S. C. Watters T. R. Banks M. E.
Impact Crater Populations on Mercury **[#1115]**
For the first time a "pure" Population 2 distribution has been found on Mercury. This result strengthens the conclusion that there are two different crater populations in the inner solar system.

Fassett C. I. Head J. W. III Baker D. M. H. Chapman C. R. Murchie S. L. Neumann G. A. Oberst J. Prockter L. M. Smith D. E. Solomon S. C. Strom R. G. Xiao Z. Zuber M. T.
Distribution, Statistics, and Resurfacing of Large Impact Basins on Mercury **[#1428]**
We map large impact basins ($D \geq 300$ km) on Mercury, whose distribution and characteristics are important to understand Mercury's geological history. The density of large basins appears lower on Mercury than the Moon, and basins are less well-preserved.

Prockter L. M. Murchie S. L. Ernst C. M. Baker D. M. H. Byrne P. K. Head J. W. III Watters T. R. Denevi B. W. Chapman C. R. Solomon S. C.
The Geology of Medium-Sized Basins on Mercury: Implications for Surface Processes and Evolution **[#1326]**
We investigate the morphology and stratigraphy of medium-sized basins (diameter 120–200 km) to determine how they are modified by volcanism, tectonics, and subsequent impacts, in order to learn about Mercury's history and surface evolution.

Gillis-Davis J. J. Markley M. M. Goudge T. A. Head J. W. Xiao Z. Gwinner K.
Large Pit Craters on Mercury: Global Distribution and Occurrence **[#2288]**
The distribution and geologic setting of large pit craters (>20 km across) on Mercury are further investigated using orbital images from the Mercury Dual Imaging System in order to retest and revise as needed our earlier hypotheses of their formation.

Gwinner K. Head J. W. Oberst J. Gillis-Davis J. J. Xiao Z. Strom R. G. Preusker F. Solomon S. C.
Morphology of Pit Craters on Mercury from Stereo-Derived Topography and Implications for Pit Crater Formation **[#1991]**
Pit craters on Mercury occur both inside impact craters and on intercrater terrain. Morphology derived from MESSENGER stereo images from orbit suggests formation by collapse above the crustal magma reservoir, a likely contribution of explosive eruptions.

Jozwiak L. M. Head J. W.
Mercury Pit-Floor Craters: Perspectives on their Origin from Lunar Floor-Fractured Craters **[#2424]**
Investigation of the presence of mercurian shallow magmatic intrusion. Mercury's floor fractured crater is similar to a lunar one, a lack of more suggests specialized formation conditions, maybe intrusion and volatile loss leading to pit floor craters.

TERRESTRIAL IMPACTS: OLD AND NEW

Wittmann A. Goderis S. Claeys P. Elburg M. Vanhaecke F. Zaiss J. Ravizza G. Deutsch A.
Depositional Record of Pristine Impactites and Traces of the Projectile in El'gygytgyn Crater **[#1999]**
Formation and emplacement constraints for a continuous section of impactites and traces of the impacting projectile from trace-element data (platinum-group elements and Os-isotopes) in drill core samples from El'gygytgyn crater.

Chen M.
Xiuyan Impact Crater, China **[#1003]**
Xiuyan crater is the first confirmed impact structure in China. It is a simple crater 1.8 km in diameter and formed before 50 kyr ago. The evidence for shock metamorphism includes PDFs in quartz, coesite, and diaplectic feldspar glass.

Ferrière L. Kaseti P. K. Lubala F. R. T. Koeberl C.
The Omeonga Structure, Democratic Republic of Congo: Geological and Petrographical Results, and Implications for its Origin **[#2054]**
For the first time, the origin of the ~38-km-diameter Omeonga structure, located in the Democratic Republic of Congo, is discussed using geological field observations and petrographic investigations on samples from our July 2011 field campaign.

Belhai D. Sahoui R. Devouard B.
New Studies about the Maadna Impact Crater (Talemzane, Algeria) **[#1111]**
The geological investigation reveals that the Maadna (Algeria) presents a set of criteria that demonstrate it is a true impact crater. Based on erosion, the age of the crater is estimated in the range from 203,000 years to 2 million years.

Glass B. Domville S. Sanjanwala1 R. Lee P.
Constrained Model Interpretations from Haughton Crater Geophysical Datasets **[#2910]**
Existing geophysical datasets have been updated and are used as constraints to create a model of the substructure of the Haughton Crater impact structure.

Tabares Rodenas P. King D. T. Jr. Ormo J. Petruny L. W. Marzen L. J.
New LiDAR Digital Elevation Model and Geologcial Map — Wetumpka Impact Structure, Alabama **[#2522]**
New geological mapping at Wetumpka impact crater (Alabama) has been aided by the use of recently obtained lidar data to make a base-map DEM and to construct new and more accurate geological cross sections, which are presented here.

Petruny L. W. King D. T. Jr. Tabares Rodenas P.
A Shallow Excavation Transect Across the Wetumpka Impact Structure, Alabama — The El Paso Gas Company Pipeline Cut **[#2546]**
We report here on the geology observed when the El Paso Gas Company reopened its existing natural gas pipeline cut going west-east across the whole of the Wetumpka impact structure, Alabama.

Misra S. Androli M. A. G.
Post-Impact Dolerite Dykes in the ~145 Ma Morokweng Crater, South Africa: Impact Related? **[#1078]**
In the present abstract we studied geochemistry of some mafic dykes emplaced along radial fractures within the Morokweng crater, South Africa, and we discuss their possible relationship with impact.

Beauford R. E.
Ferrous Minerals and Impactite Mineralization at Missouri's Crooked Creek and Decaturville Impact Craters **[#1710]**
Epigenetic hydrothermal mineralization, subsequent to the Crooked Creek and Decaturville impacts, accompanied Paleozoic dolomitization of carbonates at a regional scale in the Ozarks and produced quantities of ferrous minerals at both locations.

Azad A. S. Dypvik H. Kalleson E. Riis F.
Sedimentation in the Ritland Impact Structure, Western Norway **[#1281]**
Ritland is the most recently confirmed Norwegian impact structure. Different gravity controlled sedimentation processes; rock avalanches, and debris flows initially operated to fill the crater. Suspension deposition and turbidity currents dominated lately.

Wood C. A.
Recognition of Degraded Impact Craters on Earth, Moon and Titan **[#1637]**
Impact craters occur everywhere, but the identification of degraded ones is very difficult or even impossible on worlds like Titan with an uncertain inventory of geologic processes and an active surface.

Maziviero M. V. Vasconcelos M. A. R. Góes A. M. Crósta A. P. Reimold W. U.
The Riachão Ring Impact Structure, Northeastern Brazil: Re-Evaluation of Its Stratigraphy and Evidence for Impact **[#1511]**
Results of a field mapping and petrographic studies are discussed. We propose changes in the stratigraphy of the Riachão impact structure and present new shock deformation evidences found in the structure.

Brown P. Ens T. Edwards W. N. Silber E. A.
Global Detection of Airbursts: A Combined Satellite-Infrasound Study **[#1581]**
A total of 71 satellite detected airbursts were detected by one or more infrasound arrays. Airbursts larger than 20 kT are detectable by infrasound globally, while more than 50% of all 1 kT airbursts are detected by the current infrasound network.

Kuzmicheva M. Yu. Losseva T. V.
Simulations of the Geomagnetic Field Disturbances Caused by the Tunguska Event 1908 **[#2319]**
The phenomena explaining the main features of geomagnetic perturbations caused by the Tunguska explosion: location, start time, and signs of disturbances of the geomagnetic field have been simulated. Azimuth of trajectory of the bolide has been defined.

Steiner M. B.
Newly Discovered Iron Meteorites Within the City Limits, Laramie, WY **[#2924]**
Abundant iron meteorites in southeast Wyoming indicate a meteorite shower, with similarities to the Shikote Alin fall, i.e., breakup in the atmosphere. Evidence indicates flight very close to the land surface and a flight direction of ~N 30 E.

Shumilova T. G. Isaenko S. I. Makeev B. A. Ernstson K. Neumair A. Rappenglück M. A.
Enigmatic Poorly Structured Carbon Substances from the Alpine Foreland, Southeast Germany: Evidence of a Cosmic Relation **[#1430]**
We studied exotic carbon matter from the field composed of amorphous carbon and the monocrystalline carbyne allotrope ("chaoite"). The required PT conditions (4–6 GPa, 2500–4000 K) are evidence of a formation in a so-far unsettled shock event.

MORE HOT STUFF: INTERPLANETARY STUDIES OF IMPACT MELT

Wagner R. V. Robinson M. S. Ashley J. W.
Small-Scale Pits in Impact Melts **[#2266]**
The Lunar Reconnaissance Orbiter's Narrow Angle Camera has revealed over 150 10-m-scale collapse pits in impact melts of Copernican age craters. These pits may provide insight into the dynamics of impact melt emplacement.

Boyce J. M. Wilson L. Mouginis-Mark P. J. Tornabene L. L. Hamilton C. W.
Origin of Closely-Spaced Groups of Pits in Martian Craters **[#1017]**
A model of explosive degassing of thin deposits of suevite-like fall-back is proposed for the origin of closely-spaced pits formed in thin impactite deposits superposed on well-preserved martian impact craters.

Beach M. J. Head J. W. III Ostrach L. R. Robinson M. S. Denevi B. W. Solomon S. C.
The Influence of Pre-Existing Topography on the Distribution of Impact Melt on Mercury **[#1335]**
The objective of this study is to characterize the nature and distribution of impact melt, influenced by the pre-impact topography of the target site, enabled by the high-resolution images obtained during the MESSENGER primary orbital mission.

Öhman T. Kramer G. Y. Kring D. A.
Spectral Analysis of the Distribution of Impact Melt-Rich Lithologies in Lunar Crater Kepler Using M^3 Data **[#2257]**
Moon Mineralogy Mapper (M^3) data show Kepler impact melt to be gabbroic, and highlight an uprange splash. A halo of less-crystalline material, possibly derived from a collapsing impact plume, is shifted ~downrange. Both surficial features are invisible in visual imagery.

Kuriyama Y. Ohtake M. Haruyama J. Iwata T.
Distributions of Impact Melts Within Lunar Complex Craters Jackson and Tycho **[#1395]**
We identified impact melts on the central peaks as well as in the floors and on the wall terraces in the lunar complex craters Jackson and Tycho by MI spectral data and LROC image data. We tried to constrain the formation of the central peak.

Chanou A. Tornabene L. L. Osinski G. R. Zanetti M. Pickersgill A. E. Shankar B. Marion C. Mader M. M. Souders K. A. Sylvester P. Jolliff B. L. Shaver C.
Impact Melt-Pond Scenario Tested During the KRASH 2011 Analogue Mission at Kamestastin Impact Structure **[#2580]**
Discovery Hill is dominated by a wedge-like shaped outcrop of columnar-jointed impact melt rock. Field observations of the hill's morphology, geologic contacts and relative position within the Mistastin impact crater suggest a melt-pond origin.

Vaughan W. M. Head J. W. III Hess P. C. Wilson L. Neumann G. A. Smith D. E. Zuber M. T.
Depth and Differentiation of the Orientale Melt Lake **[#1302]**
We suggest that the central depression of the Orientale basin is an impact melt lake ~15 km deep and model the igneous differentiation of the melt lake. Impact melt differentiates may be represented in remotely-sensed data and the lunar sample suite.

Pittarello L. Koeberl C.
A Suevite in Black and White: SEM Study on the Samples from the El'gygytgyn Drill Core **[#1883]**
The El'gygytgyn structure, N-E Siberia (Russia), is the only impact crater on Earth in rhyolitic-trachytic volcanic rocks; it provides a unique opportunity to improve our knowledge of shock metamorphism at the microscopic scale in such a target.

Pickersgill A. E. Osinski G. R. Mader M. M.
A Formational Model for an Impact Melt-Bearing Breccia Dyke at the Mistastin Lake Impact Structure, Labrador, Canada **[#2473]**
Variation in shock level and glass clast morphology is drawn on to support a multi-stage dynamic flow emplacement model for an impact melt-bearing breccia dyke at the Mistastin Lake impact structure, Labrador, Canada.

Beauford R. E.
Carbonate Melts and Sedimentary Impactite Variation at Crooked Creek and Decaturville Impact Craters, Missouri, USA **[#1705]**
The Crooked Creek and Decaturville, Missouri, impact craters offer an opportunity to understand variation in impactite lithologies in carbonate and mixed sedimentary environments. Impactites involve mixes of carbonates, sandstone, chert, and shale.

Murty S. V. S. Ranjit Kumar P. M.
Noble Gas Isotopes: Tracers of Impactor Signatures in Lonar Impact Glasses **[#1423]**
Noble gas isotopes ^{21}Ne, ^{36}Ar, and ^{129}Xe reveal excesses due to the presence of cosmogenic, trapped, and radiogenic components of meteoritic origin, in the impact glasses from Lonar Crater, providing unambiguous signatures of the impactor.

Giuli G. Cicconi M. R. Eeckhout S. G. Koeberl C. Glass B. P. Pratesi G. Paris E.
North-American Microtektites are More Oxidised than Tektites **[#1921]**
Microtektites from the Australasian and Ivory Coast strewn fields (SF) show low values of the Fe^{3+}/Fe_{tot} ratio, comparable to tektites from the same SF. In contrast, microtektites from the North American SF show a wider range (from 0 to 0.75).

Giuli G. Cicconi M. R. Eeckhout S. G. Paris E. Pratesi G. Folco L.
Fe Oxidation State in Microtektites from the Transantarctic Mountains **[#1927]**
Fe oxidation state of microtektites from the Transantarctic mountains is consistent with that of Australasian tektites and microtektites. Despite the long distance from the presumed impact site, the Fe oxidation state does not show appreciable variation.

Goderis S. Simonson B. M. McDonald I. Hassler S. W. Izmer A. Vanhaecke F. Claeys Ph.
Geochemical Correlation of Two Late Archean Impact Spherule Layers Between South Africa and Western Australia: the Paraburdoo-Reivilo Link **[#1882]**
The unique geochemical compositions of the Late Archean Paraburdoo (Hamersley Basin, Western Australia) and Reivilo (Griqualand West Basin, South Africa) spherule layers confirm their proposed correlation.

Huber M. S. Crne A. E. Lepland A. McDonald I. Melezhik V. A. Koeberl C.
Chemical Analysis of Impact Spherules from the Zaonega Formation, Karelia, Russia, and Implications for Vredefort Origin **[#1970]**
Recently discovered spherules with a possible relationship to the Vredefort impact event have been shown to have a nonterrestrial geochemical signature. The relationship to the Vredefort target has been tested by analysis of silicates in spherules.

Fernandes V. A. Hopp J. Schwarz W. Trieloff M. Reimold W. U.
Re-Evaluation of the Chesapeake Bay Crater Impact Age: New ^{40}Ar-^{39}Ar Step-Heating Results for North American Tektites **[#1775]**
Reevaluation of Chesapeake Bay crater impact age is being undertaken by ^{40}Ar-^{39}Ar step-heating of NA tektites and impact melt found within the USGS-ICDP drill core Eyreville-B. Initial results suggest a slightly younger age than the accepted 35.3 Ma.

SHOCKING ROCKS: INVESTIGATING SHOCK EFFECTS IN ROCKS AND MINERALS

TUE POSTERS

Kraus R. G.   Newman M. G.   Stewart S. T.
Hugoniot Measurements on Heterogeneous Geologic Materials **[#2680]**
The Hugoniot of 8% porous Nontronite and a 25% porous sandy soil have been measured in the stress range from 0.5 to 22 GPa.

Sugita S.   Kurosawa K.   Kadono T.   Sano T.
An High-Precistion Semi-Analytical on-Hugoniot EOS for Geologic Materials **[#2053]**
Most modern EOS's for shock compression is highly complicated. Here we a new very accurate but simple semi-analytical on-Hugoniot EOS, which requires only Co, s Cp, and q. Comparison with experimental data shows very good fidelity.

Kraus R. G.   Swift D. C.   Hicks D. G.   Stewart S. T.
High Accuracy Equations of State for Planetary Collision Modeling **[#2649]**
Equation of state properties are now being measured over an extremely wide range of pressures and temperatures. We present multi-phase equations of state for MgO and SiO_2 that accurately describe the material's response to planetary collisions.

Holm S.   Ferrière L.   Alwmark C.
A Statistical Study of Shocked Quartz Grains from the Siljan Impact Structure (Sweden) — Horizontal Versus Vertical C-Axes **[#1846]**
We investigate if high-index PDF orientations are more frequent in quartz grains with vertical c-axes (determined by the U-stage) and discuss implications for the interpretation of the PDF dataset, including the derived shock pressures.

Collins G. S.   Melosh H. J.   Pasek M. A.
Can Lightning Strikes Produce Shocked Quartz? **[#1160]**
We simulated approximate P-T-t conditions in lightning strikes. In typical strikes, peak pressures in the soil are <10 GPa; however, in very high-energy, short-duration, narrow-channel strikes peak pressures can exceed 10 GPa outside the channel.

McHone J. F.   Shoemaker C.   Killgore M.   Killgore K.
Two Shatter-Coned NWA Meteorites **[#2359]**
Shatter cones are found in target rocks at more than 70 terrestrial impact sites and are regarded as reliable field criteria for meteoroid impact events. Shatter cones are now seen in chondritic meteorites and indicate early collision events.

Lindgren P.   Price M. C.   Lee M. R.   Burchell M.
Constraining the Pressure Threshold of Impact Induced Calcite Twinning **[#1934]**
To better constrain the pressure threshold of impact-induced calcite twinning, calcite targets have been experimentally impacted. This study has implications for the deformation history of carbonaceous chondrite parent bodies.

Hu J.   Sharp T. G.   Tricky R.   Leinenweber K.
Akimotoite and Silicate-Perovskite in L5-6 S6 Chondrite Acfer 040 Suggesting a High Shock Pressure of 25GPa **[#2728]**
We study the mineralogy and micro-structure of the high-pressure assemblages in the shock-induced melt veins of L5-6 S6 chondrite Acfer 040 to estimate its shock pressure and to understand the origins of silicate-perovskite and akimotoite.

Wright S. P.
Not Just Fresh Basalt: A Range of Shocked Alteration Products and Soil from Lonar Crater, India **[#2765]**
Several Deccan basalt lava flows were aqueously altered (via groundwater) prior to shock compression and emplacement as clasts in the Lonar suevite breccia. These, along with a shocked soil, are unique mixtures of glass and alteration products.

Kurosawa K. Ohno S. Sugita S. Mieno T. Hasegawa S.
Shock-Induced Decarbonation in an Open System Using a 2-Stage Light Gas Gun **[#1730]**
We present a new experimental method for gas-phase chemical analysis in an open system using a two-stage light gas gun at ISAS/JAXA to investigate the decarbonation pressure of calcite. The "effective" decarbonation pressure of calcite is ~60 GPa,.

Kowitz A. Schmitt R. T. Reimold W. U. Hornemann U.
Development of Fractures, Melt and Local Shock Effects on Shock Recovery Experiments at Low Shock Pressure with Dry Seeberger Sandstone **[#1201]**
Shock experiments were carried out with dry Seeberger sandstone at 5, 7.5, 10, and 12.5 GPa. The shocked samples show subplanar fractures, melting, and local shock features along shear zones, e.g., diaplectic quartz glass, SiO_2 melt, microbreccia, and PDF.

Moser D. Grosse C. Güldemeister N. Buhl E. Wünnemann K. Kenkmann T.
Looking Beneath an Impakt Crater — Non-Destructive Testing for Hypervelocity Impact Experiments **[#2207]**
In the framework of the "MEMIN" project, ultrasound tomography gives an overview about the inner damage zone. The comparison to numerical simulations and optical evaluation will give an association about terrestrial craters.

Stickle A. M. Schultz P. H.
Subsurface Damage Features Following Projectile Decapitation **[#1269]**
Laboratory experiments demonstrate that decapitated projectile fragments reimpacting the target control subsurface damage features. Decoupling the downrange re-impact results in a damage zone more consistent with numerical models.

Kimberley J. Ramesh K. T.
Real-Time Observation of Early Stage Damage During Hypervelocity Impacts into Basalt Targets **[#2344]**
Hypervelocity impacts were conducted on basalt targets bonded to glass allowing for the early stages of damage accumulation to be observed in real time. Results show that significant damage accumulates before the arrival of tensile wave reflections.

Takagi Y. Hasegawa S. Kurosawa K.
Cratering Experiments on Basalt Targets **[#2002]**
Impact cratering experiments using basalt target were performed. Diameters, depths, and volumes of 16 craters were measured. Preliminary analyses of these values showed scaling laws consistent with previous studies.

Munsat T. Collette A. Drake K. Grun E. Horanyi M. Kempf S. Mocker A. Northway P. Robertson S. Shu A. Sternovsky Z. Thomas E.
The Dust Accelerator Facility of the Colorado Center for Lunar Dust and Atmospheric Studies **[#2730]**
The Colorado Center for Lunar Dust and Atmospheric Studies has developed a new hypervelocity dust accelerator, which accelerates ~1 µm particles to 10's of km/s. We describe the experimental capabilities and the results of our first campaign.

EXOBIOLOGY: FROM WORLDS WE KNOW TO OTHER STARS

Thiemens M. M. Moynier F. Thiemens M. H. Shaheen R. Chong K. Koeberl C. Popp F. Gyollai I.
Zn and C Isotopic Variations Associated with Neoproterozoic Ice Ages **[#2499]**
Analysis of Marinoan glacial deposits for C and Zn isotopes shows a correlation between heavy δ^{66}Zn to characteristic light δ^{13}C, indicative of heavy biological activity post glaciation. These measurements can be used for exobiological measurements.

Steininger H. Goetz W.
Pyrolysis-GC-MS Analysis of Antarctic Lake Sediments **[#2841]**
Antarctic lake sediments were analyzed with Pyrolysis-GC-MS, a method similar to the methods used on board MSL and Exomars. This is the starting point to build a library of data from terrestrial samples to improve the analysis of martian samples.

Marnocha C. L. Dixon J. C.
Bacterial Community Structure of Sulfate Crusts, Fe/Mn Skins, and Alumina Coatings from Kärkevagge, Swedish Lapland **[#2150]**
Rock coatings could serve as biosignatures on Mars. In this work, we present the bacterial community structure of rock coatings from Kärkevagge, Swedish Lapland as a first step in assessing their feasibility as biosignatures.

Sheehan R. C. Marnocha C. L. Dixon J. C.
Bacterial Diversity of Fe/Mn and White Rock Coatings in Kärkevagge: A Potential Mars Analogue **[#1013]**
Rock coatings from Kärkevagge, a potential Mars analogue, were analyzed for their microbial diversity, yielding distinct bacterial phylogenies of wide-ranging environmental tolerations and physiologies for different rock coating morphologies.

Rodzinyak K. J. Wing B. A. Léveillé R. J.
Unexpectedly Large S Isotope Fractionation During Natural Sulfide Oxidation at Cold Temperatures **[#2067]**
If an isotopic enrichment of 10–20‰ can be produced by low-temperature sulfide oxidation, preservation of potential records of microbial sulfate reduction may be incompatible with the present martian surface environment.

McMahon S. Parnell J. Blamey N. J. F.
Analysis of Volatile Fluids in Basalt: A Possible Source of Martian Methane **[#1046]**
Terrestrial basalts commonly yield methane when crushed into a sensitive mass spectrometer. Basalts are abundant on Mars, hence may be a source of martian methane, and should be targeted for analysis accordingly.

Webster K. D. Rebholz J. A. White J. R. Douglas B. J. Pratt L. M.
Using Open-Path Laser Measurement of Atmospheric Methane Concentration Along a Major Shear Zone in Western Greenland as an Analogue for Exploration on Mars **[#1514]**
An open-path infrared laser was used to measure open air methane concentrations in west Greenland. Nine open air transects were measured across a shear zone valley. Mean measured methane concentrations ranged from 1.4 to 2.3 ppm.

Franchi F. Cavalazzi B. Rossi A. P. Pondrelli M. Barbieri R.
Kess Kess Hydrothermal Mounds in Morocco: A Unique Analog for Exploring Possible Fossil or Extant Life on Mars **[#2245]**
The recent discovery of mound fields on the surface of Mars gave new inputs to the astrobiological study of the terrestrial mounds. This work compares the Kess Kess conical mound (Earth) and the Firsoff crater mounds (Mars) and reports their affinity with fluids escape.

Fu Q.   Socki R. A.   Niles P. B.   Romanek C.   Datta S.   Darnell M.
The Origin of Carbon-Bearing Volatiles in a Continental Hydrothermal System in the Great Basin: Water Chemistry and Isotope Characterizations **[#2481]**
Two processes are proposed for the observed isotope values of carbon-bearing compounds in SVHS: thermogenic production of alkane homologs and formation of CO_2 by AOM. The geological background and fluid chemistry are used to support this scenario.

Socki R. A.   Fu Q.   Niles P. B.   Gibson E. K. Jr.
Hydrogen Isotope Measurements of Organic Acids and Alcohols by Pyrolysis-GC-MS-TC-IRMS: Application to Analysis of Experimentally Derived Hydrothermal Mineral-Catalyzed Organic Products **[#2483]**
We report results of experiments to measure the H-isotope composition of organic acids and alcohols. These experiments make use of a pyroprobe interfaced with a GC and high-temperature extraction furnace to make quantitative H-isotope measurements.

de Morais A.
A Possible Biogeochemical Model for Mars **[#2943]**
A possible biogeochemical evolution within martian subsurface using clays cataltic properties might have occured. Same organisms sources 1) great depths using geochemical energy by sulfur redox; 2) near surface using light emitted from clays.

Thompson D. R.   Allwood A. C.   Bekker D. L.   Cabrol N. A.   Fuchs T.   Wagstaff K. L.
TextureCam: Autonomous Image Analysis for Astrobiology Survey **[#1659]**
The TextureCam project will design a “smart camera” that aims to improve scientific return by increasing science autonomy and observation capabilities. An initial test demonstrates automatic recognition of stromatoform structures in outcrop.

Misra A. K.   Sharma S. K.   Acosta T. E.   Bates D. E.   Clegg S.   Wiens R. C.
Standoff Bio-Finder for Planetary Exploration with Fast Detection **[#1666]**
A new instrument “standoff bio-finder” is described that uses fluorescence imaging to detect biomaterials. In the fast (<100 ns) gated fluorescence mode the instrument provide live images of biomaterials at 10 frames/s.

Scott V. J.   Amashukeli X.   Siegel P. H.   Fisher A.   Bae Y.   Toda R.
An RF-Powered Micro-Extractor for the Detection of Astrobiological Target Molecules **[#2128]**
Sample-processing instruments for the extraction of astrobiological target molecules have been designed as part of potential in situ exploration missions. These instruments have been built and preliminary experiments demonstrate promising results.

Malespin C. A.   Glavin D. P.   ten Kate I. L.   Franz H. B.   Mumm E.   Bleacher J. E.   Rice J. W.
Volatile Analysis by Pyrolysis of Regolith in the 2011 D-RATS Field Test **[#2181]**
The Volatile Analysis by Pyrolysis of Regolith (VAPoR) instrument is a compact vacuum pyrolysis mass spectrometer designed to detect volatiles released during high temperature (up to 1300°C) heating of crushed or solid samples.

Elliott H. M.   Martinez G. M.   Halleaux D. G.   Braswell S. F.   Renno N. O.
The Michigan Mars Environmental Chamber (MMEC): Determining the Conditions at Which Liquid Brines form on Mars **[#2117]**
The MMEC will test the hypothesis that microscopic brine pockets can form and be concentrated into larger pockets by freeze-thaw cycles on Mars. This is relevant to exobiology because these brine pockets have the potential to be habitable.

TUE POSTERS

Papineau D.
Organic Matter Associated with Apatite in Martian Meteorite Chassigny **[#1549]**
Associations between organic matter and hydroxylated apatite have been found in the Chassigny meteorite. Data suggest precipitation from a low-temperature hydrothermal fluid and organic matter production from FTT synthesis on Mars.

Pavlov A. A. Vasiyev G. Ostryakov V. M. Pavlov A. K. Mahaffy P.
Degradation of the Organic Molecules in the Shallow Subsurface of Mars due to Irradiation by Cosmic Rays **[#2933]**
Degradation of organic molecules by cosmic ray irradiation on Mars is often ignored. We demonstrated that the heavy organic molecules would not survive in the shallow subsurface of Mars if the exposure age of a geologic outcrop would exceed 300 Myr.

Wimmer-Schweingruber R. F. Hassler D. M. Zeitlin C. Böttcher S. Martin C. Andrews J. Böhm E. Weigle G. Brinza D. Posner A. Burmeister S. Epperly M. Seimetz L. Reitz G. Kortmann O. Köhler J. Ehresmann B. Neal K. Rafkin S. Peterson J. Tyler Y. Smith K. Bullock M. Cucinotta F.
Determining the Martian Radiation Environment — The Radiation Assessment Detector (RAD) on Mars Science Laboratory (MSL) **[#2460]**
The Radiation Assessment Detector (RAD) onboard the Mars Science Laboratory (MSL) is performing radiation measurements en route to Mars. On Mars it will measure the broad particle spectrum and determine the dose and dose rate on the martian surface.

Oshima M. Tani A. Kitano K. Sugahara T. Ohgaki K.
Possibility of Carboxylic Acid Formation by Radiolysis of CO_2 Hydrate on Mars **[#1976]**
We have analyzed the aqueous solution after dissociation of the gamma-irradiated CO_2 hydrate by ion chromatography. Formic acid and oxalic acid are observed in aqueous solution after dissociation of irradiated CO_2 hydrate.

Sandford S. A. Nuevo M. Materese C. K. Milam S. N.
Nucleobases and Other Prebiotic Species from the Ultraviolet Irradiation of Pyrimidine in Astrophysical Ices **[#1550]**
We discuss the results of UV irradiation of ices containing pyrimidine and show that such processing efficiently forms the nucleobases uracil and cytosine, but not thymine, a pattern similar to what is seen in carbonaceous meteorites.

Sinha N. Kral T. A.
Sensitivity of Desiccated and Liquid Cultures of Methanogens to Ultraviolet Radiation **[#1702]**
The goal of this study is to determine the sensitivity of desiccated and liquid cultures of some methanogens to UV radiation in an anaerobic condition.

Stromberg J. M. Mann P. Cloutis E. A.
The Effects of Desiccation Under Mars-Like Conditions on the Spectral Detectability of Gypsum Associated Endolithic Communities **[#1224]**
Gypsum associated endolithic communities detectable by reflectance spectroscopy were subjected to “Mars-like” conditions for 75 days to examine the preservation potential of their spectral biosignatures.

Kyle J. E. Jahnke L. L. Stedman K. M.
Preservation Potential of Lipid-Containing Viruses Under Silicifying Conditions **[#2228]**
The preservation potential of lipid-containing viruses, PRD1 and PBCV1, within silicifying solutions exists. Both viruses are rapidly removed from precipitating solutions, and the lipids within PBCV1 are unique from that of their host.

Figlewski N. M. Beegle L. W. Sollitt L. S.
Laser Desorption Infrared Spectrometry for Icy Moon Surfaces **[#2642]**
We present first results of experiments to determine the suitability of laser resonant desorption as a technique to search for astrobiologically interesting molecules in planetary ices.

Aponte J. C. Tarozo R. Hallmann C. Summons R. Huang Y.
The Racemic Nature of the Free and IOM-Derived Monocarboxylic Acids in Carbonaceous Chondrites Suggests the Origin of Chirality During Parent Body Modification Processes **[#1032]**
The chirality of free and IOM-derived branched monocarboxylic acids present in three carbonaceous chondrites was studied by chemical derivatization and gas chromatography.

Boice D. C. de Almeida A. A.
Prospects for Phosphorus-Bearing Molecules in Cometary Comae **[#1887]**
Phosphorus is a key element in all known forms of life but searches for P-bearing, volatile species in comets have been unsuccessful. We present model results to identify likely P-species in comets to aid in searches for this important element.

Brock L. S. Melosh H. J.
Impact Exchange of Material Between Planets of Gliese 581 **[#2467]**
Gliese 581 d resides close to the "habitable zone" and has sparked debate on the existence of potential life. We evaluated the possibility for transfer of material between planet d and its sister planets and discovered an exchange was unlikely.

MATERIAL ANALOGS IN THE FIELD AND IN THE LABORATORY

Rull F. R. Klingelhoefer G. Martinez Frias J. Rodriguez J. A. Medina J. Lalla E.
A Combined Raman and Mössbauer Analysis of Atered Basalts in Tenerife Island: Analogies with Mars **[#2882]**
A combined Raman and Mössbauer study has been performed in different areas of Tenerife to analyze the water alteration processes of volcanic materials and the possible analogy with Mars.

McHenry L. J. Chevrier V. F. Schröder C.
Spatial vs. Temporal Distribution of K-Jarosite in a Saline-Alkaline Paleolake Deposit: Implications for the Distribution and Longevity of Jarosite on Mars **[#2010]**
A range in jarosite abundance from 0.4 to 7.9% within a single layer in an altered tuff in an East African saline-alkaline paleolake deposit suggests a spatial rather than temporal control for this unusual jarosite occurrence, with implications for Mars.

Sharma S. K. McKay C. P. Misra A. K.
Time-Resolved Raman and Laser-Induced Native Fluorescence Investigations of Carbonate Rocks as an Analogue for Martian Carbonates **[#1312]**
Martian analog carbonates are investigated with time-resolved bio-imager, and Raman and LINF spectroscopy, to understand the organic and bio-signatures.

Englert P. Bishop J. L. Hunkins L. D. Koeberl C.
Martian Soil Analogs from Antarctica: Chemical and Mineralogical Weathering Scenarios **[#1743]**
This investigation of chemical and mineralogical weathering of Antarctic Dry Valleys soils found more extensive physical than chemical alteration. This may provide insights into weathering scenarios on Mars.

Sobron P. Amundsen H. E. F. Bauer A. Bishop J. L. Jordan F. Josset J-L. Josset L. Leveille R. Pugh S. M. Schmitz N. Steele A. Wang A.
In-Situ Investigation of Devonian Redbed Sediments in Bockfjord (Svalbard, Norway) as a Martian Analogue **[#2631]**
We performed in-situ imaging and spectral analysis of redbeds in Svalbard using prototypes of mission instruments. We evaluated synergies between optical/spectroscopic instruments and characterized red sandstones in a Mars analogue site.

Stoker C. R.   Clarke J. D. A.   Valdivia-Silva J.   Foing B.
Subsurface Profiles of Organics Obtained by Core Drilling in Jurassic Sediments at a Mars Analog Site in Utah **[#2850]**
We obtained rock cores (0.6–1.6 m depth) from ancient (150 m.y. old) sediments at a Mars analog site in Utah using a prototype Mars drill. We report the depth profile of organics from these samples to illustrate the utility of drilling on Mars.

Salvatore M. R.   Mustard J. F.   Head J. W. III   Marchant D. R.   Wyatt M. B.   Seeley J.
Linking Orbital, Field, and Laboratory Analyses of Dolerites in the McMurdo Dry Valleys of Antarctica: Terrestrial Studies and Planetary Applications **[#1590]**
Primary igneous and secondary alteration signatures can be resolved using orbital spectroscopy over mafic regions of the McMurdo Dry Valleys. We assess the nature of these signatures and their link to surface stability and regional microclimates.

Salvatore M. R.   Mustard J. F.   Head J. W. III   Cooper R. F.   Marchant D. R.   Wyatt M. B.
Characterizing Widespread Oxidation Processes on Mars: Alteration Rind Development and Effects on Spectroscopic Investigations **[#1597]**
The chemical, mineralogical, and spectral products of oxidation are characterized using a variety of laboratory techniques. Orbital and in situ observations of the martian surface suggest that this process is widespread and spectrally significant.

Mandt K. E.   Patrick E. L.   Mitchell E. J.   Seifert C.   Mitchell J. N.   Libardoni M.   Younkin K. N.
In-Situ Mass Spectrometer Measurements of Cave Atmospheres as an Analogue to Future Planetary Cave Missions **[#1442]**
We built a portable mass spectrometer to survey the composition of local cave atmospheres as early instrument development for future missions to caves on the Moon and Mars. Measurement results are used in support of current Earth science research.

Rutledge A. M.   Christensen P. R.
Infrared Spectroscopy and Geochemistry of Cold Weathering Products in a Terrestrial Icy Environment: Implications for Weathering on Mars **[#2715]**
Cold weathering processes on Earth and Mars are poorly understood, despite both having an abundance of ice in contact with geologic material. We use TIR spectroscopy and geochemistry to characterize weathering processes in an icy analog environment.

McGlynn I. O.   Fedo C. M.   McSween H. Y. Jr.
Physical Modification of Synthetic Basaltic Sediment Compositions: Implications for Interpreting the Geochemistry of Martian Soils **[#1251]**
Synthetic sediment produced from the sorting of shattered basalt bedrock demonstrates the possibility for hydrodynamic compositional modification of sediment on Mars and must be considered when interpreting the composition of martian sediment.

Hallis L. J.
Weathering in Terrestrial Samples from the Miller Range and Elephant Moraine Regions of Antarctica: Comparisons with Weathering in Antarctic Martian Meteorites **[#2819]**
We compared the secondary alteration minerals in Antarctic terrestrial samples with those of the Miller Range nakhlite martian meteorites to determine the origin of the sulphates in the latter.

Brown A. J.   Bishop J. L.   Roush T. L.   Hunkins L.   Bristow T.   Blake D.
Controlled Study for Quantitative Clay Abundance on Mars **[#1747]**
We report on a laboratory-controlled study of four well-characterized martian analog samples. We have conducted SEM analysis and derived grain size distributions and shape information. We will report on VNIR spectra and RT models of these samples.

Zhou Y. Z.   Wang A. W.
Potential Existence of Al-Bearing Sulfates on Mars and Their Spectral Characteristics **[#2289]**
We anticipate a great potential existence of Al-bearing sulfates on Mars based on the evidences of extensive weathering observed by recent missions. We conducted spectroscopic characteristics of two typical Al-sulfates, alunogen and alum-(K).

Liu Y.   Wang A.
Dehydration of Na-Jarosite, Ferricopiapite, and Rhomboclase at High T and Implications on Martian Ferric Sulfates **[#2791]**
Our dehydration experiments of ferric sulfates show that OH-bearing Na-jarosite is relatively stable at 95°C and RH ≤ 11%, while H_2O/OH-bearing ferricopiapite and rhomboclase have converted entirely to anhydrous phases.

Lu Yanli.   Wang A.
Synthesis and Spectral Characterization of OH-bearing Ferric Sulfates **[#2514]**
We report the synthesis of three jarosites, $FeOHSO_4$, paracoquimbite, and their Raman, MIR-ATR, VIS-NIR-DF spectral characterizations, which is the first step to start a study of their stability field and phase transition pathways.

Graff T. G.   Morris R. V.   Achilles C. N.   Agresti D. G.   Ming D. W.   Hamilton J. C.
Mertzman S. A.   Smith J. G.
Chemical and Mineralogical Characterization of Acid-Sulfate Alteration of Basaltic Material on Mauna Kea Volcano, Hawaii: Jarosite and Hydrated Halloysite **[#2639]**
We characterized the chemical and mineralogical properties of basalt subjected to acid-sulfate weathering under natural conditions on Mauna Kea Volcano, Hawaii. Alteration products include jarosite and hydrated halloysite.

Lauer H. V. Jr.   Archer P. D. Jr.   Sutter B.   Niles P. B.   Ming D. W.
Thermal and Evolved Gas Analysis of "Nanophase" Carbonates:Implications for Thermal and Evolved Gas Analysis on Mars Missions **[#2299]**
We characterize the thermal and evolved gas properties of carbonates of varying particle size, evaluate the CO_2 releases from CO_2 treated CaO samples, and examine the secondary CO_2 release from reheated calcite of varying particle size.

Sakatani N.   Ogawa K.   Iijima Y.   Honda R.   Tanaka S.
Thermal Conductivity of Glass Beads as a Model Material of Regolith **[#2000]**
Thermal conductivity of glass beads as a model material of regolith was measured with changes in temperature. Our results indicate that the solid conductivity is dependent on the number of contact per unit volume and contact conductance.

Moroz L. V.   Starukhina L. V.   Rout S. S.   Sasaki S.   Leroux H.   Helbert L.   Baither D.
Bischoff A.   Hiesinger H.
Space Weathering of Fe-Poor Silicate Regoliths: Experimental and Theoretical Simulations **[#1488]**
We present spectral and SEM/TEM studies of a natural plagioclase irradiated with a nanosecond pulsed laser. We also employed theoretical modeling to assess optical modification of Fe^{2+}-poor regoliths due to formation of nanophase iron inclusions.

Dropmann M.   Gomringer C.   Koch H.   Peters S.   Herdrich G.   Cook M.   Schmoke J.   Laufer R.   Matthews S.
Hyde T. W.
Setup of an Inductively–Heated Plasma Generator and Diagnostics to Build a Hybrid Plasma Simulation Facility for Complex Space Environment Investigations **[#2165]**
Environmental plasma research using an inductively heated plasma generator and several subsystems for investigation in the fields of dusty plasma, catalysis, atmospheric entry, and even terrestrial applications.

Gillis-Davis J. J.   Markley M. M.   Lucey P. G.   Bradley J. P.   Ishii H. A.
Laser Space Weathering of Quartz **[#2664]**
Our pulsed laser irradiation experiments are devised to systematically examine how low-iron materials like plagioclase space weather.

Barmatz M.   Steinfeld D.   Winterhalter D.   Rickman D.   Gustafson R.   Butts D.   Weinstein M.
Microwave Permittivity and Permeability Measurements on Lunar Simulants **[#1050]**
In this investigation, we have measured the dielectric and magnetic properties of lunar simulants being developed by three companies and compared their resulting behavior to earlier measurements of representative mare and highland lunar soil samples.

Russell P. S.   Grant J. A.   Williams K. K.   Carter L. M.   Garry W. B.   Morgan G.
Daubar I.   Bussey D. B. J.
Ground Penetrating Radar Field Studies of Lunar-Analog Geologic Settings: Impact Ejecta and Volcanic Materials **[#2604]**
GPR surveys are analyzed in conjunction with "ground-truth" outcrop observations, with the goal of determining whether and how different geologic materials, processes, and settings can be uniquely distinguished and characterized with GPR.

Gurgurewicz J.   Maturilli A.   Helbert J.   Kostylew J.   Zalewska N.
Emissivity Measurements of Basaltic Analogues for Mercury **[#2124]**
Emissivity of basaltic rocks from three different terrestrial geological environments has been measured and implications for Mercury's surface composition are discussed.

Bodnarik J. G.   Schweitzer J. S.   Parsons A. M.   Evans L. G.   Starr R. D.
PING Gamma Ray and Neutron Measurements of a Meter-Scale Carbonaceous Asteroid Analog Material **[#1544]**
We compare PING experimental data from the asteroid stimulant, basalt, and granite structures with computer simulations for a homogenous carbonaceous asteroid to show that the asteroid simulant's response closely approximates a carbonaceous asteroid.

Ivliev A. I.   Kuynko N. S.
The Thermoluminescence in the Experimentally Shock Loaded Minerals **[#1273]**
The study of shock loaded matter in such experiments can appear useful for interpreting measurement results of physicochemical transformations of different minerals conditioned by the effects of high pressures and temperatures.

ElShafie A.   Heggy E.
Dielectric Properties of Volcanic Material and Their Role for Assessing Rock Hardness in the Martian Subsurface **[#2790]**
We perform dielectric permittivity and hardness measurements for martian analog rocks in an attempt to correlate between the physical and mechanical properties of volcanic rocks and its implication for optimizing ExoMars drilling and sampling activities.

Choukroun M.   Barmatz M.   Castillo-Rogez J. C.   Mielke R.   Mitchell K.   Smythe W.   Sotin C.   Young J.
Zhong F.
JPL's Capabilities for Ice Physics Experimentation with Planetary Applications **[#2774]**
We present experimental facilities developed at JPL to support geophysical models and mission data interpretation on icy bodies of the solar system, and current research that uses these facilities.

Haberle C. W.   Cabrol N. A.   Grin E. A.
Exploring Planetary Analogs: Environmental Monitoring and Lake Bottom Mapping at Planetary Lake Lander 2011 **[#2705]**
During the deployment of Planetary Lake Lander, external observations and investigations were required. Meteorological information, stream discharge data and bathymetry were critical in determining where to place the Lake Lander.

Núñez J. I.   Farmer J. D.   Sellar R. G.
Exploration at the Hand Lens Scale: Results from the 2010 ILSO-ISRU Field Test Using the Multispectral Microscopic Imager **[#2290]**
The MMI provides in situ mineralogy within a microtextural framework. We present results from the first field deployment of the MMI in support of the 2010 International Lunar Surface Operations In-Situ Resource Utilization (ILSO-ISRU) Field Test.

EDUCATION AND PUBLIC OUTREACH: HIGHER EDUCATION

Budney C. J. Lowes L. L. Sohus A. M. Wessen A. S. Stelzner T. D. Urban A.
NASA Planetary Science Summer School: Preparing the Next Generation of Planetary Mission Leaders **[#2721]**
NASA's PSSS prepares the next generation of engineers and scientists for solar system exploration missions. Each summer, PhD candidates and post-doctoral students work with JPL's Team X to develop a mission concept and present it to a review board.

Dove A. Poppe A. Fagan A. L. Neish C. Fuqua H. Kramer G. Szalay J. Horanyi M.
LunGradCon: The Lunar Graduate Student Conference **[#2713]**
LunGradCon was created to enhance the professional development of graduate students and early postdoctoral researchers by providing an opportunity to present and discuss scientific research in an environment of their peers.

Kring D. A. Mendell W. W. Shaner A. J. Shipp S. S. Tygielski J. D.
The Lunar Exploration Summer Intern Program: Plugging Students into the Lunar Science and Exploration Pipeline **[#2814]**
The Lunar Exploration Summer Intern program at the Lunar and Planetary Institute gives graduate and advanced undergraduate students the opportunity to be involved in planning future lunar missions.

de Wet A. P. Bleacher J. E. Garry W. B.
Origins of Sinuous and Braided Channels on Ascraeus Mons, Mars — A Keck Geology Consortium Undergraduate Research Project **[#2502]**
This Keck Geology Consortium project, involving four undergrad geology students, mapped and analyzed sinuous channel features on Ascraeus Mons, Mars, to better understand the role of volcanic and fluvial processes in the geological evolution of Mars.

Hegyi S. Kereszturi A.
E-Learning System to Fuse Planetary Science and Engineering Issues **[#1812]**
Based on a realized e-learning course we tested how planetary science could be integrated into the education of engineering issues under natural sciences. Several experiences are presented here based on the online course in the autumn of 2011.

Chan M. A. Robinson J. K.
Mars for Earthlings: A Higher Educational Terrestrial Analog Approach for Teaching Integrated Earth and Planetary Science **[#1184]**
"Mars for Earthlings" teaching modules use Earth analogs to explore Mars at an introductory college level. This integrated approach increases science literacy and attracts students to STEM disciplines.

Urquhart M. L. Montgomery H. A.
Designing an Earth and Space Science Course Sequence for In-Service Teachers **[#2324]**
We describe the design for a specific set of courses including a significant NASA-influenced space sciences component to provide Texas in-service precollege teachers with the knowledge and resources necessary to be successful with their own students.

Bérczi Sz. Nagy Sz. Gyollai I. Józsa S. Szakmány Gy. Varga T. N. Varga T. P. Gucsik A.
How we Used the NASA Lunar Sample Set in the Planetary and Material Analog Studies: Lunar and Industrial Implications from the Comparison of Textures and Processes **[#1399]**
NASA's lunar sample set is an ideal collection for teaching material science through textures, as a result of both natural and industrial processes, which both have comparable parameters. Exotic lunar petrography makes this subject attractive.

Allen J.   Galindo C.   Luckey M.   Reustle J.   Todd N.   Allen C.
Lunar and Meteorite Thin Sections for Undergraduate and Graduate Studies **[#2805]**
Lunar and meteorite thin sections sets are available from JSC Curation for loans to domestic university petrology classes. See the new website for information http://curator.jsc.nasa.gov/Education/index.cfm.

Hargitai H.   Simonné-Dombóvári E.   Gede M.
A 3D Planetary Neocartographic Tool in Education: A Game on Virtual Moon and Mars Globes **[#1783]**
The paper describes the educational use of online virtual globes of Mars and the Moon. The game uses topographic globes of Mars (MOLA) and the Moon (LRO DTM) that includes IAU nomenclature + informal names. Students have to position the points described.

EDUCATION AND PUBLIC OUTREACH: K–12 PROGRAMS AND PRODUCTS

Croft S. K.   Baldridge A. M.   Buxner S.   Canizo T. L.   Chuang F. C.   Crown D. A.
Kortenkamp S. J.   Lebofsky L. A.
Instructional Rock Kits for Use in Professional Development Workshops, Classrooms, and Informal Educational Events **[#1485]**
Hands-on rock kits, activities, and associated training sessions are described that allow students to explore impact, meteorite/asteroid, volcanic, and desert environments and processes.

Lebofsky L. A.   Buxner S.   Crown D. A.   Canizo T. L.   Schmitt W.   Anderson S. W.
Project WISER: Evaluation Strategies for Professional Development Workshops at the Planetary Science Institute **[#1304]**
The Planetary Science Institute offers professional development workshops for K–8 science teachers. These workshops provide teachers with in-depth content knowledge of fundamental concepts in astronomy, geology, and planetary science.

EDUCATION AND PUBLIC OUTREACH: GENERAL E/PO

Gilbert A. M.   Osinski G. R.   August T.   Mader M.   McCullough E.   Pontefract A.
Shankar B.   Singleton A.
The Continued Growth of the Education and Outreach Program at the Centre for Planetary Science and Exploration **[#1626]**
The Centre for Planetary Science and Exploration at The University of Western Ontario has seen continual growth of its education and outreach program since 2009. This presentation summarizes the approach, reach, and activities of the program.

Anand M.   Pearson V. K.   Tindle A. G.   Kelley S. P.   Koeberl C.   Smith C. L.   Whalley P. C.
Space Eyeful: A Virtual Microscope for Extraterrestrial Samples **[#2187]**
In this contribution we describe the latest developments in producing a library of virtual microscope images of a range of extraterrestrial samples for public engagement with planetary and space sciences.

Mayo L.   James N.   Lewis E.   Ng C.   Odenwald S.   Thieman J.
Sun Earth Day 2012, The Transit of Venus, "Shadows of the Sun" **[#2869]**
This year's Sun Earth Day theme is the Transit of Venus, featuring a live webcast from Mauna Kea, Hawaii and multi wavelength video observations of the transit from Hawaii and Alaska. This will produce a sufficient baseline needed to derive the AU.

EDUCATION AND PUBLIC OUTREACH: SCIENTIST PARTICIPATION IN E/PO

Halligan E. Shipp S. Shupla C. Dalton H. Buxner S. Boonstra D. Scalice D. Bleacher L. V.
The Year of the Solar System: Opportunities for Scientist Involvement **[#2503]**
Discover ways that scientists may get involved and contribute to NASA's Year of the Solar System (YSS) activities, resources, and events!

Shupla C. Shipp S.
Menu of Opportunities for Scientist Involvement in Pre-Service Science Teacher Preparation **[#2655]**
There is a widely-recognized national crisis in science education, and scientists will be an important part of the solution. This presentation will highlight a variety of opportunities for scientists to be involved in science teacher preparation.

Jones A. J. P. Hsu B. C. Bleacher L. V.
Scientist Involvement in the Lunar Reconnaissance Orbiter's Lunar Workshop for Educators Teacher Professional Development Series **[#2916]**
Scientist involvement is critical to the LRO EPO program, including the Lunar Workshops for Educators teacher professional development series.

Galindo C. Jr. Allen J. Garcia J. Herrera S.
NASA Space Science Days: An Out of School Program Using National Partnerships to Further Influence Future Scientists and Engineers **[#2919]**
NASA Space Science Days (NSSD) was established in 2004 to bring the story of the Mars Exploration Rovers (MER) to a community far removed from areas NASA traditionally serves.

POSTER SESSION II
Thursday, 6:00 p.m. Town Center Exhibit Area

DAWN OVER VESTA: GLOBAL MAPPING

Roatsch T. Kersten E. Matz K.-D. Preusker F. Scholten F. Jaumann R. Raymond C. A. Russell C. T.
High Resoltuion Vesta HAMO Atlas Derived from Dawn FC Images **[#1765]**
Dawn FC-images from the high-altitude mapping orbit were used to calculate a global mosaic of Vesta and a high-resolution atlas.

Tricarico P. Asmar S. W. Ermakov A. Gaskell R. Jaumann R. Konopliv A. S. Marchi S. Palmer E. Park R. S. Raymond C. A. Russell C. T. Schenk P. M. Smith D. E. Sykes M. V. Toplis M. J. Zuber M. T.
Geoid and Terrain Slope of Vesta from Dawn **[#1746]**
The data collected by the Dawn spacecraft at Vesta allows the study of its geophysical characteristics. We derive the shape of the geoid, and then use it estimate the elevation and slope of the terrain.

Preusker F. Scholten F. Matz K.-D. Jaumann R. Roatsch T. Raymond C. A. Russell C. T.
Topography of Vesta from Dawn FC Stereo Images **[#2012]**
The Dawn spacecraft has entered Vesta orbit and collects a few thousand stereo images following a stereo observation scheme planned in the previous years, from which we have produced digital terrain models (DTMs).

Becker K. J. Anderson J. A. Barrett J. M. Sides S. C. Titus T. N.
ISIS Support for Dawn Instruments **[#2892]**
The USGS ISIS system now includes support for the Dawn FC and VIR instruments with ingestion and camera/sensor model software. This provides the scientific community with the means to process Dawn image data into geologic maps.

Yingst R. A. Mest S. Garry W. B. Williams D. A. Berman D. C. Jaumann R. Pieters C. M. Ammannito E. Buczkowski D. L. De Sanctis M. C. Frigeri A. Le Corre L. Preusker F. Raymond C. A. Reddy V. Russell C. T. Roatsch T. Schenk P. M. Dawn Team
A Preliminary Global Geologic Map of Vesta Based on High-Altitude Mapping Orbit Data **[#1359]**
We here report on a 1:500,000-scale preliminary global map of Vesta, based on data from Dawn's high-altitude mapping orbit (HAMO). This map is part of an iterative mapping effort; the geologic map is refined with each improvement in resolution.

Ruesch O. Hiesinger H. Schmedemann N. Kneissl T. Blewett D. T. Williams D. A. Russell C. T. Raymond C. A.
Geologic Mapping of the Av-2 Bellicia Quadrangle of 4 Vesta **[#2160]**
We present the geologic mapping of the Bellicia (Av-2) quadrangle on asteroid 4 Vesta. The map is primarily based on morphologic observations in clear filter Dawn Framing Camera images.

Young B. L. Blewett D. T. Williams D. A. O'Brien D. P. Gaskell R. Yingst R. A. Garry W. B. Buczkowski D. L. Hiesinger H. McCord T. B. Combe J.-Ph. Schenk P. M. Jaumann R. Pieters C. M. Nathues A. Le Corre L. Hoffmann M. Reddy V. Roatsch T. Preusker F. Marchi S. Scully J. Russell C. T. Raymond C. A. De Sanctis M. C.
Geologic Mapping of the Av-3 Caparronia Quadrangle of Asteroid 4 Vesta **[#1245]**
We present a preliminary geological map of Vesta's northern hemisphere quadrangle Av-3 (Caparronia), based on data returned by the Dawn spacecraft.

THU POSTERS

THU POSTERS

Scully J. E. C.   Russell C. T.   Yin A.   Williams D. A.   Blewett D. T.   Buczkowski D. L.
Ammannito E.   Roatsch T.   Preusker F.   Le Corre L.   Yingst R. A.   Garry W. B.   Jaumann R.   Pieters C. M.
Raymond C. A.
Geologic Mapping of the Av-4 Domitia Quadrangle of Asteroid 4 Vesta **[#2368]**
This presentation describes the geologic mapping and interpretations of Vesta's Domitia quadrangle, which have been derived from Dawn spacecraft data. The trough and ridge system, varieties of craters, dark material, and composition are discussed.

Mercer C. M.   Williams D. A.   Scully J. E.   Blewett D. T.   Buczkowski D. L.   Jaumann R.   Schenk P. M.
Yingst R. A.   Garry W. B.   Roatsch T.   Preusker F.   Pieters C. M.   Russell C. T.   Raymond C. A.
De Sanctis M. C.   Dawn Science Team
Geologic Mapping of the Av-5 Floronia Quadrangle of the Asteroid 4 Vesta **[#1716]**
The Dawn spacecraft is characterizing the geology, surface composition, topography, and shape of the asteroid 4 Vesta during its one year of operations there. We present results from the geologic mapping of the Av-5 quadrangle, named Floronia.

Le Corre L.   Reddy V.   Nathues A.   Williams D. A.   Garry W. B.   Yingst R. A.   Jaumann R.   Roatsch T.
Preusker F.   Pieters C. M.   Russell C. T.   Raymond C. A.
Geologic Mapping of the Av-6 (Gegania) Quadrangle of Asteroid 4 Vesta **[#1629]**
This presentation concentrates on the geologic analysis and mapping of quadrangle Av-6 on Vesta using the latest data from the Dawn spacecraft. The prevailing feature observed is a set of equatorial troughs up to ~20 km wide parallel to the equator.

Reddy V.   Le Corre L.   Nathues A.   Williams D. A.   Gary W. B.   Yingst R. A.   Juamann R.   Roatsch T.
Preusker F.   Pieters C. M.   Russell C. T.   Raymond C. A.
Geologic Mapping of the Av-7 (Lucaria) Quadrangle of Asteroid (4) Vesta **[#1616]**
We present mapping results of the Av-7 quad on asteroid Vesta from the Dawn mission; this region includes the enigmatic Lucaria Tholus structure.

Williams D. A.   Schenk P. M.   Jaumann R.   Buczkowski D. L.   McCord T. B.   Yingst R. A.   Hiesinger H.
Garry W. B.   Combe J.-Ph.   Pieters C. M.   Nathues A.   Le Corre L.   Hoffmann M.   Reddy V.   Roatsch T.
Preusker F.   Marchi S.   Russell C. T.   Raymond C. A.   Neukum G.   Schmedemann N.   Ammannito E.
De Sanctis M. C.
Geologic Mapping of the Av-8 Marcia Quadrangle of Asteroid 4 Vesta **[#1534]**
This presentation will discuss our Dawn mission-based geologic mapping of the Av-8 Marcia quadrangle, one of the equatorial quadrangles of asteroid 4 Vesta.

Buczkowski D. L.   Wyrick D. Y.   Capaccioni F.   Scully J. E. C.   Williams D. A.   Hiesinger H.   Garry W. B.
Yingst R. A.   Le Corre L.   Nathues A.   Schenk P. M.   Jaumann R.   Raymond C. A.   Pieters C. M.   Roatsch T.
Preusker F.   Russell C. T.
Geologic Mapping of the Av-9 Numisia Quadrangle of Asteroid 4 Vesta **[#2263]**
We present our geologic analysis and mapping of quadrangle Av-9 Numisia.

Garry W. B.   Sykes M. V.   Buczkowski D. L.   Williams D. A.   Yingst R. A.   Mest S. C.
Jaumann R.   Pieters C. M.   Roatsch T.   Preusker F.   Russell C. T.   Raymond C. A.
Filacchione G.   Dawn Science Team
Geologic Mapping of Av-10 Oppia Quadrangle of Asteroid 4 Vesta **[#2315]**
Geologic mapping of Vesta is being conducted as series of 15 quadrangle maps. This work will present results from the geologic mapping of quadrangle Av-10 Oppia. Geologic features in this quad are Oppia Crater, Feralia Planitia, and Divalia Fossa.

Hoogenboom T. Schenk P. White O. L. Williams D. Heisinger H. Garry W. B. Yingst R. A. Buczkowski D. L. McCord T. B. Jaumann R. Pieters C. M. Gaskell R. W. Neukum G. Schmedemann N. Marchi S. Nathues A. LeCorre L. Roatsch T. Preusker F. De Sanctis M. C. Fillacchione G. Raymond C. A. Russell C. T.
Geologic Mapping of the Av-11 Pinaria Quadrangle of Asteroid 4 Vesta **[#2179]**
Dawn entered orbit of the asteroid 4 Vesta in 7/2011, to characterize its geology, elemental and mineralogical composition, topography, shape, and internal structure. This abstract describes the results from mapping quadrangle Av-11.

Krohn K. Jaumann R. Stephan K. Pieters C. M. Wagner R. Yingst R. A. Williams D. A. Schenk P. Neukum G. Schmedemann N. Kneissl T. De Sanctis M. C. Nathues A. Buczkowski D. L. Roatsch T. Preusker F. Kersten E. Russell C. T. Raymond C. A.
Geologic Mapping of the Av-12 Sextlia Quadrangle of Asteroid 4 Vesta **[#1901]**
The geologic map of Quadrangle Av-12 Sextilia shows several different units: Rheasilvia material, including scarp wall material, slump deposits and ridge and groove terrain; dark material; slump material in impact craters; and old basin material.

Kneissl T. Schmedemann N. Neukum G. Williams D. A. Garry W. B. Yingst R. A. Ammannito E. Jaumann R. Pieters C. M. Russell C. T. Raymond C. A. Schenk P. Hiesinger H. McCord T. B. Buczkowski D. L. Nathues A. Reddy V. Büttner I. Krohn K. Preusker F.
Geologic Mapping of the AV-13 Tuccia Quadrangle of Asteroid 4 Vesta **[#1899]**
This abstract reports results from the geological mapping of quadrangle Av-13, named Tuccia. We used Framing Camera (FC) monochrome and color data, Visible and InfraRed (VIR) hyperspectral data, and DTMs derived from stereo image data.

Mest S. C. Yingst R. A. Williams D. A. Garry W. B. Pieters C. M. Jaumann R. Buczkowski D. L. Sykes M. V. Tricarico P. Wyrick D. Y. Schenk P. M. Russell C. T. Raymond C. A. Neukum G. Schmedemann N. Roatsch T. Preusker F. Ammannito E. Dawn Team
Geologic Mapping of the Av-14 Urbinia Quadrangle of Asteroid 4 Vesta **[#2375]**
The Av-14 Urbinia Quadrangle of 4Vesta is being mapped using high altitude mapping orbit (HAMO) clear filter Framing Camera (FC) images, a Survey orbit FC-derived DTM, FC color ratio images, and visible and infrared (FIR) hyperspectral images.

White O. L. Yingst R. A. Berman D. Frigeri A. Jaumann R. Le Corre L. Mest S. Pieters C. M. Preusker F. Raymond C. A. Reddy V. Roatsch T. Russell C. T. Schenk P. M. Schmedemann N.
Geologic Mapping of the AV-15 Rheasilvia Quadrangle of Asteroid 4 Vesta **[#1264]**
Mapping of the Rheasilvia quadrangle has characterized the Rheasilvia mound complex, slump material originating from the mound's scarp, and cratered terrain.

Palomba E. De Sanctis M. C. Nathues A. Stephan K. Ammanito E. Longobardo A. Frigeri A. Zambon F. Capaccioni F. Yingst R. A. Jaumann R. Tosi F. Pieters C. M. Raymonds C. A. Russell C. T.
Compositional Mapping of Vesta Quadrangle V22 **[#2243]**
The results of the spectroscopic analysis achieved for the quadrangle V22, which covers Vesta's surface between 57°N–57°S and 0°–180°, are presented. In detail, band depths of the pyroxene bands are given for different terrains of the quadrangle.

Stephan K. Jaumann R. De Sanctis M. C. Ammannito E. Pieters C. M. Matz K.-D. Preusker F. Roatsch Th. Russell C. T. Raymond C. A.
Compositional Mapping of Vesta Quadrangle V-23 **[#2133]**
We present the compositional mapping results for Vesta-Quadrangle V 23 derived from VIR data.

Tosi F.   De Sanctis M. C.   Nathues A.   Ammannito E.   Frigeri A.   Zambon F.   Palomba E.   Capaccioni F.
Yingst A.   Jaumann R.   Stephan K.   Pieters C. M.   Raymond C. A.
Russell C. T.   Dawn Team
Compositional Mapping of Vesta Quadrangle V24 **[#1966]**
In this work we present the results of the spectroscopic analysis achieved on the basis of Dawn's Visible and InfraRed Imaging Spectrometer (VIR) for the quadrangle V-24, which covers Vesta's southern polar region 55°S–90°S and longitude 0°–360°.

DAWN OVER VESTA: COMPOSITION OF A TRANSITIONAL WORLD

Srinivasan P.   Delaney J. S.
The Significance of Fe Exchange Between Metal and Silicate Minerals in Mafic Clasts from the Howardites Kapoeta and Winterhaven **[#2668]**
Fe in metal and silicate minerals of mafic clasts from howardites reflects original metal composition and subsequent modifications by post igneous processes. The sequence of exchange reactions in howardites will elucidate the regolith history of Vesta.

Righter M.   Shaulis B. J.   Lapen T. J.
U-Pb and ^{207}Pb-^{206}Pb Age of Zircons from Polymict Eucrites and Howardites **[#2562]**
We have analyzed zircon and baddeleyite grains from polymict eucrites and howardites. Preliminary results shows those ages are slightly younger than those of unbrecciated eucrites reported before.

Patzer A.   McSween H. Y. Jr.
Gabbroic vs. Cumulate Eucrites: Extending the Diversity of Eucritic Lithologies **[#1227]**
In addition to the established subgroups of basaltic and cumulate eucrites, we propose the definition of a third subclass: gabbroic eucrites. This proposition is based on petrographic data from our ongoing investigation of new Antarctic howardites.

Strashnov I.   Nottingham M.   Llorca J.   Gilmour J. D.
^{81}Kr-Kr Cosmic Ray Exposure Age of the Puerto Lapice (and Other) Eucrites **[#1813]**
^{81}Kr-Kr cosmic-ray exposure ages of several eucrites including of the new fall Puerte Lapice have been determined. The Akaike information criterion has been used to assign them into "clusters" representing the impacts on parent body.

Claydon J. L.   Crowther S. A.   Gilmour J. D.
Xenon in the Anomalous Eucrites Bunburra Rockhole and Ibitira **[#1884]**
Samples show Pu-Xe ages consistent with normal eucrites but higher ^{129}I/^{244}Pu ratios indicating they formed on a more volatile-rich (or less-devolatised) parent body.

Castle N. C.   Irving A. J.   Tanaka R.   Bachmann O.
Major and Trace Element Characterization of Pyroxenes in Polymict Eucrite Northwest Africa 6475: Contrasts with Juvinas, Stannern and Igdi, and Evaluation of Models for Eucrite Magmatic Evolution **[#2647]**
We examined the range of pyroxene major, minor and trace element chemistry in the three eucrite trends, and compared them with clasts in NWA 6475, a polymict eucrite. Existing models relating the three chemical trends were examined with this new data.

van Drongelen K. D.   Tait K. T.   Gregory D. A.
Polymict Eucrite Northwest Africa 5232: Composition and Classification of Clasts **[#2056]**
The study of NWA 5232 aims at describing this 18.5 kg polymict eucrite and classifying its constituents. Six polished sections were examined with a petrographic microscope, electron microprobe, scanning electron microscope, and Raman spectrometer.

Satake W.   Buchanan P. C.   Mikouchi T.   Miyamoto M.
Redox States of Some HED Meteorites as Inferred from Iron Micro-XANES Analyses of Plagioclase **[#1725]**
We analyzed plagioclase in HED meteorites by Fe-XANES. The Fe^{3+} ratio of a cumulate eucrite was high (~0.9), while those of basaltic eucrite and diogenite were low (~0). This may be related to the heterogeneous redox environment of Vesta's crust.

Balta J. B.   Beck A. W.   McSween H. Y. Jr.
Trace Elements Reveal Complex Histories in Diogenites **[#1189]**
We report relict trace-element zoning in diogenite meteorites. Trace elements in otherwise homogeneous OPX record histories of both magmatic and impact processes. These patterns suggest previously unrecognized long thermal histories for diogenites.

Ek M.   Quinn J. E.   Mittlefehldt D. W.
In Situ Analysis of Orthopyroxene in Diogenites Using Laser Ablation ICP-MS **[#2096]**
In situ analysis of orthopyroxene in diogenites shows that the variationof trace element are several times larger than for the minor elements, and in GRO 95555 and MET 00425 the trace element concentrations increase in proximity to a silica phase.

Tarduno J. A.   Cottrell R. D.
Single Crystal Paleointensity Analyses of Olivine-Diogenites: Implications for a Past Vestan Dynamo **[#2663]**
Preliminary rock magnetic and paleointensity analyses of olivine-diogenite meteorites are presented. These data indicate that olivine hosting magnetic inclusions is a suitable magnetic recorder, and suggest Vesta once had a dynamo.

Greenwood R. C.   Barrat J-A.   Scott E. R. D.   Janots E.   Franchi I. A.   Hoffman B.
Yamaguchi A.   Gibson J. M.
Has Dawn gone to the Wrong Asteroid? Oxygen Isotope Constraints on the Nature and Composition of the HED Parent Body **[#2711]**
Oxygen isotope analyses for 122 HED samples are used to examine whether Vesta is a viable source for the HEDs. The levels of isotopic heterogeneity within the HED parent body are assessed and the origin of anomalous HED meteorites re-examined.

Lawrence D. J.   Prettyman T. H.   Feldman W. C.   Bazell D.   Mittlefehldt D. W.
Peplowski P. N.   Reedy R. C.
Geochemistry at 4 Vesta: Observations Using Fast Neutrons **[#1837]**
Fast neutrons provide a measure of the average atomic mass of planetary surface material. The GRaND instrument on the Dawn spacecraft is measuring fast neutrons from 4 Vesta and will provide constraints of Vesta's surface composition.

Zambon F.   De Sanctis M. C.   Ammannito E.   Capria M. T.   Capaccioni F.   Carraro F.   Fonte S.   Frigeri A.
Magni G.   Marchi S.   Palomba E.   Tosi F.   Blewett D. T.   Raymond C. A.
Russell C. T.   Titus T. N.
Classification of Dawn VIR hyperspectral Data of Vesta **[#1964]**
The analysis of the whole disk of Vesta gives a global overview of its surface. We have classified the whole disk image of Vesta normalized at 550 nm with an ISODATA classifier and we have compared this result with a RGB image (R: 0.44 µm, G: 0.75 µm, B: 1 µm).

Li S.   Milliken R. E.
Estimating Mineral Abundances of HED Meteorites from VIS-NIR Spectra and Implications for Dawn at Vesta **[#1459]**
A new implementation of Hapke modeling for simultaneously quantifying minerals and particle sizes of eucrite and olivine diogenite meteorites.

THU POSTERS

Cloutis E. A.   Reddy V.   Le Corre L.   Pompilio L.   Mann P.   Nathues A.   Hiesinger H.
Spectral Reflectance Properties of HED Meteorites as a Function of Grain Size and Presence of CM2 Material **[#1571]**
The spectral reflectance properties of low-albedo areas on Vesta can be attributed to either larger grain sizes of HED meteorites or the presence of CM2-type chondrites. However, these two mechanisms lead to differences in band depths vs. albedo.

Reddy V.   Le Corre L.   McCoy T. J.   Nathues A.   Mayne R. G.   Sunshine J.   Gaffey M. J.
Becker K. J.   Cloutis E. A.
Testing the Magma Ocean Model Using Distribution of Chromium on Vesta's Surface from Dawn Framing Camera Color Images **[#1588]**
We are attempting to test partial melting vs. magma ocean models for Vesta petrogenesis by detecting and quantifying the 0.6-μm chromium feature in Dawn Framing Camera color images. Initial investigation suggests this feature is rare on Vesta.

DAWN OVER VESTA: MORE CHEMISTRY, MORE ROCKS

Farina M.   Capaccioni F.   Carli C.   Consolmagno G. J.   De Sanctis M. C.   Ammannito E.   Turrini D.
Studying HED Meteorites in View of the Analysis of the VIR Spectra of Vesta **[#1992]**
Howardites, eucrites, and diogenites have been mapped, taking numerous spots on the surface of each slab. Using also Relab spectra we will discuss how spectral reflectance properties differ between powders and slabs.

Usui T.   Iwamori H.
Independent Component Analysis of HED Meteorites: Prospective Study for Interpretation of Gamma-Ray and Neutron Spectra for the Dawn Mission **[#2231]**
Our eight-component ICA model (computational statistical technique) explains compositional variations, petrographic observations, and mixing relations of the HED suite without assuming any end-member components.

Frigeri A.   De Sanctis M. C.   Ammannito E.   Yingst R. A.   Mest S.   Capaccioni F.   Garry B.   Magni G.
Palomba E.   Petro N.   Tosi F.   Williams D.   Zambon F.   Jaumann R.   Pieters C. M.   Raymond C. A.
Russell C. T.   Dawn Team
Correlation Between Preliminary Mineralogic and Geologic Maps of Vesta **[#2934]**
In this work we will report the comparison of the preliminary geologic map of Vesta with the spectral indicators synthesized from the VIR instrument data on-board the Dawn mission.

Nathues A.   Le Corre L.   Reddy V.   Hoffmann M.   Dawn Science Team
Identification of Vesta Surface Units with Principal Component Analysis by Using Dawn Framing Camera Imagery **[#1779]**
Multicolor images obtained by the Dawn Framing Camera have been used to create color cubes that have been transformed to PC space for lithology identification.

Mittlefehldt D. W.   Li J.-Y.   Pieters C. M.   De Sanctis M. C.   Schroder S. E.   Hiesinger H.   Blewett D. T.
Russell C. T.   Raymond C. A.   Yingst R. A.   Dawn Science Team
Types and Distribution of Bright Materials on 4 Vesta **[#1680]**
The surface of 4 Vesta has localized deposits of atypically high-albedo material. Here we define the types of deposits and map their distribution.

Yamashita N.   Prettyman T. H.   Mafi J.   Joy S.   Feldman W. C.   Forni O.   Lawrence D. J.   Reedy R. C.
Data Reduction and Archiving for Dawn's Gamma Ray and Neutron Detector **[#2448]**
The reduction, analysis, and archiving of data acquired by the NASA Dawn mission's Gamma Ray and Neutron Detector is presented. Processing and analysis steps for determining the abundance of Fe in the surface of Vesta are highlighted.

Palmer E. M.   Heggy E.   Russell C. T.   Asmar S. W.   Raymond C. A.
Exploring Surface and Shallow Subsurface Volatile Presence on Vesta Using a Bistatic Radar Experiment **[#2685]**
An interesting topic of concern for Vesta is the presence or lack of volatiles. A bistatic radar experiment may help address this question, where data interpretation relies on dielectric models of the surface and shallow subsurface.

Reedy R. C.   Prettyman T. H.   Yamashita N.
Backgrounds in Space Cadmium Zinc Telluride (CZT) Gamma-Ray Spectrometers **[#1284]**
Gamma rays made by energetic particles in CdZnTe detectors, such as those on Dawn, are listed and discussed. Most prompt and decay gamma rays are <2 MeV and could be backgrounds to peaks of interest.

Reedy R. C.
Update on Solar-Proton Fluxes During the Last Five Solar Activity Cycles **[#1285]**
The event-integrated fluences of energetic solar protons during the last 5 solar cycles (1954–2008) have been reevaluated. Such data are needed to plan for space missions, such as Dawn at Vesta.

Starukhina L. V.   McCord T. B.
Asteroid Shielding from Solar Wind: Calculation of the Parameters of Magnetospheres **[#1288]**
The magnetic field required to protect asteroids from solar wind is calculated as a function of asteroid diameter and heliocentric distance. For asteroid protection, moderate values of dipole magnetic moments and fields on the surfaces are sufficient.

Tosi F.   Capria M. T.   De Sanctis M. C.   Palomba E.   Grassi D.   Capaccioni F.   Ammannito E.   Combe J.-Ph.   Sunshine J. M.   McCord T. B.   Li J.-Y.   Titus T. N.   Russell C. T.   Raymond C. A.   Mittlefehldt D. W.   Toplis M. J.   Forni O.   Sykes M. V.
Analysis of Temperature Maps of Selected Dawn Data over the Surface of Vesta **[#1886]**
In this work, we present temperature maps of several unusual local-scale features that were observed by Dawn's Visible and Infrared Mapping Spectrometer under different illumination conditions and different local solar times.

Titus T. N.   Becker K. J.   Anderson A.   Capria M. T.   Tosi F.   De Sanctis M. C.   Palomba E.   Grassi D.   Capaccioni F.   Ammannito E.   Combe J.-Ph.   McCord T. B.   Li J.-Y.   Russell C. T.   Raymond C. A.   Mittlefehldt D.   Toplis M.   Forni O.   Sykes M. V.
Comparison of Observed Surface Temperatures of 4 Vesta to the KRC Thermal Model **[#2851]**
In this work, we will compare observed temperatures of the surface of Vesta using data acquired by the Dawn Visible and Infrared Mapping Spectrometer (VIR-MS) during the approach phase to model results from the KRC thermal model.

MAIN BELT ASTEROIDS: LUTETIA, IDA, AND OTHERS

Okamura N.   Hasegawa S.   Hiroi T.   Ootsubo T.   Müller T. G.   Usui F.   Sugita S.
3-µm Spectroscopic Obersvations of Asteroid 21 Lutetia Using Akari Satellite **[#1918]**
We investigate the presence of 3-µm absorption band of asteroid 21 Lutetia based on the observational results obtained by the AKARI satellite. As a result, the 3-µm absorption bands are found to have a very shallow absorption or no obvious absorption.

Andrews D. J.   Morse A. D.   Barber S. J.   Leese M. R.   Morgan G. H.   Sheridan S.   Wright I. P.   Pillinger C. T.
Ptolemy: Operations at 21 Lutetia as part of the Rosetta Mission and Future Implications **[#2113]**
Ptolemy is an evolved gas analyzer onboard the Philae lander of the Rosetta mission. Attempts were made to detect the exosphere of asteroid 21 Lutetia during a July 2010 targeted flyby; the results are presented here and future implications discussed.

Granahan J. C.
Revisiting 243 Ida Galileo Infrared Spectra **[#1162]**
Radiance spectra data files are being assembled for the Galileo Near Infrared Mapping Spectrometer observations of asteroid 243 Ida and its satellite Dactyl. These calibrated data are being prepared for archival in the NASA Planetary Data System.

Hirabayashi M.   Scheeres D. J.
Fission Limits for Bifurcated Asteroids: The Case of Kleopatra **[#2256]**
Based on radar and optical measurement of Kleopatra we show that it is spinning near, but less than, its fission limit. Our method is also applied to five other asteroids to map out their spin limits before they are susceptible to spin fission.

Blagen J. R.   Gaffey M. J.   Fieber-Beyer S. K.
Testing the Gefion Family as a Possible Parent Body for the L-Chondrite Meteorites **[#1643]**
A goal has been to find the origin of the L-chondrite meteorites. This study uses infrared spectroscopy to assess the mineralogy of Gefion family asteroids to test whether the family is a source of the L chondrites, and if it is a genetic family.

Crane K. T.   Emery J. P.   Lim L. F.
Shape and Thermal Modeling of a Selection of M-Type Asteroids **[#1425]**
We have determined the shape and thermally modeled six M-type asteroids that, because of their spectral signatures or lack thereof, radar albedos, and other thermal and physical properties, are likely candidates for metallic core progeny.

EDUCATION AND PUBLIC OUTREACH: SMALL BODIES

Cobb W. H.   Lebofsky L. A.   Ristvey J. D.   Buxner S.   Weeks S.   Zolensky M. E.
Small Bodies, Big Concepts: Bringing Visual Analysis into the Middle School Classroom **[#2327]**
Multi-disciplinary PD model digs into high-end planetary science backed by a pedagogical framework, Designing Effective Science Instruction. NASA activities are sequenced to promote visual analysis of emerging data from Discovery Program missions.

SMALL BODIES: COMETS, TROJANS, AND TNOS

Hermalyn B.   Farnham T. L.   Schultz P. H.   Kelly M. S.   Thomas P. C.   Lindler D.   Bodewits D.   A'Hearn M. F.   Meech K.   DIXI Science Team
The Detection, Localization, and Dynamics of Large Icy Particles Surrounding Comet 103P/Hartley 2 **[#2785]**
The Deep Impact spacecraft flyby of the hyperactive comet Hartley 2 revealed a field of fine grain dust and ice and hundreds of discrete larger particles enveloping the comet. Here, we present an analysis of the location and dynamics of particles.

Smith T.   Khodja H.   Raepsaet C.   Burchell M.   Flynn G. J.   Herzog G. F.   Park J.   Lindsay F.   Nakamura-Messenger K.   Keller L. P.   Taylor S.   Westphal A.
Characterization of 81P/WILD 2 Particles C2067,1,111,6.0 and C2067,1,111,8.0 **[#2198]**
We used FTIR, TEM, EDAX, and nuclear reaction analysis (NRA) to measure in Stardust particles the areal concentrations of C and N; C/N ratios ranged from 3.3 to 43.6. NRA studies of glycine shot into Al suggest loss of light elements.

Komatsu M.   Fagan T.   Mikouchi T.   Miyamoto M.   Zolensky M.   Ohsumi K.
Mineralogy of Stardust Track 112 Particle: Relation to Amoeboid Olivine Aggregates **[#1654]**
We have examined the relationships between T112 particle and amoeboid olivine aggregates. Slight enrichment of Fe in olivine rim and associated chromites suggest that T112 may have experienced a minor degree of metamorphism.

Parsons A. M.   Evans L. G.   Lim L.   Starr R.
Capabilities of Gamma Ray and Neutron Spectrometers for Studying Trojan Asteroid Subsurface Ices **[#2769]**
We present computer simulation results for gamma ray and neutron instruments located 50 km above a Trojan asteroid. Preliminary results indicate that these instruments can detect buried ices that may indicate a Kuiper Belt origin for the Trojans.

Doressoundiram A.   Liu C.-Y.   Roques F.
Discovery of Sub-Kilometer Size Trans-Neptunian Objects with the COROT Space Observatory **[#1967]**
We reexamine the COROT asteroseismology lightcurves for the search of small transneptunian objects (TNOs). The total observation time available is about 144408.3 star-hours. We aim to search for serendipitous occultations by passing TNOs.

SMALL BODIES: NEAR-EARTH ASTEROIDS AND MARS MOONS

Dunn T. L.   Burbine T. H.
Mineralogies of Near Earth Asteroids **[#2305]**
We characterize the mineralogies of four NEAs with chondrite-like infrared spectra. This is preliminary data from a larger study of ~138 NEAs with SpeX spectra that appear visually similar to ordinary chondrites.

Abell P. A.   Barbee B. W.   Mink R. G.   Adamo D. R.   Alberding C. M.   Mazanek D. D.   Johnson L. N.   Yeomans D. K.   Chodas P. W.   Chamberlin A. B.   Benner L. A. M.   Drake B. G.   Friedensen V. P.
The Near-Earth Object Human Space Flight Accessible Targets Study (NHATS) List of Near-Earth Asteroids: Identifying Potential Targets for Future Exploration **[#2842]**
The Near-Earth Object Human Space Flight Accessible Target Study (NHATS) identifies NEAs for human exploration. An updated list of NEAs identified under the NHATS criteria will be made available to the international community via a NASA website.

Bazso A.
Lunar Effects on Close Encounters of Near Earth Asteroids **[#1809]**
By numerical integrations we investigate the Moon's effects on close encounters of near-Earth asteroids. It is shown in two models that with the Moon more close encounters occur and these encounters result in lower minimal distances.

Vodniza A. Q.   Pereira M. R.
Study of 2003 YT1 Asteroid **[#1559]**
The asteroid 2003 YT1 was at approximately 25 million kilometers from Earth on May 05-2011 (U.T). From our observatory, located in Pasto-Colombia, we captured several pictures during three days and we calculated the orbital elements.

Roberts J. H.   Barnouin O. S.   Prockter L. M.   Kahn E. G.   Gaskell R. W.
Not All Ponds are Flat: A Stereophotoclinometric Analysis of Eros Topography **[#2450]**
We investigate the topography of ponds on Eros, using a new shape model derived from sterophotoclinometric analysis. We find that a significant fraction (~75%) of ponds do not have flat floors, and evaluate hypotheses for pond formation.

McMahon J. W.   Scheeres D. J.
Inferring Small-Scale Surface Variability on Near-Earth Asteroids from Itokawa's Shape Data **[#1596]**
Itokawa data shows significant surface slope variations at high resolutions relative to lower-resolution models. When Itokawa's statistics are applied to radar shape models, this implies significant surface roughness down to submeter resolution.

Abe M.   Yada T.   Fujimura A.   Okada T.   Ishibashi Y.   Shirai K.   Uesugi M.   Karouji Y.   Yakame S.
Nakamura T.   Noguchi T.   Okazaki R.   Mukai T.   Fujimoto M.   Yoshikawa M.   Kawaguchi J.
Asteroid Itokawa Sample Curation and Distribution for Initial Analyses and International AO held in the Planetary Material Sample Curation Facility of JAXA **[#1708]**
We review how a series of curation works for the Hayabusa samples (asteroid Itokawa's materials) goes in the facility and sample distribution for initial analyses and international announces of opportunity (AO) for research.

De Gregorio B. T.   Zolensky M. E.   Bastien R.   McCann B.   Frank D. R.   Warren J. L.   Allen C. C.
Developing the New Hayabusa Curation Facility at Johnson Space Center **[#2020]**
NASA Johnson Space Center will receive 10% of the asteroid grains returned by the Hayabusa mission. We describe the development, construction, and contamination control for the new Hayabusa curation facility at JSC.

Ishibashi Y.   Fujimura A.   Abe M.   Okada T.   Yada T.   Uesugi M.   Karouji Y.   Yakame S.
Design of Sample Transportation Container for the First AO Distribution of Hayabusa Samples **[#2887]**
We report the design and preparation of the sample transportation container for the first AO distribution of Hayabusa samples.

Gondet B.   Bibring J.-P.
Deimos and Phobos Compared Observations by OMEGA/MEX **[#2041]**
The OMEGA imaging spectrometer has acquired hyperspectral images of both Phobos and Deimos. These two objects exhibit distinct spectral characteristics in the visible, which could offer clues as to their origin.

Karachevtseva I.   Oberst J.   Shingareva K.   Konopikhin A.   Nadejdina I.   Zubarev A.   Willner K.   Mut N.
Wählisch M.
Global Phobos Geodatabase and GIS Analyses **[#1342]**
Geoanalysis of the Phobos surface has been made using GIS and a new global crater catalog. Our further activities are to analyse Phobos grooves and boulders in GIS, and to develope new control points for updates of the current Phobos shape and map models.

SMALL BODIES: PROCESSES, TOOLS, AND UPCOMING MISSIONS

Molaro J. L.   Byrne S.
The Effect of Rotation Rate and Semi-Major Axis on the Efficacy of Thermal Stress Weathering **[#1154]**
We explore which solar system bodies may be most susceptible to thermal stress weathering by modeling surface temperatures of near-Earth asteroids and examining how rates of temperature change vary with rotation rate, semi-major axis, and obliquity.

Moskovitz N. A.
Spectro-Photometry of Dynamically Associated Asteroid Pairs **[#2032]**
Pairs of dynamically associated asteroid pairs have recently been identified in the main belt. We will present the results of a spectro-photometric study to address the formation of these unusual objects.

Fu R. R.   Hager B. H.
Asteroid Shape as a Constraint on Early Melting and Differentiation **[#1956]**
We conduct numerical modeling of the early deformation of partially differentiated asteroids due to self gravity. Fully molten bodies relax to hydrostatic shapes in <1 m.y. while the presence of a crust can prevent relaxation for small bodies (<150 km).

Kahn E. G.   Barnouin O. S.   Ernst C. M.
Improved Estimation of the Hayabusa Spacecraft Trajectory and Lidar Tracks **[#1648]**
An algorithm is presented for improving the estimate of the Hayabusa spacecraft trajectory and lidar tracks by using a high-resolution shape model of 25143 Itokawa and a point-matching scheme to match the lidar tracks with the asteroid.

Savanevich V. E.   Kozhukhov A. M.   Bryukhovetskiy A. B.   Vlasenko V. P.   Dikov E. N.   Ivashchenko Yu. N.   Elenin L. V.
Program of Automated Asteroids Detection CoLiTec — New Features and Results of Implementation **[#1049]**
The report presents the main improvements and results of using of the CoLiTec program in 2011. By 10 December the two observatories discovered more than 700 asteroids and one comet and sent to the MPC more than 150,000 measurements using the program.

Levengood S. P.   Shepard M. K.
A GUI-Based Open-Source Program for Viewing and Illuminating Asteroid Shape Models **[#1230]**
We created an interactive opensource program that can generate brightness maps and phase curves for a given asteroid shape (.SHP) model. Images of the model are rendered using ray tracing via OpenGL.

Lauretta D. S.   OSIRIS-REx Team
An Overview of the OSIRIS-REx Asteroid Sample Return Mission **[#2491]**
The science objectives, science implementation, and mission implementation plans for the OSIRIS-REx mission will be presented.

Dickinson C. S.   Daly M.   Barnouin O.   Bierhaus B.   Gaudreau D.   Tripp J.   Ilnicki M.   Hildebrand A.
An Overview of the OSIRIS REx Laser Altimeter (OLA) **[#1447]**
The Canadian Space Agency is contributing a scanning lidar system known as the OSIRIS-REx Laser Altimeter, or OLA, to the OSIRIS REx Mission. OLA will deliver high-density three-dimensional point cloud data, enabling reconstruction of an asteroid shape model.

Helbert J.   Maturilli A.   Grott M.   Knollenberg J.   Okada T.   Kührt E.
Measurements at the Planetary Emissivity Laboratory in Support of MARA and the TIR Imager on the JAXA Hayabusa II Mission **[#1955]**
At the Planetary Emissivity Laboratory (PEL) at DLR we perform measurements on analog materials to explore the possibility of mineralogical studies with the thermal infrared imager and the radiometer MARA (MAscot RAdiometer) on MASCOT.

Okada T.   Fukuhara T.   Tanaka S.   Taguchi M.   Nakamura R.   Sekiguchi T.   Hasegawa S.   Ogawa Y.   Kitazato K.   Matsunaga T.   Imamura T.   Wada T.   Arai T.   Yamamoto Y.   Takaki R.   Tachikawa S.   Helbert J.   Mueller T. G.
Thermal Infrared Imager TIR on Hayabusa 2 to Investigate Physical Properties of C-Class Near-Earth Asteroid 1999JU3 **[#1498]**
Thermal-infrared imager TIR is being prepared to observe a C-class ENA 1999JU3 in Hayabusa 2, not only for scientific investigation of asteroid physical properties but also for landing site selection and safety descent to asteroid surface.

McCord T. B.   Combe J.-Ph.   Taffin C.
Composition of a Comet Nucleus: Preparing for Rosetta Observations **[#2449]**
Knowledge about the specific components of a comet nucleus is limited. We review the current knowledge, explore additional inferred components, and show the detectability using the IR spectrometer, VIRTIS, on the Rosetta mission.

Briani G.   Engrand C.   Duprat J.   Benoit R.   Krüger H.   Fischer H.   Hilchenbach M.   Briois C.   Thirkell L.
TOF-SIMS Analyses of an Ultracarbonaceous MicroMeteorite: Preparation of Rosetta-COSIMA Studies in 2014 **[#2584]**
We studied organic matter of an ultracarbonaceous Antarctic micrometeorite (UCAMM) by in situ high mass resolution TOF-SIMS. Results will be used to optimize the scientific return of the COSIMA mass spectrometer onboard the ESA space mission Rosetta

DAWN OVER VESTA: SURFACE AND CRATERING

Ivanov B. A.   Melosh H. J.
The Rheasilvia Crater on Vesta: Numerical Modeling **[#2148]**
The impact cratering two-dimensional numerical model is presented aimed to reproduce Rheasilvia crater formation on Vesta. The model is tuned to reproduce the prominent central mound in the crater.

Galiazzo M. A.   Souami D.   Eggl S.   Souchay J.
The Vesta Asteroid Family: Study of the Family and Close Encounters with Terrestrial Planes and Dynamical Influences by (1) Ceres and (4) Vesta **[#1424]**
The Vesta family is the largest asteroidal family known in the inner main belt, and it is believed to be a source of HED meteorites. We study its long-term evolution and investigate close encounters with Ceres, Vesta, and terrestrial planets.

Turrini D.   Coradini A.   Federico C.   Formisano M.   Magni G.
The Primordial History of Vesta and the Jovian Early Bombardment **[#2047]**
We report the first results of a joint study of the differentiation of Vesta and the bombardment triggered by the formation of Jupiter to assess the possible implications of the interpretation of the data supplied by the Dawn mission.

Marchi S.   Bottke W. F.   Cohen B. A.   De Sanctis M. C.   Wuennemann K.   McSween H. Y.   O'Brien D. P.   Schenk P.   Raymond C. A.   Russell C. T.
A New Interpretation of ^{40}Ar–^{39}Ar Ages of Eucrites and Implications for Vesta's Collisional History **[#2167]**
In this work we provide a new interpretation of Ar-Ar ages of HED meteorites that may significantly affect their implications for the collisional evolution of Vesta.

Starukhina L. V.
Global Distribution of Crater Ejecta on Asteroids **[#1791]**
Average thickness of crater ejecta is calculated for asteroids taking the surface curvature into account. Average thickness of ejecta from craters of diameters >5 km is shown to be >0.01 mm all over Vesta, which may explain its optical immaturity.

Denevi B. W.   Coman E. I.   Blewett D. T.   Mittlefehldt D. W.   Buczkowski D. L.   Combe J.-Ph.   De Sanctis M. C.   Jaumann R.   Li J. Y.   Marchi S.   Nathues A.   Petro N. E.   Pieters C. M.   Schenk P.   Schmedemann N.   Schröder S.   Sunshine J. M.   Williams D. A.   Raymond C. A.   Russell C. T.
Regolith Depth, Mobility, and Variability on Vesta from Dawn's Low Altitude Mapping Orbit **[#1943]**
We use Framing Camera images acquired by the Dawn spacecraft from its low-altitude mapping orbit to characterize regolith depth, variability, and mobility on Vesta, and to locate areas of especially thin regolith and exposures of competent material.

Hiesinger H.   Ruesch O.   Jaumann R.   Nathues A.   Raymond C. A.   Russell C. T.
Smooth Pond-Like Deposits on Asteroid 4 Vesta: Preliminary Results from the Dawn Mission **[#2487]**
We have identified smooth pond-like deposits on the surface of asteroid 4 Vesta, which might have several origins, including volcanism, impact sedimentation, impact melt deposition, dust levitation and transport, seismic shaking, or landslides.

Buratti B. J.   Hicks M. D.   Hillier J. K.   Li J. Y.   Reddy V.
The Roughness of Vestoids, Vesta, and other Small Bodies as a Clue to their Collisional History **[#1527]**
An analysis of the macroscopic roughness of Vesta and the V-type asteroids shows that their surfaces are rougher than C-type or S-type asteroids. These bodies may have have had a violent collisional history or possess unique mechanical properties.

Ermakov A. I.   Zuber M. T.   Smith D. E.
Forward Modeling of Vesta's Interior Structure Using Gravity and Shape Models from the Dawn Mission **[#2382]**
We use gravity and shape models of Vesta along with geochemical evidence from HED meteorites in order to constrain Vesta's interior structure. Least-squares adjustment of gravity anomalies is performed to estimate the interior structure parameters.

Formisano M.   Federico C.   Coradini A.   Turrini D.   Capaccioni F.
Time Scales of Accretion and Differentiation of Vesta **[#1984]**
We constrain the timescales of accretion and differentiation of Vesta, by developing several thermal and structural scenarios based on radiogenic heating. The scenarios differ for the deleay parameter in the injection of ^{26}Al by the solar nebula.

Keil K.   Wilson L.
Volcanic Eruption and Intrusion Processes on 4 Vesta: A Reappraisal **[#1127]**
A new analysis supports our earlier predictions of sizes of lava flows and pyroclast deposits on Vesta, but argues against a magma ocean, instead suggesting eruptions were fed by magma from large sill-like intrusions at the base of the lithosphere.

Horváth A.   Bérczi Sz.   Illés-Almár E.
Stratigraphy of the Rolling-Printed Groove-Fields on Dawn Images in Order to Reconstruct Paleoaxes of Vesta **[#1402]**
If we accept that the equatoral groove system is the result of surface prints of reimpacting ejecta boulders – thrown away by a huge impact – we can use it to identify the actual rotational axis of the asteroid.

IMPACTS ON SMALL BODIES

Schenk P.   Marchi S.   O'Brien D. P.   Vincent J. B.   Jaumann R.   Gaskell R.   Roatsch T.   Keller H.   Denevi B. W.   Raymond C. A.   Russell C. T.
Impact Cratering on a Mid-Sized Planetary Body: Insights from Morphology as seen by Dawn at Vesta **[#2677]**
Dawn at Vesta has revealed a transitional world with diverse crater morphologies. These examined from a solar system perspective. Impact melt, slumping, crater chains and ejecta are examined, measured and compared.

Flynn G. J.   Durda D. D.   Minnick M. A.   Lipman M. D.   Strait M. M.
Disruption of Porous Pumice Targets: Implications for Cratering on 253 Mathilde **[#1091]**
Hypervelocity impacts into porous pumice targets demonstrate that under conditions that disrupt non-porous targets a crater-like hole, with very little ejecta, results. This is likely to explain the large, overlapping craters on the asteroid Mathilde.

Bowling T. J.   Melosh H. J.
Sub-Surface Excavation of Transient Craters in Porous Targets: Explaining the Impact Delay **[#2433]**
We numerically investigate the subsurface excavation of the transient crater in the earliest moments after the Deep Impact event. At high target porosities the crater remains hidden from observation long enough to explain the "impact delay."

Schultz P. H.   Hermalyn B.   Veverka J.
The Deep Impact Crater as Seen from the Stardust-NExT Mission **[#2440]**
The Stardust-NExT mission imaged the impact crater formed by the DI impact probe. The size of the crater is estimated to be 150 m to 200 m in diameter based on the observed crater and disruption of ejecta as seen in images from the DI flyby in 2005.

Ipatov S. I.
Location of the Upper Borders of the Cavities Excavated after the Deep Impact Collision **[#1318]**
The upper border of the largest cavity excavated during ejection of material after the collision of the Deep Impact impact module with Comet 9P/Tempel 1 could be located at a depth of about 3–5 meters below the pre-impact surface of the comet.

Lorenz C. Basilevsky A. Shingareva T. Oberst J. Waehlisch M. Willner K. Noekum G.
Phobos: Impact Crater Morphology and Regolith Structure from Mars-Express Images **[#1142]**
Analysis of craters of complex morphology on the entire Phobos surface using Mars-Express images indicates local vertical variations of regolith strength in the scale 10–100 meters due to occurrence of buried layers of consolidated ejecta material.

Oklay N. Vincent J.-B. Sierks H. Wünnemann K. Elbeshausen D.
Impacts on a Differentiated Lutetia **[#1845]**
Is Lutetia differentiated? Using iSALE hydrocode simulations we investigate how the peculiar morphology of Massilia crater could be explained by an impact into a layered body. This allows to put some constrain on the asteroid inner structure.

Elbeshausen D. Wünnemann K. Sierks H. Vincent J. B. Oklay N.
The Effect of Topography on the Impact Cratering Process on Lutetia **[#1867]**
By using three-dimensional simulations we investigate whether a landslide in a crater at asteroid (21) Lutetia might be triggered by an impact that occurred at the rim of this crater. This study gives new insights into the effect of topography on crater formation.

STUDYING IMPACTS THROUGH EXPERIMENTS AND MODELING

Collette A. Horanyi M. Drake K. Mocker A. Sternovsky Z. Munsat T. Cintala M.
Experimental Investigation of Light Flash from Hypervelocity Impacts **[#2793]**
We describe laboratory investigations into the phenomenon of visible light flash generated by hypervelocity impact, and the relationship between the flash characteristics (spectrum, duration and intensity) and the characteristics of the impactor.

Zimmerman M. I. Farrell W. M. Stubbs T. J.
Characterizing Electron Oscillations in a Collisionless, Expanding Impact Plasma **[#2071]**
During a meteoritic impact on the Moon, target and impactor material can form an impact plasma. Plasma oscillations and the surface-plasma interaction are characterized via kinetic simulations, with relevance to a planned lunar impact experiment.

Hamura T. Kurosawa K. Hasegawa S. Sugita S.
A Ground-Hugging Downrange Vapor Cloud due to Oblique Impacts **[#1888]**
We experimentary modeled the dynamics of oblique impact vapor clouds as a hypersonic mixture of projectile fragments and their melts and ablated gas species.

Ohno S. Kadono T. Kurosawa K. Sakaiya T. Yabuta H. Shigemori K. Hironaka Y. Sano T. Hamura T. Sugita S. Arai T. Matsui T.
Impact-Induced Sulfur Release from a Carbonaceous Chondritic Impactor: Implication to the K/Pg Event **[#1894]**
We experimentally measure the chemical composition of the S-bearing gases in carbonaceous chondritic impact vapor using a laser gun and a QMS. Reducing S-bearing gasses were the major species and would have also released by the K/Pg impact.

Ormö J.   Rossi A. P.
Effect of Impact Angle on the Off-Set of Outer vs. Nested Crater for Concentric Impact Structures in Layered Targets: A Tool to Determine Direction of Impact **[#1138]**
We show with observation and experiments that the concentric shape of craters from oblique impacts into targets with an upper, weaker layer over a more rigid substrate is affected by the impact angle. This is useful to determine direction of impact.

Price M. C.   Burchell M.
Using Hydrocode Modelling to Track Ejecta from Oblique Hypervelocity Impacts onto Glass **[#1904]**
Hydrocode modelling has been implemented to track the ejecta from hypervelocity impacts of oblique impactors onto glass. This supports the ongoing Stardust ISPE as a method to aid discrimination between spacecraft secondary impacts and IDP/ISPs.

Miljkovic K.   Collins G. S.   Mannick S.   Bland P. A.
Hydrocode Simulations of Binary Asteroid Impacts **[#1338]**
Numerical modeling provides a unique insight into the processes and parameters that lead to single, elliptical, overlapping, and doublet craters as a result of binary asteroid impacts in different materials and gravities.

Bland P. A.   Muxworthy A. R.   Collins G. S.   Moore J.   Davison T. M.   Prior D. J.   Wheeler J.   Ciesla F. J.   Dyl K. A.
Effect of Low Intensity Impacts on Chondrite Matrix **[#2005]**
Although the majority of carbonaceous chondrites have only experienced low-intensity (<5 GPa) impacts, we show that compacting initially highly porous matrix aggregates results in large temperature excursions even at low shock pressures.

Wada K.   Nakamura A. M.
Numerical Simulations of Penetration into Porous Granular Targets **[#1803]**
We carry out numerical simulations of penetration into porous granular targets under microgravity to elucidate impact processes on asteroids. As a result of our simulations, penetration resistance is obtained and discussed.

Poelchau M. H.   Kenkmann T.   Dufresne A.
A Simple Analysis of Porosity and Pore Space Saturation Effects on Crater Volume **[#2185]**
The effect of porosity (and pore space saturation) on crater volume in strength-dominated impact experiments is investigated using calculations based on scaling laws for non-porous impacts.

Güldemeister N.   Wünnemann K.   Buhl E.   Kenkmann T.   Durr N.   Hiermaier S.
Numerical Modeling of Porosity Alteration at the Sub-Surface of Impacts in Sandstone **[#1851]**
In the framework of the MEMIN project the effects of hypervelocity impact shock compression and release in sandstone are investigated. The increase of porosity as a result of the rarefaction wave has been modeled and quantified in impact experiments.

Buhl E.   Poelchau M. H.   Kenkmann T.   Dresen G.
Porosity Reduction in the Sub-Surface of Experimentally Produced Impact Craters in Sandstone **[#1401]**
Subsurface analyses of experimental impacts in sandstone have shown a variation of pore space with increasing depth from the impact point source. Differences between dry and wet targets suggest an effect of pore fluids on deformation mechanisms.

Dufresne A.   Poelchau M. H.   Kenkmann T.   Deutsch A.   Hoerth T.   Schaefer F.
Morphology of Experimental Impact Craters into Sandstone **[#1821]**
Detailed morphometric crater analyses of hypervelocity impact experiments were carried out to investigate the influence of impact velocity and target pore space saturation on crater size and morphology.

Schultz P. H. Stickle A. M. Crawford D. A.
Effect of Asteroid Decapitation on Craters and Basins **[#2428]**
Asymmetries within and around large impact craters and basins on the Moon are interpreted as the effects of projectile failure. One result is shallow crater excavation downrange, which can support the uplifted rim downrange while collapsing uprange.

Plesko C. S. Jensen B. J. Fredenburg D. A. Wescott B. L. Skinner McKee T. E.
Quasi-Static and Dynamic Compaction of the JSC-1A Lunar Regolith Simulant **[#2746]**
Moon dust simulant / Compressed in stillness and at speed / Toward an EOS.

See T. H. Cardenas F. Montes R.
The Johnson Space Center Experimental Impact Lab: Contributions Toward Understanding the Evolution of the Solar System **[#2488]**
Impact is the only common weathering phenomenon affecting all planetary bodies in the solar system. JSC's Experimental Impact Lab includes three accelerators used in support of research into the role of impact on the evolution of the solar system.

IMPACT EJECTA: FROM PROXIMAL TO DISTAL

Seward L.M. S. Colwell J. E. Mellon M. T. Stemm B. A.
Ejecta Mass Production and Velocities in Low-Energy Impacts into Simulated Lunar Regolith **[#2509]**
We conducted low-velocity impact experiments ~ 1 m/sec into JSC-1 lunar regolith simulant in 1 g and in microgravity. We wish to understand the collision parameters that control the outcome of low-velocity impacts into regolith.

Riis F. Kalleson E. Dypvik H.
Crater Rim Development of the Ritland Impact Structure — Field Observations and Possible Mechanisms **[#1353]**
Parts of the crater rim of the 2.7-km-diameter, Cambrian, Ritland impact structure have been preserved. The rim consists of upturned and elevated basement rocks overlain by brecciated gneiss sheets resting on a thin Cambrian shale.

Kring D. A. Cole S. Craft K. Crites S. Gaither T. Jilly C. Lemelin M. Rosenburg M. Seward L. Song E. Snape J. F. Talpe M. Thaisen K. Veto M. Wielicki M. Williams F. Worsham E. Garber J.
Extensional Faulting of the Overturned Coconino Ejecta Layer and Emplacement of Fallback Breccia at Barringer Meteorite Crater (aka Meteor Crater) **[#1618]**
New sections measured at Meteor Crater indicate the extension of the ejecta blanket was partly accommodated by a series of normal faults. Those normal faults also provided a means of "burying" and protecting fallback ejecta.

Spudis P. D. Baloga S. M. Glaze L. S. Dixit V. Pantone S. M. Juvanescu I.
Radar Scattering and Block Size Properties of Lunar Crater Ejecta from Mini-RF and LROC NAC Data **[#1461]**
Block abundances around lunar craters are measured on LROC images and compared with CPR values derived from the Mini-RF SAR images. CPR tends to increase with increasing blockiness, but the correlation is not simple.

Wulf G. Pietrek A. Kenkmann T.
Ejecta Layer Deposition Chronology of a Double-Layer-Ejecta (DLE) Crater on Mars **[#1744]**
We analyzed the contact zone between the inner and outer ejecta layer of a DLE crater on Mars. The results confirm a successive deposition chronology with the inner ejecta layer overlaying the outer layer.

Sturm S. Wulf G. Jung D. Kenkmann T.
Impact Ejecta Modeling of the Bunte Breccia Deposits of the Ries Impact Crater, Southern Germany **[#1770]**
Here we present new impact ejecta modeling results of the paleo-surface and Bunte breccia ejecta outside the Ries impact crater that provide morphology and thickness variations of the Bunte breccia with increasing distance from the crater center.

Gaither T. A. Hagerty J. J. McHone J. F. Newsom H. E.
Characterization of Impact Ejecta Deposits from Meteor Crater, Arizona **[#1601]**
We present an initial assessment of physical distribution patterns and compositions of impact-generated lithologies from Meteor Crater, Arizona, and announce the availability of the USGS Meteor Crater Sample Collection to the planetary science community.

Artemieva N. Wuennemann K. Stoeffler D. Reimold W. U.
Ries Suevite — Plume Ejecta, Melt Flow or Something Else? **[#1364]**
We present results of numerical modeling applied to various aspects of Ries crater formation and compare the results with observations. We also analyze existing analog models of suevite emplacement.

Bell S. B. Schultz P. H.
Detection of a Radar Signature of the Uprange Plume in Fresh Oblique Lunar Craters **[#2824]**
We report the detection of a radar signature of the uprange plume in fresh oblique lunar craters.

Boyce J. M. Barlow N. G. Wilson L.
Model for the Emplacement of the Outer Ejecta Layer of Low Aspect-Ratio Layer Ejecta Craters by Turbulent Flow **[#1081]**
Our modeling and geomorphic analysis suggest that the outer ejecta layer of low aspect-ratio layer ejecta (LARLE) craters may be fine-grain ejecta deposited from a dilute, suspension-driven, gravity current produced by collapse of the ejecta column.

Alwmark C. Holm S. Meier M. M. M. Hofmann B. A.
A Study of Shocked Quartz in Distal Ries Ejecta from Eastern Switzerland **[#1827]**
Here we confirm the occurence of shocked quartz in the so-called Blockhorizont in eastern Switzerland by measurements and indexing of PDFs. We suggest transportation of material to the present location by ejection during impact.

Shuvalov V. V.
A Mechanism of the Production of Crater Rays **[#1030]**
The goal of this work is to propose and to study a possible mechanism of generation of the crater rays resulting from interaction between an impact induced shock wave in a target and nonuniformities of the target surface.

Carter L. M. Ghent R. R. Bandfield J. L. Bussey D. B. J.
Young, Rayed, and Radar-Bright Craters at the Lunar Poles **[#2485]**
We use radar, infrared, and optical data to study the ejecta patterns, rock abundance, and regolith development surrounding lunar craters. Mini-RF data show previously unknown ejecta features, including a crater ray that crosses Schrödinger Basin.

Artemieva N. Simonson B. M.
Elucidating the Formation of Archean-Proterozoic Boundary Spherule Layers **[#1372]**
We extrapolate the numerical results for K-Pg ejecta to bigger events that occurred around the time of the Archean-Proterozoic boundary. Spherule-rich layers from a minimum of four large impacts have been identified in W. Australia and three in S. Africa.

Ramsley K. R.
The Effects of Gravity on the Morphology and Morphometry of Ejecta and Secondary Craters on the Moon and Mercury **[#1609]**
This study applies a reference template of secondary impact patterns to compare the influence of gravitation in the formation of secondary impact features on the Moon and on Mercury and suggests additional applications of this methodology.

Fernandes V. Artemieva N.
Impact Ejecta Temperature Profile on the Moon — What are the Effects on the Ar-Ar Dating Method? **[#1367]**
Several of the lunar samples dated have demonstrated that there is a decoupling between K-Ar reset ages and their shock-related petrographic features. As shown in our model, temperatures within an ejecta blanket during the early-hot-Moon can be high.

METEORITES AND MITIGATION

Trigo-Rodriguez J. M. Madiedo J. M. Cortés J. Dergham J. Pujols P. Ortiz J. L. Castro-Tirado A. J. Alonso-Azcárate J. Zamorano J. Izquierdo J. Ocaña F. Sánchez de Miguel A. Tapia M. Martín-Torres F. J. Lacruz J. Rodríguez D. Pruneda F. Oliva A. Pastor-Erades J.
The 2011 Giacobinid Outburst: Meteoroid Flux Determination and Orbital Data by Using Video Imagery from the Spanish Fireball Network **[#1926]**
The results for the 2011 Draconid outburst are presented. The peak flux of this meteor shower was recorded in solar longitude 195.03 (Oct. 8, 2011, at 20h00m UT). Accurate orbits for 10 high-resolution selected Draconid 2011 meteors are also given.

Ashley J. W. Christensen P. R.
Thermal Emission Spectroscopy of Unpowdered Meteorites **[#2519]**
Spectral libraries are an integral part of planetary surface remote sensing. Thermal emission spectra have been collected for whole-rock specimens of meteorites representing chondritic and achondritic groups, with asteroid assessment applicability.

Clayton A. N. Lipman M. D. Strait M. M. Flynn G. J. Durda D. D.
Fabrication of Hydrous Meteorites for use in Meteorite Disruption Experiments **[#2764]**
Hydrous meteorites demonstrate fundamental differences in their disruption patterns from anhydrous samples. A method was developed to hydrate meteorites for use as analogues in disruption experiments.

Lipman M. D. Strait M. M. Flynn G. J. Durda D. D.
Analysis of Fragmentation Patterns in Disrupted Meteorites and Single Mineral End-Members **[#2724]**
NWA 869 and Allende were disrupted as asteroid analogs and compared to disrupted end-members quartz and mica. Slopes of the size-frequency curves determine the structure of the particles produced.

Korycansky D. G. Plesko C. S.
Effects of Stand-off Bursts on Rubble-Pile Targets: Evaluation of a Hazardous Asteroid Mitigation Strategy **[#1522]**
We evaluate the effects of stand-off X-ray bursts on rubble-pile asteroids as a strategy for hazard mitigation.

Bruck Syal M. Schultz P. H. Dearborn D. S. P. Managan R. A.
Porosity Controls on Asteroid Defense Strategies **[#2480]**
We report on calculations to quantify the effects of porosity on the deflection or disruption of hazardous asteroids by standoff nuclear bursts. Asteroid response to this mitigation tactic is found to be strongly dependent on porosity.

Housen K. R. Holsapple K. A.
Deflecting Asteroids by Impacts: What is Beta? **[#2539]**
Experiments are described that measure the momentum transferred to a target body during hypervelocity impact. We find that the momentum transfer is most efficient for bodies with low porosity.

ZIRCONS: A RECORD OF ANCIENT IMPACTS

Cavosie A. J. Erickson T. M. Radovan H. A. Moser D. E. Gibbon R. J.
The Cenozoic Detrital Shocked Mineral Record of Southern Africa **[#2279]**
This abstract reviews the Cenozoic detrital shocked mineral record of southern Africa.

Erickson T. M.   Cavosie A. J.   Radovan H. A.   Moser D. E.   Barker I. R.   Wooden J.
Implications of Detrital Shocked Minerals at the Mouth of the Orange River: Continental Scale Transport by Fluvial, Eolian, and Coastal Processes **[#1938]**
We document detrital shocked grains from the mouth of the Orange River in South Africa. These grains require long (1200 to 2000 km) distances of transport, diverse sedimentary processes, and originate from multiple impact basins.

Montalvo P. E.   Cavosie A. J.   Cintron N. O.   Radovan H. A.   Moser D. E.   Gibbon R. J.
Detrital Shocked Zircons in Cenozoic Fluival Terraces of the Vaal and Orange Rivers, South Africa **[#2059]**
This abstract describes the occurrence of detrital shocked zircons in Cenozoic fluvial terraces of the Vaal and Orange Rivers in South Africa.

Lugo Centeno C. M.   Cavosie A. J.   Radovan H. A.
A Search for Detrital Shocked Zircons Eroded from the Santa Fe Impact Structure, New Mexico, USA **[#2014]**
This study describes preliminary results of a search for detrital shocked zircons eroded from the Santa Fe impact structure, New Mexico, USA.

Thomson O. A.   Cavosie A. J.   Radovan H. A.   Moser D. E.
Origin of Detrital Shocked Zircons from Different Sedimentary Environments at the Sudbury Impact Structure, Ontario Canada **[#2129]**
This abstract describes the occurrence of detrital shocked zircons in fluvial and glacial deposits at the Sudbury impact basin, Ontario, Canada.

Cupelli C. L.   Moser D. E.   Barker I. R.   Darling J.   Bowman J. R.   Wooden J.   Hart R.
Zircon-Based Identification of Mafic Impact Melt Bodies at the Center of the Vredefort Dome-Remnants of the Lost Melt Sheet **[#2402]**
Analysis has led to identification of mafic impact melts at the Vredefort impact. Using microstructural analyses of zircon we were able to distinguish igneous grains for dating and the U-Pb geochronology support crystallized at the time of impact.

Wielicki M. M.   Harrison T. M.   Boehnke P.   Schmitt A. K.
Modeling Zircon Saturation Within Simulated Impact Events: Implications on Impact Histories of Planetary Bodies **[#2912]**
We model the likelihood and crystallization temperatures of impact produced zircon on Earth, the Moon and Mars.

Hopkins M. D.   Mojzsis S. J.
Early Thermal Events Recorded in Zircon U-Th-Pb Depth Profiles from Eucrite Meteorites and Lunar Impact Breccias **[#2109]**
Thermal events recorded in zircon U-Th-Pb depth profiles from Millbillillie eucrite show a core Pb-Pb age (~4560 Ma) that correlates with other reported crystallization ages for eucrites and a previously unseen younger thermal event at ~4530 Ma.

YOUNG SOLAR SYSTEM CATACLYSM

Mest S. C.   Crown D. A.   Berman D. C.
Chronology of Hesperia Planum, Mars Using Impact Craters as Stratigraphic Markers **[#2268]**
Large (D > 15 km) fresh impact craters in Hesperia Planum, Mars, are being mapped and superposed craters are being measured. These data are being used to constrain the relative ages of the craters and plains to develop a chronology of Hesperia Planum.

Korycansky D. G.   Nimmo F.   Asphaug E.
Catastrophic Disruption of Icy Satellites: Preliminary Results **[#2387]**
We report preliminary results of SPH simulations of the catastrophic impacts of icy satellites .

Corrigan C. M.   Cohen B. A.   Hodges K.   Lunning N. G.   Bullock E. S.
3.9 Billion Years Ago and the Asteroid Belt: Impact Melts in Ordinary Chondrites **[#1577]**
This project incorporates the Smithsonian's efforts of identifying and classifying ordinary chondrite impact breccias with a study of impact melt clasts in order to understand the impact history of the asteroid belt during the early solar system.

Hartmann O.   Werner S. C.   Ivanov B. A.   Neukum G.
The Mass Influx of the Inner Solar System Estimated by a Lunar-Like Chronology Model **[#1947]**
Aim of this work is to test one of the most simplest and straightforward hypothesis: What if the early highly populated asteroid belt (AB) is the main source for the masses impacted in the inner solar system, not only now, but also before 3.0 Ga?

Bell E. A.   Harrison T. M.
Trace Elements Reveal a Possible Link Between Jack Hills Detrital Zircons and the Late Heavy Bombardment **[#2736]**
The Jack Hills detrital zircons range in age 4.3–3.0 Ga. At ca. 3.9 Ga the record contains a population that appears to have recrystallized during a major thermal event. This may be circumstantial terrestrial evidence for the late heavy bombardment.

LUNAR CHRONOLOGY BY ANY MEANS NECESSARY

Seddio S. M.   Jolliff B. L.   Korotev R. L.   Carpenter P. K.
Thorite in an Apollo 12 Granite Fragment and Age Determination Using the Electron Microprobe **[#2704]**
We present the first quantitative analysis of lunar thorite. It contains a 12% xenotime component. We calculate an age of 3.88 Ga. Yttrobetafite and monazite, also present in the sample, yield similar ages.

Zhou Q.   Zeigler R. A.   Yin Q.-Z.   Korotev R. L.   Jolliff B. L.   Amelin Y.   Marti K.   Wu F. Y.   Li X. H.   Li Q. L.   Lin Y. T.   Liu Y.   Tang G. Q.
U-Pb Dating of Zircons and Phosphates in Lunar Meteorites, Acapulcoites and Angrites **[#1554]**
New zircon and phosphate dating techniques are developed and applied to two KREEPiest lunar meteorites (SaU 169 and Dhofar 1442). We also report results for Acapulco and NWA 4950 phosphates with precisely known TIMS U-Pb ages.

Shirley K. A.   Zanetti M.   Jolliff B. L.   van der Bogert C. H.   Hiesinger H.
Crater Size-Frequency Distribution Measurements at the Compton-Belkovich Volcanic Complex **[#2792]**
We present and discuss the results of CSFDs determined on areas within the Compton-Belkovich Volcanic Complex (CBVC) and surrounding areas, including immediately adjacent terrain and the nearby Copernican Hayn Crater.

Thiessen F.   Hiesinger H.   van der Bogert C. H.   Pasckert J. H.   Robinson M. S.
Surface Ages and Mineralogy of Lunar Light Plains in the South-Pole Aitken Basin **[#2060]**
In this study we obtained crater size-frequency distribution measurements to derive absolute model ages of light plains in the South Pole Aitken basin. Furthermore we analyzed their mineralogical composition.

Demidova S. I.   Nazarov M. A.   Anosova M. O.   Kostitsyn Y. A.   Brandstätter F.   Ntaflos Th.
U-Pb Dating of Zircons from the Dhofar 1442 Lunar Meteorite **[#1090]**
U-Pb dating of eight zircon grains from the Dho 1442 lunar meteorite was performed. There are two groups of different age: old and young. The age of the old group is 4309 ± 13 Ma. The young group includes two grains of 3934 ± 19 and 3998 ± 32 Ma ages.

Cho Y.   Morota T.   Yasui M.   Hirata N.   Haruyama J.   Sugita S.
Young Mare Volcanism in the Orientale Region Contemporary with ~2 Ga PKT Volcanism Peak Period **[#1575]**
Crater counting analyses with Kaguya images reveal that maria along Orientale Basin rings, far from PKT, are covered with lava erupted contemporarily with the PKT volcanic activity peak at ~2 Ga, suggesting a widespread nature of this volcanic event.

LUNAR MELTS: NEW INSIGHTS FROM ISOTOPES, IMPACTS, AND EXPERIMENTS

Vander Kaaden K. E.   Agee C. B.   McCubbin F. M.
A Comparison of Melt Density and Compressibility of the Green, Yellow, and Orange Apollo Glasses as a Function of TiO_2 Content **[#1584]**
This study investigates the density and compressibility of the green, yellow, and orange Apollo glasses. The difference in compressibility between these glasses is currently attributed to their vastly different TiO_2 contents from 0.24 to 9.12 wt%.

Gombosi D. J.   Baldwin S. L.   Watson E. B.   Swindle T. D.   Delano J. W.   Roberge W. G.
Argon Diffusion in Lunar Impact Glass **[#2364]**
Diffusion kinetics of Ar in Apollo 16 lunar impact glasses have been experimentally determined . These kinetics allow the calculation of how much radiogenic Ar has been lost by diffusion on the lunar surface, which may alter apparent $^{40}Ar/^{39}Ar$ ages.

Spicuzza M. J.   Valley J. W.   Ushikubo T.
Li Concentration and Isotope Ratio in Lunar Zircons: Li-Enriched and Depleted Magmas on the Moon **[#2878]**
Lithium concentrations and isotope ratios were measured in lunar zircons. The bimodality of [Li] suggests the presence of Li-enriched and depleted magmas on the Moon.

O'Sullivan K. M.   Neal C. R.   Simonetti A.
A Crystal Stratigraphy Approach to Understanding Melt Evolution in the Apollo 12 Ilmenite Suite Basalts **[#2431]**
Using a crystal stratigraphy approach, a detailed petrogenetic model and crystallization sequence for 12062 is presented here.

Dygert N. J.   Liang Y.   Hess P. C.
The Effect of Melt TiO_2 on Fe-Ti Oxide-Picritic Basalt HFSE Partitioning: Parameterized Models, Lunar Applications **[#2033]**
We measured HFSE partition coefficients for Fe-Ti oxides and picritic basalts, and developed parameterized partitioning models. HFSE Kd's are strongly affected by melt TiO_2. Models are applied to mare basalt petrogenesis and lunar armalcolite.

Yao L.   Liang Y.
An Experimental Study of the Solidus of a Hybrid Lunar Cumulate Mantle: Implications for the Temperature at the Core-Mantle Boundary of the Moon **[#2258]**
Solidus and phase relations of a mixture of ilmenite- and cpx-bearing cumulate and harzburgite lunar mantle are examined. Temperature of the lunar core-mantle boundary is estimated as 1360°–1400°C, based on the solidus of this study.

Sedaghatpour F. S.   Teng F.-Z.   Liu Y.   Sears D. W. G.   Taylor L. A.
Behavior of Magnesium Isotopes During Lunar Magmatic Differentiation **[#2884]**
In order to provide an internally consistent estimate of the Mg isotopic composition of the Moon, we studied 47 well-characterized lunar samples including mare basalts, highland impact melts, mare breccias and regolith samples.

de Vries J.   van Westrenen W.   van den Berg A.
Radiogenic Heat Production in the Moon: Constraints from Plagioclase-Melt Trace Element Partitioning Experiments **[#1737]**
We estimate radiogenic heat production in the Moon, and its depth distribution, by combining highland surface concentrations of U, Th, and K with experimental constraints on the distribution of these elements between anorthositic plagioclase and melt.

THU POSTERS

THU POSTERS

Sakai R.   Kushiro I.   Nagahara H.   Ozawa K.   Tachibana S.
Constraints on the Bulk Composition of Lunar Magma Ocean from Conditions of Crust Formation; Critical Reevaluation of Separation Mechanism of Anorthite **[#2849]**
The bulk composition of the lunar magma ocean was constrained to satisfy the formation condition of lunar anorthosite crust. We showed that the lunar magma ocean was likely to be enriched in FeO compared to the BSE.

Sun C.   Liang Y.
Trace Element Partitioning Between Low-Calcium Pyroxene and Lunar Picritic Glass Melts at Multiple-Saturation Points with Applications to Melting and Melt Migration in A Heterogeneous Lunar Cumulate Mantle **[#1952]**
Trace-element D values of opx or pigeonite vary by less than a factor of two for various melt and mineral compositions at multi-saturation points. We employ a simple model and show the importance of lunar source composition to mare basalt genesis.

Zhang N.   Parmentier E. M.   Liang Y.
Instability and Distribution of Ilmenite-Rich Cumulates After the Overturn of an Initially Stratified Lunar Mantle **[#2641]**
Geochemical observations suggest lunar mantle is heterogeneous. We use a thermochemical convection model to explain the distributions of ilmenite-bearing cumulates and KREEP. It provides constraints for lunar evolution.

Galenas M.   Righter K.   Danielson L.   Pando K.   Walker R. J.
Experimental Study of the Partitioning of Siderophile Elements in a Crystallizing Lunar Magma Ocean **[#2270]**
This study focuses on experimentally determining partition coefficients for a variety of elements including the highly siderophile elements. Conditions of these experiments are designed to approximate a crystallizing lunar magma ocean.

Liu J. G.   Ash R. D.   Walker R. J.
Fractionation and Remobilization of Siderophile Elements in Metal Grains of Apollo 16 Lunar Impact-Melt Breccia 67095 **[#2683]**
The metal globules in Apollo lunar impact-melt breccia 67095 exhibit fractionated surface to interior compositions of siderophile elements. The data show that the globules were derived from siderophile-rich impactor, and crystallized outward.

Schaffer L. A.   Niihara T.   Kring D. A.
Petrology of an Impact Melt Clast from Lunar Regolith Breccia 60016 **[#1174]**
The petrology and major element composition of a small-volume lunar impact melt clast are examined. Sample 60016,321 is fine-grained, porphyritic, and composed mainly of olivine (18.5 %), pyroxene (47.8 %), plagioclase (31.0 %), and metal (2.2 %).

Niihara T.   Kring D. A.
Petrology of the Centimeter-Size Impact Melt Clasts in Ancient Regolith Breccia 60016 **[#1229]**
Here we report petrological analyses of five impact clasts in 60016. The petrological texture and mineral compositions data suggest these clasts in 60016 possibly represent five different types of impact melts.

Fagan A. L.   Neal C. R.
Negative Eu Anomalies in Plagioclase: KREEP-Like Contaminant of Impact Melt? **[#1426]**
Some plagioclase crystals from several Apollo 16 impact samples display negative Eu anomalies in their REE patterns rather than the expected positive. This can be explained by contamination of the impact melt by a form of KREEP such as (W-)QMG.

Neal C. R.   Fagan A. L.
Petrogenesis of Apollo 16 Impact Melts **[#2248]**
Textures coupled with whole rock and mineral compositions of igneous textured impact melts provided heretofore unseen insights into impact melt petrogenesis.

LUNAR GEOPHYSICS AND INTERNAL STRUCTURE

Kattoum Y. K.   Andrews-Hanna J. C.
Evidence of Ring-Faults in Orientale from Gravity **[#2767]**
The internal structure of Orientale Basin is examined through means of gravity to determine the existence of ring faults and to place a constraint on their geometry.

Sasaki S.   Goossens S.   Ishihara Y.   Araki H.   Hanada H.   Matsumoto K.   Noda H.
Kikuchi F.   Iwata T.
Kaguya Selenodesy and the South Pole Aitken Basin **[#1838]**
Kaguya obtained accurate lunar farside gravity for the first time. The region with the thinnest crust is offset southward from the center of the SPA basin. Using a localized gravity analysis, we analyzed the interior structure of small basins in and around SPA.

Yang H. W.   Zhao W. J.   Wu Z. H.
Solution and Preliminary Explanations for Gravity Field of the Moon **[#1865]**
A lunar gravity model was built with the transplanted GEODYN2. A lunar Bouguer gravity anomalies field was established. With some necessary constraints, the thickness of the uplifted Moho subsurface in three mare basins was calculated respectively.

Meyer H. M.   Frey H. V.
Using a New Crustal Thickness Model to Test Previous Candidate Lunar Basins and to Search for New Candidates **[#1936]**
A new crustal thickness model was used to test the viability of 110 previously identified candidate large lunar basins and to search for new candidates. We eliminated 11 of 27 previous candidates, and found evidence for at least 8 new candidates.

Li F.   Wang W. R.   Chen W.   Hao W. F.
Lunar Global Crustal Thickness Estimation Using Compensated Terrain Gravity Effect (CTGE) Data **[#1432]**
A global lunar crustal thickness model is constructed, with the topography and gravity data from the Japanese SELENE mission. The mean thickness of the new global crustal thickness model is 42 km, with the maximum value 85.6 km, the minimum value –0.6 km.

Byrne C. J.
A Layered Model of the Moon's Far Side Bulge **[#2037]**
The Moon's farside bulge could have been created by ejecta from the nearside megabasin, depositing the bulge in two layers. The subsurface structure of the two layers after isostatic compensation is described. GRAIL data may detect the layers.

Weber R. C.   Knapmeyer M.
Deep Moonquake Focal Mechanisms: Recovery and Implications **[#1466]**
In this study, we analyze Apollo deep moonquake seismograms in an attempt to constrain their focal mechanisms using first arrival amplitudes. The goal is to asses tidal stress as a driving force behind moonquake generation.

Blanchette-Guertin J.-F.   Johnson C. L.   Lawrence J. F.
Modeling Seismic Waveforms in a Highly Scattering Moon **[#1473]**
We model lunar seismic waveforms in a highly heterogeneous media and investigate suites of scattering models of the Moon. The decay parameters of the synthetic coda are compared to those of the Apollo lunar seismic dataset.

Schmerr N. C.   Ashley J. W.   Petro N. E.
Identifying Impact Craters Recorded by the Apollo Passive Seismic Experiment **[#2220]**
We identify fresh impact craters associated with seismic recordings of meteoroid impacts on the Moon. Precise hypocenters improve seismic constraints on lunar regolith properties, crustal thickness, seismic attenuation, and elastic velocity.

Yamada R.   Yamamoto Y.   Nakamura Y.   Kuwamura J.
A New Retrieval System of Apollo Lunar Seismic Data with Data Correction **[#1712]**
We have a constructed a new retrieval system for the Apollo seismic data that enables the user to obtain the data as well as metadata necessary to use them properly. We will report on the new convenient system in this presentation.

Laneuville M.   Wieczorek M.   Breuer D.
Asymmetric Thermal Evolution of the Moon **[#1928]**
We study the thermal evolution of the Moon using a two- and three-dimensional convection code when initially concentrating most of the heat sources in the PKT region. We find that this initial asymmetry has long-lasting consequences on magmatism and gravimetry.

Fuller M.   Weiss B. P.
The Paleomagnetic Record of Melt Breccia 62235 Yields Consistent Estimates of a Lunar Field of ~100μT at 3.9 Ga **[#1690]**
The melt breccia 62235 is critical in lunar paleomagnetism because it gives a consistent paleointensity of ~100 μT by different methods for 3.9 Ga, thereby affirming a high field era at that time.

Williams J. G.   Boggs D. H.   Ratcliff J. T.
Lunar Moment, Love Number, and Core **[#2230]**
New data improves lunar science results. A fluid core and tidal dissipation are inferred from dissipation effects on orientation. Detection of core-mantle boundary flattening is also fluid core evidence. A new Love number and solid moment are given.

Fa W.
Exploration Subsurface Structure of the Moon: Potential Scientific Return from a Ground Penetrating Radar **[#1274]**
In this study, we analyzed the potential scientific return from a ground-penetrating radar to the Moon for China's Chang-E 3 lunar mission.

Salmon J. J.   Canup R. M.
Three-Stage Lunar Accretion: Slow Growth of the Moon and Implications for Earth-Moon Isotopic Similarities **[#2540]**
We have developed a new hybrid numerical model to study the accretion of the Moon from an impact-generated circumterrestrial disk: a fluid disk for material inside the Roche limit, and an N-body code to track outer solid bodies.

LUNAR MAPPING

Petro N. E.   Bleacher J. E.   Gaddis L. R.   Garry W. B.   Lam F.
ArcGIS Digitization of Apollo Surface Traverses **[#2512]**
The Apollo lunar traverses produced a large volume of data, photos, audio, film, and the samples themselves. Data created during Apollo exist in several locations. We are digitizing available traverse data to centralize this wealth of information.

De Rosa D.   Bussey D. B. J.   Cahill J. T. S.   Crawford I.   Hackwill T.   Neukum G.   van Gasselt S.   Lutz T.   Witte L.   McGovern A.   Carpenter J.
Characterisation of Potential Landing Sites for the European Space Agency's Lunar Lander Project **[#1585]**
The European Space Agency's Lunar Lander mission targets highly illuminated locations at the South Pole. Several parallel studies are being carried out in order to characterise the illumination conditions and the hazard distributions at these sites.

Kokhanov A.   Karachevtseva I.   Oberst J.   Gläser Ph.   Wählisch M.   Robinson M. S.
Cartography Support and Assessment of Candidate Landing Sites for the "Luna-Glob" Mission **[#1756]**
For cartography support of future landing mission LUNA-GLOB was development a geodatabase using data obtained by LRO. For characterization of the surface we created some examples of maps: slope, roughness, and hill-shaded relief in various scales.

Clegg R. N.   Jolliff B. L.
Photometric Analysis of the Apollo Landing Sites **[#2030]**
Apollo lander rocket exhaust caused an increase in reflectivity in areas surrounding the LMs. We use photometric characteristics to explore soil parameters that could account for differences in reflectivity of blast zones vs. undisturbed regions.

Kirk R. L.   Howington-Kraus E.   Becker T. L.   Cook D.   Barrett J. M.   Neish C. D.
Thomson B. J.   Bussey D. B. J.
Progress in Radargrammetric Analysis of Mini-RF Lunar Images **[#2772]**
Geometric errors that distorted our topomaps from Mini-RF data have been resolved. We are making controlled radar mosaics and DTMs of Constellation regions of interest at low/mid latitudes, and preparing for large controlled mosaics of the poles.

Lee E. M.   Weller L. A.   Richie J. O.   Redding B. L.   Shinaman J. R.   Edmundson K. L.   Archinal B. A.
Hare T. M.   Fergason R. L.   Astrogeology Science Center Programming Team
Controlled Polar Mosaics of the Moon for LMMP by USGS **[#2507]**
Controlled polar mosaics of the Moon were produced by USGS in support of the Lunar Mapping and Modeling Project for lunar exploration activities. Mosaics consist of images taken by Lunar Reconnaissance Orbiter Camera (LROC) Narrow Angle Cameras.

Haruyama J.   Hara S.   Hioki K.   Iwasaki A.   Morota T.   Ohtake M.   Matsunaga T.   Araki H.   Matsumoto K.
Ishihara Y.   Noda H.   Sasaki S.   Goossens S.   Iwata T.
Lunar Global Digital Terrain Model Dataset Produced from SELENE (Kaguya) Terrain Camera Stereo Observations **[#1200]**
A lunar global digital terrain model (DTM) dataset has been produced from the SELENE (Kaguya) Terrain Camera (TC) stereo data of 10-m spatial resolution.

Mattson S.   Ojha L.   Ortiz A.   McEwen A. S.   Burns K.
Regional Digital Terrain Model Production with LROC-NAC **[#2630]**
We describe the production of Digital Terrain Models (DTM) from LROC-NAC images for science use and for the Lunar Mapping and Modeling Project (LMMP) done at the University of Arizona. To date the UA has completed seven science and five regional LMMP DTM mosaics.

Stopar J. D.   Robinson M. S.   Speyerer E. J.   Burns K.   Gengl H.   LROC Team
Regolith Characterization Using LROC NAC Digital Elevation Models of Small Lunar Craters **[#2729]**
NAC DEMs provide morphometry of large populations of small craters. Such observations are used to assess morphometric variability of craters (30 < D < 300m) due to terrain and degradation with implications for populations of small secondary craters.

Laura J. R.   Miller D.   Paul M. V.
AMES Stereo Pipeline Derived DEM Accuracy Experiment Using LROC-NAC Stereopairs and Weighted Spatial Dependence Simulation for Lunar Site Selection **[#2371]**
An accuracy assessment of AMES Stereo Pipeline derived DEMs for lunar site selection using weighted spatial dependence simulation and a call for outside AMES derived DEMs to facilitate a statistical precision analysis.

Waller D. A.   Boyd A. K.   Speyerer E. J.   Robinson M. S.
Constructing NAC Polar Maps that Optimize Lunar Surface Illumination **[#2531]**
Due to the high incidence angle at the lunar poles, local topography and Sun azimuth drastically affect the amount of illuminated surface imaged by LRO Narrow Angle Cameras. Techniques are proposed to optimize polar surface illumination.

Wagner R. V. Speyerer E. J. Mahanti P. Danton J. Robinson M. S.
Pointing Corrections for the Lunar Reconnaissance Orbiter Narrow Angle Cameras **[#2372]**
Temperature-dependent pointing corrections have been derived for the Lunar Reconnaissance Orbiter's Narrow Angle Camera system. The new corrections improve the absolute pointing by 25%, and eliminate the offset between the left and right cameras.

Speyerer E. J. Wagner R. Robinson M. S. Becker K. Anderson J. Thomas P. Brylow S.
Characterizing the Geometric Distortion of the Lunar Reconnaissance Orbiter Wide Angle Camera **[#2505]**
The Wide Angle Camera (WAC) is currently acquiring synoptic views of nearly the entire Moon each month. In-flight calibration measurements and improved distortion models are improving the accuracy of map projected images.

Epps A. D. Wingo D. R.
Integrating LROC-NAC, LOLA, and LROC-WAC Derived Illumination Mosaic for Preliminary North Pole Rover Mission Planning **[#2700]**
Describes a methodology for using LRO data sets to identify potential rover driving routes from high-illumination regions on the rim of Whipple Crater to low-illumination craters on the floor of Peary.

Fortezzo C. M. Hare T. M.
Digital Renovation of the 1:5,000,000-Scale Lunar Geologic Map Series **[#2623]**
Digital renovations of the 6 1:5,000,000-scale lunar geologic maps continues with the completion of the near-side, and north and south poles. This year we are beginning the far side maps and should make them available by mid-2012.

Trang D. Gillis-Davis J. J. Hawke B. R. Issacson P. J. Spudis P. D.
The Geology of the Plato Region of the Moon **[#1792]**
The Plato region is anomalous because it shows a radar dark halo, more mature regolith than the surrounding highlands, and a spectral red spot. We used various remote sensing datasets to determine the sequence of events that formed the anomalies.

Zhang F. Zou Y. L. Zheng Y. C. Fu X. H.
Mapping Homogeneous Mare Basalt Units in the Aristarchus Quadrangle Using Clementine Spectral Parameters **[#1133]**
In our work, multi-dimensional spatial distribution of several Clementine spectral parameters was used to identify and determine basalt units, which related to the composition of the lunar interior and its thermal evolution.

Kim K. J. Dohm J. M. Williams J.-P. Ruiz J. Hare T. M. Hasebe N. Yamashita N. Karouji Y. Kobayashi S. Hareyama M. Shibamura E. Kobayashi M. d'Uston C. Gasnault O. Forni O. Reedy R. C.
GIS-Based Geological Investigation of the South Pole-Aitken Basin Using Kaguya (SELENE) Gamma-Ray Spectrometer **[#1391]**
This study confirms that the elemental signatures of major elements of SPA are key evidences in unraveling geological history of SPA when these elemental signatures obtained from Kaguya GRS are represented with respect to stratigraphic information.

Dworzanczyk A. R. Mest S. C.
Results from Scientific Characterization and Traverse Development of the Apollo 15 and Copernicus Crater Regions of Interest **[#2345]**
The Apollo 15 and Copernicus Crater Regions of Interest were studied and traverses across each region planned in order to determine the relative scientific value of each Region of Interest as defined by the Constellation Program Office.

Ling Z. C.   Zhang J.   Liu J. J.
An Empirical Nonuniformity Correction of Chang'E-1 IIM Data **[#2213]**
We have obtained an empirical model of nonuniformity correction of the IIM data using 15 spectrally homogenous standard lines. When the correction is applied on IIM data, it yields an obvious improvement for the line direction homogeneity of the IIM data.

Hao W. F.   Li F.
The Communication Accessibility of the Lunar Rover Based on Lunar DEM Derived from Kaguya/Selene **[#1278]**
The mathematical model can be established to study the communication accessibility affected by topography. Therefore, the Antarctic Great-Wall station is chosen as a deep space tracking station and the feasibility is simulated and analyzed.

Yu S. R.   Wu Y. Z.   Tang Z. S.
The Check of Topographic Correction Methods Based on CE-1 IIM **[#1446]**
Topographic relief affects the reflectance spectra. Topographic correction can reduce this effect. The visual and statistical assessments of the topographic correction results indicate that C-correction and improved C-correction yield the best result.

Mazarico E.   Neumann G. A.   Rowlands D. D.   Smith D. E.   Zuber M. T.
Topography of the Lunar Poles and Application to Geodesy with the Lunar Reconnaissance Orbiter **[#2423]**
We use the large number of LRO tracks intersecting at the poles to construct high-resolution topographic maps from LOLA data. A special adjustment technique is used that enables geodetic accuracy assessment and improved orbit reconstruction.

Byrne C. J.
Modeling the Moon's Topographic Features **[#1118]**
Models of all lunar features that are 200 km or larger, based on Kaguya LALT data, are combined to model the current topography of the Moon in great detail.

AIRLESS BODIES EXPOSED: REGOLITH PROPERTIES AND SPACE ENVIRONMENT INTERACTIONS

Mahanti P.   Robinson M. S.   Thompson S. D.   Humm D. C.
Searching for Lunar Horizon Glow Using LROC Images **[#1638]**
The LRO camera aboard the LRO spacecraft performed its first series of experiments in an attempt to detect the weak signal of putative lunar horizon glow. Imaging geometry, image analysis procedures, and results are presented in this work.

Szalay J. R.   Horanyi M.
Modeling Dust Clouds on the Moon **[#1796]**
A one-dimensional hybrid code, treating electrons and ions as fluids and the dust grains as particles, has been developed to constrain the properties of levitating dust clouds. We will discuss the preliminary results and compare these to existing observations.

Senshu H.   Kobayashi M.   Wada K.   Namiki N.   Hirata N.   Miyamoto H.   Matsui T.
Photoelectric Dust Levitation on Eros and Itokawa **[#1826]**
Photoelectric effect levitate dust particles around asteroids. Hayabusa might have captured such dust. In this study we simulate vertical motion of dust grain with various size and initial velocity launched from Eros and Itokawa.

Tankosic D. Abbas M. M.
Laboratory Measurements on Charging of Individual Micron-Size Apollo-11 Dust Grains by Secondary Electron Emission **[#1623]**
We present some examples of the complex nature of secondary electron emissions from lunar dust grains levitated in an electrodynamic balance, and show that the measurements are unaffected by the variation of the AC field employed in the experiments.

Samad R. L. Poppe A. R. Halekas J. S. Delory G. T. Angelopoulos V. Farrell W. M.
Direct Observations of Lunar Pickup Ions in the Magnetosphere Tail-Lobes by ARTEMIS **[#2352]**
We present ARTEMIS observations of pickup ions on the dayside of the Moon in the terrestrial magnetotail lobes. We attempt to determine the composition of these ions, presumably from either the surface or the exosphere, via ion tracing simulations.

Herzog G. F. Delaney J. S. Lindsay F. Alexander C. M. O'D. Chakrabarti R. Jacobsen S. B. Whattam S. Korotev R. Zeigler R. A.
Magnesium and Silicon Isotopes in HASP Glasses from Apollo 16 Lunar Soil 61241 **[#1579]**
Five HASP glasses and two lunar-impact spherules give solar system (SS) values for δ^{26}Mg; in five other HASPs δ^{26}Mg is below SS. For all samples we find δ^{30}Si<SS. Partial recondensation of vapor may be important in these samples.

Binnie S. A. Nishiizumi K. Welten K. W. Caffee M. W.
Lunar Regolith Activity Inferred from Cosmogenic Radionuclides ^{26}Al and ^{36}Cl in Core 60014/60013 **[#1900]**
Lunar surface processes are investigated by measuring cosmogenic ^{26}Al and ^{36}Cl concentrations in core 60014/60013. Our results suggest a layer of impact ejecta around 1.5 cm thick blanketed this site sometime in the last 1.1 m.y.

Cooper B. L. McKay D. S. Fruland R. L. Gonzalez C. P.
Laser Diffraction Techniques Replace Sieving for Lunar Soil Particle Size Distribution Data **[#2900]**
The laser diffraction method is rapid and reproducible, taking less than half an hour to produce a complete size distribution covering hundreds of size bins and providing size data down to 1 micrometer, an impossible task for sieving.

Fu X. H. Zou Y. L. Zheng Y. C. Zhang F.
Effects of Space Weathering on Diagnostic Spectral Features: Results from He+ Irradiation Experiments **[#1272]**
We performed ion irradiation of mineral samples with 50 keV He^+, aimed to investigate ion irradiation effects on diagnostic spectral features of minerals, including olivine, basaltic glass, and ilmenite.

Christoffersen R. Rahman Z. Keller L. P.
Solar Ion Sputter Deposition in the Lunar Regolith: Experimental Simulation Using Focused-Ion Beam Techniques **[#2614]**
Uncertainties remain about the relative roles of solar ion sputter deposition and impact vapor deposition for forming "rims" on lunar regolith grains. We have adapted FIB techniques to study the role of sputter deposition in rim formation.

Braden S. E. Robinson M. S. Denevi B. W. Solomon S. C.
Immature Craters Mature Faster on Mercury than on the Moon **[#2872]**
Mercury Dual Imaging System and Lunar Reconnaissance Orbiter Camera observations of craters with high-reflectance continuous ejecta and/or rays on the Moon and Mercury are consistent with faster space weathering on Mercury.

Schwadron N. A. Baker T. Blake B. Case A. W. Cooper J. F. Joyce C. Kasper J. Kozarev K. Mislinski J. Mazur J. Posner A. Rother O. Smith S. Townsend L. W. Wilson J. Zeitlin C. Spence H. E.
Lunar Radiation Environment and Space Weathering from the Cosmic Ray Telescope for the Effects of Radiation (CRaTER) **[#2103]**
The Sun is now emerging from a deep protracted solar minimum when galactic cosmic ray fluxes are at their highest levels. CRaTER measurements open a critical window on the history of the radiation environment, suggesting a changing space environment.

Miura Yas.
Significant Role for Regolith Soils to Produce Carbon-Bearing Gases to the Interior on the Moon and Asteroids Compared with Earth-Type Planets **[#2920]**
Cratered surface of three-type surfaces on the Moon and Earth-type planets shows voids-rich regolith soils as significant roles of light-gasses transportation in the interior on the Moon and asteroids without major evaporated atmosphere.

DATASETS AND ARCHIVES: FROM ASTROMATERIALS TO IMAGES

Todd N. S. Satterwhite C. E. Righter K.
Antarctic Meteorite Classification and Petrographic Database Enhancements **[#2935]**
Describes the Antarctic Meteorite Classification Database and the latest enhancements made to the data acquisition process used to provide updated meteorite data concurrent with the publication of the Antarctic Meteorite Newsletter twice a year.

Ferrière L. Brandstätter F.
Digitalization Project of the Meteorite Collection of the Natural History Museum, Vienna **[#1985]**
The meteorite collection of the Natural History Museum, Vienna, one of the world's largest collection (with about 2400 individual meteorites and more than 7000 registered individual specimens) is now about to be entirely digitized.

Daviau K. C. Mayne R. G. Ehlmann A. J.
An XRF Study of Meteorites **[#1306]**
Meteorites from the Oscar E. Monnig collection at TCU were scanned with a Bruker Tracer-III SD XRF machine in order to begin creating a library of XRF spectra for different groups of meteorites.

Williams D. R. Hills H. K. Guinness E. A. Taylor P. T. McBride M. J.
Restoration of Apollo Data by the NSSDC and PDS Lunar Data Node **[#2476]**
We report on the progress made by the Planetary Data System Lunar Data Node and the National Space Science Data Center retrieving and restoring Apollo data. The restored datasets are being reformatted and archived with PDS and NSSDC.

Paris K. N. Robinson M. S. Lawrence S. J. Danton J. Bowman-Cisneros E. Licht A. Close W. Ingram R.
The Apollo Digital Image Archive: Project Status **[#2273]**
Photographs acquired by the Apollo astronauts are currently being scanned at JSC and the files sent to ASU for the Apollo Digital Image Archive. The metric frames are nearing completion while the panoramic frames are in the process of being released.

McBride M. J. Williams D. R. Hills H. K.
Restoration and Reexamination of Apollo Lunar Dust Detector Data from Original Telemetry Files **[#2075]**
We have retrieved Apollo Dust Detector data from the raw ALSEP telemetry at NSSDC and are converting it into voltages and temperatures for archive through the PDS Lunar Data Node. We report on progress and preliminary examination of the data.

THU POSTERS

Berlanga G.   Richard D. T.   Marshall J.   Davis S.
Testing of a Polar Nephelometer for Use in the Creation of a Dust Database Supporting Lunar Science Applications **[#2464]**
We created a program to help develop a lab database of dust scattering measurements. The program is tailored to meet needs for spectra acquisition automation, increased measurement precision and accuracy, and real-time processing of scattering data.

Holmer C. I. II
An Overview of the Innovative Lunar Demonstration Data (ILDD) Program: NASA's Next Steps to Extending Public/Private Partnerships Beyond Earth Orbit **[#1605]**
The Innovative Lunar Demonstration Data (ILDD) program is a way to reap benefits from the knowledge from commercial attempts to return to the Moon. This paper will review the ILDD program and its goals, objectives, and benefits to the participants.

Terazono J. T.   Nakamura R. N.   Kodama S. K.   Yamamoto N. Y.   Demura H. D.   Hirata N. H.   Ogawa Y. O.   Sugawara T. S.
WISE-CAPS: Archiving, Browsing and Analyzing Environment for Lunar and Planetary Data: Current Enhancement and Future Prospect **[#1198]**
This presentation describes current enhancement and future prospects on our web-GIS-based archiving, browsing, and analyzing environment of lunar and planetary data, called "WISE-CAPS," including integrated data display and data uploading mechanism.

Hagerty J. J.   RPIF Network Node Directors and Managers
The Regional Planetary Image Facility Network **[#1548]**
NASA's Regional Planetary Image Facilities are data and information centers for browsing, studying, and selecting planetary data including images, maps, supporting documentation, and outreach materials.

Hare T. M.   Skinner J. A. Jr.   Fortezzo C. M.   Tanaka K. L.   Nava R. A.
The Astrogeology Mapping, Remote-Sensing, Cartography, Technology, and Research (MRCTR) GIS Lab **[#2871]**
This year we have formalized the MRCTR, as in "Mercator", GIS Lab, a concept we have initiated as a means to support digital mapping and development of GIS tools. We will focus on creating a technical foundation prior to the retirement of PIGWAD.

Semenov M.   Oberst J.   Malinnikov V.   Shingareva K.   Konopikhin A.   Grechishchev A.   Karachevtseva I.   Shkurov F.
Space Science Support in Moscow State University of Geodesy and Cartography (MIIGAiK) **[#1997]**
For the future science development MIIGAiK investigated the old Soviet Archives and received the access to the telemetry data of Lunokhod-1 and Lunokhod-2. That data will be used for education purposes and support in new missions.

Neakrase L. D. V.   Huber L.   Rees S.   Roybal M.   Beebe R.   Crichton D. J.   Hughes J. S.   Gordon M. K.   Mafi J.
Data Migration Strategies: Preparing for the Move to PDS4 **[#2557]**
The NASA Planetary Data System beginning late in 2012, will be publicly moving from version 3 to 4 of the archive. Maintaining data integrity and accessibility for past archived data is important to user confidence under the modernized system.

Huber L.   Neakrase L. D. V.   Rees S.   Roybal M.   Beebe R.   Crichton D. J.   Delory G. T.   DeWolf A.   Hughes J. S.   Mafi J.
LADEE and MAVEN: Active Mission Pipeline Development Using PDS4 **[#2589]**
Beginning late in 2012, the PDS will be moving from version 3 to 4 of its archival system. The first two missions to archive under the new system will be LADEE and MAVEN. These missions will exercise the new standards and aid in development of PDS4.

Stein T. C.
Accessing MER Mosaic Image Data Using PDS Analyst's Notebook Mosaic Viewer **[#1305]**
The PDS Analyst's Notebook provides access to MER data archives. The Mosaic Viewer (http://an.rsl.wustl.edu/mv) is a new interactive tool within the Analyst's Notebook for viewing MER traverse maps and image mosaics.

Bailen M. S.   Hare T. M.   Akins S. W.   Isbell C.
Astropedia — A Data Portal for Planetary Science **[#2478]**
Astropedia is a data portal that allows easy ingestion, presentation, and delivery of cartographic products housed at the USGS Astrogeology Science Center, made available in a consistent, efficient, and user-friendly manner.

Ishikawa S. T.   Gulick V. C.
Clickworkers Interactive: Towards a Robust Crowdsourcing Tool for Collecting Scientific Data **[#2927]**
We present a web-based platform for collecting massive amounts of data from a volunteer workforce tasked with analyzing data captured by the High Resolution Imaging Science Experiment (HiRISE) instrument.

Henneken E. A.   Accomazzi A.   Kurtz M. J.   Grant C. S.   Thompson D.   Di Milia G.   Luker J.
Thiell B.   Murray S. S.
Online Discovery: Search Paradigms and the Art of Literature Exploration **[#1022]**
Furthering science depends critically on discoverability of literature, and therefore on accurate and intelligent search tools. In this presentation we discuss new search paradigms and techniques explored in "ADS Labs," offered by the ADS.

Ceamanos X.   Douté S.   Fernando J.   Schmidt F.   Pinet P.   Lyapustin A.
MARS-ReCO: Multiangle Approach for Retrieval of Surface Reflectance from CRISM/MRO Observations **[#2697]**
Retrieval of surface reflectance of Mars is carried out using CRISM multi-angular observations acquired during the ongoing Mars Reconnaissance Orbiter (MRO) mission thanks to the MARS-ReCO approach that considers a non-Lambertian surface.

Cseh R.   Varga T. P.   Bérczi Sz.   Varga T. N.
Educational Relationships the Development of the Hunveyor 13 Informatics Architecture **[#1183]**
The HUNVEYOR 13 space probe model informatics system has several levels, proportioned hierarchically on the basis of function, which can be formed in a flexible way. Certain blocks of function are handled as functional units.

GEOLOGICAL ANALOGS FOR DISTANT PLANETARY SURFACES

Di Primio M.   Marinangeli L.
Radar Stratigraphy of the Northern and Central Greenland Ice Cap: Groundtruth for SHARAD Data **[#1945]**
In the Greenland ice sheet we recognized four different radar facies based on the CReSIS acquisition and correlated these units with the core microscopic analysis to provide modeling for radar interpretation of the Mars polar layered deposits (PLD).

Levy J. S.   Fountain A. G.   Nylen T. L.   Head J. W. III   Dickson J. L.
Rapid Growth and Decay of Mars-Analog Gullies in Buried Ice and Sediment-Rich Substrates: New Views of Gullies as Disequilibrium Landforms in Garwood Valley, Antarctica **[#1100]**
Garwood Valley gullies are an extreme case of rapid landscape change in response to strong disequilibria between ground ice and surface temperature conditions. They may be analogs for gully evolution on Mars driven by both "wet" and "dry" processes.

Socki R. A.   Sun T.   Niles P. B.   Harvey R. P.   Bish D. L.   Tonui E.
Antarctic Mirabilite Mounds as Mars Analogs: The Lewis Cliffs Ice Tongue Revisited **[#2718]**
We have identified massive but highly localized Antarctic mirabilite mounds that may be derived from subsurface fluids and may provide insight into the processes associated with the subsurface. These mounds may be analogous to mounds found on Mars.

THU POSTERS

Cousins C. R.   Crawford I.   Gunn M.   Harris J. K.   Steele A.
Detection and Identification of Mars Analogue Volcano — Ice Interaction Environments **[#1216]**
Volcano-ice interaction produces many environments available to microbial colonisation. Similar processes are likely to have occurred on Mars, and are prime exobiology targets. Multi-instrument analyses of volcano-ice deposits are presented.

Pina P.   Vieira G.   Christiansen H. H.   Barata M. T.   Oliva M.   Neves M.   Bandeira L.   Lousada M.   Jorge M.   Saraiva J.
Analog Studies of Ice-wedge Polygons in Svalbard: 2011 Field Campaign, Topology and Geometry **[#2353]**
A second field campaign was conducted in Svalbard to study ice-wedge polygons in the framework of project ANAPOLIS. Some results are shown from the mapping of a network, along with ideas on what they can signify for the analysis of martian polygons.

Essefi E.   Komatsu G.   Fairén A. G.   Ben Jmaa H.   Rekhiss F.   Yaich C.
Spring Mounds at Sidi El Hani Saline Environment, Eastern Tunisia: Terrestrial Analog for Mars **[#1289]**
The development of spring mounds within the Sidi El Han saline environment is a slow and continuous process, taking place according to different stages. Similarly, the formation of some putative spring mounds on Mars may be explained by the same processes.

Matsubara Y.   Howard A. D.   Burr D. M.   Williams R. M.   Moore J. M.
Meandering Channels in a Non-Vegetated Area: Quinn River, NV as a Martian Analog **[#2534]**
Meander channels require cohesive banks. On Earth, this is obtained by vegetation. Meandering channels found on Mars raises the question of this paradigm. Quinn River meanders through an area with sparse vegetation and abundant mud and salt.

Irwin R. P. III   Zimbelman J. R.
Pluvial Shore Landforms in the Great Basin, USA: Analogs to Martian Paleolake Basins **[#2061]**
Great Basin pluvial shore landforms are often topographically subtle. They should not have survived degradation since the Noachian or Early Hesperian, and detection in high-resolution data would depend on youth and ideal conditions for development.

Zheng M. P.   Kong W. G.
Application of Saline Lake Studies in Martian Geology and Paleoclimatology: Implication for Widespread Potassium Salts on Mars **[#1314]**
On the basis of current understanding of martian salts, potassium salts are proposed to be widespread on the martian surface by applying the principles of terrestrial saline lake studies.

Cannon K. M.   Fenwick L. A.   Peterson R. C.
Spotted Lake: Mineralogical Clues for the Formation of Authigenic Sulfates in Ancient Lakes on Mars **[#1989]**
Spotted Lake in British Columbia has some of the highest sulfate concentrations in the world, and serves as a valuable analog for studying evaporation and freezing crystallization processes in martian paleolakes.

Ehlmann B. L.   Kelemen P. B.   Pinet P.   Mustard J. F.   Launeau P.   Ceuleneer G.
Aqueous Alteration of Ultramafic Rocks in Oman: An Analog for Understanding Carbonate and Serpentine on Mars **[#1471]**
Abundance of carbonate and circulation of waters and geochemical reactions (serpentinization, carbonation) within ultramafic rocks are examined with hyperspectral airborne data coupled with laboratory infrared spectroscopy, XRD, and petrologic data .

Fleischer I.   Klingelhöfer G.   Schäfer M.   Panthöfer M.   Rosemann J.   Fischer T.
Alteration of Sulfate Minerals from Rio Tinto, Spain **[#2074]**
The sulfate mineral jarosite was detected at Meridiani Planum, Mars, with the Mössbauer spectrometer MIMOS II on the MER Opportunity. Analog studies were performed with a lab MIMOS II version on sulfate samples from Rio Tinto region in Spain.

Komatsu G.   Takemura K.   Goto K.   Shibuya H.   Yamagishi A.   Sekina Y.   Ishimaru R.
Beppu Hotspring, Japan, as a Terrestrial Analog for Ancient Hydrothermal Systems on Mars **[#1096]**
The Beppu Hotspring on the Kyushu Island, Japan, is an active geothermal field notable for a variety of mineralogy, geochemistry, and microbial activities. This setting maybe comparable to the hypothesized ancient martian hydrothermal systems.

Williams A. J.   Sumner D. Y.
The Development and Preservation of Filamentous Fabrics as Mineralogic Biosignatures, Iron Mountain, California **[#2337]**
This study investigates mineralogic biosignature formation in gossans related to Fe oxide precipitation in association with microbes. We explore the relevance and detection of these biosignatures within the detection limit of the Mars Science Laboratory.

McAdam A. C.   Stern J. C.   Mahaffy P. R.   Blake D. F.   Bristow T.   Steele A.
Amundsen H. E. F.   AMASE 2011 Team
Evolved Gas Analysis of Mars Analog Samples from the Arctic Mars Analog Svalbard Expedition: Implications for Analyses by the Mars Science Laboratory **[#2318]**
Data from samples collected during the Arctic Mars Analog Svalbard Expedition show that MSL SAM-like evolved gas analyses can give constraints on sample organic chemistry, organic matter-mineral associations, and volatile-bearing minerals.

Gurgurewicz J.   Mège D.   Carrère V.   Cornen G.   Gaudin A.   Kostylew J.   Morizet Y.
Purcell P. G.   Le Deit L.
Inferring Alteration Conditions on Mars: Insights from Near-Infrared Spectra of Basalts from Siberia and East Africa **[#1505]**
An attempt is made to infer climate indicators from the alteration features of terrestrial basalts altered in arid cold and arid hot environmental settings.

Bhattacharya S.   Jain N.   Parthasarathy G.   Chauhan P.   Ajai
Study of Hydrous Sulfates from the Deccan Volcanic Province (DVP) of Kutch, India: Implications for Aqueous Alteration Processes on Mars **[#1468]**
The Deccan Volcanic Province (DVP) at Gujarat, India is consider as a good analogue for the study of clay and hydrous sulphate minerals.This study can lead in interpreting the environmental conditions on the early Mars.

Jain N.   Bhattacharya S.   Chauhan P.   Ajai
Hyperspectral Study of Hydrous Magnesium Minerals (Serpentine) from Ultramafic Rocks Along the Rikhabhdev Lineament, Rajasthan, India: As an Analogue for Hydrous Magnesium Minerals on Mars **[#1474]**
The ultramafic rocks along the Rikhabhdev Lineament, Rajasthan, India is consider as a good analogue for the study study of serpentine. This study help in interpreting the environmental conditions on Mars in its past.

Gavin P.   Chevrier V. F.   Sayyed M. R. G.   Islam R.
Spectral Analysis of Deccan Intrabasaltic Bole Beds: Implications for Phyllosilicate Formation on Mars **[#1621]**
This study compares IR spectra of the Deccan bole beds with those observed in Mawrth Vallis and links their formation processes. Our data suggests changing temperatures during formation then transformation without significant ion transfer.

de Morais A.
Carbonate Diagenetic Deposits — Parallels Between Arenites at Bauru Region, South America and Rocks at Nili Fossae Region, Planet Mars **[#2942]**
It is made specific comparisons among diagenetic processes on carbonate deposits on Earth and Mars to give a contribution — via the use of biased techniques and gained experience — for future exploration and better understanding of the Earth and planet Mars.

Potter-McIntyre S. L.   Chan M. A.   McPherson B. J.
Iron (Oxyhydr)Oxide Biosignatures in the Brushy Basin Member of the Jurassic Morrison Formation, Colorado Plateau, USA: Analog for Martian Diagenetic Iron **[#1940]**
Iron precipitates in modern microbial mats compared with iron cements in Jurassic alkaline saline lake sediments show that morphological and chemical biosignatures are present and preserved in oxidized, evaporative environments analogous to Mars.

Valdueza J. E.
Selection of the Guinsaugon Rockslide in the Philippines as a Structural and Morphologic Analog to Rockslide Avalanches in Valles Marineris, Mars **[#2936]**
This paper selects the Guinsaugon landslide in the Philippines as a potential site to do terrestrial analog studies on Mars.

Halliday W. R.   Favre G.   Stefansson A.   Whitfield P.   Banks N.
Occurrence and Absence of Lava Tube Caves with Some Other Volcanic Cavities; a Consideration of Human Habitation Sites on Mars **[#1613]**
Field investigation of Hawaii's Kau Desert pit craters shows that they are not connected to lave tube caves. The Seven Sisters of Arsia Mons are unlikely to contain lave tube caves. Other types of caves on Mars may provide human habitation sites.

Edgar L. A.   Grotzinger J. P.   Southard J. B.   Ewing R. C.   Lamb M. P.
Criteria for the Identification of Pyroclastic Surge Deposits on Mars: Insight from Hunt's Hole, New Mexico **[#2638]**
We combine field observations, Terrestrial Laser Scanning (TLS), and hydrodynamic considerations to understand pyroclastic surge deposits at Hunt's Hole, New Mexico, and provide criteria for their identification on Mars.

TESTING SCIENCE MISSION OPERATIONS IN ANALOG SETTINGS

Marion C. L.   Osinski G. R.   Abou-Aly S.   Antonenko I.   Barfoot T.   Barry N.   Bassi A.   Battler M.   Beauchamp M.   Bondy M.   Blain S.   Capitan R. D.   Cloutis E. A.   Cupelli L.   Chanou A.   Clayton J.   Daly M.   Dong H.   Ferrière L.   Flemming R.   Flynn L.   Francis R.   Furgale P.   Gammel J.   Garbino A.   Ghafoor N.   Grieve R. A. F.   Hodges K.   Hussein M.   Jasiobedzki P.   Jolliff B. L.   Kerrigan M. C.   Lambert A.   Leung K.   Mader M.   McCullough E.   McManus C.   Moores J.   Ng H. K.   Otto C.   Ozaruk A.   Pickersgill A. E.   Pontefract A.   Preston L. J.   Redman D.   Sapers H.   Shankar B.   Shaver C.   Singleton A.   Souders K.   Stenning B.   Stooke P.   Sylvester P.   Tripp J.   Tornabene L. L.   Unrau T.   Veillette D.   Young K.   Zanetti M.
A Series of Robotic and Human Analogue Missions in Support of Lunar Sample Return **[#2333]**
This work represents an overview of an analogue mission campaign entitled Impacts: Lunar Sample Return (ILSR) to the South Pole–Aitken Basin (SPA) funded by the Canadian Space Agency.

Preston L. J.   Barber S. J.   Grady M. M.
CAFE — A New On-Line Resource for Planning Scientific Field Investigations in Planetary Analogue Environments **[#1874]**
The Concepts for Activities in the Field for Exploration (CAFE) project is creating a complete catalogue of terrestrial analogue environments that are appropriate for testing human space exploration-related scientific field activities.

Francis R.   Osinski G. R.   Moores J.   Barfoot T.   ILSR Team
Co-Operative Human-Robotic Exploration of Lunar Analogue Sites **[#1996]**
Operational capacity and performance comparison of lunar analogue missions using robot-only, astronaut-only, and joint robotic-astronaut mission architectures, at the Sudbury and Mistastin Lake impact structures in Canada.

Moores J. E.   Francis R.   Osinski G. R.   Mader M.   McCullough E.   Preston L. J.   Tornabene L. L.
KRASH Operations and Science Team
Surface Operations for Mission Control During Analogue Human Lunar Deployments to Mistastin and Barringer Impact Structures **[#1136]**
The pre-deployment structure is presented for Mistastin along with the evolution of that structure. The lessons learned are applied to Barringer. The value of and requirements for different cross-cutting processes and roles are considered.

Shankar B.   Osinski G. R.   Abou-Aly S.   Beauchamp M.   Blain S.   Chanou A.   Clayton J.   Francis R.
Kerrigan M.   Mader M. M.   Marion C.   McCullough E.   Moores J. E.   Pickersgill A. E.   Pontefract A.
Preston L. J.   Tornabene L. L.
Lunar Analogue Mission: Overview of the Site Selection and Traverse Planning Process for a Human Sortie Mission at the Mistastin Lake Impact Structure, Labrador, Canada **[#1143]**
This abstract summarizes the detailed approach applied in selecting sites and planning astronaut traverses for an analogue human sortie mission.

Tornabene L. L.   Osinski G. R.   Mader M. M.   Chanou A.   Francis R.   Joliff B. L.   Marion C.   McCullough E.
Pickersgill A.   Sapers H.   Souders K.   Sylvester P.   Young K.   Zanetti M.
KRASH Operations and Science Team
Utility of Remote Sensing, Robotic Precursor Data and a Focused Science Hypothesis for a Follow-On Human Exploration Lunar Analogue Mission at the Mistastin Lake (Kamestastin) Impact Structure **[#2390]**
Here we summarize how remote sensing, robotic precursor data and a focused science hypothesis augmented the results from a lunar analogue mission to the Mistastin impact structure in Labrador, Canada. Join me as we go on a magical tour of this crater.

Kerrigan M. C.   Shankar B.   Marion C.   Francis R.   Pickersgill A. E.   Capitan R. D.
Osinski G. R.   ILSR Team
Real-Time Mission Control Tracking of Astronaut Positions During Analogue Missions **[#2756]**
Here we present a simple and reliable method of real-time tracking of astronaut positions developed and implemented during recent analogue missions.

Mader M. M.   McCullough E.   Beauchamp M.   Clayton J.   Marion C. L.   Moores J.   Pickersgill A. E.
Preston L. J.   Shankar B.   Osinski G. R.   ILSR Team
Science Data Management During Real-Time Geological Lunar Analogue Missions to the Sudbury and Mistastin Lake Impact Structures: Recommendations for Future Ground Data Systems **[#1842]**
Simulating planetary missions on Earth can help test data management procedures and help identify needs and gaps in current ground data systems. We present lessons learned from three lunar analogue missions funded by the Canadian Space Agency.

Abou-Aly S.   Mader M. M.   McCullough E.   Preston L. J.   Moores J.   Tornebene L. L.   Osinski G. R.
ILSR Team
Signficance of Science-Tactical Liaison Role in Mission Control for the Krash Lunar Analogue Sample Return Mission **[#2310]**
Our team carried out an analogue mission at the Mistastin Lake. Mission Control was divided into a tactical team and a science team. The science liaison is responsible for relaying the aims and motivations of the science room to the tactical room.

Blain S.   Mader M. M.   Tornabene L. L.   Osinski G. R.   ILSR team
Significance of Mission Control Science Documentarian in the KRASH Lunar Analogue Mission **[#2079]**
Responsibilities and role of the mission control science documentarian in the KRASH lunar analogue mission.

THU POSTERS

McCullough E. Pickersgill A. E. Francis R. Bassi A. Shankar B. Mader M. M. Beauchamp M. Osinski G. R. KRASH Operations and Science Team
Scientific Application of Visual Systems Instrumentation used During Lunar Sample Return Analogue Missions **[#2687]**
We present the use of 2D and 3D visual data for situational awareness and geological interpretations from the mission control perspective of three lunar analogue missions funded by the Canadian Space Agency.

Pickersgill A. E. Osinski G. R. Beauchamp M. Marion C. Mader M. M. Francis R. McCullough E. Shankar B. Barfoot T. Bondy M. Chanou A. Daly M. Dong H. Furgale P. Gammell J. Ghafoor N. Hussein M. Jasiobedzki P. Lambert A. Leung K. McManus C. Ng H. K. Pontefract A. Stenning B. Tornabene L. L. Tripp J. KRASH Science and Operations Teams
Scientific Instrumentation for a Lunar Sample Return Analogue Mission **[#2657]**
We outline the scientific instruments used during a lunar sample return analogue mission campaign and their strengths and weaknesses from a field perspective. Recommendations are included for maximizing scientific gain with these instruments.

Pontefract A. Marion C. Osinski G. R. Francis R. Pickersgill A. E. Tornabene L. L. ILSR Team
Use of Portable XRF and Raman for In Situ Analyses in Manned Planetary Investigations: Lessons Learned from the Kamestastin Lunar Analogue Mission **[#2086]**
The development of in situ geochemical instruments is critical for use in future human-led planetary investigations. We report here on our experiences using portable XRF and Raman spectrometers in the field during the KRASH 2011 analogue mission.

Stenning B. Osinski G. R. Barfoot T. Basic G. Beauchamp M. Daly M. Dong H. Francis R. Furgale P. Gammell J. Ghafoor N. Jasiobedzki P. Lambert A. Leung K. Mader M. Marion C. McCullough E. McManus C. Moores J. Preston L.
Planetary Surface Exploration Using a Network of Reusable Paths **[#2360]**
A network of reusable paths is a powerful new concept for planetary exploration. It allows a rover to study sites in parallel. It was field tested in mock lunar sample-return mission scenarios conducted in the Sudbury impact crater in Canada.

Deans M. C. Lees D. S. Smith T. Cohen T. E. Morse T. F. Fong T. W.
Field Testing Next-Generation Ground Data Systems for Future Missions **[#2518]**
Our Exploration Ground Data System comprises tools for mission science ops, including planning, monitoring, documentation, and analysis. In 2011, we tested our tools by supporting the Pavilion Lake Research Project, NEEMO and Desert RATS.

Johnson J. E. Janoiko B. A.
Desert Research and Technology Studies (D-RATS) 2011 Mission Overview **[#1604]**
2011 marked the 14th year of NASA's Desert Research and Technology Studies (D-RATS) analog mission operations. This test integrated some of NASA's latest technologies in an operational setting to evaluate a simulated near-Earth asteroid mission.

Bleacher J. E. Hurtado J. M. Jr. Meyer J. A. Tewksbury-Christle C. M.
Desert RATS 2011 Mission Simulation: Effects of Microgravity Operational Modes on Field Geology Capabilities **[#2208]**
The 2011 Desert RATS tested delayed communications and several combinations of hardware and crew assignments for microgravity targets. We discuss the strengths and weaknesses with respect to conducting planetary field geology.

Eppler D. B.
Managing Science Operations During Planetary Surface Operations at Long Light-Delay-Time Targets: The 2011 Desert RATS Test **[#2175]**
Desert RATS 2011 Science Operations Test simulated managing of human science operations at targets beyond the light delay time experienced during low-Earth orbit and lunar surface missions, such as a mission to a near-Earth object or Mars.

Evans C. A.   Calaway M. J.   Bell M. S.
GeoLab 2011: New Instruments and Operations Tested at Desert RATS **[#1186]**
GeoLab,a prototype glovebox integrated into a habitat testbed, simulates science operations for future exploration missions. We present GeoLab results from 2011 Desert RATS analog tests with new analytical instruments and data collection interfaces.

Yingst R. A.   Cohen B. A.   Hynek B. M.   Johnson J. B.   Schmidt M. E.   Schrader C. M.
Science-Driven Strategies for Semi-Autonomous Rovers on the Moon: Field Test at an Ice-Bearing Regolith Analog **[#1674]**
We report on field tests at two glacial moraines (analogs for ice-bearing lunar regolith) where we tested science operational strategies used on Mars to determine best practices for conducting remote semi-autonomous rover geology on the Moon.

Cloutis E. A.   Whyte L.   Qadi A.   Bell J. F. III   Berard G.   Boivin A.   Ellery A.   Haddad E.   Jamroz W.   Kruzelecky R.   Mann P.   Olsen K.   Perrot M.   Popa D.   Rhind T.   Samson C.   Sharma R.   Stromberg J.   Strong K.   Tremblay A.   Wilhelm R.   Wing B.   Wong B.
The Mars Methane Analogue Mission (M3): Results of the 2011 Field Deployment **[#1569]**
The M3 mission simulated a rover mission to Mars to search for sources of methane. The 2011 campaign found that methane plumes from serpentinite are very localized and target selection based on imagery is preferred over direct methane detection.

Boivin A.   Samson C.   Holladay J. S.   Cloutis E. A.   Ernst R. E.
Mars Methane Analogue Mission (M3): Near Subsurface Electromagnetic Techniques and Analysis **[#2140]**
As part of the Canadian Space Agency's Mars Methane Analogue Mission, a micro-rover mission, an Electromagnetic Induction Sounder (EMIS) was used with the goal of demonstrating its value as a potential science instrument onboard future rovers.

Weiss D. K.   Levine N. S.   Beutel E. K.   De Munster N.   Barajas L. G.   Wynne K.   Stein A.   Runyon C.
Mapping Rover Routes and Hydrous Soil Locations on the Mars Desert Research Station **[#1950]**
We report on a two-week Mars Desert Research Station (MDRS) crew 109 rotation where satellite imagery and groundbased observations were combined to create a map of potential rover exploration routes for the area surrounding the MDRS habitat.

Rask J. C.   De Leon P.   Marinova M. M.   McKay C. P.
The Exploration of Marambio Antarctica as a Mars Analog **[#2455]**
To learn how spacesuits limit Mars exploration activities, we performed field exploration, sample collection, and instrument deployment, utilizing a pressurizable prototype spacesuit in a rocky, permafrost-rich Mars-like Antarctic location.

EDUCATION AND PUBLIC OUTREACH: MISSION ANALOGS

Gruener J. E.   McGlone M.   Allen J.   Tobola K.   Graff P.
NASA Desert RATS 2011 Education Pilot Project and Classroom Activities **[#1583]**
For the 2011 NASA Desert RATS analog activities, NASA HQ provided support to develop an education pilot project with student activities to parallel the Desert RATS mission planning and exploration activities in the classroom, as well as educator training.

Garry W. B.   Bleacher L. V.   Bleacher J. E.   Petro N. E.   Mest S. C.   Williams S. H.
The Scale of Exploration: Planetary Missions Set in the Context of Tourist Destinations on Earth **[#2166]**
What if the Apollo astronauts explored Washington, DC, or the Mars Exploration Rovers explored Disney World? We present educational versions of the traverse maps for Apollo and MER missions set in the context of popular tourist destinations on Earth.

PLANETARY BRINES AND ALTERATION

Marion G. M. Catling D. C. Crowley J. K. Kargel J. S.
Sulfite-Sulfide-Carbonic Equilibria on Earth and Mars **[#1501]**
Volcanism on a cold Mars may be the primary causes of high sulfur minerals on Mars, compared to volcanism on a warm Earth that led to high carbonate minerals.

Chevrier V. F. Lozano C. G. Altheide T. S.
Experimental Weathering of Silicates and Carbonates in a SO_2 Atmosphere: Implications for the Martian Surface Mineralogy **[#2908]**
Weathering experiments of carbonates and silicates in a SO_2 atmosphere and water or water plus hydrogen peroxide result in differences in nature and abundance of secondary phases, favoring sulfites in the first case and sulfates in the second.

Uts I. Rivera-Valentin E. G. Chevrier V. F.
Exploring Possible Brine Compositions for Martian Paleolakes **[#1731]**
We use the possible brine compositions from Tosca et al. (2011) in order to model the evolution of a martian paleolake accounting for possible initial chemistries.

Martinez G. M. Renno N. O. Elliott H. M.
Optical Evidence for Brines on Mars in Richardson Crater **[#2825]**
In this work, we show optical evidence from HiRISE images in the near infrared (NIR) for the existence of brines at Richardson Crater during the spring.

Runyon K. D. Davatzes A. K. Gulick V. C.
Putative Active Brine Flows in the Cerberus Fossae, Mars **[#2072]**
The equatorial Cerberus Fossae may currently be hydrogeologically active as evidenced by morphologic and albedo features termed slope lineae. Some lineae show significant modification between repeat HiRISE images.

Massé M. Beck P. Schmitt B. Pommerol A. McEwen A. Chevrier V. F. Brissaud O.
Nature and Origin of RSL: Spectroscopy and Detectability of Liquid Brines in the Near-Infrared **[#1856]**
The aim of our study is to test with laboratory experiments the plausibility of a brine origin for the formation of the recurrent slope linea (RSL). We thus acquire near-infrared spectra during some brine dehydration and hydration processes.

Al-Samir M. van Berk W. Kneissl T. van Gasselt S. Gross C. Wendt L. Jaumann R.
A Model Scenario for Kieserite-Dominated Evaporites in Juventae Chasma, Mars **[#2453]**
Taking evaporation as a prerequisite, we measured the "stairstep" morphology and the volume of mound B to model the mineral assamblage to reconstruct the amount of water needed to form mound B in its composition as measured by CRISM and OMEGA.

Berard G. Applin D. Stromberg J. Sharma R. Mann P. Grasby S. Bezys R. Horgan B. Londry K. Rice M. Last B. Last F. Badiou P. Goldsborough G. Bell J. F. III
A Hypersaline Spring Analogue in Manitoba, Canada for Potential Ancient Spring Deposits on Mars **[#1513]**
This study explores the characteristics of a spring complex, East German Creek, Manitoba (EGC), as a terrestrial analogue for similar environments on Mars. We focus on EGC's mineral precipitation patterns and potential for biosignature preservation.

Oehler D. Z. Allen C. C.
Fluid Expulsion, Habitability, and the Search for Life on Mars **[#1044]**
The search for evidence of past life on Mars should be concentrated on settings with potential for long-lived water, sources of nutrient and energy renewal, and sediments that would preserve organics. We provide an example of such a setting.

Loizeau D.   Werner S. C.   Mangold N.   Bibring J.-P.   Vago J. L.
Chronology of Deposition and Alteration in the Mawrth Vallis Region, Mars **[#2114]**
We have investigated ages of deposition and alteration of the clay unit of the Mawrth Vallis plateaus, through regional and local crater counts. This work provides useful boundaries for constraining the time period of water activity in this region.

DIFFERENTIATION AND COOLING HISTORIES OF PLANETARY MAGMAS: FROM ISOTOPES TO TEXTURES

Dauphas N.   Roskosz M.   Alp E. E.   Sio C. K.   Tissot F. L. H.   Neuville D.   Hu M.   Zhao J.   Tissandier L.   Medard E.
Controls on Iron Isotope Variations in Planetary Magmas **[#1525]**
Using a synchrotron technique, we have measured the equilibrium Fe-isotope fractionation factors of geological materials. This study reveals the potency of Fe isotopes to trace redox variations and magmatic differentiation in planets.

Holness M. B.   Richardson C.   Anand M.
A New Proxy for Dolerite Crystallisation Times in Planetary Samples **[#1589]**
In this contribution we introduce a new parameter for constraining solidification times in mafic rocks: the median clinopyroxene-plagioclase-plagioclase dihedral angle.

Mills R. D.   Glazner A. F.
Coarsening of Crystals During Temperature Cycling in Magmas and Icy Materials **[#1819]**
Temperature cycling during crystal growth produces large crystals and coarse texture in magmas and ices by dissolution-crystallization. This has implications for crystal growth and texture development on the Moon, Mars, and comets.

Jacob D.   Palatinus L.   Cuvillier P.   Leroux H.   Domeneghetti C.   Camara F.
Fe-Mg Ordering in Orthopyroxene Studied at a Microscopic Scale Using Precesion Electron Diffraction **[#1337]**
The ordering state of orthopyroxene is determined at a microscopic scale in a transmission electron microscope. The method allows distinguishing between a natural ordered sample from a disordered one annealed at high temperature and quenched.

McCutcheon W. A.   King P. L.   Lee R. J.   Ramsey M. S.
Understanding the Composition and Thermal History of Silicic Glasses Through Thermal Infrared Spectroscopy **[#2543]**
Thermal infrared spectroscopy of glasses, common on planetary surfaces, is complicated by the effects of composition and temperature. This contribution examines these effects in a range of natural and synthetic silicic glass compositions.

ORIGIN AND INTERNAL EVOLUTION OF PLANETS

Albalat E.   Telouk P.   Albarede F.
Er and Yb Isotope Fractionation in Planetary Material **[#1129]**
We present an investigation of Er and Yb isotopes in Earth, meteorites, and the Moon by MC-ICP-MS. The main results concern the Yb redox state, condensation of the Moon from the impact vapor, and neutron adsorption by the lunar surface.

Craddock P. R.   Warren J. M.   Dauphas N.
The Chondritic Iron Isotopic Composition of the Earth **[#1672]**
Iron isotopic fractionation in terrestrial igneous rocks did not result from early core-mantle differentiation, but by partial melting of the mantle, based on the identical composition of abyssal mantle peridotites to undifferentiated meteorites.

Arkani-Hamed J.
Delayed Activation of Martian Core Dynamo **[#1563]**
The embryo-embryo collision at the later stages of accretion could have delayed the core dynamo activation of Mars by 50–120 Myr.

Neumann W. Breuer D. Spohn T.
Differentiation of H-Chondritic Planetesimals **[#1889]**
We have studied the influence of melt migration on the thermochemical evolution of planetesimals taking into account accretion, sintering, and melt heat transport via porous flow. Our work constrains the timing and the duration of the core formation.

Swift D. C. Drummond N. D. Heuze O. Kraus R. G. Ackland G. J.
Analytic Multiphase Equation of State for MgO **[#2545]**
Analytic equations of state (EOS) of Mie-Grueneisen form were constructed for B1, B2, and liquid phases of MgO, calibrated against our previous ab initio B1–B2 EOS. The effect of kinetics on B1–B2 and melting transitions was investigated.

Gu T. Wu X. Qin S. Fei Y.
Magnetic and Structural Transitions of Fe_3P and Implications for Phosphorus in Planetary Cores **[#2301]**
In order to understand the structure type of the high-pressure phase of Fe_3P and its implications for planetary cores, we carried out ab initio calculations to explore the stability of Fe_3P in several structures.

Burkemper L. K. Agee C. B. Garcia K. A.
Molybdenum Metal-Silicate Partitioning Behavior: Constraining the Magma Ocean Hypothesis for Core Formation **[#2155]**
Mo metal-silicate partitioning experiments were performed over a P range of 3–20 GPa and a T range of 2173–2673 K. Parameterization of our new data and literature data indicates Mo is compatible with the deep (42–57 GPa) magma ocean hypothesis.

Nickodem K. Righter K. Danielson L. Pando K. Lee C.
Core-Mantle Partitioning of Volatile Siderophile Elements and the Origin of Volatile Elements in the Earth **[#2295]**
Determine the effect of Si on core-mantle partitioning of volatile siderophile elements. Analyze As, Ge, In, and Sb partitioning between metal melt and silicate liquid using partition coefficients.

Malavergne V. Charon E. Jones J. Agranier A. Campbell A.
Pt, Au, Pd and Ru Partitioning Between Mineral and Silicate Melts: The Role of Metal Nanonuggets **[#1873]**
Pt, Au, Pd, and Ru partition coefficients between olivine (or diopside) and silicate melts have been determined. In parallel, we will explain how metal nanonuggets appeared in our samples and how we will understand their formation.

Frank E. F. Maier W. D. Mojzsis S. J.
The "Late Veneer" on Earth: Evidence from Eoarchean Ultramafic Schists (Metakomatiites) **[#2890]**
Contemporary peridotites show an enhanced concentration of the highly siderophile elements (HSEs). This is believed to be due to a late accretion event called the Late Veneer. Here we show the evolution of the HSE signature using ancient komatiites.

PRESOLAR GRAINS: INSIGHT INTO STELLAR PROCESSES

Jadhav M. Nagashima K. Huss G. R. Ogliore R. C.
Nitrogen Isotopic Compositions of Mainstream SiC Grains from Chondrites with a Range of Cosmic Ray Exposure Ages **[#2826]**
We present and compare N isotopic data of mainstream SiC grains from chondrites with varying CRE ages in an attempt to explain low $^{14}N/^{15}N$ ratios. The N isotopic probability distributions overlap considerably making any correlation with CRE ages irresolvable.

Henkel T.   Sattaur A.   Lyon I. C.
Deconvoluting TOFSIMS Depth Profiles of Presolar SiC Grains **[#2135]**
The sputtering process of presolar grains is simulated to deconvolute TOFSIMS depth profiles. This helps to determine the interior structure, which provides clues about the history of the grains like shockwave implantation of trace elements.

Liu N.   Savina M. R.   Davis A. M.   Shkrob I.   Marin T.   Pellin M.   Willingham D.
Development of a Resonance Ionization Method for Isotopic Analysis of Neodymium at Trace Levels in Presolar SiC Grains **[#2401]**
We developed a resonance ionization method with enough precision for isotopic analysis of neodymium in single presolar silicon carbide (SiC) grains. We analyzed two standards and agreement between both results indicates that the method is robust.

Amari S.   Zinner E.   Gallino R.
Presolar Graphite from the Murchison Meteorite: Puzzles Related to Its Origins **[#1031]**
Carbon, O and Al isotopic ratios of many low-density grains are hard to reproduce by supernova mixing if C-rich conditions are necessary to form grains. Many grains from high-density fractions most likely formed in low-metallicity AGB stars.

Xu Y. C.   Amari S.   Gyngard F.   Zinner E.   Lin Y.
Isotopic Studies of Presolar Graphite Grains from the Murchison Meteorite **[#1094]**
Isotopic ratios of C, N, and O are compared to morphology and density of presolar graphite grains from the Murchison meteorite.

Heck P. R.   Pellin M. J.   Davis A. M.   Isheim D.   Seidman D. N.   Hiller J.   Mane A.   Elam J.   Savina M. R.   Auciello O.   Stephan T.   Larson D. J.   Lewis J.   Floss C.   Daulton T. L.
Atom-Probe Tomographic Analysis: Towards Carbon Isotope Ratios in Individual Nanodiamonds **[#1790]**
We successfully analyzed individual meteoritic and synthetic nanodiamonds with highly improved sample stability. The mass spectra have a low background and display well-defined C peaks. Tomographic reconstructions to ~100 nm depth were performed.

Lewis J. B.   Isheim D.   Floss C.   Daulton T.   Seidman D. N.   Heck P. R.   Davis A. M.   Pellin M. J.   Savina M. R.   Hiller J.   Mane A.   Elam J.   Auciello O.   Stephan T.
Meteoritic Nanodiamond Analysis by Atom-Probe Tomography **[#2192]**
We are using atom-probe tomography to clarify the origin of meteoritic nanodiamonds. We report new data and revised analytical protocols in our continuing efforts to quantitatively determine the C-isotopic ratios of individual ~3 nm nanodiamonds.

Takigawa A.   Tachibana S.   Nagahara H.   Ozawa K.
Anisotropic Evaporation and Condensation of Circumstellar Corundum **[#1875]**
We experimentally showed the evaporation and condensation anisotropy of corundum under circumstellar conditions. Calculated infrared spectra of anisotropically condensed corundum well reproduce the 13-µm peaks observed from O-rich AGB stars.

Ong W. J.   Floss C.   Gyngard F.
Negative Secondary Ion Measurements of $^{54}Fe/^{56}Fe$ and $^{57}Fe/^{56}Fe$ in Presolar Silicate Grains from Acfer 094 **[#1225]**
We measured ^{54}Fe/^{56}Fe and ^{57}Fe/^{56}Fe as negative secondary ions of Fe oxide in eight presolar grains. One AGB grain is enriched in ^{54}Fe and ^{57}Fe. Another grain is depleted in ^{57}Fe; such deficits cannot be explained by current nucleosynthetic models.

THU POSTERS

Stephan T.   Davis A. M.   Pellin M. J.   Savina M. R.   King A. J.   Liu N.   Rost D.
Trappitsch R.   Yokochi R.
CHILI — Approaching the Final Frontiers in Lateral Resolution and Sensitivity — A Progress Report **[#2660]**
CHILI, a new RIMS instrument, presently under construction at the University of Chicago, will achieve unprecedented sensitivity and lateral resolution. It will be applied to the analysis of samples from the Stardust mission and presolar dust.

McLeod A. S.   Dominguez G.   Gainsforth Z.   Kelley P.   Andreev G.   Thiemens M.
Keilmann F.   Basov D. N.
Infrared Phonon Fingerprinting of Nanocrystals Through Broadband Near-Field Spectroscopy **[#1828]**
Near-field infrared spectroscopy is applied to the study of nanometer-scale crystals of SiO_2 and SiC, revealing the spectral signatures of size effects and lattice disorder. This technique holds great promise for the analysis of returned samples.

Leitner J.   Heck P. R.   Hoppe P.   Huth J.
The C-, N-, and O-Isotopic Composition of Cometary Dust from Comet 81P/Wild 2 **[#1839]**
We investigated the C-, N-, and O-isotopic compositions of small ($d < 2$ µm) impact crater residues on Stardust Al foils. Focusing on the small crater population allows a more reliable estimate of the abundance of presolar material in 81P/Wild 2.

COSMIC DUST: INTERSTELLAR, INTERPLANETARY, AND COMETARY MATERIAL

Füri E.   Marty B.
Helium Isotopes in Stardust Cometary Matter: A Possible Record of the Early Evolution of the Solar System **[#1220]**
We reevaluate the origin of noble gases in Comet 81P/Wild 2. Helium-isotope ratios of Stardust samples fall between PSN and modern SW values, suggesting that cometary matter has recorded several snapshots of the early evolution of the solar system.

Palma R. L.   Pepin R. O.   Westphal A.   Schlutter D.   Gainsforth Z.
Helium and Neon in "Blank" Stardust Aerogel Samples **[#1076]**
Helium and neon concentrations and compositions were measured in 49 samples of "blank" aerogel from Stardust cell C2044. Five samples show interesting compositions that if related to the Track 41 impactor indicate a complicated parent particle.

Ogliore R. C.   Butterworth A.   Gainsforth Z.   Huss G. R.   Nagashima K.   Stodolna J.   Westphal A. J.
Sulfur Isotope Measurements of a Stardust Fragment **[#1670]**
We report S-isotopic measurements (^{3}2S, ^{3}3S, ^{3}4S, ^{3}6S) of a pyrrhotite grain from Comet Wild 2 returned by NASA's Stardust mission.

Snead C. J.   McKeegan K. D.   Burchell M.   Kearsley A. T.
Oxygen Isotope Measurements of Simulated Wild 2 Impact Crater Residues **[#2238]**
We discuss techniques developed to analyze the oxygen-isotopic compositions of Stardust impact crater residues, and we present results of such measurements of simulated impact crater residues of several mineral standards.

Nakashima D.   Ushikubo T.   Joswiak D. J.   Brownlee D. E.   Matrajt G.   Kita N. T.
High Precision Oxygen Three-Isotope Analysis of Crystalline Silicates of Comet Wild 2: A Genetic Link to Chondrules and AOAs in CR Chondrites **[#2196]**
Eight ferromagnesian Wild 2 particles show diverse oxygen isotope ratios and chemistry: ^{16}O-rich (Mn-rich forsterite) and ^{16}O-poor (FeO-rich and -poor), similar to AOAs and chondrules in CR chondrites. This suggests a genetic link to CR chondrites.

Nakashima D. Brownlee D. E. Joswiak D. J. Kita N. T. Ushikubo T.
Techniques for Ion Microprobe Analysis of Tiny Particles: Combination of FIB Marking and $^{16}O^{-}$ Ion Imaging and Sample Mounts Using Indium **[#2216]**
We developed new analytical protocols for high-precision oxygen-isotope analyses of tiny particles: use of indium to mount microtomed potted butt samples and combination of FIB marking and $^{16}O^{-}$ secondary ion imaging.

Silver E. Lin T. Vicenzi E. Toth M. Westphal A. Beeman J. Haller E. E. Burchell M.
Advanced Chemical Analysis of Cometary Material and Interstellar Dust Using a Microcalorimeter and a Low Vacuum Scanning Electron Microscope **[#2511]**
A microcalorimeter and an environmental scanning electron microscope modified to permit material-selective, gas-mediated, electron beam-induced etching are coupled to chemically analyze cometary particles and interstellar dust returned by Stardust.

White A. J. Ebel D. S. Greenberg M.
A New Experimental Deconvolution Technique for 3-Dimensional Laser Confocal Microscopy of Stardust Tracks in Aerogel **[#1542]**
We report successful three-dimensional deconvolution of Zeiss LSM 710 confocal microscopy data using an experimentally determined point spread function to obtain more accurate three-dimensional measurements of Stardust track morphology, grain size, and grain location.

Butterworth A. Becker N. Gainsforth Z. Lanzirotti A. Newville M. Proslier T. Stodolna J. Sutton S. Tyliszczak T. Westphal A. J. Zasadzinski J.
New Homogeneous Standards by Atomic Layer Deposition for Synchrotron X-Ray Fluorescence and Absorption Spectroscopies **[#2666]**
New homogeneous multi-layer film standards synthesized using Atomic Layer Deposition and characterized by multiple analytical methods, including ellipsometry, RBS, TEM, and synchrotron x-ray fluorescence and absorption spectroscopies.

Price M. C. Burchell M. Kearsley A. T. Cole M. J.
Alteration and Formation of Organic Molecules via Hypervelocity Impacts **[#1755]**
Raman spectral analyses of residues from polystyrene impactors on Al foils show the presence of intact polystyrene, carbon, and an unknown organic that is tentatively identified as a metal phthalate created during the hypervelocity impact.

Merouane S. Djouadi Z. d'Hendecourt L. Borg J.
IDPs' Silicate 10 µm Signature Versus Aliphatic 3.4 µm Features: A Key to Their Origin? **[#1777]**
Based on a quantification of olivine and pyroxene in the 10 µm band of IDPs, we investigate a possible link between their mineral and aliphatic components. This is probably reflecting an evolutionary pathway of the studied particles.

Matrajt G. Flynn G. J. Brownlee D. E. Joswiak D. J.
Coordinated FTIR and TEM Study of the Organic Material in the Stardust Particle Febo and the IDP Chocha **[#2576]**
We compared the organic carbonaceous material in a stardust particle and an IDP and found that texturally the material is identical but the IR data in the IDP shows many more peaks and variability than the SD particle.

Stodolna J. Gainsforth Z. Butterworth A. Westphal A. J.
TEM/STXM Characterization of Preserved Primitive Material from the Comet Wild2 **[#1214]**
We report the discovery of preserved primitive fine-grained material from Comet 81P/Wild 2. It is composed of silica-rich amorphous matrix embedded with iron sulfides and silicates. An enstatite whisker is identified inside the matrix.

Frank D. R.   Zolensky M. E.   Le L.
Using the Fe/Mn Ratio of FeO-Rich Olivine in Wild 2, Chondrite Matrix, and Type IIA Chondrules to Disentangle Their Histories **[#2748]**
We compare our data for FeO-rich olivine in matrix and Wild 2 to that of type IIA chondrules. This comparison yields implications for chondrule fragmentation, and the mixing and transport of fine-grained material to the outer solar system.

Rietmeijer F. J. M.
Sub-Micron Pyrrhotite-Taenite Grains in the Nucleus of Comet 81P/Wild 2 **[#1294]**
Chemical modeling predicts the presence of single pyrrhotite-taenite grains in the nucleus of Comet Wild 2 to explain the presence of the observed high-Ni FeNiS nanograins found in low-Mg silica glass.

Flynn G. J.   Sutton S. R.   Wirick S.   Lanzirotti A.   Rao W.
Fe- and Cr-XANES Analyses of Large Cluster Interplanetary Dust Particles **[#1089]**
Fe-XANES shows three large CI-like cluster IDPs consist of a mixture of at least two Fe-bearing phases, each dominated by Fe with a valance near Fe^{2+}. The absence of Fe-metal suggests the anhydrous IDP parent body is different from Wild 2.

THU POSTERS

Wopenka B.   Floss C.
Raman and Laser-Induced Fluorescence Signatures of Isotopically Primitive and Normal IDPs **[#1191]**
Isotopically primitive IDPs have lower laser-induced fluorescence and wider Raman D bands than normal IDPs. Combined Raman/SIMS study suggests that there may be multiple carbonaceous carriers for the N-isotopic anomalies in primitive IDPs.

Kohout T.   Suuronen J.-P.   Kallonen A.   Cuda J.   Badjukov D. D.   Skala R.
Physical Properties and X-Ray Microtomography of the Micrometeorites from Novaya Zemlya, Russia **[#2332]**
Physical properties and internal structure of cosmic dust in the form of six ~100-µm-sized micrometeorites, collected in the Novaya Zemlya glacier in Russia, were investigated using X-ray microtomography (XMT).

Schreiber K.   Stadermann F. J.   Floss C.   Rea D.   Lyle M.
Search for Extraterrestrial Particles in Sediment from the South Pacific Bare Zone **[#1112]**
The low sedimentation rate in the South Pacific Bare Zone suggests it may be a promising site for enhanced accumulation of extraterrestrial matter. Our initial search of a core from this region identified five particles with chondritic compositions.

Yabuta H.   Itoh S.   Noguchi T.   Sakamoto N.   Hashiguchi M.   Abe K.   Tsujimoto S.   Kilcoyne A. L. D.   Okubo A.   Okazaki R.   Tachibana S.   Terada K.   Nakamura T.   Nagahara H.
Finding of Nitrogen-Rich Organic Material in Antarctic Ultracarbonaceous Micrometeorite **[#2239]**
An ultracarbonaceous micrometeorite (UCMM) has been investigated using isotope microscopy, FIB-SEM, STXM, and TEM. C- and N-XANES spectra of N-rich organic region in the UCMM were similar to those of several Comet Wild 2 dust particles.

Engrand C.   Dobrică E.
Bulk Oxygen Isotopic Composition of Antarctic Micrometeorites: Effect of Atmospheric Entry **[#2636]**
The bulk O isotopic compositions of Antarctic micrometeorites are broadly compatible with that of carbonaceous chondrites, but systematic heavy O isotopic enrichments due to atmospheric entry were observed in partially melted particles.

Baecker B.   Cordier C.   Folco F.   Trieloff M.   Cartwright J. A.   Ott U.
Noble Gas Inventory of Micrometeorites from the Transantarctic Mountains **[#1824]**
We have initiated a comprehensive survey of noble gases (He, Ne, Kr, Ar, and Xe) in micrometeorites (MMs) at the MPIC, Mainz. At present, we have obtained noble gas results for 11 MMs. Solar wind and spallogenic contributions are evident in some MMs.

Yano H.   Hirai T.   Olamoto C.   Fujii M.   Tanaka M.   IKAROS-ALADDIN Team
The Multiple Round Trip Measurement of Cosmic Dust Flux Completed by Ikaros-Aladdin in the Inner Planetary Region **[#1632]**
ALADDIN onboard the IKAROS solar sail detected >2500 dust impacts in 16 months. It made ~1.5 round trips between Earth and Venus orbits and unveiled the finest dust flux above 1 μm in the region compared to records of 1970–1990s.

SECONDARY PROCESSES IN CHONDRITES

Lindgren P.   Lee M. R.   Sofe M.
Evidence for Multiple Fluid Pulses in the CM1 Carbonaceous Chondrite Parent Body **[#1949]**
We have studied the two Antarctic CM1s, MET 01070 and SCO 06043, to determine if multiple episodes of fluids can be observed and if we can distinguish between pre- and postterrestrial alteration products.

Jilly C. E.   Huss G. R.
Heterogeneous Aqueous Alteration in the CR2 Chondrite Renazzo **[#1348]**
We examine the aqueous alteration of CR2 chondrites and report on phosphates, sulfides, and other phases present in Renazzo. Various styles of alteration present in close proximity may suggest localized variations in conditions on the CR parent body.

Islam M. A.   Ebihara M.   Kojima H.
Chemical Compositions and Alteration of Primitive Carbonaceous Chondrites **[#1974]**
Chemical compositions of CI and CM/C2 chondrites were determined to study chemical alteration and thermal metamorphism experienced by them based on their volatile-element loss.

Mikouchi T.   Zolensky M.   Satake W.   Le L.
The Valence of Iron in CM Chondrite Serpentine as Measured by Synchrotron XANES **[#1496]**
We report synchrotron XANES analysis of serpentines in CM chondrites to estimate their ferric/ferrous iron ratios. Although we selected samples showing wide ranges of alteration degrees, all samples gave ~80% ferric ratios.

Jones R. H.   McCubbin F. M.
Phosphate Mineralogy and the Bulk Chlorine/Fluorine Ratio of Ordinary Chondrites **[#2029]**
Average Cl/F ratios in apatite from individual H and LL chondrites are much higher than bulk Cl/F ratios for ordinary chondrites. Either bulk F in OCs is poorly known, or F is present in other phases in addition to apatite.

Goreva Y. S.   McCoy T. J.
Is the Difference Between CVox and CVred a Function of Oxygen Fugacity? **[#2470]**
Our results show that reduced and oxidized CV chondrites were altered under very similar oxygen fugacity as calculated from composition of metal-magnetite pairs.

Bunch T. E.   Wittke J. H.   Irving A. J.   Kuehner S. M.
Estimation of Petrologic Subtypes of Unequilibrated Ordinary Chondrites from Systematics of Chromium Distribution in Ferroan Olivine **[#2193]**
We refine the systematics of fayalite and chromium contents of olivine within unequilibrated ordinary chondrites as a means of estimating petrologic subtypes and gauging their progressive thermal metamorphism.

Simon S. B.   Sutton S. R.   Grossman L.
Effects of Metamorphism on the Valence and Coordination of Titanium in Ordinary Chondrites **[#2078]**
We have undertaken a study of L and LL chondrites of grades 3–6 to see how Ti valence and coordination vary with grade and to see if the variations can be used to constrain conditions of chondrite metamorphism.

Ibrahim M. I. Hildebrand A. R.
The Elastic Properties of Carbonaceous Chondrites **[#2859]**
The elastic properties of carbonaceous chondrites indicate variation with petrologic type similar to that found in the ordinary chondrites, and apparently record damage from relatively frequent collisions with still weaker objects.

Izawa M. R. M. Moser D. E. Barker I. R. Flemming R. L. Gainsforth Z. Stodolna J. Matveev S. Banerjee N. R.
Exploring the Distribution and Nature of Shock Deformation in an Enstatite Chondrule at Submicron Resolution by a Combination of CL, Electron Backscatter Diffraction, EDS Mapping and EPMA **[#2735]**
EBSD, CL, EDS and EPMA investigations of shock-deformed enstatite in MET 00783 (EH4, S4) reveal microstructures including heterogeneous lamellar fabrics corresponding to subtle differences in Kikuchi band contrast, and amorphous feldspathic material.

Varga T. N. Bérczi Sz. Varga T. P.
Study of Thermal Metamorphism of Chondrites by Diffusional Fading of Chondrule Rims of Antarctic NIPR Meteorite Samples **[#1558]**
We studied the diffusion process in four Antarctic meteorite sample textures (L3, L4, L5, and L6 chondrites) by optical microscopy and diffusion calculations of diffusion length and times.

Miyamoto M. Kaiden H.
Maximum Temperature of Parent-Body Thermal Metamorphism for ALH 77299 (H3.7) Chondrite by Analyzing Fe-Mg Zoning of Olivine **[#1082]**
We studied maximum temperature of thermal metamorphism in the parent body for ALH77299 (H3.7) chondrite by fitting the calculated Fe-Mg zoning of olivine to observed one. The result for 600°C shows the best fit.

Friedrich J. M. Rubin A. E. Swindle T. D. Isachsen C. E. Beard S. P.
Impact Histories of Incompletely Compacted Ordinary Chondrites from Petrographic Examination and $^{40}Ar/^{39}Ar$ *Analysis* **[#1199]**
We show some petrographic evidence suggesting that incompletely compacted chondrites experienced some level of shock loading despite their poorly compacted nature. We use ^{40}Ar-^{39}Ar data to elucidate the timing of these shock episodes.

Hanna R. D. Ketcham R. A. Hamilton V. E.
Inclusion Foliation in Murchison as Revealed by High Resolution X-Ray CT **[#1242]**
Using high-resolution X-ray computed tomography we have found evidence for a preferred orientation, consistent with flattening, of a group of inclusions in a sample of CM2 Murchison chondrite.

Bérczi Sz. Nagy Sz. Gyollai I. Józsa S. Havancsák K. Dankházi Z. Varga G. Ratter K. Pál-Molnár E. Fintor K. Gucsik A.
EBSD Studies of Ringwoodite Microcrystalline Fabrics in the Shocked NWA 5011 L6 Chondritic Meteorite **[#1332]**
EBSD measurements on a 2 mm × 2 mm sample of the shocked, veined NWA 5011 L6 chondrite showed that the optically homogeneous large ringwoodite minerals in the veins consist of 2–5 µm sized, variously oriented micrograins.

Dyl K. A. Bland P. A. Muxworthy A. R. Collins G. S. Davison T. M. Prior D. J. Ciesla F. J.
Compositional Effects of Low-Pressure Impacts in Chondritic Meteorites: Oxygen Isotope Homogenization and Mg-Fe Diffusion in Matrix Olivine and Presolar Grains **[#2251]**
Recent work has explored the effects of low-intensity impacts into porous chondrite precursors. We show oxygen-isotope homogenization of presolar grains and Mg-Fe diffusion in fine-grained matrix are potential consequences of this process.

Xie Z.   Li X.   Sharp T. G.   De Carli P. S.
Shock-Induced Ringwoodite Rims Around Olivine Fragments in Melt Vein of Antarctic Chondrite GRV022321: Transformation Mechanism **[#2776]**
We study the formation of ringwoodite via diffusion at high temperatures and shock pressures in GRV022321 chondrite by using FIB/TEM techniques. The result suggests transformation occurred by a solid-state mechanism, enhanced by extreme deformation.

Acosta T. E.   Scott E. R. D.   Sharma S. K.
Micro-Raman Mapping of Mineral Phases in the Strongly Shocked Taiban Ordinary Chondrite **[#2725]**
Micro-Raman mapping of a thin-section of the highly shocked Taiban meteorite revealed new minor phases around the ringwoodite grains. These phases include wadsleyite and olivine surrounded by pyroxene and majorite.

De Carli P. S.   Xie Z.   Trickey R.   Hu J.   Weaver C. A.   Sharp T. G.
High-Pressure Minerals in RC106 Provide Evidence for a Very Large Impact **[#2877]**
Thermal analysis of a large vein in RC106 indicates that the vein solidified in about 3.3 sec at a pressure in the range of 15 to 25 GPa. Hydrocode calculations indicate that a very large impact with a 100 km diameter body is required.

Keller L. P.   McKeegan K. D.   Sharp Z. D.
The Oxygen Isotopic Composition of MIL 090001: A CR2 Chondrite with Abundant Refractory Inclusions **[#2065]**
The whole rock oxygen isotopic composition of MIL 090001 shows that it is a new member of the CR chondrite group. MIL 090001 is anomalous for a CR chondrite because of its high modal abundance of refractory inclusions compared to other members of the CR group.

Hoffmann V. H.   Hochleitner R.   Kaliwoda M.   Torii M.   Funaki M.   Mikouchi T.
Magnetic Signature of E Chondritic Lithologies of Almahata Sitta and Comparison with Neuschwanstein (EL6) **[#2342]**
The aim of our investigations is to compare mineralogy/chemistry/petrology and specifically the magnetic signature of E-chondritic lithologies of Almahata Sitta with the properties of known E-chondrite falls such as Neuschwanstein.

Meier M. M. M.   Schmitz B.   Alwmark C.   Maden C.   Wieler R.
The Ghubara (L5) Regolith Breccia as a Sample of the Source-Rock of Fossil Micrometeoritic Chromite Found in Ordovician Sediments **[#1131]**
Chromite grains extracted from the L chondrite regolith breccia Ghubara (L5, Ar-Ar-age: 470 Ma) show a similar ^{21}Ne-cosmic ray exposure (CRE) age distribution as fossil Ordovician micrometeorites. We report a new CRE age for Ghubara of only ~7 Ma.

Nishiizumi K.   Caffee M. W.
Exposure Histories of CI1 and CM1 Carbonaceous Chondrites **[#2758]**
We have extended our investigation of the cosmic ray exposure age distribution of CM2 to those CI1 and CM1 meteorites that have a high degree of aqueous alternation.

Welten K. C.   Caffee M. W.   Nishiizumi K.   Leya I.   Dalcher N.   Vogel N.   Wieler R.
Cosmogenic Radionuclides in Ordinary Chondrite Falls Selected for Calibration of the ^{81}Kr-Kr Method **[#2867]**
We present cosmogenic radionuclide results in the metal and stone fractions of 14 ordinary chondrites to calibrate the ^{81}Kr-Kr exposure age method using independent ^{36}Cl-^{36}Ar ages.

Strashnov I.   Gilmour J. D.
Cosmic Ray Exposure History of Individual Chondrules from Allegan H5 Ordinary Chondrite Probed by ^{81}Kr-Kr Chronometer **[#1820]**
The chondrules of the Allegan H5 chondrite have been separated from matrix. ^{81}Kr-Kr cosmic ray exposure ages of individual chondrules and separately the matrix have been determined.

THU POSTERS

Kubovics I.   Vizi P. G.
Trajectory and Analysis of Fireball-Meteorite "2010.02.28 Kosice" from Security Cameras and from Electomicroscopic Examination **[#2816]**
We show our investigation about the 2010.02.28. fireball and meteorite Košice. Included trajectory analysis from security cameras (meteorite cameras were off because of cloudy sky) and detailed electronmicroscopic examination of meteorite.

LOW-TEMPERATURE AQUEOUS MARTIAN GEOCHEMISTRY

Pritchett B. P.   Elwood Madden M. E.   Madden A. S.
Salinity and Temperature Effects on the Dissolution of Natrojarosite and K-Jarosite **[#2331]**
This study examines the effects of activity of water on the dissolution rates and the lifetimes of Na- and K-jarosite. It found that jarosite dissolution rates and particle lifetimes are extended in high salinity brines compared to dilute fluids.

Zahrai S. K.   Elwood Madden M. E.   Madden A. S.   Rimstidt J. D.
Comparing Na-Jarosite and K-Jarosite Dissolution Rates to Determine the Effects of Crystal Chemistry on Jarosite Lifetimes **[#1658]**
In this study, Na-jarosite dissolution experiments were conducted and compared to previous K-jarosite results. By comparing these two phases, the effect of crystal chemistry on jarosite dissolution rates can be determined.

Madden A. S.   Elwood Madden M. E.   Rimstidt J. D.   Kendall M. R.
Time-Course Mineralogy and Texture of Nanoscale Jarosite Dissolution Products **[#1684]**
Investigation of jarosite dissolution reaction products with AFM, SEM, TEM, and XRD demonstrated patterns indicative of reaction progress and solution conditions.

Sansano A.   Sobron P.   Sanz J. A.
Evaporation Pathways and Solubility of Fe-Ca-Mg-Rich Salts in Acid Sulfate Waters. A Model for Martian Ancient Surface Waters **[#2862]**
In this work we have characterized a layered deposit formed from the evaporation of stream water from Rio Tinto, Spain, a relevant Mars analog site. The minerals detected in-situ, confirmed later via high resolution Raman spectroscopy.

Sansano A.   Medina J.   Rull F.
Identification of Iron Sulfates by Raman Spectroscopy. Outcomes on the Missions to Mars **[#2784]**
Identification of iron sulfates by Raman spectroscopy using synthetic sulfates and sulfates from analogs. The results obtained with this technique on the Exomars mission could give us new data about the sequence of formation of the sulfate system on the brines of Mars and their possible implication in the habitability of that environment.

Rao M. N.   Nyquist L. E.   Ross D. K.   Asimow P. D.   See T.   Sutton S.   Cardenas F.
Montes R.   Cintala M.
Laboratory Shock Experiments on Basalt — Iron Sulfate Mixes at ~40–50 GPa and Their Relevance to the Martian Regolith Component Present in Shergottites **[#2102]**
By conducting laboratory shock experiments, we demonstrate the plausibility of iron sulfate reduction to sulfides in martian meteorites by shock.

Fortes A. D.   Browning F.   Wood I. G.
Ionic Substitution in Meridianiite ($MgSO_4 \cdot 11H_2O$): Solid Solutions and Novel Hydrates **[#1024]**
We report on an extensive study of chemical substitution in magnesium sulfate undecahydrate (meridianiite); our results may have application to the chemistry and hydration state of sulfates on Mars.

THU POSTERS

Dehouck E.   Chevrier V. F.   Gaudin A.   Mangold N.   Mathé P.-E.   Rochette P.
Experimental Weathering of Silicates and Sulfides in CO_2 Atmospheres: Implications for Sulfates Versus Carbonates on Mars **[#2621]**
We present the results of a 4-year-long experiment in which silicates and silicate/sulfide mixtures were weathered under CO_2 atmospheres, and the implications of these results about the formation of carbonates and sulfates at the martian surface.

Weber I.   Böttger U.   Jessberger E. K.   Hübers H. W.   Pavlov S. G.   Schröder S.   Tarcea N.   Dörfer Th.
Raman Spectroscopy of Mars Relevant Minerals for Planetary Exploration **[#1793]**
Different natural minerals are investigated by Raman under various temperature, pressure, and atmosphere conditions. Most of the minerals show at least one temperature dependent shift in the spectra.

Sutter B.   Ming D. W.   Niles P. B.   Golden D. C.
The Geochemical Alteration History of Clovis Class Rocks in Gusev Crater as Determined by Ti-Normailized Mass Balance Analysis **[#1518]**
Clovis rocks were exposed to high aqueous activity that resulted in the loss of 20–65% of pyroxene and feldspar, which was followed by periods of lower aqueous activity that allowed for Mg, Si, Ca, S, and Cl additions.

Viviano C. E.   Moersch J. E.   McSween H. Y.
Spectral Evidence for the Carbonation of Serpentine in Nili Fossae, Mars **[#2682]**
Spectral analysis of Nili Fossae phyllosilicates reveals evidence for the presence of talc (not saponite) and mixed-layer clay. These findings provide further evidence that carbonation of serpentine is the formation mechanism for carbonates on Mars.

Hicks L. J.   Bridges J. C.   Gurman S. J.
Ferric Iron Content of Nakhlite Hydrothermal Minerals **[#2253]**
Fe-K XANES absorption edge positions are correlated with ferric-ferrous ratios. This allows us to determine the oxidation state of the phyllosilicate (mixed ferric and ferrous) and amorphous gel (ferric) in the Lafayette nakhlite.

Gainey S. R.   Hausrath E. M.   Hurowitz J. A.
Kinetics of Nontronite Dissolution and Implications for Mars **[#2383]**
The clay mineral nontronite, which forms in liquid water, has been detected on Mars. Our dissolution rates of notronite were slow relative to basalt. Nonstoichiometric dissolution preferentially removed Al relative to the parent material.

Golden D. C.   Ming D. W.   Hausrath E. M.   Morris R. V.   Niles P. B.   Achilles C. N.   Ross D. K.   Cooper B. L.   Gonzalez C. P.   Mertzman S. A.
Dissolution of Olivine, Siderite, and Basalt at 80°C in 0.1M H_2SO_4 in a Flow Through Process: Insights into Acidic Weathering on Mars **[#2521]**
The object of this research is to determine acidic dissolution rates of olivine, siderite, and basaltic materials at 80°C using a flow-thru reactor and to characterize the weathering products.

Crouse C. B.   Bish D. L.
Acid-Sulfate Alteration of Montmorillonite and Nontronite Under Mars-Relevant Conditions **[#2283]**
Exposure of montmorillonite and nontronite to low-pH Fe- and Mg-sulfate solutions produced material resembling opal-CT in only the lowest pH experiments and only for nontronite. Montmorillonite is comparatively much more stable in these solutions.

Tu V.   Hausrath E. M.
Dissolution Rates of Amorphous Al- and Fe-Phosphates and Their Relevance to Mars **[#2609]**
Phosphorous is crucial for life on Earth and if life has ever existed on Mars it may also have required phosphorous. Measuring dissolution rates of amorphous Al- and Fe-phosphates likely constrains the bioavailability of P for life in martian soils.

Adcock C. T. Hausrath E. M.
The Dissolution Rate of Whitlockite and Implications for the Habitability of Early Mars **[#2446]**
Phosphate is an essential element for life. The dissolution rate of whitlockite indicates that phosphate minerals common to Mars may dissolve faster than common terrestrial phosphates. This has implications for the habitability of the planet.

Zhao Y. S. McLennan S. M.
Experimental Constraints on Partitioning Behavior of the Halogen Elements During Sedimentary Processes on Mars: A Progress Report **[#1958]**
We make a progress report on our experimental investigation of possible controls on Cl and Br partitioning behaviors during sedimentary processes on Mars, including evaporative, diagenetic, and photochemical processes relevant to martian conditions.

Clark A. S. Cull S. C.
Mapping the Distribution of Perchlorates on the Martian Surface at the Phoenix Landing Site **[#2171]**
Mapping the distribution of perchlorates near the Phoenix landing site is accomplished using the Phoenix's Surface Stereo Imager (SSI). Images were chosen for analysis based on the trenching activity of the Phoenix's Robotic Arm.

MARS FLUVIAL

Howard A. D. Moore J. M.
Enigmatic Valley in Northern Arabia: 800 km Long, Constant Width, Undulating Profile, and No Tributaries **[#1106]**
This unnamed Arabian valley may have been formed subglacially as a tunnel valley. It formed near the Noachian-Hesperian boundary and suggests ice coverage of much of Arabia at this time.

Williams R. M. E. Chuang F. C.
Mapping of Sinuous Ridges in Oxia Palus, Mars: New Insight into the Aqueous Record **[#2156]**
New geomorphic mapping of sinuous ridges and associated features (inferred preservation styles of valley networks) reveals correlation of certain types with stratigraphic units and record of multiple periods of fluvial events in the Noachian.

Jacobsen R. E. Burr D. M.
Paleo-Fluvial Features in the Western Medusae Fossae Formation, Aeolis and Zephyria Plana, Mars: Elevations and Implications **[#2398]**
Sinuous ridges interpreted as inverted channelized flow features are classified, delineated, and measured. Gathering sinuous ridge elevations enable initial interpretations of relative stratigraphy and spatio-temporal history of fluvial processes.

Penido J. C. Fassett C. I.
Comparison of Small Valley Networks on Earth and Mars Through Scaling Laws **[#2274]**
Using HRSC DEMs, we measure small valley networks on Mars to determine whether scaling laws derived for valley systems on Earth adequately describe catchment and valley properties on Mars, and our data support earlier observations that they do not.

Peel S. E. Fassett C. I.
Central Pit Craters with Interior Valley Networks on Mars: Characteristics and Formation Processes **[#1250]**
Valley networks in central pit craters are examined to characterize their morphology and morphometry, assess their hydrology and formative conditions, and investigate the relationship of valley initiation to the formation of the host craters.

Rauhala A. I.   Kostama V.-P.
Origins and Age Constraints of the Palos Crater Floor Deposits and Tinto Vallis, Mars **[#2261]**
Our observations indicate that the previously hypothesized volcanic origin of Tinto Vallis is very unlikely. Palos crater records variety of events and it likely served as a conduit for water and material transfer from Hesperia to Amenthes Planum.

Goddard K.   Gupta S.   Warner N. H.   Kim J-R.   Muller J-P.
Transient Landscape Evolution in the Amazonian-Age Mojave Crater, Mars **[#1393]**
Mojave Crater likely records an unusual morphology that represents an early and transient stage of crater rim degradation by precipitation. We describe how the growth of catchment-fan systems on intracrater ranges influences crater rim evolution.

MARS GLACIAL, PERIGLACIAL, AND GROUNDWATER/ICE

Komatsu G.   Okubo C. H.   Wray J. J.   Gallagher R.   Orosei R.   Cardinale M.   Chan M. A.   Ormo J.
Small Mounds in Chryse Planitia, Mars: Testing a Mud Volcano Hypothesis **[#1103]**
Our ongoing investigation of small mound features in Chryse Planitia, Mars, using imaging and spectral data is in general agreement with a mud volcano hypothesis but some notable characteristics uncommon in terrestrial counterparts are identified.

Ivanov M. A.   Hiesinger H.   Erkeling G.   Reiss D.
Evidence for Effusive Mud Volcanism in Utopia Planitia on Mars **[#1490]**
In Utopia Planitia we have found features strongly resembling extensive flows of mud.

Nunes D. C.
A Survey of Southeastern Utopia Planitia with SHARAD Data **[#2233]**
Presented is a survey of SHARAD data over Utopia Planitia, Mars. Numerous subsurface reflectors are detected, and they likely reflect the interface between Elysium volcanic flows and the underlying Vastitas Borealis Formation.

Séjourné A.   Costard F.   Gargani J.   Soare R. J.   Fedorov A.   Marmo C.
Degradation of the Periglacial Landscape of Utopia Planitia Under Global Warming: Comparison Earth-Mars **[#1881]**
Our results show that the assemblage of landforms in UP indicates the presence of an ice-rich permafrost like on Earth. This permafrost was degraded during a relatively recent (< 10 Ma) high-obliquity periods of Mars inducing a major climate change.

Kerrigan M. C.   Osinski G. R.   Capitan R. D.   Barry N.   Blain S.   Van De Wiel M.
The Distribution and Stratigraphy of Periglacial Landforms in Western Utopia Planitia, Mars **[#2716]**
This study focuses on the largest periglacial unit identified in Western Utopia Planitia and aims to introduce a clearer understanding of the large-scale geographical context of the multiple episodes of periglacial activity on Mars.

Johnsson A.   Reiss D.   Hauber E.   Zanetti M.   Hiesinger H.   Johansson L.   Olvmo M.
Periglacial Mass-Wasting Landforms on Mars Suggestive of Transient Liquid Water in the Recent Past: Insights from Solifluction Lobes on Svalbard **[#2073]**
Superposition relationships of landforms suggest a young age for the lobes.Morphometric relationships and morphology suggest a solifluction origin that may indicate transient liquid water within the regolith in the recent past.

El Maarry M. R.   Kodikara J.   Markiewicz W. J.   Wijessoriya S.   Thomas N.
Modeling the Formation of Large Desiccation Polygons on Earth: Possible Relation to Intermediate-Sized Polygons on Mars and Implications to Mars Hydrology **[#1063]**
We present a pre-fracture model to constrain the models of formation of giant desiccation cracks on Earth as a possible analog to intermediate-sized (70–350 m large) polygons located in many impact craters on Mars.

Hecht M. H. Head J. W.
Stability of Shallow Buried Ice on Mars **[#2260]**
Measured column water abundances and the measured vertical distribution of the column are consistent with humidity measured by Phoenix, subsurface ice temperature at the Phoenix site, and a 40° latitudinal limit of ice stability.

Sizemore H. G. Zent A. P. Rempel A. W.
Ice Lens Formation and Unfrozen Water at the Phoenix Landing Site **[#2397]**
We employ numerical simulations of climate and soil-ice interactions to place quantitative constraints on the growth of segregated ice lenses at the Phoenix landing site, Mars.

Beach M. J. Head J. W. III
Debris-Covered Glacier Deposits in a Trio of Impact Craters in the Southern Mid-Latitudes of Mars: Evidence for Ice Accumulation and Intercrater Flow in Connected Concentric Crater Fill **[#1140]**
Three closely spaced craters offer a unique opportunity to study Amazonian intracrater and intercrater ice-related deposits and their evolution within adjacent and overlapping crater interiors in a narrow latitude band.

Souness C. J. Hubbard B.
Crevasse-Like Openings as Indicators of Flow in Martian Glacier-Like Forms **[#1070]**
Crevasse-like openings occur on some martian mid-latitude glacier-like forms. On Earth, the position and morphology of crevasses reflects a glaciers basal and flow characteristics. We extend this model to Mars to better understand martian ice flow.

Bernhardt H. Hiesinger H. Reiss D. Ivanov M. Erkeling G.
Possible Glacio-Fluvial Landforms in Southern Argyre Planitia, Mars: Implications for Glacier Thickness and Depositional Settings **[#1830]**
We conducted a detailed geomorphologic mapping and analysis of the southern rim of the Argyre basin, Mars. We reconstructed the glacial load potentially associated with esker-like ridges and propose new formation mechanisms for their surroundings.

Fastook J. L. Head J. W. III
Mid-Latitude Amazonian Glaciation on Mars: Controls on Accumulation and Glacial Flow Patterns **[#1296]**
A model of flow into a crater from episodic layering events driven by obliquity demonstrates that even at Amazonian temperatures, concentric crater fill can be formed in as little as 50 m.y., whereas flow from a single persistent layer takes 450 m.y.

Franchi F. Rossi A. P. Pondrelli M. Barbieri R.
Ancient Fluid Escape and Conical Mound Fields in Firsoff Crater, Arabia Terra (Mars) **[#1062]**
In this study we report the occurrence of a mounds field in the southern Arabia Terra and present data from the Firsoff crater and its neighborhood where the mounds are exposed within the hydrothermal equatorial layered deposits (ELDs).

Chuang F. C. Crown D. A.
Surface Textures on Martian Lobate Debris Aprons: Comparison of Regional Populations Using CTX Images **[#2235]**
Using CTX images, we are in the process of reevaluating surface textures identified and characterized in earlier studies of the major lobate debris apron populations on Mars.

Scanlon K. E. Head J. W.
Volcano-Ice Interactions Recorded in the Arsia Mons Fan-Shaped Glacial Deposits: Synthesis and Astrobiological Importance **[#2183]**
We have mapped the glaciovolcanic features in the Arsia Mons fan-shaped glacial deposit and assessed the astrobiological implications of their type and their distribution in time and space.

Berman D. C.   Crown D. A.   Joseph E. C. S.
Constraints on the Formation and Modification of Lobate Debris Aprons Through Categorized Crater Counts **[#1593]**
Compilation of crater counts using CTX images and analysis of SFD, coupled with categorization of crater morphologies, provides important insights into interpretation of the formation and modification of lobate debris aprons.

Atkins C. M.   Barlow N. G.
Impact Crater Morphologies as Indicators of Volatiles in Northeastern Arabia Terra, Mars **[#2122]**
We are investigating the influence of volatiles on impact craters in the northeastern quadrant of Arabia Terra, Mars. Preliminary results show high concentrations of morphologies indicative of subsurface volatiles at high latitudes.

Schon S. C.   Head J. W.
Decameter-Scale Pedestal Craters in the Tropics of Mars: Evidence for the Recent Presence of Very Young Regional Ice Deposits in Tharsis **[#1669]**
We document very small pedestal craters in the tropics of Mars.The characteristics of these small pedestal craters provide evidence that meters-thick ice accumulations existed in the tropical Tharsis region of Mars in the last few million years.

Skinner J. A. Jr.
Constraining the Origin of Pitted Cones in Chryse and Acidalia Planitiae, Mars, Based on Their Statistical Distributions and Marginal Relationships **[#2905]**
Despite the fact that pitted cones are common landforms in the martian northern plains, there is still ambiguity regarding their origin. This study addresses these ambiguities by assessing their spatial variations and marginal relationships.

Cull S. C.   Dundas C.   Mellon M. T.   Byrne S.
CRISM Observations of Fresh Icy Craters in Mid- to High-Latitudes on Mars **[#2145]**
Byrne et al. (2009) reported exposed ice in five new mid-latitude impact craters that had formed between HiRISE observations taken a few months to a few years apart. Here, we report on analyses of CRISM observations taken over these 13 fresh craters.

Bapst J.   Wood S. E.
The Long-Term Effects of Surface Frosts, Seasonal Atmospheric Water Variation and Ice Fraction-Dependent Thermal Conductivity on Martian Ground Ice **[#2808]**
We use a 1-D time-dependent model to simulate martian ground ice evolution over the past ~1 Myr. Our goal is to quantify and understand the effects of some known processes (see title) on ground ice growth/retreat rates.

Saper L. M.   Mustard J. F.
Orientations and Morphology of Linear Ridges in Nili Fossae: Mineralized Fracture Zones and Implications for Crustal Fluid Transport **[#1119]**
A total of 2283 ridges were mapped in Nili Fossae bedrock at CTX resolution. We propose that the ridges represent impact-generated fracture zones that facilitated fluid flow, were preferentially hardened, and exhumed by differential erosion.

Schon S. C.   Head J. W.   Fassett C. I.
Recent High-Latitude Resurfacing by a Climate-Related Latitude-Dependent Mantle: Constraining Age of Emplacement from Counts of Small Craters **[#1811]**
A chronology for the deposition of the latitude-dependent mantle is revealed by superposed crater densities, which show that the overall age and age trend of mantling deposits is consistent with first-order control by obliquity variations.

MARS POLAR PROCESSES

Dixon E. M.   Calvin W. M.   James P. B.   Cantor B. A.
New Observations of the Martian Northern Seasonal Cap Recession with MARCI **[#2798]**
Data from the 2008 north cap recession has been analyzed and compared to data from the 2000 recession. The recession rate was found to be very similar for the two years but the 2008 recession began earlier in the year compared to the 2000 recession.

Russell P. S.   Byrne S.   Pathare A.   Herkenhoff K. E.
Active Erosion and Evolution of Mars North Polar Scarps **[#2747]**
Four years of observations confirm that north polar scarps are highly active places. The distribution and rates of mass-wasting are presented and the link between powder avalanches and block mass-wasting is tested.

Mount C.   Titus T. N.
Time Evolution and Inter-Annual Variability of Seasonal Ice on the Mars Northern Polar Cap **[#1043]**
We explore the temporal density variations of Mars' NPSC and use ice depth and density estimates to constrain the CROCUS date for a specific location and compare it to the CROCUS dates from three previous Mars years.

Mellem B. A.   Brown A. J.   Kahre M. A.   Hollingsworth J. L.   Schaefer J. R.
Investigation of Asymmetric H_2O Ice Distribution During Northern Spring on Mars Using a Modified NASA Ames Global Climate Model **[#1724]**
We attempt to use the NASA Ames Global Climate Model to test whether a source of water ice in the location of residual ice deposits could lead to asymmetric condensation of water ice over the top of the residual ice cap.

Smith I. B.   Holt J. W.
The Northern Spiral Troughs of Mars as Cyclic Steps: A Theoretical Framework for Calculating Average Migration and Accumulation Rates **[#2116]**
We interpret the spiral troughs of the NLPD to be depositional forms of cyclic steps, features that have been well characterized on Earth. Within this framework we estimate migration rates for the troughs to be tens of millimeters per Mars year.

Steel L. E.   Holt J. W.
Characterization of Large-Scale Sequence Boundaries and Erosional Events Within the North Polar Layered Deposits, Mars **[#2355]**
This study examines large-scale erosional events in the north polar layered deposits in order to constrain their number, location, and extent. Based on radar stratigraphy, deposits are broken into three sequences bounded by unconformities.

Rodriguez J. A. P.   Tanaka K. L.   Platz T.
Types and Formational Mechanisms of South Polar Troughs, Mars **[#2613]**
Our investigation reveals three distinct morphologic types of south polar troughs, each with a distinct formational history involving unique modes of basement and atmospheric controls.

Cowan T. C.   Holt J. W.
Quantifying Accumulation Patters in the Uppermost North Polar Layered Deposits, Mars Using Internal Radar Stratigraphy **[#2834]**
We map radar reflectors in the upper portions of Gemina Lingula to quantify accumulation patterns in that region. Results show latitude dependent spatial patterns and agreement with recent climate models.

Milkovich S. M.
Correlating Images and Radar at the Surface of Promethei Lingula in the South Polar Layered Deposits of Mars **[#2587]**
Promethei Lingula contains numerous subsurface SHARAD radar reflectors; some of these reflectors intersect with the surface. The locations of such intersections are mapped and compared with images to determine which layers create radar reflections.

Milkovich S. M.   Byrne S.   Russell P. S.
Variations in Surface Texture of the North Polar Residual Cap of Mars **[#2226]**
The rough surface texture of the martian north residual ice cap shows quasi-periodic patterns. Spectral analysis of this texture allows us to map out variations in its orientation and size and look for processes controlling resurfacing of the cap.

Moore M. W.   Holt J. W.   Campbell B. A.
Internal Structure of the Domed Deposit Within Korolev Crater, Mars from Radar Sounding **[#2894]**
First radar investigation into the Korolev Crater on Mars. Korolev is a larger martian crater located near the north polar layered deposit and contains up to 1.8 kilometers of ice.

MARTIAN (ALLUVIAL) FANS AND (DEBRIS) FLOWS

Morgan A. M.   Beyer R. A.   Howard A. D.   Moore J. M.
The Alluvial Fans of Saheki Crater **[#2815]**
Characteristics of the Saheki Crater fans suggest that they formed during the late Hesperian to early Amazonian periods, possibly under conditions similar to those that were prevalent during the formation of fans in the Atacama Desert, Chile.

Johnsson A.   Reiss D.   Zanetti M.   Hauber E.   Hiesinger H.
Recent Debris Flow Deposits in a Pristine Impact Crater, Mars: Insights from Terrestrial Analogous on Svalbard **[#2111]**
We have identified well-preserved debris-flow deposits within a pristine crater on Mars. The deposits show several diagnostic features of being formed by water-bearing sediment flows. Crater retention age suggest a very young age for the deposits.

Wilson S. A.   Grant J. A.   Howard A. D.
Distribution of Intracrater Alluvial Fans and Deltaic Deposits in the Southern Highlands of Mars **[#2462]**
CTX images were used to expand on the previously mapped distribution of alluvial deposits in craters across the southern highlands of Mars. We identified 78 additional craters with fans or deltas in the study region from 0–360E between 0–40S.

MARS AEOLIAN PROCESSES

Rossman B.   Wilson R.   Schieber J.
Eolian Erosion Experiments on Soft Sedimentary Rocks — Measurements of Erosion Rates, Textural Observations, and Implications for Mars Rover Geology **[#2837]**
Eolian erosion experiment with various lithologies in a wind-chamber to assess abrasion rates in soft sedimentary rocks.

Howard A. D.   Spiga A.   Moore J. M.
The Deepest Basin on Mars is Formed by Aeolian Erosion **[#1105]**
The trough forming NW floor of Hellas Planita has been deepened by at least 1 km by wind erosion as evidenced by geomorphic evidence and mesoscale atmospheric modeling.

Lang N. P.   DeFazio E.   Schneider R.
Erosional Modification of Apollinaris Mons, Mars **[#2788]**
In this contribution we examine erosion that has occurred at Apollinaris Mons, Mars. The goal is to provide additional constraints on the evolution of this volcanic construct.

THU POSTERS

Statella T.   Pina P.   Silva E. A.
Automated Detection of Martian Dust Devil Tracks **[#1026]**
This is a novel method to detect martian dust devil tracks automatically in orbital images. It is mainly based on mathematical morphology and we present the results for 200 NA MOC and HiRISE images. The mean global accuracy was 92.02% ± 4.87%.

Reiss D.   Zanetti M.   Neukum G.
Multitemporal Observations of Identical Active Dust Devils on Mars with the High Resolution Stereo Camera (HRSC) and Mars Orbiter Camera (MOC) **[#2015]**
We present dust devil lifetimes and dust entrainment calculations based on retraced active dust devils observed by two different orbiter cameras with a time delay of 26 minutes.

Neakrase L. D. V.   McHone J.   Whelley P. L.   Greeley R.
Terrestrial Analogs to Mars: East-Central Saharan Dust Devil Tracks **[#2009]**
Seen abundantly on Mars, dust devil tracks are rare features on Earth due to the active surface processes. Using the publicly available images from Google Earth, we describe four sites in the east-central Saharan Desert (Libya, Chad, and Egypt).

Sullivan R.   Zimbelman J. R.   Greeley R.
Coarse-Grained Ripples on Earth and Mars: Field Studies and Wind Tunnel Experiments **[#2161]**
We report fieldwork and wind tunnel experiments investigating coarse-grained ripples (aeolian bedforms common at VL-2 and at both MER sites), and their sedimentary structures likely to be preserved in martian sedimentary rocks.

Berman D. C.   Balme M. R.
Investigations of Transverse Aeolian Ridges on Mars **[#1598]**
We are examining transverse aeolian ridges on Mars in terms of their morphology/morphometry, mapping surficial deposits, comparing their distribution with local/regional meteorology, topography, and composition, and their age and changes in time.

de Silva S. L.   Burr D. M.   Ortiz A.   Spagnuolo M.   Zimbelman J. R.   Bridges N. T.
Dark Aeolian Megaripples from the Puna of Argentina: Sedimentology and implications for Dark Dunes on Mars **[#2038]**
The sedimentology of aeolian dark gravel megaripples in the Argentinean Puna indicate local derivation from volcaniclastic bedrock. Their similarity to aeolian dark dunes on Mars suggests local derivation of dark aeolian sediment in Mars.

Burr D. M.   de Silva S. L.   Zimbelman J. R.   Bridges N. T.
Aeolian Dunes from Volcaniclastic Sediments: The Medusae Fossae Formation, Mars, and Andean Ignimbrites, Earth **[#1692]**
One hypothesis for the source of dark dune sediments on Mars is volcaniclastic sediments. Comparison between dark dunes in the western Medusae Fossae Formation and dark dunes derived from an Andean ignimbrite supports this hypothesis.

Das S.   Amara S.   Aclese D.   Castany D.   Prejean Cole T.   Jordan Z.   Schuman S.
Analysis of Aeolian Processes and Morphological Effects in the Medusa Fossae Region of Mars **[#1673]**
We look to measure specific dimensions of yardangs and determine whether the major to minor axis ratio correlates with thermal inertia. We suspect that the unique morphology of yardangs is essential to discover the ancient wind patterns of Mars.

Christian S.   Kocurek G.
Combining Mesoscale Wind Modeling with Dune Field Analysis to Constrain Modern Wind Regime, Hyperboreae Undae, Mars **[#1450]**
Wind modeling of Planum Boreum, Mars has been used to confirm that the unusual dune morphologies of Hyperboreae Undae are consistent with the modern wind regime. Dune orientations in this region can now be used to inform modeling efforts.

Fenton L. K. Michaels T. I. Beyer R. A.
Aeolian Sediment Sources and Transport in Ganges Chasma, Mars: Morphology and Atmospheric Modeling **[#2441]**
We present first results from aeolian bedform mapping and atmospheric modeling in Ganges Chasma that suggest (1) sand sources are widespread throughout the chasma and (2) saltation threshold friction velocities may be lower than expected.

Chojnacki M. Moersch J. E. Burr D. M. Wray J. J.
Valles Marineris Dune Fields: Sediment Pathways and Provenance **[#2444]**
We test the hypothesis that Valles Marineris dune fields are derived from multiple local sources. Supporting spectral, thermophysical, and morphological evidence for local provenance argues for a relatively low degree of sediment homogenization.

Cardinale M. Silvestro S. Komatsu G. Vaz D. A. Michaels T. I.
Evidences for Sand Motion in the Equatorial Region of Mars **[#2452]**
In this work we investigate HiRISE images that allow multi-temporal analysis of an erg in Herschel basin. We observed dune activity suggesting that the dark dunes in the studied area are movable under the present-day wind conditions.

Craddock R. A. Needell Z. A. Rose T. R.
Characteristics of Basaltic Sand: Size, Shape, and Composition as a Function of Transport Process and Distance **[#1460]**
We document the physical and geochemical changes that take place as basaltic materials are transported by a variety of geologic processes, including wind, water, and ice. We will present results from quantitative, microscopic, and SEM analyses.

Bandeira L. Saraiva J. Pina P. Marques J. S.
Evaluating Dune Delineation on Images from Mars **[#1988]**
The results produced by an automated approach to delineate dunes on high-spatial-resolution images of Mars are presented and evaluated by type of dune, showing that the methodology is robust, even for dune types poorly represented in the dataset.

Hayward R. K. Fenton L. K. Titus T. N.
Mars Global Digital Dune Database: Wind Direction Analysis in South Polar Region (MC-30) **[#1185]**
We discuss and compare wind directions, as derived from dune centroid azimuth, slipface, and wind streak observations in the south polar region of Mars. We also compare those groundbased wind directions to GCM-modeled wind directions.

ROVING ON MARS: CURRENT AND FUTURE SITES

Saper L. M. Allen C. C. Oehler D. Z.
Rover Exploration of Acidalia Mensa and Acidalia Planitia: Probing Mud Volcanoes to Sample Buried Sediments and Search for Ancient and Extant Life **[#1218]**
Mud volcanoes are provocative targets for exploration because they concentrate sedimentary materials from depth that are otherwise inaccessible to a rover. We propose a plan to explore possible mud volcanoes observed in Acidalia Planitia.

Schurmeier L. R. Heldmann J. L. Stoker C. McKay C. Davila A. Marinova M. Karcz J. Smith H. Wilhem M.
Characterization of a Mid-Latitude Ice-Rich Landing Site on Mars to Enable In Situ Habitability Studies **[#1271]**
We developed a set of criteria to rank landing sites for a Mars lander mission to study permafrost. We ranked sites based on the presence of polygonal ground, rock density and landing dangers seen in HiRISE images. An optimal landing site was found.

Weitz C. M.   Bishop J. L.
Investigation of Layered Sediments at a Proposed Future Landing Site in Ladon Valles **[#1243]**
We have identified candidate rover traverses and scientific targets within two proposed landing ellipses at the distal end of Ladon Valles. Both sites would enable potential access to sedimentary units of diverse morphologies and mineralogies.

Ruff S. W.
Evidence for an Extended Carbonate-Bearing Unit in the Columbia Hills of Gusev Crater, Mars **[#2898]**
Spectra from Mini-TES reveal outcrops on Haskin Ridge and boulders from McCool Hill that are spectrally intermediate between those of olivine-rich Algonquin and carbonate-rich Comanche outcrops, consistent with a larger carbonate occurrence.

Cole S. B.   Watters W. A.   Squyres S. W.
Structure of Husband Hill and the West Spur of the Columbia Hills, Gusev Crater **[#1134]**
We measure bedding plane orientations of outcrops across the West Spur and Husband Hill. The measured dips are steeper than the local topography, and are consistent with the hypothesis that the exposures drape an underlying structure.

Watters W. A.   Squyres S. W.
Pattern and Distribution of Shrinkage Fractures at Meridiani Planum **[#2915]**
We assess the significance of the pattern and distribution of shrinkage fractures at the Opportunity landing site in terms of the role of desiccation and mineral dehydration in the evolution of the Meridiani sandstones.

Li R.   Wang W.   Lin L.   Gong W.   Li D.   Wu R.   Meng X.   Matthies L. H.
Recent Topographic Mapping of the NASA MER 2003 Opportunity Landing Site Using HiRISE and Rover Imagery **[#2385]**
This abstract presents recent high-precision mapping and localization efforts at the Mapping and GIS Laboratory of The Ohio State University for the NASA 2003 MER mission, particularly the Opportunity rover.

Shaw A.   Arvidson R. E.   Wolff M. J.   Seelos F. P.   Wiseman S. M.   Cull S.
Determining Surface Roughness and Additional Terrain Properties: Using Opportunity Mars Rover Results to Interpret Orbital Data for Extended Mapping **[#1644]**
The Opportunity rover traverse is ideal for observing the relation between surface properties and orbital data because we have ground truth for a part of each orbital image. We use this information to make conclusions over extensive orbital coverage.

Fernando J.   Schmidt F.   Ceamanos X.   Pinet P. C.   Douté S.   Daydou Y.   Souchon A.
Martian Surface Photometry Properties from Orbit by CRISM/MRO at Gusev Crater and Meridiani Planum **[#1960]**
The physical parameters at the MER landing sites were estimated from retrieved surface BRDF by using CRISM multiangle images, correcting the atmospheric contributions and inverting the Hapke model. They were compared to Pancam photometric results.

MARS SCIENCE LABORATORY INSTRUMENT AND METHODS DEVELOPMENT

Anderson R. B.   Bell J. F. III
Correlations Between Multispectral Imaging and Compositional Data from the Mars Exploration Rovers and Implications for Mars Science Laboratory (MSL) Data Analysis **[#2284]**
We used several methods to seek relationships between Pancam multispectral observations and APXS and Mossbauer data. Gusev correlations were weak, but Meridiani was slightly better, likely because of lower dust cover and several outlier compositions.

Bell J. F. III   Malin M. C.   Caplinger M. A.   Ravine M. A.   Godber A. S.   Jungers M. C.
Rice M. S.   Anderson R. B.
Mastcam Multispectral Imaging on the Mars Science Laboratory Rover: Wavelength Coverage and Imaging Strategies at the Gale Crater Field Site **[#2541]**
We describe the multispectral imaging capabilities and science strategies of the Mars Science Laboratory rover "Curiosity" Mastcam multispectral imaging system, which can obtain color images in 13 medium or narrowband wavelengths from 445 to 1013 nm.

Bennett K. A.   Bell J. F. III   McConnochie T. H.   Wolff M. J.
Extending CRISM Spectral Coverage in Gale Crater Using THEMIS-VIS and HiRISE **[#2761]**
In this study, we investigate whether HiRISE color and THEMIS-VIS images can be used to identify clay and/or sulfate deposits at finer spatial scales and/or in areas not yet measured by CRISM within Gale Crater and elsewhere.

Fraeman A. A.   Arvidson R. E.   Ehlmann B. L.   McGovern J. A.   Milliken R. E.   Murchie S. L.   Seelos F. P.
Seelos K. D.
Increasing the Spatial Resolution of Oversampled CRISM Images at Gale Crater **[#2123]**
CRISM has gathered data which is oversampled in the along-track direction. We describe characteristics of these observations, discuss techniques for processing them, and highlight results from an oversampled observation acquired over Gale Crater.

Beyer R. A.   Kirk R. L.
HiRISE Photoclinometry of Final MSL Landing Sites **[#2694]**
We present the results of point photoclinometry on HiRISE images of three of the four finalist MSL landing sites. We also provide calibration to previous photoclinometry results and to slope information from stereo terrain models.

Parker T. J.   Golombek M. P.   Calef F. J. III   Hare T. M.
High-Resolution Basemaps for Localization, Mission Planning, and Geologic Mapping at Meridiani Planum and Gale Crater **[#2535]**
We recently updated the Opportunity location map to include Endeavour Crater, using CTX and HiRISE images at 25 cm/pixel (http://goo.gl/pSuFZ, http://goo.gl/ydjT2). A similar base mosaic is nearing completion for the Gale Crater landing site.

Fairen A. G.   Davila A.   Uceda E. R.   Dohm J. M.   Baker V. R.   McKay C. P.   Stokes C. R.
Glacial Paleomorphologies in Gale Crater, Mars **[#2182]**
We identify large-scale glacial morphologies in Gale Crater, Mars. We propose to use MSL instrumentation to search for and identify small-scale glacial features.

Yakovlev V. V.
The Ice Nature of the Gale Crater Central Structure **[#1454]**
Morphometric and other data substantiate the ice origin of the central structure of Gale Crater. It is offered as the mechanism of the considerable changes of the piezometric surface of the underfrost hydrosphere of Mars.

Golombek M. P.   Bellutta P.   Calef F. J. III   Fergason R. L.   Hoover R. H.   Huertas A.   Kipp D.   Kirk R. L.
Parker T. J.   Sun Y.   Sladek H. L.
Surface Characteristics and Traversability of the Gale Crater Mars Science Laboratory Landing Site **[#1608]**
Comparison of remote sensing data of Gale crater with the existing six landing sites on Mars allows predictions of likely surface characteristics at the Mars Science Laboratory landing site.

Newsom H. E.   Blaney D.   Wiens R. C.   Clegg S.   Lanza N.   Vaniman D.   Maurice S.   Gasnault O.   King P.
Bridges N.   Dyar M. D.   Melikechi N.   Blank J. G.   Cousin A.   Ollila A.   Baxter A.   Vasavada A.   Mangold N.
Le Mouelic S.   ChemCam Team
Operational Strategies for the ChemCam LIBS Experiment on MSL **[#2477]**
The ChemCam LIBS on the Mars Science Lab can analyze a single target (within an RMI image), producing a depth profile on a single point, rasters consisting of ~9 separate points, or a line of points to characterize fine-grain layered materials.

THU POSTERS

Cousin A.   Sautter V.   Fabre C.   Maurice S.   Wiens R.
ChemCam Technique: A Powerful Tool for Textural Comparison of DAG 476 Meteorite and Picritic Basalt **[#1841]**
ChemCam optical measurement will be blind for fine-grained textured rock. We test the capability of ChemCam to distinguish rocks with different grain size distribution using key elemental ratios.

Cousin A.   Forni O.   Sautter V.   Fabre C.   Maurice S.   Wiens R.
Classification of Non-Homogeneous Basalts Using Independent Component Analysis Technique for MSL/ChemCam Data **[#2891]**
Independent Component Analysis technique, concerning ChemCam data, is usually performed using calibration standards spectra, which are usually homogeneous compacted powders. Here we test the capability of this technique using heterogeneous basalts.

Gasnault O.   Mazoyer J.   Cousin A.   Meslin P.-Y.   Lasue J.   Lacour J.-L.   Ollila A.   Berger G.   Forni O.   Maurice S.   Wiens R.-C.   Clegg S.   Blank J.
Deciphering Sample and Atmospheric Oxygen Contents with ChemCam on Mars **[#2888]**
Use of oxgen line calibration with ChemCam, LIBS instrument on Curiosity, Mars.

Clegg S.   Lasue J.   Forni O.   Bender S.   Wiens R. C.   Maurice S.   Barraclough B.   Blaney D.   Cousin A.   DeFlores L.   Delapp D.   Dyar M. D.   Fabre C.   Gasnault O.   Lanza N.   Morris R. V.   Nelson T.   Newsom H.   Ollila A.   Perez R.   Sautter V.   Vaniman D. T.
ChemCam Flight Model Calibration **[#2076]**
ChemCam is an integrated Remote LIBS and remote micro-imager (RMI) on the Mars Science Laboratory Rover. This paper will describe the ChemCam flight model calibration and report the elemental accuracy, precision, and detection limits.

Thompson L. M.   King P. L.   Spray J. G.   Elliott B. E.   Gellert R.
Characterization of BT-2: Calibration Target for Mars Science Laboratory Alpha Particle X-Ray Spectrometer **[#2427]**
This work describes the ongoing effort to fully characterize BT-2 (the calibration standard for the APXS instrument onboard MSL) using a variety of techniques and instrumentation to aid in the interpretation of APXS data.

Yen A. S.   Bish D. L.   Blake D. F.   Vaniman D. T.   Treiman A. H.   Ming D. W.   Morris R. V.   Farmer J. D.   Downs R. T.   Chipera S. J.   Des Marais D. J.   Chen C. W.
Definitive Mineralogy from the Mars Science Laboratory CheMin Instrument **[#2741]**
CheMin is on its way to Mars to provide detailed, in situ measurements of mineralogy. Laboratory work with the flight hardware and related instruments characterize the performance capabilities.

Achilles C. N.   Ming D. W.   Morris R. V.   Blake D. F.
Effects of Kapton Sample Cell Windows on the Detection Limit of Smectite: Implications for CheMin on the Mars Science Laboratory Mission **[#2786]**
The CheMin IV laboratory instrument measured the detection limit of smectite in Kapton sample cells along with the effects of the Kapton diffraction peak for both hydrated and dehydrated smectite samples.

Minitti M. E.   McCoy T. J.
Assessing the Longwave Ultraviolet Fluorescent Characteristics of Martian Meteorites **[#2349]**
We investigate the occurrence and importance of mineral fluorescence in the martian meteorites utilizing 365-nm ultraviolet light. The results provide “ground truth” for observations that can be carried out by the MSL Mars Hand Lens Imager (MAHLI).

Maki J. N.   Thiessen D.   Pourangi A.   Kobzeff P.   Scherr L.   Elliott T.   Dingizian A.   St. Ange B.
The Mars Science Laboratory (MSL) Hazard Avoidance Cameras (Hazcams) **[#2828]**
The Mars Science Laboratory (MSL) Rover, scheduled to land on Mars on August 6th 2012 UTC, utilizes eight Hazard Avoidance Cameras (Hazcams). This abstract describes the MSL Hazcams.

McCanta M. C.   Dyar M. D.   Dobosh P. A.   Newsom H. E.
Using the LIBSSIM Program to Calculate Rock Composition: Testing the Potential of LIBS Analyses **[#1993]**
We use the LIBSSIM program to examine sampling strategies for the LIBS instrument (ChemCam) on MSL. Grain size, phase proportions, and numbers of analyses are investigated to determine the accuracy and precision of the calculated compositions.

Ozanne M. V.   Dyar M. D.   Carmosino M. L.   Breves E. A.   Clegg S.   Wiens R. C.
Comparison of Lasso and Elastic Net Regression for Major Element Analysis of Rocks Using Laser-Induced Breakdown Spectroscopy (LIBS) **[#2391]**
Results of using the LASSO (least absolute shrinkage and selection operator) and elastic net regression techniques for quantitative elemental analysis of rocks are compared.

Maurice S.   Cousin A.   Wiens R. C.   Gasnault O.   Parès L.   Forni O.   Meslin P.-Y.
Clegg S.   ChemCam Team
Laser Induced Breakdown Spectroscopy (LIBS) Spot Size at Stand-Off Distances with ChemCam **[#2899]**
First measurements of spot size for a Laser Induced Breakdown Spectroscopy (LIBS) experiment at Stand-off distances (MSL/ChemCam).

Carmosino M. L.   Breves E. A.   Dyar M. D.   Ozanne M. V.   Clegg S.   Wiens R. C.
Behavior of Feature Selection in LIBS Spectroscopy as a Function of Varying Distance and Data Pre-Processing **[#2285]**
This study uses the lasso approach to examine the importance of varying distance and data pre-processing (baseline subtraction) on results of multivariate elemental analysis of LIBS data on geological samples.

MARS WATER: OTHER

Birnie C.   Fueten F.   Stesky R.   Cheel R.   Rossi A. P.
Lithified Aeolian Bedforms as Evidence for Ancient Water Circulation in West Candor Chasma, Mars **[#1292]**
In West Candor Chasma, corrugated, curvilinear features (CCF) that display evidence of brittle deformation also display many characteristics common to aeolian dunes, suggesting they originated as dunes but were lithified by ancient water circulation.

Baioni D.   Sgavetti M.   Wezel F. C.
Karst Landforms in Northern Sinus Meridiani, Mars **[#1052]**
The abstract shows the results of geomorphologic study in great detail of the northern part of Sinus Meridiani. Here karst-like landforms are observed. Based on the kind and degree, three morpho-units are identified.

Morgan G. A.   Campbell B. A.   Carter L. M.   Plaut J. J.
Mapping the Three Dimensional Stratigraphy of the Amazonian Geological Record of Mars as Preserved in Elysium Planitia **[#2605]**
We have used SHARAD to map and characterize the range of Amazonian subsurface deposits preserved within Elysium Planitia. This has included identifying the relationships between outflow channel erosion, volcanic activity and aeolian deposition.

Erkeling G.   Reiss D.   Hiesinger H.   Ivanov M. A.   Bernhardt H.
Relief Inversion at the Deuteronilus Contact of the Isidis Basin, Mars: Implications for the Formation of the Isidis Interior Plains **[#2016]**
Valleys that occur on the Isidis exterior plains continue across the Deuteronilus contact and occur then as ridges. We propose a fluvio-glacial scenario for the formation of relief inversion at the Deuteronilus contact.

Golder K. B.   Gilmore M. S.
Evolution of Chaos Terrain in the Eridania Basin, Mars **[#2796]**
We performed a geomorphological analysis of the Eridania Basin in order to better understand the history of water and chaos in the region and to constrain models for chaos formation.

Iijima Y.   Goto K.   Minoura K.   Komatsu G.   Imamura F.
Exploring Sedimentological Evidence of an Ancient Ocean on Mars **[#1753]**
Distribution of boulders on surface of Mars, which can be altered by impact-induced tsunami, may become best candidates as the sedimentological feature of past existence of ancient ocean on Mars.

Salzman B. J.   Gafinowitz S.   Regnerus B.
Phyllosilicates in Nili Fossae **[#1995]**
This is an abstract about an area on Mars called Nili Fossae. It describes how we have found a way to locate phyllosilicates through geomorphology. Our analysis is based on the Jezero crater delta and geological features associated with it.

EDUCATION AND PUBLIC OUTREACH: MARS EXPLORATION

THU POSTERS

Shaner A. J.   Shipp S. S.   Wiens R. C.   Maurice S.   Gasnault O.   Newsom H.   Anderson R.
ChemCam Education and Public Outreach: Zapping the Public into Awareness of ChemCam, the Mars Science Laboratory, and Mars Science and Exploration **[#2835]**
The Chemistry and Camera (ChemCam) instrument EPO program utilizes a public website and educator professional development to capture the public's interest and imagination in Mars science and exploration.

Jones A. J. P.   Bleacher L. V.
Education and Public Outreach for the Mars Science Laboratory Curiosity Rover's Sample Analysis at Mars **[#2930]**
Poster summarizes the EPO goals and programs of the Sample Analysis at Mars (SAM) instrument.

Vizi P. G.
Simulated Mars Rover Model Competition 2011–-2012 **[#1825]**
This is a report about the organization and management of the Simulated Mars Rover Model Competition events of 2011 and 2012. Presented are results for 2011 and plans for 2012.

Aubele J. C.   Stanley J.   Grochowski A.   Jones K.   Aragon J.
Mars Curriculum for K–12 Science Education, 2nd Edition, Making Tracks on Mars Teacher Resource and Activity Guide **[#1266]**
A Mars K–12 curriculum, created by the New Mexico Museum of Natural History & Science, is now in 2nd edition DVD, approved by NASA educational review, 508 compliant to ensure accessibility for people with disabilities, and applicable to MSL.

Albin E. F.
Mars 2012: Opposition and Educational Opportunities at Fernbank Science Center **[#2045]**
On March 3, 2012, Mars reaches opposition and is well placed for public viewing. The opposition timeline and educational opportunities are considered, with emphasis on programs presented at the Fernbank Science Center in Atlanta, Georgia.

MARS ATMOSPHERE

Lognonne P.   Spiga A.   Hurst K.   Gabsi T.   Banfield D.   de Raucourt S.   Mimoun D.
Banerdt W. B.   Hecht M.
Martian Atmospheric Induced Micro-Seismic Noise Generation: Large Eddy Simulations **[#1994]**
The surface of planets with an atmosphere or ocean has continuous vibrations generated by the fluid envelop circulations and turbulences, generating a microseismic noise. This is estimated for Mars by modeling the interaction of large eddies.

Madeleine J.-B.   Head J. W.   Spiga A.   Dickson J. L.   Forget F.
A Study of Ice Accumulation and Stability in Martian Craters Under past Orbital Conditions Using the LMD Mesoscale Model **[#1664]**
The goal of this study is to better understand the climate conditions under which ice-related features present in impact craters formed, using geological observations and mesoscale climate simulations of the corresponding regions.

Soto A.   Mischna M. A.   Richardson M. I.
Climate Dynamics of Atmospheric Collapse on Ancient Mars **[#2783]**
Using a general circulation model (GCM), we investigate the details of the three-dimensional, time varying climate dynamics at the threshold for atmospheric collapse.

Chaffin M. S.   Chaufray J. Y.   Schneider N. M.   Stewart I.
Mars Express Measurements of Water Loss from Mars **[#2282]**
Mars Express Observations of hydrogen Lyman α are used to infer an escape rate of hydrogen, with implications for the time-integrated loss of water from the surface of Mars and the evolution of the martian climate.

Teodoro L. F. A.   Elphic R. C.   Hollingsworth J. I.   Haberle R. M.   Kahre M. A.   Eke V. R.   Roush T.   Marzo G. A.   Brown A. J.   Feldman W. C.   Maurice S.
Constraining the Mars General Circulation Model with Realistic Distributions of Polar Ice **[#2617]**
We constrain the Mars General Circulation Model with realistic distributions of polar ice drawn from the most recent MONS. We apply an image reconstruction algorithm to the epithermal neutron data with the aim of improving its spatial resolution.

Chevrier V. F.   Rivera-Valentin E. G.
Regolith Control of Atmospheric Water Vapor on Mars from Analysis of the Phoenix TECP Data **[#2370]**
Numerical modeling of mass and heat transfer in the martian regolith and analysis of the humidity and temperature data returned by the TECP onboard Phoenix show that the regolith probably controls the diurnal cycle through diffusion and adsorption.

Dickinson C. S.   Komguem L.   Whiteway J. A.
Clouds and Precipitation at the Phoenix Mars Lander Site **[#1916]**
Observations of clouds within the planetary boundary layer on Mars was made using the lidar on the Phoenix mission. A regular Sol-to-Sol pattern of cloud formation was observed to occur each night and completely dissipate before midday.

Sefton-Nash E.   Teanby N. A.   Calcutt S. B.   Hurley J.   Irwin P. G. J.
Detection and Mapping of Ice Clouds in Mars' Mesosphere **[#1817]**
We map ice cloud occurrence in Mars' mesosphere using > 2 Mars years worth of limb spectra acquired by the Mars Climate Sounder. We find two distinct seasonal regimes with short periods/latitudes of increased formation and limited longitudinal bias.

Santiago D. L.   Colaprete A.   Kreslavsky M.   Kahre M. A.   Asphaug E.
Cloud Formation and Water Transport on Mars After Major Outflow Events **[#2438]**
The triggering of a robust water cycle on Mars might have been caused by the gigantic flooding events evidenced by outflow channels. We use the Ames Mars General Circulation Model (MGCM) to test this hypothesis.

Barth E. L.   Farrell W. M.   Rafkin S. C. R.
Modeling Electric Field Generation in Martian Dust Devils **[#2794]**
We have added triboelectric dust charging physics to the Mars Regional Atmospheric Modeling System (MRAMS) in order to simulate the electrodynamics of dust devils and dust disturbances on Mars.

Baragiola R. A.   Dukes C. A.
Ozone Production by Colliding Dust in the Martian Atmosphere **[#2471]**
Laboratory studies show that ozone is produced by electrical discharges when rocks fracture. We propose that a similar process should occur in the collision of dust particles during dust storms in Mars and discuss implications.

THU POSTERS

INSIGHT: A PROPOSED MARTIAN GEOPHYSICS DISCOVERY MISSION

Banerdt W. B. Smrekar S. Alkalai L. Hoffman T. Warwick R. Hurst K. Folkner W. Lognonné P. Spohn T. Asmar S. Banfield D. Boschi L. Christensen U. Dehant V. Giardini D. Goetz W. Golombek M. Grott M. Hudson T. Johnson C. Kargl G. Kobayashi N. Maki J. Mimoun D. Mocquet A. Morgan P. Panning M. Pike W. T. Tromp J. van Zoest T. Weber R.
Wieczorek M. InSight Team
InSight: An Integrated Exploration of the Interior of Mars **[#2838]**
InSight is a proposed Discovery mission to Mars that will illuminate the fundamental processes of terrestrial planet formation and evolution by performing the first comprehensive surface-based geophysical investigation of Mars.

Van Hoolst T. Dehant V. Folkner W. Asmar S. Rivoldini A. Banerdt W. B.
Interior of Mars form Geodesy **[#2157]**
Within the InSight mission, the radioscience experiment RISE (Rotation and Interior Structure Experiment) determines Mars' length-of-day variations, precession, and nutation and constrains the interior structure and atmosphere.

Folkner W. M. Asmar S. W. Dehant V. Warwick R. W.
The Rotation and Interior Structure Experiment (RISE) for the InSight Mission to Mars **[#1721]**
The goals of the Rotation and Interior Structure Experiment (RISE) are to deduce the size and density of the martian core through estimation of the precession and nutation of the spin axis.

Spohn T. Grott M. Knollenberg J. van Zoest T. Kargl G. Smrekar S. E. Banerdt W. B.
Hudson T. L. HP^3 Instrument Team
INSIGHT: Measuring the Martian Heat Flow Using the Heat Flow and Physical Properties Package (HP^3) **[#1445]**
HP^3 is being developed for an application on the InSight mission to Mars, and the design is currently changed to increase the penetration performance of the instrument. If selected it will conduct the first heat flow measurement on Mars.

Grott M. Spohn T. Smrekar S. E. Banerdt W. B. Hudson T. L. Morgan P. v. Zoest T.
Kargl G. Wieczorek M. A.
InSight: Constraining the Martian Heat Flow from a Single Measurement **[#1382]**
If selected as a Discovery mission, InSight will land a geophysical station on Mars. We discuss what can be learned from a single heat flow measurement conducted at the candidate landing site in the Elysium region.

Panning M. P. Mocquet A. Beucler E. Banerdt W. B. Lognonné P. Boschi L. Johnson C. Weber R. C.
InSight: Using Earth Data to Demonstrate Inversion Techniques for Mars' Interior **[#1515]**
InSight is a proposed Discovery mission to deliver a seismometer package to the martian surface. Earth data from a single station is used to demonstrate the single-station techniques that will be used to constrain the interior structure of Mars.

Mimoun D. Lognonné P. Banerdt W. B. Hurst K. Deraucourt S. Gagnepain-Beyneix J. Pike T. Calcutt S. Bierwirth M. Roll R. Zweifel P. Mance D. Robert O. Nébut T. Tillier S. Laudet Ph. Kerjean L. Perez R. Giardini D. Christenssen U. Garcia R.
The InSight SEIS Experiment **[#1493]**
This abstract presents the design of the SEIS instrument, which is the main instrument of the InSight mission; the InSight mission has been pre-selected in the frame of the 2012 Discovery mission selection.

Robert O. Gagnepain-Beyneix J. Nebut T. Tillier S. Deraucourt S. Hurst K. Gabsi T. Lognonne P. Banerdt W. B. Mimoun D. Bierwirth M. Calcutt S. Christenssen U. Giardini D. Kerjean L. Laudet Ph. Mance D. Perez R. Pike T. Roll R. Zweifel P. SEIS Team
The InSight Very Broad Band (VBB) Seismometer Payload **[#2025]**
This paper exposes the last developments made on the martian VBB (very broad band seismometer) sensor made by an international consortium under the management of CNES, currently part of the core payload for the martian project InSight from JPL.

PLANETARY MISSION CONCEPTS

Szatkowski G. P.
ULA Rideshare to Support Lunar and Planetary Missions **[#1149]**
This provides the rideshare capabilities for EELVs. Details will be provided; launch operations; development schedules; and launch opportunities. Concept delivery missions using Rideshare will be suggested for the Moon, Mars, and NEOs.

Szentesi J.
Electro-Magnetic Propulsion System (EMPS) for Spacecrafts and Satellites **[#1202]**
The electro-magnetic propulsion system (EMPS) for driving satellites and other spacecraft has smaller mass, smaller volume, and more efficiency compared with the known systems applied in space technology.

Klesh A. T. Castillo-Rogez J. C.
Applicability of Nanosatellites to Deep Space Exploration **[#2326]**
We present recent work on the use of secondary nanospacecraft on deep space missions to provide in situ measurements in risky and inhospitable locations, including high science/high risk sites, like cometary vents, Enceladus' jets, and Io's volcanos.

Allton J. H. Allen C. C. Burkett P. J. Calaway M. J. Oehler D. Z.
Toward Lower Organic Environments in Astromaterial Sample Curation for Diverse Collections **[#2439]**
Changes in organic contamination control and monitoring at Johnson Space Center Astromaterials curation facilities, from Apollo to Hayabusa, are documented to support improvements for the diverse collections and future sample return missions.

McNutt R. L. Jr. Solomon S. C. Anderson B. J. Blewett D. T. Evans L. G. Gold R. E. Murchie S. L. Nittler L. R. Phillips R. J. Prockter L. M. Slavin J. A. Vervack R. J. Jr. Zuber M. T. MESSENGER Team
MESSENGER's Extended Mission **[#2422]**
MESSENGER is completing its primary one-year mission at Mercury. It has been selected for a one-year-long extension by NASA. We give an overview of the extended-mission science questions and the plans for carrying out the required observations.

Choo T. H. Perry M. E. Steele R. J. Nair H. Nguyen L. Skura J. F. Lucks M. Bedini P. D. Solomon S. C.
SciBox and Observation Planning for MESSENGER's Extended Mission at Mercury **[#1262]**
The MESSENGER spacecraft will begin its extended mission in March 2012 for one Earth year. The MESSENGER team has used SciBox software to rapidly develop a 12-month science observation packed operation schedule.

Stickle A. M. Banks M. E. Benecchi S. D. Bradley B. K. Budney C. J. Clark G. B. Corbin B. A. James P. B. Kumar K. O'Brien R. C. Rivera-Valentin E. G. Saltman A. Schmerr N. Seubert C. R. Siles J. V. Stockton A. M. Taylor C. Zanetti M.
VULCAN: A Concept Study for a New Frontiers-Class Venus Lander **[#1939]**
VULCAN is a concept study for a New Frontiers mission to Venus to analyze atmospheric and surface composition. The mission would provide ~1 hr of atmospheric descent data and ~2 hrs of surface measurements, including detailed imaging and chemistry.

Schmidt G. R. Landis G. A. Oleson S. R.
HERRO Missions to Mars and Venus using Telerobotic Surface Exploration from Orbit **[#1543]**
This paper presents concepts for human missions to the orbits of Mars and Venus that feature direct robotic exploration of the planets' surfaces via teleoperation from orbit.

Raftery M. Hoffman J. Klaus K.
International Space Station as an Exploration Platform for Deep Space **[#1448]**
We will introduce concepts for how ISS could be fully utilized to support exploration. Pressure on program budgets will only intensify the need to use existing assets to their fullest extent. Meaningful progress on exploration can be made using ISS.

Lester D. Klaus K. Hodges K. Ower C. Jasiobedzki P.
On-Orbit Telerobotics as a Strategy for Lunar Exploration **[#1417]**
On-orbit telerobotic control is a strategy for near-term lunar exploration, allowing astronauts near the Moon, ideally at EM L1/L2, low-latency control of surface assets. It provides real telepresence, and is highly extensible to other destinations.

Carmona Reyes J. A. Peters S. Herdrich G. Srama R. Schmoke J. Cook M. Matthews L.
Laufer R. Hyde T. W.
Multi Wall Carbon Nano Tubes as Material for a Space Elevator on the Moon **[#2106]**
In order to determine the effects that plasma has on Carbon Nano Tubes (CNTs), a gaseous electronics conference reference cell (GEC reference cell) is employed to investigate how they react under varying plasma environments.

Eubanks T. M.
Sample Return from Shackleton Crater with the Deep Space Tether Pathfinder (DSTP) **[#2870]**
The Deep Space Tether Pathfinder (DSTP), a 5000 km rotating tether, will demonstrate the scientific utility of planetary scale tethers by collecting and returning a surface sample from the floor of Shackleton Crater near the lunar south pole.

Vondrak R. R. Keller J. W. Chin G. Garvin J. B. Rice J. W. Petro N. E.
The Lunar Reconnaissance Orbiter: Plans for the Extended Science Phase **[#1931]**
Update of the Lunar Reconnaissance Orbiter mission detailing plans for the extended science phase.

Carpenter J. D. Fisackerly R. Pradier A. Houdou B. De Rosa D. Gardini B.
Science and Payload Activities in Support of the ESA Lunar Lander **[#1990]**
We report on the status of the ESA Lunar Lander mission, emphasizing related science and payload activities.

Látos T. Deák M. Bérczi Sz.
Landing Site Modelling for the Puli/Hunveyor-15 Lunar Rover Prototype **[#1748]**
The Team Puli Space first GLXP rover tests on the new ground-modeling table.

Stern S. A. Gladstone G. R. Horanyi M. Kutter B. Goldstein D. B. Tapley M.
Synthetic Lunar Atmosphere Experiments and Base Resupply Mission Concept **[#1008]**
We describe a mission concept called SLAM to generate temporary, artificial lunar atmospheres for experimentation. This concept also has important applications to supplying water to lunar outposts.

Crites S. Quintana S. Przepiórka A. Santiago C. Trabucchi T. Kring D. A.
Lunar Landing Sites that will Enhance our Understanding of Regolith Modification Processes **[#1086]**
As part of the LPI-JSC 2011 Lunar Exploration Summer Intern Program we conducted a global survey of the Moon to identify possible mission landing sites where regolith processes and weathering on anhydrous airless bodies could be studied.

Quintana S.   Crites S.   Przepiórka A.   Santiago C.   Trabucchi T.   Kring D. A.
Moscoviense Basin: A Landing Site to Study Science Goals Associated with Lunar Regolith Processes and Space Weathering **[#1215]**
Moscoviense Basin represents an exceptional site to study lunar regolith processes, including space weathering. The site proposed here provides access to a fresh crater, a lunar swirl, and both mare and highland surfaces, all within a 20 km radius.

Przepiórka A.   Crites S.   Quintana S.   Santiago C.   Trabucchi T.   Kring D. A.
Tycho Crater: A Potential Landing Site to Study a Diversity of Regolith Processes and Space Weathering **[#1387]**
The paper describes the potential landing site on the Moon, Tycho Crater, where four goals identified in the NRC 2007 report can be addressed. The work was produced during the 2011 LPI-JSC Lunar Exploration Summer Intern Program.

Trabucchi T.   Crites S.   Przepiórka A.   Quintana S.   Santiago C.   Kring D. A.
Identifying Regions of Interest Needed to Characterize the Diverse Physical Properties of the Lunar Regolith **[#1679]**
In the NRC 2007 report, Science Goal 7b states: "Determine the physical properties of the regolith at diverse locations of expected human activity." To respond to this goal we prioritized regions of interest on the Moon to defined potential landing sites.

Roberts C. E.   Blair D. M.   Lemelin M.   Nowka D.   Runyon K. D.   Paige D. A.
Spudis P. D.   Kring D. A.
The Potential for Volatiles in the Intercrater Highlands of the Lunar North Pole **[#1371]**
A mission concept for volatile exploration in the intercrater polar highlands near the lunar north pole.

George J. A.   Mattes G. W.   Rogers K. N.   Magruder D. F.   Paz A. J.   Vaccaro H. M.   Baird R. S.   Sanders G. B.
Smith J. T.   Quinn J. W.   Larson W. E.   Colaprete A.   Elphic R. C.   Suaris T. R.
RESOLVE Mission Architecture for Lunar Resource Prospecting and Utilization **[#2583]**
Design Reference Mission 2.2 is presented for proposed flight of the RESOLVE payload for lunar resource groundtruth and utilization. The rover/payload deploys on a ten day surface mission to the Cabeus Crater near the lunar south pole in May of 2016.

Tanaka S.   Mitani T.   Iijima Y.   Otake H.   Ogawa K.   Kobayashi N.   Hashimoto T.   Otsuki M.   Kimura J.
Kuramoto K.
Overview of Candidate Instruments On Board the Lunar Lander Project SELENE-2 **[#1651]**
We report on the updated status of investigation and development of candidate instruments onboard the SELENE-2 lunar landing mission.

Garrick-Bethell I.   Lin R.   Sanchez H.   Hemingway D.
Lunar Swirl Impactors: A Low-Cost Mission to Study Swirls, Magnetism, Water, Space Weathering, Dust, and Plasma Physics **[#2650]**
Releasing several cubesat probes into the heart of Reiner Gamma swirl can address a number of open problems in lunar science for very low cost.

Clark P. E.   Cox R.   Vassant A.   Scharfstein G.
LunarCube: A Concept for Advancing Solar System Exploration **[#1123]**
We propose LunarCube, an extension of the affordable and successful CubeSat approach to facilitate access to the Moon. CubeSat has already encouraged and increased access to Earth orbital space over the last five years.

Clark P. E.   Rilee M. L.   Curtis S. A.   Bailin S.
Evolving a Method to Capture Science Stakeholder Inputs to Optimize Instrument, Payload, and Program Design **[#1124]**
We are developing Frontier, a highly adaptable, stably reconfigurable, web-accessible intelligent decision engine capable of optimizing design as well as the simulating operation of complex systems in response to evolving needs and environment.

THU POSTERS

Chicarro A. F.
MNSM — A Future Mars Network Science Mission **[#1066]**
A Mars Network Science Mission of several surface stations is being studied by ESA, to investigate the interior of the planet, its rotational parameters and its atmospheric dynamics, which have not been fully addressed by previous Mars exploration.

Murchie S. L. Chabot N. L. Yen A. S. Arvidson R. E. Maki J. N. Trebi-Ollennu A. Wang A. Gellert R. Daly M. Rivkin A. S. Seelos F. P. Eng D. Guo Y. Adams E. Y.
MERLIN: Mars-Moon Exploration, Reconnaissance and Landed Investigation **[#2569]**
MERLIN, an orbital and landed investigation of Deimos, would begin landed robotic exploration of Mars' moons and of D-type bodies, and collect information valuable to the planning of future human exploration of the Mars system.

Blaney D. L. Staehle R. L. Betts B. Friedman L. Hemmati H. Lo M. Mouroulis P. Pingree P. Puig-Sauri J. Svitek T. Wilson T.
Interplanetary CubeSats: Small, low cost Missions Beyond low Earth Orbit **[#1868]**
Interplanetary CubeSats provide a platform for small low-cost missions beyond low-Earth orbit. The initial mission studied is an asteroid flyby with a small compact imaging spectrometer.

McCarthy J. F.
A Low Cost Approach to Close-Up Examination of Multiple Near Earth Asteroids **[#1016]**
A mission concept combining a small, inexpensive, but capable solar electric propulsion spacecraft with low cost launch vehicles to provide close-up examination of multiple near Earth asteroids within the cost cap of NASA's Discovery program.

Straub J. Fevig R. Borzych T. Church C. Holmer C. Komus A. Perrin T.
NEOSat: An Architecture for Small Interplanetary Craft Development **[#2797]**
Earth impactors may present the greatest natural threat to the Earth and its inhabitants. This paper describes a precursor mission at the University of North Dakota to test and validate technologies required for assessment of a near Earth object.

Bernal J. A. Wegel D. C. Nuth J. A. III
Harpoon-Based Sample Acquisition System **[#1182]**
A way to acquire core samples from low-gravity objects without the need for landing gear.

Barucci M. A. Michel P. Cheng A. Böhnhardt H. Brucato J. R. Dotto E. Ehrenfreund P. Franchi I. A. Green S. F. Lara L. -M. Marty B. Koschny D.
MarcoPolo-R: Near Earth Asteroid Sample Return Mission Selected for ESA Assessment Study Phase **[#1457]**
MarcoPolo-R is a sample return mission to a primitive near-Earth asteroid (NEA) selected in February 2011 for the assessment study phase at ESA in the framework of ESA's Cosmic Vision 2 program. MarcoPolo-R is a European-led mission with a proposed NASA contribution.

Klaus K. Lawrence S. .J. Elsperman M. S. Smith D. B. Horsewood J.
Innovative Stratiges for Asteroid Precursor Exploration **[#1441]**
We support technology advances to reduce the cost and increase the flight rate of planetary missions, while actively developing a scientific and engineering workforce to achieve national space objectives. This is a low-cost asteroid mission concept.

Smith D. B. Klaus K. Behrens J. Bingaman G. Elsperman M. Horsewood J.
Trojan Tour Enabled by Solar Electric Based Mission Architecture **[#2632]**
To the greatest extent possible, we will utilize the PS Decadal Trojan concept as a basis for examining the feasibility of a Solar Electric Propulsion (SEP) mission using a Boeing bus and Advanced Modular Power System (AMPS) solar power generation.

Nahm A. L. Potter S. L. Sayanagi K. M. Diniega S. Gil S. Balcerski J. Carande B. Diaz-Silva R. Fraeman A. A. Hudson J. S. Guzewich S. D. Livi R. Route M. Urban K. D. Vasisht S. Williams B. Budney C. J. Lowes L. L.
TASTER: Trojan ASteroid Tour, Exploration, and Rendezvous, a JPL Planetary Science Summer School Mission Design Exercise **[#2857]**
We present a mission concept to explore Trojan asteroids recommended by the Planetary Science Decadal Survey as target candidates for a future New Frontiers class mission.

Dougherty M. Grasset O. Erd C. Titov D. Bunce E. Coustenis A. Blanc M. Coates A. Drossart P. Fletcher L. Hussmann H. Jaumann R. Krupp N. Prieto-Ballesteros O. Tortora P. Tosi F. Van Hoolst T.
JUpiter ICy moons Explorer (JUICE): An ESA L-Class Mission Candidate to the Jupiter System **[#1806]**
JUICE is the next step for an in-depth exploration of the geophysical and environmental characteristics of Ganymede and exploration of Callisto and Europa, and will provide an in-depth understanding of Jupiter's atmosphere and magnetosphere.

Pappalardo R. T. Bagenal F. Barr A. C. Bills B. G. Blaney D. L. Blankenship D. D. Brinckerhoff W. Connerney J. E. P. Hand K. Hoehler T. Kurth W. McGrath M. Mellon M. Moore J. M. Prockter L. M. Senske D. A. Shock E. Smith D. E. Gavin T. Garner G. Magner T. Cooke B. C. Crum R. Mallder V. Adams L. Klaasen K. Patterson G. W. Vance S.
Mission Concepts for Exploring Europa's Habitability **[#1714]**
The Europa Science Definition Team reports on its study of three Europa mission concepts: a Europa orbiter, a Europa multiple-flyby mission, and a Europa lander.

Noll K. S. Simon-Miller A. A. Wong M. H. Choi D. S.
JESTR: Jupiter Exploration Science in the Time Regime **[#2007]**
We describe a mission concept for a dedicated space telescope designed to observe Jupiter at diffraction-limited resolution over a two-year mission. The small-scale sources of Jupiter's large-scale circulation will be studied in unprecedented detail.

Simon-Miller A. A. Lunine J. I. Atreya S. K. Spilker T. R. Coustenis A. Atkinson D. H. Colaprete A. Reh K.
Scientific Value of a Saturn Atmospheric Probe Mission **[#1114]**
A shallow Saturn probe mission can obtain the key noble gas and isotopic abundances, plus vertical abundance profiles for other constituents, critical to enabling a full comparison of composition and dynamical processes on Jupiter and Saturn.

Cabrol N. A. Grin E. A. Haberle C. Moersch J. E. Jacobsen R. E. Sommaruga R. Fleming E. D. Detweiler A. M. Echeverria A. Blanco Y. Rivas L. A. Pedersen L. Smith T. Wettergreen D. S. Demergasso C. Parro V. Fong T. Bebout L.
Planetary Lake Lander: Using Technology Relevant to Titan's Exploration to Investigate the Impact of Deglaciation on Past and Present Planetary Lakes **[#2147]**
The Planetary Lake Lander project deploys and remotely operates a lake lander to gain operational experience for future lake lander missions. Its scientific mission in the Chilean Andes is focused on the study of deglaciation.

Benfield M. P. J. Hakkila J. Blevins E. R. Turner M. W. Farrington P. A. Runyon C. J.
Cronus and Oceanus — Two Undergraduate Titan Lake Lander Mission Concepts **[#1660]**
Two student concepts for a Titan Lake Lander Mission.

INSTRUMENT AND PAYLOAD CONCEPTS

Reach W. T.
Stratospheric Observatory for Infrared Astronomy: First Full Proposal Call **[#2753]**
The Stratospheric Observatory for Infrared Astronomy had first light in 2010 and during 2011 performed its first series of scientific observations. The Cycle 1 proposal call, with a due date of January 27, 2012, solicits a full year of observing.

Anderson R. C. Nesnas I. A.
Enabling New Exploration Opportunities on Planetary Surfaces **[#2907]**
Recent water ice discoveries emanate from sites that are currently inaccessible for in-situ exploration. The rich science return has motivated the investigation of novel robotic explorers that would be able to access, measure and sample such sites.

Palmer E. E. Gaskell R. W. Vance L. D. Sykes M. V. McComas B. K. Jouse W. C.
Location Identification Using Horizon Matching **[#2325]**
We developed a system that autonomously determines a rover's location. It uses a digital elevation model derived from orbital imagery. Then, it finds the best match between the synthetic panoramas generated by the DEM and a rover's panoramic image.

Kooshesh K. A. Lineberger D. H.
Automated Thermal Sample Acquisition with Applications **[#2524]**
We created an Arduino®-based robot to detect samples subject to an experiment, perform measurements once each sample is located, and store the results for further analysis. We then relate the robot's performance to an experiment on thermal inertia.

Lo A. S. Trinidad M. Guilmette T. Segura T.
Using the Mars Ascent Vehicle as a Stand-Alone Sample Return System **[#1570]**
Northrop Grumman is participating in a Phase I study of a Mars Ascent Vehicle (MAV) design. As part of internal R&D, we conducted a feasibility study of using the MAV as a stand-alone sample return vehicle for the Moon. We discuss our results.

Iwata T. Matsumoto K. Ishihara Y. Kikuchi F. Harada Y. Sasaki S.
A Study on the Satellite-to-Satellite Tracking to Detect Mars Rotation Variations **[#1308]**
We plan the precise observations of Mars rotation using the Doppler measurements by satellite-to-satellite tracking (SST) for the Japanese future exploration for Mars: MELOS (Mars Exploration with Lander-Orbiter Synergy).

Sollitt L. S. Beegle L. W.
Off-Nadir LIDAR to Detect Bouguer Anomaly on Airless Worlds **[#1236]**
We present a concept for a novel LIDAR to detect Bouguer anomalies and associated mass concentrations beneath the surfaces of planetary bodies. Our approach uses off-nadir beams at large angles into and away from the spacecraft direction of motion.

Ismail S. Clancy R. T. Sharma S. K. Refaat T.
A 3-D Aerosol Profiling Lidar for Planetary Rover Missions **[#1540]**
A conceptual study is presented for an advanced three-dimensional profiling lidar for aerosols and clouds. This instrument will have a form factor suitable for future Mars and other planetary lander and rover missions.

Abedin M. N. Bradley A. T. Hibberd J. Refaat T. F. Ismail S. Sharma S. K. Misra A. K. Garcia C. S. Mau J. Sandford S. P.
Planetary Surfaces and Atmosphere Characterization Using Combined Raman, Fluorescence, and Lidar Instrument from Rovers and Landers **[#1219]**
Develop a remote Raman-fluorescence spectroscopy and LIDAR multi-sensor instrument capable for investigation and identification of minerals, organics, and biogenic materials as well as conducting atmospheric studies of Mars from rovers and landers.

Du H.   Wang A.
Raman Imaging of Extraterrestrial Materials **[#2221]**
We report the first Raman imagery study on a thin section of Apollo sample 14161-7062 and on a sawn rock slice from the new lunar meteorite Dhofar 1672, using a state-of-art Raman imaging system with five laser wavelengths.

Rull F. R.   Martinez Frias J.   Rodriguez-Losada J. A.   Sanz A.
A Micro Raman Study of the Erupted Pyroclasts from El Hierro (Spain) **[#2822]**
A Raman spectroscopic analysis has been performed on the recent volcanic materials erupted in October 2011 at the El Hierro Island (Spain). This analysis is at our knowledge the first Raman study performed on such pristine materials.

Blacksberg J.   Maruyama Y.   Choukroun M.   Charbon E.   Rossman G. R.
New Microscopic Laser-Coupled Spectroscopy Instrument Combining Raman, Libs, and Fluorescence for Planetary Surface Mineralogy **[#1510]**
We present a time-resolved laser spectroscopic technique that can collect microscopic Raman spectra as well as additional and complementary elemental information (LIBS, fluorescence), all with the same instrument.

Wang A.
In Situ Laser Raman Spectroscopy for Mars Sample Return Mission **[#2149]**
We describe the scientific advantages brought by the four characters of Mars Microbeam Raman Spectrometer (MMRS), thus demonstrate a powerful technology with high TRL for in situ mineralogy and biomarker detection for the first MSR mission in 2018.

Wiens R. C.   Maurice S.   Clegg S.   Sharma S.   Misra A.   Bender S.   Newell R.   Dallmann N.   Lanza N.   Forni O.   Lasue J.   Rull F.
Compact Remote Raman-LIBS Instrument for Mars or Titan **[#1699]**
A combined remote Raman and LIBS instrument is a natural outgrowth of ChemCam and the in situ Raman spectroscopy instruments currently being developed. It would be significantly lighter than ChemCam and would have the advantage of both techniques.

Schröder S.   Pavlov S.   Hübers H.-W.   Jessberger E. K.
LIBS Studies of Ferric Salts in Frozen Solutions Under Martian Conditions **[#1980]**
Laser-induced breakdown spectroscopy (LIBS) is capable of investigating pure salts and frozen salt solutions. Ferric chloride can be distinguished from ferric sulfate by applying multivariate data analysis methods.

Ishibashi K.   Arai T.   Wada K.   Kobayashi M.   Ohno S.   Senshu H.   Namiki N.   Matsui T.   Kameda S.   Cho Y.   Sugita S.
Analysis Method for Minerals with Laser-Induced Breakdown Spectroscopy (LIBS) for In-Situ Lunar Mineral Measurement **[#1786]**
We confirmed that the elemental composition of olivine and plagioclase are predicted with LIBS by using PLS regression. It is important to prepare reference samples with various physical properties to achieve high precision and accuracy.

Dobosh P. A.   Breves E. A.   Dyar M. D.   McCanta M.
LIBSSIM: Simulation of LIBS Sampling on Rock Surfaces **[#1480]**
A Javascript-HTML5 model has been built to simulate LIBS sampling of a rock surface. The model allows construction of arbitrary rock slabs of chosen grain size and laser beam size (both in pixels) and reports mineral and oxide percentages.

Lanza N. L.   Wiens R. C.   Newsom H. E.   McInroy R. E.   Clegg S.   Bender S. C.
A Preliminary Examination of Meteorites with Laser-Induced Breakdown Spectroscopy (LIBS) **[#2780]**
A suite of meteorites are measured under low vacuum conditions with Laser-Induced Breakdown Spectroscopy (LIBS).

THU POSTERS

Clegg S.   Sharma S. K.   Misra A. K.   Dyar M. D.   Dallmann N.   Wiens R. C.   Vaniman D. T.   Speicher E. A.   Smrekar S. E.   Wang A.   Maurice S.   Esposito L.
Raman and Laser-Induced Breakdown Spectroscopy (LIBS) Remote Geochemical Analysis Under Venus Atmospheric Pressure **[#2105]**
A remote Raman-LIBS spectrometer (RLS) is a rapid method to determine Venus surface chemistry and mineralogy without collecting samples and bringing them into the lander. The RLS results from 18 synthetic samples will be presented.

Hunter G. W.   Ponchak G. E.   Beheim G. M.   Scardelletti M. C.   Meredith R. D.   Taylor B.   Beard S.   Kiefer W. S.
The Development of a High Temperature Venus Seismometer **[#1259]**
This paper describes efforts to design, fabricate, and demonstrate a proof-of-concept seismometer operating at Venus temperatures. Seismometer design and fabrication are discussed, as well as preliminary results.

Noda H.   Kunimori H.   Araki H.   Fuse T.   Hanada H.   Katayama M.   Otsubo T.   Sasaki S.   Tazawa S.   Tsuruta S.   Funazaki K.   Taniguchi H.   Murata K.
Lunar Laser Ranging Experiment for SELENE-2 **[#1855]**
We present the development status of the Lunar Laser Ranging experiment proposed for the Japanese SELENE-2 lunar landing mission.

Morse A. D.   Barber S. J.   Dewar K. R.   Pillinger J. M.   Sheridan S.   Wright I. P.   Gibson E. K.   Merrifield J. A.   Howe C. J.   Waugh L. J.   Pillinger C. T.
Searching for Lunar Sater: The Lunar Volatile Resources Analysis Package **[#2320]**
The Lunar Volatile Resources Analysis Package is a provisional payload for the ESA Lunar Lander. It is designed to analyse the chemical and isotopic composition of volatiles extracted from rock samples and the tenuous lunar atmosphere.

Gerasimov M. V.
Gas-Analytic Package for the Russian Lunar-Resource and Luna-Globe Missions **[#2223]**
The paper describes the architecture of the Gas Analytic Package, which is now under development for the Russian Lunar-Resource and Lunar-Globe missions. The package is a combination of thermal analyzer, gas chromatograph, and mass-spectrometer.

Anderson F. S.   Nowicki K.   Hamilton V.   Whitaker T. J.
Portable Geochronology with LDRIMS: Learning to Date Meteorites like Zagami with the Boulder Creek Granite **[#2844]**
We demonstrate a rapid, portable in-situ dating technique on granite in preparation for dating lunar and martian materials.

Cohen B. A.
Development of the Potassium-Argon Laser Experiment (KArLE) Instrument for In Situ Geochronology **[#1267]**
How to date a rock? / Use potassium-argon / Or bring it flowers.

Young K. E.   Evans C. A.   Hodges K. V.
Evaluating Handheld X-Ray Fluorescence (XRF) Technology in Planetary Exploration: Demonstrating Instrument Stability and Understanding Analytical Constraints and Limits for Basaltic Rocks **[#2628]**
Handheld X-ray fluorescence instruments show great promise in enhancing the science return of planetary surface missions. Examining their stability and trace element detection limits is crucial in establishing this technology.

Jackson T. L.   Farrell W. M.   Bleacher J. E.
xPED: The Exploration Portable Electrostatic Detector **[#1545]**
The Exploration Portable Electrostatic Device (xPED) will allow astronauts to determine their charge state and characterize the electrical environment from their excursions. Testing at the DRATS site provided an opportunity to obtain new results.

Dove A. Robertson S. Wang X. Horanyi M.
Surface Effects on Photoelectron Sheath Characteristics **[#2421]**
Photoelectron sheaths are generated by shining ultraviolet radiation on Zr and CeO_2 surfaces. We use Langmuir probes to measure the electron density and temperature within the sheath and compare the results for the conducting and insulating surfaces.

Hobosyan M. A. Martirosyan K. S.
Sintering of Regolith by Activated Thermites: A Novel Approach for Lunar In-Situ Resource Utilization **[#1019]**
The concept of sintering of lunar regolith with activated thermites is provided. The thermodynamic calculations and experimental procedures are provided to demonstrate the effectiveness of new route of regolith sintering under the lunar environment.

Varga T. P. Szilágyi I. Bérczi Sz. Varga T. N.
Process for Producing Building Elements with Multilayer Structure from Lunar Regolith by Microwave Heating **[#1560]**
Arbitrarily large building elements can be created from lunar regolith, if the elements are produced layer by layer in a way that every layer is heated individually by microwave, and the newer layers are placed over the older ones.

Nagihara S. Zacny K. Hedlund M. Taylor P. T.
A Compact In-Situ Thermal Conductivity Probe as Part of a Lunar Regolith Excavation System **[#1135]**
We propose a design for a compact in situ thermal conductivity probe intended for lunar network geophysical missions. The probe is attached to the penetrating cone of the newly developed low-power, low-mass lunar regolith excavation system.

Skocki K. Seweryn K. Kuciński T. Grygorczuk J. Rickman H. Morawski M.
Experimental Determination of Geotechnical Parameters of Planetary Bodies — CHOMIK Sampling Device Example **[#2298]**
The CHOMIK planetary sampler designed for the Phobos-Soil mission was developed at the Space Research Centre PAS. Tests show the capability of in situ recognition of basic rock/soil types and parameters of planetary bodies.

Zacny K. Paulsen G. Mellerowicz B. Craft J. McKay C. Glass B. Davila A. Marinova M. Dave A. Thompson S.
The Icebreaker: Mars Drill and Sample Delivery System **[#1153]**
We present development and testing of a 1-meter-class rotary-percussive drill and associated sample delivery system for future Mars missions.

Paulsen G. Zacny K. Steele A. Conrad P. Chu P. Craft J. Hedlund M. McCarthy T. Schad C.
Demonstration of the Acquisition and Caching for the Mars Sample Return Missions **[#1151]**
We present results of the end-to-end demonstration of the core acquisition and caching for the Mars Sample Return mission.

Zacny K. Paulsen G. Mellerowicz B. Craft J. Beegle L. Bar-Cohen Y. Sheritt S. Badescu M.
Wireline Rotary-Percussive Coring Drill for Deep Exploration of Planetary Bodies **[#1173]**
We present a wireline drilling system for acquisition of core samples from great depths in planetary bodies containing water-ice deposits.

De Sanctis M. C. Coradini A. Ammannito E. Boccaccini A. Di Iorio T. Battistelli E. Capanni A.
Micro Imaging Spectrometer for Subsurface Studies of Martian Soil: Ma_Miss **[#2855]**
Ma_Miss (Mars Multispectral Imager for Subsurface Studies) is a spectrometer devoted to observe the lateral wall of the borehole generated by the drill installed on the ExoMars Pasteur Rover to perform in situ investigations in the Mars subsurface.

THU POSTERS

Li R.   Li D.   Lin L.   Meng X.   Di K.   Paar G.   Coates A.   Muller J. P.   Griffiths A.
Oberst J.   Barnes D. P.
ExoMars: Pre-Launch PanCam Modeling and Accuracy Assessment **[#2437]**
The goal of this research is pre-launch quantitative analysis of the localization accuracy of the Panoramic Camera (PanCam) vision system designed to be carried onboard the European Space Agency (ESA) ExoMars rover mission for launch in 2018.

McElhoney K.   Chaniotakis N.   O'Neil G. D.   Bauer J.   Harjes D.   Traviglia D.
Hecht M. H.   Kounaves* S. P.
The In-Situ Wet Chemical Analysis Laboratory and Sensor Array (CHEMSENS): The Next Generation Mars Soil Chemistry Analyzer **[#2329]**
CHEMSENS builds on the heritage and success of the Phoenix wet chemistry laboratory (WCL). It will provide the ability to perform analyses over a variety of geological surfaces, materials, soil chemistry, and the lifetime of a rover or lander.

Lorenz R. D.   Stofan E.   Lunine J. I.   Zarnecki J. C.   Harri A.-M.   Karkoschka E.   Newman C. E.   Bierhaus E. B.
Clark B. C.   Yelland M.   Leese M. R.   Boldt J.   Darlington E.   Neish C. D.   Sotzen K.   Arvelo J.   Rasbach C.
Kretsch W.   Strohbehn K.   Grey M.   Mann J.   Zimmerman H.   Reed C.
MP3 —- A Meteorology and Physical Properties Package to Explore Air-Sea Interaction on Titan **[#2768]**
Neat gadget to gauge / Heat, moisture, and momentum / Sailing Ligeia.

Wolf A.   Laufer R.   Lightsey G.   Herdrich G.   Srama R.   Röser H.-P.   Hyde T. W.
Piezo Dust Detector (PDD) — A Modular Miniaturized In-Situ Measurement Instrument for Dust Research **[#2136]**
The Piezo Dust Detector (PDD) is a modular miniaturized in situ measurement instrument for submillimeter dust and orbital debris particles based on piezo sensor element technology, which can be flown on a large number of space-borne platforms.

Daly R. T.   Kerby J. D.   Austin D. E.
Steps Toward an Innovative Electrospray-Based Particle Source for Dust Accelerators **[#1917]**
We are developing a new particle source for dust accelerators that charges particles regardless of their electrical conductivity. This overcomes a major limitation of current dust accelerator particle sources.

Westphal A. J.   Blum J.   Gainsforth Z.   Lee A. T.   Sandford S. A.
Silicon Nitride Spiderwebs for Cometary Coma Dust Capture **[#1156]**
Here we describe a cometary coma dust collector based on silicon nitride "spiderwebs." The basic technology is already flight-proven on the Planck cosmic microwave background mission.

Kobayashi M.   Miyachi T.   Nakamura M. H.
Cosmic Dust Detector Using Piezoelectric PZT with Current-to-Voltage Conversion Amplifier **[#1411]**
This paper describes the concept of a dust monitor with a large detection area but less resource using PZT ceramics, and the possibility is experimentally demonstrated. We suggested the use of a current-to-voltage converting amplifier for it.

Kobayashi M.   Senshu H.   Wada K.   Namiki N.   Hirata N.   Miyamoto H.
Circumasteroid Dust Monitor Instrument for Future Missions **[#1418]**
Dust particles may exist even on or around asteroids. We propose direct observations of such dust particles for future missions to asteroids.

Sternovsky Z.   Gruen E.   Horanyi M.   Kempf S.   Postberg F.   Schmidt J.
Dust Spectroscopy of the Jovian Satellites **[#2929]**
Dust instruments can be used for surface composition measurements of Europa and Ganymede.

Amini R. B.   Beegle L.   Castillo-Rogez J. C.   Giapis K.   Snyder J. S.
Electric Propulsion Induced Secondary Mass Spectroscopy (EPI-SMS) **[#2781]**
We posit electric propulsion's ability to serve as a source for sputtering experiments at small bodies to determine surface composition. In the abstract we depict expected sputtering return and outline two validating experiments.

Zinovev A.   Baryshev S.   Tripa E.   Veryovkin I.
Laser Setup for Multi-eElement RIMS of GENESIS Returned Samples **[#2911]**
Laser setup for multi-element RIMS analysis is described. This approach is the compromise between sensitivity and complexity of the instrument and allowed us to get more data within single experiment thereby decreasing the samples consumption.

Mahaffy P. R.   Hodges R. R.   Harpold D. N.   King T. T.   Jaeger F.   Raaen E.   Lyness E.   Collier M.   Benna M.
Calibration of the Neutral Mass Spectrometer for the Lunar Atmosphere and Dust Environment Explorer (LADEE) Mission **[#2144]**
The calibration of the Neutral Mass Spectrometer for the Lunar Atmosphere and Dust Environment Explorer Mission designed to measure the composition of the lunar exosphere has been completed prior to environmental tests and the results will be presented.

Wilson E. L.   Georgieva E. M.   Blalock G. W.   Marx C. T.   Heaps W. S.
Development of a Miniaturized Hollow-Waveguide Gas Correlation Radiometer for Trace Gas Measurements in the Martian Atmosphere **[#1603]**
We present the development of a miniaturized gas correlation radiometer (GCR) for column trace gas measurements in the martian atmosphere. Designed as an orbiting instrument, the GCR maps multiple gases to identify active regions on the surface.

Blaney D. L.   Mouroulis P.   Green R.   Rodriquez J.   Sellar G.   Van Gorp B.   Wilson D.
The Ultra Compact Imaging Spectrometer (UCIS): In Situ Imaging Spectroscopy for Mars, the Moon, and Asteroids **[#2593]**
The Ultra Compact Imaging Spectrometer (UCIS) can map mineralogy in situ on Mars, the Moon, asteroids, and comets.

Bowles N. E.   Calcutt S. B.   Reininger F. M.
The Asteroid Thermal Mapping Spectrometer: An Imaging Mid-IR Spectrometer for the Marco Polo–R NEO Sample Return Cosmic Vision Candidate Mission **[#2334]**
This paper describes the Asteroid Thermal Mapping Spectrometer (ATMS) development model currently under test at the Department of Physics, University of Oxford.

Edwards C. S.   Christensen P. R.
Development of a Microscopic Thermal Emission Spectrometer: Analysis of Primary Igneous Materials for Planetary Analogs **[#2658]**
We present initial results from the development of a microscopic thermal emission spectrometer and its application to igneous planetary analog materials. Additionally, we also illustrate its utility as a non-destructive micro-analysis technique.

Okada T.
Reanalysis of Possible Degraded XRS and Remote X-Ray Spectroscopy in the Future Missions **[#2057]**
Planetary remote X-ray fluorescence spectroscopy is proposed by showing the new concept of XRS instrument using a standard sample by considering the lessons learned from the previous missions.

Schmanke D.   Hasebe N.   Blumers M.   Heinl M.   Klingelhöfer G.   Brückner J.
Preliminary Experiments with a Pyroelectric X-Ray-Source for the Development of AXS for the Scientific Payload of the SELENE-2 Mission **[#2831]**
The further development of the successful APXS leads to the Active X-ray Spectrometer (AXS) as candidate for scientific payload for the JAXA SELENE-2 mission. A new on-demand X-ray generator source is examined by preliminary usability tests.

Kim K. J.   Amano Y.   Boynton W. V.   Klingelhöfer G.   Brückner J.   Hamara D.   Starr R. D.   Lim L. F.
Hasebe N.   Ju G.   Fagan T. J.   Ohta T.   Shibamura E.
Introduction to the Scientific Investigation of an Active X-Ray Spectrometer for the SELENE-2 Rover **[#1282]**
This presentation introduces the proposed Active X-ray Fluorescence Spectrometer for SELENE-2 rover mission using a pyroelectric crystal to generate X-rays; a silicon drift detector would minimize radiation hazard and provide good XRF performance.

Shanmugam M.   Vadawale S.   Acharya Y. B.   Goyal S. K.   Arpit Patel   Bhumi Shah   Murty S. V. S.
Solar X-Ray Monitor (XSM) On-Board Chandrayaan-2 Orbiter **[#1858]**
The Solar X-ray Monitor will provide real time X-ray spectra for the CLASS experiment on the Chandrayaan-2 Orbiter. In this experiment, the SDD detector has been used for the first time. The developmental status of XSM will be discussed in this paper.

PRINT-ONLY PRESENTATIONS

MERCURY

Hughes E. T.   Vaughan W. M.
Albedo Features of Mercury **[#2151]**
The albedo features of Mercury as observed from Earth are considered. We conclude that they have broadly similar origins to those of the Moon but reflect unique mercurian crustal chemistry and volatile-related surface processes.

Lopes F. C.   Barata T.
Morpho-Tectonic Analysis of the Surface of Mercury **[#1204]**
This paper intends to give a contribution to the tectonic geomorphologic studies of Mercury, by the identification of structural lineaments and possible cinematic criteria.

Weihs G. T.   Leitner J. J.   Firneis M. G.
Polygonal Impact Craters on Mercury **[#1083]**
This study proves the existence of polygonal impact craters on Mercury. Furthermore, the assumption was confirmed that PICs are an integral part of impact craters and common on the Moon, all terrestrial planets, and several asteroids and icy moons.

MOON

Abdrakhimov A. M.   Ivanov M. A.   Basilevsky A. T.   Dickson J. L.   Head J. W. III   Zuber M. T.   Smith D. E.   Mazarico E.   Neish C. D.   Bussey D. B. J.
The Luna-Glob Candidate Landing Region: Geological Mapping Based on the Lunar Reconnaissance Orbiter Data **[#1331]**
The new regional detailed geologic map was made using recent LRO data for the Luna-Glob mission. The most probable unit that could be sampled by the lander is a feldspathic Imbrian highland plains-forming material, resembling the Cayley Formation.

Anosova M. O.   Nazarov M. A.   Demidova S. I.   Kostitsyn Yu. A.   Ntaflos Th.   Brandstätter F.
Trace Element Chemistry of a Silicon-Bearing Association in the Dhofar 280 Lunar Meteorite **[#1079]**
Trace elements were measured in silicon-bearing objects of the Dhofar 280 lunar meteorite. Such objects are enriched in volatiles and elements that can be easily reduced. The volatile elements could be condensed from an impact-generated vapor.

Berezhnoy A. A.   Kozlova E. A.   Shevchenko V. V.
Stability of Volatile Species at the Poles of the Moon **[#1396]**
Areas of thermal stability of Ca, Mg, and Na deposits are estimated. Complex species NH_3, C_2H_4, CH_3OH, and CH_4 can be destroyed during meteoroid bombardment. Polar species with maximal content in the impact-produced cloud are proposed.

Cortés J.   Trigo-Rodriguez J. M.   Llorca J.
The Lunar Breccia NWA 2700: Origin, Description, and Its UV to NIR Reflectance Spectrum **[#1455]**
We present here a precise UV to NIR reflectance spectra of NWA 2700. We wish to explore the relation between the mineralogy, the size of the grains, and the reflectance. Interesting links between lunar soil mineralogy and reflectance are found.

Grumpe A.   Wöhler C.
Image-Based Construction of Lunar Digital Elevation Models of very High Lateral Resolution **[#2597]**
This abstract describes a method to create Digital Elevation Models (DEMs) of high lateral resolution from imagery of high lateral resolution and DEMs of lower lateral resolution.

Kaydash V. G.   Shkuratov Y. G.
Phase-Ratio Imagery Identification of the Surface Altered in the Apollo-16 Landing Site **[#1484]**
The phase ratio technique reveals the photometric anomalies in the vicinity of the Apollo 16 landing site. We interpret them as surface smoothing caused by the engine jets of the lander and regolith loosening by astronauts and the vehicles.

Khisina N. R.   Wirth R.   Riede D.
Oriented Chromite-Diopside Symplectic Inclusions in Lunar Olivine from the "Luna-24": Hydrogenation-Dehydrogenation as a Mechanism of Simplectic Formation? **[#1068]**
Diopside-chromite symplectitic lamellae in olivine from the "Luna-24" soil are studied with FIB/TEM and FE-EMPA and suggested to be formed by two-step solid-state reaction involving exsolution, oxidation, cellular decomposition, and dehydrogenation.

Krishna Sumanth T.   Nagasubramanian V.   Radhadevi P. V.   Sudheer Reddy D.   Solanki S. S.   Jyothi M. V.   Saibaba J.   Geeta Varadan
Comparison of DEMs from Terrain Mapping Camera Images with LOLA **[#2026]**
DEMs generated from the TMC camera are compared with LDEM-256. TMC DEMs are of high quality and accurate, which enables the contruction of three-dimensional models. They are representative of the stability of the platform and the potential of CH-1 for accurate lunar referencing.

Lena R.   Phillips J.
Lunar Domes in Cauchy Region: Morphometry and Mode of Emplacement **[#1005]**
We provide an analysis of four domes located in Mare Tranquillitatis, near Rima Cauchy, termed as C14-17.

Liu D.   Li L.
An Improved Radiative Transfer Model for Estimating Mineral Abundance of Immature and Mature Lunar Soils **[#2011]**
Introduce an improved Hapke's radiative transfer model to estimate the mineral abundance of both immature and mature lunar soils.

Lu Ya.   Shevchenko V. V.
Current Events on the Moon: LROC and Chang'E-2 Data **[#1207]**
Slope movements of material in lunar craters are investigated based on remote spectral studies carried out onboard the Clementine spacecraft, and data obtained during the large-scale survey onboard the LRO and Change'e-2 spacecrafts.

Mitrofanov I. G.   Golovin D. V.   Kozyrev A. S.   Litvak M. L.   Malakhov A. A.   Sanin A. B.
Solar Water Permafrost: Is It Detected on the Moon? Is It Expected on the Mercury? **[#2083]**
In addition to neutron data from LRO for the Moon, the data from MESSENGER should be studied for testing and understanding the physical origin of polar water ice deposits at the Moon and at Mercury.

Moggi-Cecchi V.   Caporali S.   Pratesi G.   Franchi I. A.   Greenwood R. C.
NWA 6687: A New Lunar Meteorite from Northwest Africa **[#2710]**
NWA 6687 is a new meteorite recovered in Northwest Africa. The presence of medium-grained inclusions with intersertal texture, oxygen isotopic data and various minerochemical features suggest a classification as lunar feldspathic breccia.

PRINT ONLY

Nazarov M. A.   Demidova S. I.   Ntaflos Th.   Brandstätter F.
Native Silicon, Fe-Silicides and a Condensate Lithology in the Dhofar 280 Lunar Meteorite **[#1073]**
Native silicon and Fe-silicides were found in the lunar meteorite Dhofar 280. The phases associate with a Si-rich melt. The association could be formed by condensation of an impact-induced vapor, remelted and mixed with the host rock.

Petrova N. K.   Abdulmyanov T. R.   Hanada H.
Inverse Problem of the Lunar Physical Libration by Observing Stars from the Lunar Surface **[#1027]**
Method of solution of the inverse problem is suggested. The dependence of accuracy of libration angles on the measuring error of selenographic coordinates of stars is estimated. Their sensitivity to deformability of the Moon is verified.

Radhadevi P V.   Sudheer Reddy D.   Saibaba J.   Geeta Varadan
Suitability of LOLA DEMs for Processing TMC Images of Chandrayaan-1 **[#2303]**
In this paper, we study the impact of height error in combination with view angle of the TMC cameras on planimetric accuracy. Our study reveals that height errors in LDEM-256 is minimum and is suitable for processing TMC data.

Saran S.   Das A.   Mohan S.   Chakraborty M.
Scattering Properties of Jackson Crater in the Lunar Far Side **[#1234]**
Scattering properties of the lunar farside crater “Jackson” have been analyzed using Mini-SAR data of Chandrayaan-1 mission supported by high-resolution optical datasets from the NAC of the LRO.

Shevchenko V. V.
Interstellar Matter on the Moon **[#1275]**
We know that other stars have circumstellar clouds of dust or icy bodies that may be analogous to the Kuiper Belt in the solar system. So, we propose that dust particles may be brought to the Moon by a giant comet from another star system.

Shkuratov Y. G.
Forgotten Solar-Wind Iron Implanted in Lunar Regolith **[#1286]**
The SW-Fe suggests an additional source of npFe0 in the lunar regolith. This source can be important, since much more volatile helium-3, having lower SW-concentartion than SW-Fe, is nevertheless detected in the lunar regolith and suggested as a fuel.

Sinitsyn M. P.
Correlations of Hydrogen Concentration and Surface Formations on the Moon According to the Lunar Prospector Neutron Spectrometer **[#1108]**
As a result of neutron spectrometer LEND new information was received about distribution of thermal and epithermal neutrons on the lunar surface.In this paper, we propose to compare some of the correlations found earlier LPNS device with new data.

Sposetti S.   Lena R.   Iten M.
Detection of Meteoroidal Impacts on the Moon **[#1012]**
During our surveys carried out on February 11, 2011, and April 9–10, 2011, four impacts were simultaneously recorded by two independent and distant (13 km apart) observatories.

Svetsov V. V.   Pechernikova G. V.   Vityazev A. V.
A Model of Moon Formation from Ejecta of Macroimpacts on the Earth **[#1808]**
We suggest a statistical model of Moon formation, assuming that initially thin prelunar swarm of particles grows due to capture of material ejected after impacts of large planetesimals on growing Earth. Numerical simulations of impacts are made.

PRINT ONLY

Thomas-Keprta K. L. Clemett S. J. Ross D. K. Le L. McKay D. S. Gibson E. K. Gonzalez C.
Indigenous Carbon Embedded in Apollo 17 Volcanic Black Glass Surface Deposits **[#2561]**
We report for the first time the identification of arguably indigenous carbonaceous matter present within surface deposits of a black glass grain collected on the rim of Shorty Crater during the Apollo 17 mission.

Todd N. S. Lofgren G. E.
Apollo Lunar Sample Photograph Digitization Project Update **[#2860]**
Update on the progress and availability of data from a 4-year data restoration project effort to digitize photographs of the Apollo lunar rock samples and create high resolution digital images.

Wöhler C. Grumpe A.
Correction of Chandrayaan-1 M^3 Lunar Hyperspectral Image Data with Respect to Local Topography **[#1906]**
In this study we propose an empirical method to correct Chandrayaan-1 M^3 hyperspectral image data with respect to the local topography based on a digital elevation model (DEM) of high lateral resolution.

MARS

Barata T. Pina P. Saraiva J. Alves E. I. Machado A. Vaz D. A. Bandeira L. Ori G. G.
The Camel Project — Characterization and Classification of Dune Fields on Mars Based on Earth **[#1141]**
Two Portuguese research groups together with one Italian group will develop a methodology to automatically delineate and extract dimensional and morphological features of dune fields in images of the martian surface.

Centeno J. D. de Pablo M. A.
Preliminary Analysis of Surface Temperature in the Depression at the Lower NW Flank of Hecates Tholus Volcano, Mars **[#1097]**
In search for evidence of glacial ice in Hecates Tholus slopes, we have tested the use of THEMIS-derived brightness temperature record (BTR) data in order to analyze surface temperature.

Coleman N. M.
Megaflood Erosion on Mars — How a Lava-Filled Crater Became a Mesa **[#1117]**
A round mesa exists on the floor of the Elaver Vallis outflow channel. How was the mesa formed in this zone of intense erosion? I theorize the mesa began as a crater that filled with basaltic lava, then later was exhumed and eroded by a megaflood.

Guallini L. Lauro S. Marinangeli L. Pettinelli E. Seu R.
SHARAD Analysis of Promethei Lingula (Mars): Evidences of Angular Unconformities and Possible "Crevasse-Like" Structures Within South Polar Layered Deposits **[#1412]**
We observed angular unconformities and crevasse-like structures within SPLD in Promethei Lingula through SHARAD. Unconformities are consistent with two stratigraphic units, divided by one regional hiatus. Possible crevasses suggest past ice flow .

Hobbs S. W. Paull D. Clark J. D. A.
What Lake George Can Tell Us About Martian Gullies **[#1101]**
We analysed the morphology of gullies and debris flows within a fresh martian crater located in Noachis Terra and compared them to four gullies in Lake George, Australia. Evidence of liquid water erosion was observed at both sites.

Jiang Y. Hsu W.
In Situ U-Pb Geochronology of Baddeleyite in the Enriched Lherzolitic Shergottite Grove Mountains (GRV) 020090 **[#1741]**
GRV 020090 is a new geochemically enriched lherzolitic shergottite after RBT 04261/04262. In situ U-Pb dating of baddeleyite demonstrates that shergottites have young crystallization age.

PRINT ONLY

Leppänen L. I.   Kostama V. -P.   Raitala J.
Oval Structures on the Floor of Hellas Basin, Mars **[#1784]**
Observing locations, structures, and positions of the Hellas floor ovals, depth of the ovals can be estimated. This information may be used to determine the formation mechanisms of the oval structures.

Martin-Torres F. J.   Moyano-Cambero C. E.   Trigo-Rodriguez J. M.
Evolution of Mars Atmospheric Pressure and Temperature Modeling and Constraints from Meteorites **[#2840]**
We have developed a 1D model of the evolution of martian mass, near surface temperature and pressure considering the main production and loss processes of Mars atmosphere and the radiative conditions on Mars.

Morley J. G.   Lin N.   Muller J-P.   Shin D.   Paar G.
PRoGIS: A Web Tool to Understand and pProcess Mars Rover Imagery in a Planetary Context **[#2896]**
The PRoGIS system described below is an output from an EU FP7 project, PRoVisG (Planetary Robotics Vision Ground processing). ProGIS provides access to MER rover data, photogrammetric processing, and viewing of data in a planetary contex.

Moyano-Cambero C. E.   Trigo-Rodriguez J. M.   Martin-Torres F. J.   Llorca J.
Martian Meteorites: Reflectance Properties, Atmosphere-Implantation Ages, and the Climatic Evolution of Mars **[#1132]**
SNC meteorites are the only martian samples available to be studied in terrestrial laboratories. We will use them to corroborate an evolutionary climatic model for Mars. UV to visible reflectance spectra of Nakhla and Zagami are also presented.

Nussbaumer J. W.
Elongated Deposits in Southern Elysium Planitia, Mars **[#1208]**
In the Elysium Planitia region, deposits have elongated elevations that resemble terrestrial drumlins or yardangs. Drumlins and drumlin clusters are glacial landforms that have been extensively studied. In contrast, Yardangs are formed by wind.

Papike J. J.   Burger P. V.   Shearer C. K. Jr.   McCubbin F. M.   Elardo S. M.
Experimental Martian Eclogite with a QUE 94201 Composition **[#1010]**
High-pressure techniques were used to synthesize a martian eclogite based on the composition of martian meteorite QUE 94201. The resultant eclogite may be representative of martian melts whose ascent has been arrested in the upper mantle.

Pedersen G. B. M.   Head J. W. III
Evidence of Complex Ice-Volcano Interactions in the Transition Zone Between Elysium Rise and Utopia Basin **[#1169]**
We report on morphologic evidence of a complex succession of ice-volcano interactions in the Galaxias region, Mars, and reconsider the emplacement properties of volcanoclastic outflow deposit under martian conditions.

Roush T. L.   Maturilli A.   Helbert J.   Mannstein H.
Optical Constants of Eyjafjallajökull Volcanic Ash: Analogs for Mars **[#1464]**
We estimate optical constants of Eyjafjallajökull volcanic ash as analogs for Mars ash deposits.

Soare R. J.   Conway S. J.   Pearce G. D.   Costard F.
Ice-Enriched Loess and the Formation of Periglacial Terrain in Mid-Utopia Planitia, Mars **[#1311]**
Landforms suggestive of periglacial processes are commonplace in mid-Utopia Planitia, Mars. They form syngenetically in ground-ice comprised of loess transported by katabatic wind from the NPLDs and enriched by ice through the thaw-freeze cycling of obliquity-driven precipitation.

Valenciano A.   de Pablo M. A.
Geological Cartography of Inner Materials of an Impact Crater on Nepenthes Mensae, Mars **[#1038]**
We present the geological map and a brief description of the materials, its geological history and an approach to their astrobiological and exopaleontological implications from sedimentary materials located into impact crater, in Nepenthes Mensae, Mars.

PRINT ONLY

Zent A. P.   Hecht M. H.   Hudson T. L.   Wood S. E.   Chevrier V. F.
A Revised Calibration Function for the TECP Humidity Sensor of the Phoenix Mission **[#2846]**
A revised calibration function for the RH sensor on the Phoenix mission TECP is presented.

de Pablo M. A.   Centeno J. D.
Geomorphological Map of the Lower NW Flank of Hecates Tholus Volcano, Mars **[#1098]**
We present our 1:100,000-scale geomorphological map of the NW flank of Hecates Tholus volcano, Mars, by the use of CTX images and HRSC-derived DTM. This map will allow us to study in detail the geology and glacial history of this volcano.

IGNEOUS PROCESSES

Brož P.   Hauber E.
Amenthes Cones, Mars: Hydrovolcanic (Tuff) Cones from Phreatomagmatic Explosive Eruptions? **[#1321]**
Aim of the study is a field of pitted cones located along the dichotomy boundary in the Amenthes region. We tested the hypothesis of a hydrovolcanic origin of the cones because the regional context displays lines of evidence for subsurface water ice.

Richter F. M.   Watson E. B.   Chaussidon M.   Mendybaev R. A.   Ruscitto D. M.
Experimental Determination of the Rate of Cooling and Isotope Fractionation of Li Diffusing into Augite and Constraints on the Cooling Rate of Martian Meteorite MIL 03346 **[#2094]**
Laboratory experiments demonstrating isotopic fractionation of lithium diffused into an augite grain are in good agreement with the lithium abundance and isotopic profiles in an augite grain from martian meteorite MIL 03346.

CHONDRITES AND THEIR COMPONENTS

Alexander C. M. O'D.   Bowden R.   Fogel M. L.   Howard K. T.   Greenwood R. C.
The Classification of CM and CR Chondrites Using Bulk H Abundances and Isotopes **[#2799]**
We show that H abundances and isotopes are a useful tool for classifying the CM and CR chondrites.

Bendel V.   Pack A.   O'Neill H.
Rare Earth Elements in CI1-Chondrites and Planetary Samples **[#2578]**
We present high-precision LA-ICPMS data about rare earth elements, which show that planetary samples have a Tm-anomaly compared to CI1-chondrites. We conclude that a Tm-rich refractory phase was added to the CI1-chondrites.

Gorin V. D.   Alexeev V. A.   Ustinova G. K.
Peculiarities of the 23-th Solar Cycle According to Cosmogenic Radionuclides in the Tamdakht and Ash Creek Chondrites **[#1020]**
Cosmogenic radionuclide measurements in the fresh-fallen chondrites Tamdakht and Ash Creek are used for evaluation of the galactic cosmic ray intensity along the chondrite orbits during the transitional minimum between 23rd and 24th solar cycles.

Weidenschilling S. J.   Hood L. L.
Some Implications of Meteoritic Constraints for Chondrule Formation Models Including the Bow Shock Model **[#1551]**
The lack of chemical and isotopic fractionation in chondrules implies that they formed in a uniform nebular midplane layer, not in turbulence. If melted by bow shocks, the supersonic bodies were large, i.e., Moon- to Mars-sized.

PRINT ONLY

ACHONDRITES

Badjukov D. D. Raitala J.
Ablation Spherules of the Sikhote-Alin Iron Meteorite Shower **[#1759]**
We report textures, mineralogy, and compositions of the meteorite ablation spherules collected at the crater field of the Sikhote-Alin iron shower. Using specific features of the spherules we give constraints on formation parameters of the spherules.

Baghdadi B. Godard G. Jambon A.
Metamorphic Reactional Coronas in the Peridotitic Angrite NWA 3164, Interpretations and Implications **[#2188]**
The NWA 3164 angrite shows some unique metamorphic features that consist in various complex coronas developing at mineral interfaces. Thermodynamic calculations permit to constrain P,T conditions of formation.

Bartoschewitz R. Tagle R. Nolze G. Spettel B. Greshake A.
The Dermbach Meteorite — A Relict of the IVA Parent Body? **[#1192]**
Dermbach might be a Ni-rich member of the IVA group that formed during parent body core crystallization.

Caporali S. Moggi-Cecchi V. Pratesi G. Franchi I. Greenwood R. C.
NWA 6685: A New Lodranite from Northwest Africa **[#1935]**
In this communication we provide the petrographic and minerochemical description of a new achondrite meteorite. The coarse texture, as well as the minerochemical and oxygen isotope data, suggest the classification of this meteorite as lodranite.

Teplyakova S. N. Artemov V. V. Vasiliev A. L.
Unusual Siderite-Bearing Dendrites in Melt Pockets of the Elga IIE Iron **[#1064]**
The Elga iron contains melt pockets with dedritic texture not only inside Fe,Ni-metal but also inside silicate inclusions (SI). The unusual siderite-bearing melt pockets inside SIs has never been previously observed in any types of meteorites.

Wright A. J. Parnell J.
Raman Characterization of Thermally Altered Carbon and Implications for the Evolution of Ureilite Carbon **[#1018]**
This study used carbon in terrestrial, CC, and ureilte samples to show that the diversity of terrestrial and extraterrestrial carbon is broadly comparable in both datasets and that thermal alteration follows similar inferred evolutionary pathways.

THE SPANISH METEOR NETWORK

Alonso-Azcárate J. Madiedo J. M. Trigo-Rodriguez J. M. Zamorano J. Izquierdo J. Ocaña F. Sánchez de Miguel A. Lacruz J. Toscano F. M.
Orbit and Radiant of a Sporadic Fireball Imaged by the Spanish Meteor Network **[#1177]**
we have imaged on April 17, 2011, a four-station sporadic fireball with an absolute magnitude of about –7. The analysis of this bolide is presented here.

Dergham J. Trigo-Rodriguez J. M. Cortés J. Alonso-Azcárate J. Pujols P. Ortiz J. L. Castro-Tirado A. J. Madiedo J. M. Montanyà J. van der Velde O.
Large Meteoroids from the 2P/Encke Complex: Orbital Data of 2010 Taurids Recorded in the Framework of the Spanish Fireball Network **[#1137]**
Orbital data for seven Taurid fireballs are presented. The main orbital elements of such orbits are compiled and compared to 2P/Encke. The orbital data indicate that most of the brightest 2010 Taurid events were associated with the northern branch.

PRINT ONLY

Diez F.   Madiedo J. M.   Toscano F. M.   Trigo-Rodriguez J. M.
A Bright Bolide Produced by a Meteoroid Following a Jupiter Family Comet Orbit **[#1171]**
We have imaged on April 27, 2011, a double-station sporadic fireball with an absolute magnitude of about –7. The analysis of this bolide is made here. The meteoroid followed a JFC orbit.

Docobo J. A.   Madiedo J. M.   Trigo-Rodriguez J. M.
A Bright Fireball Witnessed on August 17, 2011 Over the Iberian Peninsula **[#1164]**
The preliminary analysis of a meteorite-dropping fireball witnessed on August 17, 2001, over the Iberian Peninsula is presented.

Garcia J. M.   Madiedo J. M.   Castro-Tirado A. J.   Jelinek M.   Trigo-Rodriguez J. M.
Analysis of Large Sporadic Meteoroids in the Framework of the Spanish Meteor Network **[#1165]**
We have imaged on October 13, 2009, a double-station sporadic fireball with an absolute magnitude of about –10. The analysis of this event is presented here.

Martinez L.   Madiedo J. M.   Toscano F. M.   Castro-Tirado A. J.   Trigo-Rodriguez J. M.
Pastor S.   de los Reyes J. A.
Orbital Elements and Emission Spectrum of a Comae Berenicids Fireball **[#1167]**
We present here the analysis of a three-station Comae Berenicids fireball with an absolute magnitude of about –8 imaged on January 14, 2011.

Toscano F. M.   Madiedo J. M.   Ortiz J. L.   Castro-Tirado A. J.   Trigo-Rodriguez J. M.
Pastor S.   de los Reyes J. A.
On the Chemical Composition and Orbit of a Diurnal Fireball **[#1163]**
We present here the preliminary analysis of a three-station sporadic diurnal fireball with an absolute magnitude of about –8, imaged at dawn on June 1, 2011.

SMALL BODIES

Abdulmyanov T. R.
The Problem of the Gravitational Accretion of Particles **[#1015]**
In this paper we attempt to detail the process of accretion using the more general equations of the motion with the law of egual areas for revolving orbits.

Alexeev V. A.
Extraterrestrial and Terrestrial Chromite Grains in Middle Ordovician Limestones of Sweden and China: Some Peculiarities of Distributions **[#1001]**
The flux of extraterrestrial micrometeorites on all Earth after disruption of the L-chondrite parent body has increased approximately 2–3 times, but not in two orders of magnitude.

Busarev V. V.
An Oceanic Source of Icy, Hydrosilicate and Organic Grinded Materials as One of the Main Factors Sculptured the Early Asteroid Belt **[#1453]**
Intensive fluxes of grinded materials from neighboring formation zones of giant planets might have considerably influenced chemical and mineralogical content of asteroid parent bodies at the time of their accretion and shortly thereafter.

Giuppi S.   Coradini A.   Capaccioni F.   Capria M. T.   De Sanctis M. C.   Erard S.   Filacchione G.   Tosi F.
Virtis/Rosetta: Temperature Analysis During Lutetia Dynamic Rehearsal as an Input in Lutetia Fly-By Planning **[#1053]**
In this paper we show how, taking into account the different spacecraft/Sun distances during the Lutetia dynamic rehearsal and Lutetia fly-by, it was possible to predict within one degree the temperature trend on VIRTIS during the Lutetia fly-by.

PRINT ONLY

Iwasa K.   Ohtsuki K.
On the Orbital Evolution of Planetary Embryos Under the Influence of GiantPlanet Scattering **[#1903]**
We investigated orbital behavior of small bodies under the influence ofthree giant planets that undergo dynamical instability, focusing on orbitalevolution of small bodies whose perihelion distances become rather small.

Konovalova N. A.   Madiedo J. M.   Trigo-Rodriguez J. M.
Meteorite-Dropping Bodies from Cometary Meteoroid Streams and Their Physical Properties **[#1205]**
Some meteoroids with orbits clearly associated with two cometary meteoroid streams o-Draconid and June Bootid and its physical properties.

Kuzmin R. O.   Zabalueva E. V.
Daily Temperature Regime of the Surficial Regolith of Phobos in the Landing Site Region for the Phobos-Grunt Mission Lander in Different Seasons: The Model Predictions **[#1769]**
We present the results of the numerical modeling of the thermal regime of the Phobos surface regolith layer (on daily and seasonal timescale) within the selected landing site for the Phobos-Grunt mission in the Lagado Planitia.

Madiedo J. M.   Trigo-Rodriguez J. M.   Konovalova N.   Castro-Tirado A. J.
A 13 kg Meteoroid from Comet 21p/Giacobini-Zinner Recorded as a Bolide During the 2011 Draconid Outburst **[#1298]**
We present here the analysis of an extraordinarily bright Draconid event (mag. –10.5) recorded together with its spectrum during the 2011 Draconid outburst. The mass of the meteoroid was about 13 kg.

Mousis O.   Guilbert-Lepoutre A.   Lunine J. I.   Cochran A. L.   Petit J.-M.
Radiogenic Heating as the Cause of the Nitrogen Deficiency in Comets **[#1891]**
We find that radiogenic heating provides a viable mechanism to account for the origin of the nitrogen deficiency observed in comets. This mechanism is also found consistent with the presence of nitrogen-rich atmospheres around Pluto and Triton.

Narziev M.   Konovalova N. A.
Bulk Density of Meteoroids on Combined Radar-Optical Observations **[#1373]**
Fragmentation and physical properties of the meteoroids from combined radar-optical observations.

Okamoto T.   Nakamura A. M.   Hasegawa S.   Kurosawa K.   Ikezaki K.   Tsuchiyama A.
Capture of Hypervelocity Dusts by Highly Porous Small Bodies **[#1782]**
We conducted dust impact experiments into highly porous brittle targets using a flash X-ray system and showed that the deceleration process of projectiles and the cavity morphology is similar to those reported for aerogel targets.

Petit J.-M.   Mousis O.   Kavelaars J. J.
Formation Location of Enceladus and Comets from D/H Measurements **[#1937]**
The nearly-isotropic comets and Enceladus have similar D/H ratios. Thus they were formed in the same region as Uranus and Neptune, at less than ~15 AU. As 103P/Hartley 2 is D-poor compared to these bodies, the current models are called into question.

Rodriguez A.   Madiedo J. M.   Konovalova N.
Analysis of Large Meteoroids Produced by Comet 7P/Pons-Winnecke **[#1301]**
Two of the meteor observing stations operated by the Spanish Meteor Network (SPMN) simultaneously imaged a June Bootid fireball with an absolute magnitude of about –9 on July 5, 2009. The analysis of this event is presented here.

Slyusarev I. G.   Shevchenko V. G.   Belskaya I. N.   Krugly Yu. N.   Chiorny V. G.
Magnitude Phase Angle Dependences of Jupiter Trojans and Hilda Asteroids **[#1885]**
Results of photometric observations of 6 Jupiter Trojans and 11 Hilda asteroids are presented. The detailed magnitude phase dependences were obtained for the Hilda asteroid (1748) Mauderli and the Trojans (2207) Antenor and (2357) Phereclos.

PRINT ONLY

Slyuta E. N.
Shape Distribution of Ordinary Chondrite, Iron Meteorites and Metallic Asteroids **[#1088]**
The shape of metal asteroids strongly differs from the shape of fragments of iron meteorites. Such distinction may be caused by different mechanics of formation of these bodies' shape.

Szurgot M.
On the Heat Capacity of Asteroids, Satellites and Terrestrial Planets **[#2626]**
Specific heat capacity and heat capacity of selected asteroids,natural satellites and terrestrial planets have been estimated.

Tielieusova I. M.   Lupishko D. F.
The YORP-Effect and Axis Rotation of Near-Earth Asteroids **[#1491]**
Using statistical approach it is shown that the available observational data indicate the noticeable influence of the YORP-effect on the rotation rates distribution of the whole population of near-Earth asteroids.

Trigo-Rodriguez J. M.   Llorca J.   Madiedo J. M.   Alonso-Azcárate J.   Rivkin A. S.   Fornasier S.   Belskaya I.   Binzel R. P.   Moyano-Cambero C. E.   Dergham J.   Cortés J.
IR Reflectance Spectra of Antarctic Carbonaceous Chondrites to Better Characterize the Surfaces of Asteroids Targeted by Sample Return Missions **[#1443]**
IR reflectance spectra for NASA Antarctic carbonaceous chondrites from the CM, CO, CH, and CK groups are presented. The location and relative depth of OH bands could be used to identify pristine regions of NEOs selected for future spacecraft missions.

Zamorano J.   Madiedo J. M.   Trigo-Rodriguez J. M.   Izquierdo J.   Ocaña F.
Sánchez de Miguel A.   Toscano F. M.
Large Meteoroids Belonging to the α-Capricornid Meteoroid Stream **[#1181]**
We present here the analysis of a very bright α-Capricornid fireball simultaneously registered from three meteor observing stations on July 31, 2011, with an absolute magnitude of –9.

DAWN OVER VESTA

Carraro F.   Fonte S.   Coradini A.   De Sanctis M. C.   Capaccioni F.   Capria M. T.   Filacchione G.   Ammannito E.   Tosi F.   Cartacci M.   Noschese R.
Calibration Pipeline for VIR Data **[#1439]**
The VIR-MS instrument team has realized a calibration tool that has the goal of producing calibrated (1b level) data starting from the raw (1a level) ones. This tool, developed by using the Java language, has been called "VIR Calibration".

Fonte S. F.   Carraro F. C.   Ammannito E. A.   Coradini A.   De Sanctis M. C.   Magni G. M.
A Validator for SASF (Spacecraft Activity Sequence File) NASA Language Interface in Dawn/VIR Experiment **[#1810]**
VIRV is a tool to checks the VIR instrument sequences during the Dawn campaign. This is a syntax and grammar language checker; the development guidelines of VIRV are the idea of usual compiler, as C/C++ or fortran compilers.

EXOBIOLOGY: FROM WORLDS WE KNOW TO OTHER STARS

Keszthelyi Zs.
Effect of Impact Angle on the Off-Set of Outer vs. Nested Crater for Concentric Impact Structures in Layered Targets: A Tool to Determine Direction of Impact **[#1095]**
The abstract discusses the astrobiology potential of the jovian moon, Europa. Surface features were investigated, especially focusing on possibly uprising material from the putative ocean. Pressure calculation was done for the ocean.

PRINT ONLY

Schuerger A. C. Ming D. W. Golden D. C.
Low Biotoxicities of Analog Soils Suggest that the Surface of Mars May Be Habitable for Terrestrial Microorganisms **[#1507]**
Bacillus subtilis and Enterococcus faecalis were exposed to six Mars analog soils under martian conditions. Only high-salt soils were observed to be moderately biotoxic to both species, suggesting regoltih may be habitable to terrestrial microorganisms.

Schuerger A. C. Moores J. E. Clausen C. Barlow N. G. Britt D. T.
A Proposed UV/CH4 Linked Model for the Global Methane Budget on Mars **[#1911]**
The UV/CH_4 model for Mars is now supported by four studies that demonstrate the evolution of CH_4 from UV-irradiated organics under simulated martian conditions. The UV/CH_4 model predicts a global average up to 11 ppbv from accreted IDP organics.

Swain R. K. Behera D. Sahoo P. K. Swain S. K. Sasmal A.
Lunar Gene Bank for Endangered Species **[#1084]**
In the face of failure of conservation programs, a Gene Bank in the lunar PSR, preferably the Shoemaker crater incorporating natural cryopreservation will provide permanent preservation of germplasms to protect endangered species from extinction.

IMPACT CRATERING STUDIES

Burrer B. Povenmire H.
A Unique Bicolored Bediasite from Bazos County, Texas **[#1257]**
A uniquely bicolored bediasite is described. Generally, bediasites are noted for their homogeneous color and composition. This is a unique specimen as no other similar bediasite has been reported in many thousands of bediasite finds.

McMahon S. Parnell J. Burchell M. Blamey N. J. F.
Methane Retention by Rocks Following Simulated Meteorite Impacts: Implications for Mars **[#1040]**
A high-velocity impact was simulated in the laboratory and methane-retention in the crater quantified by mass spectrometry. The results are consistent with the possibility that impact events could store methane in the martian crust.

Michel P. Schwartz S. R. Richardson D. C. Machii N. Nakamura A. M.
Numerical Simulations of Low-Speed Impact Disruption of Cohesive Aggregates Using the Soft-Sphere Discrete Element Method and Comparison with Experiments on Sintered-Glass-Bead Agglomerates **[#1320]**
We show that simulations using an adapted version of the N-body code pkdgrav to model the behavior of cohesive aggregates under various kinds of stresses can reproduce the outcome properties of low-speed impacts on spherical glass bead agglomerates.

Naumov M. V.
Sulfide Mineralization in the Kara Impact Structure, Russia **[#1313]**
Data on distribution and composition of sulfide mineralization in the 60-km Kara impact structure are given. Both geochemical and isotope data indicate that sulfides in impact melt lithologies arise at the expense of pre-impact sulfides.

Povenmire H. Burrer B. Cornec J. Harris R. S.
The Central American Tektites and Strewn Field Update **[#1260]**
A description of Central American tektite specimens found in Belize including electron microprobe analysis.

PRINT ONLY

Povenmire H. Doss A.
The Second Georgia Tektite Worked Into An Indian Projectile Point **[#1263]**
A Cotaco Creek asymmetrical projectile point made from a Georgia tektite found along the Dodge-Bleckley County line in the middle of the Georgia Tektite strewn field.

Salamunićcar G. Lončarić S.
Crater Detection from Venus Digital Topography and Comparison with Martian and Lunar Craters **[#1159]**
We used a crater detection algorithm (CDA) for detection of craters from Venus digital topography and computation of the depth/diameter ratio. The results were compared with the accompanying results for martian and lunar craters.

Schwartz S. R. Michel P. Richardson D. C.
Numerical Simulations of Low-Speed Impact Cratering into Granular Materials Using a High-Performance Parallel Gravity Tree Code Including both the Soft- and Hard- Sphere Discrete Element Methods **[#2533]**
We carry out N-body simulations of low-speed impact events into beds of granular material using two different collisional routines. Boundary effects are explored by simulating over a small variety of confinement conditions and particle sizes.

Sjöqvist A. S. L. Lindgren P. Mansfeld J. Sturkell E. F. F. Ormö J. Lee M. R.
Carbonate Melt Fragments in Resurge Deposits from the Lockne Impact Structure, Sweden **[#1962]**
The loftarstone resurge deposits from the Lockne impact crater in Sweden contain abundant carbonate and silicate melt fragments.

Valter A. A. Maschak M. S.
About the Same Geological Age and Possible Simultaneous Formation of Obolon' (Ukraine) and Puchezch-Katun' (Russia) Impact Structures **[#1080]**
Structures have Bajocian ages of primary crater sediments and the K-Ar ages of impact glasses: 168 ± 5 Ma (Obolon') and 167 ± 3 Ma (Puchezch- Katun'). Direction of O elongation coincides with (O)-(P) line. They might be formed by the same projectile.

Vishnevsky S. A.
Popigai Astrobleme (Russia), Water and Diamond Potential of the Impactites-Tagamites: Data on Gas Chromatography **[#1315]**
There are "dry" and "wet" Popigai diamond-bearing impactites-tagamites. The general petrology of the rocks and the data regarding their water amount vs. diamond content are presented with the goal of quest of the rocks with the economic potential of diamond.

Whymark A.
Were Australian Tektites Plastically Deformed Prior to Re-Entry? **[#1045]**
Australites are oriented, almost without exception. This constitutes evidence that they were plastically deformed during atmospheric exit. Strong evidence exists for proximal and medial tektites being plastically deformed during atmospheric exit.

PRINT ONLY

MOVERS AND SHAKERS: PLANETARY DYNAMICS AND TECTONICS

Gold M. W. Leitner J. J. Firneis M. G.
Self-Sustaining Dynamos in Massive Terrestrial Exoplanets? **[#1065]**
Do massive terrestrial exoplanets have the ability to generate and sustain magnetic fields over geological time? A simple model shows that due to dominance of conduction, caused by increased pressure and density, this seems to be rather unlikely.

Musiol S. Neukum G.
Finite Element Models of Lithospheric Flexure and Volcanic Spreading at Olympus Mons, Mars **[#1772]**
The formation of Olympus Mons upper-flank terraces, its circumferential scarp, and aureole deposits is investigated with the finite element method. First results for an instantaneous load are given.

OUTER PLANETS: ENCELADUS AND RINGS

Annex A. M.   Verbiscer A. J.   Helfenstein P.
Photometric Properties of Enceladus' South Polar Terrain **[#2698]**
Differences in the photometric properties of terrains near the south pole of Enceladus can be correlated with proximity to source locations of plume activity and anomalously high thermal emission.

Perov N. I.
On a Model of Spokes Origin in the Celestial Mechanical Systems **[#1002]**
It is shown in the celestial mechanical system of nine major massive bodies, which form central configuration, for mass ratio $m_i/m_1 > 0.1$, the bodies of mass m_i, m_5, and m_6 and six points of libration form a spoke's structure.

Taubner R.-S.   Leitner J. J.   Firneis M. G.
The Contribution of Radiogens to the Thermal Budget of Enceladus **[#1206]**
We estimated the radiogenic heat release in Enceladus, which is mainly driven by ^{232}Th, ^{235}U, ^{238}U, and ^{40}K, and concluded that even with more detailed values for those radiogens the amount of radiogenic heat release is just about 0.3 GW.

Yasui Y.   Ohtsuki K.   Daisaka H.
Influence of Formation of Temporary Gravitational Aggregates on Ring Viscosity **[#1698]**
Using local N-body simulation, we examine viscosity of planetary rings consisting of spinning, self-gravitating particles for a wide range of parameters, including the cases of dense rings with temporary aggregate formation.

COSMIC DUST

Fisenko A. V.   Verchovsky A. B.   Semjonova L. F.
The Study of Kinetics of C, N and Xe Release During Isothermal Pyrolysis and Subsequent Oxidation of Nanodiamonds from Orgueil **[#1437]**
The results on kinetics of release of C, N, and Xe under different conditions during pyrolysis of two aliquots from intermediate-grain-sized fraction of nanodiamonds from the meteorite Orgueil are discussed.

Kortenkamp S. J.
Trapping of Interplanetary Dust Particles in Earth's Quasi-Satellite Resonance: Dependance on Particle Size **[#2779]**
Numerical simulations are used to model the orbital evolution of interplanetary dust particles decaying into the inner solar system under PR drag. Trapping in Earth's 1:1 quasi-satellite resonance is studied as a function of dust particle diameter.

PRINT ONLY

COSMOLOGY AND THE EARLY SOLAR SYSTEM

Wilson T. L.   Blome H.-J.
Possible Effects of Cosmological Evolution on the Origin of the Solar System **[#1042]**
The deceleration parameter, Hubble tidal term, and onset of acceleration in Friedmann-Lemaitre cosmology are shown to have remarkable correlations with the origin of the solar system. These are related to existing studies of the protoplanetary disk.

EXOPLANETS

Futó P.
Possible Structure Models for the Transiting Super-Earths:Kepler-10b and Kepler-11b **[#1290]**
It was expected that the mass of Kepler-10b and Kepler-11b would be similar, but they differ in respect to the average density due to their dissimilar compositions.

Futó P.
Coreless Water Ice Planets **[#1293]**
It is expected that outside the snow-line of protoplanetary disks, the formation of a water ice planet with no core is probably more frequent than one with a metallic core.

Marzari F.   Picogna G.   Desidera S.   Vanzani V.
Planetesimal Accumulation Around Kepler-16 (AB) **[#1093]**
We model the planetesimal accretion process and planet migration in the KEPLER-16 (AB) system. The dynamics of both planetesimals and the fully formed planet are investigated with up to date numerical algorithms.

Vidmachenko A. P.   Ivanov Yu. S.   Kostogryz N. M.
Spectropolarimetric Observations of Transiting Extrasolar Planetary System HD189733 **[#1280]**
Spectropolarimetric observations were carried out with spectropolarimeter mounted in the Cassegrain focus at the 70-cm telescope of Golosiiv (Kyiv). We observed the extrasolar planetary system HD189733 during the planet-crossing of the host star.

INSTRUMENT AND PAYLOAD CONCEPTS

Blamey N. J. F.   Parnell J.   Longerich H. P.
Understanding Detection Limits in Fluid Inclusion Analysis Using an Incremental Crush Fast Scan Method for Planetary Science **[#1035]**
We propose formulae for the determination of the detection and reporting limits applied to fluid inclusion volatile analysis, adapted from LA-ICP-MS formulae, and applicable to samples of limited size that are available in planetary science studies.

Cable M. L.   Stockton A. M.   Mora M. F.   Willis P. A.
In Situ Titan Instruments and the Case for Microfluidics-Based Sample Processing and Analysis **[#2206]**
We explore the potential for sample handling and interrogation using microfluidics as an enabling technology for an in situ Titan mission. Benefits include low mass and power, small sample size, and the capability of gas or liquid processing.

JayantaLaha   Dinesh B.   Selvaraj P.   Subhalakshmi Krishnamoorthy
Challenges in the Design of Space Grade State of the Art Navigation Cameras for Lunar Environment **[#1789]**
This paper describes the challenges in the design of navigation cameras for the lunar rover, Chandrayaan-2. These are state-of-the art space-grade cameras designed to withstand the lunar environment. The protomodel is integrated and tested with rover.

EDUCATION AND PUBLIC OUTREACH

Buxner S.   Orchard A.   Colodner D.   Schwartz K.   Crown D. A.   King B.   Baldridge A.
Laurel Clark Earth Camp: A Program for Teachers and Students to Explore Their World and Study Global Change Through Field-Experience and Satellite Images **[#2820]**
The Laurel Clark Earth Camp program provides middle and high school students and teachers opportunities to explore local environmental issues and global change through field-experiences, inquiry exercises, and exploring satellite images.

Grigsby B.   Turney D.   Patterson W.   Bussey D. B. J.   Neish C.   Spudis P.   Beisser K.
Student Planetary Investigators: Students Exploring the Moon Through Mini-RF **[#1862]**
The Student Planetary Investigator Program was created by the Johns Hopkins University Applied Physics Laboratory (APL) Space Department EPO office, where teams of high school students analyze data from the Moon through the Mini-RF insturment.

Horvai F. H.
Connections Among Planetology, Astrobiology and Natural Sciences — Educational Book Project for Universities **[#1733]**
An educational book on astrobiology was published in Hungary, containing background information, figures, connection tables, and references to help the teaching of astrobiology at university level. We show examples of the used educational materials.

Kabai S. Fenyvesi K. Szabó I. Stettner E. Szilassi L. Vörös L. Lénárt I. Bérczi Sz.
Experience-Workshop in Mathematics and Space Education: Joyful Teaching Program in Hungary **[#2611]**
During the last years a program of Experience Workshop on Mathematics organized creative day meetings for teachers and students on the topics of joyful, constructing mathematics. One region of the mathematical construction was the space.

Kereszturi A. Pentek K.
New Planetary Science Course at the University of Western Hungary **[#1778]**
We present examples from a new planetary science course in Hungary, focusing on the comparative issues of various surface processes. The educational materials were tested with undergraduate students at Earth science during the course.

Lebofsky L. A. Higgins M. L. McCarthy D. W. Lebofsky N. R.
Bringing Astronomy Activities and Science Content to Girls Locally and Nationally: A Girl Scout NIRCam Collaboration **[#1303]**
A long-term collaboration between the JWST's NIRCam E/PO team and the Girl Scouts of Southern Arizona brings STEM activities and concepts to Girl Scout leaders, staff, and volunteers, and in turn to their councils and girls.

Madiedo J. M.
The Virtual Museum for Meteorites: An Online Resource for Students, Educators and Researchers **[#1300]**
A Virtual Museum for Meteorites has been created. A description of this on-line tool is given here.

PROGRAM AUTHOR INDEX

** Denotes speaker. WW = Waterway Ballroom; MB = Montgomery Ballroom; TC = Town Center Exhibit Area.*

INDEX

INDEX

INDEX

INDEX

INDEX

INDEX

INDEX

INDEX

INDEX

INDEX

INDEX

INDEX

INDEX

INDEX

INDEX

INDEX

INDEX

INDEX

INDEX

INDEX

INDEX

INDEX

INDEX

INDEX

INDEX

INDEX

INDEX

INDEX

INDEX

INDEX

INDEX

INDEX

INDEX

INDEX

INDEX

NOTES

NOTES

NOTES

NOTES

RADIOISOTOPE POWER SYSTEMS: FUTURE RPS CONCEPTS
Friday, 3:30 p.m. Waterway Ballroom 3

Chairs: **Steve Howe** *(*Center for Space Nuclear Research) and **Rodger Dyson** (NASA Glenn Research Center)

3:30 p.m. Dugala G. M. * Oriti S. M. Meer D. W.
Small Radioisotope Power System Testing at (NASA Glenn Research Center) **[#3044]**
The testing of a small radioisotope power system for use on a lunar mission is described. The system includes an advanced Stirling convertor with a passive balancer, advanced Stirling convertor controller, and a lunar lander simulated test stand.

3:50 p.m. Dyson R. W. *
Novel Stirling Power Systems for Extreme Environments **[#3001]**
This report will describe the development of a combined power and cooling system that enables the exploration of high-temperature solar system bodies.

4:10 p.m. DeChristopher M. J. Tarau C. * Anderson W. G.
Diode Heat Pipes for Long-Lived Venus Landers **[#3101]**
Cooling of long-lived Venus landers can be provided with a radioisotope Stirling power converter and Stirling coolers. The waste heat is transported by a gas charged alkali metal diode heat pipe to the radiator. Test results demonstrate the concept.

4:30 p.m. Ferrulli R. * Howe S. Hundley J. Kaczmarowski A.
Review of $^{250}W_t$ *Radioisotope Powered Thermophotovoltaic Systems* **[#3085]**
Analyzes enabling technologies for thermophotovoltaic power conversion of a radioisotope heat source for performance improvements emphasizing considerations for the heat source, spectral control mechanisms, thermionics, photovoltaics, and radiators.

ADVANCED CONCEPTS: LENR, ANTI-MATTER, AND NEW PHYSICS
Friday, 3:30 p.m. Waterway Ballroom 2

Chair: **Harold White Jr.** (NASA Johnson Space Center)

3:30 p.m. Kim Y. E. *
Cryogenic Ignition of Deuteron Fusion in Micro/Nano-Scale Metal Particles **[#3006]**
Possibility of cryogenic ignition of deuteron fusion in micro/nano-scale metal particles is described based on nuclear fusion theory for Bose-Einstein condensation of deuterons in metal. Experimental tests of hypothesis and predictions of the theory are also discussed.

3:50 p.m. Yang X. Miley G. *
A Game-Changing Power Source Based on Low Energy Nuclear Reactions (LENRs) **[#3051]**
Excess heat generation from our gas-loading LENR power cell has been verified, confirming nuclear reactions provide output energy. Neglecting unlikely chemical reaction contributions, the energy gain is virtually unlimited due to negligible power input with gas loading.

4:10 p.m. White H. * March P.
Advanced Propulsion Physics: Harnessing the Quantum Vacuum **[#3082]**
NASA/JSC is implementing an advanced propulsion physics laboratory, “Eagleworks,” to pursue propulsion technologies necessary to enable human exploration of the solar system over the next 50 years, and interstellar flight by the end of the century.

4:30 p.m. Obousy R. K. * Long K. F. Smith T.
Project Icarus: Antimatter Catalyzed Fusion Propulsion for Interstellar Missions **[#3104]**
This paper will explore the possibility for using antimatter catalyzed fusion propulsion for interstellar missions. This includes direct anti-proton and magnetically insulated ICF schemes.

RADIOISOTOPE POWER SYSTEMS: ALTERNATIVE FUELS AND METHODS
Friday, 1:30 p.m. Waterway Ballroom 3

Chairs: **Ryan Bechtel** (DOE Headquarters) and **Ronald Lipinski** (Sandia National Laboratories)

1:30 p.m. Katalenich J. A. * Hartman M. R. O'Brien R. C. Howe S. D.
Fabrication of Sol Gel Microspheres for Space Nuclear Power **[#3024]**
A testing rig has been developed to investigate a sol-gel process for the fabrication of actinide microspheres for encapsulation in tungsten. Applicability for space fission systems and radioisotope thermoelectric generators is being explored.

1:50 p.m. Williams H. R. * Ambrosi R. M. Ning H. Reece M. J. Bannister N. P. Sarsfield M. J. Stephenson K.
Novel Composite Materials for Primary Containment of Radioisotope Fuel in Spacecraft Energy Systems **[#3040]**
A feasibility study into a Spark Plasma Sintered composite primary containment structure for future radioisotope power systems is reported, including matrix selection, manufacture and mechanical test of a fuel composite with a non-active surrogate.

2:10 p.m. Tinsley T. P. * Sarsfield M. J. Clough M. Rhodes C. Stephenson K.
Design Requirements for a Plant to Produce ^{241}Am Suitable for Use in an European RTG **[#3029]**
Production of ^{238}Pu requires considerable facilities including a nuclear reactor and reprocessing plants that are very expensive to build and operate. ESA plan to use ^{241}Am as an alternative isotope to power future European RTGs and RHUs.

2:30 p.m. Tinsley T. P. * Sarsfield M. J. Cordingley L. Stephenson K.
Development of an Am_2O_3 Fuelled Encapsulated Pellet for Use in RTGs or RHUs **[#3028]**
The ESA has assessed the options for post-launch power generation in future missions and has made the decision to pursue the use of ^{241}Am as an alternative isotope. An item on the ESA roadmap is the design of an Am_2O_3 fuelled encapsulated pellet for use in RTGs or RHUs.

2:50 p.m. Ambrosi R. M. * Williams H. R. Samara-Ratna P. Bannister N. P. Vernon D. Crawford T. Bicknell C. Jorden A. Slade R. Deacon T. Konig J. Jaegler M. Stephenson K.
Development and Testing of Americium-241 Radioisotope Thermoelectric Generator: Concept Designs and Breadboard System **[#3043]**
This paper reports development of an RTG system breadboard to validate design and design methodologies for ^{241}Am spacecraft power sources.

3:10 p.m. BREAK

ADVANCED CONCEPTS: ANEUTRONIC FUSION POWER AND PROPULSION
Friday, 1:30 p.m. Waterway Ballroom 2

Chair: **John Scott** (NASA Johnson Space Center)

1:30 p.m. Chapman J. J. *
Aneutronic Fusion Topics for In-space Applications **[#3027]**
Aneutronic Fusion for In-Space thrust, power. Promise of clean energy and potential nuclear gains. Fusion plant concepts, potential to use advanced fuels. Methods to harness ionic momentum for high Isp thrust plus direct power conversion into electricity will be presented.

1:50 p.m. Krishnamurthy A. Chen G. Ulmen B. A. Keutelian P. Orcutt J. Miley G. H. *
Helicon Injected Inertial Plasma Electrostatic Rocket, HIIPER **[#3045]**
HIIPER (Helicon Injected Inertial Plasma Electrostatic Rocket) is a unique electric thruster where a helicon source produces high density plasma and an IEC grid accelerates ions to produce thrust.

2:10 p.m. Sedwick R. J. *
Magnetic Core Multi-Grid IEC Concept for Burning p-11B **[#3098]**
A natural instability, coupled with trap kinematics, may offer a way to slow thermalization, allowing for the exploitation of a low-energy resonance in p-11B and a subsequent reduction in Bremsstrahlung losses to allow for breakeven operation.

2:30 p.m. Long K. F. * Obousy R. K. Crowl A.
Project Icarus: Specific Power for Interstellar Missions Using Inertial Confinement Fusion Propulsion **[#3103]**
This is an examination of specific power for fusion-propelled intersellar missions looking 1–100 kW/kg from NASA studies and 40–100 MW/kg from BIS Project Daedalus. This work is part of Project Icarus.

2:50 p.m. BREAK

MISSIONS AND ARCHITECTURES: SPACE POLICY AND RISK ANALYSIS
Friday, 1:30 p.m. Waterway Ballroom 1

Chairs: **Jeffrey Nosanov** (Jet Propulsion Laboratory) and **Dave Woerner** (Jet Propulsion Laboratory)

1:30 p.m. Bechtel R. D. * Lipinski R. J.
Radioisotope Power Systems and Launch Approval Overview **[#3086]**
Radioisotope power systems are enabling for exploration of the outer planets and other advanced missions. Approval by the Executive Branch is required for launch. This paper describes power systems and the process for obtaining launch approval.

1:50 p.m. Smith T. E. R. *
International Export Control Law and Reform Applied to Nuclear Space Technologies **[#3039]**
International partnerships are feasible and could save the U.S. money on nuclear space projects. This paper will strive to demystify the export control regime, with discussions on the President's Reform Initiative and potential projects with Russia.

2:10 p.m. Robinson D. G. *
An Advanced Risk Analysis Framework **[#3017]**
This paper provides a summary of the framework developed for the Mars Science Laboratory launch risk analysis.

2:30 p.m. BREAK

RADIOISOTOPE POWER SYSTEMS: STIRLING ENERGY CONVERSION
Friday, 10:30 a.m. Waterway Ballroom 3

Chairs: **Scott Wilson** (NASA Glenn Research Center) and **Wayne Wong** (NASA Glenn Research Center)

10:30 a.m. Williams Z. D. *
ASC-E2 Testing to Characterize Sensitivity of Parameters to AC Bus Voltage Changes **[#3062]**
Testing was conducted on an Advanced Stirling Convertor to see how varying the AC bus voltage will affect other parameters of the convertor. Data from this test was analyzed and compared to previous tests on other convertors.

10:50 a.m. Meer D. W. *
Advanced Stirling Convertor Durability Testing: Plans and Interim Results **[#3022]**
This abstract summarizes the plans, analysis, and initial results for the planned durability testing of the Advanced Stirling Convertor. These tests will exercise the convertor at conditions beyond the design specification.

11:10 a.m. Wilson S. D. *
Heat Transfer Measurement Uncertainty for Stirling Heat Addition Predictions **[#3087]**
In an effort to improve the accuracy of ASC net heat input calculations, validation testing was carried out to provide direct comparison of numerical results and validate net heat input predictions. The combined standard uncertainty is discussed.

11:30 a.m. Bagg S. D. *
Linear Alternator Technologies Used for Free Piston Stirling Engines **[#3047]**
NASA GRC is conducting in-house research on linear alternators used in Stirling convertors for radioisotope space power systems. This abstract summarizes the existing and potential linear alternators that may be used with Stirling power convertors.

11:50 a.m. BREAK

NUCLEAR THERMAL PROPULSION: NTP FUELS II
Friday, 10:30 a.m. Waterway Ballroom 2

Chairs: **Jonathan Webb** (Idaho National Laboratory) and **Stan Borowski** (NASA Glenn Research Center)

10:30 a.m. Cavender D. P. * Mireles O. R. Broadway J. W.
Design of A Uranium-Dioxide Plasma Spheroidization System **[#3041]**
UO_2 Plasma Spheroidization System is NASA's first major process in the development of NTR fuel cermets. Processed powders show significant improvement in mechanical properties and surface morphology for eventual CVD coating.

10:50 a.m. Mireles O. R. * Broadway J. W. Hickman R. R.
Development of a Fluidized Bed CVD System for Coating UO_2 Particles with Tungsten **[#3021]**
Nuclear thermal propulsion (NTP) is under consideration for use in deep space exploration. Tungsten-UO_2 cermet fuel forms require UO_2 powders coated with tungsten to improve fuel properties. This paper details the development of a chemical vapor deposition (CVD) system.

11:10 a.m. Valentine P. G. * Allen L. R. Shapiro A. P.
Advanced Ceramics for Use as Fuel Element Materials in Nuclear Thermal Propulsion Systems **[#3026]**
A variety of ceramic materials, primarily carbides, are being considered for use in the fabrication of two of the three fuel element designs being considered under the NASA NCPS Program — the graphite composite and the advanced carbide approaches.

11:30 a.m. Moran R. P. * Emrich W. J.
Modeling and Simulation of a Nuclear Fuel Element Test Section **[#3050]**
The Nuclear Thermal Rocket Element Environmental Simulator (NTREES) test section closely simulates the internal operating conditions of a thermal nuclear rocket. An extensive thermal fluid analysis was performed in support planned upgrades to NTREES.

FISSION POWER SYSTEMS: TESTING AND VALIDATION
Friday, 10:30 a.m. Waterway Ballroom 1

Chairs: **A. Lou Qualls** (Oak Ridge National Laboratory) and
J. Boise Pearson (NASA Marshall Space Flight Center)

10:30 a.m. Qualls A. L. * Joseph R. A. III Chadwell C. S. Hancock E. F.
The Fission Power System Control Drive Motor Testing **[#3063]**
This study seeks to understand the conditions under which available motor technology can be expected to perform and to determine when and to what extent the motors and control drives may require thermal management.

10:50 a.m. Thomas Godfroy T. G. * Boise Pearson B. P. Kenny Webster K. W.
Build Status of Reactor Simulator for Fission Surface Power Technology Demonstrator Unit **[#3092]**
Currently being developed is a reactor simulator (RxSim) for incorporation into the Technology Demonstrator Unit for the Fission Surface Power System Program. This paper will discuss the current build status of the RxSim.

11:10 a.m. Gibson M. A. * Jaworske D. A. Sanzi J. L. Ljubanovic D. Sechkar E. A.
Flight Experiments of Planetary Gravitational Effects on Thermosyphon Flooding Limits **[#3048]**
This experiment was designed to set precedence on determining the flooding limitations of thermosyphons in reduced gravity environments and compile the results into correlation models.

11:30 a.m. Sanzi J. L. * Jaworske J. A.
Titanium-Water Thermosyphon Gamma Radiation Effects **[#3055]**
Titanium-water thermosyphons are being considered for use in heat rejection systems for fission power systems.

RADIOISOTOPE POWER SYSTEMS: STIRLING GENERATORS
Friday, 8:30 a.m. Waterway Ballroom 3

Chairs: **Rebecca Onuschak** (DOE Headquarters) and **Wayne Wong** (NASA Glenn Research Center)

8:30 a.m. Withrow J. P. *
Advanced Stirling Radioisotope Generator Flight Development **[#3107]**
Radioisotope-based generators have powered missions to collect planetary science data since the launch of an astronaut-deployed generator on the Moon's surface during Apollo 12 in 1969.

8:50 a.m. Wong W. A. * Wilson K. Smith E. Collins J.
Pathfinding the Advanced Stirling Convertor Flight Design with the ASC-E3 **[#3076]**
Sunpower, NASA GRC and Lockheed Martin are developing the flight ASC-F in parallel with the ASC-E3 pathfinders. The ASC-E3 units reduce risk by validating the flight design prior to implementation on the ASRG flight convertors.

9:10 a.m. Collins J. * Wong W. Wilson K. Smith E. Dunlap M. A.
A Dynamic Path to Flight — Sunpower and the Advanced Stirling Convertor (ASC-F) **[#3083]**
For the flight project, Sunpower has transformed from R&D to a flight-qualified vendor. A review and status will be presented for Sunpower capabilities, design status, and production progress.

9:30 a.m. Oriti S. M. * Schmitz P. C.
Test Hardware Design for Flight-Like Operation of Advanced Stirling Convertors (ASC-E3) **[#3064]**
NASA Glenn Research Center is preparing test hardware for upcoming extended operation of ASC-E3 units that will emulate the ASRG flight design. An overview of the test hardware and its engineering are presented here.

9:50 a.m. Noravian H. * Carpenter R. T.
ASRG/DASRG Electrical Power Predictions in Lunar Environment **[#3105]**
This paper shows the use of Small Stirling RPS or modified Advanced Stirling Radioisotope Generator (ASRG) for the International Lunar Network (ILN) missions, on the surface of the Moon.

10:10 a.m. BREAK

NUCLEAR THERMAL PROPULSION: NTP FUELS I
Friday, 8:30 a.m. Waterway Ballroom 2

Chairs: **Robert Hickman** (NASA Marshall Space Flight Center)
Omar Mireles (NASA Marshall Space Flight Center)

8:30 a.m. Webb J. A. *
A Review of Historical Tungsten CERMET Fuel Development Programs and Lessons Learned **[#3054]**
This presentation outlines the actions and results of previous tungsten cermet fuel programs and presents a list of recommendations for future cermet fuels programs.

8:50 a.m. Broadway J. W. * Hickman R. R. Mireles O. R.
The Manufacture of W-UO_2 Fuel Elements for Nuclear Thermal Propulsion Using the Hot Isostatic Pressing Consolidation Process **[#3020]**
The purpose of this paper is to discuss current cermet fuel material development being performed at NASA's Marshall Space Flight Center. Specifically, cermet is fabricated using the hot isostatic press consolidation process.

9:10 a.m. Webb J. A. * Harp J. Werner J.
W-UO_2 CERMET Fuel Development Via Pulsed Eleectric Current Sintering **[#3058]**
This presentation outlines the objectives and accomplishiments of a Tungsten-UO_2 development program at the Idaho National Laboratory for the previous year.

9:30 a.m. O'Brien R. C. * Jerred N. D. Howe S. D. Samborsky R. Brasuell D. Zillmer A.
Recent Research Activities at the Center for Space Nuclear Research in Support of the Development of Nuclear Thermal Rocket Propulsion **[#3060]**
The CSNR is undertaking activities in collaboration with the Aerojet Corporation to further the development of safe, practical and affordable nuclear thermal propulsion systems. A summary is presented with the progress made and the challenges ahead.

9:50 a.m. BREAK

FISSION POWER SYSTEMS: POWER CONVERSION, MANAGEMENT, AND DISTRIBUTION
Friday, 8:30 a.m. Waterway Ballroom 1

Chairs: **Maxwell Briggs** (NASA Glenn Research Center) and **Thomas Godfroy** (Maximum Technology Corp.)

8:30 a.m. Wood J. G. * Holliday E. S. Stanley J. C.
First Operation of a 12 kWe Stirling Power Conversion Unit for Fission Power Technology Demonstration **[#3072]**
Sunpower is developing a 12 kW dual-opposed Stirling Power Conversion Unit (PCU) with controller. This work is funded by NASA-Glenn Research Center (GRC) and is to be used as part of a fission power technology demonstration.

8:50 a.m. Briggs M. H. *
Dynamic Behavior of Kilowatt Class Stirling Convertors with Coupled Expansion Spaces **[#3032]**
A small power oscillation was observed during the testing of two Stirling convertors in a thermodynamically coupled configuration. This paper investigates the cause of the oscillation and ways to control and/or eliminate it.

9:10 a.m. Birchenough A. Hervol D. * Geng S. Briggs M.
Operational Test Results of a 2 kW Stirling Power Conversion Unit with a GRC Developed Engine Controller and PMAD System **[#3042]**
A NASA GRC designed PMAD and control system was built and connected to a Stirling engine pair. Testing demonstrated successful control during different phases of engine operation.

9:30 a.m. Guimaraes. L. N. F. * Placco. G. M. Barrios A. G. Jr. Borges. E. M. Nascimento. J. A.
Alternative Technologies for Power Conversion on the TERRA Project **[#3013]**
This paper will present the developments that have been accomplished on the TERRA Project regarding Tesla turbine and Stirling engine. The TERRA project aims to prepare the Brazilian space program to take advantage of the nuclear space technology.

9:50 a.m. Andreev P. V. Gulevich A. V. Zaritsky G. A. Legostaev V. P. Nikonov A. M. Ovcharenko M. K. Pyshko A. P. Sinyavsky V. V. Yarygin V. I. *
Physical and Engineering Potential of Thermionics for Advanced Projects of Sub-Megawatt SNPS **[#3014]**
The second-generation sub-megawatt class nuclear thermionic power systems that will be used to supply power for energy-intensive spacecraft and complexes, including lunar and martian outposts, advanced spacecrafts with nuclear power and propulsion systems, etc., are discussed.

10:10 a.m. BREAK

POSTER SESSION: NUCLEAR AND EMERGING TECHNOLOGIES FOR SPACE
Thursday, 6:00 p.m. Town Center Exhibit Area

Hu X. Aghara S. K.
Assessment of Geometry Effects in Monte Carlo Simulations to Evaluate Neutron Albedo on the Lunar Surface **[#3036]**
Developing the small spherical and cylindrical geometry to study geometric effects. Placing water and human tissue cylinders above the cylindrical surface to study energy deposition of neutron albedo.

Tarditi A. G. Miley G. H.
Fission Fragment Direct Energy Conversion into Low-Frequency Alternating Current **[#3090]**
A different approach to fission fragments direct energy conversion is here considered by investigating the possibility of converting the fission fragment kinetic energy into alternating current via a traveling wave coupling.

Myers S. C. Porterfield D. R. Carver N. R. Jump R. K. Foster L. A.
Gamma-Ray Isotopic Analysis of Heat Source Plutonium Using FRAM Software **[#3007]**
An alternative method for the determination of plutonium isotopic abundances in heat source plutonium (>80% ^{238}Pu) uses high-purity germanium detectors in conjunction with the LANL developed FRAM software package.

Howe T. M. O'Brien R. C. Stoots C. M.
Development of a Small-Scale Radioisotope Thermo-Photovoltaic Power Source **[#3059]**
Overview of an RTPV space power system utilizing variable emitter shapes, temperatures, and materials to allow for a customizable power source with high efficiency and low mass to be housed safely in proximity to instruments and equipment.

Fraeman M. E. Frankford D. P. Shamkovich A. L. Denissen R. A.
Single Stirling Convertor Controller Spacecraft Interface **[#3012]**
The interface between an active controller for a single Stirling convertor and a spacecraft is described. The controller can detect a wide variety of interface faults and then implement corrective actions that allow the mission to continue.

Thelander S. D. Lohman K. T. Schmidt E. A. Williams C. H.
Initial Vibration Analysis of the ASRG's Effect on Spacecraft Instruments **[#3010]**
A vibration analysis was performed to investigate the vibration impact of the Advanced Radioisotope Stirling Generator (ASRG) on spacecraft instruments. Analysis, results, and recommendations to future ASRG users are provided.

Peterson J. R. Kurwitz R. C. Carron I.
MCNP Modeling of Photo-Neutronic Methods for Gauging Fluid Levels in Cryogenic Hydrogen Propellant Tanks **[#3099]**
Accurately gauging the fluid level in propellant tanks is critical. Many hydrogen gauging methods in place today are inaccurate or require excessive time to obtain readings. Photon sources and detectors can create quick and accurate gauging systems.

Stoots C. O'Brien R. McKellar M.
Nuclear-Powered Co-Electrolysis for Mars Combined Life Support and Methanol Production **[#3002]**
High temperature co-electrolysis can be used to reduce H_2O and CO_2 simultaneously in an integrated nuclear-powered concept for combined life support and *in situ* resource utilization for space applications.

Tarditi A. G. Miley G. H. Scott J. H.
Investigation on Enabling Technologies for a Near-Term Aneutronic Fusion Propulsion Experiment **[#3089]**
The present study explores the feasibility of direct energy conversion from the products of aneutronic fusion reactions directly into propulsive thrust.

RADIOISOTOPE POWER SYSTEMS: THERMOELECTRIC ENERGY CONVERSION
Thursday, 3:30 p.m. Waterway Ballroom 3

Chairs: **Jean-Pierre Fleurial** (Jet Propulsion Laboratory) and **Joseph Sholtis (**Consultant)

3:30 p.m. Caillat T. * Firdosy S. Li B. C- Y. Huang C. -K. Cheng B. Paik J. Chase J. Arakelian T. Lara L. Fleurial J. -P.
Progress Status of the Development of High-Efficiency Segmented Thermoelectric Couples **[#3077]**
Advanced thermoelectric couples have demonstrated 11 to 15% conversion efficiencies with cold and hot side temperatures in the 150°–200°C and 800°–1000°C range, respectively.

3:50 p.m. Fleurial J. P. * Bux S. K. Li B. C. Y. Huang C. K. Cheng B. J. Vo T. VonAllmen P. Caillat T. Pei Y. Lalonde A. Snyder G. J. King D. Star K. Ma J. Kaner R. B. Dunn B. S. Cox C. Kauzlarich S. M.
Progress Towards High Efficiency Thermoelectric Materials for Space Power **[#3080]**
An overview of collaborative research efforts to identify and characterize advanced bulk thermoelectric materials capable of quadrupling average ZT values and achieving at least 20% efficiency while maintaining long-term reliable power generation operation.

4:10 p.m. LaLonde A. D. * Pei Y. Wang H. Snyder G. J.
Lead Telluride Alloy Thermoelectrics **[#3071]**
Key aspects for achieving maximum performance and successful band structure engineering strategies for further improvements in PbTe based materials are identified based on past and present successes of the material.

4:30 p.m. Paik J. * Firdosy S. Fleurial J. -P. Caillat T.
Life Testing of Advanced of Advanced Thermoelectric Components **[#3078]**
Life test data for advanced thermoelectric materials (n-type $La_{3-x}Te_4$, p-type $Yb_{14}MnSb_{11}$, and n- and p-type filled skutterudites) and associated components is presented.

NUCLEAR THERMAL PROPULSION: MODELING
Thursday, 3:30 p.m. Waterway Ballroom 2

Chairs: **Stan Borowski** (NASA Glenn Research Center) and
Jeramie Broadway (NASA Marshall Space Flight Center)

3:30 p.m. Litchford R. * Luo W. Cassibry J.
Physics Based Modeling for Nuclear Rocket Fuel Development **[#3061]**
Physics based modeling for nuclear rocket fuel development.

3:50 p.m. Appel B. C. *
Combined Neutronics and Thermal-Hydraulics Simulation of the Argonne National Lab 10 klbf-Thrust Cermet Nuclear Thermal Rocket **[#3067]**
In the 1960s, the Argonne National Lab demonstrated the feasibility of tungsten-cermet fuel for a nuclear thermal rocket. This study evaluates a 10 klbf-thrust design developed at ANL by combining neutronics simulations with CFD models.

4:10 p.m. Harrison T. J. * Qualls A. L.
Analysis of Burnup Effects on Reactor Control Strategies **[#3057]**
Most proposed space applications use small, fast-spectrum cores. This paper describes calculational methods to include burnup effects to better optimize the control strategy.

4:30 p.m. Shipley K. Sudderth L. * Deason W. Casey D. Fischhaber L. Marquis J. Saleem R.
High Performance Bimodal Nuclear Thermal Rocket **[#3025]**
A high performance BNTR achieves 100 kWe using W-Re cermet fuel, with peak fuel temperature of 3000 K. A thrust to weight ratio of 1.3 is achieved with 6000 lbf thrust. The system mass is 3600 kg, including the reactor, shield, Brayton components, and radiators.

FISSION POWER SYSTEMS: HEAT TRANSFER AND THERMAL CONTROL
Thursday, 3:30 p.m. Waterway Ballroom 1

Chairs: **Marc Gibson** (NASA Glenn Research Center) and
Omar Mireles (NASA Marshall Space Flight Center)

3:30 p.m. Gu H. * Shouzhi Z. Zhiyong S. Gang C. Chengzhi Y. Yunpeng S. Hong Y.
A Heat Pipe Cooled Modular Reactor Concept for Manned Lunar Base Application **[#3015]**
A lithium heat pipe cooled modular fast reactor (HPCMR) power system concept has been developed for manned lunar base application. The system is designed to use the static thermoelectric conversion module to produce over 100 kW electricity for up to ten years.

3:50 p.m. Geng S. M. * Niedra J. M. Polzin K. A.
Magnetic Analysis of an Annular Linear Induction Pump for Fission Power Systems **[#3033]**
A 3-D magnetostatic model was created of a prototypic annular linear induction pump (ALIP) for fission power systems. This paper presents the model along with performance predictions generated at various ALIP operating conditions.

4:10 p.m. Flanders J. M. * Eades M. J. Blue T. E. Sun X.
Heat Exchanger Considerations for a Space Molten Salt Reactor **[#3075]**
Research at the Ohio State University has identified molten salt reactors as a potentially appealing technology for high-power, high-temperature space fission systems. The design aspect of the heat exchangers for a Brayton cycle is discussed.

4:30 p.m. Jaworske D. A. * Gibson M. A. Hervol D. S.
Heat Rejection from a Variable Conductance Heat Pipe Radiator Panel **[#3016]**
A titanium-water heat pipe radiator panel was evaluated in vacuum. Variable conductance heat pipes were sandwiched between two polymer matrix composite face sheets. Heat rejection was calculated utilizing the Stefan-Boltzmann equation.

4:50 p.m. Briggs M. H. *
Conceptual Design of an Affordable Radiator for the Fission Power System Technology Demonstration Unit **[#3031]**
Results of a trade study on affordable radiator designs for the Fission Power System (FPS) Technology Demonstration Unit (TDU).

RADIOISOTOPE POWER SYSTEMS: RPS DESIGN SAFETY
Thursday, 1:30 p.m. Waterway Ballroom 3

Chairs: **Ronald Lipinski** (Sandia National Laboratories) and **Ryan Bechtel** (DOE Headquarters)

1:30 p.m. Clayton D. J. Lucas G. M. * Radel T. E. Wiberg B. D.
Accident Sequence Modeling for Radioisotope Power Systems **[#3008]**
Radioisotope power systems have extended our knowledge of the solar system. Due to the hazardous material that can be released during a launch accident, the potential health risk of an accident must be quantified.

1:50 p.m. Clayton D. J. * Lucas G. M. Radel T. E.
Resulting Source Term from the Mars Science Laboratory Safety Analysis **[#3009]**
An updated Final Safety Analysis Report was prepared for the MSL launch. A summary of the results of the source term analysis from the updated Final Safety Analysis Report are presented here.

2:10 p.m. Lipinski R. J. * Tikare V.
Model for Grain Growth in DOP-26 Iridium Clad **[#3004]**
The nuclear fuel in a radioisotope power system is contained within an iridium alloy. To avoid brittle behavior, the iridium grains must be small compared to the clad thickness. This paper describes an improved model for grain growth.

2:30 p.m. Clayton D. J. * Lucas G. M.
Solid Propellant Behavior in Radioisotope Power Systems Accident Sequence Modeling **[#3046]**
Observations from accident videos have enabled a closer look into the solid propellant processes that occur during a launch accident. Modifications to the fragment distribution model, along with a secondary fragmentation model are discussed.

2:50 p.m. Gelbard F. *
Analysis of Aluminum Drop Combustion in the Gap Region Below a Burning Propellant **[#3003]**
The temperature below a burning propellant during a hypothetical accident is of interest for determining possible vaporization of hazardous materials. The conditions for aluminum drop oxidation that would affect the temperature below the propellant are analyzed.

3:10 p.m. BREAK

NUCLEAR THERMAL PROPULSION: PROGRAM OVERVIEW
Thursday, 1:30 p.m. Waterway Ballroom 2

Chairs: **Bruce Schnitzler** (Idaho National Laboratory)
Jonathan Webb (Idaho National Laboratory)

1:30 p.m. Borowski S. K. * Lapointe M. R. Houts M. G. Warren J. W.
Nuclear Thermal Rocket (NTR) Propulsion: "Before the Decade is Out" **[#3088]**
The NTR has demonstrated all the key performance parameters needed for a human Mars mission. NASA task activities are reviewed and a development strategy is presented aimed at ground testing a small, scalable engine before 2020 with a flight test shortly thereafter.

1:50 p.m. Houts M. G. * Borowski S. K. George J. A. Kim T. Emrich W. J. Hickman R. R. Broadway J. W. Gerrish H. P. Adams R. B.
Nuclear Cryogenic Propulsion Stage **[#3093]**
The fundamental capability of Nuclear Thermal Propulsion (NTP) is game changing for space exploration. A first-generation Nuclear Cryogenic Propulsion Stage (NCPS) based on NTP could provide high thrust at a specific impulse above 900 s.

2:10 p.m. Hickman R. R. * Broadway J. W. Mireles O. R. Webb J. A. Qualls L. A.
Nuclear Cryogenic Propulsion Stage Fuel Materials Design and Fabrication **[#3019]**
Nuclear Thermal Propulsion (NTP) is currently being developed on a NASA/DOE project. The purpose of this paper is to provide an overview of the project including development needs, test goals, and relevance to future efforts.

2:30 p.m. Manning B. T. * Allen R. E. Chlapek T. M. Shipley K. J.
Affordable Development and Implementation of Nuclear Thermal Rockets for Mars Missions **[#3049]**
Utilizing technology derived from the NERVA program in the 1960s along with the SAFE engine testing facility, a NTR-driven Mars sample return mission could be completed on a schedule and budget competitive with current chemical architectures.

2:50 p.m. BREAK

FISSION POWER SYSTEMS: REACTOR DESIGN AND SIMULATION
Thursday, 1:00 p.m. Waterway Ballroom 1

Chairs: **Shannon Bragg-Sitton** (Idaho National Laboratory) and
Sterling Bailey (Bailey Engineering and Management)

1:00 p.m. Rogerson W. T. Jr. * Brown S. W. Smith D. R.
Y-12 National Security Complex's Contribution to Nuclear Space Applications: Past, Present, and Future **[#3030]**
Y-12 has a history of contributions to NASA programs, and has been a part of every mission that carried a nuclear package. Paper details relationship between Y-12 and NASA, and discusses opportunities for future contributions to nuclear systems for deep space travel.

1:20 p.m. Bragg-Sitton S. M. * Bess J. D. Poston D. I. Bailey S.
Criticality Testing Needs for a Small Fast-Spectrum Reactor Design for Space Power Application **[#3037]**
This paper reviews possible reactor physics and criticality testing needs to support development and qualification of a fission reactor design that could be employed on lunar, martian or asteroid surfaces.

1:40 p.m. Poston D. *
Overview of MRPLOW: A Design Tool for Surface Reactor Power Systems **[#3097]**
MRPLOW is the driver for a design process that creates and/or evaluates fission surface power (FSP) system concepts. MRPLOW is used in conjunction with several other tools to complete an automated, versatile, and high-fidelity design process.

2:00 p.m. Eades M. J. * Flanders J. M. Sun X. Blue T. E.
Space Molten Salt Reactor Design Considerations and Research Needs **[#3070]**
The unique design considerations of a space molten salt reactor are discussed. A focus is given on how the design considerations of a space molten reactor compare to that of more familiar solid fueled reactors.

2:20 p.m. Miller C. G. * Lin T. F.
Experimental Study of Lithium Capillary Flow and Evaporative Processes Under Simulated Reactor Conditions **[#3084]**
Under experimentally simulated reactor conditions a capillary pore structure was shown to sustain rigorous liquid lithium flow up to a capillary limit, to sustain evaporative heat transfer, and to replace evaporated lithium with fresh liquid lithium.

2:40 p.m. BREAK

RADIOISOTOPE POWER SYSTEMS: MISSION SIMULATION, INTEGRATION AND TEST
Thursday, 10:30 a.m. Waterway Ballroom 3

Chairs: **June Zakrajsek** (NASA Glenn Research Center) and **Karla Clark** (Jet Propulsion Laboratory)

10:30 a.m. Johnson S. G. * Dwight C. C. Lively K. L.
So Exactly How Do You Get a Radioisotope Power System into Space for a NASA Mission? **[#3034]**
Radioisotope power systems (RPSs) are an enabling technology for deep space and various planetary missions. This paper describes the various activities conducted by the Department of Energy to provide a RPS to a NASA center for launch into space.

10:50 a.m. Giglio J. C. * Jackson A. A.
Enhanced Thermal Vacuum Test Capability for Radioisotope Power Systems at the (Idaho National Laboratory) *Better Simulates Environmental Conditions of Space* **[#3011]**
The thermal vacuum test chamber located at the Idaho National Laboratory is the first of its kind capable of accurately simulating the space environment while testing a fueled radioisotope power system.

11:10 a.m. Cataldo R. L. * Tatro C. A. Colozza A. J. Wang X. Y. Rusick J. J.
Concept of Operations for the Advanced Stirling Radioisotope Generator **[#3074]**
Description of the concept of operations of the ASRG on a surrogate mission highlighting new potential possibilities provided by the Advanced Stirling Radioisotope Generator (ASRG) and possible spacecraft accommodations required for its use.

MISSIONS AND ARCHITECTURES: SPACE RADIATION SHIELDING AND LUNAR SURFACE CONCEPTS
Thursday, 10:30 a.m. Waterway Ballroom 2

Chairs: **Jacklyn Green** (Jet Propulsion Laboratory) and
Yasunori Miura (Yamaguchi University/Al.I. Cuza University)

10:30 a.m. Rukhadze L. Kutelia E. R. Maisuradze N. Eristavi B. Bakhtiyarov S. I. *
A Novel Radiation Shielding Nano-Composite Material for Space Exploration **[#3018]**
Although nanomaterials have found broad applications in the exploration of space, the emerging new generation of carbon nanoparticles doped with neutron absorbing clusters (for example, boron carbide) is not well characterized.

10:50 a.m. Sriprisan S. I. * Aghara S. K. Singleterry R. C.
Optimization of Shielding Design for Secondary Particle Radiations from SPEs **[#3052]**
The simulation based on the MCNPX code has been developed to analyze multi-material-layer shielding materials (Al and CH_2) for shielding optimization. The study presents the development of the preliminary optimal shielding configuration.

11:10 a.m. Miura Yas. *
Surface Regolith Breccias Formed by Shock Evolution on the Moon and Asteroids Related with Huge Nuclear Explosions **[#3100]**
Glassy regolith with carbon on the Moon is similar to formation at nuclear explosions, which are checked on the Hiroshima and Nagasaki nuclear explosion samples. This result can be applied to the regolith mixing process on asteroids and some planetary surfaces.

ADVANCED CONCEPTS: ADVANCED FISSION CONCEPTS AND SYSTEMS
Thursday, 10:30 a.m. Waterway Ballroom 1

Chair: **Jeffrey George (**NASA Johnson Space Center)

10:30 a.m. Mason L. S. * Oleson S. R. Mercer C. R. Palac D. T.
Nuclear Power System Concepts for Electric Propulsion Missions to Near Earth Objects and Mars **[#3066]**
This paper examines the fission power concepts developed to support recent studies for nuclear electric propulsion (NEP) missions to near Earth objects (NEOs) and Mars.

10:50 a.m. Cliquet E. * Ruault J.-M. Roux J.-P. Paris N. Cazalé B.
Study of a Megawatt Level Power Generation System for Exploration Missions **[#3005]**
CNES and AREVA have done a study of a megawatt level power generation system. The paper will describe the method used and results obtained.

11:10 a.m. George J. A. *
Solid-State Nuclear Power **[#3095]**
A strategy for "solid-state" nuclear power is proposed to guide development of technologies and systems into the second 50 years of nuclear spaceflight. The strategy is based upon a simplified integrated system architecture with few moving parts or fluid loops.

11:30 a.m. O'Brien R. C. * Stoots C. M. McKellar M. G.
In-Situ Resource Utilization and Cabin Atmosphere Revitalization Via the Use of Nuclear Process Heat and Electrical Power Generation **[#3079]**
In situ resource utilization on planetary surfaces may be considered to be beneficial under future manned or robotic space exploration missions. In this presentation, example *in situ* processes that may be coupled to "nuclear enabled" mission architectures are presented.

RADIOISOTOPE POWER SYSTEMS: ^{238}PU PRODUCTION AND ANALYSIS
Thursday, 8:30 a.m. Waterway Ballroom 3

Chair: **Alice Caponiti** (DOE Headquarters)

8:30 a.m. Wham R. M. *
Plutonium-238 Technology Demonstration Project **[#3053]**
This paper reports plans and current status of target design qualification, target fabrication, irradiation, and chemical processing development tasks have begun in order to develop appropriate technology to supply new ^{238}Pu.

8:50 a.m. Stoll M. E. * Spengler D. J. Vigil M. L.
Processing and Purification of Heat-Source $^{238}PuO_2$ (HS-PuO_2) at Los Alamos National Laboratory **[#3038]**
Aqueous processing of reclaimed PuO_2 scrap and residues is an integral first step in the ultimate production of fueled clads as heat sources for Radioisotope Thermoelectric Generators and Radioisotope Heater Units (RHU). Our current processing methods will be discussed.

9:10 a.m. Whiting C. E. * Kramer D. P. Cairns-Gallimore D. Barklay C. D.
PuO_2 — A Powerful Oxidizing Agent? **[#3069]**
PuO_2 typically contains strong oxidizing agents that are outgassed under conditions found in fuel pellet processing and space flight. Reactions of these agents with materials found near PuO_2 during processing and flight are modeled and discussed.

9:30 a.m. Brockman R. A. Kramer D. P. * Barklay C. D. Cairns-Gallimore D.
Finite Element Analysis of Temperature and Stress Fields During Fabrication of $^{238}PuO_2$ Fuel Pellets **[#3035]**
Modeling of $^{238}PuO_2$ fuel pellet unit operations can be beneficial in the understanding and control of the processing parameters with the goal of further enhancing the desired characteristics of the RPS fuel.

9:50 a.m. Richardson P. D. Jr. Mulford R. N. * Chavarria R. Gower J. S.
Iridium Welds on Simulant Fuel Clads, Characterizations and Qualification **[#3056]**
Qualification of iridium welds is described, and consistency of welds demonstrated, and discussed in terms of welding behavior of iridium alloys.

10:10 a.m. BREAK

FISSION POWER SYSTEMS
Thursday, 8:30 a.m. Waterway Ballroom 1

Chairs: **Don Palac** (NASA Glenn Research Center) and **James Werner** (Idaho National Laboratory)

8:30 a.m. Palac D. T. *
Space Fission Power: A New Opportunity for Systems Technology Leadership **[#3023]**
Fission Space Power System Technology represents an opportunity to reestablish leadership in systems technology development by completing the Technology Demonstration Unit now being built and demonstrating readiness for mission applications.

8:50 a.m. Poston D. * Kapernick R. Dixon D. Reid R. Mason L.
Reactor Module Design for a Kilowatt-Class Space Reactor Power System **[#3094]**
A simple fission system can provide robust, long-lived space power in the range of 1 to 10 kWe. This study examines a heat-pipe cooled reactor that could provide power to a 1-kWe thermoelectric power system or a 3-kWe Stirling power system.

9:10 a.m. Dixon D. D. * Poston D. I. McClure P. R.
Fission Power Systems and Vehicle Technologies to Enable Significant Ground-Based Exploration of the Martian Surface **[#3096]**
A fission power system, transported (or "towed") by a vehicle, could enable large-scale ground exploration of the martian surface.

9:30 a.m. Ilin A. V. * Chang Diaz F. R. Glover T. W. Carter M. D. Cassady L. D. White H.
Nuclear Electric Propulsion Mission Scenarios Using VASIMR Technology **[#3091]**
This paper will present resent results using VASIMR-NEP for missions including (1) a robotic mission to Mars, (2) a human mission to Mars, (3) robotic missions to Jupiter, and (4) a precursor interstellar mission.

9:50 a.m. BREAK

NETS TUTORIAL: BUILDING THE BRIDGE BETWEEN SCIENCE MISSIONS AND NUCLEAR POWER SOURCES
Wednesday, 12:15 p.m. Panther Creek

Introduction to Nuclear Systems and Nuclear Technology: This tutorial is designed to better prepare attendees who are unfamiliar with nuclear systems to attend the NETS technical sessions. This goal will be accomplished by first providing an overview of nuclear terminology and discussing the capabilities and attributes of radioisotope power systems and fission power systems currently available and being designed to provide both power and propulsion for space missions. The tutorial will also provide a general overview describing the unique aspects of space nuclear missions with regard to the general manufacture, assembly, testing, and delivery of a nuclear unit to the launch site and the associated safety assessments.

Moderator: **James Werner**

Panel Members: **James Werner, Ryan Bechtel, Stephen Johnson**

The Audience is Encouraged to Bring a Lunch to Enjoy During the Tutorial!

James Werner (Idaho National Laboratory, Space Reactor Technology Program)
Introduction to Radioisotope and Reactor System Designs for Power and Propulsion Applications

Ryan Bechtel (DOE NE-75, Space Nuclear Systems Program Manager)
Discussion of the Safety Aspects Involved in the System Design and Launch Approval for Nuclear Systems

Stephen Johnson (INL, Space Nuclear Systems and Technology Division Director)
Overview of Manufacturing and Assembly, System Testing and Delivery of a Nuclear Unit to the Launch Site

NUCLEAR AND EMERGING TECHNOLOGIES FOR SPACE: OPENING PLENARY
Wednesday, 5:30 p.m. Waterway Ballroom 4/5

What Can Nuclear Power Sources Do for Science?

Moderators: **Leonard Dudzinski** (NASA Headquarters) and **Wade Carroll** (Department of Energy Headquarters)

Panel Members: **Ralph L. McNutt Jr., Michael Meyer, Steve Squyres**

The NETS opening plenary will take an in-depth look at what nuclear power sources have offered to science missions in the past, how they are being employed today, and what might be on the horizon for the future.

5:30 p.m. ***Ralph L. McNutt Jr.*** (Science and Analysis Branch, Chief Scientist for Space Science, Johns Hopkins University Applied Physics Laboratory)
Historical Overview of RPS-Enabled Planetary Science Missions

5:55 p.m. ***Michael Meyer*** (Lead Scientist for NASA's Mars Exploration Program, NASA Headquarters)
Current Applications of Radioisotopes in Science Missions

6:20 p.m. ***Steve Squyres*** (Goldwin Smith Professor of Astronomy, Cornell University)
What Does the Future Hold?

Guide to Technical Program

LPSC WEEK AT A GLANCE

Day and Time	Waterway Ballroom 1	Waterway Ballroom 4	Waterway Ballroom 5	Waterway Ballroom 6	Montgomery Ballroom
Monday Morning, 8:30 a.m.	**SPECIAL SESSION:** A Season in the Saturn System I	New Views on Lunar Volatiles	Hot Stuff: Interplanetary Studies of Impact Melt	Chemical Processes in the Solar Nebula and Latest Genesis Results	Achondrites: From Core to Crust
Monday Afternoon, 1:30 p.m.		**PLENARY SESSION:** Masursky Lecture and Dwornik Award Presentations			
Monday Afternoon, 2:30 p.m.	**SPECIAL SESSION:** A Season in the Saturn System II	Mind the Gap: Lunar Petrology and Remote Sensing	Movers and Shakers: Planetary Dynamics and Tectonics	Recent Slope Processes on Mars: Sliding, Flowing, and Falling Down	
Monday Evening, 5:30 p.m.		**NASA Headquarters Briefing**			
Tuesday Morning, 8:30 a.m.	**SPECIAL SESSION:** Planetary Hydrology: Wet Worlds	Diverse Views of the Lunar Crust: An Orbital Perspective	Solar Nebula Mixing and CAIs	New Martian Meteorites and New Perspectives on Old Favorites	Venus Volcanism Viewpoints: Vague or Viable?
Tuesday Afternoon, 1:30 p.m.	Ice is Nice: Icy Satellite Landforms, Processes, and Structure	Opportunities for Scientist Participation in Education and Public Outreach	Isotopic Constraints on Early Solar System Chronology	Martian Hydrated Minerals and Volatiles from Mantle to Surface	
Tuesday Evening, 6:00 p.m. Town Center Exhibit Area Poster Session I					
Wednesday Morning, 8:30 a.m.	**SPECIAL SESSION:** MESSENGER's First Year in Orbit About Mercury	Airless Bodies Exposed: Space Environment Conditions and Surface Interactions	Impact Ejecta: Processes and Products	Primary and Secondary Martian Geochemistry	Primary and Secondary Martian Geochemistry
Wednesday Afternoon, 12:15 p.m. Panther Creek **NETS Tutorial: Building the Bridge Between Science Missions and Nuclear Power Sources**					
Wednesday Afternoon, 1:30 p.m.	Mercury Composition and Evolution from the Inside Out	Impact Craters: Peaks, Rings, and Basins	Small Body Studies I: Formation, Regolith, and Rubble Piles	Roving on Mars: Current and Future Sites	Chondrite Components and Primary Processes
Wednesday Evening, 5:30 p.m.		**Nuclear and Emerging Technologies for Space: Opening Plenary (Joint LPSC/NETS Plenary Session)**			
Thursday Morning, 8:30 a.m.	NETS SESSIONS	Lunar Chronology By Any Means Necessary	Small Body Studies II: Earth-Crossing to Main Belt	Water on Mars: Flowing, Flooding, and Freezing	Secondary Processes in Chondrites
Thursday Afternoon, 1:30 p.m.	NETS SESSIONS	Lunar Petrology and Geochemistry: From Core to Crust	**SPECIAL SESSION:** Dawn Over Vesta I	Planetary Brines and Alteration	Presolar Grains: Insight into Stellar Processes
Thursday Evening, 6:00 p.m. Town Center Exhibit Area Poster Session II					
Friday Morning, 8:30 a.m.	NETS SESSIONS	Lunar Geophysics and Internal Structure	**SPECIAL SESSION:** Dawn Over Vesta II: The HED-Vesta Connection	Mars Aeolian Processes: Prepare to be Blown Away! ***Followed at 10:00 a.m. by*** Mars Polar Processes: Very Cold and Really Cool	Cosmic Dust: Interstellar, Interplanetary, and Cometary Material
Friday Afternoon, 1:30 p.m.	NETS SESSIONS	Lunar Mapping ***Followed at 10:00 a.m. by*** Mars Climate Tales: Meteorites, Morphology, Models	**SPECIAL SESSION:** Dawn Over Vesta III: Regolith of a Transitional Planet	Young Solar System Cataclysm	Planetary Interiors: Dynamics and Differentiation

NETS Week at a Glance

Day and Time	Waterway Ballroom 1	Waterway Ballroom 2	Waterway Ballroom 3	Waterway Ballroom 4/5	Panther Creek
Wednesday Afternoon, 12:15 p.m.					NETS Tutorial: Building the Bridge Between Science Missions and Nuclear Power Sources
Wednesday Evening, 5:30 p.m.				Nuclear and Emerging Technologies for Space: Opening Plenary	
Thursday Morning, 8:30 a.m.	Fission Power Systems		Radioisotope Power Systems: Pu-238 Production and Analysis		
Thursday Morning, 10:30 a.m.	Advanced Concepts: Advanced Fission Concepts and Systems	Missions and Architectures: Space Radiation Shielding and Lunar Surface Concepts	Radioisotope Power Systems: Mission Simulation, Integration and Test		
Thursday Afternoon, 1:00 p.m	Fission Power Systems: Reactor Design and Simulation	Nuclear Thermal Propulsion: Program Overview	Radioisotope Power Systems: RPS Design Safety		
Thursday Afternoon, 3:30 p.m	Fission Power Systems: Heat Transfer and Thermal Control	Nuclear Thermal Propulsion: Modeling	Radioisotope Power Systems: Thermoelectric Energy Conversion		
Thursday Evening, 6:00 p.m. Town Center Exhibit Area Poster Session: Nuclear and Emerging Technologies for Space					
Friday Morning, 8:30 a.m.	Fission Power Systems: Power Conversion, Management, and Distribution	Nuclear Thermal Propulsion: NTP Fuels I	Radioisotope Power Systems: Stirling Generators		
Friday Morning, 10:30 a.m.	Fission Power Systems: Testing and Validation	Nuclear Thermal Propulsion: NTP Fuels II	Radioisotope Power Systems: Stirling Energy Conversion		
Friday Afternoon, 1:30 p.m.	Missions and Architectures: Space Policy and Risk Analysis	Advanced Concepts: Aneutronic Fusion Power and Propulsion	Radioisotope Power Systems: Alternative Fuels and Methods		
Friday Afternoon, 3:30 p.m.		Advanced Concepts: LENR, Anti-Matter, and New Physics	Radioisotope Power Systems: Future RPS Concepts		

Smithsonian/NASA ADS
adslabs.org
Smithsonian Astrophysical Observatory
60 Garden Street, MS 83
Cambridge MA 02138

Contact: Donna Thompson
617-496-7660
dthompson@cfa.harvard.edu

The NASA Astrophysics Data System (ADS) is a Digital Library portal offering access to 9 million bibliographic records in Astronomy and Physics. The ADS provides access and links to a wealth of external resources, including electronic articles, data catalogs, and archives. Please stop by our booth for a demonstration of ADS Labs, our new search interface featuring filtering of results, visualization of bibliographic networks, article recommendations, and full-text searching. Find us online at http://adslabs.org.

Space Science in Wikipedia
www.lpi.usra.edu
Lunar and Planetary Institute
3600 Bay Area Blvd
Houston TX 77059

Contact: Mary Ann Hager
281-486-2136
mhager@hou.usra.edu

The Lunar and Planetary Institute (LPI) is a research institute that provides support services to NASA and the planetary science community, and conducts planetary science research under the leadership of staff scientists, visiting researchers, and postdoctoral fellows. LPI is available to assist the science community in sharing their knowledge and expertise worldwide on the world's most successful online encyclopedia, Wikipedia.

Springer
www.springer.com
233 Spring St.
6th Floor
New York NY 10013

Contact: Megan Ernst
212-460-1511
megan.ernst@springer.com

Our business is publishing. Throughout the world, we provide scientific and professional communities with superior specialist information — produced by authors and colleagues across cultures. We foster communication among our customers — researchers, students, and professionals. We think ahead, move fast, and promote change: Creative business models, inventive products, and mutually beneficial international partnerships have established us as a trusted supplier and pioneer in the information age.

The Boeing Company
www.boeing.com
Advanced Space Exploration
13100 Space Center Blvd
MC HB4-20
Houston TX 77059

Contact: Kurt Klaus
281-226-5707
kurt.k.klaus@boeing.com

Boeing Defense, Space & Security's Phantom Works group includes advanced programs, pursues new business, and executes new programs prior to their reaching the System Design and Development phase. In close collaboration with Boeing Research & Technology, Boeing's advanced research and development unit, Phantom Works develops and transitions advanced programs into the BDS business areas and ultimately to BDS' defense and space customers.

The University of Arizona Press
www.uapress.arizona.edu
1510 E. University Blvd
Tucson AZ 85721-0055

Contact: Arin Cumming
520-621-4913
acumming@uapress.arizona.edu

The University of Arizona Press publishes important research that bears great significance to the field of Space Science, including publications in our Space Science Series. Please visit our website, www.uapress.arizona.edu, for more information and visit us in our booth during to see a great selection of our books available for order at a special conference discount.

U.S. Geological Survey Astrogeology Science Center
astrogeology.usgs.gov/
2255 N. Gemini Dr
Bldg. 6
Flagstaff AZ 86001

Contact: Corey Fortezzo
928-556-7133
cfortezzo@usgs.gov

The United States Geological Survey Astrogeology Science Center is a community leader in planetary science research, image processing, cartography, geologic mapping, and geographic information system (GIS). Our mission is to serve the planetary community and public with research and technical expertise, analytical software, image products, digital and print maps, technical training, and education and public outreach programs.

NASA Radioisotope Power Systems

rps.nasa.gov
NASA/JPL
4800 Oak Grove Drive
Mail Stop 180-112
Pasadena CA 91109-8001

Contact: Eddie Gonzales
818-354-2326
edward.v.gonzales@jpl.nasa.gov

The Radioisotope Power Systems Program is an ongoing partnership between NASA and the U.S. Department of Energy to develop the next generation of reliable radioisotope power systems (RPS), enabling a broad range of science missions that could operate more widely and efficiently than their predecessors. This mission-driven technology development program is developing and validating two basic RPS units: the Multi-Mission Radioisotope Thermoelectric Generator (MMRTG) and the Advanced Stirling Radioisotope Generator (ASRG).

NASA's Eyes on the Solar System

solarsystem.nasa.gov/eyes
NASA/JPL
4800 Oak Grove Drive
Mail Stop 180-112
Pasadena CA 91109-8001

Contact: Eddie Gonzales
818-354-2326
edward.v.gonzales@jpl.nasa.gov

Almost everyone with a computer can now "ride along" with our planetary missions in a video-game like fashion. Using "Eyes on the Solar System," people everywhere can experience NASA and some ESA missions in real time or travel through time viewing missions from 1950 through 2050 using real mission data. New features and operation of NASA's "Eyes on the Solar System" and "Eyes on the Earth" online tools will be demonstrated.

National Nuclear Laboratory (UK)

www.nnl.co.uk
Chadwick House (5th Floor)
Birchwood Park
Warrington WA3 6AE
United Kingdom

Contact: Tim P Tinsley
tim.p.tinsley@nnl.co.uk

The UK's National Nuclear Laboratory (NNL) offers an unrivalled breadth of technical products and services to our customers across the whole nuclear industry. NNL covers the complete nuclear fuel cycle from fuel manufacture and power generation, to reprocessing, waste treatment, and disposal and including defence, new nuclear builds, and Homeland Security. NNL provides these services supported by an impressive range of facilities and links with international research organisations, academia, and other national laboratories.

NLSI-Center for Lunar Science and Exploration

www.lpi.usra.edu/nlsi/
USRA
3600 Bay Area Boulevard
Houston TX 77058

Contact: Julie Tygielski
281-486-2122
tygielski@lpi.usra.edu

The Center for Lunar Science and Exploration is an integral member of the NASA Lunar Science Institute and is designed to address the highest science priorities identified by the National Research Council for NASA, integrate lunar science with exploration activities to enhance mission productivity, generate expertise to meet the nation's needs, and provide a pipeline of knowledge for students and the public.

PDS Geosciences Node

pds-geosciences.wustl.edu
NASA
Washington University in St. Louis
One Brookings Dr., Campus Box 1169
St. Louis MO 63130

Contact: Susan Slavney
314-935-9295
geosci@wunder.wustl.edu

The Geosciences Node of NASA's Planetary Data System (PDS) archives and distributes data related to the study of the surfaces and interiors of terrestrial planetary bodies. We work with NASA missions to help them generate well-documented, permanent data archives. We provide data to NASA-sponsored researchers upon request, make data available using Analyst's Notebooks and Orbital Data Explorers, and provide expert assistance in using the data.

Regional Planetary Image Facility (RPIF) Network

science.nasa.gov/planetary-science/planetary-science-data/regional-planetary-image-facilities-rpif/
USGS Astrogeology Science Center
2255 N. Gemini Dr.
Flagstaff AZ 86001

Contact: David Portree
928-556-7037
dportree@usgs.gov

NASA's 17 U.S. and overseas Regional Planetary Image Facilities (RPIFs) supply planetary data to researchers, students, and the public. The RPIF Network was founded in 1977 to maintain photographic and digital data and mission documents. RPIF facilities, which are open to the public, are reference centers for browsing, studying, and selecting planetary data including images, maps, documents, and outreach materials. Experienced staff at each facility assist scientists, educators, students, media, and the public in accessing materials.

Hamilton Sundstrand Rocketdyne

www.utc.com/units/hamilton.htm
6633 Canoga Ave.
Canoga Park CA 91309

Contact: Mike Tosca
818-586-0432
Mike.Tosca@hsr.utc.com

Hamilton Sundstrand Rocketdyne is currently working with NASA and the Department of Energy in defining and developing the latest radioisotope generators and nuclear power systems to power spacecraft and lunar surface systems, as well as advanced terrestrial nuclear power plants. We have been instrumental in bringing the necessary experience to energy and space exploration programs including innovative electrical power conversion, power management and distribution, heat transport, and thermal management as well as large-scale system integration, reliability and safety, and payload solutions.

Jacobs Technology

www.jacobstechnology.com
2224 Bay Area Blvd
Houston TX 77058

Contact: Glenn Ellis
281-461-5732
Glenn.Ellis@escg.jacobs.com

Jacobs Technology is the advanced technology division of Jacobs Engineering, one of the nation's largest engineering and technical services-only companies. With 70+ years of experience supporting government and commercial clients, we have earned a reputation for excellence and outstanding technical and managerial achievements in quality, performance, and safety. Our clients include the DOD, NASA, the U.S. Special Operations Command, the DOE, and dozens of commercial clients, such as Boeing, Lockheed Martin, Rolls-Royce, and General Motors.

JHU/Applied Physics Laboratory

civspace.jhuapl.edu
11100 Johns Hopkins Road
Laurel MD 20723

Contact: Margaret Simon
240-228-7150
Margaret.Simon@jhuapl.edu

The Johns Hopkins University's Applied Physics Laboratory (APL) leads several NASA planetary missions and conducts significant grant-based research on planetary, space, and Earth science interests. APL has built more than sixty-four spacecraft and instruments, including New Horizons, MESSENGER, STEREO, and RBSP.

JMARS — Mars Space Flight Facility — Arizona State University

jmars.mars.asu.edu
201 E. Orange Mall
Tempe AZ 85287

Contact: Scott Dickenshied
sdickens@mars.asu.edu

JMARS (Java Mission-planning and Analysis for Remote Sensing) is a Java-based geospatial information system developed by the Mars Space Flight Facility at Arizona State University. It is currently used for mission planning and scientific data analysis by several NASA missions, including Mars Odyssey, Mars Reconnaissance Orbiter, and the Lunar Reconnaissance Orbiter.

Lockheed Martin

www.lockheedmartin.com
P.O. Box 179
Mail Stop S8110
Denver CO 80201

Contact: Melissa Croswhite
303-971-9646
melissa.croswhite@lmco.com

Headquartered in Bethesda, Maryland, Lockheed Martin is a global security company that employs about 126,000 people worldwide and is principally engaged in the research, design, development, manufacture, integration, and sustainment of advanced technology systems, products, and services. Expanding our knowledge and understanding of the universe is a challenging endeavor that Lockheed Martin has been actively engaged in for five decades. We have developed and deployed numerous spacecraft and products supporting our understanding of Earth and Planetary Science, Heliophysics, and Astrophysics. We're accountable to one standard — 100% mission success. We understand the risks and will not shy away from the hard challenges associated with this mission.

NASA In-Space Propulsion Technology Program

spaceflightsystems.grc.nasa.gov/Advanced/ScienceProject/ISPT/
NASA Glenn Research Center
21000 Brookpark Rd, Mail Stop 142-5
Cleveland OH 44136

Contact: Daniel Vento
216-433-2834
Daniel.M.Vento@nasa.gov

Design Your Mission! NASA's In-Space Propulsion Technology program is sponsoring an opportunity to design your mission with the latest in NASA's Mission Design tools. Mission designers will be available to discuss your concept, potential methods of implementation, and design a notional trajectory to determine delivered capabilities and mission class estimate. The NASA ISPT Project provides advanced propulsion technology for planetary science missions. Technologies include advanced ion propulsion, advance chemical propulsion, and planetary ascent vehicles, as well as aerocapture and Earth entry vehicles.

LIST OF EXHIBITORS

Cambridge University Press
www.cambridge.org/us
32 Avenue of the Americas
New York NY 10013-2473

Contact: James Murphy
212-924-3900
jmurphy@cambridge.org

Cambridge's publishing in books and journals combines state-of-the-art content with the highest standards of scholarship, writing and production. Visit our stand to browse new titles, available at a 20% discount, and to pick up sample issues of our journals. Visit our website to see everything we do: www.cambridge.org/us/.

Center for Space Nuclear Research
www.usra.csnr.edu
Universities Space Research Association
995 University Blvd.
Idaho Falls ID 83401

Contact: Delisa Rogers
208-526-5309
drogers@usra.edu

The Center for Space Nuclear Research (CSNR) is operated by the Universities Space Research Association (USRA) and Idaho National Laboratory (INL). The CSNR is a focus for engaging university research scientists in research and development of advanced space nuclear systems, including power/propulsion systems and radioisotope power generators. The CSNR creates opportunities for university researchers to collaborate with their counterparts at NASA and INL in projects to advance nuclear technologies for space exploration and other space applications.

Centre for Planetary Science and Exploration
www.cpsx.uwo.ca
Department of Earth Science
The University of Western Ontario
1151 Richmond Street
London Ontario N6A5B7 Canada

Contact: Alyssa Gilbert
519-661-2111
amoldow@uwo.ca

The goal of the Centre for Planetary Science and Exploration (CPSX) is to make The University of Western Ontario (Western) the focus for planetary science and exploration research in Canada, and to establish Western as a leading school for space systems design. The CPSX boasts the largest planetary science research group in Canada, consisting of over 50 faculty members and researchers, 10 post-docs, and 35 graduate students from 10 academic departments across the university.

Google Lunar X PRIZE
www.googlelunarxprize.org
X PRIZE Foundation
5510 Lincoln Blvd, Suite 100
Playa Vista CA 90094

Contact: Alexandra Hall
alex.hall@xprize.org

Before the end of 2015, robots will be landing on the surface of the Moon as competitors in the Google Lunar X PRIZE, vying to win some of a $30 million prize purse, and establish new efficient and effective ways to reach the Moon. Our 26 teams, from 16 countries, have a variety of options for taking small science payloads to the surface and are now seeking to partner with interested scientists!

ABOUT NETS-2012

The 2012 Nuclear and Emerging Technologies for Space (NETS-2012) meeting is the first topical meeting held in conjunction with the Lunar and Planetary Science Conference. NETS-2012 is organized by the Aerospace Nuclear Science and Technology Division (ANSTD), a professional division of the American Nuclear Society (ANS). Sponsored by the ANSTD and co-sponsored by the American Institute of Aeronautics and Astronautics (AIAA), NETS-2012 is the premier conference covering advanced power and propulsion systems for landed and in-space applications in 2012.

With authors hailing from universities, national laboratories, NASA centers and industry, NETS-2012 will provide an excellent communications network and forum for information exchange. The unique NETS venue attracts presentations from a wide range of experiences and expertise. NETS attendees range from engineers designing space power and propulsion systems, to those completing mission planning and analysis for proposed space missions, to scientists who are designing payloads for those missions. NETS-2012 will allow nuclear professionals to learn about missions that require high power or advanced propulsion systems — conversely, it will allow mission designers opportunities to learn more about what advanced power and propulsion systems are available or could be developed to meet the needs of those missions. Establishing these lines of communication — and then working to keep them open through collaborative work — will more rapidly advance technology development, as it will be developed to specifically meet the needs of the user community.

The conference will include an opening plenary session, a tutorial on nuclear systems, and numerous technical sessions organized into five technical track areas:

Missions and Architectures ❖ Fission Power and Propulsion ❖ Radioisotope Power Systems
Nuclear Thermal Propulsion ❖ Advanced Concepts

LOGISTICAL INFORMATION

Venue Address and Phone Number
The meeting is being held at The Woodlands Waterway Marriott Hotel and Convention Center, which is located at 1601 Lake Robbins Dr., The Woodlands TX 77380. The phone number for the hotel is 281-367-9797. Messages may be left for attendees by phoning the hotel and asking for the conference registration desk.

Internet Access
Complimentary Wi-Fi service will be available throughout the duration of the conference in the Creekside Park and College Park rooms (open only during conference hours), and in the Town Center Exhibit Area and immediate vicinity. Wi-Fi service will NOT be available in the oral session rooms. This restriction is (and has been) in place to curtail activities that could be distracting to speakers during their presentations.

Conference Shuttle Service
Conference shuttle bus service between the venue and the approved list of hotels will be provided on Sunday evening during the registration time and throughout the duration of the conference. Shuttle service will run before and immediately following all evening activities. Detailed shuttle schedules are available in the registration area.

NEW THIS YEAR!!!

AlphaGraphics will have a staffed booth at The Woodlands Waterway Marriott, just outside the Town Center Exhibit Area. Poster presenters can pick up pre-ordered posters or place orders for posters beginning on Sunday, March 18, at 4:00 p.m. The desk is located just outside the Town Center Exhibit Area on the first floor. For more information, visit their website at http://www.txagprinting.com/.

Create your own personal meeting schedule using the Personal Schedule tool found in the USRA Meeting Portal! Select the sessions you want to attend or talks you want to hear, then create a shareable schedule that can be viewed on your smart phone or shared with a colleague.

Announcing NETS-2013

NETS-2013 will return to Albuquerque as a stand-alone conference sponsored by the American Nuclear Society, the Aerospace Nuclear Science and Technology Division, and the Trinity Section of ANS and co-sponsored by the American Institute of Aeronautics and Astronautics (AIAA). Mark your calendars for **February 25–28, 2013,** and join us at the Albuquerque Marriott!

NETS-2013 Organizing Committee
General Chairs: Shannon Bragg-Sitton, INL and Lee Mason, NASA GRC; Local Chair: Tom Conboy, SNL; Program Chairs: Rob O'Brien, CSNR and John Bess, INL.

If you are interested in knowing more about NETS-2013, including participation as part of the organizing committee, please send an e-mail to NETSconf@gmail.com.

NUCLEAR AND EMERGING TECHNOLOGIES FOR SPACE (NETS)

Program of Technical Sessions

March 21–23, 2012

The Woodlands Waterway Marriott Hotel and Convention Center
The Woodlands, Texas

Sponsored by
American Nuclear Society (ANS)
American Institute of Aeronautics and Astronautics (AIAA)
Aerospace Nuclear Science and Technology Division of ANS

General Co-Chairs
Leonard Dudzinski, *NASA Headquarters*
Wade Carroll, *U.S. Department of Energy Headquarters*
George Schmidt, *NASA Glenn Research Center*

Logistics
Shannon Bragg-Sitton, *Idaho National Laboratory*

Local Chair/LPI Liaison
John Scott, *NASA Johnson Space Center*

Publications Chair
Martin Sattison, *Idaho National Laboratory*

Technical Program Track Chairs
Radioisotope Power Systems: Tom Sutliff (*NASA GRC*) and Dirk Cairns-Gallimore (*DOE HQ*)
Fission Power Systems: Michael Houts (*NASA MSFC*) and Lee Mason (*NASA GRC*)
Nuclear Thermal Propulsion: Jonathan Webb (*INL*) and Stanley Borowski (*NASA GRC*)
Advanced Systems (Fusion): John Scott (*NASA JSC*) and Robert O'Brien (*Center for Space Nuclear Research*)
Mission Applications: Jackie Green (*JPL*)

Session Chairs

Steven Howe, CSNR/INL
Rodger Dyson, NASA GRC
Sterling Bailey, Bailey Engineering & Management
John Scott, NASA JSC
Scott Wilson, NASA GRC
Jeffrey Nosanov, JPL
Dave Woerner, JPL
James Werner, INL
Don Palac, NASA GRC
Jacklyn Green, JPL
Bruce Schnitzler, INL
Ron Lipinski, SNL
Ryan Bechtel, DOE HQ
Harold White, NASA JSC
Stan Borowski, NASA GRC
Jeramie Broadway, NASA MSFC
J. Boise Pearson, NASA MSFC

A. Louis Qualls, ORNL
Marc Gibson, NASA GRC
Omar Mireles, NASA MSFC
Maxwell Briggs, NASA GRC
Jonathan Webb, INL
Thomas Godfroy, Maximum Technologies, Inc.
Jean-Pierre Fleurial, JPL
Joseph Sholtis, Consultant
Alice Caponiti, DOE HQ
Jeffrey George, NASA JSC
June Zakrajsek, NASA GRC
Karla Clark, JPL
Shannon Bragg-Sitton, INL
Robert Hickman, NASA MSFC
Rebecca Onuschak, DOE HQ
Wayne Wong, NASA GRC
Yasumori Miura, Yamaguchi University

Produced by the Lunar and Planetary Institute (LPI), 3600 Bay Area Boulevard, Houston TX 77058-1113. Logistics, administrative, and publications support for the meeting were provided by the Meeting and Publication Services Department of the LPI. The LPI is operated by the Universities Space Research Association under a cooperative agreement with the Science Mission Directorate of the National Aeronautics and Space Administration.

Woodlands Waterway Convention Center Map

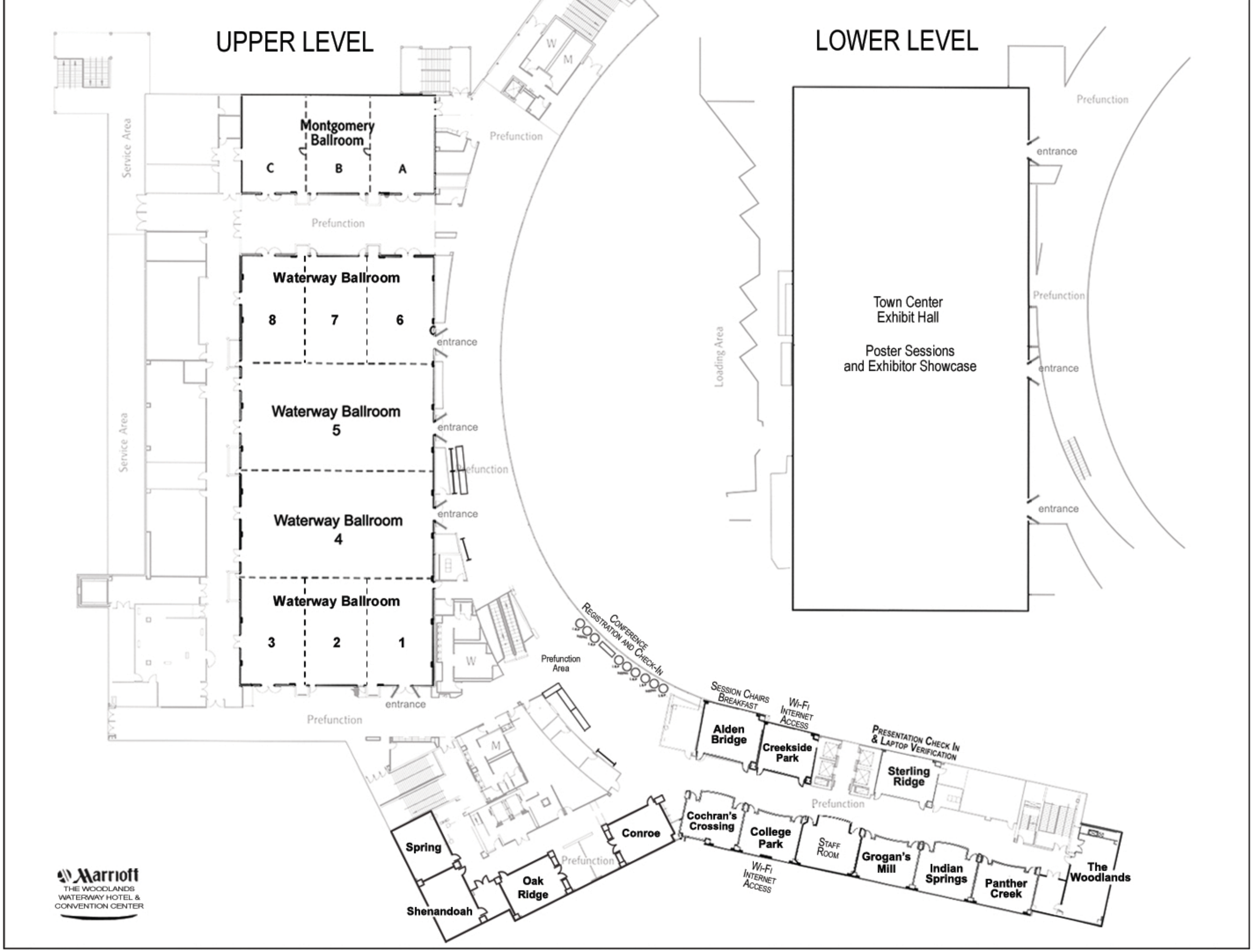

NETS 2012

Nuclear and Emerging Technologies for Space

March 21–23, 2012
The Woodlands, Texas

PROGRAM OF TECHNICAL SESSIONS

The World's Forum for Aerospace Leadership